



University of
Sheffield



Institute of
Molecular and
Cell Biology

IMCB

Dissecting Extracellular Matrix Internalisation Mechanisms using Functional Genomics

Montserrat Llanses Martínez

This thesis is submitted in partial fulfilment
of the requirements for the degree of
Doctor of Philosophy

School of Biosciences
Faculty of Science
The University of Sheffield

January 2023

ABSTRACT

Breast and ovarian malignancies account for one third of female cancers. The role of the stroma in supporting invasive growth in breast cancer has become clear. Breast cancer cells interact and respond to the cues from the surrounding extracellular matrix (ECM). Integrins are main cell adhesion receptors and key players in invasive migration by linking the ECM to the actin cytoskeleton. In addition, integrins mediate distinctive biochemical and biomechanical signals to support cancer invasion. The role of matrix proteases in promoting ECM degradation and cancer dissemination has been extensively studied; however, cancer cells possess additional means to support those processes, such as integrin-mediated ECM endocytosis and consequent degradation in the lysosomes. Internalisation of the extracellular matrix is upregulated in invasive breast cancer. Nonetheless, the mechanisms by which cancer cells regulate this process are poorly understood. We developed a high throughput pH sensitive system to detect ECM uptake. Here, we show that MDA-MB-231 breast cancer cells converge in macropinocytosis to internalise diverse ECM components and we confirm that this process is modulated by PAK1. To unravel which ECM components breast cancer cells internalise in a complex environment (namely, cell derived matrices), we performed mass spectrometry. Proteomic analysis identified Annexin A6, Collagen VI, Tenascin C and fibronectin, among other matrisome proteins, to be internalised by invasive breast cancer cells. Following ECM endocytosis, ECM is targeted for lysosomal degradation. To unravel the molecular mechanisms behind this process, we performed a trafficking screen and identified the AP3 complex, VAMP7, Arf1 and ARFGEF2. Our results suggest that the AP3 complex may regulate ECM-integrin delivery to lysosomes.

To gain more insight on the signalling pathways governing macropinocytosis in breast cancer cells, we performed a kinase and phosphatase screen that unravelled MAP3K1 and PPP2R1A, a subunit of protein phosphatase 2A (PP2A) as relevant regulators of ECM endocytosis. Furthermore, our data suggests that p38 mitogen-activated protein kinase (MAPK) activation upon binding to the ECM is required for ECM macropinocytosis. Outstandingly, inhibiting p38 MAPK led to profound changes in the ability of breast cancer cells to migrate in cell derived

matrices. Previous work from the Rainero lab focused on characterising the receptors involved in ECM internalisation; $\alpha 2\beta 1$ integrin was identified as the main regulator of ECM uptake in MDA-MB-231 cells. In particular, $\alpha 2\beta 1$ integrin has been shown to activate p38 MAPK pathway. Taken together, we hypothesise that binding of ECM to $\alpha 2\beta 1$ integrin results in the activation of PAK1 and MAP3K1, which in turn leads to ECM endocytosis. p38 MAPK activity may induce changes in actin polymerisation via PPP2R1A and/or focal adhesion turnover, which consequently promotes ECM macropinocytosis and invasive migration.

ACKNOWLEDGEMENTS

I would like to thank my supervisors, **Dr Elena Rainero** and **Dr Frederic Bard** for providing me with the opportunity to work within their laboratories to complete my PhD. I am truly and sincerely grateful to Elena for entrusting me with this project and keeping her door always open for discussion. I am much obliged for her constant guidance, motivation, confidence in my work and support with my hundreds of hypotheses. She is a great mentor.

My gratitude is extended to **Dr Xavier Le Guezennec**, who enabled this project to succeed. I would like to thank him for his trust in me to overcome the constraints of this project, as well as his help to make this project work through covid. Xavier was always willing to give advice to my latest results and problems; he was a true supervisor in Singapore. I would like to extend my gratitude to the members of my Singaporean lab. Thank you to **Pei Ling (Felicia) Tay, Trinda Anne Ting, Keit Min (Jasmine) Tham, Hui Hui Wong** and **Sze Hwee Seet** for their support, chats together, snacks and baked goods to cheer me up. I really appreciated it. Thank you to **Dr Rebecca Bennion** for always lending an ear when I needed it. Becca you were a great lab mate. I really enjoyed our chats over coffee and our lunches together. We indeed got each other through our stay in Singapore. I am truly grateful for your friendship. I wish you all the best for your postdoc life in Marseille. Thank you to **Dr Poonam Shah** for her friendship in the lab. Our video calls during Circuit breaker made me truly happy. I really enjoyed ladies' night in Cé la vie. Massive thanks for taking me to Kanchanaburi (Thailand) to see elephants. My thanks are extended to **Laura Andrea Berrio Correa** for exploring Singapore with me and making my life so much better. She is the best flatmate I have ever had.

I would also like to thank my advisors, **Professor Elizabeth Smythe** and **Dr Vincent Cunliffe** for their support during my PhD. I would also like to thank **Dr Mark Collins** (Mass Spectrometry Centre, The University of Sheffield) for troubleshooting through the mass spec protocol with me. I would like to thank **Dr Carl Harrison** for his help with Single molecule localisation microscopy. In addition, I would like to express my deep thanks to past and present members of **Kathryn Ayscough, Steve Winder, Helen Matthews** and **Elena Rainero** labs. I would like to thank **Dr Stella Christou, Dr Mona Nazemi** and **Dr Keqian Nan** for becoming my first friends in Sheffield. Stella,

see you in Vienna. Thank you to **Rachele Bacchetti** for her help with Western Blots; as well as our conversations over dinner and bubble tea after late evenings in the lab. Thank you to **Dr Victoria H. Hart** for being very helpful and an excellent desk neighbour. Thank you to **Shengnan Yuan** for her willingness to help and also for walking me home. Simply thank you to **Bian Yanes, Shahd M Alhadid, Haya Alomaim** and **Zhe Bao** for being such good lab mates.

I would like to specially thank my partner, **Nicolas Smetacek**, for always being by my side despite the distance, for his daily advice, constant encouragement and support. I am extremely thankful for his willingness to help me overcome my challenges. I truly appreciate his daily smile, especially in my darkest days. Nick has always listened to my concerns, my complaints but also celebrated my achievements. I truly know he sincerely felt my emotions. In spite of the distance across countries, continents and time zones, we always made time for video calls.

I would like to extend my thanks to my mother, **Maribel Martínez Arce**, for her constant support throughout the years and her blind trust in me, for believing I can achieve anything I set my mind to. I am extremely grateful to her for considering my education and my sister's her greatest investment. I am extremely fortunate to have such a great mother, I could not have done this without her unconditional encouragement. (Catalan: M'agradaria ampliar el meu agraïment a la meva mare, Maribel Martínez Arce, pel seu suport al llarg dels anys i la seva confiança cega en mi, per creure que puc aconseguir tot el que em proposi. Estic extremadament agraïda a ella per considerar la meva educació i la de la meva germana la seva inversió de futur més gran. Soc extremadament afortunada per tenir una mare excel·lent, no podria haver fet tot això sense el seus ànims incondicionals.)

Ultimately, I would like to dedicate this PhD thesis in loving memory of my grandma **Maria Teresa Arce González**, who told me when I was six years old to study to either become a doctor or a lawyer. Despite not becoming an MD, I know she would have been proud of me. (Spanish: En último lugar, me gustaría dedicar esta tesis doctoral en memoria de mi querida "padrina Tere", quien me dijo a los seis años que estudiara para convertirme en doctora o abogada. A pesar de no ser una doctora/médica, sé que estaría orgullosa de mí.)

DECLARATION

I, Montserrat Llanses Martínez, hereby declare that this thesis is the result of my sole work, except where explicitly stated otherwise, after registration for the degree of Doctor of Philosophy at the University of Sheffield, and it has not been previously submitted to this or any other institution. I am aware of the University's guidance on the Use of Unfair Means (www.sheffield.ac.uk/ssid/unfair-means). I confirm that where I have quoted from the work of others, the source is always given.

The work presented in Figure 3-16, Figure 3-23, Figure 3-24 and Figure 3-26 (Chapter 3) is published in the form of a BioRxiv paper and it is under review as "The extracellular matrix supports cancer cell growth under amino acid starvation by promoting tyrosine catabolism" by Mona Nazemi, Bian Yanes, **Montserrat Llanses Martínez**, Heather Walker, Frederic Bard* and Elena Rainero*. This study was conceived by all of the authors.

*Supervisors

Montserrat Llanses Martínez

31st January 2023

Table of contents

ABSTRACT	I
ACKNOWLEDGEMENTS	III
DECLARATION	V
Table of contents	VI
List of figures	XII
List of tables	XVI
Abbreviations	XVII
Chapter 1 – Introduction	1
1.1. CANCER BIOLOGY	1
1.1.1. An introduction to cancer	1
1.1.1.1. The hallmarks of cancer	1
1.1.2. An overview to Breast cancer	2
1.1.2.1. Epidemiology	2
1.1.2.2. Breast cancer progression and subtypes	3
1.1.3. The tumour microenvironment	5
1.1.4. A brief introduction to signal transduction pathways in cancer	11
1.2. ENDOCYTOSIS AND ENDOSOME TRAFFIC IN CANCER	14
1.2.1. The plasma membrane and endocytic membrane traffic	14
1.2.1.1. Clathrin-mediated endocytosis	14
1.2.1.2. Lipid raft-mediated endocytosis	15
1.2.1.3. Phagocytosis, macropinocytosis and the CLIC-GEEC pathway	17
1.2.2. Endolysosomal trafficking	20
1.2.3. Dysregulation of membrane traffic in cancer	21
1.3. THE EXTRACELLULAR MATRIX IN CANCER	26
1.3.1. Post-translational modifications of the extracellular matrix	27
1.3.1.1. Disulphide cross links in the ECM	27
1.3.1.2. Hydroxylation crosslinks in the ECM	28
1.3.1.3. Glycosylation, glycation and phosphorylation of the ECM proteins	29
1.3.2. ECM proteins in the tumour microenvironment	30
1.3.2.1. Collagens: Fibrous ECM proteins	30
1.3.2.1.1. The formation of the triple helix	31

1.3.2.1.2. Network-forming collagens	32
1.3.2.1.2. Collagens assembling into beaded filaments	33
1.3.2.1.3. Anchoring fibril collagens	33
1.3.2.1.4. Transmembrane collagens	34
1.3.2.2. Laminins: Network basement membrane proteins	36
1.3.2.3. Other ECM proteins	37
1.3.2.3.1. Fibronectins	37
1.3.2.3.2. Tenascin-C	38
1.3.2.3.3. Elastin	38
1.3.2.3.4. Vitronectin	39
1.3.2.3.5. Thrombospondins	39
1.3.2.4. Interactions within the ECM meshwork	40
1.3.2.4.1. Collagen interactions	40
1.3.2.4.2. Linking the gap: basement membrane- stroma interactions	42
1.3.2.4.2. Basement membrane ECM interactions	44
1.4. EXTRACELLULAR MATRIX DEGRADATION IN CANCER	46
1.4.1. Invadopodia: specialised structures for ECM degradation	46
1.4.1.1. Signalling regulators of invadopodia	46
1.4.1.2. Integrins and invadopodia	47
1.4.2. Matrix metalloproteinases	49
1.4.2.1. Regulation of MMPs through membrane trafficking	51
1.4.3. Beyond the MMP monopoly: cathepsins, ADAMs, serine proteases and oxidoreductases	54
1.4.3.1. Cathepsins: cysteine, serine and aspartyl proteases	54
1.4.3.2. Serine proteases, ADAM and ADAMTS family	55
1.4.3.3. Protein disulfide isomerases, proteases and ECM degradation	56
1.4.4. Mechanical aspects of ECM degradation	57
1.5. EXTRACELLULAR MATRIX RECEPTORS IN CANCER	58
1.5.1. Integrins	59
1.5.2. Other ECM receptors	63
1.6. INTERNALISATION OF EXTRACELLULAR MATRIX	65
1.6.1. Collagen I internalisation	65
1.6.1.1. Integrin-mediated phagocytosis	65

1.6.1.2. Non-phagocytic pathway of collagen uptake: uPARAP/Endo180-dependent endocytosis	67
1.6.2. Fibronectin internalisation	68
1.6.2.1. Integrins, migration and fibronectin internalisation	69
1.6.3. Laminin internalisation	70
1.6.3.1. Normal mammary epithelial cells endocytose laminin in a Dystroglycan-dependent manner	71
1.6.3.2. Laminin internalisation supports cell survival under starvation conditions	72
1.6.3.3. 67kDa laminin receptor (67LR) is linked to cancer progression	73
1.6.4. Elastin internalisation	73
1.6.5. The ECM meshwork - ECM internalisation in in vivo-like complex matrices	74
1.7. AIMS AND OBJECTIVES OF THE THESIS	75
Chapter 2 – Materials and methods	77
2.1. MATERIALS	77
2.1.1. Reagents and suppliers	77
2.1.2. Solutions	81
2.2. METHODS	81
2.2.1. Cell culture	81
2.2.2. 2.5D collagen I, matrigel and laminin endocytosis assay for confocal microscopy	83
2.2.2.1. Assessment of lysosomal degradation	83
2.2.2.2. Assessing the role of MAPK inhibitors on 2.5D uptake	83
2.2.3. Generation of cell-derived matrices	84
2.2.3.1. CDM endocytosis assay	85
2.2.3.2. Assessing the role of inhibitors on CDM uptake	86
2.2.3.3. Cell migration assay in CDM	86
2.2.4. Transferrin uptake	87
2.2.5. Lactosylceramide uptake	87
2.2.6. Rhodamine-dextran uptake	88
2.2.7. siRNA transfection	88
2.2.7.1. Transfection in 6-well plate	88
2.2.7.2. Transfection in 96-well plate	89
2.2.7.3. Transfection in 384-well plate	89
2.2.8. DNA transfection	91
2.2.8.1. Transient transfection	92

2.2.9. Generation of MDA-MB-231-dCas9-CRISPRi cells	92
2.2.10. RNAi screen	93
2.2.10.1. Knockdown in high throughput systems	93
2.2.10.2. Matrigel coating and labelling in high content imaging plates	94
2.2.10.3. Collagen coating and labelling in high content imaging plates	96
2.2.10.4. Cell detachment in high content imaging plates	97
2.2.10.5. Assessing the role of inhibitors in collagen I and matrigel uptake	99
2.2.11. Assessing 3D uptake in spheroid assay	102
2.2.12. Immunofluorescence	103
2.2.12.1. Quantification	105
2.2.13. Western Blotting	107
2.2.14. Mass spectrometry of internalised ECM proteins	108
2.2.14.1. CDM internalisation assay using biotinylation	108
2.2.14.2. Western blot analysis	109
2.2.14.3. Streptavidin-agarose beads pulldown	110
2.2.14.4. On-beads tryptic digestion	111
2.2.14.5. Desalting and desiccation of digested peptides	111
2.2.14.6. Mass spectrometry analysis	112
2.2.15. Statistical analysis and SuperPlots	112
Chapter 3 – The use of small molecules as a tool to characterise ECM internalisation in high throughput systems.	114
3.1. INTRODUCTION	114
3.2. RESULTS	118
3.2.1. Dynasore and MiTMAB reduce transferrin endocytosis in MDA-MB-231 cells	118
3.2.2. Filipin blocks caveolae-dependent endocytosis of Lactosylceramide in MDA-MB-231 cells	120
3.2.3. Rhodamine-dextran endocytosis is reduced upon EIPA treatment in MDA-MB-231 cells	122
3.2.4. Matrigel and collagen I coating in 384 high content imaging plates	123
3.2.5. Optimisation of ECM internalisation in 384 high content imaging plates	128
3.2.6. Blocking endo-lysosomal acidification impacts on ECM visualisation	132
3.2.7. Assessing the role of cysteine cathepsins in lysosomal degradation of ECM proteins	134

3.2.8. MDA-MB-231 cells converge in macropinocytosis to internalise the diverse ECM components	138
3.2.9. Optimisation of siRNA-mediated downregulation of target genes	144
3.2.10. Regulators of ECM internalisation: β 1-integrin is required for macropinocytosis of ECM	148
3.2.11. Optimisation of a high content screening ECM internalisation assay using pHrodo red	151
3.2.12. PAK1 regulates macropinocytosis of ECM components	156
3.2.13. Extracellular proteolysis by cysteine cathepsins and matrix metalloproteinases is partially required in ECM internalisation	160
3.2.14. MDA-MB-231 breast cancer cells internalise extracellular matrix in 3D culture	162
3.3. DISCUSSION	163
Chapter 4 – Dissecting extracellular matrix internalisation using proteomics	172
4.1. INTRODUCTION	172
4.2. RESULTS	173
4.2.1. Breast cancer cells internalise more ECM components from CDM than normal mammary epithelial cells	173
4.2.2. Proteomic analysis identifies that breast cancer cells internalise pro-tumorigenic ECM-related proteins	176
4.2.3. Optimisation of protein extraction using phospholipase A2	183
4.3. DISCUSSION	185
Chapter 5 – A trafficking screen identifies the AP3 complex as a novel regulator of ECM-bound integrin traffic to lysosomes	195
5.1. INTRODUCTION	195
5.2. RESULTS	198
5.2.1. The internalised ECM components are degraded in the lysosomes in MDA-MB-231 cells	198
5.2.2. An siRNA trafficking screen identifies regulators of ECM traffick to lysosomes	201
5.2.3. Preliminary hit validation confirmed AP3D1 reduced matrigel and collagen I uptake index	204
5.2.4. Downregulation of the AP3 complex promotes β 1-integrin endosomal accumulation in MDA-MB-231 cells	208
5.2.5. Downregulation of the AP3 complex promotes matrigel accumulation in early endosomes	210
5.2.6. The AP3 complex is recruited to Rab5 and Arf1-positive early endosomes containing matrigel	212

5.2.7. Optimisation of single-molecule localisation microscopy	214
5.2.8. Disrupting ligand-bound integrin traffic to lysosomes impinges MDA-MB-231 cell migration on cell derived matrices and poor prognosis in breast cancer patients	216
5.3. DISCUSSION	220
Chapter 6 – A Kinase and Phosphatase functional screen unravels p38 mitogen-activated protein kinase pathway to promote macropinocytosis of integrin-bound extracellular matrix	226
6.1. INTRODUCTION	226
6.2. RESULTS	227
6.2.1. A kinase and phosphatase screen identifies EPH receptors and MAPK cascade as regulators of matrigel uptake	227
6.2.2. A secondary screen confirms that MAP3K1 and PPP2R1A are required for the endocytosis of matrigel	235
6.2.3. Chemical inhibition of EphB4 slightly decreased internalisation of ECM in MDA-MB-231 cells	238
6.2.4. Pharmacological inhibition of EphB4 impairs MDA-MB-231 cell migration	242
6.2.5. p38 MAPK is required for ECM macropinocytosis in MDA-MB-231 cells	243
6.2.6. p38 is required for macropinocytosis of dextran	257
6.2.7. MAP3K1, MAPK11, PPP2R1A and α 2-integrin promote macropinocytosis of ECM	259
6.2.8. Inhibition of p38 MAPK impairs migration of MDA-MB-231 cells	263
6.3. DISCUSSION	266
Chapter 7 – Final Discussion	275
7.1. SUMMARY: PUTTING KEY FINDINGS INTO PERSPECTIVE	275
7.2. ARE INTEGRINS NOVEL REGULATORS OF MACROPINOCYTOSIS?	277
7.3. EXTRACELLULAR AND INTRACELLULAR DEGRADATION IN ECM INTERNALISATION	279
7.4. INVASIVE AND ANCHORAGE INDEPENDENT GROWTH	282
7.5. THERAPEUTIC OPPORTUNITIES	283
7.6. CONCLUSIONS AND FUTURE DIRECTIONS	284
Chapter 8 – References	287
Chapter 9 – Appendix	336
9.1. Supplementary figures	336
9.2. Supplementary tables	349

List of figures

Chapter 1 - Introduction

Figure 1-1. (A) Schematic representation of breast cancer progression. (B) Breast cancer subtypes	5
Figure 1-2. The tumour microenvironment	10
Figure 1-3. (A) Conventional Mitogen-activated protein kinase signalling (MAPK) pathways. (B) PI3K/Akt/mTOR pathway.	13
Figure 1-4. Schematic representation of the foremost endocytic pathways	19
Figure 1-5. Dysregulations of membrane traffic during tumorigenesis	25
Figure 1-6. (A) Collagen biosynthesis. (B) Proteolytic and oxidoreductase cleavage of human collagen IV	35
Figure 1-7. Laminin structure	37
Figure 1-8. Schematic representation of the ECM meshwork	43
Figure 1-9. Diagram of the mechanisms employed by cancer cells to degrade the ECM	53
Figure 1-10. Integrin heterodimers	59
Figure 1-11. Integrin regulation at endosomal level	62
Figure 1-12. Schematic representation of ECM endocytic pathways	71

Chapter 2 - Materials and methods

Figure 2-1. Schematic diagram for generation of CDMs.	85
Figure 2-2. Representative pipeline to assess the knockdown efficiency in Columbus software	90
Figure 2-3. Schematic workflow depicting the key instruments used for high throughput knockdown, matrigel coating and cell splitting	98
Figure 2-4. Schematic pipeline for analysis of ECM endocytosis in high throughput	100
Figure 2-5. Schematic pipeline for analysis of ECM endocytosis in fixed samples	101
Figure 2-6. Spheroid analysis for ECM uptake in 3D	103
Figure 2-7. ECM and integrin internalisation analysis	106
Figure 2-8. Schematic representation of the mass spectrometry workflow	110

Chapter 3 - The use of small molecules as a tool to characterise ECM internalisation in high throughput systems

Figure 3-1. Schematic representation of the foremost endocytic pathways	116
Figure 3-2. Dynasore and MiTMAB reduce transferrin internalisation in MDA-MB-231 cells	119
Figure 3-3. Filipin treatment diminishes LacCer internalisation in MDA-MB-231 cells	121
Figure 3-4. EIPA blocks Rhodamine-dextran internalisation in MDA-MB-231 cells	123
Figure 3-5. Generating matrigel matrices in high content imaging plates	125

Figure 3-6. Generating Collagen I matrices in high content imaging plates	126
Figure 3-7. Generating cell-derived matrices in high content imaging plates	127
Figure 3-8. Fluorescence of endocytosed ECM is dependent on pHrodo concentration	129
Figure 3-9. ECM internalisation is independent of collagen I and matrigel concentration in high throughput systems	131
Figure 3-10. Blocking endo-lysosomal acidification impairs visualisation of intracellular pHrodo-labelled ECM	133
Figure 3-11. Matrigel is trafficked to acidic lysosomes, where cysteine cathepsins mediate its degradation	135
Figure 3-12. Inhibition of cysteine cathepsins results in accumulation of ECM in enlarged vesicles	137
Figure 3-13. Dynasore, filipin and EIPA reduce matrigel internalisation	139
Figure 3-14. Collagen I uptake is inhibited by EIPA in MDA-MB-231 cells	141
Figure 3-15. TIF-CDM uptake is inhibited by EIPA and Dynasore in MDA-MB-231 cells	142
Figure 3-16. The invasive breast cancer cell line MDA-MB-231 converges in macropinocytosis to internalise ECM	143
Figure 3-17. Dharmafect IV and I enable transfection and siRNA mediated downregulation of PLK1 and ITGB1 in MDA-MB-231 cells	145
Figure 3-18. Dharmafect IV enables siRNA mediated downregulation of PLK1 and ITGB1 in MDA-MB-231 cells	147
Figure 3-19. β 1-integrin mediates matrigel internalisation in MDA-MB-231 cells	149
Figure 3-20. β 1-integrin mediates internalisation of collagen I in MDA-MB-231 cells	151
Figure 3-21. Optimisation of cell transfer	153
Figure 3-22. Optimisation of high throughput imaging for matrigel uptake	155
Figure 3-23. DNM2/3, CAV1/2 and PAK1 mediate matrigel internalisation in MDA-MB-231 cells	158
Figure 3-24. PAK1 mediates macropinocytosis of collagen-rich ECM in MDA-MB-231 cells	159
Figure 3-25. Inhibition of cysteine cathepsin reduces ECM uptake	161
Figure 3-26. The invasive breast cancer cell line MDA-MB-231 internalises ECM in 3D	163
Figure 3-27. Schematic summary of the endocytic pathways regulating ECM internalisation	168

Chapter 4 - Dissecting extracellular matrix internalisation using proteomics

Figure 4-1. Invasive MDA-MB-231 cells internalise more CDM than normal mammary MCF10A cells by western blot analysis	175
Figure 4-2. Western blot analysis of internalised CDM in MDA-MB-231 cells on unlabelled and biotinylated CDMs	177
Figure 4-3. Mass spectrometry of internalised CDM in MDA-MB-231 cells	178
Figure 4-4. Western blot for optimisation of protein extraction	185
Figure 4-5. Schematic summary of the hits obtained by mass spectrometry	193
Figure 4-6. Schematic mass spectrometry protocol	194

Chapter 5 - A trafficking screen identifies the AP3 complex as a novel regulator of ECM-bound integrin traffic to lysosomes

Figure 5-1. (A) Schematic representation of AP3 structure and (B) localization in tubular endosomes	197
Figure 5-2. Endocytosed ECM is degraded in the lysosomes by cysteine cathepsins	200
Figure 5-3. A trafficking screen identifies the AP3 complex, ARF1, ARFGEF2 and VAMP7 to regulate matrigel traffic	203
Figure 5-4. Preliminary validation confirms the role of AP3D1 and ARFGEF2 in matrigel traffic	205
Figure 5-5. Preliminary validation confirms the role of AP3D1 and ARFGEF2 in collagen traffic	207
Figure 5-6. AP3D1 knockdown affects cell morphology and promotes a slight increase in the internal pool of ITGB1	209
Figure 5-7. AP3D1 knockdown promotes accumulation of matrigel and ITGB1 in early endosomes	211
Figure 5-8. The AP3 complex is recruited to Arf1 and Rab5 positive early endosomes containing matrigel	213
Figure 5-9. Optimisation of Single-molecule localisation microscopy	215
Figure 5-10. Disrupting the AP3 complex impinges on the directionality and average velocity of MDA-MB-231 cells on CDM	217
Figure 5-11. Comparison of AP3D1 RNA expression in tumour and normal tissues	219
Figure 5-12. Schematic representation of the working model	223

Chapter 6 - A kinase and phosphatase functional screen unravels p38 mitogen-activated protein kinase pathway to promote macropinocytosis of integrin-bound extracellular matrix

Figure 6-1. Kinome and phosphate-wide screen for regulators of matrigel internalisation in the invasive breast cancer cell line MDA-MB-231	228
Figure 6-2. siRNA-mediated downregulation of EphB4, EphA4, DGKE, PKIB, MAP3K1 and PPP2R1A impairs matrigel internalisation	231
Figure 6-3. siRNA-mediated downregulation of BLNK, DLG4, STYK1, PI3KC2A, ABI1 reduce matrigel internalisation	233
Figure 6-4. siRNA-mediated downregulation of AKAP11, RAPGEF3 and AURKB promotes matrigel internalisation	234
Figure 6-5. Secondary validation screen	236
Figure 6-6. Effect of NVP-BHG712 treatment on matrigel internalisation	237
Figure 6-7. 1 μ M NVP-BHG712 slightly reduced collagen I internalisation	239
Figure 6-8. 1 μ M NVP-BHG712 slightly reduced CDM internalisation	241
Figure 6-9. 1 μ M NVP-BHG712 reduced velocity and directionality of MDA-MB-231 cells migrating on CDMs	242
Figure 6-10. p38 β showed a trend towards reduced matrigel uptake index in the kinome and phosphate screen	243
Figure 6-11. Effect of MAPK inhibition on matrigel internalisation	244
Figure 6-12. Effect of MAPK inhibition on collagen I internalisation	246
Figure 6-13. Effect of MAPK inhibition on TIF-CDM internalisation	248

Figure 6-14. Effect of MAPK inhibition on matrigel internalisation	249
Figure 6-15. Effect of MAPK inhibition on collagen I internalisation	251
Figure 6-16. Effect of MAPK inhibition on TIF-CDM internalisation	252
Figure 6-17. p38 MAPK inhibition on reduced collagen I internalisation	254
Figure 6-18. Effect of p38 MAPK inhibition on TIF-CDM internalisation	256
Figure 6-19. SB202190 blocks Rhodamine-dextran internalisation in MDA-MB-231 cells	258
Figure 6-20. MAP3K1, MAPK11, PPP2R1A and α 2-integrin (ITGA2) are required for collagen I internalisation	260
Figure 6-21. sgRNA against PPP2R1A reduced matrigel uptake index in MDA-MB-231 cells	261
Figure 6-22. MAP3K1, MAPK11, PPP2R1A and α 2-integrin (ITGA2) are required for collagen I internalisation	262
Figure 6-23. p38 inhibition reduces velocity and directionality in MDA-MB-231 cells migrating on CDMs	264
Figure 6-24. siRNA downregulation of MAP3K1 and MAPK11 reduces velocity and directionality in MDA-MB-231 cells migrating on CDMs	265
Figure 6-25. Schematic representation of the proposed mechanism promoting ECM internalisation	274

Chapter 7 - Final discussion

Figure 7-1. Schematic summary on the mechanism behind ECM internalisation	276
---	-----

Chapter 9 - Appendix

Figure S1-1. Transferrin, Lactosylceramide and Rhodamine-dextran uptake (non-normalised data related to Figure 3-2, 3-3 and 3-4)	336
Figure S1-2. Cell permeabilization decreases the fluorescence intensity of endocytosed pH-rodo labelled matrigel in MDA-MB-231 cells	337
Figure S1-3. PAK1 mediates macropinocytosis of collagen-rich ECM in MDA-MB-231 cells (non-normalised data related to Figure 3-24)	338
Figure S1-4. Endocytosed ECM is degraded in the lysosomes by cysteine cathepsins (non-normalised data related to Figure 5-2)	338
Figure S1-5. STRING Analysis: Trafficking screen	339
Figure S1-6. KEGG analysis- SNARE interactions in vesicular transport	340
Figure S1-7. KEGG analysis- Lysosome	341
Figure S1-8. Sequence analysis of ITGB1, ITGA2 and LIMP2	342
Figure S1-9. KEGG pathways enriched in the primary screen	343
Figure S1-10. KEGG pathway: FcR-mediated phagocytosis	344
Figure S1-11. KEGG pathways: MAPK Signalling pathway	345
Figure S1-12. STRING Analysis: Kinome and Phosphatome	346
Figure S1-13. Effect of synchronisation by serum starvation on ECM uptake	347
Figure S1-14. Effect of double thymidine block synchronisation on ECM uptake	348

List of tables

Chapter 2 - Materials and methods

Table 2-1. Reagents and suppliers	77
Table 2-2. Recipes of solutions	81
Table 2-3. Cell seeding values for generation of cell derived matrices	85
Table 2-4. siRNA and sgRNA for low throughput screening	91
Table 2-5. List of antibodies in immunofluorescence	104
Table 2-5. List of antibodies in Western blotting	108

Chapter 3 - The use of small molecules as a tool to characterise ECM internalisation in high throughput systems

Table 3-1. Fixative conditions tested	156
---------------------------------------	-----

Chapter 4 - Dissecting extracellular matrix internalisation using proteomics

Table 4-1. Core-matrisome and matrisome-associated proteins detected in the 214 common proteins in biotinylated CDM samples	179
Table 4-2. Extraction buffers used for optimisation of protein extraction	184

Chapter 9 - Appendix

Table S1-1. Heat map table that shows the median and arithmetic mean values for TF uptake index upon dynasore treatment	349
Table S1-2. Heat map table with the median and arithmetic mean values for TF uptake upon MiTMAB treatment	349
Table S1-3. Heat map table with the median and arithmetic mean values for lactosylceramide uptake upon Filipin treatment	349
Table S1-4. List of 214 proteins identified by mass spectrometry and differentially regulated between biotinylated and unlabelled CDMs	350
Table S1-5. Heat map table showing the differences in the median and arithmetic mean values for ECM uptake	356
Table S1-6. Raw data values (related to Figure 5-3) for matrigel uptake index (of at least 4 technical replicates), normalisation between NT5+BafA1 and Z-score calculated for data value	357
Table S1-7. Raw data values (related to Figure 6-1) for matrigel uptake index and normalisation between NT5+BafA1 (-1) and NT5 (0)	363
Table S1-8. Normalised data values (related to Figure 6-5) between NT5+BafA1 (-1) and NT5 (0)	387

Abbreviations

67kDa laminin receptor	67LR
A2780 overexpressing Rab25	A2780-Rab25
Abl Interactor 1	ABI1
<u>A</u> <u>d</u> isintegrin <u>a</u> nd <u>m</u> etalloprotease	ADAM
<u>A</u> <u>d</u> isintegrin <u>a</u> nd <u>m</u> etalloprotease with <u>t</u> hrombospondin motifs	ADAMTS
Advanced glycation end products	AGEs
A-Kinase Anchoring Protein 11	AKAP11
AMP-protein activated kinase	AMPK
Adaptor protein	AP
Adaptor-related protein complex 2 subunit alpha 1	AP2A1
Adaptor-related protein complex 3 subunit beta 2	AP3B2
Adaptor-related protein complex 3 subunit delta 1	AP3D1
Adaptor-related protein complex 4 subunit epsilon 1	AP4E1
ADP ribosylation factor 1	Arf1
ADP ribosylation factor guanine nucleotide exchange factor 2	ARFGEF2
Actin Related Protein 2/3	Arp2/3
ArfGAP with SH3 Domain, Ankyrin Repeat and PH Domain 1	ASAP1
Adenosine triphosphate	ATP
Aurora Kinase B	AURKB
Bovine aortic endothelial cells	BAEC
Bafilomycin A1	BafA1
Bin-Amphiphysin-Rvs	BAR
Branched-chain amino acid	BCAA
Branched Chain Amino Acid Transaminase 1	BCAT1
Branched-chain α -ketoacid	BCKA
Bet1 Golgi vesicular membrane trafficking protein	BET1
B-Cell Linker protein	BLNK
Basement membrane	BM
BCL2 interacting protein 1	BNIP1
Breast cancer 1	BRCA1
Bovine serum albumin	BSA
Cancer associated fibroblasts	CAFs
Cyclic adenosine monophosphate	cAMP
Caveolin	CAV/Cav
Clathrin-coated pits	CCPs
Clathrin-coated vesicles	CCVs
Cell division cycle 42	Cdc42
Cyclin Dependent Kinase Inhibitor 3	CDKN3
Cell derived matrix	CDM

Clathrin-independent endocytosis	CIE
CDC42-interacting protein 4	CIP4
Casein kinase 2	CK2
Clathrin light-chain	CLCb
Clathrin-independent carriers and GPI-Enriched Endocytic Compartments	CLIC-GEEC
Chloride Intracellular Channel Protein 3	CLIC3
Clathrin heavy chain	CLTC/CHC17
Clathrin-mediated endocytosis	CME
Conserved oligomeric golgi	COG
COPI Coat complex subunit beta 2	COPB2
Class C core vacuole/endosome tethering	CORVET
Clustered regulatory interspaced short palindromic repeats interference	CRISPRi
Coefficient of variation	CV
CYFIP Related Rac1 Interactor A	CYRI-A
CYFIP Related Rac1 Interactor B	CYRI-B
Dialised foetal bovine serum	D-FBS
Ductal carcinoma in situ	DCIS
Discoidin domain receptors	DDR
Dystroglycan	DG
Diacylglycerol kinase α	DGK- α
Diacylglycerol kinase epsilon	DGKE
Discs Large MAGUK Scaffold Protein 4	DLG4
Dulbecco's modified eagle medium	DMEM
Dimethyl sulfoxide	DMSO
Dynamin	DNM/Dyn
Dye-quenched collagen	DQ-Collagen
Dithiothreitol	DTT
Dual Specificity Phosphatase 8	DUSP8
Extracellular matrix	ECM
Ethylenediaminetetraacetic acid	EDTA
Early endosomes	EE
Early endosomal antigen 1	EEA1
Ephrin ligand	EFN
Epidermal growth factor	EGF
Epidermal growth factor Receptor	EGFR
EH domain-containing protein 2	EHD2
Ethyl-isopropyl amiloride	EIPA
Eker Leiomyoma Tumour-3	ELT-3
Elastin microfibril interface 1	EMILIN-1
Epithelial-to-mesenchymal transition	EMT
Urokinase plasminogen activator receptor-associated protein	Endo180/uPARAP

Ephrin receptor	Eph
Ephrin A4 (receptor)	EphA4
Ephrin B2 (receptor)	EphB2
Ephrin B4 (receptor)	EphB4
Epidermal growth factor receptor substrate 15	EPS15
Epidermal growth factor receptor substrate 15-like 1	EPS15R
Oestrogen receptor	ER
Extracellular signal regulated kinase	ERK
Endosomal sorting complex required for transport	ESCRT
Extracellular vesicles	EVs
Focal adhesions	FAs
Fibril-associated collagens with interrupted triple helices	FACITs
fluorescence activated cell sorting	FACS
Focal adhesion kinase	FAK
fibroblast activation protein	FAP α
Foetal bovine serum	FBS
F-BAR domain only protein 1/2	FCHO1/2
Fibroblast growth factor 2	FGF2
Flotillin	Flot
Fibronectin	FN
fluorescence resonance energy transfer	FRET
RNA-DNA binding protein fused in sarcoma	FUS
GalNac transferases	GALNTs
GTPase activating protein	GAP
Glyceraldehyde-3-phosphate dehydrogenase	GAPDH
Golgi-specific brefeldin A-resistance guanine nucleotide exchange factor 1	GBF1
Guanine nucleotide exchange factor	GEF
Green fluorescent protein	GFP
Glucose transporter 8	GLUT8
GTPase Regulator Associated with Focal Adhesion Kinase	GRAF1/ARHGAP26
G Protein-Coupled Receptor Kinase 1	GRK1
Glycogen synthase kinase 3 β	GSK3 β
human epidermal growth factor receptor 2	HER2 or c-erbB2
Hepatocyte growth factor	HGF
hypoxia-inducible factor 1	HIF-1
Homotypic fusion and vacuole protein sorting complex	HOPS
Horse serum	HS
Heat shock protein	HSP
Heat shock protein 47	HSP47
Human umbilical vein endothelial cells	HUVEC
Invasive ductal carcinoma	IDC

Interleukin	IL
Integrin-linked kinase	ILK
Intraluminal vesicles	ILVs
inducible nitric oxide synthase	iNOS2
Insulin Receptor tyrosine kinase substrate protein 53kDa	IRSp53
α 2-integrin	ITGA2
β 1-integrin	ITGB1
C-Jun N-terminal kinase	JNK
Laminin type IV domains	L4 & LF
Lactosylceramide	LacCer.
Lysosomal transmembrane protein I and II	LAMP1/2
Laminin-type epidermal growth factor-like repeats	LE
G-like globular domain	LG
Lysyl hydroxylase	LH
Lysosomal integral membrane protein 2	LIMP2
Linker of the nucleoskeleton and cytoskeleton	LINC
Globular laminin domain	LN
Lysyl oxidase related enzyme	LOXL2
Lysyl oxidases	LOXs
MAP kinase	MAP2K
MAPK kinase kinase	MAP3K
Mitogen-activated protein kinase kinase kinase 1	MAP3K1
Mitogen-activated protein kinase	MAPK
Mitogen-activated protein kinase 11	MAPK11/p38 β
Microtubule Affinity Regulating Kinase 3	MARK3
Myristyl trimethyl ammonium bromide	MiTMAB
Myosin light chain	MLC
Myosin light chain kinase	MLCK
Matrix metalloproteinases	MMPs
Mouse mammary tumour virus-polyoma middle T (tumour) antigen	MMTV-PyMT
MAGUK P55 Scaffold Protein 2	MPP2
Mechanistic target of rapamycin	mTOR
Mechanistic/mammalian target of rapamycin complex 1	mTORC1
Multivesicular bodies	MVBs
sodium bicarbonate	NaHCO ₃
Na ⁺ /H ⁺ exchanger type 1	NHE1
Nemo-like kinase	NLK
Non-muscle myosin IIA	NMMIIA
Non-small-cell lung cancer	NSCLC
Non-targeting	NT5
p38 MAPK	p38

Prolyl 3-hydroxylase	P3H
Prolyl 4-hydroxylase	P4H
Phosphatidic acid	PA
p21-activated kinase 1	PAK1
Phosphate buffer saline	PBS
Phosphate buffer saline containing calcium and magnesium	PBS++
Pancreatic ductal adenocarcinoma	PDAC
Platelet derived growth factor	PDGF
Disulphide isomerase	PDI
Paraformaldehyde/formaldehyde	PFA
pHrodo iFL Red STP ester	pHrodo
Phosphatidylinositol 3-phosphate	PI(3)P
Phosphatidylinositol-3-kinase	PI3K
Phosphatidylinositol-4-Phosphate 3-Kinase Catalytic Subunit Type 2 Alpha	PIK3C2A
Phosphatidylinositol 4,5-bisphosphate	PIP2 or PI(4,5)P2
Phosphatidylinositol (3,4,5)-trisphosphate	PIP3
Phosphatidylinositol-3,4,5-triphosphate	PIP3
Phosphatidylinositol phospholipids	PIPs
Protein kinase A	PKA
Protein kinase C alpha	PKC α
cAMP-Dependent Protein Kinase Inhibitor Beta	PKIB
Phospholipase A2	PLA2
Polo-Like Kinase 1	PLK1
Plasma membrane	PM
Phorbol 12-myristate 13-acetate	PMA
Protein Phosphatase 2A	PP2A
Protein Phosphatase 2 scaffold subunit A alpha	PPP2R1A
Progesterone receptor	PR
Protein Kinase cAMP-Dependent Type I Regulatory Subunit Alpha	PRKAR1A
PTM-disrupting mutations	PTMmut
Post-translational modifications	PTMs
Protein tyrosine phosphatase 1B	PTP-1B
Pyrroline-5-carboxylate reductase 1	PYCR1
FAK-related proline-rich tyrosine kinase 2	Pyk2
Quiescin sulfhydryl oxidase 1	QSOX1
Rap Guanine Nucleotide Exchange Factor 3	RAPGEF3
Rab11-coupling protein	RCP
Recessive dystrophic epidermolysis bullosa	RDEB
Rab7-interacting protein	RILP
RNA sequencing	RNAseq
Rho associated coiled-coil containing protein kinase	ROCK

Soluble NSF attachment protein	SNARE
Serine/Threonine Kinase 39	STK39
STE20 Related Adaptor Beta	STRADB
Syntaxin	STX
Serine/Threonine/Tyrosine Kinase 1	STYK1
Tumour associated macrophages	TAMs
Tricarboxylic acid	TCA
T Cell immune regulator 1	TCIRG1
Tumour endothelial cells	TECs
Type 2 transglutaminase	TG2
Transforming growth factor β	TGF- β
Transforming growth factor β 1	TGF- β 1
Transforming growth factor-beta-induced protein ig-h3	TGFBI
Trans Golgi network	TGN
Thrombospondin-1	THBS1
Telomerase-immortalised fibroblasts	TIFs
Tissue inhibitors of metalloproteinases	TIMPs
Tyrosine kinase substrate with 5 SH3 domains	Tks5
Melting temperature	TM
Tumour microenvironment	TME
Triple negative breast cancer	TNBC
Tenascin-C	TNC
Tensin 3	TNS3
Trafficking protein particle complex subunit 9	TRAPPC9
TrypLE Express	TrypLE
Thrombospondin repeats	TSR type I
Vesicle associated membrane protein	VAMP
Vascular endothelial growth factor	VEGF
Vascular endothelial growth factor A	VEGFA
von Willebrand Factor type A	VWA
von Willebrand Factor type C	VWC
Yes-associated protein	YAP
Alpha-smooth muscle actin	α -SMA

Chapter 1 – Introduction

1.1. CANCER BIOLOGY

1.1.1. An introduction to cancer

Cancer is frequently defined as a disorder in which a group of cells abnormally proliferate on account of dysregulation of the standard rules of cell cycle (Hanahan and Weinberg, 2000; Pucci, Kasten and Giordano, 2000). Non-cancerous cells are constantly being submitted to regulatory signals that force cells to divide, differentiate into another cell type or undergo apoptosis (Pucci, Kasten and Giordano, 2000). On the contrary, cancer cells become autonomous from these signals and, as a consequence, cell growth and proliferation are unrestrained (Hanahan and Weinberg, 2000; Pucci, Kasten and Giordano, 2000). In point of fact, cells may trespass their natural boundaries, invade the surrounding stroma and disseminate to distal regions, a process known as metastasis, which could be lethal (Hanahan and Weinberg, 2000). Actually, nearly 90% of cancer-related deaths are due to tumour dissemination (Chaffer and Weinberg, 2011).

Notwithstanding, cancer goes beyond being a mass of multiplying tumour cells. Instead, it is a complex tissue constituted by a huge variety of different cell types (e.g. cancer associated fibroblasts, tumour associated macrophages, among other types), which heterotypically interact with one another (Baghban *et al.*, 2020). Importantly, the phenotypic characteristics of the stromal cell types, its abundance and its histologic organisation, together with the extracellular matrix (ECM), change over cancer progression, consequently permitting primary, invasive and, thereafter, metastatic growth (Winkler *et al.*, 2020).

1.1.1.1. The hallmarks of cancer

The terminology cancer does not just denote one disease but a set of malignancies which mainly originate from epithelial cells (*i.e.*, *breast carcinoma, pancreatic carcinoma, colorectal carcinoma, etc.*). Despite the highly heterogeneity of cancers, tumour cells share some features or rationalised organising principles denoted as *The Hallmarks of Cancer* (Hanahan and Weinberg,

2000). These characteristics could be defined as distinctive and complementary abilities that enhance tumour growth and metastatic dissemination (Hanahan and Weinberg, 2000). These trademarks imply cellular and physiological alterations, such as sustaining proliferative signalling, evasion of growth suppressors, non-mutational epigenetic reprogramming, avoiding immune destruction, enabling replicative immortality, promotion of tumour inflammation, polymorphic microbiomes, activation of invasion and metastasis, induction of angiogenesis or access to vasculature, senescence, genomic instability and mutation, resistance to cell death and deregulation of cell metabolism (Hanahan and Weinberg, 2000, 2011; Hanahan, 2022).

More importantly, these hallmark principles could be contemplated as possible mechanism-based targeted therapies (Hanahan and Weinberg, 2011). Thus, drugs interfering with these characteristics have been developed. Inhibitors targeting angiogenesis, for instance, have been developed for treating glioblastoma (Schulte, Aghi and Taylor, 2021). Nevertheless, it has been observed that as a response cancer cells become dependent on other hallmarks. In the context of glioblastoma, it has been reported to increase invasion of the surrounding tissue, which leads to extravasation of cancer cells in blood vessels nearby and local metastasis (Lucio-Eterovic, Piao and de Groot, 2009). This highlights the need to develop therapies targeting simultaneously several hallmarks of cancer.

1.1.2. An overview to Breast cancer

1.1.2.1. Epidemiology

Breast cancer is the most frequently diagnosed malignancy in 154 out of 185 countries (~83%) in women and, in addition, it is the major cause of cancer death in over 100 countries (Bray *et al.*, 2018). In 2020, 2.3 million women were diagnosed with breast cancer and it caused 685,000 deaths worldwide (*Cancer today, GLOBOCAN 2020*, no date). Breast cancer is the most prevalent cancer globally, 7.8 million cases were diagnosed since 2015 (*Cancer today, GLOBOCAN 2020*, no date). In the UK, breast cancer accounts for 30% of female cancers diagnosed and it is expected that between 2014 to 2035 breast cancer incidence rate will increase by 2%, meaning 210 new cases per 100,000 women will be diagnosed by 2035 (*Breast cancer statistics, CRUK 2015*, 2015).

Furthermore, the vast majority of breast cancer deaths are due to breast cancer metastasis (Scully *et al.*, 2012).

1.1.2.2. Breast cancer progression and subtypes

Tumour progression is a multistep process accompanied by alterations in tissue structure; breast tissue, for instance, becomes *hyperplastic* (i.e. there is an increase in cell number) at early stages of cancer development (Khamis, Sahab and Sang, 2012). Besides, cells acquire many mutations during the process and these hyperplastic lesions may give place to dysplasia (i.e. abnormal growth within the tissue), which further evolves into *ductal carcinoma in situ (DCIS)* (Khamis, Sahab and Sang, 2012). Outstandingly, throughout tumorigenesis, cells acquire mutations that promote invasive traits, including a mesenchymal phenotype and secretion of proteases. These features enable degradation of the basement membrane and invasion of the surrounding stroma, which results in an *invasive ductal carcinoma (IDC)*. Finally, cells may disseminate through the lymphatic and blood circulatory system to distal regions, also known as metastasis (Khamis, Sahab and Sang, 2012) (see [Figure 1-1A](#)).

Additionally, breast cancer can be classified into four different subtypes depending on the expression of oestrogen (ER) and progesterone receptor (PR), as well as the proliferation marker Ki67 and the human epidermal growth factor receptor 2 (HER2 or c-erbB2) (Khamis, Sahab and Sang, 2012; Yersal and Barutca, 2014) (see [Figure 1-2B](#)). Luminal A accounts for 50 to 60% of breast cancer cases, it is ER⁺, PR⁺, HER2⁻ and presents low levels of Ki67 (< 14%). This Luminal A breast cancer has better prognosis than other subtypes; if recurrence occurs, bone metastasis is frequently observed in these patients (Kennecke *et al.*, 2010). Luminal B is more aggressive, has a lower survival rate and worse prognosis compared to Luminal A subtype; it comprises 15 to 20% of breast cancers. Histological samples are ER⁺, PR⁺, HER2⁻ and present higher levels of Ki67 (≥ 14%) (Kennecke *et al.*, 2010). Similarly, HER2-positive patients comprise 15-20% of total breast cancer cases. They show high expression levels of HER2; approximately half of the patients express low levels of ER and 40% are p53-mutant (Yersal and Barutca, 2014). Histological samples are stained by high levels of Ki67 (≥ 15%) (Soliman and Yussif, 2016). HER2 confers biological and clinical aggressiveness and, in the absence of trastuzumab treatment (anti-HER2 monoclonal

antibody), chemo- and radiotherapy, these tumours display poor prognosis (Yersal and Barutca, 2014; Yu *et al.*, 2017). Lastly, tumours that do not express ER, PR and HER2 are classified into the category of Basal-like subtype; it is thus also known as Triple negative breast cancer (TNBC) and it represents 8 to 37% of breast cancers (Yersal and Barutca, 2014). Three fourths of TNBC are breast cancer 1 (BRCA1) and p53 mutant (Yersal and Barutca, 2014). They usually display high expression of Ki67 and have poor clinical outcome (Yersal and Barutca, 2014). A subtype of TNBC is distinguished to express low levels of tight junctions and cell-cell adhesions, namely claudins 3, 4 and 7, occludin and E-cadherin and have undergone epithelial-to-mesenchymal transition (EMT) (Yersal and Barutca, 2014). This subtype is known as low claudin TNBC and is highly metastatic; however, little is known on the signalling drivers of this subtype (Rädler *et al.*, 2021). Nevertheless, it has been recently reported that K-Ras enhances cellular plasticity and mesenchymal/stem-like characteristics in this cancer subtype (Rädler *et al.*, 2021). The breast cancer cell line MDA-MB-231 is commonly used as a model for this subtype (Rädler *et al.*, 2021).

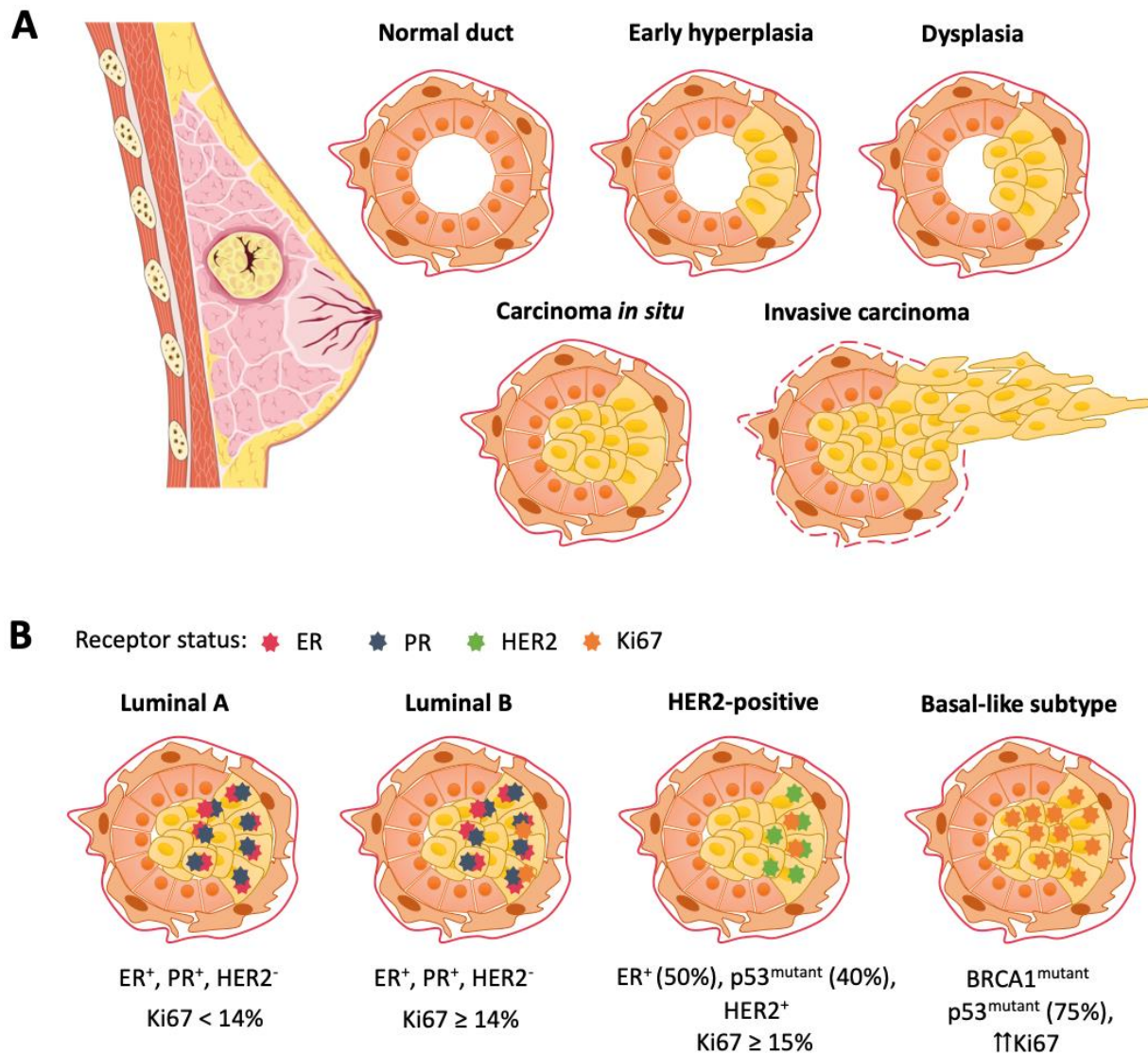


Figure 1-1. (A) Schematic representation of breast cancer progression. In the mammary duct, normal breast epithelial cells are surrounded by myoepithelial cells and the basement membrane. At the beginning of tumorigenesis, few breast cells overgrow, become hyperplastic and lead to dysplasia of the mammary duct. If proliferation continues, cells acquire more mutations and tissue homeostasis is lost, cells become malignant. This is known as ductal carcinoma in situ. Finally, few cancer cells are able to degrade the basement membrane and invade the surrounding stroma: known as invasive carcinoma. **(B) Breast cancer subtypes** depending on the receptor status of oestrogen (ER), progesterone (PR), human epidermal growth factor receptor 2 (HER2) and the proliferation marker Ki67. Image made using items from Servier medical Art.

1.1.3. The tumour microenvironment

The tumorigenic process is shaped by genetic and epigenetic factors (Timp and Feinberg, 2013). However, other factors participate in tumorigenesis, such as changes in the surrounding extracellular matrix and stromal cells, known together as the tumour microenvironment (TME)

(Baghban *et al.*, 2020) ([Figure 1-2](#)). Having a deep comprehension on how cancer cells interact with the TME is essential to understand what governs tumour growth and metastasis. Nevertheless, the study of the TME has remained challenging. This section will outline the foremost cellular types that comprise the TME. While the non-cellular components will be discussed in section [1.3. The extracellular matrix in cancer](#).

Tumour endothelial cells (TECs) assemble into a stratified squamous epithelial layer (as opposed to the healthy simple squamous epithelial monolayer) to form blood vessels in a growing tumour in response to hypoxia (Nagl *et al.*, 2020). Hypoxia-inducible factors promote vessel sprouting by secreting proangiogenic factors, namely platelet derived growth factor (PDGF) and vascular endothelial growth factor (VEGF) (Semenza, 1998; Carmeliet and Jain, 2000; Nagl *et al.*, 2020) ([Figure 1-2](#)). On the one hand, blood vessel formation increases water and nutrient supply to tumours. However, high levels of VEGF leads to the formation of fenestrated blood vessels, highly characteristic of tumours (Esser *et al.*, 1998; Carmeliet and Jain, 2000). This results in a leaky vasculature, reduced blood flow and further causes tumour hypoxia. Simultaneously, TEC organisation influences infiltration of immune cells and how stromal cells arrange (Nagl *et al.*, 2020).

Another important cell type within the TME are Tumour associated macrophages (TAMs), which can be classified into inflammatory M1 macrophages and immune-suppressive M2 macrophages (Atri, Guerfali and Laouini, 2018; Boutilier and ElSawa, 2021) ([Figure 1-2](#)). The first ones are in charge of phagocytosing and inducing cell death, while the second group participates in wound healing (Atri, Guerfali and Laouini, 2018). The conditions within the TME (e.g. hypoxia and cytokine secretion, such as interleukin 4 (IL-4)) promotes the M2 phenotype, which supports tumour growth and progression (Atri, Guerfali and Laouini, 2018; Ke *et al.*, 2019). High levels of macrophage infiltration correlate with poor prognosis in breast, lung, ovarian and prostate cancers (Larionova *et al.*, 2020). TAM, in addition, secrete VEGF, which contributes to angiogenesis (Ke *et al.*, 2019). Other cells in charge of carrying out the innate immune response and found in the TME are neutrophils and dendritic cells (antigen presenting cells) (Piccard, Muschel and Opdenakker, 2012; Masucci, Minopoli and Carriero, 2019). Depending on the

tumour type, neutrophils have been described as tumour promoting or suppressive. At early stages of tumour formation, neutrophils release cytokines and matrix metalloproteinase 8 (MMP-8) that prevent chronic inflammation, thus reducing genomic instability and tumour development (Piccard, Muschel and Opdenakker, 2012). However, in later stages of tumour development, neutrophils seem to have a promoting role by modifying the ECM, producing MMP-9 and VEGF to stimulate angiogenesis, tumour progression and local invasion (Piccard, Muschel and Opdenakker, 2012; Masucci, Minopoli and Carriero, 2019).

Cancer associated fibroblasts (CAFs) usually originate from fibroblasts that reside in the tissue, where cancer cells start proliferating/invading. However, they may additionally derive from cells of different origin, such as adipocytes, endothelial cells, pericytes, bone-marrow-derived mesenchymal stem cells and stellate cells in pancreatic and hepatocellular carcinomas (Gunaydin, 2021). Cancer cells and other stromal cells release transforming growth factor β (TGF- β), PDGF and fibroblast growth factor 2 (FGF2), which promote fibroblast activation into CAFs (Bordignon *et al.*, 2019; Gunaydin, 2021) ([Figure 1-2](#)). Fibroblast activation leads to deposition of ECM proteins. A hallmark and driver of tumour aggressiveness is deposition of collagen-rich ECM (Kay *et al.*, 2022). Pyrroline-5-carboxylate reductase 1 (PYCR1) is upregulated and highly expressed in CAFs and in the stroma of breast carcinoma patients (Kay *et al.*, 2022). PYCR1 is an essential enzyme for proline synthesis and thus the formation of pro-tumorigenic proline-rich collagen fibres (Kay *et al.*, 2022). The authors of this study conclude that targeting PYCR1 may be a novel strategy to fight both cancer and stromal cells (Kay *et al.*, 2022). Moreover, PYCR1 inhibition may ameliorate drug delivery and immune cell recruitment (Kay *et al.*, 2022).

Furthermore, CAFs promote tumour progression by different means. On the one hand, CAFs release to the extracellular environment several growth factors, namely FGF2 and vascular endothelial growth factor A (VEGFA), which lead to angiogenesis (Wang *et al.*, 2019). On the other hand, CAFs influence proliferation and metabolism of cancer cells. In fact, pancreatic stellate cells, specifically myofibroblasts, internalise ECM under branched-chain amino acid (BCAA)-limiting conditions (Z. Zhu *et al.*, 2020). In this system, myofibroblasts catabolise BCAAs to branched-chain α -ketoacid (BCKA) in a process dependent on the enzyme BCAT1 (Z. Zhu *et al.*,

2020). Following that, BCKAs are secreted and used by pancreatic cancer cells to promote cell proliferation (Z. Zhu *et al.*, 2020). The TGF- β - SMAD5 axis upregulates DQ-collagen I internalisation in myofibroblasts (Z. Zhu *et al.*, 2020) ([Figure 1-2](#)).

In addition, cancer ECM derived from CAFs has been reported to be tumour suppressive by either recruiting immunosuppressive cells, including TAMs and Regulatory T cells (Treg), or by secreting a dense ECM barrier that impairs immune infiltration (Liu *et al.*, 2019). Nevertheless, a recent bioRxiv study suggested that CAFs may limit, confine and compress tumours (Barbazan *et al.*, 2021). This process is dependent on actomyosin contractility (Barbazan *et al.*, 2021). Another characteristic of CAFs is their ability to deposit large amounts of fibronectin and myosin IIA-mediated contractility by CAFs is required for its fibrillogenesis (Attieh *et al.*, 2017). Fibronectin deposition at the boundary between CAFs and tumour cells is critical to build a mechanical scaffold to enable actomyosin-driven compression of cancer cells (Barbazan *et al.*, 2021). Of note, cancer cells sense and respond to CAF compression by shuttling the mechanosensor Yes-associated protein (YAP) to the cytosol (Barbazan *et al.*, 2021). In fact, cytoplasmic YAP has been associated with mediating cell contact inhibition (Zhao *et al.*, 2007). This suggests that CAF-mediated compression of cancer cells may reduce tumour cell growth, partially by inhibiting proliferation of cancer cells.

These studies indicate that CAFs are a heterogeneous population that will either promote or constrain tumour growth/progression. Two populations of CAFs have been described in human colorectal tumours, one subgroup expressed genes related to activated myofibroblasts while the second subgroup expressed genes related to ECM remodelling (Li *et al.*, 2017). Another example of CAF heterogeneity is found in non-small lung cell carcinoma (NSCLC). In these tumours, 7 different subtypes of CAFs have been described, which express distinctive collagen types (Lambrechts *et al.*, 2018). Cluster 1 expressed high levels of COL10A1, while cluster 2 expressed COL4A1 (Lambrechts *et al.*, 2018). Non-malignant fibroblasts, which were not tumour derived, expressed high levels of elastin and low levels of collagen I, III, V and VIII, but not other types, such as collagen VI (Lambrechts *et al.*, 2018). Four distinct CAFs subtypes were reported in tumours derived from the mouse mammary tumour virus-polyoma middle tumour-antigen

(MMTV-PyMT) (Bartoschek *et al.*, 2018). These 4 subpopulations could be distinguished by: genes regulating vascular development/angiogenesis, genes related to ECM and Matrisome, genes related to cell cycle (S, G2 and M phase) and CAFs that promoted differentiation, development and morphogenesis (Bartoschek *et al.*, 2018). The degree of CAF activation may lead to producing quiescent CAFs, tumour-restraining CAFs or tumour promoting CAFs, all of which display different expression patterns (Wang *et al.*, 2021). The two former are predominantly present in early-stage cancer, while tumour-promoting CAFs are associated with advance-stage disease (Wang *et al.*, 2021). In point of fact, it is suggested that acquisition of pro-tumorigenic traits by quiescent CAFs is essential for tumour development (Wang *et al.*, 2021). In several cancer types, namely breast, head and neck and prostate malignancies, CAFs undergo pro-catabolic reprogramming (Giatromanolaki *et al.*, 2012; Witkiewicz *et al.*, 2012; Curry *et al.*, 2013; Wang *et al.*, 2021). However, it is not clear whether changes in metabolism may trigger tumour-restraining and quiescent fibroblasts to become tumour promoting (Wang *et al.*, 2021).

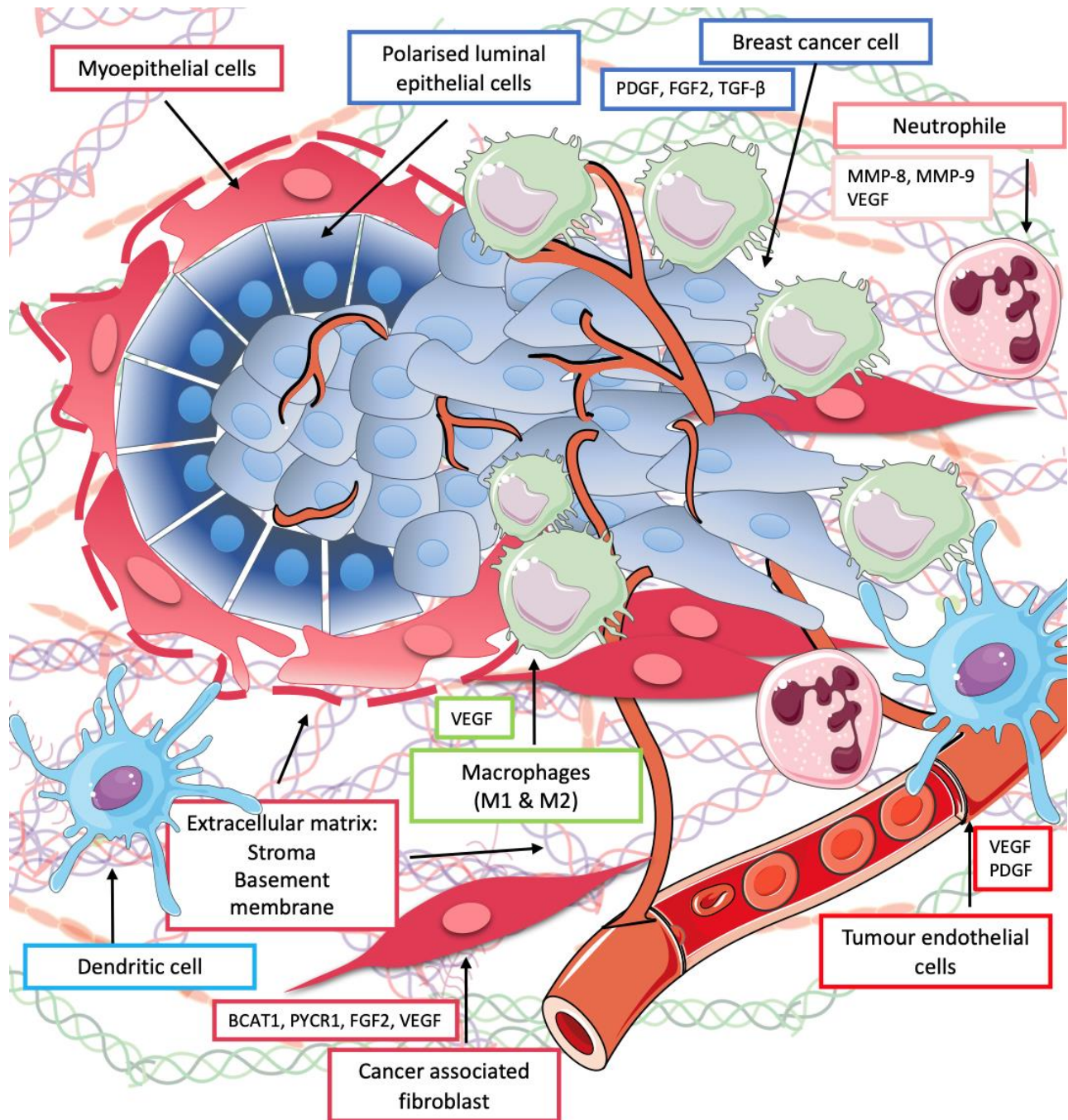


Figure 1-2. The tumour microenvironment. Cancer cells interact with the extracellular matrix, stromal and immune cells. Tumour endothelial cells (TECs) secrete VEGF and PDGF to promote angiogenesis and nutrient supply to tumours (red, bottom right corner). Macrophages in the tumour can either be tumour-suppressor (M2) or tumour-promoter (M1) (green). Macrophages and neutrophils aid cancer cells and induce angiogenesis by secreting VEGF. In addition, neutrophils produce MMP-9 to facilitate local invasion of cancer cells at later stages, while they secrete MMP-8 at early stages to prevent chronic inflammation (pink, upper right corner). During tumour progression, cancer cells secrete diverse molecules, including FGF2, PDGF and TGF- β (blue, upper right corner). This promotes the activation of fibroblasts into cancer associated fibroblasts (CAFs), which support cancer growth by secreting growth factors or upregulating diverse metabolic pathways (red, bottom left corner). Image made using items from Servier medical Art.

1.1.4. A brief introduction to signal transduction pathways in cancer

Sustaining proliferative signalling is one of the hallmarks of cancer (Hanahan and Weinberg, 2000). Growth signals and cell cycle progression are tightly regulated in normal tissues. Malignant tumours, however, characteristically display deregulations of intracellular signalling (Hanahan and Weinberg, 2011). In fact, 40% of human melanomas contain activating mutations of B-Raf (V599E), leading to constitutive signalling of mitogen-activated protein kinase (MAPK) (Davies *et al.*, 2002; Davies and Samuels, 2010). MAPK signalling cascade is a sequential action of three protein kinases. The pathway is classically initiated by phosphorylation or a small GTP-binding protein of the Ras/Rho family (Cargnello and Roux, 2011). This results in activation of the first kinase in the signalling cascade pathway: MEKK or MAP3K (MAPK kinase kinase), which phosphorylates and positively regulates the second kinase of the pathway: MEK, MAP2K or MKK (MAPK kinase) (Bardwell, 2006; Cargnello and Roux, 2011). The last effector kinase is a MAPK, phosphorylated and activated by MEK (Bardwell, 2006; Cargnello and Roux, 2011) ([Figure 1-3A](#)). In mammalian cells, there are four distinct conventional MAPK signalling pathways according to the terminal tier kinase: Extracellular signal regulated kinase (ERK) 1/2, c-Jun N-terminal kinase (JNK) 1/2/3, p38 $\alpha/\beta/\delta/\gamma$ and ERK5 (Bardwell, 2006; Cargnello and Roux, 2011). Furthermore, there are atypical MAPK signalling enzymes, including ERK3/4, ERK7 and Nemo-like kinase (NLK) (Cargnello and Roux, 2011; Kciuk *et al.*, 2022). These pathways are essential in numerous cellular processes, namely gene expression, metabolism, proliferation, apoptosis, invasion and metastasis (Cargnello and Roux, 2011; Kciuk *et al.*, 2022). The Ras - Raf - MEK - ERK pathway is disrupted in 40% of human cancers, frequent mutations being B-Raf (10%) and its upstream activator Ras (30%) (Kciuk *et al.*, 2022). The JNK and p38 MAPK pathways are activated upon cellular stress (Bardwell, 2006) ([Figure 1-3A](#)). Importantly, the p38 pathway has recently gained considerable attention in the context of carcinogenesis. p38 activity has been associated with EMT, proliferation, migration, invasion and metastasis of cancer cells (del Barco Barrantes and Nebreda, 2012; Koul, Pal and Koul, 2013; Lin *et al.*, 2016; Ling *et al.*, 2016).

Another important signalling pathway dysregulated in cancer and downstream of K-Ras is phosphatidylinositol-3-kinase (PI3K)/Akt/mTOR signalling (Mortazavi *et al.*, 2022). This signalling

cascade leads to cell growth, proliferation and survival, cytoskeletal remodelling, migration and invasion (Karami Fath *et al.*, 2022) ([Figure 1-3B](#)). Pancreatic cancers have hyperactivated this pathway (Payne *et al.*, 2015). In fact, point mutations in PI3K have been described to initiate pancreatic ductal adenocarcinoma in mice models (Payne *et al.*, 2015). In addition, Ras signalling contributes to upregulating macropinocytosis in cancer. Actually, Ras localises in the interior of the macropinocytic cup in mammalian and *Dictyostelium* cells (Veltman *et al.*, 2016). Ras activity leads to production of phosphatidylinositol-3,4,5-triphosphate (PIP3) by PI3K followed by Akt activation, which culminates in macropinocytosis events (Castellano and Downward, 2011; Veltman *et al.*, 2016) ([Figure 1-3B](#)).

The following sections will deepen into the diverse endocytic pathways and trafficking dysregulations in cancer, the ECM components and the mechanism to degrade them. The final sections will focus on the main ECM receptors and the endocytic pathways described to internalise the different ECM components.

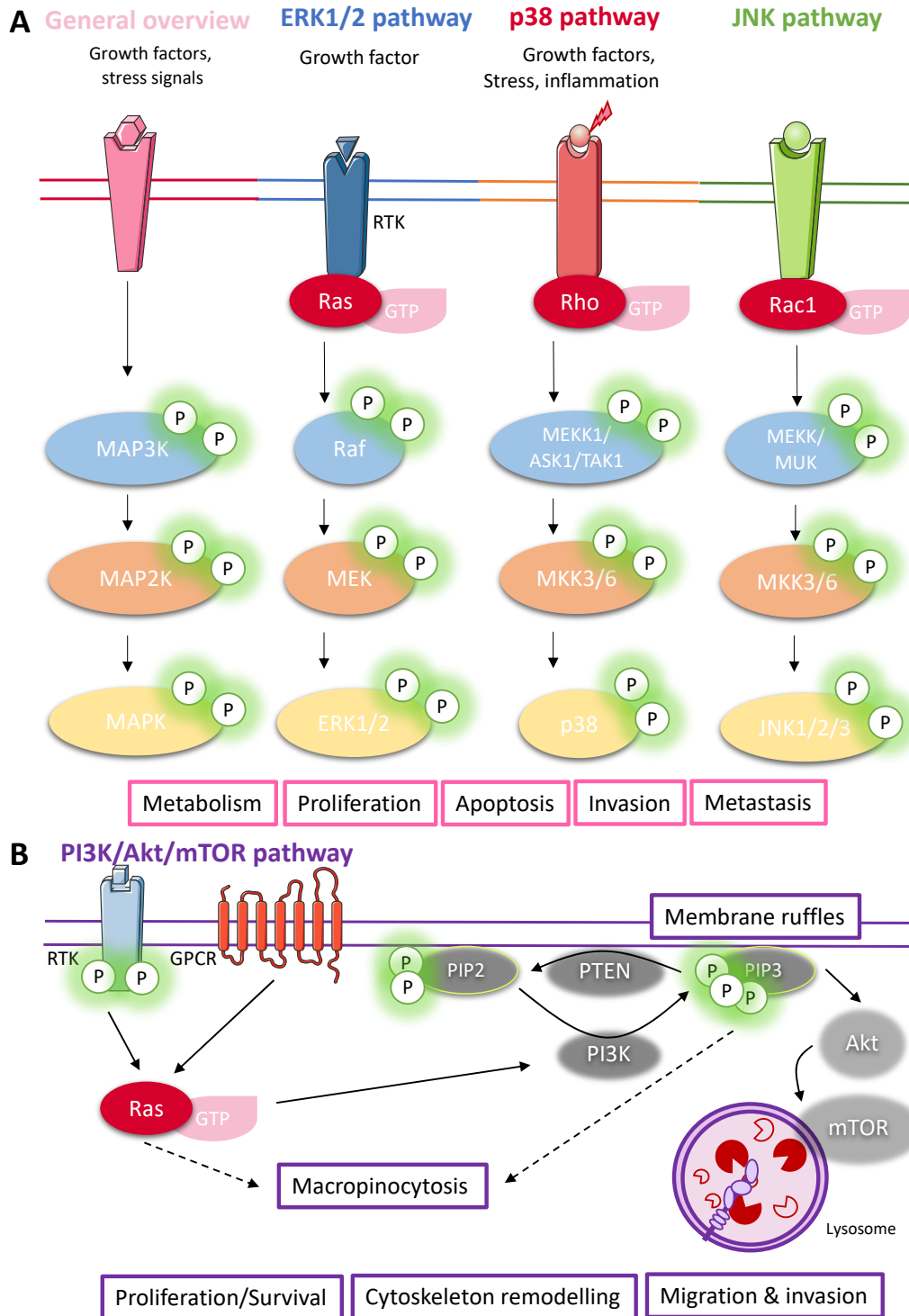


Figure 1-3. (A) Conventional Mitogen-activated protein kinase signalling (MAPK) pathways. The sequential action of three protein kinases activated by phosphorylation leads to changes in gene expression, metabolism, proliferation and apoptosis. In addition, MAPK signalling promotes cancer invasion and metastasis. **(B) PI3K/Akt/mTOR pathway.** PI3K activation leads to the phosphorylation of PIP2 into PIP3, which results in Akt and mTOR activation. This pathway results in proliferation, survival, migration and invasion of cancer cells. PI3K can be activated by Ras, which is a known regulator of macropinocytosis. Image made using items from Servier medical Art.

1.2. ENDOCYTOSIS AND ENDOSOME TRAFFIC IN CANCER

1.2.1. The plasma membrane and endocytic membrane traffic

The plasma membrane (PM) consists of an asymmetric bilayer of phospholipids, which hydrophilic head groups face the aqueous intra- and extracellular compartments; while the hydrophobic acyl chains are arranged horizontally to form the hydrophobic core of the bilayer (Ma *et al.*, 2017). Of note, the PM is not just a mere barrier that separates the cell from its environment but mediates the interaction between the cell and its surrounding environment; the PM is involved in endocytosis and exocytosis (Ivanov, 2008), as well as signal transduction (Ma *et al.*, 2017).

The terms endocytosis and exocytosis respectively refer to the inward or outward movement of plasma membrane vesicles (Mayor and Pagano, 2007; Ivanov, 2008). Notably, endocytosis (broadly defined as the internalisation of extracellular molecules and cell surface proteins) is an extremely regulated biological process. Endocytosis is an essential process, which is involved in multiple functions; some examples include nutrient uptake (Ivanov, 2008; Kaksonen and Roux, 2018), regulation of cell shape and volume, transcellular transport, cell migration (Ivanov, 2008) and termination of receptor signalling (Ivanov, 2008; Barbieri, Di Fiore and Sigismund, 2016). The term endocytosis comprises multiple pathways that differ regarding their morphology and mechanics (Elkin, Lakoduk and Schmid, 2016). In brief, the main endocytic pathways can be sub-categorised as clathrin-mediated endocytosis, caveolin-dependent endocytosis, clathrin and caveolin-independent endocytosis, macropinocytosis and phagocytosis (Ivanov, 2008).

1.2.1.1. Clathrin-mediated endocytosis

Clathrin-mediated endocytosis (CME) is the most well-known form of receptor-mediated internalisation (Ivanov, 2008; Schreij, Fon and McPherson, 2016). CME is mechanistically defined by the assembly of icosahedral clathrin lattices and bending of the PM into clathrin-coated pits (CCPs). At early stages, clathrin-adaptor proteins containing Bin-Amphiphysin-Rvs (BAR) domains, such as the AP2 complex and F-BAR domain only protein 1/2 (FCHO1/2) are recruited to the PM

(Henne *et al.*, 2010; Umasankar *et al.*, 2012; Ma *et al.*, 2016) ([Figure 1-4A](#)). In addition, together with the scaffold proteins epidermal growth factor receptor (EGFR), epidermal growth factor receptor substrate 15-like 1 (EGFRS15) and intersectin 1/2 form a “pioneer core” that initiates endocytosis (Taylor, Perrais and Merrifield, 2011; Umasankar *et al.*, 2012; Ma *et al.*, 2016). AP2 complex binding to phosphatidylinositol 4,5-bisphosphate, known as PIP2 or PI(4,5)P2, triggers a conformational change that exposes its clathrin-binding site (Kadlecova *et al.*, 2017). The YxxΦ motif of the transferrin receptor can additionally co-activate the AP2 complex, which results in clathrin being recruited to the assembling coat (Kadlecova *et al.*, 2017). Different models have been proposed on how the clathrin pit is formed. The first model suggested that clathrin would first assemble into flat lattices, which would gradually reorganise into an icosahedron that promotes membrane bending (Heuser, 1980). Nevertheless, the transition between the flat lattice to the 3D icosahedral lattice is energetically costly; thus, an alternative model proposed that clathrin initially polymerises into a curve lattice (Nossal, 2001). Subsequently, scission proteins participate in the invagination of CCPs into the cytoplasm to form clathrin-coated vesicles (CCVs) ([Figure 1-4A](#)). BAR domain proteins (e.g. endophilin) recruit the GTPase dynamin, which oligomerizes into tight helical rings that constrict the neck of CCPs (Hohendahl *et al.*, 2017). However, overexpression of endophilin impairs membrane fission by inhibiting interactions between dynamin (Hohendahl *et al.*, 2017). Concomitantly to this multistep assembly of CCPs, actin polymerisation generates pulling forces that contribute to membrane bending and internalisation of CCPs (Merrifield *et al.*, 2002). Lastly, the clathrin lattices disassemble from CCVs (Mousavi *et al.*, 2004; Kaksonen and Roux, 2018), allowing the trafficking of the cargo molecule (Kaksonen and Roux, 2018) ([Figure 1-4A](#)).

1.2.1.2. Lipid raft-mediated endocytosis

Caveolae are specialised and dynamic PM domains that contain a characteristic lipid profile with high levels of cholesterol, sphingomyelin and ceramides (Matthaeus and Taraska, 2020). These regions are stabilised by several key proteins, namely Caveolin 1-3 (Cav), Cavin 1-4, the BAR proteins syndapin/Pacsin2 and the dynamin-related ATPase EHD2 (Matthaeus and Taraska, 2020). Receptors accumulating in caveolae and binding of certain ligands induce signalling

cascades that trigger caveolar endocytosis. Integrins were shown to regulate caveolin-mediated endocytosis (del Pozo *et al.*, 2005). Actually, Cav-1 has been found to co-localise with vinculin at focal adhesions (FA) (del Pozo *et al.*, 2005). What triggers caveolin-mediated internalisation? In detail, Cav-1 phosphorylation on tyrosine residue 14 by Src-family tyrosine kinases results in caveolar internalisation (Li, Seitz and Lisanti, 1996; Lee *et al.*, 2000). Interestingly, phosphotyrosine 14 localises at FA (Lee *et al.*, 2000). Simultaneously, Cav-2 is also phosphorylated on tyrosine 19 by Src (Lee *et al.*, 2002). In addition, Cav-2 is phosphorylated at serine 23 and 36 in the N-terminal region by Casein kinase 2 (CK2) or CK2-like kinase (Sowa *et al.*, 2003). This contributes to the formation of deep PM invaginations (Sowa *et al.*, 2003) ([Figure 1-4B](#)). Likewise clathrin-dependent endocytosis, the GTPase dynamin is recruited to caveolae. Subsequent to GTP hydrolysis, dynamin constricts the neck of the caveolae invagination and triggers the fission of the caveolae to the cytoplasm (Oh, McIntosh and Schnitzer, 1998). During this process, reorganisation of the actin cytoskeleton is critical. The cortical actin network depolymerises, while actin monomers are recruited near the invaginating caveolae where they form actin patches (Kiss and Botos, 2009). The newly formed vesicles are transported along microtubules and trafficked to early endosomes in a Rab-5 dependent manner (Mundy *et al.*, 2002) ([Figure 1-4B](#)).

Flotillins were originally thought to associate with caveolae (Bickel *et al.*, 1997), but later studies showed that flotillins form specific non-caveolar microdomains or lipid rafts (Glebov, Bright and Nichols, 2006; Fernow, Icking and Tikkanen, 2007). Flotillin-1/reggie-2 and flotillin-2/reggie-1 (abbreviated to Flot-1/2) associate with particular PM microdomains by acylation (single palmitoylation of Flot-1; single myristoylation and triple palmitoylation of Flot-2) (Neumann-Giesen *et al.*, 2004). Flotillins establish their own clathrin-independent endocytosis (CIE) pathway (Glebov, Bright and Nichols, 2006). In the lipid rafts, flotillins form hetero-oligomers that assemble into large flotillin platforms (Solis *et al.*, 2007). Flot-1/2 internalisation is triggered by Fyn-dependent phosphorylation on tyrosine 160 and 163 respectively (Riento *et al.*, 2009). In addition, Src phosphorylation of Flot-2 on tyrosine 163 is also required for its hetero-oligomerisation (Babuke *et al.*, 2009). Flotillins are upregulated in carcinomas and sarcomas, and this correlates with poor prognosis in patients (Gauthier-Rouvière *et al.*, 2020). In fact, H-Ras

expression in the MCF10A mammary cell line results in high levels of flotillin-1 expression and increase in tumour aggressiveness (Koh *et al.*, 2016). Overexpression of flotillin causes its oligomerization, which leads to membrane curvature and high levels of endocytosis in cancer (Gauthier-Rouvière *et al.*, 2020). In cells overexpressing flotillins, MT1-MMP (MMP14) is endocytosed and found in flotillin late endosomes, from where it will be recycled and delivered to degradation sites, i.e. invadopodia (Planchon *et al.*, 2018).

1.2.1.3. Phagocytosis, macropinocytosis and the CLIC-GEEC pathway

Phagocytosis is an endocytic pathway that leads to the internalisation of relatively large insoluble antigens, including opsonized pathogens, necrotic and apoptotic cells (Cardelli, 2001). This pathway is predominantly carried out by professional phagocytes, such as neutrophils, macrophages and dendritic cells (Cardelli, 2001). The process can be summarised in the following stages: (I) Recognition of the particle by cell surface receptors. (II) This leads to activation of signalling cascades that induce temporal and spatial regulation of F-actin polymerisation. (III) Actin-dependent pseudopod extension to internalise the particle. (IV) Depolymerisation of F-actin from the newly generated phagosome. (V) Trafficking and fusion to form a mature phagolysosome (Cardelli, 2001).

On the contrary, **macropinocytosis** is regarded as a non-specific uptake of soluble molecules, nutrients and antigens. Nevertheless, pretreatment with the mannose receptor-agonist mannan revealed that dextran and ovalbumin are partially internalised in a mannose receptor-mediated endocytosis (Sallusto *et al.*, 1995; Burgdorf, Lukacs-Kornek and Kurts, 2006). This suggests that cells are able to concentrate macromolecules prior to macropinocytosis (Sallusto *et al.*, 1995). The pathway initiates with the formation of the macropinocytic cup or circular ruffles (Levin, Grinstein and Schlam, 2015). Similar to phagocytosis, considerable actin remodelling is required to enable the formation of extended protrusions to englobe and close the cup (Levin, Grinstein and Schlam, 2015). Finally, scission of the PM results in a sealed macropinosome. In immature dendritic cells, macropinocytosis is regulated by the Rho GTPase Cdc42 and Rac, which mediate actin remodelling (Garrett *et al.*, 2000; West *et al.*, 2000). p21-activated kinase 1 (PAK1) is a downstream effector of Cdc42 and Rac. PAK1 activity promotes circular ruffles on the dorsal

surface of cells and actin-myosin cytoskeleton remodelling, altogether stimulates dextran macropinocytosis (Dharmawardhane *et al.*, 2000) ([Figure 1-4C](#)). Another relevant regulator of this process is PI3K, which is critical at later stages to enable actin-dependent macropinocytosis (West *et al.*, 2000). The metabolism of PIP2 is strikingly similar between phagocytosis and macropinocytosis during the endocytic process (Levin, Grinstein and Schlam, 2015). However, susceptibility to PI3K inhibitors is one of the hallmarks of macropinocytosis (Levin, Grinstein and Schlam, 2015).

Similar to macropinocytosis, **Clathrin-independent carriers (CLICs) and GPI-Enriched Endocytic Compartments (GEECs)** endocytosis is heavily dependent on actin polymerization (Rennick, Johnston and Parton, 2021). CLIC-GEEC endocytosis is regulated by the small GTPases ADP ribosylation factor 1 (Arf1) and Cdc42, the GTPase activating factor GRAF1, the actin nucleation factor Arp2/3 and the BAR domain protein IRSp53 (Sabharanjak *et al.*, 2002; Kumari and Mayor, 2008; Lundmark *et al.*, 2008; Sathe *et al.*, 2018) ([Figure 1-4D](#)). It has been involved in the uptake of the hyaluronic acid receptor (CD44) and it can also mediate the internalisation of fluid and cell membrane (Rennick, Johnston and Parton, 2021).

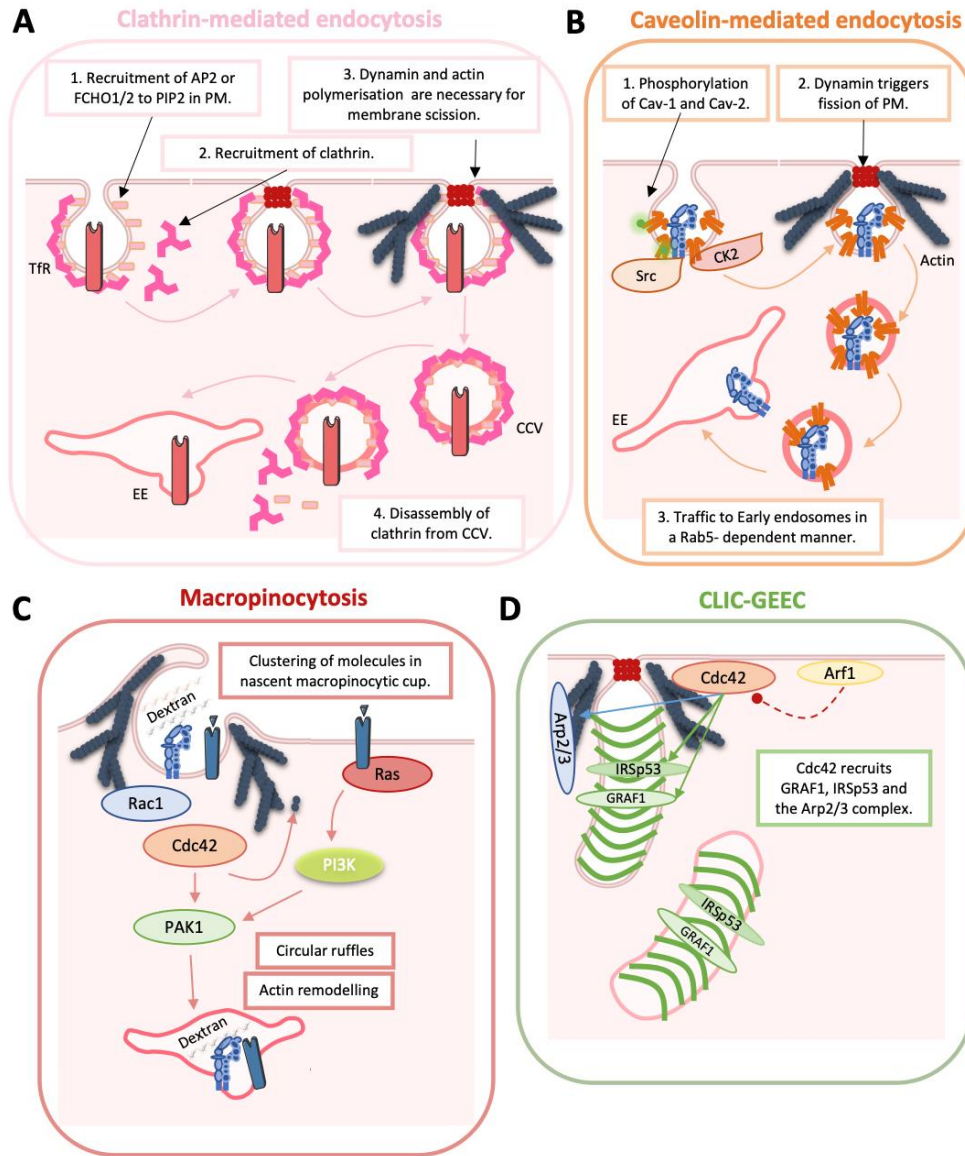


Figure 1-4. Schematic representation of the foremost endocytic pathways. (A) Schematic summary of clathrin-mediated endocytosis. Adaptor proteins, namely AP2 complex and F-BAR domain only protein 1/2 (FCHO1/2) are first recruited. Binding to membrane bound PIP2 induces conformational changes that expose the clathrin-binding site of the AP2 complex. Following clathrin assembly into an icosahedral structure, the small GTPase dynamin is recruited and together with actin forces promotes the scission of the clathrin coated pit (30-100nm; (Arpino et al., 2022)).(B) Receptor clustering at caveolae triggers signalling cascades (Cav-1 and Cav-2 phosphorylation by Src and CK2 respectively) that result in caveolin-mediated endocytosis. Dynamin is recruited at the neck of the invaginated PM and mediates its fission. The newly formed caveosomes (60nm; (Rennick, Johnston and Parton, 2021)) are trafficked in Rab5-mediated manner. (C) Scheme of the signalling regulators of macropinocytosis. PAK1 activation downstream of Rac1 and Cdc42 lead to actin remodelling and formation of circular ruffles on the dorsal surface. Changes in the lipid composition and further activation of PAK1 is mediated by PI3K, downstream of Ras, is also critical for macropinocytosis (0.2µm to 5µm; (Garrett and Mellman, 2001)). (D) Cdc42 activity leads to recruitment of IRSp53 and GRAF1 to promote tubular invaginations, which characterise the CLIC-GEEC pathway (100nm; (Rennick, Johnston and Parton, 2021)). In addition, Cdc42 recruits the Arp2/3 complex, which leads to changes in actin remodelling. Finally, the GTPase Arf1 (activated by GBF1, Golgi-specific brefeldin A resistance factor 1) recruits the RhoGAP for Cdc42: ARHGAP21. This results in accelerated cycling of Cdc42, its removal from the PM and actin-dependent endocytosis.

1.2.2. Endolysosomal trafficking

Following endocytosis, cargoes and their respective receptors are incorporated into the endosomal network. Once internalised, primary endocytic vesicles fuse and form early or sorting endosomes (Elkin, Lakoduk and Schmid, 2016). These receptors will be ultimately recycled back to the PM, sent to the trans-Golgi network via retrograde traffic or sorted to the lysosomes for degradation (Elkin, Lakoduk and Schmid, 2016).

Endosomal sorting is tightly regulated by spatial and temporal control of endosomal identity. Internalised receptors can be recycled via Rab4-dependent short-loop from early endosomes or via the Rab11-dependent long loop via the perinuclear recycling compartment (Stenmark, 2009). Different mechanisms have been described during maturation of early endosomes into late endosomes. One way is through the acidification of the endosomal lumen via the v-type vacuolar H⁺ ATPase found in the membrane bilayer (Mellman, Fuchs and Helenius, 1986; Fuchs, Mâle and Mellman, 1989). Another way is through alterations in the phosphatidylinositol phospholipids (PIPs) and the recruitment of Rab family GTPases. PIP kinases and phosphatases are Rab effectors, Rab5-dependent synthesis of phosphatidylinositol 3-phosphate (PI(3)P) on early endosomes is controlled by VPS34, class III PI3-kinase (Schu *et al.*, 1993; Futter *et al.*, 2001; Elkin, Lakoduk and Schmid, 2016). Several Rab effectors contain PI(3)P binding motifs, including early endosomal antigen 1 (EEA1) (Elkin, Lakoduk and Schmid, 2016). Another important partner in defining early endosomes is the class C core vacuole/endosome tethering (CORVET) complex, which associates with Rab5 (Balderhaar *et al.*, 2013). The CORVET complex is additionally required for endosomal fusion to generate sufficient surface area for enabling the formation of intraluminal vesicles (ILVs) (Balderhaar *et al.*, 2013). During endosomal maturation, an upstream Rab, e.g. Rab5, recruits a guanine nucleotide exchange factor (GEF) that activates a downstream Rab, e.g. Rab7, which subsequently recruits a GTPase activating protein (GAP) for the upstream Rab (Elkin, Lakoduk and Schmid, 2016). This results in endosomal maturation or Rab conversion of the membrane identity, from Rab5 to Rab7. The endosomal sorting complex required for transport (ESCRT) acts on late endosomes and executes: (I) generation of ILVs/ multivesicular bodies (MVBs) and (II) sorting ubiquitinated membrane proteins/receptors for lysosomal

degradation (Raiborg and Stenmark, 2009). The MVBs fuse with the lysosomes and cargo proteins and the intraluminal vesicles are degraded. The homotypic fusion and vacuole protein sorting (HOPS) complex, associated with Rab7, and the Rab7-interacting protein (RILP) mediate the fusion of mature endosomes with lysosomes by recruiting VAMP7 and syntaxin 7 (Rainero and Norman, 2013). In addition, RILP binds to components of ESCRT II leading to the formation of ILVs in the late endosomes (Wang and Hong, 2006).

1.2.3. Dysregulation of membrane traffic in cancer

Dysregulations of endocytic traffic have been associated with malignancies. In fact, genes encoding regulators of endocytic trafficking have been identified as drivers of tumorigenesis and acquisition of prometastatic features. The latter usually involves: increase in invasive migration, survival and resistance to environmental stress. Rho-like GTPases, including Rac1 and Cdc42, are critical for cancer invasion by means of reorganising the actin and tubulin cytoskeleton. The regulatory circuit of Rac1 involved the Rab5A/Rab4 axis. Rab5A overexpression correlates with poor clinical outcome in breast cancer patients (Frittoli *et al.*, 2014). Clathrin- and Rab5-dependent endocytic traffic of Rac1 promote its re-localisation to early endosomes, where the GEF Tiam1 activates Rac1 (Palamidessi *et al.*, 2008) ([Figure 1-5](#)). Rac1 is thereafter recycled back to the specific regions of the PM, where it regulates polarisation of lamellipodia protrusion and directed cell migration (Palamidessi *et al.*, 2008). Rab4 is also overexpressed in invasive breast carcinomas (Lanzetti and Di Fiore, 2017). Rab5A promotes the Rab4-mediated fast recycling of MT1-MMP and $\beta 3$ integrin to invadosomes, to enable extracellular proteolytic degradation (Frittoli *et al.*, 2014) ([Figure 1-5](#)). Dynamin-2 is overexpressed in pancreatic cancer (Eppinga *et al.*, 2012; Razidlo *et al.*, 2013). In this model, dynamin-2 stabilises and impairs proteasomal degradation of Vav1, a Rac1 GEF (Razidlo *et al.*, 2013). This presumably results in Rac1 activation, lamellipodia protrusion and invasive migration of pancreatic cancer cells (Razidlo *et al.*, 2013) ([Figure 1-5](#)). Vav1 is also overexpressed in pancreatic tumours due to demethylation of the gene promoter (Fernandez-Zapico *et al.*, 2005; Eppinga *et al.*, 2012; Razidlo *et al.*, 2013).

CDC42-interacting protein 4 (CIP4), a BAR domain protein, is a Cdc42 effector. CIP4 is overexpressed in breast cancer and its expression correlates with poor prognosis and metastasis

(Cerqueira *et al.*, 2015). CIP4 increases E-cadherin endocytosis, which leads to cell scattering by regulating actomyosin contractility (Rolland *et al.*, 2014) ([Figure 1-5](#)). However, other studies suggested that it reduces invadopodia-mediated ECM proteolysis and invasion in breast cancer by promoting MT1-MMP endocytosis (Hu *et al.*, 2011).

Rab25 belongs to the Rab11 subfamily, which is involved in the long loop endosomal recycling. Rab25 is amplified in ovarian and breast cancers, interestingly, its overexpression is linked to resistance to apoptosis and anoikis (Cheng *et al.*, 2004). Mechanistically, Rab25 interacts with the cytoplasmic tail of β 1-integrin (Caswell *et al.*, 2007). In fibronectin containing ECM, Rab25 promotes recycling of α 5 β 1 integrin to the tips of extending pseudopodia and, in addition, invasive migration in 3D matrices (Caswell *et al.*, 2007) ([Figure 1-5](#)). Nonetheless, Rab25 guides α 5 β 1 integrin bound to fibronectin to Chloride Intracellular Channel Protein 3 (CLIC3) lysosomes (Dozynkiewicz *et al.*, 2012) ([Figure 1-5](#)). Interestingly, α 5 β 1 integrin is not degraded but rather recycled back to the PM in a CLIC3-dependent manner (Dozynkiewicz *et al.*, 2012). However, in the absence of CLIC3, α 5 β 1 integrins are ubiquitinated and degraded in the lysosomes (Lobert *et al.*, 2010; Dozynkiewicz *et al.*, 2012). In addition, Rab25 drives association of tensin-1/2/3 with α 5 β 1 in fibronectin-containing fibrillar adhesions beneath the nucleus (Rainero *et al.*, 2015). In A2780 cells, overexpressing Rab25, tensin-1/2/3 interacts with Arf4 and both are required for α 5 β 1 integrin internalisation and traffic to lysosomes (Rainero *et al.*, 2015). Of note, this pathway is upregulated under glucose starvation and inhibition of this pathway blocks mTORC1 recruitment to lysosomes (Rainero *et al.*, 2015) ([Figure 1-5](#)). In line with these results, macropinocytosis enables pancreatic cancer cells to scavenge extracellular proteins as a source of nutrients in starvation conditions (Commisso *et al.*, 2013). Accordingly, our lab has shown that breast cancer cells internalise different ECMs and sustain cancer cell growth under amino acid starvation (Nazemi *et al.*, 2021). Hypoxia is a universal hallmark of solid tumours. A recent study showed that hypoxia-inducible factor 1 (HIF-1) activates the transcription of EH domain-containing protein 2 (EHD2) to initiate macropinocytosis in hepatocellular carcinoma cells (Zhang *et al.*, 2022). More studies are needed to assess whether hypoxia could also participate in scavenging of ECM components and fuel the tricarboxylic acid (TCA) cycle to promote tumour growth.

p53 is considered a major tumour suppressor, however gain of function mutations result in its transformation into oncogenic p53 (Soussi and Wiman, 2015). Interestingly, mutant/oncogenic p53 promotes invasive migration by promoting $\alpha 5\beta 1$ integrin recycling (Caswell *et al.*, 2008; Muller *et al.*, 2009). Rab11 regulates $\alpha 5\beta 1$ integrin recycling (Roberts *et al.*, 2001; Caswell *et al.*, 2007); interestingly, Rab11- coupling protein (RCP) is essential to link mutant p53 and recycling of $\alpha 5\beta 1$ integrin (Muller *et al.*, 2009). Mechanistically, this process is dependent on the generation of phosphatidic acid (PA) by Diacylglycerol kinase α (DGK- α) (Rainero *et al.*, 2012). PA at the leading edge of migrating cells is essential to tether recycling vesicles via the PA-binding C2 domain of RCP (Rainero *et al.*, 2012) ([Figure 1-5](#)).

Rab1A GTPase is overexpressed in colorectal carcinomas, it predicts poor outcome and cancer invasion (Thomas *et al.*, 2014). Rab1A GTPase is involved in trafficking from the endoplasmic reticulum to the Golgi Apparatus. In addition, Rab1A senses amino acid signalling to mTORC1. Amino acids stimulate GTP binding to Rab1A (Thomas *et al.*, 2014). Rab1A regulates Rheb-dependent activation of mTORC1 in the golgi (Thomas *et al.*, 2014). Altogether, this leads to oncogenic advantage and tumour growth. Another regulator of endoplasmic reticulum to golgi traffic is Rab2A, which is overexpressed and hyperactivated in breast cancer (Luo *et al.*, 2015). On the one hand, Rab2A promotes recycling of MT1-MMP to invadopodia, where it enhances ECM degradation (Kajiho *et al.*, 2016) ([Figure 1-5](#)). On the other hand, it impinges on E-cadherin traffic to the PM, therefore reducing cell-cell adhesion and boosting invasion (Kajiho *et al.*, 2016). In agreement with the latter results, Rab2A potentiates EMT by binding to ERK1/2 and inhibiting its deactivation (Luo *et al.*, 2015) ([Figure 1-5](#)).

Clathrin light-chain (CLCb) is overexpressed in NSCLC cells and it correlates with poor prognosis (Chen *et al.*, 2017). Epidermal growth factor receptor (EGFR) endocytosis in cells overexpressing CLCb leads to activation of Akt/Glycogen synthase kinase 3β (GSK3 β) axis, which in turns activates Dynamin-1 (Reis *et al.*, 2015). EGFR endocytosis results in altered signalling and increased metastasis (Chen *et al.*, 2017). In addition, CLCb has been described to promote the rapid, gyrating clathrin-dependent recycling of EGFR (Majeed *et al.*, 2014).

Cav-1 has been reported to be a tumour suppressor at early stages of tumorigenesis, while high expression is associated with tumour progression and metastasis at later stages (Goetz *et al.*, 2008). In fact, downregulation of Cav-1 in breast and prostate cancer cells impaired velocity, directionality and persistence of cell migration (Joshi *et al.*, 2008; Urra *et al.*, 2012). These studies showed that Src kinase phosphorylates Cav-1 at tyrosine 14, which in turn activates Rho/ROCK signalling, FA turnover and cell migration (Joshi *et al.*, 2008; Urra *et al.*, 2012). In line with these results, rear retraction is controlled by caveolae in 3D matrix and durotaxis (Hetmanski *et al.*, 2019). Caveolae are formed as a consequence of low membrane tension at the cell rear (Hetmanski *et al.*, 2019). Caveolae drives the RhoA-ROCK/PKN2 signalling axis through Ect2, a RhoA GEF. Ect2 regulates F-actin organisation and contractility and promotes forward movement of the cell rear (Hetmanski *et al.*, 2019). In this system the role of Cav-1 is independent of its effects on endocytosis (Hetmanski *et al.*, 2019). Cav1 expression is higher in small cell lung cancer compared to NSCLC, its expression decreases in high grade tumours however cell-level variability is observed within the tissue (Y.-B. Shi *et al.*, 2020). High levels of Cav-1 correlate with high Ki67 levels and mutant p53, markers of poor prognosis and high histopathology grade in pancreatic ductal adenocarcinoma (Tanase *et al.*, 2009). Cav1 has been reported to regulate certain aspects of metabolism, including glycolysis (Nwosu *et al.*, 2016). Overexpression of Cav1 may drive glycolysis by providing docking sites for certain metabolic enzymes, namely phosphofructokinase and aldolase (Nwosu *et al.*, 2016). Cav1 downregulation has been shown to decrease glycolysis, induce metabolic switch towards lipid metabolism and induce production of reactive oxygen species (Shiroto *et al.*, 2014). It has been proposed that high caveolin 1 expression may correlate with tumours *addicted* to glucose (Nwosu *et al.*, 2016). In pancreatic tumours, high glucose promotes AMP-activated protein kinase (AMPK) inhibition, which in turn activates the signalling axis Bmi1-GATA2, which in turn reduces the expression of MHC class I chain-related protein A/B, resulting in immune evasion (Duan *et al.*, 2019).

The role of other endocytic proteins in driving cell migration has been reviewed elsewhere (Llanses Martinez and Rainero, 2019); this section provides evidence that cancer cells hijack the endocytic and endosomal system to promote proliferation, migration and invasion of cancer

cells. Thus, studying how cancer cells use endocytic traffic to survive and metastasise may open new avenues for therapeutically treating malignancies.

So far, the sections above have focused on introducing breast cancer, the main endocytic pathways and endosomal traffic. The section below aims to introduce the ECM as a complex protein scaffold, but also how cancer cells are able to remodel it.

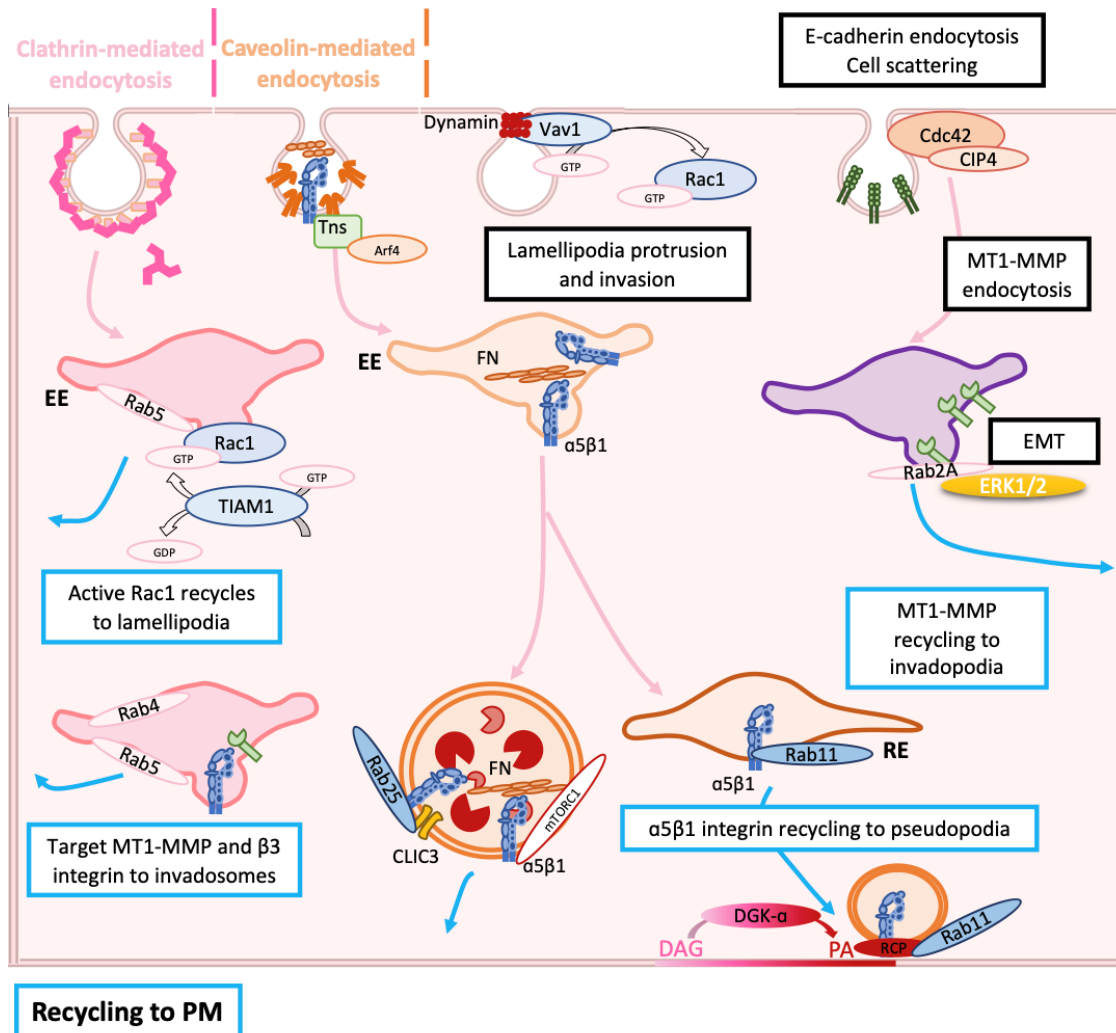


Figure 1-5. Dysregulations of membrane traffic during tumorigenesis. Diagram of how cancer cells hijack the endocytic and endosome system to promote ECM degradation and migration.

1.3. THE EXTRACELLULAR MATRIX IN CANCER

The ECM is the utmost non-cellular three-dimensional structural component of tissues. The ECM can be classified into two types concerning tissue organisation: the interstitial connective tissue and the basement membrane (BM). The first one acts as a structural scaffold, while the latter separates the epithelium from the stroma. In addition to providing tissue integrity and elasticity, the ECM is essential for morphogenesis, differentiation and homeostasis of tissues by inducing biomechanical and biochemical signals. The ECM is a dynamic structure, which can be remodelled depending on the requirements of the tissue, such as in the physiological process of wound healing. Therefore, deregulations of ECM remodelling (synthesis, deposition and degradation) are fundamental for the development of pathological conditions (e.g. fibrosis, tumour growth, invasion and metastasis). Matrigel is an ECM preparation derived from the Engelbreth-Holm-Swarm mouse tumour, a poorly differentiated chondrosarcoma (Merceron and Murphy, 2015). Matrigel is predominantly composed of laminin (approximately 60%), collagen IV (30%), entactin (8%) and other proteoglycans, including perlacan (Corning® Matrigel® Matrix, no date; Merceron and Murphy, 2015). It is commonly used in cell culture applications as a BM-like substrate; additionally, it has extensively been used for 3D cell culture (Merceron and Murphy, 2015).

The ECM is constituted by an intricate network of approximately 300 secreted proteins, including collagens, proteoglycans and glycoproteins, referred to as core matrisome (Hynes and Naba, 2012). These proteins are incorporated into the network via several intra- and intermolecular interactions. ECM proteins are additionally altered through post-translational modifications (PTMs), which may participate in cross-linking reactions that contribute to the formation of the ECM network. Of note, ECM composition, organisation and function differs depending on the tissue type; this ensures a physiological cellular regulation and organ function. On the contrary, tumour progression is chaperoned by aberrant changes in the tumour microenvironment. In fact, cancer-associated ECM extremely differs from normal ECM. Malignant tumours, for example, are frequently fibrotic or desmoplastic. Desmoplasia is well characterised by histological changes that comprise an increment in both the deposition and PTMs of ECM proteins. Correspondingly, breast cancer predictive prognosis is worse when collagen cross-linkers and matrix remodelling

genes are expressed. Further evidence is that fibrotic conditions, such as cirrhosis of the liver and cystic fibrosis, in which collagen is aberrantly accumulated, have a higher risk of developing cancer (Pickup, Mouw and Weaver, 2014).

1.3.1. Post-translational modifications of the extracellular matrix

PTMs are defined as modifications that generate a protein that is functionally and immunologically different. PTMs are classified into hydroxylation, phosphorylation, N- and O-glycosylation, acetylation, ubiquitylation, sumoylation and methylation. Actually, few of these PTMs confer structural and functional features that are required for the formation and stability of the ECM meshwork, as well as receptor recognition of ECM proteins (Leeming *et al.*, 2011; Holstein *et al.*, 2021). However, whether PTMs are drivers or consequences of disease remains unresolved. A recent bioinformatic analysis study of the TCGA Pan-Cancer Atlas mutation database showed that matrisome encoding genes are mutated roughly as frequently as the genome (Izzi, Davis and Naba, 2020). Mutations that affect residues that can be post-translationally modified are known as PTM-disrupting mutations (PTMmut) (1811, 1,19% of matrisome mutations). Interestingly, PTMmut are less frequent than for the rest of the genome, perhaps on account of the structural importance of these PTMs (Holstein *et al.*, 2021).

The following subsections will outline some of the key PTMs that contribute to the properties and structure of the ECM.

1.3.1.1. Disulphide cross links in the ECM

Disulphide bonds (S-S) are a type of cross-linking PTMs copiously found in secreted and extracellular proteins (Bošnjak *et al.*, 2014). They are typically formed in the endoplasmic reticulum by oxidoreductases, such as protein disulphide isomerase (PDI), ERp57 (PDIA3), PDIA4, PDIA6, and associated chaperones such as the collagen-binding protein heat shock protein 47 (HSP47) (Jessop and Bulleid, 2004), calnexin and calreticulin (Oliver *et al.*, 1999). Disulphide bonds on ECM proteins confer the necessary stability to withstand extracellular conditions and acidic endocytic recycling. Within the ECM, disulphide bonds are needed for an accurate processing, secretion and incorporation of peptides into their respective protein conformation.

As an example, mutations in the protein disulphide isomerase PDI-2 in *Caenorhabditis elegans* cause anomalous collagen deposition and extracellular matrix formation (Winter, McCormack and Page, 2007).

1.3.1.2. Hydroxylation crosslinks in the ECM

Hydroxylation is a modification to proline residues of collagens by prolyl 4-hydroxylase (P4H) (Pihlajaniemi, Myllylä and Kivirikko, 1991) and prolyl 3-hydroxylase (P3H) (Vranka, Sakai and Bächinger, 2004). This modification augments the stability of the collagen triple helix.

To a lesser extent, lysines are also altered by lysyl hydroxylase 1, 2 and 3 (LH1, LH2 and LH3) (Valtavaara *et al.*, 1997, 1998; Yeowell and Walker, 1999). Lysine hydroxylation is important for connective tissue development, with mutations causing defects in bones, joints and skin. In humans, mutations in LH1 cause Ehlers-Danlos syndrome and LH2 causes Bruck syndrome type 2. LH2 hydroxylates lysine residues in the collagen telopeptides, i.e. the N- and C-terminus in fibrillar collagens. Following hydroxylation of proline and lysines, lysyl oxidases (LOXs) can oxidatively deaminate lysine and hydroxylysine residues, consequently generating lysine aldehydes. Those lysine aldehydes react with unmodified lysines and hydroxylysines to form intra- and intermolecular cross-links within the collagen and elastin fibres (Yamauchi and Sricholpech, 2012).

Cross-linking of collagens is functionally important since LOXs mutations are associated with vascular disease, including aortic aneurysms, presumably due to a weak blood vessel wall (Lee *et al.*, 2016). Actually, patients with vascular disease have been associated with connective tissue disorders, such as Marfan syndrome, Ehlers-Danlos type IV, Loeys-Dietz syndrome or TGF- β vasculopathy (Lee *et al.*, 2016). Conversely, LOXs are highly expressed and upregulated in solid tumours, where they increase ECM stiffness, which contributes to tumour progression by modulating cell growth, proliferation and invasion (Levental *et al.*, 2009; Chaudhuri *et al.*, 2014; Santamaría *et al.*, 2018). The role of LOXs in cancer has been extensively reviewed elsewhere (Setargew *et al.*, 2021). The upstream enzyme, LH2 has also been involved in tumours that present high crosslinking levels (Chen *et al.*, 2015).

1.3.1.3. Glycosylation, glycation and phosphorylation of the ECM proteins

Glycosylation is a PTM that annexes complex saccharides (glycans) to proteins, which may consequently affect protein conformation, cell signalling and cancerous transformation (Fuster and Esko, 2005). The two most frequent glycosylation pathways are N-linked glycosylation and O-GalNAc linked O-glycosylation. However, several other glycosylation pathways, such as O-mannosylation, have critical functions for the ECM and interaction with cells (Schjoldager *et al.*, 2020).

BM and other stromal ECM proteins are O-glycosylated (Steentoft *et al.*, 2013). Actually, aberrant glycosylation results in structural changes to the ECM. In fact, GALNT1 has been found to be involved in the secretion of BM proteins (Tian, Hoffman and Ten Hagen, 2012). Glycoproteomic analysis of pancreatic cancer and chronic pancreatitis tissue has identified over-expression of many ECM associated glycoproteins (Pan *et al.*, 2014). The identified glycoproteins are implicated in organisational and structural changes to ECM and activation of stellate cells involved in the regulation of pancreatic fibrosis (Pan *et al.*, 2014).

Glycation is an unregulated non-enzymatically catalysed modification, which can also affect ECM proteins. It is known as Maillard or browning reaction and it results from reducing saccharides, e.g. glucose, and proteins (John and Lamb, 1993). Other reactions lead to the formation of Advanced glycation end products (AGEs), which can form cross-links, for example, in collagen molecules (Fu *et al.*, 1994; Verzijl *et al.*, 2002). AGE-crosslinking of collagen IV and laminin within the BM induces invasive behaviour in prostate cancer (Rodriguez-Teja *et al.*, 2015).

Protein phosphorylation is a reversible PTM on serine, threonine and tyrosine sites; it affects several cellular processes and it has been described in several diseases (Ubersax and Ferrell, 2007; Holstein *et al.*, 2021). Protein phosphorylation is known to affect protein-protein interactions (Betts *et al.*, 2017), which could have an effect on the ECM meshwork. Osteopontin is an extracellular structural protein mainly found in the bone. Phosphorylation negatively charges osteopontin; this impinges on its binding to multivalent positive ions found in hydroxyapatite and ultimately impacts on bone mineralisation. Osteopontin is overexpressed in several cancers, such as melanoma, breast, colorectal, lung, ovarian and stomach cancer

(Rodrigues *et al.*, 2007), and, in addition, microcalcification is commonly described in breast cancer (Cox and Morgan, 2013).

1.3.2. ECM proteins in the tumour microenvironment

ECM proteins and other associated factors are termed matrisome. The matrisome can be classified into two categories: 1) core matrisome proteins (e.g. proteoglycans, laminins, collagens, fibronectins, etc.) and 2) matrisome-associated proteins (Naba *et al.*, 2012). The latter group is additionally divided into 3 subgroups: A) ECM regulators/remodelling enzymes (e.g. transglutaminases, lysyl oxidases, MMPs and cross-linking enzymes among others), B) ECM-affiliated proteins, which are architecturally and/or biochemically similar to core ECM proteins, and C) secreted growth factors and cytokines (Naba *et al.*, 2012). The following section focuses on the core matrisome proteins, with special focus on collagens and laminins.

1.3.2.1. Collagens: Fibrous ECM proteins

The most abundant proteins in mammals are collagens, comprising around 30% of protein mass (Svoboda, 1991; Ricard-Blum, 2011). Collagens are characterised by fibrillar triple helix domains. Three polypeptide α chains form a triple helix, which distinctively contain Gly-Xaa-Yaa repeats, with proline (Pro) and 4-hydroxyproline (Hyp) being the most common amino acids at Xaa and Yaa sites respectively (Barth, Musiol, *et al.*, 2003; Bachmann *et al.*, 2005) ([Figure 1-6A](#)). Collagens are diverse in molecular structure: for example, collagen I is a heterotrimer of two $\alpha 1(I)$ and one $\alpha 2(I)$ chains (Svoboda, 1991; Ricard-Blum, 2011), collagen XI comprises $\alpha 1(XI)$, $\alpha 2(XI)$ and $\alpha 3(XI)$ (Ricard-Blum, 2011), while collagen II is a homotrimer of $\alpha 1(II)$ (Svoboda, 1991; Ricard-Blum, 2011). Interestingly, $\alpha 3(XI)$ chain has the same amino acid sequence as the $\alpha 1(I)$ chain, but differs in its PTMs and cross-linking (Ricard-Blum, 2011). Another layer of variability comes from hybrid collagen molecules, such as the type V/type XI collagen - $\alpha 1(XI)$ and $\alpha 2(V)$ – in the bovine vitreous humour (Mayne *et al.*, 1993). The possible triple helix combinations, as well as PTMs, result in a wide variety of collagen types. Several collagens have been reported to be overexpressed in cancers (e.g. COL3A1, COL4A2, COL7A1, COL11A1, COL17A1) and have been

shown to potentiate tumorigenicity (Wu *et al.*, 2014; Liu, Liao and Li, 2017; C.-C. Liu *et al.*, 2018; Z. Zhang *et al.*, 2018).

1.3.2.1.1. The formation of the triple helix

The formation of the triple helix is an intricate process that requires intermolecular and intramolecular interactions (Barth, Musiol, *et al.*, 2003; Bachmann *et al.*, 2005). Within the endoplasmic reticulum, the procollagen propeptides assemble into a triple helix. Nascent procollagen molecules characteristically consist of three domains: N-terminal, collagenous triple helix and a C-terminal non collagenous domain (Middleton and Bulleid, 1993). Before the triple helix formation, the recently synthesised procollagen α chains are further post-translationally modified in the endoplasmic reticulum: namely, hydroxyproline residues. The addition of hydroxyl groups stabilises the collagen triple helix and increases the melting temperature (TM) (Berg and Prockop, 1973; Rosenbloom, Harsch and Jimenez, 1973; Ying Chow *et al.*, 2015). Hydroxylysines, together with lysines, are needed for intra- and inter-collagen crosslinking (Knott and Bailey, 1998). Hydroxylation, in addition, is required for the formation of some disulphide bonds, which additionally stabilise many collagen molecules, at the C-terminal non-collagenous domain propeptide (C-propeptide) (Bulleid, Wilson and Lees, 1996). Prolyl hydroxylase 4 has been reported to hydroxylase type XIII collagen and further promote the formation of disulphide bonds (Snellman *et al.*, 2000). On the one hand, intrachain disulphide bonds on C-propeptides stabilise the folded structure of single chains (Lees, Tasab and Bulleid, 1997). On the other hand, the nascent collagen triple helix is stabilised by the formation of knot-like disulphide bonds between the C-propeptide chains of the same trimer (Koivu, 1987). Biochemical experimentation with small collagen peptides demonstrated that disulphide bonds enhance the folding rate and stability, whilst reducing thermo-degradation of collagen peptides (Barth, Kyrieleis, *et al.*, 2003; Barth, Musiol, *et al.*, 2003).

After the procollagen molecules are secreted into the extracellular compartment, both C- and N-terminal propeptides are cleaved ([Figure 1-6A](#)), which leads to the self-assembly of collagen into fibrils (Kadler *et al.*, 1990); this is especially true for fibrillar collagen I, II and III (Kessler *et al.*, 1996). The N- and C-terminal telopeptides generated undergo oxidative deamination by LOX on

specific lysines and hydroxylysines, which are destined to form intra- and intermolecular crosslinks (Yamauchi and Sricholpech, 2012).

While the most abundant collagens are fibrillar/fibril-forming, such as Collagen type I, there are other types of collagens. Collagens can thus be classified into: fibril-associated collagens with interrupted triple helices (FACITs), which are covalently link or associated to fibrillar collagens, network-forming collagens, beaded filaments and anchoring fibrils (Ricard-Blum, 2011). Conversely, these non-fibrillar collagens (e.g. type IV, XV and XVII) require the cysteine-rich C-terminal non-collagenous domains and N-terminal domains to maintain their structure (Ortega and Werb, 2002).

1.3.2.1.2. Network-forming collagens

Collagen IV is a network-forming collagen that is essential for the integrity, stability and function of the BM (Pöschl *et al.*, 2004). It is one of the main BM components and it is regarded as the most primitive ECM protein, having evolved up to six distinct chains: COL4A1, COL4A2, COL4A3, COL4A4, COL4A5, COL4A6 (Fidler *et al.*, 2017). Collagen IV contains 26 non-triple helix fragments as a consequence of misalignments between the sequences on α chains (Brazel *et al.*, 1988). This results in non-fibrillar loops in the native collagen IV conformation, which may be recognised by specific receptors and promote cell adhesion. Collagen IV molecules are highly cross-linked to one another by disulphide bonds (Brazel *et al.*, 1988). This permits the assembly of a branched polygonal supramolecular network that acts as a scaffold for other BM proteins (Yurchenco and Ruben, 1987). This may be consistent with the role of cysteines in crosslinking *Ascaris lumbricoides* (a human intestinal parasitic worm) collagen units together (McBride, Wesley McBride and Harrington, 1967). The presence of disulphide bonds in such primitive organisms may reflect the importance of cysteine-mediated crosslinks in ECM proteins. However, it is not clear if collagen IV is disulphide-bond crosslinked to other ECM proteins.

The abundance of cross-linking of collagen IV may influence ECM properties and stimulate cancer cells. In pancreatic tumour ECM collagen IV surrounds the cancer cells and stimulates proliferation and migration (Öhlund *et al.*, 2013).

1.3.2.1.2. Collagens assembling into beaded filaments

Collagen VI is classified as a beaded filament collagen. Its expression is ubiquitous and it is a highly disulphide cross-linked ECM protein. Comparably to collagen IV, its structure comprises collagenous and non-collagenous domains (Engel *et al.*, 1985). The C-terminal and N-terminal non globular regions show homology to the collagen-binding Von Willebrand factor A (VWA) domains (Chu *et al.*, 1989). The $\alpha 1$ (VI) and $\alpha 2$ (VI) subunits are similar in size and contain one N-terminal and two C-terminal domains. The $\alpha 3$ (VI) chain is bigger with up to ten N-terminal VWA domains, depending on alternative splicing, and C-terminal domains that contain type III fibronectin repeats (Zanussi *et al.*, 1992) and Kunitz domains (Zweckstetter *et al.*, 1996; Beecher *et al.*, 2011). Intramolecular disulphide bonds form between the C-terminal domains, as well as the five N-terminal $\alpha 3$ VWA domains so that it assembles into microfibrils (Fitzgerald *et al.*, 2001; Lamandé *et al.*, 2006). The other N-terminal $\alpha 3$ domains could participate in other ECM interactions (Beecher *et al.*, 2011). Abnormalities in collagen VI result in defective autophagy in myofibers (differentiated post-mitotic muscle cells), which leads to myofiber apoptosis and muscular dystrophy (Grumati *et al.*, 2010). Likewise, collagen VI expression protects neurons from apoptosis (Cheng *et al.*, 2011). Interestingly, collagen VI is upregulated in angiofibromas (Gramann *et al.*, 2009) and it shows aberrant expression, as well as a tumour-specific splicing in pancreatic cancer (Arafat *et al.*, 2011). Endotrophin, a peptide originated from cleaving collagen VI, promotes proliferation, angiogenesis, inflammation and fibrosis (Park and Scherer, 2012). Studies in vivo using the MMTV-PyMT breast cancer model showed that knocking out collagen VI increased tumour cell apoptosis (Park and Scherer, 2012).

1.3.2.1.3. Anchoring fibril collagens

Collagen VII is a major anchor of fibrils (Keene *et al.*, 1987). It connects the epidermis to the basal lamina, dermis and the connective tissue underneath (Gupta, Woodley and Chen, 2012; Wegener, Paulsen and Seeger, 2014). The non-collagenous domains show similarity to VWA or type III fibronectin domains. These domains mediate interaction to other ECM proteins, such as laminin-332, collagen type I and IV (Brittingham, Uitto and Fertala, 2006; Wegener, Paulsen and Seeger, 2014). After being exocytosed, procollagen VII fibres are organised in antiparallel dimers,

which are stabilised by disulphide bonds between the C-terminal domain and cysteines in the triple helix (Colombo *et al.*, 2003). A cysteine knot in the N-terminal to collagen triple helix has been suggested to hinder collagen unfolding; this disulphide bond is also present in FACIT collagen type IX (Wegener, Paulsen and Seeger, 2014). Recessive dystrophic epidermolysis bullosa (RDEB) is a skin disorder that is caused by biallelic/null mutations in collagen VII and it is associated with epidermal tumours (Ortiz-Urda *et al.*, 2005). RDEB-derived primary keratinocytes were transformed with oncogenic Ras and I κ B α , an inhibitor of the NF κ B pathway, in order to study how mutations in collagen VII promoted tumorigenesis (Ortiz-Urda *et al.*, 2005). Keratinocytes lacking collagen VII did not form tumours in nude mice, however mutant cells that conserved the NC1 domain of collagen VII generated tumours (Ortiz-Urda *et al.*, 2005).

1.3.2.1.4. Transmembrane collagens

Collagen XIII likely contains intrachain disulphide bonds in the NC4 domain (Snellman *et al.*, 2007). Disulphide bonds in collagen XIII have been described to participate in pepsin and trypsin/chymotrypsin resistance (Snellman *et al.*, 2007). Collagen XIII expression is high in breast cancer and it promotes TGF- β 1 signalling in a β 1-integrin-dependent manner (H. Zhang *et al.*, 2018). In mice models, collagen XIII promotes metastasis and resistance to anoikis (H. Zhang *et al.*, 2018).

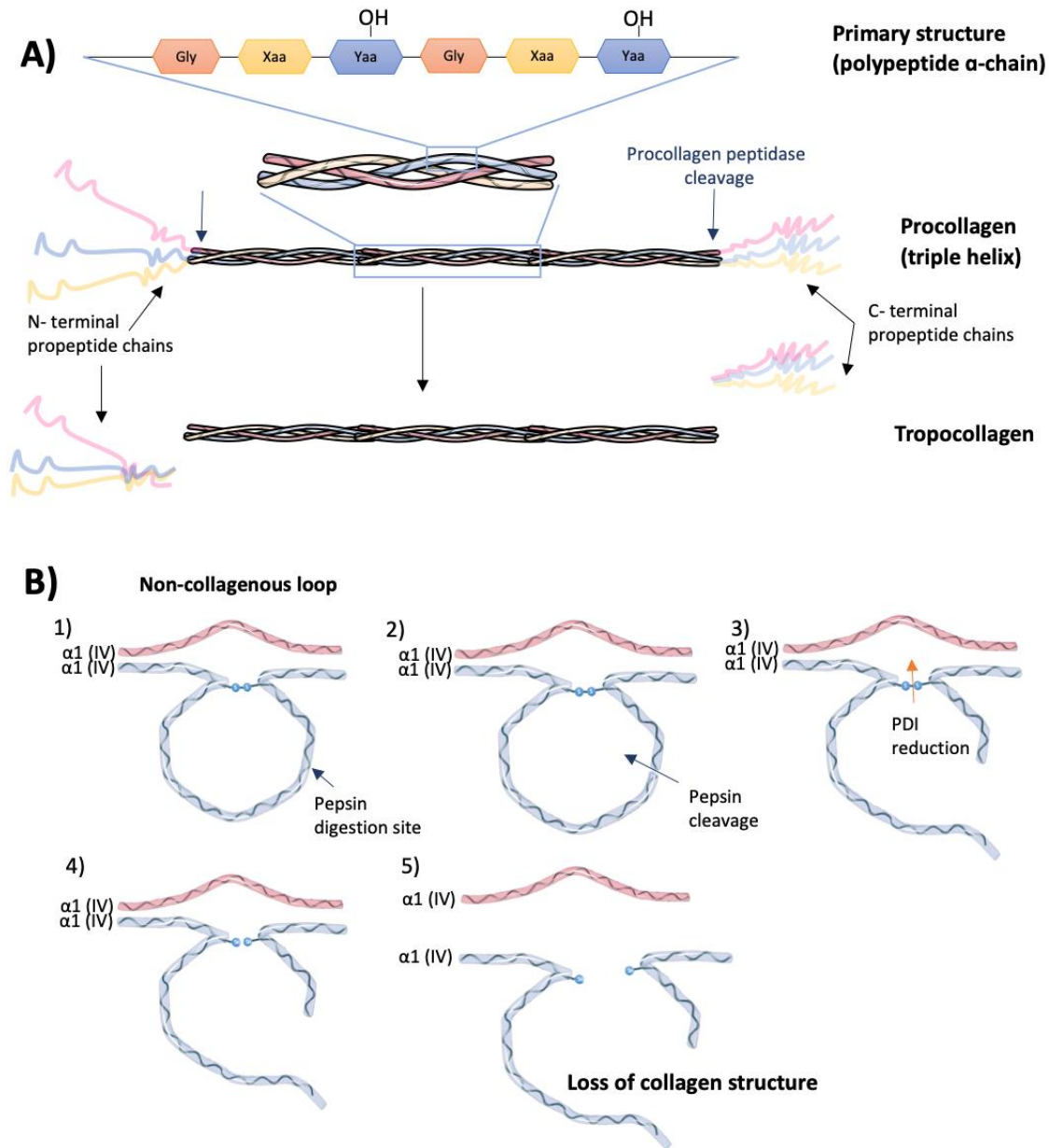


Figure 1-6. (A) Collagen biosynthesis. The primary structure of the polypeptide α -chains consists of the Gly-Xaa-Yaa repeats, where Xaa and Yaa are commonly proline and 4-hydroxyproline. In the endoplasmic reticulum, three polypeptide α -chains assemble into a triple helix: procollagen. Once secreted, the N- and C-terminal propeptide chains are cleaved by a procollagen peptidase. Specific residues of the tropocollagen molecule undergo oxidative deamination by LOX. These residues are required for the formation of intra and inter crosslinks between tropocollagen molecules. **(B) Proteolytic and oxidoreductase cleavage of human collagen IV.** (1) The non-triple helix segment of collagen IV (interruption XIII) presents a stabilising intrachain disulphide bridge. (2) In vitro studies showed that the presence of the disulphide bond in interruption XIII confers resistance to its proteolytic cleavage. Pepsin action in this disulphide-linked non-collagenous loop does not result in loss of collagen IV structure. (3-5) Following the reduction of the collagen IV segment, it is possible to see the different peptides generated from pepsin cleavage. This reduction is mediated by PDIs. PDI-mediated reduction of the intrachain disulphide bond leads to disassembly of the non-collagenous segment, which results in loss of ECM architecture (Adapted from Brazel et al., 1988). Collagen helix adapted from Servier medical art.

1.3.2.2. Laminins: Network basement membrane proteins

Laminins are major BM glycoproteins that assemble into networks. This influences tissue architecture and cellular adhesion (Erhard Hohenester, 2013; Armony *et al.*, 2016). Laminin molecules are cross-like shape heterotrimers (Engel *et al.*, 1981), consisting of one α chain, one β chain and one γ chain (Burgeson *et al.*, 1994) (Figure 1-7). Laminins contain up to 12% cysteine residues which influence the formation of stabilising disulphide bonds (Karimi *et al.*, 2016). The three laminin chains assemble together into a coiled-coil α helix structure at their C-termini (long arm of laminin) (Paulsson *et al.*, 1985). The chains are covalently linked by 3 disulphide bonds towards the N-terminal of the α helix (Frenette *et al.*, 1988) and another disulphide bond is present at the C-terminal of β 1 and γ 1 chains (Paulsson *et al.*, 1985).

In vitro, laminin-111 (Kammerer *et al.*, 1995), laminin-211 (Nomizu *et al.*, 1994) and laminin-332 (Phan *et al.*, 2008) require first the assembly of β and γ heterodimer. In Drosophila, the disulphide bonds between the dimeric β and γ chain befall prior α chain assembly; were this disulphide bond not be present, the α chain would not assemble (Kumagai, Kadowaki and Kitagawa, 1997). The C-terminal five G-like globular (LG) domains in the α chain mediate adhesion to heparin and α calcium-dependent adhesion to α -dystroglycan (Hohenester *et al.*, 1999) (Figure 1-7). At the end of the long arm, the LG domains bind to integrins; the LG3 domain of the α 3 chain of laminin-332 binds to integrin α 3 β 1 (Shang *et al.*, 2001) (Figure 1-7). The LG5 domain is conserved in the proteoglycans perlecan and agrin (Hohenester *et al.*, 1999). The N-terminal domain is comparable in the 3 laminin chains (α , β and γ). The N-terminal domains are composed of a globular laminin domain (LN), followed by laminin-type epidermal growth factor-like (LE) repeats, in between which there may be additional laminin type IV (termed L4 and LF) domains (Hohenester, 2019). The high content of disulphide bonds on LN and LE domains results in resistance to proteolysis (Ott *et al.*, 1982).

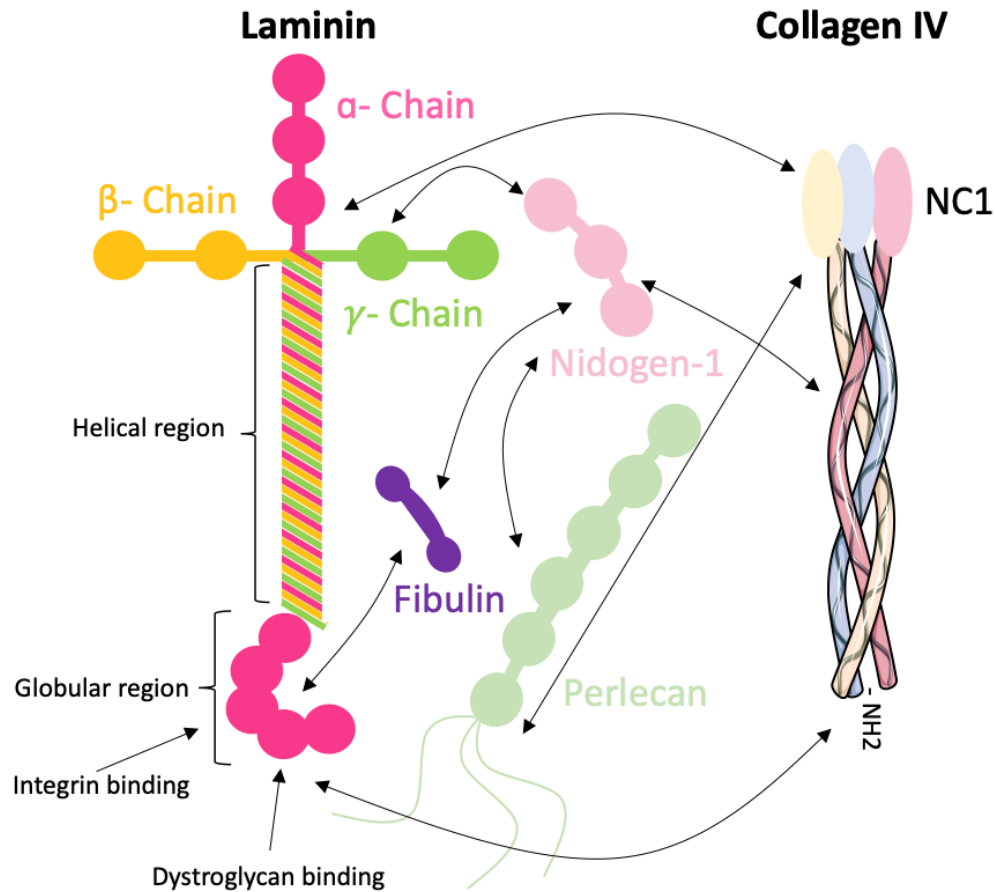


Figure 1-7. Laminin structure. Laminin is composed of an α chain, a β chain and a γ chain that are assembled into a cross-like shape. Within the basement membrane, laminin interacts with several proteins and cell receptors, including fibulin, perlecan, nidogen 1/2, collagen IV, integrins and dystroglycan (Adapted from Harvey and Thorner, 2005). Image created with items from the Servier medical art.

1.3.2.3. Other ECM proteins

1.3.2.3.1. Fibronectins

Fibronectins are glycoproteins (Hynes and Yamada, 1982), which are formed by three types of homologous repeats (Patel *et al.*, 1987). Fibronectin has twelve type I repeats, two type II repeats and fifteen to seventeen type III repeats (Pankov and Yamada, 2002). Fibronectins usually form a symmetric antiparallel dimer that is covalently linked by intramolecular disulphide bonds in its C-termini (Kar *et al.*, 1993). Extracellular fibronectin stability and aggregation depends on disulphide cross-linking (McKeown-Longo and Mosher, 1983; Langenbach and Sottile, 1999). Interestingly, the twelfth type I repeat comprises a Cys-Asp-Asn-Cys sequence with protein

disulphide isomerase activity, which may be required to incorporate fibronectin into the ECM (Langenbach and Sottile, 1999). Similarly, quiescin sulfhydryl oxidase 1 (QSOX1) is required in fibronectin incorporation and organisation in the ECM (Javitt *et al.*, 2019). Fibronectin expression is upregulated by the breast cancer cell line MDA-MB-231. In 3D suspension cultures, fibronectin expression upregulation depends on p38 activation. p38-dependent fibronectin expression facilitates attachment to two-dimensional cell cultures following activation of integrin $\beta 5$ and Src (Park and Helfman, 2019). In the SW480 colorectal cancer cell, nicotinic-acetylcholine receptor mediates upregulation of cyclooxygenase 2 and fibronectin, which in turn promotes cell migration (Wei *et al.*, 2011). $\alpha 5\beta 1$ integrin and fibronectin are required for invasion of the human ovarian cancer cell lines SKOV3ip1 and HeyA8 (Kenny *et al.*, 2014). In addition, as previously mentioned, fibronectin internalisation in the endometrioid ovarian cancer cell A2780, overexpressing Rab25, results in mTORC1 activation and invasive migration (Rainero *et al.*, 2015).

1.3.2.3.2. Tenascin-C

Tenascin-C is a disulphide-bond crosslinked mesenchymal glycoprotein that forms hexamers, a structure known as hexabrachion (Chiquet-Ehrismann *et al.*, 1986; Jones and Jones, 2000; Midwood *et al.*, 2016; Chiquet, 2020). Tenascin-C also consists of EGF-like repeats (Zanuttin *et al.*, 2004), which hinder cell adhesion on fibronectin by binding to the fibronectin type III repeats (Huang *et al.*, 2001). Tenascin-C contains fibronectin type III-like repeats, which are easily cleaved by cathepsin G, leukocyte elastase and MMP1, MMP3, MMP7 (Imai *et al.*, 1994; Siri *et al.*, 1995). The fifth fibronectin type III repeat binds to several growth factors, such as PDGF, FGF, TGF- β , IGF-BPs, which may additionally promote cell proliferation, migration (De Laporte *et al.*, 2013) and angiogenesis through VEGF (Tanaka *et al.*, 2004). Tenascin-C possibly induces amoeboid-like migration and metastasis by inhibiting YAP in a $\alpha 9\beta 1$ integrin mediated manner (Sun *et al.*, 2018).

1.3.2.3.3. Elastin

Elastin is a highly cross-linked ECM protein on its lysine residues, similar to collagen (Pinnell and Martin, 1968). It is the most abundant component of elastic fibres and provides structural support and mechanical stretching (Vindin, Mithieux and Weiss, 2019). The monomeric unit of elastin fibres is tropoelastin and mutations on this gene can cause arteriopathies, cardiovascular

and pulmonary disease, skin disease and joint hypermobility (Callewaert *et al.*, 2011). Elastin was reported to regulate proliferation and migration of colorectal cancer cells in culture. In macrophages, it increases secretion of tumour necrosis factor α (TNF α), which contributes to inflammation in cancer (Li *et al.*, 2020).

1.3.2.3.4. Vitronectin

Vitronectin is an ECM and plasma glycoprotein that participates in cell adhesion and migration upon integrin engagement (Seiffert and Smith, 1997). The N-terminal domain of vitronectin is known as somatomedin B and it provides a binding surface to stabilise plasminogen activator inhibitor-1 (PAI-1) activity and for the binding of the urokinase receptor (uPAR) (Kamikubo, Okumura and Loskutoff, 2002). Vitronectin further contains six hemopexin domains (Jenne and Stanley, 1987; Schwartz, Seger and Shaltiel, 1999); hemopexin is a glycoprotein that contains six intrachain disulphide bonds, which reduction is required for its proteolysis (Takahashi, Takahashi and Putnam, 1985). These hemopexin domains are also found in MMPs, where they have been described to regulate MMP activation and/or inhibition; for a review see (Piccard, Van den Steen and Opdenakker, 2007).

1.3.2.3.5. Thrombospondins

Thrombospondins are extracellular oligomeric glycoproteins that are classified into two subgroups: subgroup A/trimeric (thrombospondin 1 and 2) and subgroup B/pentameric (thrombospondin 3 to 5) (Adams and Lawler, 1993). The monomers contain an N-terminal domain, a coiled coil oligomerization domain, variable number of EGF-like repeats (type II), seven calcium binding TSR type 3 repeats and a globular C-terminus as reviewed in (Adams and Lawler, 2004). Subgroup A additionally contains a von Willebrand Factor type C (VWC) domain and properdin thrombospondin repeats (TSR type I) (Adams and Lawler, 2004). The N-terminal heparin-binding domain of thrombospondin 1 associates with cell surface calreticulin, this triggers PI3K and subsequently FA disassembly in bovine aortic endothelial cells, bovine embryonic fibroblasts and the uterine smooth muscle cell line (Eker Leiomyoma Tumour-3; ELT-3) (Goicoechea *et al.*, 2000). Disassembly of FA is indispensable during cell migration (Hamadi *et al.*, 2005; D'Souza *et al.*, 2020).

1.3.2.4. Interactions within the ECM meshwork

The extracellular space contains a complex meshwork of proteins, where ECM proteins, growth factors, remodelling enzymes and cell surface receptors interact. These interactions are required for ECM assembly and preservation of the tissue architecture. As a consequence, dysregulations in any of the ECM components can alter tissue homeostasis and lead to disease. The section above aimed to raise awareness of diversity of core matrix proteins and their importance in disease. This section focuses on some of the interactions described between the different ECM components and how imbalances in their structure or protein-protein interactions result in loss of ECM architecture and may facilitate certain cancer cell behaviours: namely, invasive migration.

1.3.2.4.1. Collagen interactions

Collagens assemble into fibrils *in vitro* (Gross and Kirk, 1958), however *in vivo* or in fibroblast cultures, assembly of collagen type I and type III is chaperoned by fibronectin (Grinnell, Billingham and Burgess, 1981; McDonald, Kelley and Broekelmann, 1982; Kadler, Hill and Canty-Laird, 2008), collagen V (Wenstrup *et al.*, 2004; Moriya *et al.*, 2011), $\alpha 5\beta 1$ fibronectin- and $\alpha 2\beta 1$ collagen-binding integrins (Li *et al.*, 2003). Conversely, elongation of fibronectin fibril requires binding to collagen type I (Dzamba *et al.*, 1993). Collagen and gelatin binding to fibronectin is dependent on the presence of disulphide bonds in type II fibronectin domains (Steffensen *et al.*, 2002); these domains decrease gelatinase (MMP-2 and MMP-9) activity (Steffensen *et al.*, 2002). The triple helical region of collagens I, II, III, IV, V and VI bind to the hemopexin domain 1 and 2 of vitronectin, which binding partially impairs fibronectin binding to native collagen (Gebb *et al.*, 1986; Yoneda *et al.*, 1998).

Thrombospondins can interact with several ECM proteins, such as fibronectin, laminin and collagens; for a review see (Tan and Lawler, 2009). Those interactions may be relevant to aid thrombospondin-mediated ECM assembly and remodelling (Frolova *et al.*, 2012; Subramanian and Schilling, 2014; Yamashiro *et al.*, 2020).

The NC3 domain in fibril associated collagen XII interacts with the disulphide-linked trimer tenascin-X (Veit *et al.*, 2006). This trimeric confirmation is required for ECM organisation by

bridging collagen fibrils, collagen associated fibrils, including collagen I, III, V, XII and XIV, and elastin (Lethias *et al.*, 2006; Egging *et al.*, 2007). Mutations in tenascin-X cause connective tissue disorders, such as Ehlers Danlos syndrome (characterised by joint hypermobility and skin and blood vessel fragility) (Kaufman and Butler, 2016). Tenascin-X expression is downregulated during tumorigenesis (Liot *et al.*, 2020). Tenascin-X downregulation and mutations may disrupt the collagen fibril organisation within tumour stroma and facilitate invasion. Additionally, links have been made between tenascin-X overexpression and a reduction in MMP2 and MMP9 expression (Yan *et al.*, 2019), further supporting a role in ECM network disruption and invasion.

The N- and C-telopeptides of collagen II are pyridinoline crosslinked to different sites of the triple helix COL2 domain of collagen IX in human, chick and bovine cartilage (Diab, Wu and Eyre, 1996). Collagen XI are further crosslinked between either the $\alpha 1(XI)$ or $\alpha 3(IX)$ COL2 domains and the $\alpha 3(IX)$ C-terminal (NC1) domain (Diab, Wu and Eyre, 1996). Collagen II and IX polymerise together with collagen XI, which regulates collagen fibril thickness (Mendler *et al.*, 1989). Collagen XI fibrils are crosslinked to one another between the N-telopeptide and the C-terminal of another collagen XI helix (Wu and Eyre, 1995). Collagen IX and XI are required to maintain tissue structure. Upregulation of the TGF- β ->Ets1->MMP3 axis by collagen XI in ovarian cancer promotes tumour growth, invasion and metastasis (Wu *et al.*, 2014). Interestingly, degradation of collagen IX and XI by MMP3 causes defects in ECM architecture (Wu *et al.*, 1991; Wu and Eyre, 1995). This suggests that keeping the homeostasis of the ECM is crucial; an imbalance in any of its components may cause a chain reaction that may affect contiguous ECM proteins. In fact, mutations in collagen IX destabilise the cartilage structure and have been associated with arthritis (Carlsen, Nandakumar and Holmdahl, 2006); a disbalance in collagen fibril structure further facilitates the access of anti-collagen II immunoglobulins (Carlsen, Nandakumar and Holmdahl, 2006). Similarly, mutations in collagen XI increase collagen type II degradation in cartilage (Rodriguez *et al.*, 2004). Collagen XI has been related to tumorigenesis in multiple cancers, such as colorectal (Fischer *et al.*, 2001), ovarian (Wu *et al.*, 2014), neck squamous (Sok *et al.*, 2013) and breast carcinomas (Vargas *et al.*, 2012), among others.

1.3.2.4.2. Linking the gap: basement membrane- stroma interactions

Collagen II fibres, as well as aggrecan and other procollagens, are connected to collagen VI microfibrils through linker complexes constituted by matrillin-1 and biglycan (Wiberg *et al.*, 2003); both proteins contain intrachain disulphide bonds in their structure (Wu and Eyre, 1998; Scott *et al.*, 2004). Matrillin-1 can contain additional interchain disulphide bridges with matrilin-3 (Wu and Eyre, 1998). Mutations in biglycan cause osteopenia, the phenotype of which is similar to osteoporosis and premature arthritis (Chen *et al.*, 2004). Biglycan is upregulated in many cancers, including pancreatic (Weber *et al.*, 2001), gastric (Hu *et al.*, 2014), ovarian (Kocbek *et al.*, 2014), colorectal (Xing *et al.*, 2015) and prostate cancers (Jacobsen *et al.*, 2017), and its expression correlates with tumour aggressiveness, invasion and metastasis. Biglycan expression in pancreatic cancer was proposed to act as tumour suppressor by arresting cancer cells in G1 (Weber *et al.*, 2001). Nevertheless, other studies indicated that biglycan correlates with poor survival in pancreatic tumours (Aprile *et al.*, 2013). In fact, it is worth mentioning that the breast cancer cell line MDA-MB-231 showed increased invadopodia and ECM degradation in G1 phase (Bayarmagnai *et al.*, 2019), while invasive MKN45 stomach adenocarcinoma cell line showed resistance to chemotherapy in G1 (Yano *et al.*, 2014). The differences observed between studies may be due to either early or late stage carcinomas. It could be that cell cycle arrest at early stages of tumour development is a mechanism to restrain tumour growth, but at later stages it may promote tumorigenesis.

The N-terminal domain of collagen VI $\alpha 3$ chain has further been described to interact with other ECM proteins, such as heparin and hyaluronan (Specks *et al.*, 1992). Other possible interactors of collagen type VI include collagen I, II and IV (Bonaldo *et al.*, 1990; Bidanset *et al.*, 1992; Kuo *et al.*, 1997). Nonetheless, an in vitro study reported that collagen I does not bind to collagen VI (Specks *et al.*, 1992); this difference may be on account of the experimental conditions used. Collagen VI has an important role in anchoring the BM components, such as collagen IV to the stromal ECM proteins, like collagen I ([Figure 1-8](#)). Upregulation of collagen VI and hyaluronan in breast (Wishart *et al.*, 2020; Wu *et al.*, 2020), pancreatic (Sugahara *et al.*, 2006; Owusu-Ansah *et al.*, 2019) and glioblastoma (Turtoi *et al.*, 2014; J.-W. E. Chen *et al.*, 2018) tumours promote cancer progression, invasion and dissemination.

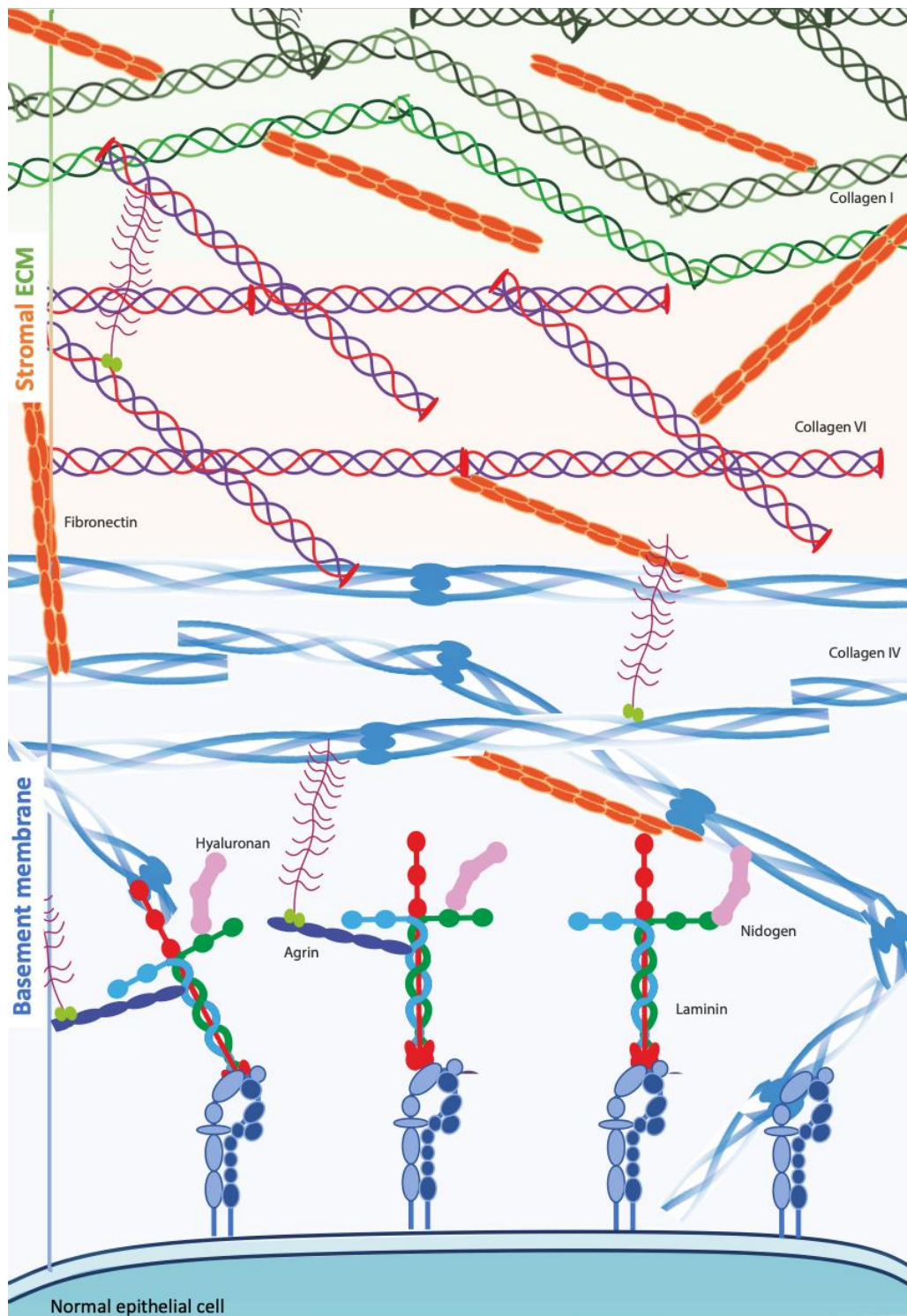


Figure 1-8. Schematic representation of the ECM meshwork. A non-transformed epithelial cell interacting with basement membrane proteins, such as laminin and collagen IV. The diagram also represents other interactions between the basement membrane proteins, namely collagen IV to the stromal ECM Collagen VI and later collagen I.

1.3.2.4.2. Basement membrane ECM interactions

Nidogen is a BM protein involved in supramolecular organisation since it complexes with laminin, collagen IV and perlecan (heparan sulfate proteoglycan) (Fox *et al.*, 1991; Battaglia *et al.*, 1992) (see [Figure 1-7](#) and [Figure 1-8](#)). Nidogen consists of three globular domains: N-terminal G1 and G2 and the C-terminal G3 (Fox *et al.*, 1991). The first two domains are connected through a flexible linker region, while the third domain is connected to G2 by rigid EGF-like repeats (Fox *et al.*, 1991). The second domain binds to collagen IV and perlecan (Fox *et al.*, 1991; Reinhardt *et al.*, 1993). Nidogen binding to collagen IV and perlecan requires the presence of a disulphide loop. The G3 domain of nidogen-1 binds to the EGF-like repeats of the laminin γ 1 chain (Mann, Deutzmann and Timpl, 1988; Fox *et al.*, 1991; Gerl *et al.*, 1991; Lössl *et al.*, 2014). Complexes between laminin and nidogen partially protect against thrombin, leukocyte elastase and MMP3-mediated proteolytic cleavage, in particular in the G3 domain (Mayer *et al.*, 1993). The CpG islands of nidogen-1/2 promoter were shown to be aberrantly methylated in colon and gastric cancers, leading to loss of gene transcription. Loss of nidogen-1/2 may favour invasion and metastasis by weakening cell-BM interactions, as well as facilitating the degradation of the BM (Ulazzi *et al.*, 2007). Similarly, degradation of nidogen by cysteine cathepsin S is associated with NSCLC (Willumsen *et al.*, 2017). On the other hand, nidogen overexpression correlates with poor prognosis and it promotes lung metastasis of melanoma and breast cancer cells (Alečković *et al.*, 2017). Nidogen-1 is increased in the serum of ovarian serous cancer (Li *et al.*, 2015).

Quiescin sulfhydryl oxidase 1 (QSOX1) is a disulphide bond catalyst found in the Golgi (Chakravarthi *et al.*, 2007) or in the secretome of confluent quiescent culture fibroblasts (Coppock *et al.*, 2000). QSOX1 is required for the incorporation of laminin α 4 into the ECM network as QSOX1 deficient fibroblasts display reduced adhesion (Ilani *et al.*, 2013). Laminin-411 and laminin-421 have been described to promote cell migration in glioma, melanoma, pancreatic and other carcinomas (Nagato *et al.*, 2005; Ishikawa *et al.*, 2014), suggesting its role in building a pro-migratory ECM. Laminin-411 has also been described to promote tumour cell growth in glioma cells by increasing Notch signalling and β 1-integrin (Sun *et al.*, 2019). Therapy using anti-QSOX1 antibody alone or together with doxorubicin decreases the tumour volumes and metastasis in the B16F10 melanoma model and in the MDA-MB-231 xenograft model (Feldman

et al., 2020). These mice showed less weight loss and weakness (Feldman *et al.*, 2020). QSOX1 could be a possible therapeutic target to modulate the laminin assembly into the ECM, as well as modulating laminin effects on cancer cells (Ilani *et al.*, 2013). QSOX1 secretion is increased in CAFs and TGF- β 1 released by cancer cells stimulates QSOX1 secretion in normal fibroblasts (Feldman *et al.*, 2020). Alpha-smooth muscle actin (α -SMA) is a sign of an activated microenvironment. Blocking antibodies against QSOX1 results in a decrease in α -SMA in myofibroblasts (Feldman *et al.*, 2020).

All above suggests the complex nature of ECM assembly and structure, as well as the relevance of ECM interactions in regulating ECM remodelling and degradation. Maintaining the balance between the matrisome components is important for the architecture of the ECM, one disturbance in one of the proteins, such as the ECM linker complexes, can perturb the structure of the meshwork and lead to pathological conditions. ECM components and the surrounding cells are constantly interacting, producing signals that influence both the ECM and cells.

The extent of ECM cross-linking can promote an invasive phenotype in cancer cells and can affect ECM remodelling (Pourfarhangi, Bergman and Gligorijevic, 2018). Tumour-associated stiffness and collagen cross-linking promote tumorigenesis in breast cancer, hepatocellular carcinomas, as well as in pancreatic ductal adenocarcinoma (PDAC) by augmenting mechanotransduction signals (Levental *et al.*, 2009; Rice *et al.*, 2017; Liu *et al.*, 2020). Nonetheless, the ECM in cancer is regarded as a two-edged sword: the ECM not only promotes tumorigenesis but also represents a barrier to cell migration and invasion; as an example, the BM is the first obstacle carcinoma cells encounter prior to invasion (Rowe and Weiss, 2008). Further evidence that sustains the tumour suppressive role of the ECM is that compressive stress, as a result of high density ECM, limits multicellular spheroid growth (Delarue *et al.*, 2014). Nonetheless, tumour cells display remodelling mechanisms to overcome the ECM barrier. Cancer cells are able to transmigrate and expand themselves through the BM and the surrounding stroma. The secretion or expression of proteases on the cell membrane is well-known to enable cancer cell movement and subsequent invasion (Hotary *et al.*, 2006). Protease-mediated degradation is known as the extracellular degradation, which is most likely complemented by and co-exists with the lysosomal degradation, which involves endocytosis of ECM (Rainero, 2016). The reorganisation of the ECM,

together with its enzymatic-mediated degradation, promotes matrix expansion (or stretching), which is required for tumour growth and local invasion (Provenzano *et al.*, 2006). However, these are complex processes that can be by-passed. Breast cancer cells, for example, can undergo mesenchymal to amoeboid migration when cell-matrix adhesions are hindered (Khoo *et al.*, 2019). Similarly, inhibiting ECM proteolysis induces invasive amoeboid phenotype in glioblastoma via Rho signalling activation (Yan *et al.*, 2016).

So far this section has discussed the structural aspects of the ECM and how imbalances in those have been associated with disease. The next part will focus on the mechanisms that cancer cells acquire in order to overcome the restrictive environment that the ECM can generate, focusing on the extracellular degradation.

1.4. EXTRACELLULAR MATRIX DEGRADATION IN CANCER

The most studied remodelling mechanism in cancer is degradation of ECM. Understanding the complexity of ECM remodelling mechanisms may open new avenues for therapeutically treating and preventing invasive growth and ultimately metastasis.

1.4.1. Invadopodia: specialised structures for ECM degradation

Following integrin-mediated adhesion to the ECM, cells of the monocytic myeloid lineage, osteoclasts, stimulated endothelial cells and cancer cells initiate the assembly of actin-rich protrusion inwards the ECM (Murphy and Courtneidge, 2011; Grafinger *et al.*, 2020). These protrusions, known as invadosomes, possess proteolytic enzymes that facilitate directional migration by promoting ECM degradation (Murphy and Courtneidge, 2011). Invasive tumours and transformed cells display specialised invadosomes, called invadopodia (Chen, 1989; Murphy and Courtneidge, 2011).

1.4.1.1. Signalling regulators of invadopodia

TGF- β (Rottiers *et al.*, 2009), vascular endothelial growth factor (VEGF) (Wang *et al.*, 2009; Lucas *et al.*, 2010), hepatocyte growth factor (HGF) (Rajadurai *et al.*, 2012) and epidermal growth factor

(EGF) (Mader *et al.*, 2011) trigger signalling cascades that result in Src kinase, PI3K and Rho family GTPases activation and positively regulate invadopodia formation (Chen, 1989; Mader *et al.*, 2011; Yamaguchi *et al.*, 2011; Spuul *et al.*, 2014). Simultaneously, EGFR and HGF signalling increases transcription and secretion of MMPs, actin aggregation and integrin distribution, which hence leads to ECM degradation (Porter and Barbieri, 2015).

Src, for instance, is a non-receptor tyrosine kinase that is frequently overexpressed and activated in many malignancies (Guarino, 2010). It is a well-known oncogene that has been described to promote ECM degradation and invasion (Guarino, 2010; Eckert *et al.*, 2011). Src-mediated phosphorylation of cortactin, Arg/Abl tyrosine kinase and tyrosine kinase substrate with 5 SH3 domains (Tks5) promote invadopodia assembly (Beaty *et al.*, 2013). The presence of Tks5 exclusively characterises invadopodia in cancer cells. Downregulation of Tks5 in Twist1- and Ras-transformed mammary epithelial cells reduced local invasion and dissemination to the lungs; while it did not affect growth of the primary tumours (Eckert *et al.*, 2011). Accordingly, overexpression of cortactin in a non-metastatic hepatocellular carcinoma cell line increased metastasis (Chuma *et al.*, 2004).

1.4.1.2. Integrins and invadopodia

Integrins are the main ECM receptors; they are heterodimers constituted by an α and β subunit (see [Figure 1-10](#) and section [1.5.1. Integrins](#)). Integrins sense the surrounding ECM and enable cells to respond to microenvironmental cues. Integrins facilitate cell adhesion, migration and invasion through the intricate ECM network; therefore, upregulated integrin expression leads to cancer invasion and vascular dissemination. Integrins cluster in invadopodia, β 1-integrin in MDA-MB-231 and MTLn3 breast adenocarcinoma cells is required for invadopodia maturation (Beaty *et al.*, 2013). β 1-integrin was reported to induce Arg kinase activation, which stimulates cortactin phosphorylation at Tks5-positive invadopodia (Beaty *et al.*, 2013). Cortactin phosphorylation leads to the recruitment of Na⁺/H⁺ exchanger type 1 (NHE1) (Magalhaes *et al.*, 2011). NHE1 activity induces an increase in the intracellular pH, which triggers release of cofilin from cortactin (Magalhaes *et al.*, 2011). Cofilin severs actin filaments and assists Arp2/3-complex dependent actin polymerisation to stabilise invadopodia (Oser *et al.*, 2009; Magalhaes *et al.*, 2011).

In breast and prostatic cancer cell lines, MDA-MB-231 and PC-3 respectively, β 1-integrin recruits integrin-linked kinase (ILK) upon engagement to the ECM (Greco *et al.*, 2021). ILK recruitment to β 1-integrin positive invadopodia activates NHE1, which leads to ECM proteolysis by acidification of the peri-invadopodia space (Greco *et al.*, 2021). The latter may be important in cathepsin-mediated ECM degradation (see section [1.4.3.1. Cathepsins: cysteine, serine and aspartyl proteases](#)).

In invadopodia, α 3 β 1 integrin associates with fibroblast activation protein (FAP α), a cell surface protease that cleaves collagen I into smaller fragments following its digestion by MMP1 (Mueller *et al.*, 1999; Fan *et al.*, 2016). In addition, α 3 β 1 integrin engagement to laminin-332 suppressed invadopodia-mediated degradation in 804G rat bladder carcinoma cells (Liu *et al.*, 2010). Paradoxically, knocking down laminin γ 2 chain boosts invadopodia assembly, as well as invadopodia-mediated degradation (Liu *et al.*, 2010). This suggests that specific ECM ligands may lead to the activation of distinctive signalling pathways, resulting in a unique biological outcome. However, more studies are required to understand the signalling cascades which are triggered by integrins in a context dependent manner.

Conversely, integrins are also well-known to activate focal adhesion kinase (FAK), which was described to negatively regulate invadopodia formation by sequestering Src to FAs (Chan, Cortesio and Huttenlocher, 2009; Kolli-Bouhafs *et al.*, 2014), while FAK-related proline-rich tyrosine kinase 2 (Pyk2), a non-receptor tyrosine kinase, was shown to recruit Src to nascent invadopodia in breast cancer cells (Genna *et al.*, 2018).

The ability of ECM degradation mediated by invadopodia resides in the proteolytic activity of MMPs, A disintegrin and metalloprotease (ADAM) and serine protease families. Of these proteases, MMPs are the most prominent family associated with invadopodia and ECM degradation in cancer cells. The next section highlights the role of MMPs and their ECM targets in cancer.

1.4.2. Matrix metalloproteinases

MMPs are regarded as the main family of proteolytic enzymes involved in ECM degradation. MMPs are often associated with the PM: MMP-1 is recruited by $\alpha 2\beta 1$ integrin, more specifically, $\alpha 2$ interacts with the linker plus hemopexin domain of MMP-1, and MMP-9 associates with CD44 (Yu and Stamenkovic, 2000; Stricker *et al.*, 2001). Interestingly, association between MMP-7 and cholesterol sulphate shifts substrate binding preference, promoting degradation of pericellular laminin-332 and fibronectin (Yamamoto, Miyazaki and Higashi, 2010). A balanced regulation of MMPs is required for normal tissue function (Ueno *et al.*, 1997; Löffek, Schilling and Franzke, 2011). Tissue inhibitors of metalloproteases (TIMPs) inhibit and regulate MMP activity (Gomez *et al.*, 1997). Not only TIMPs regulate MMPs, but MMP regulation also occurs at: (i) transcriptional and post-translational level, (ii) PTMs, including citrullination, glycosylation and nitrosylation, (iii) pro-enzyme activation by cleavage of the pro-domain and (iv) compartmentalisation within the cell (Löffek, Schilling and Franzke, 2011; Boon *et al.*, 2021). In cancer, the equilibrium becomes unbalanced, which results in increased ECM degradation, invasive growth and metastasis. Actually, expression of proteolytic enzymes, namely MMP family enzymes, positively correlates with tumour aggressiveness, while low activity is observed in normal tissues (Gress *et al.*, 1995; Murray *et al.*, 1996; Zhang *et al.*, 2008). Expression of MMPs is higher in both lymph node metastasis and dissemination to distal regions compared to ductal carcinomas in situ (Ueno *et al.*, 1997).

MMPs have been reported to participate at the initial stages of invasion by allowing cancer cells to invade through the BM and into the interstitial tissue (Bejarano *et al.*, 1988; Zeng, Cohen and Guillem, 1999). Degradation by MMPs unravels diverse molecules (e.g. growth factors) that were immersed within the ECM. Decorin degradation, for instance, leads to release of TGF- β (Imai *et al.*, 1997). While TGF- β acts as a tumour suppressor in early stages of cancer by inducing cell cycle arrest and apoptosis, at later stages it can promote EMT, metastasis and chemoresistance (Colak and Ten Dijke, 2017). Simultaneously, TGF- β has been linked to the formation of actin structures that resemble invadopodia and ECM degradation in human breast cancer cells (Mandal, Johnson and Wheelock, 2008). TGF- β is additionally implicated in the synthesis and release of

collagenases, such as MMP-13, and plasminogen activators; which on the one hand stimulate collagenolysis-dependent angiogenesis and, on the other, they further activate latent MMPs (Edwards *et al.*, 1987; Zijlstra *et al.*, 2004; Santibanez, 2013). MMP-induced cleavage of ECM molecules may further uncover latent TGF- β and other growth factors (Santibanez, 2013), as well as hidden ECM receptor binding sites. $\alpha\beta 3$, for instance, binds to denatured collagen through RGD binding sites, which are hidden within the collagen triple helix structure and are revealed following collagen denaturation (Davis, 1992).

There are twenty four types of MMPs, which can be classified into different types depending on their substrate; collagenases (MMP-1, -8 and -13), gelatinases (MMP-2 and -9), stromelysins (MMP-3 and -10), matrilysins (MMP-7 and -26), and membrane-type (MMP-14, -15, -16, -17, -24 and -25), among others; for a review see (Jabłońska-Trypuć, Matejczyk and Rosochacki, 2016). MMPs are highly specific: as an example, MMP-2 and MMP-9 are involved in the degradation of collagen type I and IV (Nikolov and Popovski, 2021). Actually, reducing MMP-2 expression results in inhibition of invasion, tumour growth and proliferation of laryngeal squamous cell carcinoma (Sun *et al.*, 2008). Similarly, MMP-9 is highly expressed in laryngeal carcinoma, which results from a disbalance in TIMP-1 expression (Matulka *et al.*, 2019). MT1-MMP (also known as MMP-14) enables cells to invade through high density cross-linked collagen I regions (Chun *et al.*, 2006). Of note, MT1-MMP has been shown to have triple helicase activity and disrupt the secondary structure of collagen molecules, as well as inducing its partial proteolysis (Tam *et al.*, 2004). On the contrary, MMP-2 is incapable of degrading densely crosslinked fibres, but it complements MT1-MMP to enable collagen cleavage into smaller soluble fibrils (Tam *et al.*, 2004). In addition, MMP-2 is activated by MT1-MMP (Tam *et al.*, 2002; Zigrino *et al.*, 2016). This ratifies that MMPs cooperate to successfully degrade the ECM.

The role of MMPs within the tumour microenvironment is complex: (i) Not only do cancer cells produce MMPs, but stromal cells, inflammatory and immune cells also contribute (Szabova *et al.*, 2008; Niland, Riscanevo and Eble, 2021). (ii) Some studies imply that there are anti-tumorigenic MMPs (MMP-3, -8, -9, -11, -12, -19 and -26). It has been reported that these play a role in inhibiting angiogenesis and metastasis in vivo (McCawley *et al.*, 2004; Montel *et al.*, 2004; Konstantinopoulos *et al.*, 2008; Dufour and Overall, 2013). (iii) The role of MMPs is distinctive

depending on the cancer grade. Broad spectrum inhibition of MMPs is inefficient to promote tumour regression in clinical trials, this may be explained by the dual function of MMPs: promoting and inhibiting tumour progression (Devy *et al.*, 2009). MMPs with anticancer functions should not be therapeutically targeted. MMP inhibition may be bypassed by alternative mechanisms. For instance, quintuple knockout of MMP in P6.p vulval precursor cells of the urinary tract in *Caenorhabditis Elegans* promotes acquisition of an adaptive mechanism to breach through the BM; actin-driven physical force enables cancer cells to breach through the BM by displacing it (Kelley *et al.*, 2019). Particularly, these cells display large protrusions enriched in Arp2/3 complex, F-actin and mitochondria, which generates high levels of ATP (Kelley *et al.*, 2019). It may be possible that in the absence of MMPs, cancer cells display similar enlarged-actin protrusions (Strzyz, 2019).

1.4.2.1. Regulation of MMPs through membrane trafficking

Malignant cells exploit the endomembrane trafficking machinery to promote cancer invasion. MMP activity can be regulated via endocytosis from or recycling to the PM. MT1-MMP, for instance, was reported to be internalised in a clathrin-dependent and clathrin-independent manner, probably caveolin-mediated endocytosis (Remacle, Murphy and Roghi, 2003); in fact, Src-dependant phosphorylation of caveolin-1 and MT1-MMP is required for their interaction, which regulates MT1-MMP turnover (Nyalendo *et al.*, 2007). Following its endocytosis, MT1-MMP co-localises with EEA1 and Rab5, localising MT1-MMP in early endosomes (Remacle, Murphy and Roghi, 2003). In addition, MT1-MMP can be recycled back to the PM through Rab4-positive endosomes (Remacle, Murphy and Roghi, 2003). Moreover, MT1-MMP colocalises with CLIC3 in late endosome/lysosome; knocking down CLIC3, Rab27A and B inhibit rapid recycling of MT1-MMP (Macpherson *et al.*, 2014). Primary cultures of invasive breast cancer cells using the PyMT model metabolise glutamine to glutamate (Dornier *et al.*, 2017). Glutamate is released via the Xc antiporter and extracellularly activates the glutamate receptor GRM3, which promotes MT1-MMP recycling in a Rab27-dependent manner (Dornier *et al.*, 2017). Additionally, vesicles containing MT1-MMP are propelled to mature invadopodia along microtubules via kinesins, including KIF1B, KIF5B and KIF3A/KIF3B (Schnaeker *et al.*, 2004; Wiesner *et al.*, 2010; Dong *et al.*, 2013; Wang *et al.*, 2017). In highly invasive breast cancer, KIF5B was identified as upregulated,

along with MT1-MMP (Marchesin *et al.*, 2015). This reinforces the important role of MMP trafficking upregulation and cancer invasion. Integrin β 1-mediated adhesion to collagen I drives MT1-MMP polarisation and its exocytosis to the PM via Rab8 activation; reducing the expression of Rab8 results in decreased ECM degradation and invasion in MDA-MB-231 breast cancer cells (Bravo-Cordero *et al.*, 2007). During invadopodia formation, Rab40b participates in the sorting of MMP-2 and MMP-9 into VAMP-4 secretory vesicles in MDA-MB-231 cells (Jacob *et al.*, 2013). In the MCF-7 breast adenocarcinoma cell line, Rab27 is found at the fusion sites in the PM, where it mediates the last stages of MMP-9 exocytosis (Stephens *et al.*, 2019). During constricted migration, the size of the matrix pore and lamin A expression, which modulates nuclear stiffness, coordinate pericellular collagenolysis in cancer cells (Infante *et al.*, 2018). The linker of the nucleoskeleton and cytoskeleton (LINC) complex protein nesprin-2 and the dynein adaptor Lis1 regulate the position of the centrosome, which contributes to the nucleo-anterior polarisation of MT1-MMP and Tks5 positive invadopodia (Infante *et al.*, 2018).

Frequent signalling pathways upregulated in cancer increase ECM degradation by affecting MMP trafficking; FAK/Src-mediated phosphorylation of Endophilin A2 inhibits endocytosis of MT1-MMP in Src transformed cells (Wu *et al.*, 2005). Conversely, MT1-MMP phosphorylation induces its internalisation, together with α 5 β 1 integrin, to Rab5 positive endosome (Williams and Coppolino, 2011). The complex formed by α 5 β 1 integrin and MT1-MMP is later trafficked to Rab7 and VAMP7 endosomes (Williams and Coppolino, 2011). The authors suggest that MT1-MMP is then recycled back to the PM, which consequently enhances degradation of ECM (Williams and Coppolino, 2011). Of note, phosphorylation of MT1-MMP by Src has been shown to promote migration in culture, as well as invasion and tumour growth in mice (Nyalendo *et al.*, 2007, 2008). Blocking MT1-MMP phosphorylation does not alter its proteolytic activity towards collagens and pro-MMP-2 (Nyalendo *et al.*, 2008). However, phosphorylation of the short cytoplasmic domain found in MT1-MMP is required for migration of the fibrosarcoma cell line HT-1080, human umbilical vein endothelial cells (HUVEC) and bovine aortic endothelial cells (BAEC) (Nyalendo *et al.*, 2007). This supports the yet unexplored role of MT1-MMP in cancer, which is independent of its proteolytic activity (Nyalendo *et al.*, 2007). The cytosolic domain of MT1-MMP recruits p130Cas to the PM of macrophages; this association contributes to Rac1 activation (Gonzalo *et*

al., 2010). In addition, MT1-MMP has been shown to regulate HIF-1 α and adenosine triphosphate (ATP) production in macrophages (Sakamoto and Seiki, 2010).

Factors other than MMPs play a role in the progression of cancer and invasion. The following section will outline other ECM proteolytic-based remodelling mechanisms used by cancer cells.

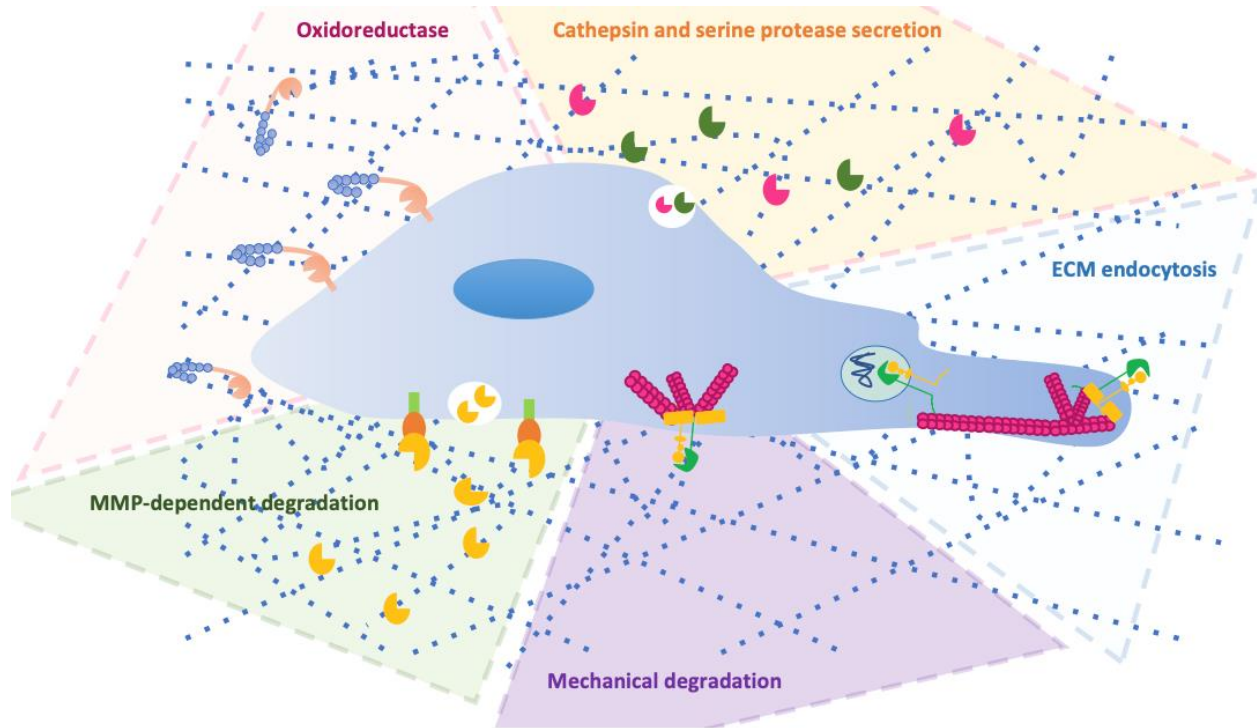


Figure 1-9. Diagram of the mechanisms employed by cancer cells to degrade the ECM. Cancer cells possess several mechanisms to overcome the constraints that the ECM may generate. While the MMP-mediated extracellular degradation has been extensively studied, cancer cells upregulate other proteolytic enzymes, namely serine and cathepsin proteases. Additionally, cancer cells internalise the diverse ECM components and degrade them in the lysosomes by cysteine cathepsins. In addition, the ECM components are highly crosslinked by disulphide bonds. Invasive cancer cells upregulate cell surface expression of oxidoreductases and protein disulphide isomerases to complement the proteolytic extracellular degradation. Moreover, cancer cells do not only rely on extracellular proteases, but they can mechanically remodel the extracellular matrix through actin-mediated pulling forces.

1.4.3. Beyond the MMP monopoly: cathepsins, ADAMs, serine proteases and oxidoreductases

1.4.3.1. Cathepsins: cysteine, serine and aspartyl proteases

Cathepsins are proteolytic enzymes, categorised into three families: cysteine (cathepsin B, C, F, H, K, L, O, S, V, X and W), serine (cathepsin A and G) and aspartyl proteases (cathepsin D and E) (Patel *et al.*, 2018; Yadati *et al.*, 2020). Cathepsins were once regarded mainly as lysosomal proteases, having a key role in intracellular protein degradation and energy metabolism (Fonović and Turk, 2014; Yadati *et al.*, 2020). These enzymes show highest activity and are active in acidic compartments, e.g. lysosomes (Patel *et al.*, 2018; Yadati *et al.*, 2020). However, it has become clear that cathepsins are secreted and expressed in the cell surface; interestingly, cathepsins remain functionally active in the extracellular space (Frosch *et al.*, 1999; Roshy, Sloane and Moin, 2003). Extracellular cathepsins are commonly found in pathology, such as cancer, neurological and cardiovascular disease (C.-L. Liu *et al.*, 2018; Bunk *et al.*, 2021).

Acidification of pericellular space promotes redistribution of lysosomes towards the PM, which results in secretion of active cathepsin B by malignant cells (Rozhin *et al.*, 1994). In the extracellular space, cathepsins are capable of degrading diverse ECM components (Fonović and Turk, 2014) ([Figure 1-9](#)). In cancer, cathepsins have been identified to cleave targets such as tenascin-C, nidogen-1, fibronectin, osteonectin, laminin, periostin, collagen IV, collagen I and elastin (Guinec, Dalet-Fumeron and Pagano, 1993; Mai *et al.*, 2002; Yasuda *et al.*, 2004; Boraschi-Diaz, 2017; Vizovišek, Fonović and Turk, 2019). Their activity results in changes to both the ECM structure and, in addition, it affects ECM-related signalling pathways. Cathepsin B and X, for instance, have been shown to promote EMT in the breast cancer cell line MCF-7 (Mitrović, Pečar Fonović and Kos, 2017). Similarly, cathepsin B and cathepsin S have been shown to be involved in the progression of pancreatic ductal adenocarcinoma and gastric cancer, respectively (Gopinathan *et al.*, 2012; da Costa *et al.*, 2020), while increased expression of cathepsin B, D and S by microglial cells has been observed in Alzheimer's disease (Lowry and Klegeris, 2018). Several cysteine cathepsins, including H, L, C, B and S are overexpressed during human papillomavirus HPV16-induced cervical carcinogenesis (Joyce *et al.*, 2004).

In addition to cathepsins degrading ECM extracellularly, cysteine cathepsins are also involved in ECM degradation in the lysosomes following its endocytosis (Nazemi *et al.*, 2021). Internalised ECM has been further described to be degraded by the proteasomes in pancreatic stellate cells to support PDAC cell growth in culture (Z. Zhu *et al.*, 2020). Together with MMPs and cathepsins, there are other key enzymes that aid cancer cells to degrade the proteins that shape the surrounding stroma ([Figure 1-9](#)).

1.4.3.2. Serine proteases, ADAM and ADAMTS family

In addition to MMPs and cathepsins, other proteases orchestrate ECM degradation. Serine proteases have been involved in cell growth and differentiation (Rakash, 2012). Similar to MMPs, serine proteases are zymogens and they are activated by proteolysis (Rakash, 2012). The best characterised serine protease is trypsin, which plays diverse roles in food digestion, coagulation, atherosclerosis, inflammation and cancer (Eagle and Harris, 1937; Soreide *et al.*, 2006; J.-Y. Shi *et al.*, 2020). Trypsin is involved in colorectal carcinogenesis by promoting proliferation, invasion and later metastasis of colorectal cancer cells (Soreide *et al.*, 2006). It has additionally been associated in activation of protease cascades, leading to MMP activation. Fibrin, fibronectin and laminin, for example, have been identified to be degraded by thrombin and plasmin serine proteases (Liotta, Goldfarb and Terranova, 1981). Another type of serine proteases are Urokinase-type plasminogen activator, whose expression positively correlates with tumour invasion and metastasis (Henneke *et al.*, 2010). Serine proteases can also be transmembrane proteins, such as matriptase, which is involved in progression of epithelial carcinomas, extracellular degradation of ECM and angiogenesis (Zoratti *et al.*, 2015).

Some ECM degrading enzymes have been shown to have anti-tumour properties or have a protective role in cancer. A disintegrin and metalloprotease with thrombospondin motifs (ADAMTS) and ADAMs, known together as adamalysins, are zinc-dependent metalloproteases, which are activated by furin (Przemyslaw *et al.*, 2013). There are 19 ADAMTS and 21 ADAMs, the former are usually secreted while the latter are transmembrane proteins (Przemyslaw *et al.*, 2013). ADAMTS1, for example, is an anti-angiogenic and tumour protective protease in breast cancer (Martino-Echarri *et al.*, 2013). ADAMTS1 expression is reduced in breast cancer; it

increases degradation of nidogen-1/2 and it ultimately affects vascular integrity (Martino-Echarri *et al.*, 2013). Nevertheless, it could be that lower levels of this enzyme are required in the process of extravasation during metastatic dissemination. Similarly, ADAMTS15 and ADAMTS18 expression is downregulated in breast, gastric, colorectal and pancreatic cancer (Porter *et al.*, 2006; Li *et al.*, 2010). ADAMTS8 expression is higher in breast carcinomas (Porter *et al.*, 2006).

1.4.3.3. Protein disulphide isomerases, proteases and ECM degradation

In malignancies, PDIs and endoplasmic reticulum chaperones are shuttled to the cell surface, where they are retained by C-terminal KDEL endoplasmic reticulum retention sequence (Bartels *et al.*, 2019). Endoplasmic reticulum stress has been reported to trigger Src activation, which consequently phosphorylates ArfGAP with SH3 Domain, Ankyrin Repeat And PH Domain 1 (ASAP1) (Tsai *et al.*, 2018). This promotes the formation of a complex with Golgi-specific brefeldin A-resistance guanine nucleotide exchange factor 1 (GBF1), which enhances its activity and leads to phosphorylation of Arf1 (Tsai *et al.*, 2018). The Src-ASAP1-GBF1-Arf1 axis or any downstream pathway promotes KDEL Receptor (KDELRL) 1 dispersion and cell-surface localisation of endoplasmic reticulum chaperones, such as the chaperones GRP78/CD109 (Tsai *et al.*, 2018). Similarly, Src- GBF1- Arf1 signalling was reported to promote relocation of GalNAc transferases (GALNTs) from the Golgi to the endoplasmic reticulum: known as GALNTs Activation (GALA) pathway (Chia *et al.*, 2020). Interestingly, the GALA pathway promotes traffic of the oxidoreductases calnexin and ERp57 (PDIA3) to the PM (Ros *et al.*, 2020). The authors consider that oxidoreductase traffic from endoplasmic reticulum to the PM originates from a modification in the O-glycosylation status at the N-termini of calnexin (Ros *et al.*, 2020). However, this raises the hypothesis that O-glycosylation in the endoplasmic reticulum may result in endoplasmic reticulum stress, which may consequently promote localisation of oxidoreductases to the PM. Concretely, PDIA3 and calnexin colocalise to invadopodia rosette-like structures, positive for cortactin, in v-Src transformed NIH/3T3 fibroblasts (Ros *et al.*, 2020). The authors postulate that calnexin and PDIA3 on the surface of invadopodia catalyse the reduction of disulphide bonds in extracellular proteins (Ros *et al.*, 2020), which therefore may affect the structure of the ECM meshwork. Reduction of disulphide bonds may enable the access of proteases, such as MMPs, to cleavage sites hidden within the protein conformation (see [Figure 1-6B](#)). Alternatively, PDI-

mediated disulphide bond formation of MMP9 is involved in regulating its activity and secretion to facilitate ECM degradation, metastasis and tumour angiogenesis (Khan *et al.*, 2012). This suggests a potential role for PDIs in orchestrating ECM degradation at multiple levels, through direct interaction with the ECM meshwork and regulation of MMPs.

1.4.4. Mechanical aspects of ECM degradation

In addition to proteolytic degradation, mechanical forces produced by cells drive ECM degradation. Invadopodia exert oscillating mechanical forces on the ECM in the order of 3 to 5pN, which further supports the proteolytic degradation of ECM (Dalaka *et al.*, 2020). Cross-linking is a PTM that modifies the mechanical properties of ECM and ECM-cell signalling. Heavily cross-linked ECM was actually found to promote the formation of invadopodia (Pourfarhangi, Bergman and Gligorijevic, 2018). This study identified that medium levels of type 2 transglutaminase (TG2) cross-linking of collagen I (0.39 as a ratio of cross-linked lysines to total number of lysine residues) resulted in increased invadopodia protrusions, MT1-MMP delivery and utmost ECM degradation (Pourfarhangi, Bergman and Gligorijevic, 2018). Similarly, the mechanical stimuli increase proteolytic collagen degradation in pancreatic cancer upon activation of ROCK1/2 activity (Rath *et al.*, 2017). Protease-independent mechanisms, i.e. mediated by matrix plasticity and actin polymerisation driven force, have been suggested to play an important role in cell invasion through covalently cross-linked BM (Wisdom *et al.*, 2020). Conversely, in breast cancer the lysyl oxidase related enzyme (LOXL2) orchestrated invasion *in vivo* and in inverted transwell collagen plugs through upregulation of MMP9 and TIMP1 (Barker *et al.*, 2011).

Other forces may affect remodelling, such as the pulling forces induced by contractility of FA of tumour cells (Provenzano *et al.*, 2006). The effects of these forces can be observed, for instance, when breast cancer cells radially re-organise collagen fibres, leading to facilitated migration and invasion at the tumour-stroma boundary in mouse breast tumour models (MMTV-Wnt-1 and MMTV-PyMT) (Provenzano *et al.*, 2006). Integrins are the molecular mediators of these mechanical forces, connecting the ECM to the actin cytoskeleton via linker proteins, such as talin and vinculin (Hu *et al.*, 2007) ([Figure 1-9](#)). This linkage to the actin cytoskeleton is known to be necessary during cell migration (Hu *et al.*, 2007) but could also move ECM fibres. Using

fluorescence resonance energy transfer (FRET) to assess changes in fibronectin conformation, it has been observed that cytoskeletal tension is a requisite to disrupt or unfold fibronectin in culture (Baneyx, Baugh and Vogel, 2002). It is not clear yet if these forces may facilitate the unfolding and disentangling of ECM proteins and help ingest ECM proteins for its intracellular degradation in lysosomes.

1.5. EXTRACELLULAR MATRIX RECEPTORS IN CANCER

Another aspect to consider is that the cellular components can interrelate with the ECM through cell-surface receptors, such as integrins, syndecans, dystroglycan, discoid domain receptors and mannose receptors. These interactions facilitate proliferation, cell polarity and migration (Rainero, 2016) by transducing cellular signals and modulating gene transcription. These ECM-binding receptors also collaborate on cell adhesion, actin cytoskeleton polymerisation and migration through the ECM (Frantz, Stewart and Weaver, 2010).

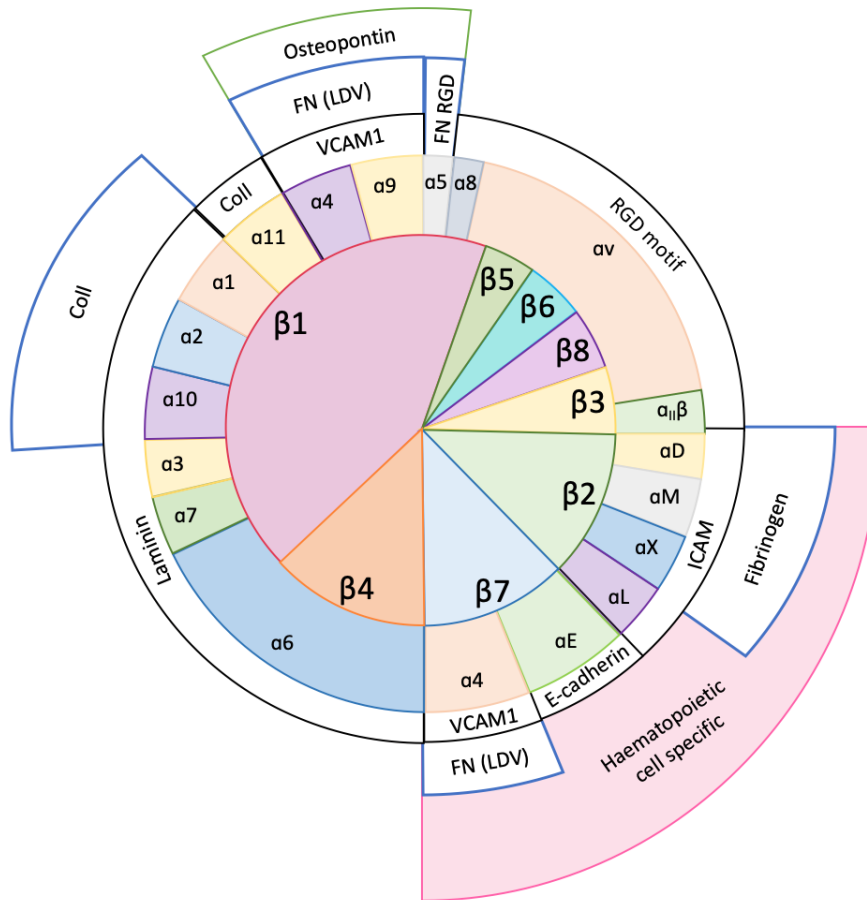


Figure 1-10. Integrin heterodimers. Reported pairing between the 18 α - and 8 β - integrin subunits and the ECM ligand in mammalian cells (Adapted from Moreno-Layseca et al., 2019).

1.5.1. Integrins

Integrins are the main cell-surface receptors that mediate cell adhesion to the extracellular matrix (Hynes, 2002). FA containing integrins are in charge of transmitting extracellular cues to regulate cell adhesion, signalling and survival. Integrins are heterodimers, which form stable non-covalent interactions between an α subunit and a β subunit (Hynes, 2002; Humphries, Byron and Humphries, 2006). Both subunits are type I transmembrane proteins, which characteristically have a large extracellular domain, a single pass transmembrane helix and a short cytoplasmic tail (Calderwood, Shattil and Ginsberg, 2000). In Mammalian cells there are 18 α -subunits and 8 β -subunits, which combine into 24 different heterodimers that bind distinct ECM components (Hynes, 2002) (Figure 1-10). Some integrins are promiscuous and interact with several ECM proteins, such as $\alpha v \beta 3$ (interacts with fibronectin, thrombospondin, fibrillin, LAP-TGF- β ,

fibrinogen, vitronectin, PCAM-1, Tenascin, osteopontin, MFG-EB Del-1 and BSP), $\alpha 4\beta 1$ (binds to fibronectin, VCAM1 and osteopontin) and $\alpha 2\beta 1$ (binds to collagens, laminins and thrombospondins) (Humphries, Byron and Humphries, 2006; Moreno-Layseca *et al.*, 2019). However, how do these integrins select ligand binding in complex environments? A recent study has shown that $\alpha v\beta 3$ integrin preferably binds to vitronectin when simultaneously exposed to vitronectin and fibronectin (Bachmann *et al.*, 2020). Interestingly, force-mediated conformational changes boost ligand promiscuity and its binding to fibronectin (Bachmann *et al.*, 2020). Other integrins, nonetheless, are highly specific and interact with a single ECM ligand; $\alpha 5\beta 1$ specifically binds to the RGD repeats of fibronectin (Humphries, Byron and Humphries, 2006; Moreno-Layseca *et al.*, 2019) ([Figure 1-10](#)).

ECM engagement to the diverse integrin family triggers distinctive signalling pathways (Hughes *et al.*, 1997; Schlaepfer and Hunter, 1997; Miranti and Brugge, 2002; Castelló-Cros *et al.*, 2009); as a consequence, integrin expression and activation at the cell surface will lead to a unique biological outcome (cell migration, invasion, proliferation and differentiation) depending on the environment and the cell type (Castelló-Cros *et al.*, 2009; Brafman *et al.*, 2013; Hou *et al.*, 2016; Bachmann *et al.*, 2020).

Integrin activity is regulated at different levels, namely integrin conformation, protein-protein interactions and its intracellular traffic (Moreno-Layseca *et al.*, 2019). One way integrins are activated is through their binding to an extracellular protein, which results in recruitment of scaffold proteins, kinases and phosphatases to modulate cell behaviour. This is known as “outside-in signalling” (Moreno-Layseca *et al.*, 2019). Conversely, integrins can be activated through “inside-out signals”, meaning that intracellular signalling promotes the recruitment of talin and kindlin to the cytoplasmic tail of β subunits (Moreno-Layseca *et al.*, 2019).

Integrin function can be regulated by its endocytosis and recycling back to the cell surface ([Figure 1-11](#)). Integrins are internalised via diverse endocytic pathways depending on integrin conformation, the ECM ligand and ECM stiffness. Integrin $\beta 3$ recruits the clathrin adaptor protein Dab2 on RGD (Arg-Gly-Asp) ligand-bound to mobile lipid bilayer, suggesting that clathrin-mediated endocytic machinery is recruited in the absence of traction forces (Yu *et al.*, 2015).

Clathrin-dependent integrin endocytosis has been extensively studied. Indeed, several α integrin subunits (i.e. $\alpha 2$, $\alpha 4$, $\alpha 9$, αM , αX , αD , αE , $\alpha 3$, $\alpha 6$ and $\alpha 7$) contain a putative Yxx Φ motif (Φ being a leucine, isoleucine, methionine or a valine) that interact with the $\mu 2$ C-terminal subdomain of the AP2 complex (De Franceschi *et al.*, 2016). Mutation on Yxx Φ motif impaired endocytosis of $\alpha 2$ and $\alpha 4$ integrin in HEK293 and MDA-MB-231 cells (De Franceschi *et al.*, 2016). Of note, 5 μ g/ml collagen I was used in this study, indicating that low collagen I concentrations may promote clathrin-dependent endocytosis of integrins. More recently, $\alpha 2\beta 1$ has been shown to be endocytosed via the clathrin- and dynamin-independent endocytic (CLIC-GEEC) pathway on MDA-MB-231 cells seeded on 0.3mg/ml collagen I (Moreno-Layseca *et al.*, 2021). This endocytic process is mediated by Rab21 (Pellinen *et al.*, 2006), which binds the cargo-specific adaptor Swip1 and $\beta 1$ -integrin (Moreno-Layseca *et al.*, 2021), while $\alpha 5\beta 1$ integrin endocytosis is dependent on caveolin-1 (Shi and Sottile, 2008). Integrins can also be internalised via phagocytosis to mediate clearance of apoptotic cells ($\alpha v\beta 3$ and $\alpha v\beta 5$) (Hanayama *et al.*, 2002), as well as internalisation of ECM components (see section [1.6. Internalisation of extracellular matrix](#)). Ultimately, integrin $\beta 3$ has been shown to be internalised via macropinocytosis, which leads to a rapid disassembly of FAs (Gu *et al.*, 2011). Similarly, $\alpha 5\beta 1$ integrin can be internalised via a macropinocytic process dependent on CYRI-A and CYRI-B (Le *et al.*, 2021). The diverse mechanisms controlling integrin internalisation may be cell type specific, however, ECM concentration and stiffness could dictate the signalling pathways activated downstream of integrins, which in turn may promote activation of distinct endocytic pathways.

Following internalisation integrins are trafficked to Rab5-positive early endosomes (Sandri *et al.*, 2012) ([Figure 1-11](#)); they can be later recycled back to the PM via Rab4 and Rab11 pathways (Roberts *et al.*, 2001; Caswell *et al.*, 2008). Additionally, integrins can be trafficked to lysosomes; the cytoplasmic tail of $\alpha 5$ is ubiquitinated and $\alpha 5\beta 1$ associates with TSG101, a component of the ESCRT complex in fibroblasts (Lobert *et al.*, 2010). Interestingly, internalised or endomembrane integrins are capable of recruiting FAK and other effectors and transmit intracytoplasmic signals, known as “inside-in signalling” (Alanko *et al.*, 2015). Additionally, integrins may also boost signalling of co-trafficking growth factor receptors (Ivaska and Heino, 2010). Interestingly, integrin signalling from early endosomes is essential for anchorage-independent survival and cell

growth of cancer cells, as well as dodging cell death in anchorage-dependent cells, a process known as anoikis (Alanko *et al.*, 2015).

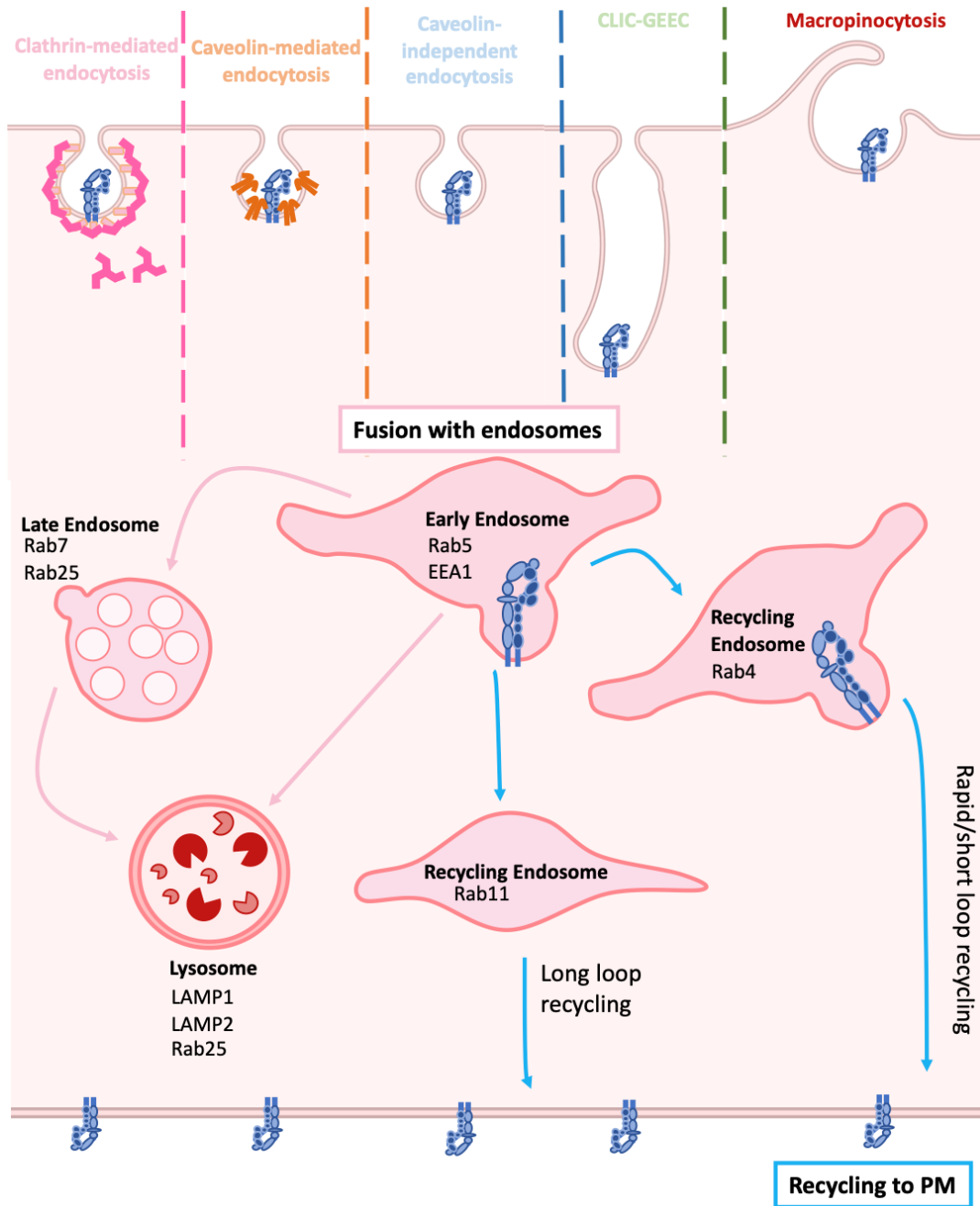


Figure 1-11. Integrin regulation at endosomal level. Traction forces and ligand availability trigger distinct endocytic pathways for the diverse integrin heterodimers. Once internalised, integrins fuse with Rab5-positive early endosomes (EE). They can be recycled in a Rab4-dependent manner (rapid/short loop recycling) and in a Rab11 and Rab25-dependent manner (slow/long loop recycling) or be traffic to late endosomes and lysosomes.

1.5.2. Other ECM receptors

Other relevant ECM receptors include the mannose receptor uPARAP/Endo180, CD44, discoidin-domain receptors (DDR) and syndecans.

uPARAP (urokinase plasminogen activator receptor-associated protein), also known as Endo180, is a 180kDa transmembrane glycoprotein (Sheikh *et al.*, 2000). It is expressed on fibroblasts, endothelial cells and macrophages (Sheikh *et al.*, 2000). It has been described to cluster in clathrin-coated pits in fibroblasts in culture; while 10 to 30% localises to the cell surface, 70-90% co-localises with the transferrin receptor in intracellular vesicles (Sheikh *et al.*, 2000). In addition to 8 C-type carbohydrate recognition domains, the receptor contains a putative collagen-binding fibronectin type II domain (Behrendt *et al.*, 2000). The receptor binds several collagens, including collagen V, collagen IV, collagen II, folded and denatured collagen I (Behrendt *et al.*, 2000; Wienke, MacFadyen and Isacke, 2003; Kjølner *et al.*, 2004).

CD44 is a transmembrane adhesion molecule that binds to hyaluronan (Vachon *et al.*, 2006). It is involved in inflammatory and immune responses by inducing phagocytosis of apoptotic cells (Vachon *et al.*, 2006). It mediates hyaluronan metabolism and induces phagocytosis of hyaluronan-coated beads in the murine macrophage RAW 264.7 (Vachon *et al.*, 2006). Hyaluronan phagocytosis is dependent on Syk, Rac1 and phosphatidylinositol 3-kinase (Vachon *et al.*, 2006). CD44 activates several signalling pathways that induce proliferation, survival, cytoskeleton changes and cell motility in cancer (C. Chen *et al.*, 2018). As a result, the use of hyaluronan-coated nanoparticles has been proposed for targeting activated CD44 for cancer therapy (Guo, Yang and Gao, 2021).

Discoidin domain receptors (DDR) are a distinctive subfamily of receptor tyrosine kinases (RTKs) that transduce a signalling cascade in response to collagens (Leitinger, 2014). Two kinases comprise the DDR subfamily: DDR1 and DDR2 (Leitinger, 2014). Alternative splicing of DDR1 gives rise to 6 different isoforms; DDR1a, DDR1b and DDR1c are full length and highly homologous, while DDR1d and DDR1e are kinase-deficient receptors (Alves *et al.*, 2001; Fu *et al.*, 2013). DDR1f contains the kinase domain but misses most of the extracellular domains (Müllenbach, Walter and Dressel, 2006). DDR1 recognises fibrillar and non-fibrillar collagens, such as collagen I and

type IV, while DDR2 only recognises fibrillar collagens, namely collagen type I and III (Vogel *et al.*, 1997; Xu *et al.*, 2011). DDR1 is mainly expressed in epithelial tissues or cancers of epithelial origin, whereas DDR2 is expressed in mesenchymal cells or cancer of mesenchymal origin. DDR1 enhances invadosome assembly and MMP activity in cancer cells via Cdc42 (Juin *et al.*, 2014). Furthermore, it has been described to promote collective migration of cancer cells and 3D amoeboid migration of Th17 cells (subpopulation of T helper cells) (Chow *et al.*, 2016; El Azreq *et al.*, 2016). Silencing DDR1 in elongated mesenchymal cells, such as the melanoma cell lines WM983A and A375P, decreases adhesion to collagen I (Sanz-Moreno *et al.*, 2022). This induces amoeboid features that lead to amoeboid 3D invasion.

Another important family of ECM receptors are syndecans. Syndecans are type I transmembrane proteoglycans that mediate cell-cell and cell-matrix interactions through glycosaminoglycan chains in the N-terminal domain (Afratis *et al.*, 2017). There are four syndecan types classified into 2 subfamilies. Syndecan-1 and syndecan-3 belong to the same subfamily, while syndecan-2 and syndecan-4 form another one (Couchman, 2003). Syndecan 1 is expressed in epithelial and plasma cells and its expression is altered in malignancies, such as myeloma, head and neck, lung, breast and colorectal carcinomas (Anttonen *et al.*, 1999, 2001; Bayer-Garner *et al.*, 2001; Wei *et al.*, 2015; Chute *et al.*, 2018). Upon binding to a ligand, syndecan-1 triggers ERK and Src phosphorylation leading to its internalisation in lipid-rafts (Chen and Williams, 2013). Syndecan-1 has been described to activate $\alpha v \beta 3$ and $\alpha v \beta 5$ integrin heterodimers in human vascular endothelial cells, which thus promotes angiogenesis during tumorigenesis (Beauvais *et al.*, 2009). Syndecan-2 is expressed in mesenchymal cells, including fibroblasts, smooth muscle cells and the mesenchymal breast cancer cell line MDA-MB-231 (Lim and Couchman, 2014; Afratis *et al.*, 2017). Its expression correlates with the metastatic potential or overall survival of head and neck, breast, colorectal and pancreatic cancer (De Oliveira *et al.*, 2012; Lim and Couchman, 2014; Farnedi *et al.*, 2015). In colorectal carcinomas, syndecan-2 expression is increased following its interaction with stromal fibroblast ECM, especially fibronectin (Vicente *et al.*, 2013). Syndecan-3 is expressed in neural tissues and developing musculoskeletal tissues (Afratis *et al.*, 2017). High syndecan 3 expression correlates with perineural invasion and poor prognosis of pancreatic carcinomas, while it promotes EMT in prostate cancer (Diamantopoulou *et al.*, 2012; Yao *et al.*,

2014). Syndecan-4 is ubiquitously expressed. High levels of syndecan-4 are associated with ER⁺ and PR⁺ breast tumours (Lendorf *et al.*, 2011). Syndecan-4 can act as a co-receptor of $\alpha 5\beta 1$ integrin to mediate PKC α activation, which leads to FA formation and cell migration (Mostafavi-Pour *et al.*, 2003; Lendorf *et al.*, 2011). Similarly, ADAM12 and syndecan-4 promote cell spreading via PKC α and RhoA in a $\beta 1$ -integrin-dependent manner (Thodeti *et al.*, 2003).

The sections above have focused on the foremost endocytic pathways, core matrisome proteins and the main ECM receptors. The following subsections comprise an overview of the described ECM endocytic pathways.

1.6. INTERNALISATION OF EXTRACELLULAR MATRIX

1.6.1. Collagen I internalisation

Collagen internalisation is hitherto reported to be under the control of three endocytic pathways: $\beta 1$ -integrin-mediated phagocytosis, Endo180-dependent uptake and macropinocytosis (Madsen *et al.*, 2011; Rainero, 2016; Yamazaki *et al.*, 2020). The first is involved in the uptake of fibrillar collagen, while the latter is responsible for the endocytosis of soluble collagen (Madsen *et al.*, 2011).

1.6.1.1. Integrin-mediated phagocytosis

Phagocytosis is a cellular process in which large extracellular particles (> 0.5 μ m) or microorganisms are receptor- and actin-dependent internalised into large vesicles, named phagosomes (Coopman *et al.*, 1996; Gordon, 2016). These vesicles eventually fuse to lysosomes and form phagolysosomes (Gordon, 2016). Particularly, $\alpha 1\beta 1$ and $\alpha 2\beta 1$ integrins are implicated in native collagen I binding and its subsequent phagocytosis in fibroblasts (Abraham *et al.*, 2007). Further studies are however needed since these results were obtained by the uptake of collagen fluorescent beads, which may not be the best scenario to recapitulate the architecture of an *in vivo* ECM.

Interestingly, denatured collagen I activates $\alpha v\beta 3$ integrin (Abraham *et al.*, 2007) which evidences that collagen phagocytosis is strongly dependent on collagen morphology (Rainero, 2016).

Congruently with these findings, it has been suggested that the intricate 3D structure of the ECM may control internalisation (Rainero, 2016).

Cells are attached to collagen through FAs, which are complex specialised adhesions constituted by integrins (Arora *et al.*, 2013; Rainero, 2016). Collagen I specifically binds to $\alpha 2\beta 1$ and increases intracellular calcium concentration $[Ca^{2+}]_i$ via the activation of stretch-sensitive, calcium-permeable channels (Arora *et al.*, 2013; Rainero, 2016). Importantly, the increase in Ca^{2+} concentration in FAs recruit Gelsolin and non-muscle myosin IIA (NMMIIA) (Arora *et al.*, 2013; Rainero, 2016) ([Figure 1-12](#)).

On the one hand, NMMIIA is needed for the phagosome formation and, in addition, it plays a role in cell migration since it is an actin-based motor protein. Activation of the integrin-signalling pathway induces phosphorylation of the NMMIIA. More particularly, the myosin light chain (MLC) subunit is phosphorylated by Myosin light chain kinase (MLCK) and consequently filament assembly is enhanced. Besides, MLC phosphorylation allows the binding of the small GTPase Rap1 to NMMIIA and Rap1 further enhances $\beta 1$ -integrin-mediated adhesion, which positively feedbacks collagen adhesion to cells (Arora *et al.*, 2013) ([Figure 1-12](#)).

On the other hand, gelsolin is a Ca^{2+} -dependent actin-binding protein involved in filament nucleation (Arora *et al.*, 2013), which is required for phagosome formation and collagen uptake to early endosomes (EEs) (Rainero, 2016). Further evidence suggests that an increase in $[Ca^{2+}]_i$ and gelsolin activation are important for the activation of the small GTPase Rac. Rac belongs to the Rho small GTPase family and it plays a role in regulating the extension of filopodia and lamellipodia. More outstandingly, the latter is required in collagen phagocytosis and cell spreading (Arora *et al.*, 2013) ([Figure 1-12](#)).

In general, GTPases are regulated by guanine nucleotide exchange factors (GEFs) and GTPase-activating proteins (GAPs), which stimulate its GTPase activity and, as a result, signalling terminates. During collagen phagocytosis, Src kinase mediates Vav2 GEF phosphorylation, subsequently activating Vav2, which enhances Rac1 activation (Arora, Marignani and McCulloch, 2008). Interestingly, Src has been reported to be associated with gelsolin and activate gelsolin-

downstream pathways (Chellaiah *et al.*, 1998). Finally, collagen is degraded in the lysosome (Arora *et al.*, 2013; Rainero, 2016) ([Figure 1-12](#)).

More recently, it has been reported that DQ-fluorescein-conjugated collagen type I is internalised via macropinocytosis in cancer cells (Yamazaki *et al.*, 2020). This process is dependent on Rac1 (Yamazaki *et al.*, 2020). Collagen I internalisation leads to mTOR activation and results in resistance against EGFR tyrosine kinase inhibitor treatment in the EGFR-mutated lung cancer cell line PC-9 (Yamazaki *et al.*, 2020).

1.6.1.2. Non-phagocytic pathway of collagen uptake: uPARAP/Endo180-dependent endocytosis

Another significant collagen internalisation route that has been described is dependent on the mannose receptor uPARAP/Endo180 (Madsen *et al.*, 2011). This receptor binds several soluble collagens, such as type I, IV and V (Rainero, 2016). Congruently, so that this specific endocytic pathway efficiently befalls, the collagen fibres must be previously cleaved by either MMPs or the cysteine protease cathepsin K (Madsen *et al.*, 2011). Collagen fragments then bind to the Fibronectin type-II domain of uPARAP/Endo180 (Engelholm *et al.*, 2001) and trigger the activation of clathrin-mediated endocytosis (Madsen *et al.*, 2011; Rainero, 2016). Following internalisation, collagen fragments are delivered to the lysosomes (Kjøller *et al.*, 2004; Rainero, 2016) where cysteine cathepsins degrade it (Mohamed and Sloane, 2006) ([Figure 1-12](#)).

Moreover, the process not only requires of uPARAP, but also the assembly of a trimolecular complex with *uPA receptor* (uPAR) and the *pro-form of the urokinase-type plasminogen activator* (pro-uPA) (Engelholm *et al.*, 2001; Mohamed and Sloane, 2006). uPAR is critical for the proteolysis of pro-uPA into active uPA and, more notably, the union of uPAR to uPA enables the conversion of plasminogen to plasmin. Plasmin degrades the ECM and releases active MMPs, thereby enhancing tumour invasion and metastasis (Noh, Hong and Huang, 2013) ([Figure 1-12](#)).

Prominently, the trimolecular complex promotes directional cell migration in mammary cancer cells since it enhances filopodia and lamellipodia formation (Takahashi *et al.*, 2011). Additionally,

uPAR promotes EMT in the breast cancer cell line MDA-MB-468 (Noh, Hong and Huang, 2013). Utilisation of uPA RNA interference (RNAi) prevented invasion, migration, proliferation and angiogenesis in glioma cells (Takahashi *et al.*, 2011).

uPARAP/Endo180 is highly expressed in several malignancies (Takahashi *et al.*, 2011), while normal human mammary cells present low levels of uPARAP (Curino *et al.*, 2005). More promisingly, uPARAP system could be considered as a novel therapeutic target in cancer because of its involvement in tumour progression and its expression in advanced tumours (Noh, Hong and Huang, 2013).

1.6.2. Fibronectin internalisation

Fibronectin polymerization into the ECM is vital to maintain the proper architecture, composition, stability and function of tissues (Sottile and Chandler, 2005). Fibronectin is also required for the correct deposition and maintenance of ECM proteins, such as collagen I, collagen III and fibrinogen (Sottile and Chandler, 2005; Rainero, 2016). It can interact with and regulate the deposition of glycoproteins found in the ECM (e.g. thrombospondin-1, tenascin C and fibulin) (Sottile and Chandler, 2005). More significantly, fibronectin fibrils regulate cell proliferation and migration (Sottile and Chandler, 2005). Therefore, preservation of fibronectin homeostasis, both synthesis and degradation, is essential.

$\alpha 5\beta 1$ integrin is paradoxically responsible for both fibronectin polymerization and caveolae-mediated endocytosis of fibronectin (Rainero, 2016). More specifically, Cav-1 is constantly regulating fibronectin internalisation (Sottile and Chandler, 2005; Shi and Sottile, 2008; Rainero, 2016) ([Figure 1-12](#)) and downregulating Cav1 results in inhibition of matrix and soluble fibronectin internalisation. Moreover, Cav1 has been reported to be a major modulator of cell migration by maintaining the homeostasis of fibronectin turnover (Shi and Sottile, 2008). Congruently, high levels of $\alpha 5\beta 1$ integrin promote motility and survival on human fibroblasts (Lobert *et al.*, 2010). Other evidence suggests that soluble fibronectin can be endocytosed in absence of $\beta 1$ -integrins (Shi and Sottile, 2008).

After endocytosis, fibronectin together with $\alpha 5\beta 1$ is trafficked into early endosomes and it is subsequently degraded in the lysosomal compartment (Lobert *et al.*, 2010). Fibronectin-bound integrins are ubiquitinated, the ESCRT machinery is activated and drives formation of ILVs (Lobert *et al.*, 2010; Rainero, 2016). Finally, fibronectin is degraded by lysosomal enzymes (Rainero, 2016) ([Figure 1-12](#)).

1.6.2.1. Integrins, migration and fibronectin internalisation

Cell migration requires the formation of new adhesion sites to the substrate at the leading edge and the loss of those at the trailing edge so that the cell detaches. Importantly, the process requires the recycling of integrins, which is regulated by Rab4, Rab11 or Rab25 small GTPases (Lobert *et al.*, 2010). $\alpha 5\beta 1$ recycling to the tip of invasive protrusions is mediated by Rab Coupling Protein – a Rab11 effector – and it improves invasion in fibronectin-rich matrices (Caswell *et al.*, 2008).

Other evidence nonetheless suggests that degradation of fibronectin-activated $\alpha 5\beta 1$ integrins, after being sorted to the MVBs, is essential for the correct migration of fibroblasts (Lobert *et al.*, 2010). One possible explanation is that integrin degradation is balanced by boosting integrin synthesis, which would be important for the proper formation of functional adhesion sites. Another possibility is that both integrin and fibronectin degradation is needed to weaken integrin signalling since increased adhesion to the substrate and higher levels of ECM impair cell motility. Notwithstanding, $\alpha 5\beta 1$ integrin has been described to directly recycle from late endosomes and lysosomes to the plasma membrane in the ovarian cancer cell line A2780, expressing Rab25, and in pancreatic tumours (Dozynkiewicz *et al.*, 2012). Moreover, traffic to lysosomes of ligand-occupied $\alpha 5\beta 1$ integrin is required for mTORC1 recruitment to these organelles (Rainero *et al.*, 2015); which links nutrient signalling to invasive migration and metastasis (Rainero *et al.*, 2015). In addition, $\alpha 5\beta 1$ -positive ILVs may also be exocytosed as exosomes, which can later fuse to their own or vicinity membrane (Lobert *et al.*, 2010). Importantly, exosome secretion can modify the tumour microenvironment and contribute to tumour growth, angiogenesis and metastasis. Indeed, ILVs secretion is controlled by cortactin, which also regulates cell motility and invasion (Sinha *et al.*, 2016). Furthermore, cortactin has been related to the secretion of fibronectin- and

collagen I-containing exosomes (Sung *et al.*, 2011; Rainero, 2016; Sinha *et al.*, 2016). Remarkably, cell motility and lamellipodia are impaired in cortactin defective cells and, more outstandingly, autocrine secretion of ECM is fundamental in cell migration (Sung *et al.*, 2011). Nonetheless, further studies are indispensable to unravel if those exosomes contain a modified form of ECM proteins.

1.6.3. Laminin internalisation

Laminins are the most abundant BM constituents (Leonoudakis *et al.*, 2014; Rainero, 2016). BM is a vital modulator of tissue architecture and function (e.g. cell polarity, survival and hormone signalling); therefore, altering cell-BM interaction contributes to the progression of human diseases, such as cancer (Leonoudakis *et al.*, 2014). Laminin-rich BMs are proteolytically degraded and, in addition, BM could be potentially remodelled by laminin internalisation (Rainero, 2016). Importantly, uptake of extracellular matrix constituents is crucial for the regulation of cell function and its interaction with the microenvironment (Leonoudakis *et al.*, 2014).

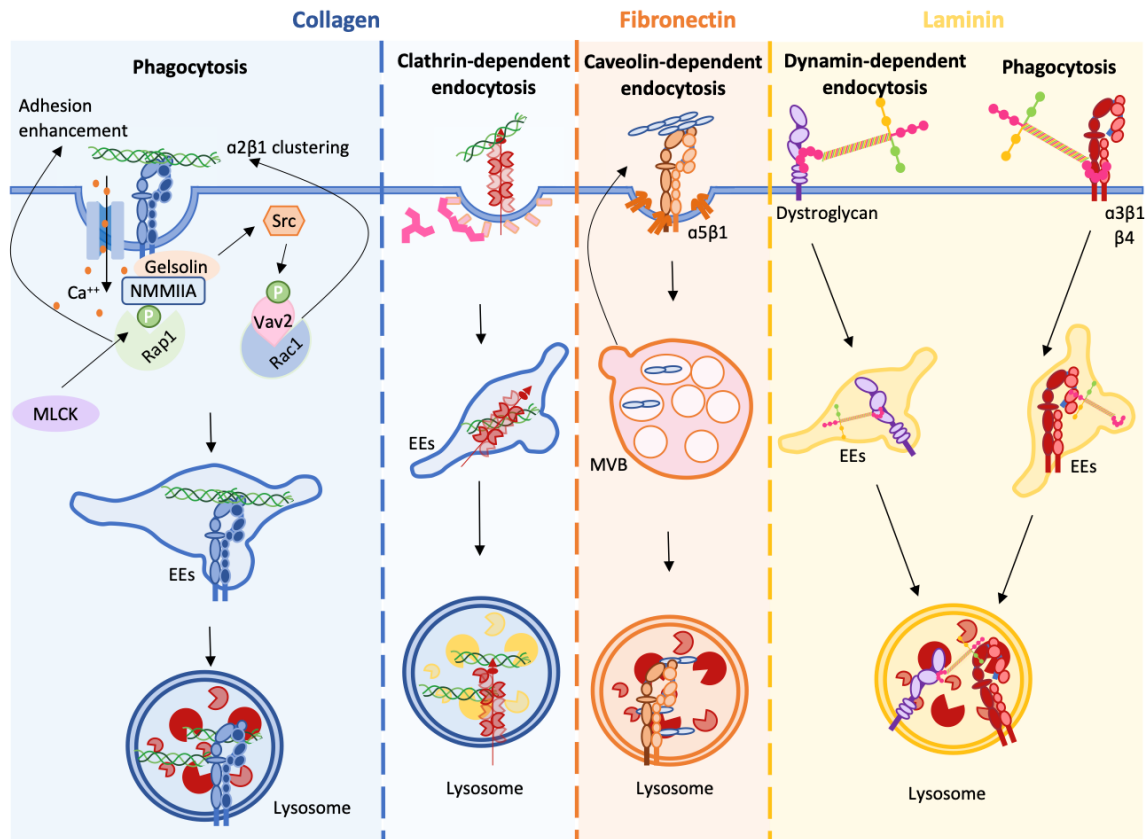


Figure 1-12. Schematic representation of ECM endocytic pathways. The diverse ECM ligands and their conformation will trigger the activation of distinct integrins. While unfolded collagen I (gelatin) is phagocytosed in an $\alpha\text{v}\beta 3$ integrin manner, fibrillar collagen I is internalised via $\alpha 2\beta 1$. Endocytosis of soluble collagen fragments is dependent on the Endo180 receptor and clathrin. Fibronectin is endocytosed in caveolae and $\alpha 5\beta 1$ integrin mediates this internalisation. $\alpha 5\beta 1$ integrin is trafficked to late endosomes, from where it can be secreted as exosomes. Interestingly, laminin internalisation has been reported to differ between cancer cells and normal cells. Normal cells internalise laminin through dystroglycan in a dynamin-dependent process and $\beta 4$ integrin, while cancer cells rely on $\alpha 3\beta 1$ integrin to phagocytose laminin. Finally, the internalised molecules are degraded in the lysosomes. Multivesicular body, MVB. Early endosomes, EE.

1.6.3.1. Normal mammary epithelial cells endocytose laminin in a Dystroglycan-dependent manner

Dystroglycan (DG) is a crucial regulator of laminin assembly and, in addition, *Leonoudakis et al., 2014* identified DG as the major receptor for laminin dynamin-dependent endocytosis in normal mammary epithelial cells (MECs). In those cells, laminin-111 is trafficked to MVBs of the late endosomes and it is later degraded in the lysosomes. More prominently, their findings suggest that integrins do not play a significant role in the internalisation of laminin in MECs, however $\beta 1$ -integrins could be potential co-receptors in DG-dependent laminin endocytosis (*Leonoudakis et al., 2014*) ([Figure 1-12](#)).

Interestingly, DG loses its ability to bind laminin in multiple congenital muscular dystrophies and laminin binding is frequently defective in breast, prostate, colon and brain cancer. DG capacity to bind to laminin depends on its glycosylation status, specially, by the glycosyltransferase LARGE (Briggs *et al.*, 2016). More promisingly, re-expression of this glycosylation enzyme in several carcinomas and glioblastoma cells restore the laminin-binding properties of DG (Leonoudakis *et al.*, 2014).

These results differ from previous ones in which the promiscuous receptor $\alpha 3\beta 1$ integrin mediated the phagocytosis of a collagenous matrix, such as gelatin, and Matrigel, a BM-like matrix in the malignant human breast carcinoma cell line MDA-MB-231 (Coopman *et al.*, 1996) ([Figure 1-12](#)). Another possible endocytic process involved in laminin internalisation may be macropinocytosis (Rainero, 2016), which has also been described to internalise hyaluronan in melanoma cells (Greyner *et al.*, 2010; Rainero, 2016).

Considering all above, DG-mediated endocytosis may be vital for normal MECs homeostasis and it is however compromised in cancer cells, in which $\alpha 3\beta 1$ integrin is responsible for laminin internalisation. Integrin-mediated laminin endocytosis is therefore concomitant with cancer progression (Rainero, 2016).

1.6.3.2. Laminin internalisation supports cell survival under starvation conditions

Under starvation conditions, laminin has been reported to be internalised in an integrin $\beta 4$ -dependent manner in the non-transformed mammary epithelial cell line MCF10A. Laminin is later transported to and degraded in the lysosomes, which provides the cells with essential amino acids and maintains cell survival (Muranen *et al.*, 2017). Nonetheless, soluble laminin secreted by starved fibroblasts was used to test this hypothesis, which implies that tissue architecture is not recapitulated. Interestingly, their findings were additionally confirmed using mice models (Muranen *et al.*, 2017). Moreover, collagen I, matrigel and CDM derived from TIFs and CAFs promote proliferation of the invasive breast cancer cell lines MDA-MB-231 and MCF10A-CA1 (Nazemi *et al.*, 2021). Interestingly, this study shows that the non-invasive breast cancer cell line MCF10A-DCIS relies on matrigel, a reconstituted BM, to proliferate under glutamine starvation

(Nazemi *et al.*, 2021). Further investigation is however required in this field in order to elucidate the role and regulators of laminin uptake in undernourished breast cancer cells, such as glucose starvation and in hypoxia, highly characteristic of tumours.

1.6.3.3. 67kDa laminin receptor (67LR) is linked to cancer progression

Another well-known laminin receptor is 67LR, which is highly expressed in several malignancies and it is widely associated with invasion and metastasis (Montuori *et al.*, 2016). 67LR was thought to play a role in cell adhesion to the ECM. A soluble peptide of the receptor, peptide G, increases adhesion to laminin, while it inhibits haptotaxis towards laminin (Taraboletti *et al.*, 1993). These receptors are probably shed from the cell membrane to the surrounding stroma, where they may interfere in the contact between cancer cells and laminin (Karpatová *et al.*, 1996).

More recently, Gopalakrishna *et al.*, 2018 showed that soluble laminin-1 and YIGSR peptide (sequence of laminin-1 β 1 chain that binds to 67LR) bind to 67LR and induce its internalisation into early endosomes in Neuroscreen-1 cells. Culturing Neuroscreen-1 cells in serum-depleted medium revealed that protein kinase A (PKA) and high levels of cAMP by increasing adenylyl cyclase signalling promote 67LR endocytosis (Gopalakrishna *et al.*, 2018). Under those conditions, internalisation of soluble laminin together with 67LR promotes cell survival and inhibits apoptosis. To confirm the results were mediated by 67LR, the authors of the study used the YIGSR peptide (Gopalakrishna *et al.*, 2018). Altogether, laminin internalisation through 67LR promotes sustained signalling that protects from cell death (Gopalakrishna *et al.*, 2018).

1.6.4. Elastin internalisation

Elastin, an insoluble polymer of tropoelastin, is abundantly present and provides elasticity and mechanical strength to a wide range of tissues and organs, such as cartilages, lungs, skin and arteries. Likewise, the elastic tissue is tightly related to desmoplasia; indeed, elastins are copious in breast carcinoma ECM (Kao, Wong and Stern, 1982).

Kao, Wong and Stern, 1982 showed that several human breast cancer cell lines presented a high elastolytic activity under serum free conditions. Remarkably, those cells also displayed

vacuolization and granularity of their cytoplasm (Kao, Wong and Stern, 1982). These results may suggest that breast cancer cells proteolyse elastin and they could potentially internalise it in order to supply nutrients to starved cells, similarly to laminin. Actually, elastin is extracellularly cleaved and internalised in elastosis conditions, in which elastin is abnormally accumulated. Skin fibroblasts exposed to UV light traffick elastin into lysosomes, where it is at least partly degraded by cathepsin K (Codriansky *et al.*, 2009).

1.6.5. The ECM meshwork - ECM internalisation in *in vivo-like* complex matrices

PTMs can modulate the intracellular degradation pathway by affecting ECM-receptor binding/recognition. Collagen IV glycosylation, for instance, has been reported to enhance Endo180-mediated endocytosis, which suggests a role of collagen glycosylation in ECM turnover (Jürgensen *et al.*, 2011). ECM protein conformation can also impact on endocytosis; disulphide crosslinked multimeric vitronectin but not monomeric, for example, can be recognised by $\alpha\beta 5$ integrin (Panetti and McKeown-Longo, 1993; Wilkins-Port and McKeown-Longo, 1998). Macrophages have been described to participate in ECM turnover during tissue remodelling and repair (Werb, Bainton and Jones, 1980; Jürgensen *et al.*, 2019). One way macrophages remodel the ECM is through its endocytosis. Tumour associated macrophages contribute to ECM degradation by upregulating cathepsins, collagenases and gelatinases, as well as mannose receptor endocytosis of collagen (Madsen *et al.*, 2017). Of note, this ECM degradation pathway is highly dependent on the ECM protein conformation, since phagocytosis of denatured collagen by macrophages during wound tissue remodelling is abolished (Madsen *et al.*, 2017). Nevertheless, phagocytosis of denatured collagen (gelatin) is rescued by fibronectin binding (Molnar *et al.*, 1979). This highlights the importance of studying ECM internalisation using matrices that recapitulate *in-vivo* like conditions.

Thrombospondin-1 has been reported to be internalised in a Endo180/uPARAP manner in dermal fibroblasts; and it is targeted for lysosomal degradation (Völker, Schön and Vischer, 1991; Nørregaard *et al.*, 2022). Interestingly, heparin competitively binds to thrombospondin and inhibits its internalisation, however heparin does not block collagen I internalisation (Nørregaard

et al., 2022). The authors of this study did not report whether collagen I could compete and block thrombospondin internalisation by competing with the uPARAP receptor.

The ECM meshwork is a complex environment, therefore it could be that interactions between ECM proteins could lead to the internalisation of more than one ECM component. Further research should focus on using intricate matrices, such as cell derived matrices from normal fibroblasts or CAFs, to unravel which components breast cancer cells internalise in a complex environment.

1.7. AIMS AND OBJECTIVES OF THE THESIS

Having a deep understanding of the mechanisms governing cancer dissemination and metastasis is fundamental for the development of targeted therapeutic strategies. As cancer cells migrate and invade through the surrounding stroma, escaping from the primary tumour, to successively intravasate into the blood or lymphatic vessels, they encounter an intricate ECM meshwork. Throughout this process, cancer cells degrade the surrounding ECM to facilitate invasive migration. Nonetheless, the ECM is not only a cellular scaffold but, in addition, it is a major signalling component for cell survival. Endosomal integrins engaged to the different ECM components are key in promoting the survival of cancer cells in the bloodstream or lymphatic system. Indeed, inside-in signalling from those integrins has been shown to suppress anoikis so that metastasis befalls (Alanko *et al.*, 2015). More promisingly, dissemination can be impeded by obstructing any of the sequential steps needed in the process (Scully *et al.*, 2012), such as cell migration and invasion. For this reason, a deep comprehension of the molecular mechanisms regulating ECM endocytosis in breast cancer cells may be crucial to prevent metastatic processes. This knowledge may be translated to develop novel cancer-specific therapies so that future patients can be beneficially treated and, therefore, reduce breast cancer mortality.

Altogether, this project aims to elucidate the molecular mechanisms controlling ECM uptake in breast cancer and understand how ECM internalisation influences cell migration and invasion. In order to study the regulators of this process we aim to:

- Develop a high throughput imaging-based screen.
- Characterise the endocytic pathways controlling internalisation of ECM in breast cancer cells.
- Identify the molecular mechanisms that promote traffic of ECM-bound integrins to lysosomes.
- Investigate the signalling effectors that promote ECM internalisation in breast cancer cells. More promisingly, a kinase and phosphatase functional screen will unravel potential targets for the development of novel cancer therapies.
- Explore whether endocytosis of ECM is required for breast cancer invasion, as well as migration.
- Elucidate if ECM-bound integrin traffic to lysosomes is required for invasive growth in breast cancer.
- Examine which integrin receptors and its corresponding ECM ligands are internalised in breast cancer cells using an unbiased mass spectrometry screen.

Chapter 2 – Materials and methods

2.1. MATERIALS

2.1.1. Reagents and suppliers

Table 2-1. Reagents and suppliers.

Reagents	Supplier
0.45µm syringe filter	Gilson
0,22µm syringe filter	Gilson
10cm petri dishes	Greiner bio-one
T75 flask	Thermofisher
6-well tissue culture plates	Greiner bio-one
12-well tissue culture plates	Greiner bio-one
PhenoPlate 96-well, black, optically clear flat-bottom 96-well glass-bottom microplates	Perkin Elmer Greiner bio-one
PhenoPlate 384-well, black, optically clear flat-bottom (formerly named CellCarrier Ultra microplates)	Perkin Elmer
3.5cm glass-bottom dishes	SPL Life Science
Foetal bovine serum (FBS)	Gibco
Dialysed Foetal bovine serum (D-FBS)	Gibco
Horse serum (HS)	Gibco
Phosphate buffer saline (PBS)	Gibco
Phosphate buffer saline, containing calcium and magnesium (PBS ⁺⁺)	Gibco and Sigma
Distilled water	Gibco
RNase-free water	Cleaver scientific and Horizon Discovery
5X siRNA buffer	Horizon Discovery by Perkin Elmer
Antibiotic-antimycotic	Gibco
Trypan Blue stain 0.4%	Gibco by life technologies

Trypsin EDTA solution 1X	Gibco
0.5% Trypsin-EDTA solution 10X	Gibco
Dulbecco's Modified Eagle Medium (DMEM), high glucose, pyruvate	Gibco and HyClone
Dulbecco's Modified Eagle Medium (DMEM), high glucose, pyruvate and Glutamax	Gibco
Dulbecco's Modified Eagle Medium / nutrient Mixture F12 (DMEM-F12)	Gibco
Epidermal growth factor (EGF)	Sigma
Hydrocortisone	Sigma
Insulin solution human	Sigma
Opti-MEM (1X), reduced serum medium	Gibco
Dharmafect I	Dharmacon/Horizon Discovery by Perkin Elmer
Dharmafect IV	Dharmacon/Horizon Discovery by Perkin Elmer
Lipofectamine™ 2000 transfection reagent	Invitrogen
Lipofectamine™ 3000 and p3000 transfection reagents	Invitrogen
Scienceware® cloning discs	Sigma-Aldrich
Dextran Rhodamine lysine fixable	LifeTech
Transferrin from human serum, Alexa Fluor™ 555	Invitrogen
BODIPY™ FL C 5 -Lactosylceramide	Thermofisher scientific
Dimethyl sulfoxide (DMSO)	Fisher Scientific
E64d (Aloxistatin)	Generon
GM6001	MedChem express
Bafilomycin A1	MedChem express
5-(N-Ethyl-N-isopropyl)-Amiloride (EIPA)	Sigma
Dynasore	Sigma
MiTMAB	Calbiochem
Filipin	Sigma
Collagen I high concentration (HC) rat tail	Corning

Matrigel basement membrane (BM) matrix, growth factor (GF) reduced	Corning
Laminin/entactin complex	Corning
Soluble collagen I	Bio Engineering
Methylcellulose	Sigma
Gelatin	Sigma
Glutaraldehyde solution	Sigma Aldrich
Glycine	Sigma
L-ascorbic acid	Sigma
Ammonium hydroxide (NH ₄ OH)	Sigma
Triton X-100	Sigma
Deoxyribonuclease I /DN25 (DNase I)	Sigma
Phospholipase A2 (PLA2)	Sigma
Tween-20	Sigma
Tris(hydroxymethyl)aminomethane (Tris)	Sigma-Aldrich
Sodium chloride	Sigma-Aldrich
Magnesium chloride	Sigma-Aldrich
Sodium deoxycholate	Sigma-Aldrich
NHS-fluorescein	Thermofisher
EZ-Link™ Sulpho-NHS-SS-Biotin	Thermo Fisher Scientific
Streptavidin Agarose conjugate beads	Merck
IRDye 680LT Streptavidin	LiCOR Biosciences
Alexa Fluor™ 555 NHS Ester (Succinimidyl Ester)	Invitrogen
Alexa Fluor™ 647 NHS Ester (Succinimidyl Ester)	Invitrogen
pHrodo™ iFL Red STP ester	Thermo Fisher Scientific
Formaldehyde 16% (w/v), Methanol-free (PFA)	Thermofisher
Saponin	Sigma
VECTASHIELD Antifade Mounting Medium with DAPI	VECTOR laboratories

VECTASHIELD Antifade Mounting Medium without DAPI	VECTOR laboratories
Alexa Fluor™ 488 Phalloidin	Invitrogen
Alexa Fluor™ 555 Phalloidin	Invitrogen
Alexa Fluor™ 647 Phalloidin	Invitrogen
Bovine serum albumin (BSA)	Sigma
NuPAGE™ LDS Sample buffer (NuPAGE)	Thermo Fisher
4-15% Mini-PROTEAN precast polyacrylamide gels	Bio-Rad
Qia-Shredder columns	QIAGEN
FL-PVDF membrane	IMMOBILON-FL
Protease inhibitor cocktail	Cell signalling
Sodium hydroxide (NaOH)	Fisher Chemical
Dithiothreitol (DTT)	Melford
Sodium 2-mercaptoethanesulfonate	Sigma Aldrich
Wizard Minicolumns	Promega
Pierce™ C18 spin columns	Thermo Fisher
Iodoacetamide	Sigma Aldrich

2.1.2. Solutions

Table 2-2. Recipes of solutions.

Solutions	Recipes
Cell extraction buffer	20mM NH ₄ OH, 0.5% Triton X-100 (v/v) in PBS with calcium and magnesium
PLA2 extraction buffer	50mM Tris-HCl pH 8, 150mM NaCl, 1mM MgCl ₂ , 1mM CaCl ₂ , 0.5% sodium deoxycholate and 20U/ml PLA2
SDS lysis buffer	1% SDS (v/v), 50mM Tris-Hcl pH7
Loading buffer	Cell lysate, 1mM DTT, 1X NuPAGE
TBST	10mM Tris-HCl pH 7.4, 150mM NaCl, 0.1% (v/v) Tween-20
Towbin buffer 10X	1.92M Glycine, 0.25M Tris
Transfer buffer	10% Towbin buffer 10X, 20% methanol in deionised water
Antibody dilution buffer	Primary or secondary antibody, 1% (w/v) BSA and 0.1% (w/v) saponin in PBS
Urea buffer	2M Urea prepared in HPLC-grade dH ₂ O
Ammonium bicarbonate solution	50mM Ammonium bicarbonate prepared in HPLC-grade dH ₂ O
TCEP	0.5M Tris(2-carboxyethyl) phosphine hydrochloride prepared in HPLC-grade dH ₂ O
Trifluoroacetic acid	0.1% trifluoroacetic acid prepared in HPLC-grade dH ₂ O
Trifluoroacetic acid /acetonitrile	0.1% trifluoroacetic acid and 50% acetonitrile prepared in HPLC-grade dH ₂ O

2.2. METHODS

2.2.1. Cell culture

The metastatic breast cancer cell line MDA-MB-231, telomerase-immortalised human dermal fibroblasts (TIFs) and cancer-associated fibroblasts (CAFs) were grown in high glucose Dulbecco's modified Eagle medium (DMEM) supplemented with 10% (v/v) foetal bovine serum (FBS), hereafter referred to as complete medium. CAFs were extracted and derived from a breast cancer tumour in Professor Akira Orimo's lab (Paterson Institute, Manchester). MCF10A is an immortalised mammary epithelial cell line, from which the premalignant MCF10AT cell line was

generated by H-Ras transformation (Dawson *et al.*, 1996; Kadota *et al.*, 2010). MCF10CA1a derives from poorly differentiated malignant xenografts tumours derived from MCF10AT (Rhee, Park and Jang, 2008; Kadota *et al.*, 2010). MCF10A and MCF10CA1a cells were cultured in DMEM/F12 media supplemented with 5% Horse serum (HS), 20ng/ml EGF, 0.5mg/ml hydrocortisone and 10µg/ml insulin. The endometrioid ovarian cancer cell line A2780 overexpressing Rab25, hereafter A2780-Rab25 cells, were cultured in RPMI media containing 10% FBS. All cell lines were maintained at 37°C in 5% CO₂ and split every 3 to 4 days. To passage or split the cells, media was removed and cells were washed twice with phosphate buffer saline (PBS). Cells were then incubated with 0.25% (w/v) trypsin-EDTA for 2 to 5 minutes at 37°C in 5% CO₂. Following detachment of cells, cells were resuspended in complete medium and reseeded in tissue culture dishes.

For long term storage, all cell lines were cryopreserved once they reached 80 to 90% confluency in a 10cm dish. Cells were trypsinized and resuspended in complete media, centrifuged at 1000 rpm for 5 min at room temperature (RT). The pellet was resuspended in solution A (500µl), containing 50% complete media (250µl) and 50% FBS or HS (250µl), and pipetted into a cryovial. The same volume of solution B (500µl), which contained 80% FBS (400µl) or HS and 20% DMSO (100µl), was added drop-by-drop in the cryovial. The cryovial was mixed gently by inverting it and later stored in Corning™CoolCell™LX Cell freezing vial container at -80°C for a few days. Vials were then transferred to liquid nitrogen (LN2 or N₂ (l)).

To recover the cells from cryopreservation, the cryovial was thawed in the water bath until fully thawed. The cell suspension was transferred into a 15ml falcon tube containing 5ml of complete media and spun down for 5 minutes at 1000 rpm. The supernatant containing DMSO was then removed. Afterwards, complete media was added and the solution was transferred into a 10cm dish.

2.2.2. 2.5D collagen I, matrigel and laminin endocytosis assay for confocal microscopy

Collagen I, Matrigel and Laminin-111/Entactin were dissolved in ice-cold PBS to a final concentration of 1mg/ml for collagen I and matrigel and 2mg/ml for Laminin-111/Entactin. 100µl of each solution was used to coat a 35mm glass-bottom dish with the help of a pipette tip. The coated ECM dishes were incubated at 37°C and 5% CO₂ for 1h for polymerisation. ECM dishes were labelled with 300µl of 10µg/ml NHS-fluorescein, 5µg/ml Alexa fluor™555 NHS ester or 5µg/ml Alexa Fluor™647 NHS ester. The dishes were incubated for 1 hour at RT on gentle rocking. The chemical group NHS ester reacts with the primary amino groups of proteins, leading to the formation of an amide bond (Nanda and Lorsch, 2014). The labelled ECM dishes were washed twice with PBS prior to cell seeding. To avoid evaporation, PBS was added into each dish to keep in the incubator.

2.2.2.1. Assessment of lysosomal degradation

To assess lysosomal degradation, 3x10⁵ MDA-MB-231 cells per dish were seeded on NHS-fluorescein-labelled matrix in the presence of DMSO (control/vehicle) or 20µM E64d, a cysteine protein inhibitor that prevents lysosomal degradation. Cells were incubated at 37°C in 5% CO₂ for 24 hours. Afterwards cells were fixed and stained for nuclei (DAPI) and the actin cytoskeleton (phalloidin); see section [2.2.12. Immunofluorescence](#).

2.2.2.2. Assessing the role of MAPK inhibitors on 2.5D uptake

MDA-MB-231 cells were serum starved overnight to block MAPK signalling. TrypLE™ Express Enzyme, henceforth TrypLE, was used to detach cells, cells were neutralised with serum free media. TrypLE is a recombinant enzyme (animal origin-free) used for dissociating adherent cells by cleaving peptide bonds on the C-terminal side of lysines and arginines and it is more gentle on cells than trypsin (*TrypLE™ Express Enzyme (1X), phenol red*, no date). 3x10⁵ MDA-MB-231 cells per dish were seeded on the NHS-Alexa fluor 555-labelled matrix. MDA-MB-231 cells were treated with DMSO or two concentrations (10µM and 50µM) of SB203580 and SB202190. Cells

were cultured in 5% FBS and incubated at 37°C in 5% CO₂ for 6 hours. Afterwards cells were fixed and stained for nuclei and α 2-integrin; see section [2.2.12. Immunofluorescence](#).

2.2.3. Generation of cell-derived matrices

Cell-derived matrices (CDMs) were generated as previously described (Kaukonen *et al.*, 2017), see [Figure 2-1](#). CDMs were generated either in a 10cm dish, a 35mm glass bottom dish, six-well plate, twelve-well plate, 8-well chamber or a 384-well plate. Tissue culture plates were first coated with 0.2% (v/v) gelatin for 1 hour at 37°C. Following that time, plates were washed twice with PBS and crosslinked with 1% (v/v) sterile glutaraldehyde (dissolved in PBS) for 30 minutes at RT. Plates were thereafter washed twice with PBS and the remaining glutaraldehyde was quenched with 1M sterile glycine for 20 minutes at RT. Subsequently, plates were washed twice with PBS and equilibrated for 30min in complete medium at 37°C. Confluent TIFs and CAFs were seeded onto the gelatin coated plates ([Table 2.3](#)). TIFs and CAFs were incubated at 37°C in 5% CO₂ until being fully confluent. The following day or the day after, the media was changed to complete media supplemented with 50µg/ml ascorbic acid, the media was refreshed every other day. TIFs and CAFs were kept secreting CDM for 9 days in a 10cm dish, six-well plate, twelve-well plate and 35mm glass bottom dish. While, only 7 days were required for CDM production in 384-well plates. Following that time, cells were washed once with PBS containing CaCl₂ and MgCl₂ (PBS⁺⁺). Cells were incubated with the extraction buffer (20mM NH₄OH and 0.5% triton X-100 in PBS⁺⁺) for 2 to 5 minutes at RT until no visible cells remained. For the 384-well plates, cells were extracted twice for 2min. Extracted CDMs were subsequently washed twice with PBS⁺⁺ and residual DNA was digested with 10µg/ml DNase I in PBS⁺⁺ at 5% CO₂, 37°C for 1h or overnight for the 384 well plates. CDMs were then washed with PBS⁺⁺ and stored at 4°C in PBS⁺⁺ supplemented with 1% Penicillin/Streptomycin.

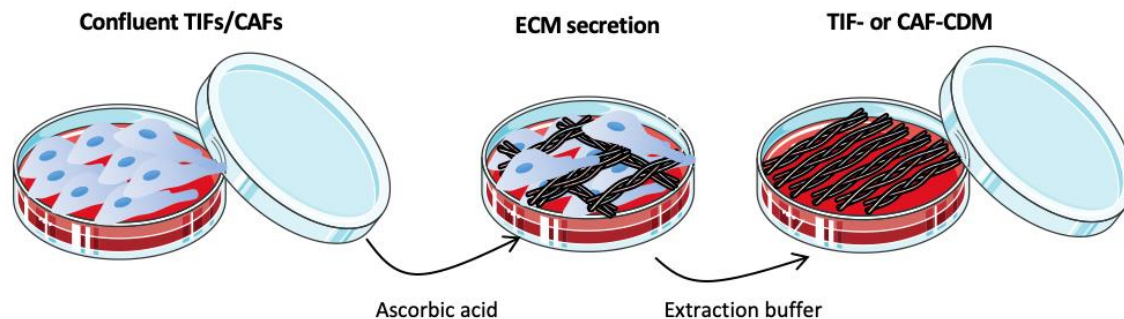


Figure 2-1. Schematic diagram for generation of CDMs. Once TIFs or CAFs reach confluency, cell media is supplemented with 50µg/ml ascorbic acid. Cell media is refreshed every other day for a period between 7 to 9 days. CDMs are extracted with 20mM NH₄OH and 0.5% Triton X-100, subsequently DNA is digested with 10µg/ml DNase I. Image made using items from Servier medical Art.

Table 2-3. Cell seeding values for generation of cell derived matrices.

Plate/dish type	Cell seeding numbers	Volume
35mm	5x10 ⁵ cells/well	Between 1ml to 1.5ml
12-well plate	2.5x10 ⁵ or 3x10 ⁵ cells/well	1ml
6-well plate	5x10 ⁵ cells/well	1.5ml
8-well chamber	10 ⁴ cells/well	200µl
384-well plate	3000 cells/well	50µl

2.2.3.1. CDM endocytosis assay

CDM dishes were labelled with 300µl (for 35mm glass-bottom dishes) and 30µl/well (384 well plate) of 20µg/ml pHrodo™ iFL Red, succinimidyl ester; hereafter, pHrodo. The dishes were incubated for 1 hour at RT on gentle rocking. The chemical group STP ester reacts with the primary amino groups of proteins, leading to the formation of an amide bond (Nanda and Lorsch, 2014). The labelled ECM dishes were washed thrice with PBS prior to cell seeding. To avoid evaporation, PBS was added into each dish to keep in the incubator. 3x10⁵ MDA-MB-231 cells per 35mm glass-bottom dish, 10⁵ MDA-MB-231 or A2780-Rab25 cells/well per 8-well chamber and 10⁴ cells/well per 384 well plate were seeded on labelled CDM in presence of vehicle or the inhibitors. Cells were incubated at 37°C in 5% CO₂ for a period of 6 hours for assessment of endocytosis experiments or 24-hour experiments for experiments related to lysosomal

degradation. After the time period, cells were labelled with 1µg/ml hoechst to visualise the nuclei and imaged live.

2.2.3.2. Assessing the role of inhibitors on CDM uptake

For 384-well plates, 10^4 MDA-MB-231 cells per well were seeded on pHrodo-labelled CDM. For 35mm glass-bottom dishes, 3×10^5 MDA-MB-231 and A2780-Rab25 cells were seeded per dish. For endocytic inhibitors, cells were cultured for 6 hours in the presence of DMSO, 20µM dynasore, 40µM dynasore, 3.75µg/ml filipin, 5µg/ml filipin, a combinatory inhibition with 20µM dynasore and 3.75µg/ml filipin, 25µM EIPA and 35µM EIPA. Inhibitors were added 2h after seeding the cells. For E64d experiments, cells were cultured for 24h in the presence of DMSO and 20µM E64d. For E64d and GM6001 experiments, cells were cultured in the presence of either DMSO, 20µM E64d or 10µM GM6001. E64d and GM6001 inhibitors were added 2h after cell seeding. For MAPK inhibitors, MDA-MB-231 and A2780-Rab25 cells were serum starved overnight to block MAPK signalling. Cells were detached with TrypLE and neutralised with serum free media. Cells were cultured in 0% FBS for 6h in presence of DMSO and SB203580, SB202190, FR180204 and PD98059. Three concentrations were used: 2µM, 10µM and 50µM. These inhibitors were added at the moment of seeding or after 2h. Cells were stained with hoechst and imaged live. A 40X water-immersion objective from an Opera Phenix microscope was used for imaging. Additionally, for MDA-MB-21 cells, 10µM and 50µM SB203580 and SB202190, were also tested in 5% FBS conditions for 6 hours (added during cell seeding). For A2780-Rab25 cells, 10µM and 50µM SB202190 were assessed. A 60X oil-immersion objective of the Nikon A1 confocal microscope was used.

2.2.3.3. Cell migration assay in CDM

For inhibitor experiments, cells were serum starved for 16 to 18h. Cells were detached using TrypLE and neutralised with serum free media. 5×10^4 MDA-MB-231 cells per well were seeded into a *CDM-coated* 12-well plate. Migration experiments were carried with 5% FBS DMEM. DMSO, MAPK inhibitors (10µM and 50µM SB202190 and SB203580) and EphB4 inhibitor (1µM NVP-BHG712) were added at the moment of cell seeding, however cells were allowed to adhere

for 4 hours before adding the α 2-integrin inhibitor, BTT-3033 (final concentration 10 μ M). Time-lapse imaging was done after a 6h-incubation with the MAPK inhibitors or 2h-incubation with BTT-3033. For knockdown experiments, cells were plated in complete media; cells were allowed to adhere for 6h before imaging.

Plates were imaged in Nikon dual cam widefield live-cell system microscope with a 10X/NA objective. Cells were incubated at 37°C and 5% CO₂; images were acquired every 10 minutes for at least 7h (more than 40 cells per well were quantified). Individual cell migration was manually tracked using MTrack2, a plugin found in ImageJ. The chemotaxis tool plugin in Image J (<https://ibidi.com/chemotaxis-analysis/171-chemotaxis-and-migration-tool.html>) was used to calculate velocity and directionality of migrating cells.

2.2.4. Transferrin uptake

35mm glass-bottom dishes were coated with 100 μ l of 0.1mg/ml collagen I for 1h at 37°C and 5% CO₂. 1 ml PBS was added on top of the dishes and dishes were kept overnight. The following day, 3x10⁵ MDA-MB-231 cells were seeded on collagen-coated dishes for 6h and then pre-treated for 30min with 3 different concentrations of two different dynamin inhibitors: DMSO, 10 μ M, 20 μ M, 40 μ M Dynasore in 2% FBS and H₂O, 15 μ M, 25 μ M, 35 μ M MiTMAB. Following pre-treatment, cells were incubated in the presence of 5 μ g/ml Transferrin for another 30min. Cells were then fixed with 4% paraformaldehyde and stained with Phalloidin Alexa Fluor 647 to visualise F-actin and DAPI for the nuclei. Cells were imaged with a 60X objective Nikon A1 confocal microscope. Image J was used to analyse Transferrin uptake index.

2.2.5. Lactosylceramide uptake

3x10⁵ MDA-MB-231 cells were seeded on 35mm glass-bottom dishes coated with 0.1mg/ml collagen I for 6h. Cells were then pre-treated with DMSO, 2.5 μ g/ml, 3.75 μ g/ml and 5 μ g/ml Filipin for 30min. Media was then aspirated and cells were further incubated for 10min on ice with ice-cold 0.5 μ M BODIPYTMFL C₅-Lactosylceramide media, which additionally contained either DMSO, 2.5 μ g/ml, 3.75 μ g/ml or 5 μ g/ml Filipin. The dishes were later incubated for 90 seconds at 37°C.

Afterwards dishes were put on ice and fixed with 4% paraformaldehyde. Phalloidin Alexa Fluor 555 was used to label the actin cytoskeleton and Vectashield mounting medium with DAPI for the nuclear staining. Imaging was done with a 60X objective Nikon A1 confocal microscope. Image analysis was performed with Image J.

2.2.6. Rhodamine-dextran uptake

MDA-MB-231 cells were seeded at a density of 3×10^5 cells/ml on 35mm glass-bottom dishes coated with 0.1mg/ml collagen I for 6h. For dextran uptake optimisation, cells were pre-treated with DMSO, 25 μ M, 35 μ M and 50 μ M EIPA for 30min. To assess the effect of p38 MAPK on dextran uptake, 10^5 MDA-MB-231, MCF10A and MCF10CA1 cells were seeded for 6h in a collagen I-coated 8-well chamber. 8-well chambers were coated with 0.1mg/ml collagen I (50 μ l/well). All cell types were pre-treated with DMSO and 50 μ M SB202190. Cells were later incubated for another hour with 0.25mg/ml Rhodamine dextran in the presence of the inhibitor and the vehicle. Cells were then fixed with 4% paraformaldehyde and stained for human β 1-integrin. Vectashield mounting medium with DAPI allowed the visualisation of the nuclei. Cell imaging was carried with a 60X objective Nikon A1 confocal microscope and Image J was used to analyse Dextran uptake index.

2.2.7. siRNA transfection

2.2.7.1. Transfection in 6-well plate

10 μ l 5 μ M siRNA were mixed with 190 μ l Opti-MEM per well of a 6-well plate. 2 μ l Dharmafect I were mixed with 198 μ l Opti-MEM and incubated for 5 minutes at RT. 200 μ l of the Opti-MEM-Dharmafect I mix were added on top of the siRNA and incubated for 20 minutes on a gentle rocker. 4×10^5 cells in 1.6ml were seeded into each well. Cells were incubated at 37 $^\circ$ C and 5%CO₂ for 72h.

To assess knockdown efficiency of PAK1 and AP3D1 by western blot, cells were washed twice with PBS and lysed with 100 μ l lysis buffer. Lysates were spined down in a Qia-Shredder column. Lysates were loaded into a 4-12% acrylamide gel and later transferred into a FL-PVDF membrane. After blocking, membranes were incubated with PAK1 antibody (1:1000), AP3D1 (1:100000) and

GAPDH (1:1000) for MDA-MB-231. Band intensity was quantified with Image Studio Lite software. See section [2.2.13. Western Blotting](#).

2.2.7.2. Transfection in 96-well plate

For knockdown optimisation, 5µl of 500nM siGENOME siRNA smart pool and 5µl Opti-MEM was added into each well of a 96-well plate. 9.9µl Opti-MEM was mixed with 0.1µl Dharmafect IV for 5min. 10µl of the latter solution was added into each well and incubated at RT for 20 minutes on a rocker. For optimisation experiments, 8000 to 12000 cells/well were seeded in 80µl 10% FBS DMEM. Final siRNA concentration was 25nM. Cells were kept at 5% CO₂ and 37°C for 72h before fixation. β1-integrin knockdown efficiency was analysed in Columbus software using the pipeline shown in [Figure 2-2](#).

2.2.7.3. Transfection in 384-well plate

2.5µl of 500nM siGENOME siRNA or sgRNA smart pool and 2.5µl Opti-MEM were added into each well of a 384 well plate. 4.95µl Opti-MEM were mixed with 0.05µl Dharmafect IV and incubated for 5 minutes at RT. 5µl of the Dharmafect IV solution were added per well. Plates were incubated for 20 minutes on a rocker at RT. 3x10³ cells were seeded in 40µl complete medium. The final concentration of the siRNA or sgRNA was 25nM. Cells were kept at 5% CO₂ and 37°C for 72h. β1-integrin knockdown efficiency was analysed in Columbus software using the pipeline shown in [Figure 2-2](#). For functional ECM endocytosis assays, cells were transferred into coated plates as described in [2.2.10.4. Cell detachment in high content imaging plates](#).

Calculate knockdown efficiency

siRNA Non-targeting

siRNA against ITGB1

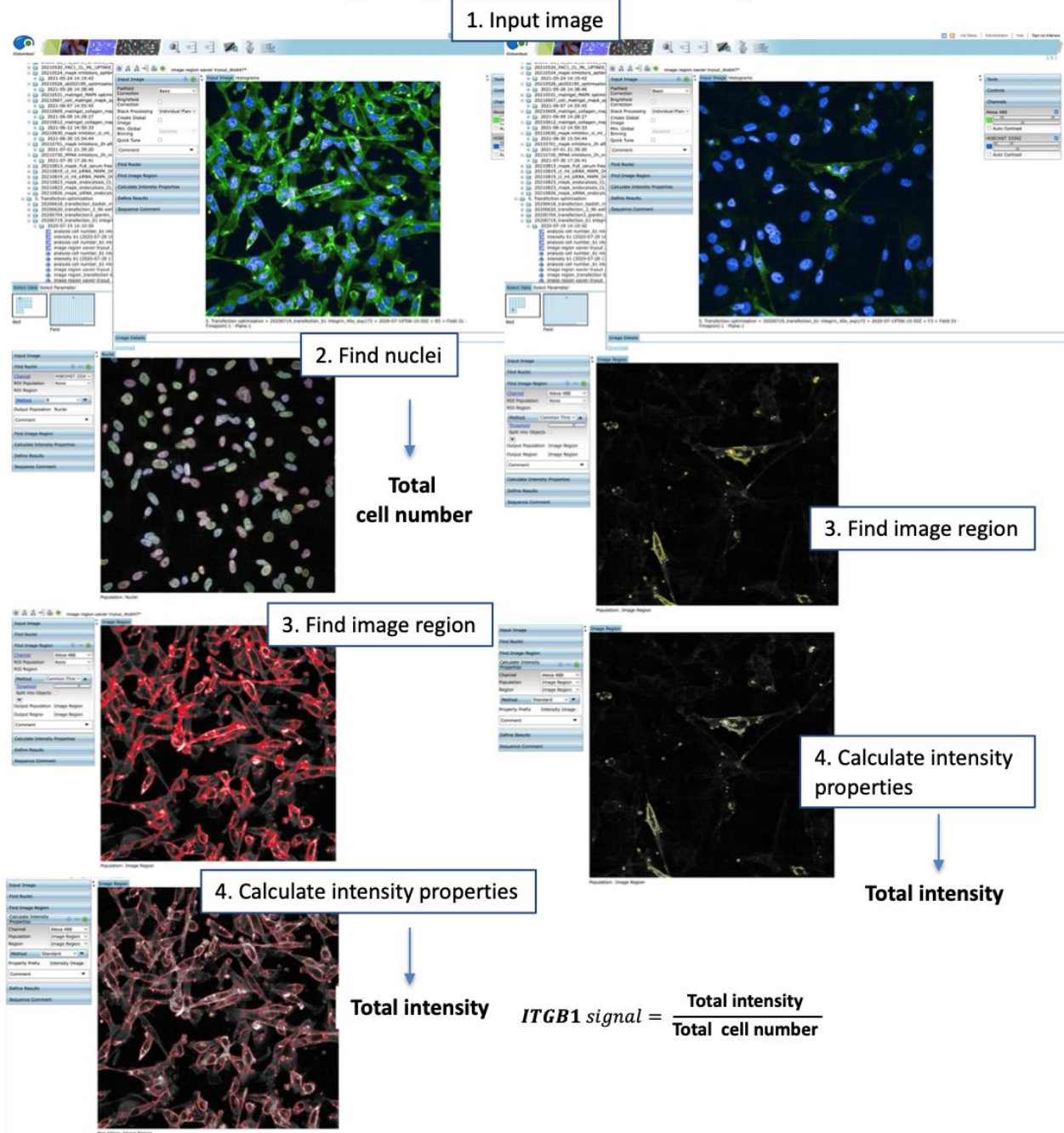


Figure 2-2. Representative pipeline to assess the knockdown efficiency in Columbus software. In short, nuclei were selected using the tool Find nuclei and total number of nuclei per well were selected. Image region enabled the detection of integrin staining. The total intensity from the picture was calculated for non-targeting conditions. The same threshold and analysis was applied for knockdown cells. Knockdown efficiency was calculated as a ratio of the total intensity per well divided into total cell number per well.

Table 2-4. siRNA and sgRNA for low throughput screening. siRNAs and sgRNAs were supplied by Dharmacon Horizon discovery through the Singaporean distributor Research Instruments.

siRNA name	Reference number	Type
NT5	D-001210-05-05	siGENOME Non-targeting control siRNA #5
NT4	D-001810-04-20	ON-TARGETplus Non-targeting control siRNA #4
NT	U-009550-10-05	CRISPRmod CRISPRi sgRNA
siGLO Red	D-001630-02-05	siGLO Red Transfection Indicator
ITGB1	M-004506-00-0005	siGENOME siRNA SMARTpool
TNS3	M-009997-02-0005	siGENOME siRNA SMARTpool
PAK1	M-003521-04-0005	siGENOME siRNA SMARTpool
CLTC/CHC17	M-004001-00-0005	siGENOME siRNA SMARTpool
DNM1	M-003940-01-0005	siGENOME siRNA SMARTpool
DNM2	M-004007-03-0005	siGENOME siRNA SMARTpool
DNM3	M-013931-00-0005	siGENOME siRNA SMARTpool
CAV1	M-003467-01-0005	siGENOME siRNA SMARTpool
CAV2	M-010958-00-005	siGENOME siRNA SMARTpool
FLOT1	M-010636-00-0005	siGENOME siRNA SMARTpool
FLOT2	M-003666-01-0005	siGENOME siRNA SMARTpool
GRAF1/ARHGAP26	M-008426-01-005	siGENOME siRNA SMARTpool
AP2A1	M-012492-00-0005.	siGENOME siRNA SMARTpool
AP3B2	M-021444-01-0005	siGENOME siRNA SMARTpool
AP3D1	M-016014-02-0005.	siGENOME siRNA SMARTpool
AP4E1	M-021474-01-0005.	siGENOME siRNA SMARTpool
ARFGEF2	M-012208-02-0005	siGENOME siRNA SMARTpool
BET1	M-012085-01-0005	siGENOME siRNA SMARTpool
BNIP1	M-011222-01-0005	siGENOME siRNA SMARTpool
COG8	M-008575-01-0005	siGENOME siRNA SMARTpool
STX12	M-018246-01-0005	siGENOME siRNA SMARTpool
TRAPPC9	M-019414-02-0005	siGENOME siRNA SMARTpool
MAP3K1	M-003575-02-0005	siGENOME siRNA SMARTpool
PPP2R1A	L-010259-00-0005	ON-TARGETplus siRNA SMARTpool
PPP2R1A	CF-010259-01-0002	CRISPRmod CRISPRi sgRNA
MAPK11	M-003972-03-0005	siGENOME siRNA SMARTpool
ITGA2	L-004566-00-0005	ON-TARGETplus siRNA SMARTpool

2.2.8. DNA transfection

For the stable generation of MDA-MB-231 expressing GFP (henceforth GFP-MDA), 8×10^5 cells/well were seeded into a 6-well plate in 2ml of complete media without antibiotics. Confluent cells were transfected with 2.5 μ g of pSBtet-GB GFP Luciferase plasmid and 0.25 μ g of the sleeping beauty transposon plasmid, pCMV(CAT)T7-SB100. 250 μ l of OptiMEM, 5 μ l p3000 and 3.75 μ l Lipofectamine 3000, together with both plasmids was added on top of the 2ml. Media

was changed after 6h. Following 48h, cells were selected with 2µg/ml blasticidin and fluorescence activated cell sorting (FACS) sorted.

2.2.8.1. Transient transfection

For the transient expression of mcherry-Arf1 and mcherry-Rab5, 1.2×10^6 cells per well were seeded into a 6-well plate. On the next day, 5µl Lipofectamine 2000 was mixed with 250µl Opti-MEM. 2.5µg of the mcherry-Arf1 or Rab5 plasmids were mixed with 250µl OptiMEM. 250µL of the lipofectamine Opti-MEM solution was mixed with 250µl of the DNA plasmid Opti-MEM solution. The lipofectamine-DNA plasmid mix was incubated for 20min at RT. Cells were washed twice with PBS. 500µl of the lipofectamine-DNA plasmid mix was added on top of the cells for 6h. Following this time, the transfection media was aspirated and complete media was added on top. The next day cells were seeded on 1mg/ml matrigel, labelled with 5µg/ml NHS-Alexa fluor 647. Cells were incubated for a period of 3h, fixed and stained with a primary antibody against AP3D1 (secondary Alexa fluor 488) and DAPI. see section [2.2.12. Immunofluorescence](#).

2.2.9. Generation of MDA-MB-231-dCas9-CRISPRi cells

3×10^5 cells/well were seeded into a 12-well plate. Confluent cells were transduced with CRISPRmod CRISPRi dCas9-SALL1-SDS3 lentivirus particles, whose expression is under the hCMV promoter (cat# VCAS10124), as per protocol (Dharmacon Edit-R CRISPR Cas9 gene engineering with Lentiviral particles, Horizon Discovery). Cells were incubated at 37°C for 6h with 250µl of serum free media containing CRISPRi lentivirus at a multiplicity of infection (abbreviated as MOI) of 0.3. After that time, 750µl of complete media was supplemented on top of the cells. Following 48h, cells were collected and a serial dilution was performed. Clone cells were grown for 2 weeks in the presence of 15µg/ml blasticidin. 12 clones were isolated with Scienceware® cloning discs (Z374431-100EA). Selected clones were allowed to grow. Clone 8 was picked for future assays based on modulation of ITGB1 expression.

2.2.10. RNAi screen

For this part, please note that Singapore is a tropical country and additional steps have been implemented to avoid fungi or bacterial contamination for these experiments. The automated methods below were optimised in [Chapter 3](#) and used for the trafficking screen in [Chapter 5](#), as well as in the kinome and phosphatome screen and deconvolution of hits in [Chapter 6](#). Plates were pre-printed with 2.5µl of 500nM siRNA by Dr Xavier Le Guezennec and Felicia Tay.

2.2.10.1. Knockdown in high throughput systems

MDA-MB-31 cells were split in 1/5 or 1/10 ratio, 4 to 5 days before transfection in high throughput. On the day of transfection, high grade tips were used for dispensing the reagents to avoid contamination. All the reagents were added in a high throughput fashion by using the Multidrop™ Combi Reagent dispenser (Thermofisher), hereafter multidrop combi. Multidrop combi enables to dispense reagents in a high throughput manner over a 0.5 to 2500µl range. It accommodates 6 to 1536 well plates by adapting a range of multi dispenser cassettes. The small cassette, which accurately dispenses volumes ranging from 2µl to 20µl, was used to dispense smaller volumes, including OptiMEM and OptiMEM-Dharmafect IV mixture. The large cassette, which is able to dispense more between 20-100µl of reagents, was used for cell seeding. The multidrop combi were used in sterile conditions underneath the tissue culture hood.

First, the small dispensing cassette was thoroughly washed and sterilised with 50 to 100ml of 70% ice-cold ethanol for at least 30 minutes at room temperature and under the hood. The small cassettes were then rinsed with sterile water (Gibco). Before proceeding to dispense the desired volume, the dispensing nozzles were assessed to ensure adequate dispensation in the corresponding well. The multidrop combi was set up to dispense 2.5µl OptiMEM per well at medium speed. The pipes of the combi were purged and washed once with sterile water. Afterwards, 5µl of the Dharmafect IV-OptiMEM solution (0.05µl Dharmafect IV and 4.95µl OptiMEM) was dispensed in each well ([Figure 2-3](#)). The cassette was then rinsed with sterile water (Gibco) and sterilised with 70% ethanol.

For the second part of this protocol, the multidrop combi with the large cassette was sterilised with 70% ethanol for 30 minutes and washed with sterile water (Gibco). During this time, cells were detached, neutralised and spun down to remove traces of trypsin. Fresh media was added on top and 1ml of the cell solution was counted using VI-Cell XR Cell viability analyser (Beckmann Coulter). After cell counting, a solution with a concentration of 7.5×10^5 cells/ml was achieved. The solution was mixed several times and flushed inside the pipes from the cassette to ensure all the pipes contained cell solution. Nozzles were checked and assessed whether they were dispensing the liquid straight into the corresponding well. 40 μ l of the cell solution was added per well (in a 384 well plate), resulting in seeding 3000 cells/well ([Figure 2-3](#)). MDA-MB-231 cells were cultured for 72h for effective knock down efficiency.

2.2.10.2. Matrigel coating and labelling in high content imaging plates

Low throughput experiments:

This method was based on a previously published protocol for 3D cell culture (Ko, Tsai and Frampton, 2019), but has been further optimised for matrigel uptake in 384-well plates. 50 μ l ice-cold PBS was added in each well using an E1-ClipTip Equaliser pipette (15-1225 μ l, Thermofisher). Plates were kept on ice and 2 μ l of 0.5mg/ml matrigel was spiked in each PBS well using an E1-ClipTip Equaliser pipette (2-125 μ l). For this step, the tip should be kept in the middle of the PBS solution, and avoid contacting the bottom of the plate. To ensure collection of matrigel at the bottom, plates were subsequently centrifuged at 500 rpm for a few seconds and kept for 8 min at 4 degrees. Matrigel was polymerised for 15 min at RT. 40 μ l/well were removed using an E1-ClipTip Equaliser pipette (2-125 μ l). Plates were then stained with 30 μ l/well of 20 μ g/ml pHrodo for uptake experiments and 10 μ g/ml NHS-fluorescein to assess matrix homogeneity. For matrix homogeneity, plates were imaged with a 20X air objective Opera Phenix microscope, while uptake experiments were imaged using a 40X or 60X water immersion objective Opera Phenix microscope. Figure legends state the objective used.

High content screening:

Matrigel coating:

Matrigel preparations were handled using high grade dispensing pipette tips (E1-ClipTip Equaliser pipette) to minimise possible contamination. All the reagents were added in a high throughput fashion by using the multidrop combi. The multidrop combi was set up to dispense at slow or medium speed. The small (only for matrigel) and large combi (for PBS) multi dispenser cassettes, henceforth small or large cassettes, were thoroughly washed and sterilised with 50 to 100ml of 70% ice-cold ethanol for at least 20 minutes. Cassettes were then rinsed with sterile ice-cold water (Gibco). Before proceeding to dispense the desired volume, the nozzles of both cassettes were assessed on how they performed on dispensing PBS and matrigel. This ensured an equal dispensation across the plate. The multidrop combi with the large cassette was kept inside the tissue culture hood and it was set to dispense 50µl ice-cold PBS in a 384-well plate ([Figure 2-3](#)). PBS plates were kept at 4°C for 15 minutes. The multi combi assembled to the small/matrigel cassette was kept at 4°C (outside the tissue culture hood). To minimise contamination, reagents and plates were carefully handled and lids were put rapidly back on after matrigel dispensing was completed. The multidrop combi was set to dispense 2µl ice-cold matrigel in the 384-well plates containing PBS. Plates were centrifuged for a few seconds at 500rpm, kept at 4°C for 8 minutes and then polymerised for 2h 30 minutes.

Matrigel labelling:

Bravo liquid handling system (Agilent Technologies, hereafter Bravo) was used to perform matrigel washes ([Figure 2-3](#)). Bravo was calibrated to ensure the pipette tips did not reach the bottom of the plate and could scratch the matrix. In addition, the pipeline included several popup messages to ensure refill the PBS reservoirs during the washing process. Reservoirs were sterilised for at least 20 minutes by ethanol and UV light. After polymerisation time was completed, 40µl PBS were pipetted up and deposited into the waste reservoir.

Prior to removing the PBS, the large cassette was thoroughly washed and sterilised with 50 to 100ml of 70% ice-cold ethanol for at least 20 minutes. Similar to before, the cassette was then

rinsed with sterile ice-cold water (Gibco). Again, the nozzles were assessed on how they performed on dispensing pHrodo solution. 30µl/well of 20µg/ml pHrodo was dispensed into 384-well plates. Plates were kept in the dark on gentle rocking for 1h for efficient matrigel labelling. Following that time, Bravo was used for washing pHrodo off. The pipeline was well designed to use a waste reservoir and two PBS reservoirs. It was important that the waste reservoir contained PBS in it to avoid formation of bubbles at the edge of the tip after releasing the waste. All washes were performed with PBS containing 1% antibiotic-antimycotic to avoid contamination. Firstly, 30µl were pipetted out and added into the waste reservoir. Three washes were performed, each with 50µl of PBS per well. To avoid any remaining unbound pHrodo, we performed two more washes with a new PBS reservoir. In addition, the waste reservoir was emptied and fresh PBS (1% (v/v) antibiotic-antimycotic) was added. Plates were kept in 50µl PBS at 37°C overnight.

2.2.10.3. Collagen coating and labelling in high content imaging plates

50ul ice-cold PBS was added in each well using an E1-ClipTip Equaliser pipette (15-1225µl, Thermofisher). Plates were kept on ice and 15µl of 0.5mg/ml collagen I was spiked in each PBS well using an E1-ClipTip Equaliser pipette (2-125µl). For this step, the tip should be kept in the middle of the PBS solution, and avoid contacting the bottom of the plate. To ensure collection of collagen I at the bottom, plates were subsequently centrifuged at 500rpm for a few seconds and kept for 8 min at 4 degree. Collagen I polymerisation is batch sensitive, so it should be optimised for each batch. Usually, overnight or 1 hour polymerisation at 37°C were used for experiments performed in [Chapter 3](#). Polymerisation at 37°C for 1h was used for [Chapter 6](#). 60µl/well were removed using an E1-ClipTip Equaliser pipette (2-125µl). Plates were then stained with 30µl/well of 20µg/ml pHrodo for uptake experiments and 10µg/ml NHS-fluorescein to assess matrix homogeneity. For matrix homogeneity, plates were imaged with a 20X air objective Opera Phenix microscope, while uptake experiments were imaged using a 40X water immersion objective Opera Phenix microscope. Figure legends state the objective used.

2.2.10.4. Cell detachment in high content imaging plates

VIAFLO-384 well head (Integra) was used for cell transfer. High was adjusted to ensure optimal height for pipetting. Cell media in transfected plates was automatically pipetted and released in a waste reservoir containing sterile PBS. Transfected plates were washed with 80µl PBS once and 20µl of TrypLE was used to ensure detachment of cells. Cells were incubated for 5 minutes at 37°C. Cells were then vortexed every 1 minute thrice. TrypLE™ Express Enzyme was neutralised with 80µl 10% FBS DMEM. Cells were pipetted up and down 50 times with VIAFLO-384 well head (Integra) before transferring 80µl of the cell solution to ECM-coated 384 well plates ([Figure 2-3](#)). Transfected and transferred cells were incubated for 6 hours. After 2 hours, cell media was changed to 200nM Bafilomycin A1 in some wells containing NT5. After 5h 45 minutes, hoechst was spiked into a final concentration of 0.5 to 1µg/ml to avoid cell toxicity. Hoechst concentration should be optimised depending on the batch or date the hoechst bottle was opened.

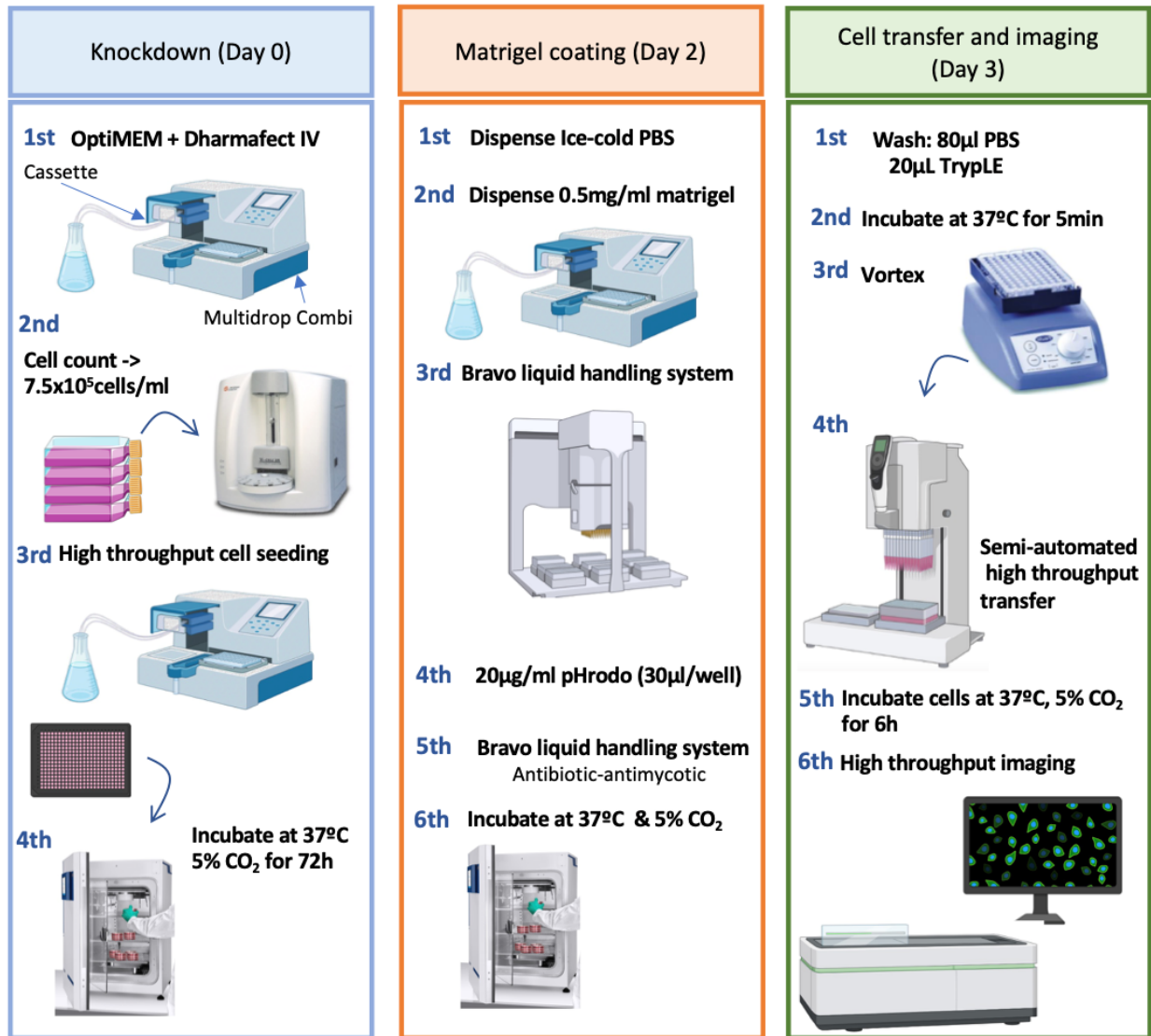


Figure 2-3. Schematic workflow depicting the key instruments used for high throughput knockdown, matrigel coating and cell splitting. Cells were transfected by siRNA and after 3 days transferred into 0.5mg/ml matrigel coated plates, labelled with pHrodo. For a demonstration on how Multidrop combi works, see the Thermo Fisher Scientific protocol in the link: <https://www.youtube.com/watch?v=qcNkm2Qs-iM>. For a representation of Bravo liquid handling system, see the following link: <https://www.youtube.com/watch?v=ByxA2H4SPj4>. For applications of ViaFlo 96- and 384- head, see: <https://www.youtube.com/watch?v=S3tFqB0yzso>. Image made using items from Bioicons.

2.2.10.5. Assessing the role of inhibitors in collagen I and matrigel uptake

10⁴ MDA-MB-231 cells per 384-well plate were seeded on pHrodo-labelled matrigel and collagen I. Cells were treated with inhibitors as described in [2.2.3.2. Assessing the role of inhibitors on CDM uptake](#). Cells seeded on collagen I were stained with hoechst and imaged live. Cells on matrigel were either fixed, labelled with hoechst and stained for β 1-integrin conjugated to Alexa fluor 488 (that is the case for some endocytic inhibitor experiments and a set of E64d and Bafilomycin A1 experiments). In addition, cells on matrigel were also stained with hoechst and imaged live. The 40X water-immersion objective of Opera Phenix microscope was used for live imaging ([Figure 2-3](#)). Live imaging analysis was performed in Columbus software using the pipeline shown in [Figure 2-4](#). A 60X water-immersion objective from an Opera Phenix microscope was used for fixed imaging. Fixed samples were analysed in Columbus software as shown in [Figure 2-5](#).

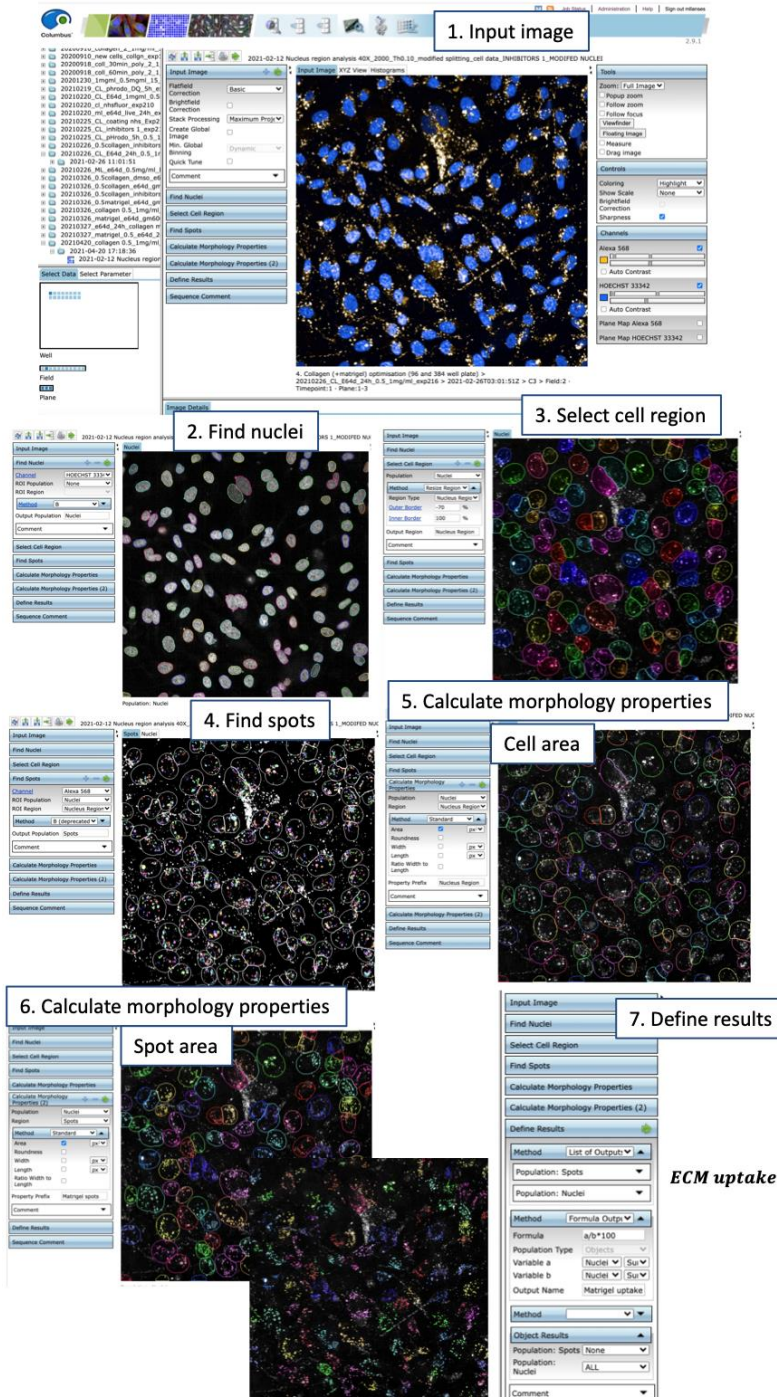


Figure 2-4. Schematic pipeline for analysis of ECM endocytosis in high throughput. For live imaging plates, the nuclei were selected. The parameter cell region enabled the selection of the area around the nuclei as an approximation of the cytoplasm. ECM spots were detected by selecting the tool find spots, specially designed for endocytosis assays. The area for the cell region was calculated using the tool morphology properties, which was also used to calculate the area for ECM spots. Results were defined as a percentage between the ECM spot area and the cell region area.

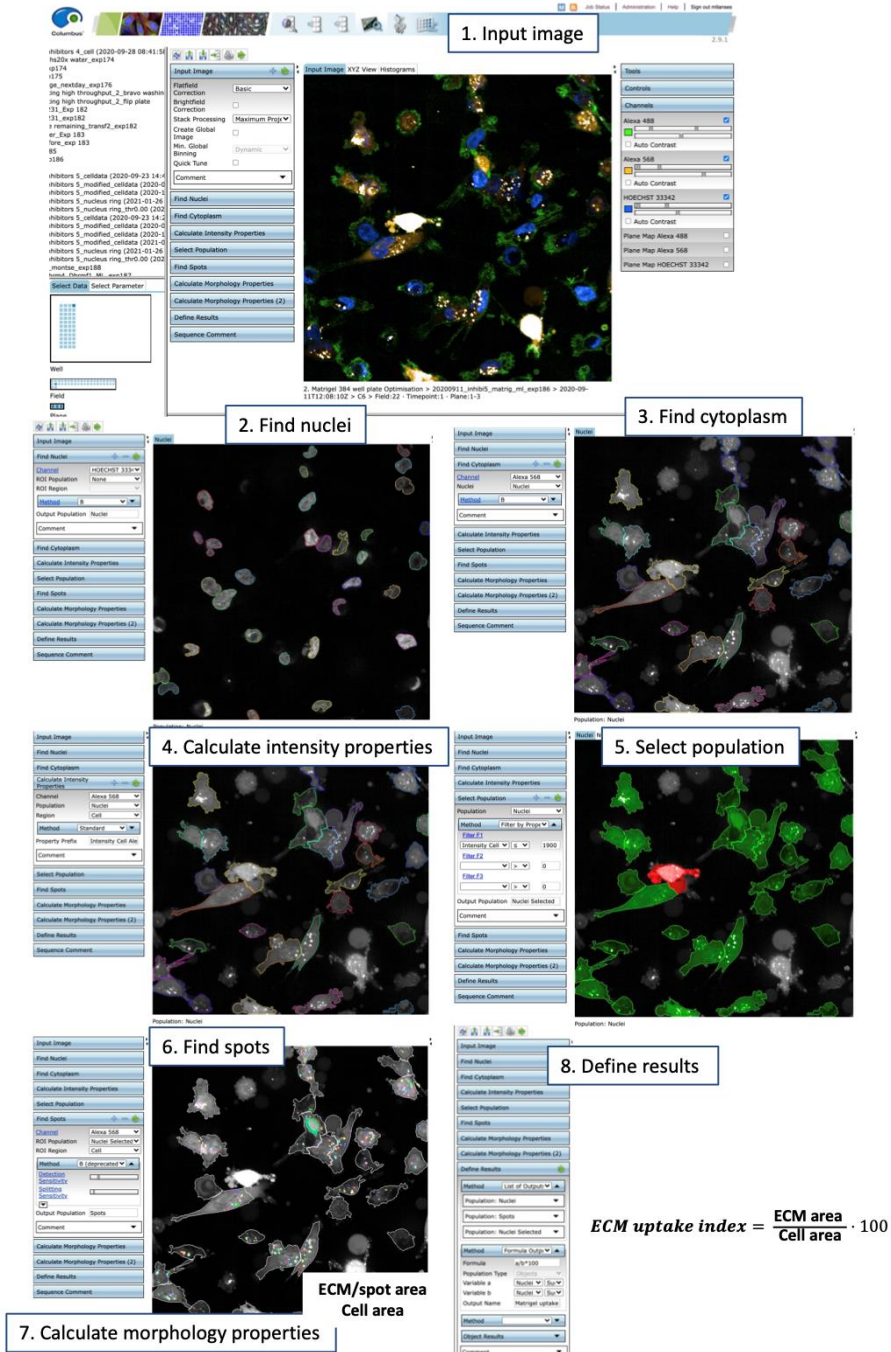


Figure 2-5. Schematic pipeline for analysis of ECM endocytosis in fixed samples. Nuclei were selected based on hoechst staining. ITGB1 staining enabled it to recognise the cytoplasm of cells. Intensity properties from each cell were calculated. Cells with high intensity signal of pHrodo were discarded to avoid an error-prone quantification. ECM spots were found in the cytoplasm of each cell. The morphology properties for cytoplasm and spots were calculated. Results were defined as a percentage between the ECM spot area and the cytoplasm area.

2.2.11. Assessing 3D uptake in spheroid assay

3D spheroids were generated by the hanging drop method, previously described in (Bayarmagnai *et al.*, 2019). 10^5 GFP-MDA cells were harvested and resuspended in 2ml of compaction media, containing 4.8mg/ml methylcellulose (Sigma- Aldrich) and 20 μ g/ml soluble collagen I (BioEngineering) in complete media. Then, 20 μ l of compaction media with cells was added on the lid of tissue culture dishes. Lids were turned and put on top of the bottom reservoir of the dish, which was filled with PBS to prevent evaporation. This resulted in the generation of spheroids containing approximately 1000 GFP-MDA cells per 20 μ l drop. Following 48h incubation at 37°C in 5% CO₂, spheroids were gently collected by flushing 800 μ l of complete media, which enabled spheroids to accumulate at the edge of the lid. Spheroids were transferred into a 1.5ml microcentrifuge tube and allowed to slowly sediment at the bottom by gravity. Supernatant was removed, spheroids were washed twice with 800 μ l of complete media before being individually collected. For 3D uptake assays, $\frac{1}{5}$ (v/v) of the matrix solution was labelled with a final concentration 20 μ g/ml pHrodo containing 0.1M sodium bicarbonate (NaHCO₃). Single spheroids were embedded into 45 μ l of 3mg/ml rat tail collagen I (Corning) and 3mg/ml geltrex (Gibco). 40 μ l of the spheroid-Collagen I-geltrex mix was deposited into a 35mm glass bottom dish. In order to prevent the embedded spheroid from reaching either the bottom of the dish or the upper edge of the collagen I-geltrex droplet, the dishes were rapidly kept for 3 to 5 minutes at 37°C upright. Following this time, dishes were flipped and incubated at 37°C for 2-3 minutes upside-down. Dishes were additionally incubated upright for 2-3 minutes at 37°C. Afterwards, dishes were kept upside-down and the matrix mixture was allowed to polymerise at 37°C for 13 to 15 minutes. Following that time, media was added into the dishes. Media was changed to 10% dialysed FBS (D-FBS) DMEM and 10% D-FBS amino acid free DMEM after 44h of embedding. Cells were imaged live at 0h, 24h, 44h, 48h and 72h post-embedding. A 10X air objective Nikon A1 confocal was used to image whole spheroids and for analysis. A 10X air objective Airyscan microscope was used for obtaining higher resolution microscopy images. 3D uptake was assessed by quantifying the pHrodo-ECM integrated intensity per spheroid, data was normalised to day 0 to better assess the fold change in uptake ([Figure 2-6](#)).

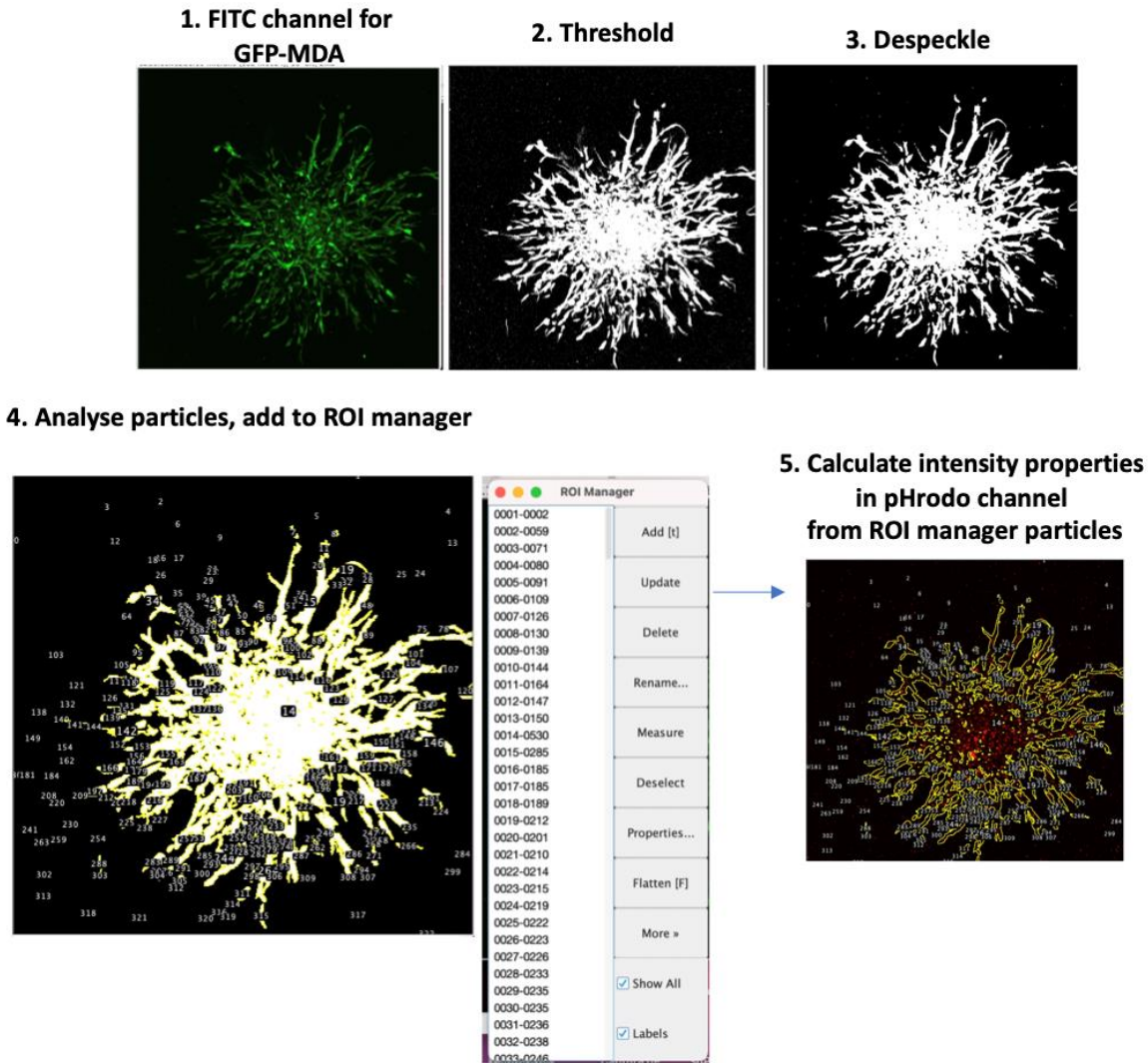


Figure 2-6. Spheroid analysis for ECM uptake in 3D. GFP-MDA cell spheroid was selected by applying a threshold and despeckling the thresholded image. Particles were then analysed and added into the ROI manager. To assess changes in ECM internalisation, the intensity properties of the pHrodo channel within the ROIs selected were calculated.

2.2.12. Immunofluorescence

Cells were fixed with 4% (w/v) paraformaldehyde (PFA) in PBS for 15 minutes. Then, cells were permeabilised with 0.25% (v/v) Triton X-100 in PBS for 5min and washed twice with PBS. For dextran internalisation assays, cells were not permeabilised.

For 2.5D ECM internalisation assays, cells were stained for the actin cytoskeleton with Phalloidin conjugated with either Alexa Fluor 555 (mainly for NHS-fluorescein labelled ECM assays), Alexa Fluor 488 (for NHS-Alexa fluor 555 labelled matrices) or Alexa Fluor 647 (for transferrin

endocytosis assays). Phalloidin was diluted 1:500 in PBS; cells were incubated for a period of 10 minutes at room temperature.

For antibody staining, cells were blocked in 1% (w/v) bovine serum albumin (BSA) for 1 hour at room temperature. Cells were then incubated with the respective primary antibodies for 1 hour at room temperature. Anti-human β 1-integrin antibody conjugated to Alexa fluor 488 (1:400 in PBS) was used for siAP3D1 knockdown experiment. Anti-human β 1-integrin antibody conjugated to Alexa fluor 647 (1:400 dilution in PBS) was utilised for colocalisation experiments and to assess endosomal integrin. To assess the internal pool of α 2-integrin, cells were incubated in FITC anti-human CD49b antibody (1:200 dilution) in PBS. For non-fluorescently conjugated antibodies, cells were first incubated with the primary antibody (EEA1, 1:100 in PBS) for 1h at room temperature. Cells were then washed thrice with PBS and incubated with the secondary antibodies (1:1000) for 45 minutes at room temperature. Cells were washed three times with PBS and incubated with Alexa fluor 647 β 1- integrin antibody as described above. For AP3D1 staining, cells were simultaneously permeabilised, blocked and stained with a solution containing the primary AP3D1 antibody (1:50000 dilution), 1% (w/v) BSA and 0.1% (w/v) saponin in PBS. Incubation time was 1h at room temperature. Cells were then washed thrice and incubated for 30 minutes with the secondary antibody in 1% (w/v) BSA and 0.1% (w/v) saponin.

Table 2-5. List of antibodies in immunofluorescence.

Primary antibodies	Supplier	Dilution ratio
Alexa Fluor 488 Anti-human (IgG) CD29	BioLegend (303016)	1:400
Alexa Fluor 647 Anti-human (IgG) CD29	BioLegend (303018)	1:400
FITC-Anti Human CD49b	BioLegend (359306)	1:200
Purified mouse Anti-EEA1 (IgG1)	BD Bioscience (610457)	1:100
AP3D1 (Mouse anti delta antibody (SA4))	Gift from Professor Andrew Peden (Available in Developmental studies hybridoma bank, Antibody Registry ID: AB_2056641)	1:50000
Secondary antibodies	Supplier	Dilution ratio
Alexa Fluor 488 Donkey Anti-mouse (IgG H+L)	Fisher Scientific (A-21202)	1:1000

For dishes and 8-well chambers, following antibody staining, cells were washed twice with PBS and washed once with deionized water, Vectashield antifade mounting medium containing DAPI was added for nucleus staining and sample preservation. The sample dishes were sealed with parafilm and kept at 4°C. A 60X objective from a Nikon A1 confocal microscope was used for cell imaging and colocalisation experiments for uptake assays. A 60X objective from Airyscan (Zeiss) was used for colocalisation experiments with Arf1-mcherry, Rab5-mcherry and AP3D1.

For high content imaging plates, cells were stained with 1µg/ml hoechst for 15min, washed twice with PBS and kept in PBS. Plates were stored at 4°C. Three different objectives were used for those plates 20X (for nuclei counting), 40X (for ITGB1 staining; knockdown optimisation in 96-well plates) and 60X (ITGB1 staining and matrigel uptake in fixed cells) using the Opera Phenix microscope (Perkin Elmer).

2.2.12.1. Quantification

A Nikon A1 Confocal microscope (Nikon Instruments Inc, Japan) with Plan-Apochromat 60X NA 1.4 oil immersion objective was used to image ECM internalisation and colocalisation experiments. The channels used throughout these experiments were: DAPI ($\lambda_{ex}=403.5\text{nm}$), FITC and Alexa Fluor 488 ($\lambda_{ex}=480.0\text{nm}$), Alexa Fluor 555 ($\lambda_{ex}=562.0\text{nm}$), Alexa Fluor 647 ($\lambda_{ex}=620.0\text{nm}$).

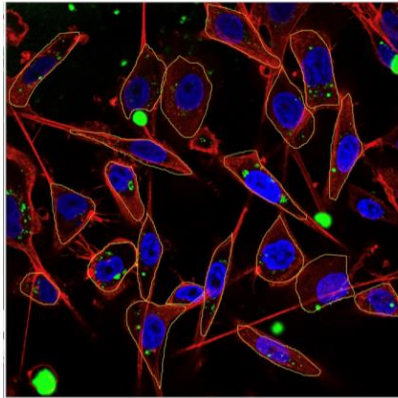
Quantification of soluble ligands (transferrin, dextran, lactosylceramide), ECM and integrin internalisation assays

All images acquired with the Nikon A1 confocal microscope were analysed using ImageJ software as previously described in (Commisso, Flinn and Bar-Sagi, 2014). Z-stacked images were maximum-projected. Phalloidin or β 1-integrin staining enabled the identification of single cells. Cells were outlined and recorded in the region of interest (ROI) manager. Cell area was measured. ECM or β 1-integrin channels were also Z-stacked; a threshold was applied to specifically select internalised ECM, α 2- or β 1-integrin internal pools. The total area of internalised soluble ligands/ECM/integrin per ROI region (or cell) was then measured. The soluble

ligands/ECM/integrin uptake index is a percentage calculated by dividing the area of internalised soluble ligands/ECM/integrin by the cell area (Figure 2-7).

1. Maximum-projected image:

Outline the cells and add to ROI manager



2. Cell area

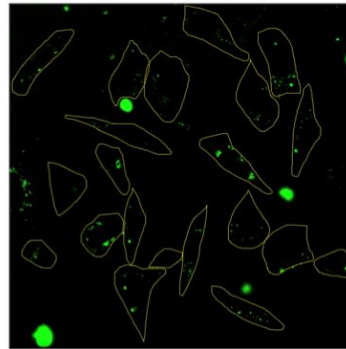
	Area	Circ.	IntDen	RawIntDen	AR	Round	Solidity
1	580.223	0.687	10725.742	251163	1.781	0.561	0.924
2	850.115	0.863	11178.706	261770	1.566	0.639	0.979
3	599.654	0.561	10368.819	242805	2.701	0.370	0.909
4	684.934	0.679	42188.610	987924	2.417	0.414	0.918
5	654.016	0.712	10582.255	247803	1.885	0.531	0.951
6	555.540	0.456	18534.481	434019	3.570	0.280	0.918
7	542.985	0.459	75805.313	1775121.000	3.600	0.278	0.880
8	404.367	0.354	16715.619	391427.000	5.491	0.182	0.944
9	582.828	0.816	8525.445	199639.000	1.342	0.745	0.970
10	674.771	0.829	16156.876	378343.000	1.240	0.806	0.934
11	301.151	0.823	17222.220	403290.000	1.512	0.661	0.974
12	436.267	0.458	16939.987	396681.000	4.648	0.215	0.942
13	699.240	0.537	30026.124	703117.000	1.611	0.621	0.817
14	159.629	0.743	217.835	5101.000	1.862	0.537	0.972
15	388.951	0.492	14813.996	346897.000	3.501	0.286	0.956
16	340.524	0.646	28836.724	675265.000	2.639	0.379	0.944
17	498.744	0.301	5379.889	125980.000	5.627	0.178	0.860
18	535.854	0.493	24126.140	564958.000	4.380	0.228	0.912
19	480.253	0.756	2306.118	54002.000	1.309	0.764	0.977
20	250.119	0.893	11488.612	269027.000	1.531	0.653	0.985
21	470.004	0.882	59226.945	1386908.000	1.506	0.664	0.972

3. "Total" Internalised area:

- A. Select channel of interest: ECM/integrin.
- B. Applied maximum projection (z-stack).
- C. Apply threshold and despeckle.
- D. Calculate total area for internalised particles.

ImageJ Macro:

```
//Z project
selectWindow("Laminin synchronised e64d 1.nd2 - C=2");//NAME!!
run("Z Project...", "projection=[Max Intensity]");
//Threshold
setAutoThreshold("MaxEntropy dark");
setOption("BlackBackground");
//Noise
run("Despeckle");
//Particle analysis
//Change number according to the number of ROIs, i<number of ROIs+1!!
for (i=0; i<50; i++) {
roiManager("Select",i);
run("Analyze Particles...", "clear summarize");
}
```



Total internalised area Uptake index

Count	Total Area	Average Size	%Area	Circ.	Solidity	IntDen
14	8.242	0.589	1.420	0.903	0.873	500.107
16	11.189	0.699	1.316	0.910	0.877	505.688
21	9.950	0.474	1.659	0.905	0.850	337.474
18	30.107	1.673	4.396	0.797	0.824	2128.981
11	10.591	0.963	1.619	0.904	0.896	819.620
11	11.146	1.013	2.006	0.892	0.875	1533.939
9	38.519	4.280	7.094	0.805	0.854	8101.648
8	17.082	2.135	4.224	0.675	0.775	1815.622
13	7.217	0.555	1.238	0.916	0.885	562.702
7	9.053	1.293	1.342	0.945	0.891	2223.357
14	7.431	0.531	2.467	0.970	0.904	1126.399
14	9.096	0.650	2.085	0.946	0.868	1161.478
14	19.772	1.412	2.828	0.860	0.818	2007.536
2	0.171	0.085	0.107	1.000	1.000	37.751
8	8.028	1.004	2.064	0.900	0.867	1746.275
6	15.117	2.520	4.439	0.918	0.863	4619.389
11	5.338	0.485	1.070	0.952	0.919	373.973
15	16.484	1.099	3.076	0.878	0.862	1316.910
4	2.178	0.544	0.453	0.872	0.889	281.283
4	11.146	2.786	4.456	0.745	0.818	2511.205
12	34.676	2.890	7.378	0.773	0.830	4721.100

$$\text{Uptake index} = \frac{\text{Total internalised area}}{\text{Cell area}} \times 100$$

Figure 2-7. ECM and integrin internalisation analysis. Images were maximum projected and the outline of each cell was recorded into the ROI manager. Cell areas were calculated. To determine the "total" internalised area, the channel of interest was selected and maximum-projected. Images were thresholded and despeckled. Uptake index is a percentage between the total ECM/integrin area and the cell area.

Quantification of colocalisation

More than 20 cells were imaged and quantified per biological replicate. Colocalisation Colormap plugin in ImageJ (<https://sites.google.com/site/colocalizationcolormap>) applies the Jaskolski algorithm (Jaskolski, Mülle and Manzoni, 2005) to measure the correlation between pairs of pixels from two images, which enables a quantitative visualisation of colocalisation. The plugin correlates two corresponding pairs of pixels by calculating the normalised mean deviation product (nMDP). This results in a spatial map of colocalisation by representing the distribution of nMDPs in a colour scale from -1 to 1. Blue colours correspond to no colocalisation, whereas red colours indicate high levels of colocalisation. In addition, the algorithm calculates the index of correlation (Icorr) to indicate the fraction of pixels that positively correlate or colocalise.

2.2.13. Western Blotting

Samples for western blot analysis were seeded in 6 well plates. For knockdown experiments, see section [2.2.7. siRNA transfection](#). Confluent 6-well plates were harvested with 100µl of lysis buffer (50mM Tris-HCl pH 7 and 1% SDS). Cell lysates were collected and transferred into QiaShredder columns (Qiagen), which were spun at 4°C for 10 minutes at 13000rpm. Extracted proteins were mixed in a 4:1 ratio with the NuPAGE buffer (for example, 75µl of extracted protein: 25µl of NuPAGE), which contained a final concentration of 1mM DTT. 15µl to 25µl of extracted proteins in NuPAGE buffer and 0.5µl protein ladder (BioLabs) were loaded into a Bio-Rad 4-15% Mini-PROTEAN precast polyacrylamide gel, which enables the separation of proteins with a molecular weight ranging from 5kDa to 200kDa. The gels were run at 100V constant voltage for 1h 15 minutes. The composition of the running buffer was the following: 3g Tris base, 14.4g glycine and 1g SDS in 1l deionised water. Afterwards, proteins were transferred to a FL-PVDF membrane using the Towbin transfer buffer (composition: 25mM Tris, 192mM glycine, 20% methanol (v/v) pH 8.3). The transferring process was performed at room temperature and at a constant voltage of 100V for 1h 15 minutes. Transferred membranes were blocked in 5% milk for 1 hour at room temperature. Membranes were washed twice TBST (50mM Tris HCl, 150mM NaCl and 0.5% (w/v) Tween 20) and incubated overnight with the primary antibodies in TBST (see [Table 2-5](#)). The membranes were washed thrice in TBST for 10 minutes with gentle rocking.

Secondary antibodies were then applied for 1h at room temperature. Anti-mouse IgG secondary LiCOR IR Dye 800 antibody was diluted 1:30000, while anti-rabbit IgG secondary LiCOR IRDye 680LT antibody was diluted 1:20000. Both antibodies were diluted in TBST supplemented with 0.01% (w/v) SDS. Afterwards, three more TBST washes were performed and a last wash with deionized water. The LiCOR Odyssey system was used for imaging the membranes. The intensity of the bands was quantified with Image Studio Lite software. Bands were normalised to GAPDH intensity. Western blotting for mass spectrometry is found in [2.2.14.2. Western blot analysis](#).

Table 2-5. List of antibodies in Western blotting.

Primary antibodies	Supplier	Dilution ratio
GAPDH	Santa Cruz Biotechnology (SC-47724)	1:1000
PAK1	Proteintech (21401-1-AP)	1:1000
AP3D1 (Mouse anti delta antibody (SA4))	Gift from Professor Andrew Peden.	1:100000
Secondary antibodies	Supplier	Dilution ratio
IR Dye 680LT anti-rabbit antibody	LiCOR Biosciences	1:20000
IR Dye 800 anti-mouse antibody	LiCOR Biosciences	1:30000

2.2.14. Mass spectrometry of internalised ECM proteins

2.2.14.1. CDM internalisation assay using biotinylation

CDMs were generated in 10cm as in section [2.2.3. Generation of Cell-derived matrices](#). CDMs were incubated with 0.13mg/ml Sulpho-NHS-SS-biotin in PBS⁺⁺ at 4°C with gentle rocking (5ml per 10cm dish). Sulpho-NHS-SS-biotin is a NHS-ester biotinylation reagent that is cell-impermeable. Similar to NHS-fluorescein, it reacts with free amine groups of proteins but, in addition, it contains a cleavable disulphide bond. Labelled CDMs were washed twice with PBS⁺⁺. For optimisation experiments, 1.2x10⁶ MDA-MB-231 and MCF10A cells were seeded per 10cm dish. For mass spectrometry, cell number was increased to 2.2x10⁶ MDA-MB-231 cells. Both cell lines were incubated in presence of 20µM E64d for 16h. Following this time, cells were washed once with ice-cold PBS⁺⁺ (5ml). Extracellular biotin was reduced with a cell-impermeable reducing

agent, 15mg/ml sodium 2-mercaptoethanesulfonate in 3mN (equals 3mM) NaOH solution (5ml), for 1h 30 minutes at 4°C. Reduced cysteines were alkylated by adding 17mg/ml iodoacetamide (5ml) for 10 minutes at 4°C. Reduction and alkylation steps were carried out on a gentle rocker. Following this, cells were kept on ice and washed once with ice cold PBS. Subsequently, MDA-MB-231 and MCF10A cells were washed and extracted with ice-cold 20mM NH₄OH and 0.5% Triton X-100 (400µl/10cm dish), containing a protease inhibitor cocktail (1:100 dilution). Cells were lysed on ice and gently rocking for 15-20 minutes. Cells were visualised under the microscope to confirm cell lysis. Afterwards, cell lysates were transferred into a Qia-shredder column and spun down at 13000rpm for 10 minutes at 10°C. The supernatant was then collected. 30µl of the cell lysates were mixed with 10µl NuPAGE buffer (¼ dilution, without a reducing agent) and heated up at 70°C for 5 minutes ([Figure 2-8](#)). The mix was stored at -20°C for western blot analysis. The remaining cell lysates were used for Streptavidin pull down assay.

2.2.14.2. Western blot analysis

15 to 20µL of the cell lysates in NuPAGE buffer and 1µl of the protein ladder were loaded into a 4-12% acrylamide gel and later transferred into a FL-PVDF membrane. Membranes were blocked with 5% (w/v) BSA in TBST for 1 hour at room temperature. After blocking, membranes were incubated with an antibody against GAPDH (1:1000 dilution in 5% (w/v) BSA in TBST) overnight at 4°C. Membranes were then washed thrice with TBST for 10 minutes on gentle rocker. Membranes were incubated with the secondary anti-mouse IgG LiCOR IR Dye 800 (1:30000 dilution) and streptavidin conjugated to LiCOR IR Dye 680LT (1:20000 dilution) in TBST, containing a final concentration of 0.01% (w/v) SDS, for 1 hour at room temperature. Lastly, membranes were washed thrice with TBST and once with deionized water. Membranes were imaged in the LiCOR Odyssey system. Band intensity was quantified with Image Studio Lite software. Streptavidin signal was normalised to GAPDH intensity. For better comparison of biological replicates, samples were normalised to the non-biotinylated group.

Detection of Biotinylated proteins by Mass spectrometry

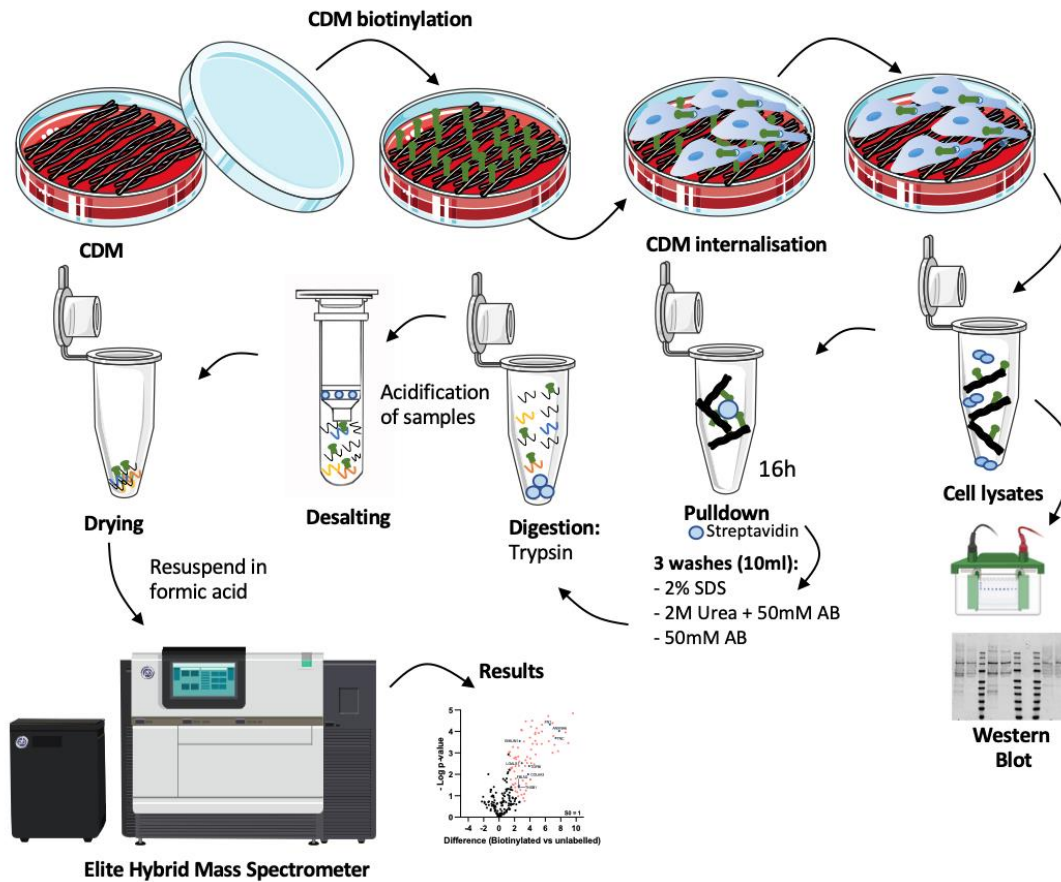


Figure 2-8. Schematic representation of the mass spectrometry workflow. Image made using items from Servier medical Art.

2.2.14.3. Streptavidin-agarose beads pulldown

The ratio of streptavidin-agarose beads (hereafter streptavidin beads) needed per lysate was 1:10 (streptavidin bead volume: cell lysate volume). Streptavidin beads were equilibrated by washing with PBS⁺⁺ (ratio 16:100, streptavidin bead volume: PBS⁺⁺ volume) and quickly spun down. This step was repeated twice. Cell lysates were incubated with equilibrated streptavidin beads at 4°C overnight under constant rotation. Afterwards, streptavidin beads were collected into a Wizard Minicolumn. These columns contain a filter that enables the flowthrough to be discarded, while streptavidin beads remain on top of the filter. Streptavidin beads were washed consecutively with 10ml of 2% (w/v) SDS solution, 10ml of 2M Urea and 50mM ammonium bicarbonate solution and 10ml of 50mM ammonium bicarbonate. These serial washes enabled

removing non-specific bound proteins. Biotinylated proteins, bound to streptavidin beads, were then collected in 100µl of 50mM ammonium bicarbonate ([Figure 2-8](#)).

2.2.14.4. On-beads tryptic digestion

In order to denature the disulphide bonds present within the biotinylated proteins-beads (contained in 100µl ammonium bicarbonate), 1µl 0.5M Tris(2-carboxyethyl)phosphine (TCEP) was added. Samples were incubated at 37°C and shaken at constant speed (850rpm) for 15 minutes. Afterwards, 2µl of 0.5M iodoacetamide, which was freshly prepared, were added to alkylate reduced cysteines. Samples were incubated in the dark for an additional 15 minutes at 37°C and kept in constant movement (850rpm). After this time, 2µl trypsin at a concentration of 1µg/µl was added into the reduced and alkylated samples. The reaction was allowed to occur at 37°C and constant shaking (850rpm) for a span of 3 hours ([Figure 2-8](#)). The supernatant was then collected with a gel-loading tip to ensure harvesting all the peptides. At this point, samples were stored at -20°C.

2.2.14.5. Desalting and desiccation of digested peptides

Traces of salt and urea may be found in the tryptic digestion solution, which may have an impact on data analysis. Digested peptides were then desalted before Orbitrap injection. Pierce™ C18 spin columns were equilibrated. Firstly, 200µl of 100% acetonitrile was allowed to flow through the columns, followed by addition of 200µl of a solution that consisted of 50% (v/v) acetonitrile and 0.1% trifluoroacetic acid. The final step was acidifying the pH of the column with 200µl of 0.1% trifluoroacetic acid to ensure peptide binding. Digested samples were acidified by adding 4µl of neat 10% trifluoroacetic acid ([Figure 2-8](#)). Afterwards, the acidified samples were added into the equilibrated columns. The flow-through was collected and added three more times into the equilibrated columns to minimise peptide loss. Peptides bound to the columns were washed thrice with 100µl of 0.1% trifluoroacetic acid. Peptides were then eluted in 100µl of 50% (v/v) acetonitrile/0.1% (v/v) trifluoroacetic acid. The desalted peptides were desiccated by spinning them in SpeedVac (Eppendorf) for 90 minutes at 45°C. Eppendorf tubes were opened to enable

the evaporation of the solution. Desiccated peptides were reconstituted in 0.5% (v/v) formic acid. Reconstituted peptides were vortexed for 10 minutes at low speed.

2.2.14.6. Mass spectrometry analysis

Peptides were analysed in Orbitrap Elite Hybrid Mass Spectrometer (ThermoFisher). Mass spectrometry data was analysed in Perseus software version 1.6.10.50. Dr Mark Collins (Senior Lecturer and Deputy Director of the Biological Mass Spectrometry Facility at The University of Sheffield) performed both analyses.

2.2.15. Statistical analysis and SuperPlots

After image analysis with ImageJ or Columbus software, we obtained quantitative data. All the gathered data was normalised to the control population. Data representation and statistical analysis were performed in Graphpad prism (Version 9.4.1) software. Scatter plot data are represented by SuperPlots, which enables the incorporation of cell level data and experimental repeatability in a single diagram (Lord *et al.*, 2020). Cell level data is represented by dots. For images acquired at Nikon A1 confocal, cell data is colour-coded in blue, red and green to display individual biological replicates. For images acquired in Opera Phenix microscope, cell data is colour-coded based on conditions due to the high number of cells analysed (at least 2000 cells/condition per biological replicate). SuperPlots in addition include the average (mean) data in each biological replicate for Nikon A1 confocal data. While, well data is included to show repeatability of technical and biological replicates for high throughput data. Average values or well data is represented by squares. Data acquired using Nikon A1 was analysed using cell data, while well data was used for the statistical analysis of images obtained in Opera Phenix microscope. To compare two datasets, unpaired t-test was used; to compare more than two datasets, nonparametric one-way ANOVA was performed. High throughput screening data was normalised between the NT5 and NT5 in presence of Bafilomycin A1 (Normalised index = (Matrigel uptake index - mean NT5)/(Mean NT5-Mean Bafilomycin A1)). In addition, for the trafficking screen ([Chapter 5](#)), Z-scores (also known as standard scores) were calculated. The Z-score is a statistical parameter or measurement that describes the relationship of a certain value

to the mean of the group of values. It is measured in terms of standard deviations from the mean. If the Z-score is 0, it indicates that the data point is identical to the mean score (Saisana, 2014). The Z-score is calculated as follows: $Z = (X - \mu)/\sigma$; where X is the raw score to be standardised, μ is the mean of the population and σ is the standard deviation of the population (Saisana, 2014). Statistical analysis for mass spectrometry was performed in Perseus software, Student T-test was calculated. Data was exported and Graphpad was used to represent the volcano plots.

Chapter 3 – The use of small molecules as a tool to characterise ECM internalisation in high throughput systems.

Montserrat Llanses Martinez conceived, planned, carried out and analysed all the experiments. Dr Xavier LeGuezennec (IMCB, Singapore) printed the siRNA plates and helped in the design of the workflow for the Bravo-liquid handling system and Integra 384-well head ([Figure 3-21](#) and [Figure 3-22](#)). This Chapter has been written using the inclusive first-person plural.

3.1. INTRODUCTION

Small molecules are powerful tools to study the molecular mechanisms behind biological processes (Stockwell, 2004), internalisation of extracellular particles being an example. Endocytosis or internalisation of extracellular particles is an intricate and diverse biological process that can be categorised into three groups: clathrin-dependent endocytosis, lipid raft/caveolae-mediated endocytosis and phagocytosis (solid particles)/micropinocytosis (extracellular liquid) (Mayor and Pagano, 2007; Ivanov, 2008). Interestingly, these endocytic pathways present a distinctive sensitivity to biological inhibitors, which allows a simple, reliable and affordable analysis of endocytosis *in vitro* and *in vivo* (Ivanov, 2008).

Dynamin is a small GTPase involved in the invagination and scission of clathrin-coated pits (Ivanov, 2008; Vercauteren *et al.*, 2010; Preta, Cronin and Sheldon, 2015), in addition to mediating the plasma membrane scission in endocytic events that occur in caveolae. The latter is referred to as caveolar endocytosis and occurs due to changes in membrane tension (Henley *et al.*, 1998; Ivanov, 2008; Parton, Kozlov and Ariotti, 2020). Three dynamin genes are present in mammals: Dynamin I (primarily expressed in the brain), Dynamin II (ubiquitously expressed) and the least characterised Dynamin III (mainly expressed in neurons and testes) (Kockx *et al.*, 2014; Preta, Cronin and Sheldon, 2015). Dynasore and myristyl trimethyl ammonium bromide (MiTMAB) are reversible inhibitors of dynamin I and II (Quan *et al.*, 2007; Preta, Cronin and Sheldon, 2015). Dynasore blocks endocytosis by inhibiting the GTPase activity of dynamin, whereas MiTMAB thwarts the recruitment of dynamin PH-domain to the plasma membrane (PM) (Kockx *et al.*, 2014; Preta, Cronin and Sheldon, 2015). These small molecules have thus been

extensively used for the inhibition of dynamin-mediated endocytosis, including transferrin (TF) uptake (see [Figure 3-1A](#)) (Kockx *et al.*, 2014; Preta, Cronin and Sheldon, 2015).

Filipin is a polyene antibiotic that interacts with and aggregates in cholesterol-rich membranes, which consequently limits cholesterol accessibility from the PM. These filipin-cholesterol interactions lead to a deformation of the cholesterol domains, affecting caveolar shape, GPI-anchored proteins and ultimately lipid raft mediated endocytosis (Ivanov, 2008). Remarkably, filipin does not affect clathrin-mediated endocytosis nor macropinocytosis, which denotes its suitable use in studying lipid raft mediated endocytosis. Lactosylceramide (LacCer), for example, is a sphingolipid that has been described to be exclusively internalised via caveolae-mediated endocytosis ([Figure 3-1A](#)) (Rejman, Bragonzi and Conese, 2005).

Ethyl-isopropyl amiloride (EIPA) is an analogue of amiloride, an inhibitor of Na⁺/H⁺ exchangers (Ivanov, 2008; Koivusalo *et al.*, 2010). Interestingly, the activation of amiloride-sensitive Na⁺/H⁺ exchangers was shown to be required in epidermal growth factor (EGF)-mediated pinocytosis in A341 carcinoma (West, Bretscher and Watts, 1989). As a result, the use of Na⁺/H⁺ exchangers inhibitors were proposed as a tool for blocking macropinocytosis and phagocytosis (Ivanov, 2008). Inhibition of Na⁺/H⁺ exchangers acidifies the submembrane cytosol. Consequently, Rac1 and Cdc42 fail to be recruited at the plasma membrane (Koivusalo *et al.*, 2010). The polysaccharide dextran is a well-established marker for the study of macropinocytosis as represented in [Figure 3-1A](#) (Moreau *et al.*, 2018).

Fluorescent cargoes facilitate the study of endocytosis, yet those particles that reside on the plasma membrane cannot be easily separated from those that have been fully endocytosed (Lindner, Burkard and Schuler, 2020). As a consequence, a diverse variety of pH-sensitive dyes (such as CypHer5E, TPE-Cy and pHrodo) are available (Lindner, Burkard and Schuler, 2020). pH Rodo™ Red succinimidyl (NHS/STP) ester is a pH-sensitive and an amine-reactive dye that reacts with primary amines of proteins. Interestingly, the *Intracellular pH (pHi) Detection* data sheet (Molecular probes by Life technologies) states that pHrodo™ dye fluorescence is considerably weak at neutral pH, but fluorescence is increased at lower pH as shown in [Figure 3-1B](#). In other words, the proteins conjugated to the dye are non-fluorescent in the extracellular environment,

but after being internalised and as the endosomal content is progressively acidified, pHrodo-conjugated proteins will be increasingly fluorescent.

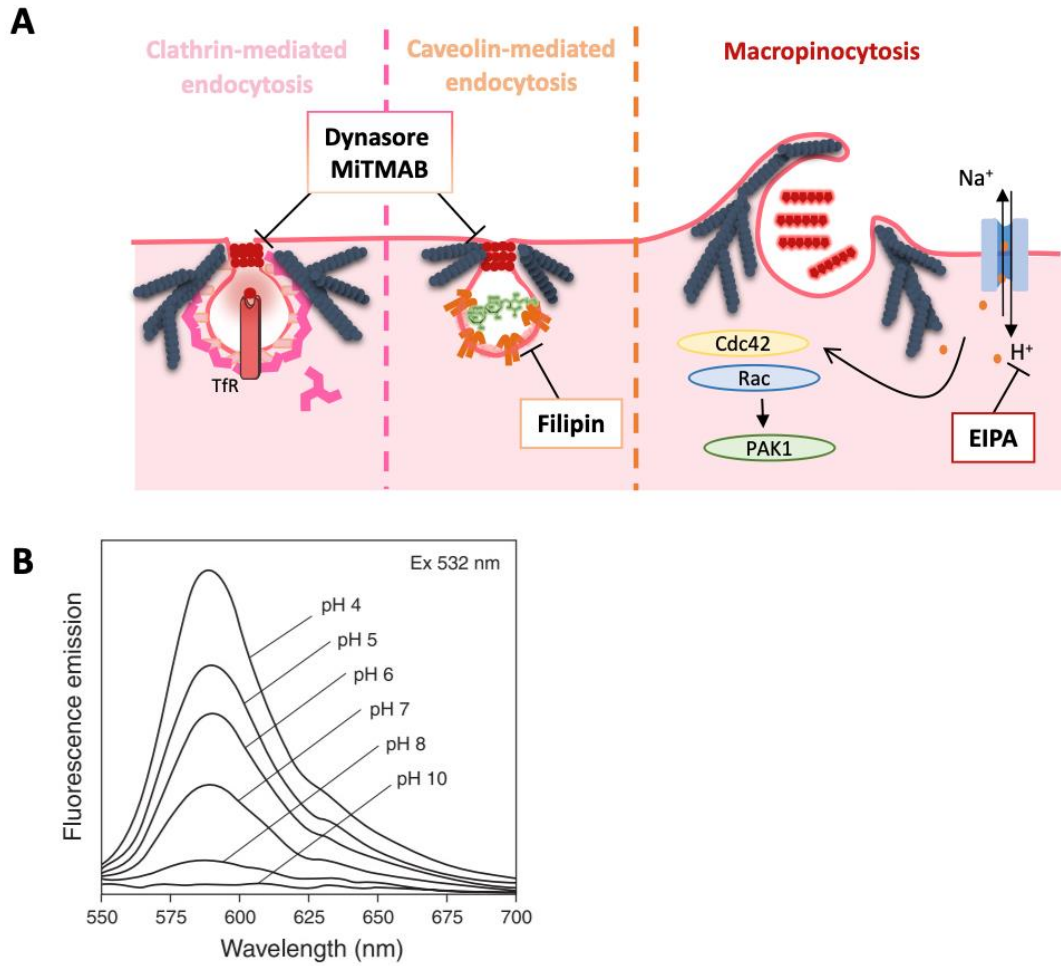


Figure 3-1. Schematic representation of the foremost endocytic pathways. (A) The small GTPase dynamin participates in the scission of the plasma membrane in clathrin- and caveolin-dependent endocytosis. To study these processes, the small molecule inhibitors dynasore and MiTMAB have been widely used. To further distinguish the endocytic pathway, the polyene macrolide filipin has been utilised since it specifically binds to lipid-rafts and specifically blocks endocytosis that occurs in these lipidic domains in the plasma membrane. EIPA treatment results in inhibition of Na⁺/H⁺ exchangers, leading to acidification of the submembrane cytosol and failure to recruit Cdc42 and Rac1. (B) Fluorescence emission diagram of pHrodo-labelled *E. coli* in solutions at different pHs (ranging from pH 10 to pH 4). Graph source: Intracellular pH (pHi) Detection data sheet, Molecular probes by Life technologies.

In the lysosomal or intracellular ECM degradation pathway, the diverse ECM components are internalised via different means. However, previous studies mostly used soluble matrices or collagen-coated beads which do not recapitulate the complex *in vivo* architecture found in tissues. This is mainly due to the lack of available methods, thus the study of cell-ECM interactions in high throughput systems has remained challenging. There is the necessity to develop reproducible and homogeneous matrices in a high-content fashion to investigate the role of the ECM in pathology. Here, we established an automated and reproducible matrigel and collagen I coating protocol in 384 well plates, as well as the generation of an *in vitro* tissue-stroma-like substrate, known as cell derived matrix (CDM) in high content imaging plates. One main problem when working with small volumes is that the meniscus of liquids is more evident. This results in generating matrices that are not homogeneous and with high variability between technical and biological replicates. In order to minimise this, we used a similar approach as previously described (Ko, Tsai and Frampton, 2019). In short, prior to coating with the matrices, we added PBS in the high content screening plates and then we spiked the ECM of interest. The presence of a high volume of PBS created a density gradient that concentrated the ECM at the bottom of the plate. Besides, this methodology also decreases the ECM-air surface tension and minimises evaporation.

This chapter aims to characterise ECM endocytosis and show the results of the optimisation process prior to performing a high throughput screening on ECM internalisation. The first sections include the optimisation of inhibitors that could potentially modulate ECM internalisation. The following sections include the generation of a thin homogeneous matrigel and collagen I matrices in 384-well plates, in addition to the generation of CDM in high content systems. This chapter also shows optimisation of matrigel labelling with pHrodo. Moreover, the last sections include assessment of the endocytic pathways implicated in ECM uptake, by siRNA-mediated downregulation of known endocytosis regulators.

3.2. RESULTS

3.2.1. Dynasore and MiTMAB reduce transferrin endocytosis in MDA-MB-231 cells

Transferrin (TF) is an iron-binding protein that is internalised into the cell via clathrin-dependent endocytosis (Mayle, Le and Kamei, 2012). We thus rationalised to use fluorescent TF as a cargo to establish the concentration range at which dynasore and MiTMAB could reduce endocytosis in MDA-MB-231 cells prior to evaluating dynamin inhibition on ECM uptake. Owing to dynamin inhibition reported cytotoxicity (Vercauteren *et al.*, 2010), we sought to determine the two lowest inhibitory concentrations that would ensure minimum toxicity and reproducible inhibition of dynamin-mediated endocytosis in MDA-MB-231 cells. Preliminary experiments showed that cell adherence to glass was severely impaired upon treatment with dynasore (data not shown), therefore 0.1mg/ml collagen I-coated dishes were required to enhance cellular adherence and spreading to the substrate for both dynamin inhibitors. In addition, dynasore has been reported to bind to serum proteins (Preta, Cronin and Sheldon, 2015) which affected experimental reproducibility (data not shown); the FBS concentration for dynasore optimisation experiments was therefore reduced to 2% in order to improve the reproducibility of independent experiments. Another layer of variability was TF fluorescence, which differed across experiments depending on the aliquot used; consequently, the mean TF uptake index per replicate was highly variable ([Figure S1-1A and B](#)). In order to address this, we normalised the TF uptake index to the control (DMSO or H₂O) (see [Figure 3-2](#)). As expected, the treatments with the different inhibitor concentrations had a similar effect on TF uptake ([Figure 3-2](#)) and the observed difference in the absolute values may be on account of TF fluorescence. The internalisation of TF was reduced in approximately 35% in the presence of 20µM and 40µM dynasore (see [Figure 3-2A and 3-2C](#) and [Table S1-1](#)), confirming its inhibitory effect on dynamin-dependent endocytosis in MDA-MB-231 cells. Similarly, 15µM and 25µM MiTMAB resulted in a 35% and 50% reduction of TF uptake respectively, while 35µM significantly diminished (~70% reduction) TF endocytosis ([Figure 3-2B and 3-2D](#) and [Table S1-2](#)). These results show that dynasore and MiTMAB reduce dynamin-mediated endocytosis in MDA-MB-231 cells and validate their usage in assessing the role of dynamin in ECM internalisation.

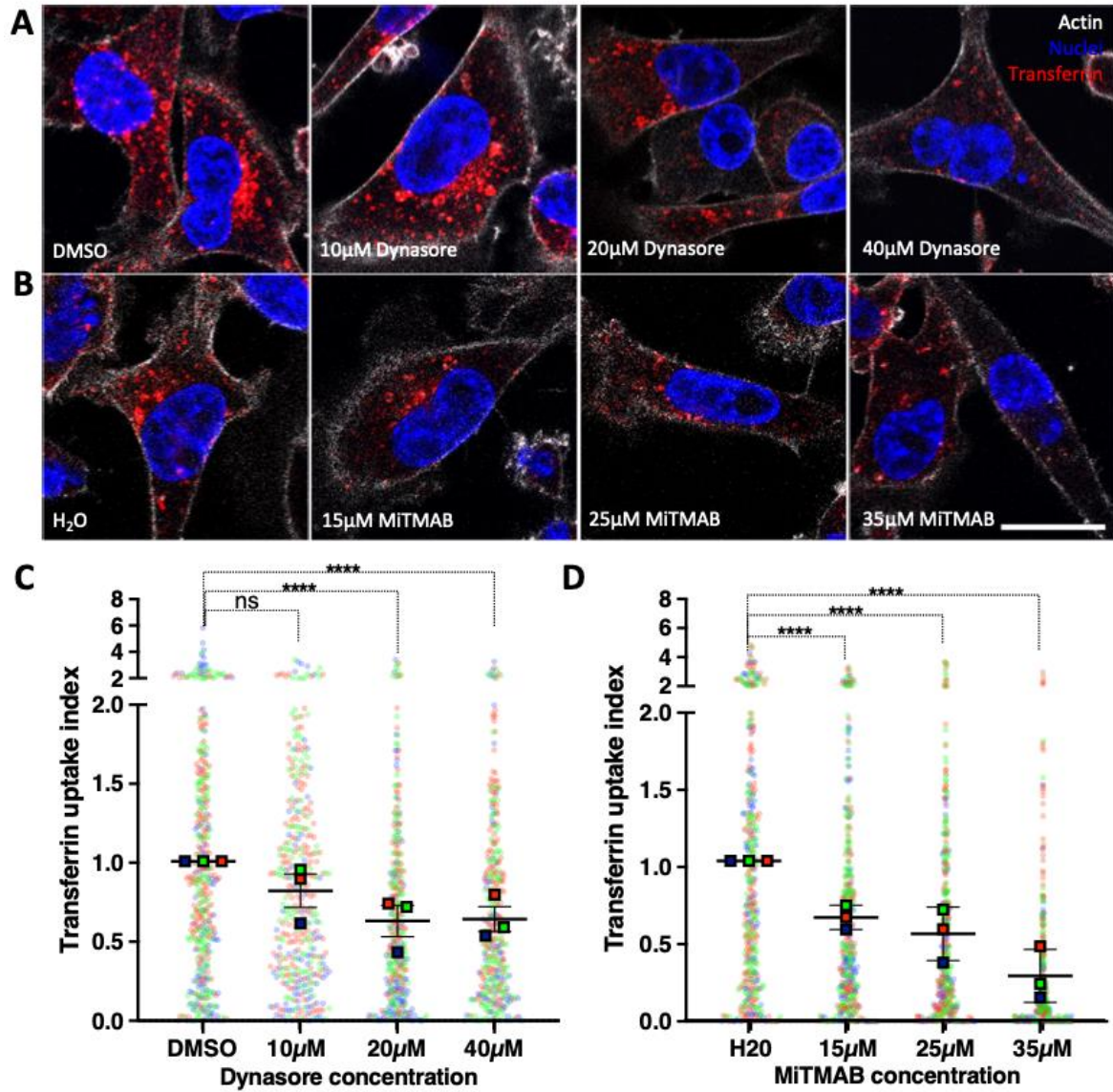


Figure 3-2. Dynasore and MiTMAB reduce transferrin internalisation in MDA-MB-231 cells. 3×10^5 MDA-MB-231 cells were seeded on 35mm glass-bottom dishes coated with 0.1mg/ml collagen I for 6h and then pre-treated with the indicated concentrations of the dynamin inhibitors (10µM, 20µM, 40µM Dynasore in 2% FBS (A,C); 15µM, 25µM, 35µM MiTMAB (B,D)) and the corresponding vehicle controls (DMSO or H₂O respectively) for 30min. Following pre-treatment, cells were incubated in the presence of 5µg/ml Transferrin (red) for another 30min and then fixed and stained with Phalloidin Alexa Fluor 647 and DAPI to visualise F-actin (white) and the nuclei (blue). Cell imaging was carried out with a 60X objective Nikon A1 confocal microscope. Image J was used to analyse the TF uptake index. Scale bar, 20µm. The SuperPlot shows the normalised cell-level data and mean values \pm SEM from N=3 independent experiments; **** $p < 0.0001$, ns (not significant); Kruskal-Wallis test.

3.2.2. Filipin blocks caveolae-dependent endocytosis of Lactosylceramide in MDA-MB-231 cells

To evaluate if filipin blocked caveolae-dependent internalisation in MDA-MB-231 cells, we took advantage of fluorescent LacCer, which is exclusively taken up in lipid rafts ([Figure 3-1A](#)). MDA-MB-231 cells were incubated with DMSO (control) and a range of filipin concentrations in presence of LacCer. Similar to dynamin inhibition, cell adhesion to glass-bottom dishes was significantly compromised in the presence of filipin (data not shown); for this reason, 0.1mg/ml collagen I coated dishes were used in order to enhance cell adhesion. To ensure that all the replicates followed a similar trend, the data was normalised. The range of tested concentrations significantly diminished the uptake of LacCer. 2.5µg/ml and 3.75µg/ml Filipin respectively decreased ~ 60% and 65% LacCer internalisation (see [Figure 3-3](#) and [Table S1-3](#)). Remarkably, 5µg/ml Filipin reduced LacCer uptake by 80% ([Figure 3-3](#) and [Table S1-3](#)). These experiments hence suggest that 3.75µg/ml and 5µg/ml Filipin are the optimum minimal concentrations to assess the role of caveolae-mediated endocytosis in ECM uptake.

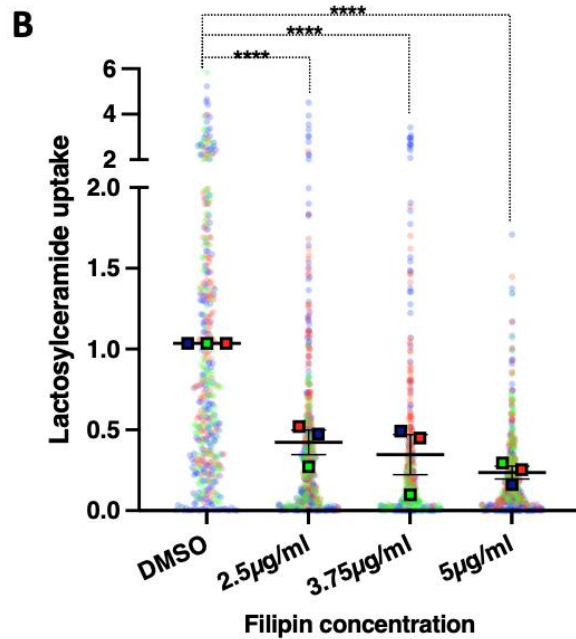
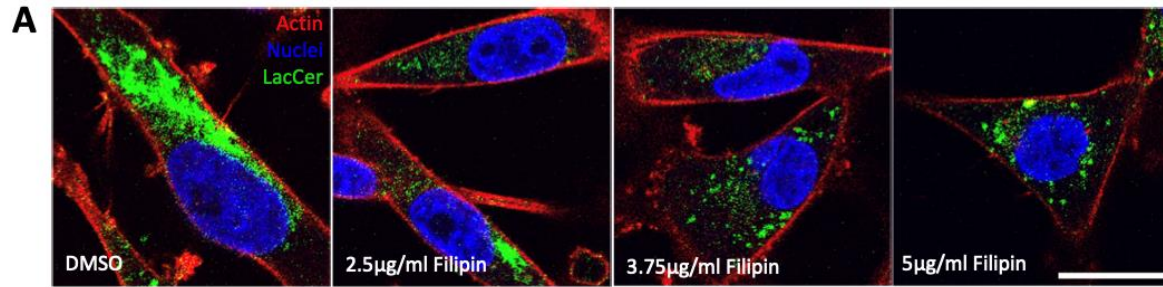


Figure 3-3. Filipin treatment diminishes LacCer internalisation in MDA-MB-231 cells. 3×10^5 MDA-MB-231 cells were seeded on 35mm glass-bottom dishes coated with 0.1mg/ml collagen I for 6h. Cells were then pre-treated with DMSO (vehicle), 2.5µg/ml, 3.75µg/ml and 5µg/ml Filipin for 30min; media was then aspirated and cells were further incubated for 10min on ice with ice-cold 0.5µM Lactosylceramide-GFP (LacCer; green) media, which additionally contained either DMSO (vehicle), 2.5µg/ml, 3.75µg/ml or 5µg/ml Filipin. The dishes were later incubated for 90 seconds at 37°C. Phalloidin Alexa 555 was used to label the actin cytoskeleton (red) and Vectashield mounting medium with DAPI for the nuclei (blue) staining. Imaging with a 60X objective Nikon A1 confocal microscope was followed by Image J analysis. Scale bar, 20µm. The scatter plot shows the normalised cell level data together with the mean and SEM from N= 3 independent experiments (blue, red, green); **** $p < 0.0001$; Kruskal-Wallis test.

3.2.3. Rhodamine-dextran endocytosis is reduced upon EIPA treatment in MDA-MB-231 cells

To assess the minimum inhibitory concentration required to block macropinocytosis in invasive breast cancer, MDA-MB-231 cells were incubated with 0.2mg/ml 70kDa Rhodamine-dextran and treated with the vehicle (DMSO) and three different concentrations of EIPA. Similar to dynasore, MiTMAB and filipin treated cells, glass bottom plates were coated with 0.1mg/ml collagen I to ensure cells were adhered and spread. Preliminary experiments showed that 30 minute incubation with dextran resulted in just a few dextran macropinosomes per cell (data not shown). Therefore, incubation time was increased to 60 minutes to boost accumulation of dextran inside the cells; this enabled us to better evaluate changes upon macropinocytosis when cells were treated with EIPA. The three tested concentrations significantly impinged on macropinocytosis. While 35 μ M and 50 μ M EIPA diminished rhodamine-dextran uptake by 70%, 25 μ M EIPA just reduced macropinocytosis by 50% ([Figure 3-4](#)). DMSO-treated cells displayed enlarged vesicles that corresponded to macropinosomes. It is noteworthy to mention that increasing concentrations of EIPA seemed to have an effect on macropinosome size as seen in [Figure 3-4A](#). The effect on macropinosome size suggests that EIPA concentration may have a distinct impact on bulk fluid phase cargoes depending on its molecular weight. This data indicates that 25 μ M and 35 μ M EIPA may be appropriate concentrations to continue studying the contribution of macropinocytosis in internalisation of ECM in invasive breast cancer.

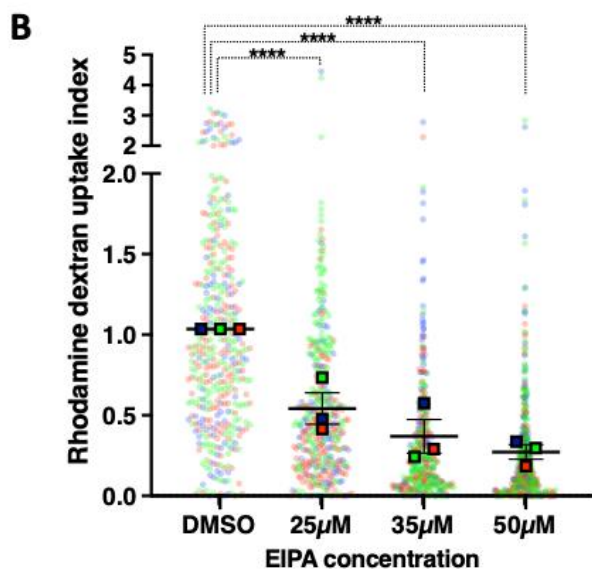
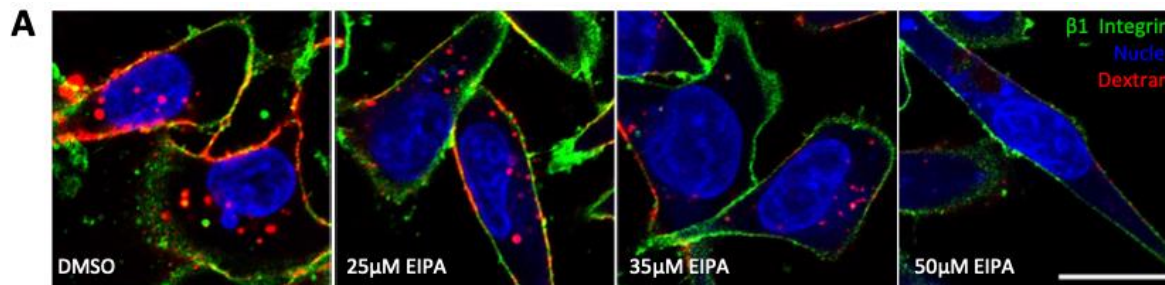


Figure 3-4. EIPA blocks Rhodamine-dextran internalisation in MDA-MB-231 cells. 3×10^5 MDA-MB-231 cells were seeded on 35mm glass-bottom dishes coated with 0.1mg/ml collagen I for 6h. Cells were then pre-treated with DMSO (vehicle), 25µM, 35µM and 50µM EIPA for 30min. Following pre-treatment, cells were incubated in the presence of 0.2mg/ml Rhodamine-dextran (red) for another 60min. Cells were then fixed and stained with an antibody against $\beta 1$ -integrin to visualise the PM (green) and the nuclei (blue). Cell imaging was carried out with a 60X objective Nikon A1 confocal microscope. Image J was used to analyse the dextran uptake index. Scale bar, 20µm. The scatter plot shows the cell-level data and mean values \pm SEM from N=3 independent experiments; **** $p < 0.0001$; Kruskal-Wallis test.

3.2.4. Matrigel and collagen I coating in 384 high content imaging plates

To determine the optimal coating conditions, different ECM concentrations, polymerisation time, temperature and different ECM volumes were tested. In order to assess ECM homogeneity across the well, different parameters were calculated. The first way to address this was to calculate the dispersion of the mean intensity values across the different fields per well, a parameter known as coefficient of variation (CV). Based on preliminary optimisation, for commercially available ECM preparations, highly homogeneous matrices would display CV values around between 13 to 20. The CV for fairly organised matrices would range from 20 to 30, while non-homogenous or highly disorganised matrices would score a CV higher than 50. On the one hand, matrigel is a BM-like commercial ECM and its polymerisation results in a sheet-like homogeneous coat on the

well, but it can also polymerise in aggregates. On the other hand, rat-tail collagen I is a fibrillar commercial ECM. Because of the two different observed morphologies, we included two additional parameters, number of particles and their total area, to have a better idea of how these matrices were polymerised. The number of particles was particularly useful to assess the number of aggregates in matrigel, while the particle area seemed to reflect the collagen porosity and density of the fibres. Taking into consideration all these parameters, matrigel seemed more homogeneous when polymerised between 15 to 150min at room temperature (data not shown). These conditions significantly reduced the matrigel aggregates, which in turn showed that the matrices were more homogeneous and had a lower CV. For collagen, overnight polymerisation at 37 degrees seemed to generate less fragile matrices and enabled better liquid handling. Another important parameter to optimise was the volume of ECM used per well. Matrigel coating was achieved with 2ul per well, however the fibrillar morphology of collagen I required 15ul per well to be assembled into fibrils (data not shown). Once the polymerisation time, temperature and volume were established for each ECM, we aimed to assess which concentration would further improve the coating conditions. For matrigel, four different concentrations were tested. Overall, it looked like all the matrices were homogeneous (see [Figure 3-5A](#)), however it was noticeable that matrigel was more variable at higher concentrations and displayed a higher number of aggregates. This was reflected by a higher CV and higher particle number (see [Figure 3-5B](#)), being 1mg/ml the one with highest values. To validate that reduced matrigel concentration resulted in more homogeneity, that is to say show lower CV, we assessed 0.1mg/ml matrigel. Although the CV was higher in 0.3mg/ml and 0.5mg/ml compared to 0.1mg/ml, the number of particles was lower in the former ([Figure 3-5C](#)). The high variability we observed among technical replicates may reflect that 0.1mg/ml may not be distributed equally between the different wells. This suggested that 0.3mg/ml and 0.5mg/ml were potentially the best conditions to perform an assay in high throughput. The area of those particles was very similar across the different concentrations ([Figure 3-5D](#)), this suggested that the different concentrations resulted in similar coating on the surface of the well.

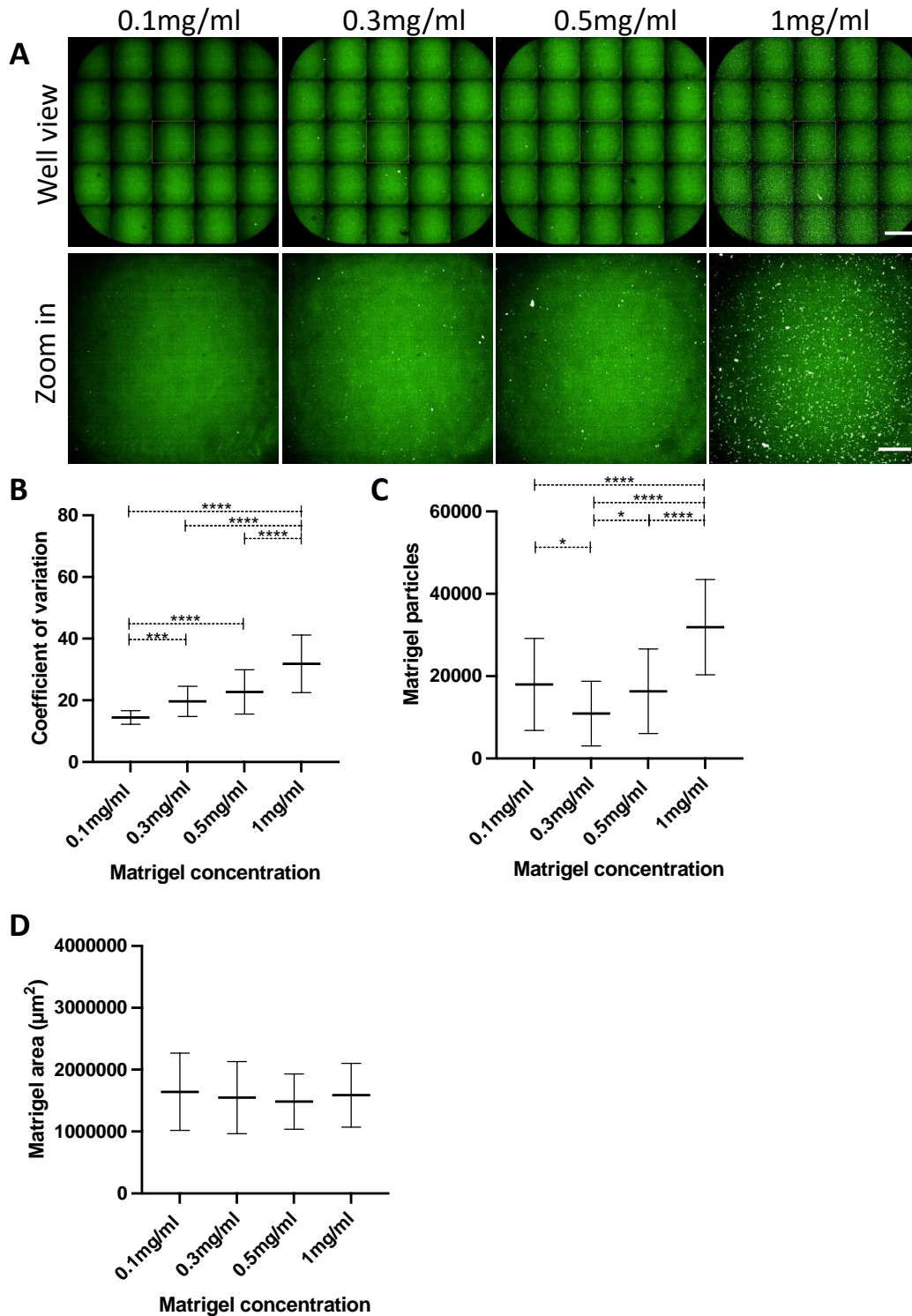


Figure 3-5. Generating matrigel matrices in high content imaging plates. (A-D) Matrigel coating in 384 well plates. 50ul ice-cold PBS was added in each well, afterwards 2ul of 0.1mg/ml, 0.3mg/ml, 0.5mg/ml and 1mg/ml matrigel was spiked in each PBS well. The plates were centrifuged at 500rpm for a few seconds and kept for 8 min at 4 degrees. Matrigel was polymerised for 15 min at RT. Plates were then stained with 10 $\mu\text{g}/\text{ml}$ NHS-fluorescein (green) and imaged with a 20X air objective Opera Phenix microscope. Columbus software was used for analysis. Scale bar: well view (stitched images): 400 μm ; zoom in: 100 μm . Values are mean well data + SD of forty to seventy well replicates from at least three independent experiments; * $p \leq 0.0189$, *** $p=0.0001$, **** $p<0.0001$; Kruskal-Wallis test.

For collagen I, we assessed two different concentrations 0.5mg/ml and 1mg/ml. No difference was observed when calculating the CV nor the particle number ([Figure 3-6](#)). This may be due to the fibrillar nature of collagen, which may be similar regardless of the concentration used in high throughput. However, the area of the fibres was higher in 1mg/ml compared to 0.5mg/ml ([Figure 3-7B](#)), this reflects the dense network and smaller fibres in higher concentrations.

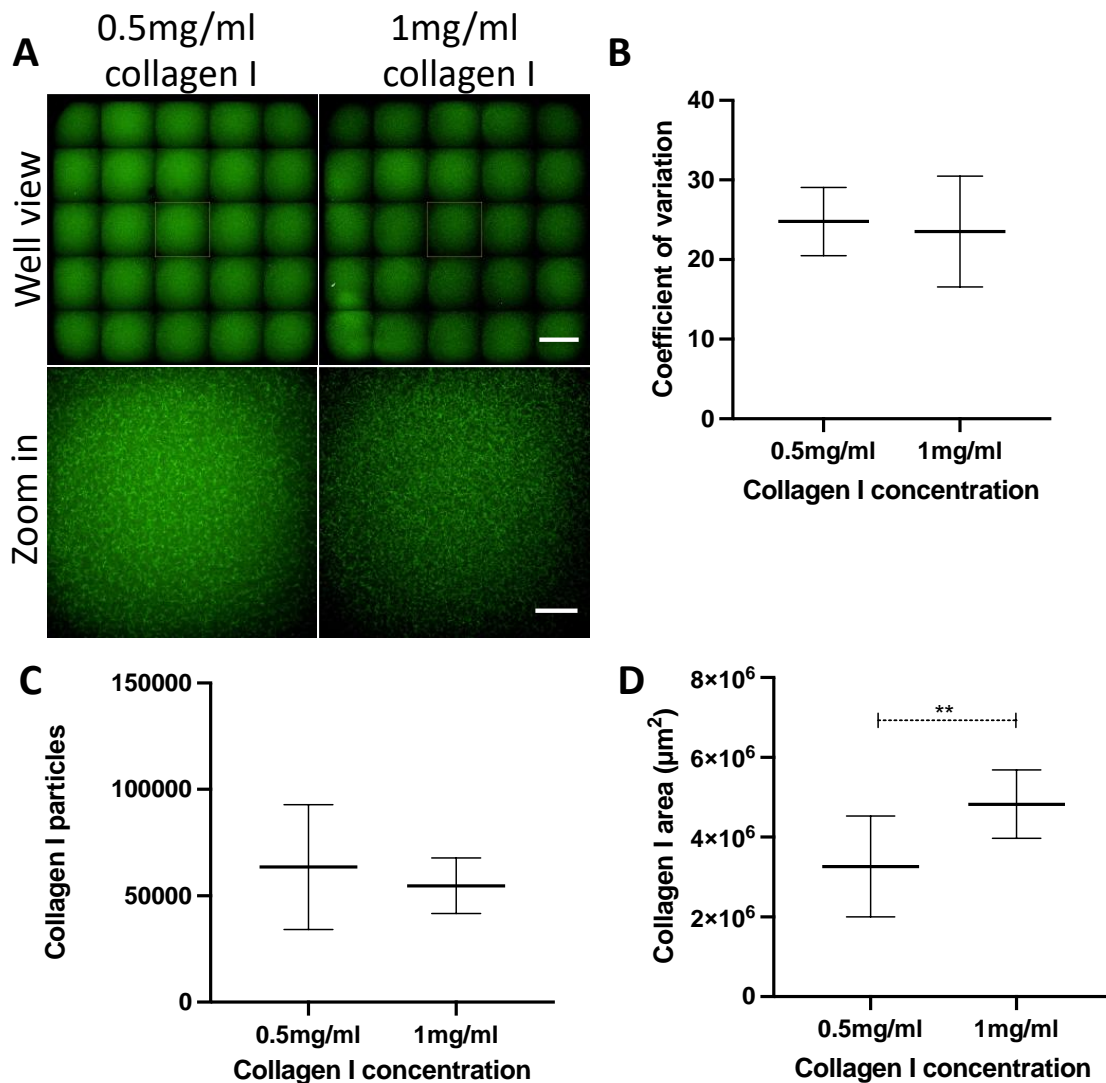


Figure 3-6. Generating Collagen I matrices in high content imaging plates. (A-D) Collagen I coating in 384 well plates. 50ul ice-cold PBS was added in each well, afterwards 15 μ l of 0.5mg/ml and 1mg/ml collagen I (green) was spiked in each PBS well. The plates were centrifuged at 500rpm for a few seconds and kept for 8 min at 4 degrees. Collagen I was polymerised for 1h15 min at 37°CRT. Plates were then stained with 10 μ g/ml NHS-fluorescein and imaged with a 20X air objective Opera Phenix microscope. Scale bar: well view (stitched images): 400 μ m; zoom in: 100 μ m. Columbus software was used for analysis. Values are mean well data + SD of forty to seventy well replicates from at least three independent experiments; * $p \leq 0.0189$, *** $p=0.0001$, **** $p<0.0001$; Kruskal-Wallis test.

In spite of the increasing evidence on the role of ECM in disease; under certain conditions, commercial ECMs fail to recapitulate the in-vivo microenvironment (Rubí-Sans *et al.*, 2021). As a result, the usage of CDMs has emerged as a great tool to reproduce the stroma of tissues or a fibrotic microenvironment (Rubí-Sans *et al.*, 2021). We assessed whether high throughput production of CDM was feasible and its variability in terms of technical and biological reproducibility. The generated matrices were highly fibrillar ([Figure 3-6A](#)), probably due to the high levels of fibronectin and collagen I. Although the variability between technical and batch/biological replicates was minimal, the CV from these matrices was almost thrice as much compared to collagen I. The high CV levels may be on account of the fibrillar nature of CDMs, in addition to its variability based on its generation by fibroblasts. Despite this, variability between batches was minimal and only a small, but significant, difference was seen between Batch 2 and 3 ([Figure 3-7B](#)). Taking everything into account, additional and complementary experiments from a biological perspective may further discern which condition is optimal to assess ECM uptake in high throughput.

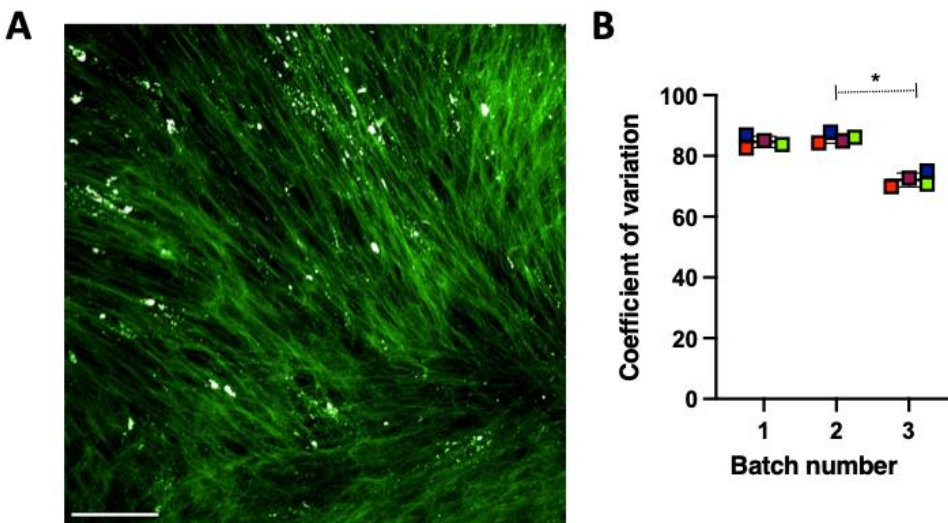


Figure 3-7. Generating cell-derived matrices in high content imaging plates. (A-B) CDMs (green) were generated as previously described in (Kaukonen *et al.*, 2017). Plates were incubated with 50 μ l pre-warmed gelatin at 37 $^{\circ}$ for 1h. Plates were then washed twice and crosslinked with 1% glutaraldehyde for 30min at room temperature. Plates were washed twice and quenched with 1M glycine. 3000 TIFs per well were added in a final volume of 50 μ l. Cell media was changed every other day with complete media containing 50 μ g/ml ascorbic acid. After 7 days, cells were extracted with 20mM NH $_4$ OH and 0.5% Triton X-100 in PBS $^{++}$. Plates were washed twice with PBS $^{++}$ and DNA was digested with 15 μ g/ml DN-25 (DNase). Plates were kept at 4 $^{\circ}$ for storage. Prior to imaging, CDMs were labelled with 10 μ g/ml NHS-fluorescein and imaged with a 20X air objective Opera Phenix microscope. Columbus software was used for analysis. Scale bar, 100 μ m. Values are mean well data + SD of four well replicates per batch; * p = 0.0243; Kruskal-Wallis test.

3.2.5. Optimisation of ECM internalisation in 384 high content imaging plates

At this point, we aimed to see if we could detect ECM uptake from the generated matrices. We took advantage of a pH sensitive dye, pHrodo iFL Red STP ester (from now on pHrodo-red). This pH-dependent fluorescence resides in the protonation of pHrodo-red molecules in low pH environments, such as in late endosomes and lysosomes. This guarantees minimum background fluorescence from the thin ECM layer underneath MDA-MB-231 cells. So that we could determine differences in ECM uptake, we quantified endocytosis using an approach described for Dextran macropinocytosis (Commisso, Flinn and Bar-Sagi, 2014). This quantification consists of a percentage ratio between the internalised ECM area versus cell area. We referred to this ratio as the ECM uptake index. Of note, preliminary data suggested that cell permeabilisation significantly impaired visualisation of pHrodo-labelled matrigel ([Figure S1-2](#)), as a result samples were not permeabilised to assess uptake in following experiments. We then aimed to determine the minimum concentration that allowed quantification of ECM uptake. Three different pHrodo concentrations were assessed for optimal visualisation of endocytosed matrigel. More specifically, 20µg/ml, 10µg/ml and 6.7µg/ml were picked based on previous optimisation using non-pH sensitive dyes, including NHS-fluorescein, NHS-Alexa fluor 647 and 555. While the three concentrations enabled visualisation of pHrodo-labelled matrigel inside the cells, higher concentrations, such as 10µg/ml and 20µg/ml, displayed better results ([Figure 3-8](#)). Indeed, the ECM uptake index in 20µg/ml pHrodo was respectively 45% and 70% higher than 10µg/ml and 6.7µg/ml pHrodo. These results are in agreement with preliminary optimisation, in which the uptake is approximately 50% more in 40µg/ml pHrodo compared to 20µg/ml ([Figure S1-2](#)). Despite this, 40µg/ml showed higher extracellular background and particles ([Figure S1-2](#)). Overall, 20µg/ml pHrodo enabled the highest visualisation of ECM inside the cell, with minimal extracellular background. It was thus selected for additional optimisation experiments.

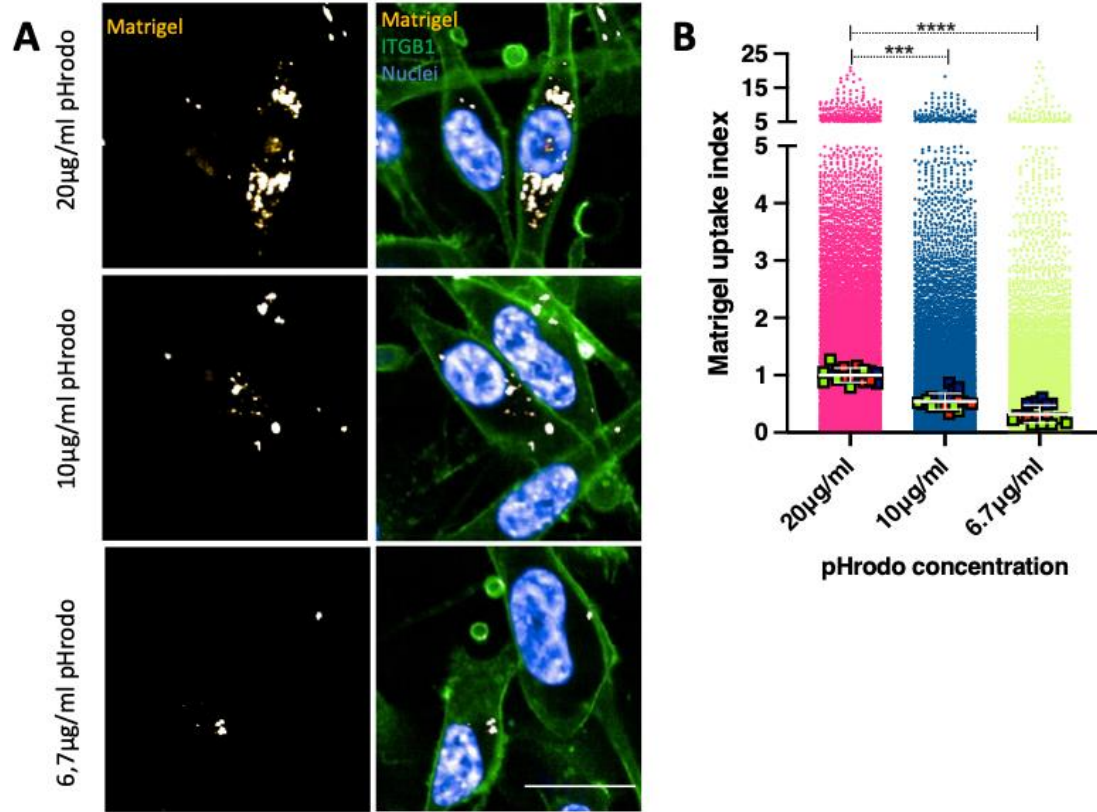


Figure 3-8. Fluorescence of endocytosed ECM is dependent on pHrodo concentration. 384-well plates were coated as previously described. 50 µl ice cold PBS was added into each well and 2 µl 0.5mg/ml matrigel (golden) was spiked in. Plates were centrifuged at 500rpm and kept at 4° for 10min. Plates were then polymerised for 15min at room temperature and labelled with 20 µg/ml, 10 µg/ml and 6.7 µg/ml pHrodo. 10.000 cells were seeded and cultured for 4h before fixation. Cells were stained with hoechst (blue) and β 1-integrin (ITGB1; green). 60X water-immersion objective Opera Phenix microscope was used for imaging. Scale bar, 20 µm. Cell data analysis was performed with Columbus software. Values represented are cell data (dots) and well data (squares) + SD from three independent experiments; mean data was used for the statistical test; *** $p=0.0002$ **** $p<0.0001$; Kruskal-Wallis test.

MDA-MB-231 cells internalise ECM in a concentration-dependent manner. MDA-MB-231 cells display more and bigger vesicles containing matrigel and collagen I when seeded on high concentration ECM preparations (Rainero, unpublished). We thus aimed to recapitulate this with the established method in this chapter. No significant differences in matrigel uptake index were detected between 0.3mg/ml and 0.5mg/ml and between 0.5mg/ml and 1mg/ml matrigel ([Figure 3-9A,B](#)). Notwithstanding that, 0.3mg/ml matrigel showed a small, but statistically significant, decrease (10%) in uptake compared to 1mg/ml matrigel ([Figure 3-9A,B](#)). Taking everything into account, 0.5mg/ml matrigel was picked for future work. In the first place, no significant differences in uptake were seen compared to 1mg/ml matrigel. In the second, 0.5mg/ml matrigel displayed less aggregates than 1mg/ml, thus being the highest concentration that allowed a homogeneous and reproducible coating ([Figure 3-5](#)).

Polymerisation with 1mg/ml collagen I was less reproducible to use in a high content screen. Some wells in 1mg/ml collagen I over-polymerised and formed a thick 3D gel that impeded imaging of the cells (therefore, the quantification of one replicate is missing for 1mg/ml collagen I, see [Figure 3-9D](#)). However, taking into account the analysed replicates, no difference in collagen I uptake index was observed. As a result, 0.5mg/ml collagen I was chosen to ensure reproducibility in high throughput.

Altogether, this data suggests that under the coating settings established above, matrigel and collagen I uptake did not depend on the concentration used, which may indicate that polymerisation using this density-gradient method differs from the conventional approach.

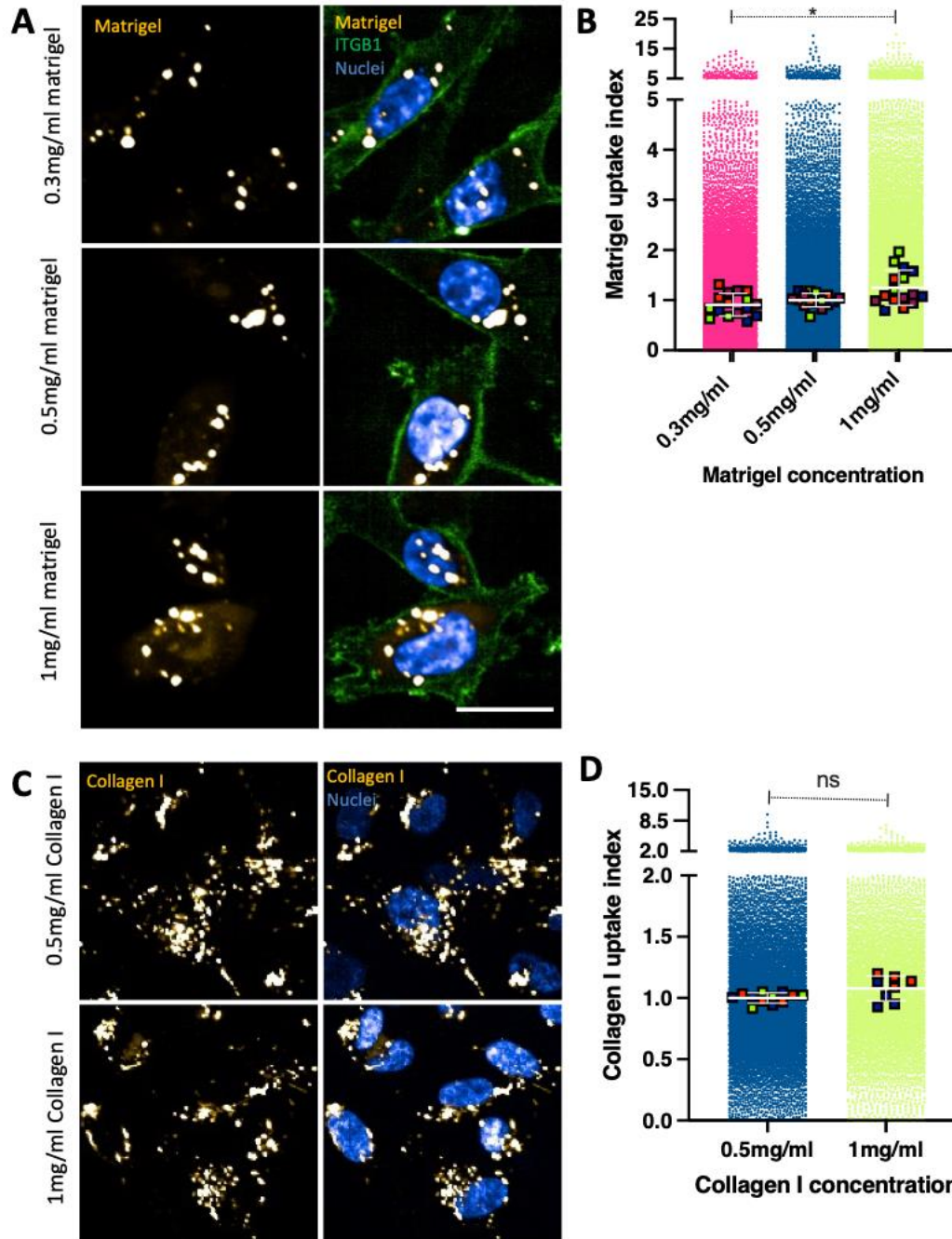


Figure 3-9. ECM internalisation is independent of collagen I and matrigel concentration in high throughput systems. 50 μ l ice cold PBS was added into each well. For matrigel coating (A-B): 2 μ l 1mg/ml, 0.5mg/ml or 0.3mg/ml matrigel (golden) was spiked in. For collagen I coating (C-D): 15 μ l 1mg/ml or 0.5mg/ml collagen I (golden) was added per well. Plates were centrifuged at 500rpm and kept at 4 $^{\circ}$ for 10min. Matrigel plates were then polymerised for 15min at room temperature; collagen I was polymerised at 37 $^{\circ}$ C overnight. Both matrices were labelled with 20 μ g/ml pHrodo. 10.000 cells were cultured for 6h prior to fixation with 4% PFA for cells cultured on matrigel. Cells seeded on matrigel were stained with hoechst (blue) and β 1-integrin (ITGB1; green). Cells on collagen were stained with hoechst (blue; high intensity signal is white) and imaged live. 60X and 40X water-immersion objectives from Opera Phenix microscope were respectively used for imaging Matrigel and collagen I. Scale bar, 20 μ m. Cell data analysis was performed with Columbus software. Values represented are cell data (dots) and well data (squares) + SD from three independent experiments; well data was used for the statistical test; (B) * p =0.0115; Kruskal-Wallis test. (D) ns (non-significant), Mann-whitney test.

3.2.6. Blocking endo-lysosomal acidification impacts on ECM visualisation

Bafilomycin A1 is a macrolide antibiotic that targets the vacuolar type-ATPase H⁺ (v-ATPase). Treatment with Bafilomycin A1 severely impairs endolysosomal acidification, resulting in lysosomal dysfunction and endocytosed proteins cannot be degraded. Owing to the pH-sensitive nature of pHrodo, if particles were truly internalised, rather than being mere extracellular background, pHrodo-ECM would be highly fluorescent in the most acidic endosomal compartments. We thus sought to corroborate whether bafilomycin A1 treatment would result in a decrease in the ECM uptake index, suggesting that the signal is emitted from intracellular vesicles. Bafilomycin A1 treatment for 6h abolished the intracellular pHrodo red signal for collagen I and TIF-CDM ([Figure 3-10](#)). Indeed, collagen I and TIF-CDM did not display bright endosomes ([Figure 3-10A,C](#)). Under certain circumstances, only few small vesicles were observed upon bafilomycin A1 treatment, however their fluorescence was highly reduced compared to control. Overall, these experiments confirmed that the detected signal is emitted from vesicles with high levels of v-ATPase proton pump activity that result in low pH, rather than being extracellular. This assay is thus reliable for the study of ECM internalisation in high throughput systems with minimal background noise.

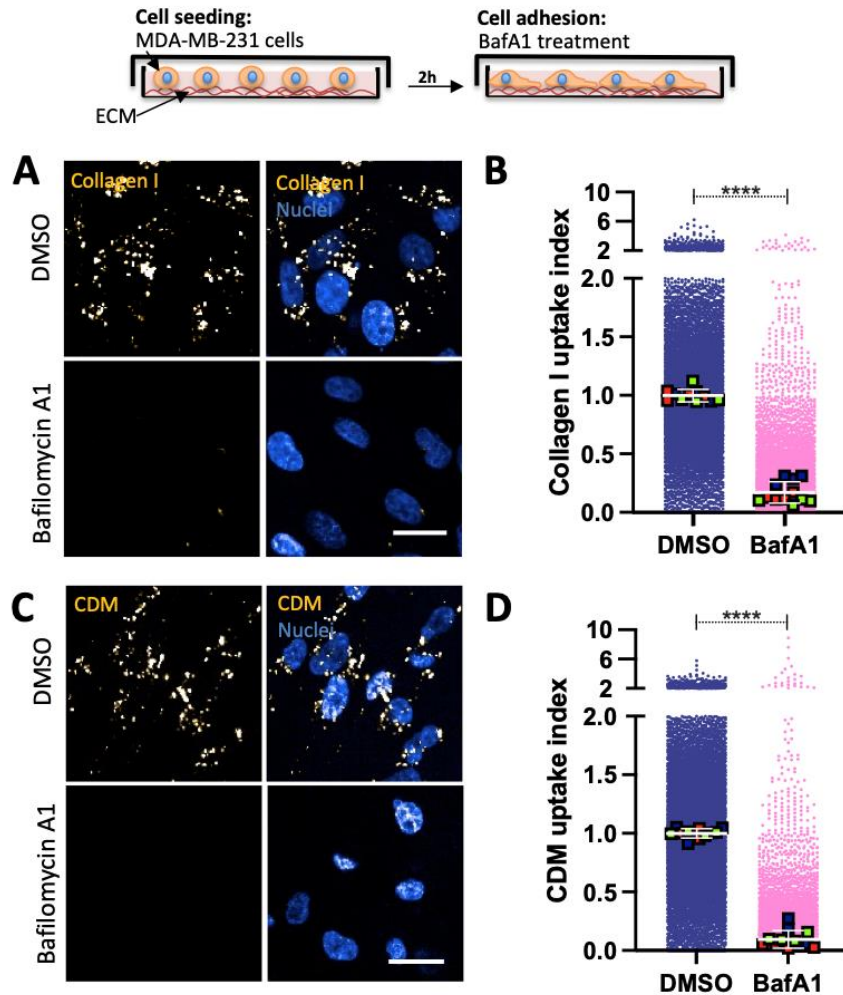


Figure 3-10. Blocking endo-lysosomal acidification impairs visualisation of intracellular pHrodo-labelled ECM. (A-B) 50 μ l ice cold PBS was added into each well. 15 μ l 0.5mg/ml collagen I (golden) was spiked per well. Plates were centrifuged at 500rpm and kept at 4 $^{\circ}$ for 10min. Plates were then polymerised overnight at 37 $^{\circ}$ C and labelled with 20 μ g/ml pHrodo. (C-D) CDMs (golden) were generated by seeding TIFs on crosslinked gelatin. TIFs were allowed to secrete and deposit ECM for 7 days before extraction. CDMs were labelled with 20 μ g/ml pHrodo. 10.000 cells were cultured for 6h in presence of DMSO or 200nM Bafilomycin A1 (BafA1), stained with hoechst (blue) and imaged live. 40X water-immersion objective Opera Phenix microscope was used for imaging. Scale bar, 20 μ m. Cell data analysis was performed with Columbus software. Values represented are cell data (dots) and well data (bigger squares) + SD from three independent experiments; well data was used for the statistical test; ****p<0.0001; Mann-whitney test.

3.2.7. Assessing the role of cysteine cathepsins in lysosomal degradation of ECM proteins

Following endocytosis of the ECM components, breast cancer cells traffic integrin-engaged ECM to the lysosomes (this will be further discussed in Chapter 5), where the internalised components are degraded by cysteine cathepsins. To validate this in this assay, we assessed how E64d, a cell permeable cysteine cathepsin inhibitor, impacted on ECM degradation for a period of 24h. We first tested the effect of E64d on 4 different concentrations of matrigel. Contrary to previous results using the conventional coating method ([see Chapter 5, Figure 5-2](#)), no significant differences in intracellular ECM between control and E64d-treated cells were observed for 0.5mg/ml and 1mg/ml matrigel ([Figure 3-11](#)). Interestingly, for the lower concentrations (0.1mg/ml and 0.3mg/ml) E64d treatment led to increased matrigel uptake index with a respective p-value of 0.0597 and 0.0082 ([Figure 3-11](#)). We have previously shown that endolysosomal acidification plays a key role in this assay. In addition, as receptors and ligands are traffic to other endosomal compartments, the endolysosomal system is acidified. We thus included bafilomycin A1 treatment for 24h as a control of downregulation of matrigel uptake index, but also to confirm that ECM was trafficked to acidified endosomes or lysosomes regardless of the matrix concentration. Indeed, bafilomycin A1 treatment resulted in a significant decrease in the uptake index for 0.1, 0.3 and 0.5mg/ml ([Figure 3-11](#)). Although statistically insignificant, bafilomycin A1 treatment also reduced matrigel uptake index in 1mg/ml matrigel with a p-value of 0.0746 ([Figure 3-11](#)). This data confirmed that ECM was trafficked along the endolysosomal system and suggested that cysteine cathepsins may be responsible for its intracellular degradation.

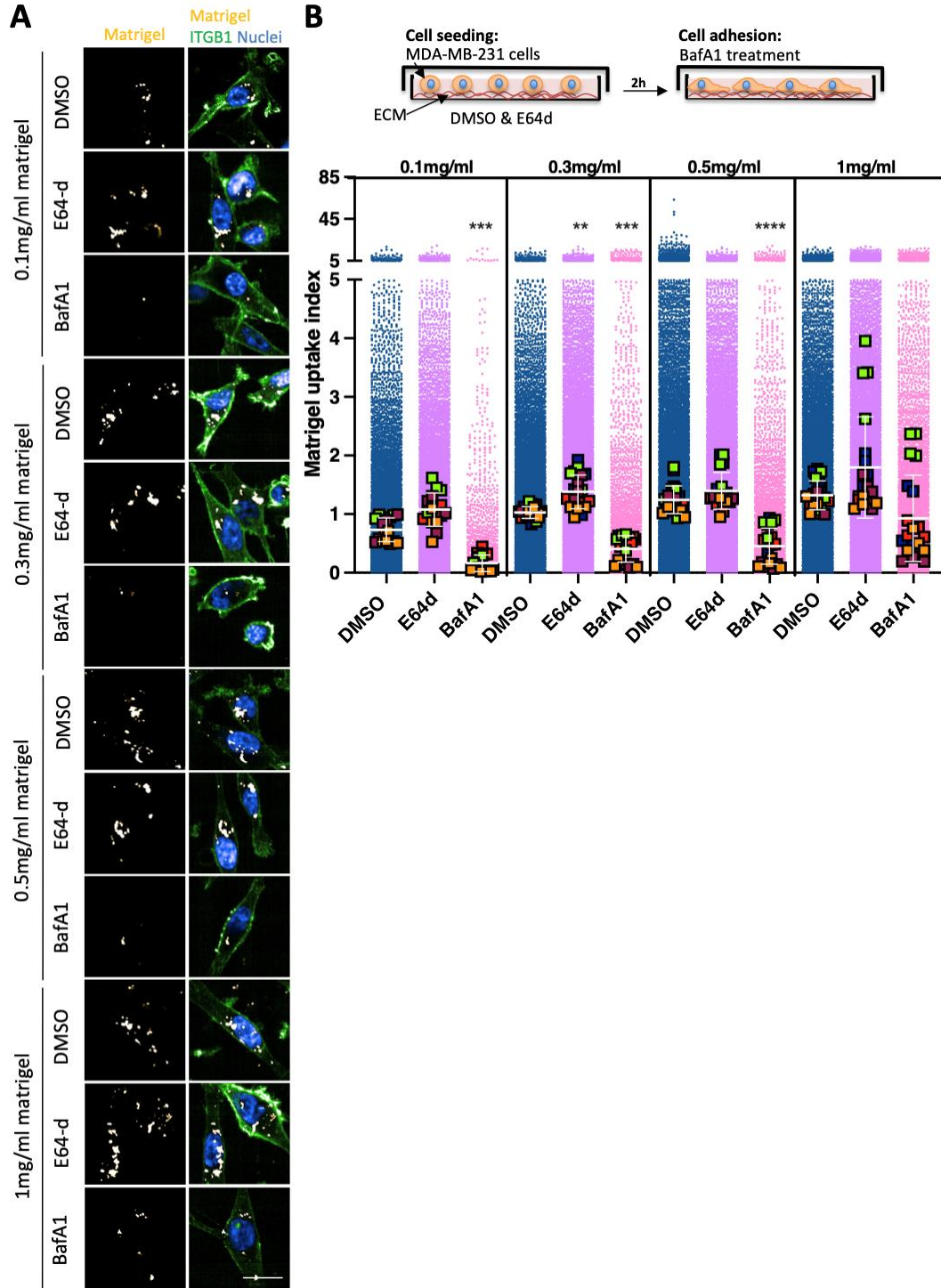


Figure 3-11. Matrigel is trafficked to acidic lysosomes, where cysteine cathepsins mediate its degradation. 50 μ l ice cold PBS was added into each well. 2 μ l of the indicated matrigel (golden) concentrations were spiked in. Plates were centrifuged at 500rpm and kept at 4 $^{\circ}$ for 10min. Matrigel plates were then polymerised for 15min at room temperature and labelled with 20 μ g/ml pHrodo. 10,000 cells were cultured for 24h prior to fixation with 4% PFA. Cells were stained with hoechst (blue; high intensity signal is white) and β 1-integrin (ITGB1; green). Imaging was performed by a 60X water-immersion objective Opera Phenix microscope. Scale bar: 20 μ m. Cell data was analysed with Columbus software. Values represented are cell data (dots) and well data (squares) + SD from at least N=4 independent experiments; well data used for statistical test; **p=0.0082, ***p<0.0003, ****p<0.0001; Kruskal-Wallis test.

To further corroborate these results, we seeded MDA-MB-231 cells on collagen I and CDM for 24h in presence of E64d. Following this time, we assessed collagen I and CDM internalisation using live imaging to avoid any effect fixation with 4% PFA could have on endosomal pH. Since the effect of E64d in intracellular degradation depended on matrigel concentration, two different collagen I concentrations were tested. Similar to previously shown optimisation data, no significant differences in intracellular ECM were seen between concentrations nor in the presence of E64d ([Figure 3-12](#)). On the contrary, CDM uptake index in presence of E64d did not result in intracellular accumulation of CDM, but resulted in a minor decrease ([Figure 3-12C,D](#)). However, it was clear that the morphological properties of the endosomes highly differed. Control cells displayed small dotted vesicles across the whole cytoplasm, while E64d treated cells presented big blobs ([Figure 3-12](#)). This suggested that E64d had an effect at the intracellular level, suggesting that the endocytosed matrix accumulated in enlarged vesicles ([Figure 3-12](#)). To better understand if these changes were occurring for matrigel, we recapitulated the conditions using live imaging for 0.5mg/ml matrigel. As in [Figure 3-11](#), E64d had no effect on matrigel uptake index ([Figure 3-12](#)), suggesting that the effect previously observed was not due to cell fixation. However, live imaging enabled better visualisation of the small vesicles containing matrigel in the control group, while enlarged endosomes were displayed upon E64d treatment ([Figure 3-12E](#)). Altogether, this data suggests that the ECM is internalised and transported through the endolysosomal system, however no clear conclusions can be drawn regarding the role of cysteine cathepsins in ECM degradation in the lysosomes using this assay.

3.2.8. MDA-MB-231 cells converge in macropinocytosis to internalise the diverse ECM components

To have a better understanding of the endocytic pathways governing ECM internalisation in breast cancer, we assessed how pharmacological inhibition of endocytosis impinged on matrigel, collagen and TIF-CDM uptake. Four different inhibitors, dynasore, MiTMAB, filipin and EIPA were used. MiTMAB induced changes in cell morphology during the 6h of treatment; in fact, cells were rounded and with a high number of membrane blebs. It was thus discarded from the analysis to circumvent off target effects or toxicity induced by dynamin inhibition (data not shown). 20 μ M dynasore only reduced matrigel uptake by an insignificant 15% ([Figure 3-13](#)). Conversely, treatment with 40 μ M dynasore impinged matrigel internalisation by 45% ([Figure 3-13](#)). Likewise, 5 μ g/ml filipin almost halved (~45% reduction) matrigel internalisation. However, no effect was observed in the presence of 3.75 μ g/ml filipin. Given the effect of dynasore and filipin in matrigel uptake, we sought to unravel whether filipin and dynasore were cooperating in the same endocytic pathway. To avoid cellular toxicity, MDA-MB-231 cells were cultured in presence of 20 μ M dynasore and 3.75 μ g/ml filipin. Interestingly, while these two concentrations alone had a minimum effect on matrigel internalisation, the combination significantly reduced matrigel internalisation by approximately 40% ([Figure 3-13](#) and [Figure 3-16](#)). This data suggests that filipin and dynasore are not cooperating within the same pathway, but participate in distinct separate pathways. In addition, incubation with 25 μ M and 35 μ M EIPA decreased matrigel internalisation 40% and 50%, respectively ([Figure 3-13](#)). Collectively, this data suggests that matrigel is internalised via multiple endocytic pathways.

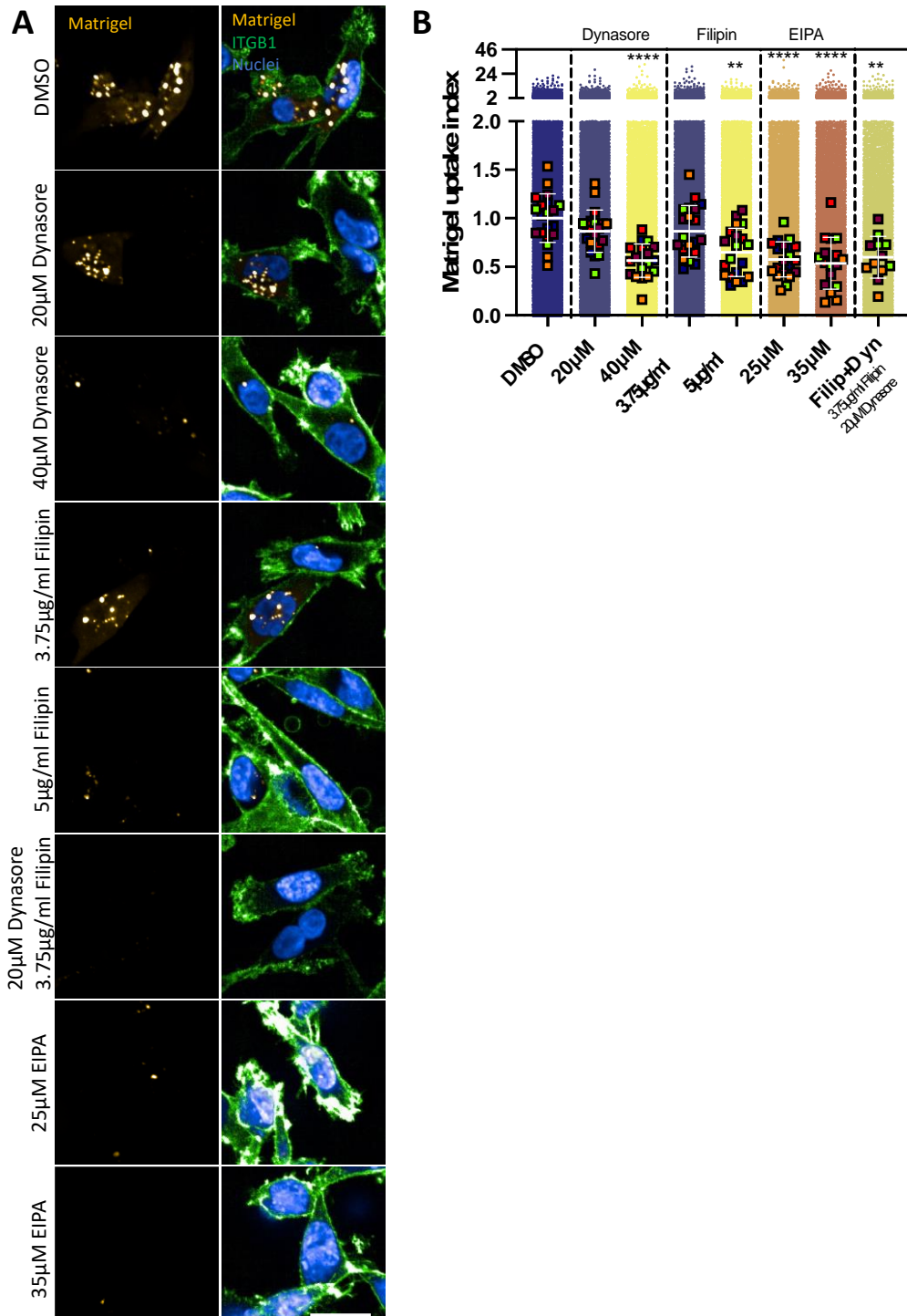


Figure 3-13. Dynasore, filipin and EIPA reduce matrigel internalisation. 50µl ice cold PBS was added into each well. 2µl 0.5mg/ml matrigel was spiked in. Plates were centrifuged at 500rpm and kept at 4°C for 10min. Matrigel (golden) plates were then polymerised for 15min at room temperature and labelled with 20µg/ml pHrodo. 10.000 cells were cultured for 6h in the presence of the indicated inhibitors prior to fixation with 4% PFA. Cells were stained with hoechst (blue; high intensity signal is white) and β1-integrin (ITGB1; green). Imaging was performed by a 60X water-immersion objective Opera Phenix microscope. Scale bar:20µm. Cell data analysis was performed with Columbus software. Values represented are cell data (dots) and well data (squares) + SD from at least four independent experiments; well data was used for the statistical test; **p=0.0012, ***p=0.0009, ****p<0.0001; Kruskal-Wallis test.

Collagen I internalisation was reduced approximately 40% in presence of 25 μ M and 35 μ M EIPA ([Figure 3-14](#)). Neither 20 μ M and 40 μ M dynasore nor 3.75 μ g/ml and 5 μ g/ml decrease internalisation of collagen I ([Figure 3-14](#) and [Figure 3-16](#)). We have previously shown that combinatory treatment of 20 μ M dynasore and 3.75 μ g/ml filipin further decreases matrigel internalisation compared to dynasore and filipin alone ([Figure 3-13](#)). To ensure this effect was not due to toxicity of combining both pharmacological inhibitors, we tested whether collagen I internalisation was reduced with the combinatory treatment. Of note, no effect was observed in collagen I internalisation, agreeing with the results obtained in presence of a single inhibitor ([Figure 3-14](#)). Altogether, this data suggests that collagen I is internalised via macropinocytosis in MDA-MB-231 cells.

We also tested the endocytic inhibitors on TIF-CDM, a complex stromal ECM. 20 μ M and 40 μ M dynasore respectively resulted in a 30% and 40% reduction in TIF-CDM uptake ([Figure 3-15](#)). But similarly to collagen I, neither 3.75 μ g/ml nor 5 μ g/ml filipin decreased internalisation of TIF-CDM ([Figure 3-13](#), [Figure 3-14](#), [Figure 3-15](#) and [Figure 3-16](#)). Again, we aimed to examine whether combining both pharmacological inhibitors had any off-target effect on TIF-CDM uptake. Actually, combinatory inhibition had the same reduction as 20 μ M dynasore only for TIF-CDM ([Figure 3-15](#)). This data suggests that the combination of 20 μ M dynasore and 3.75 μ g/ml filipin do not have an off-target effect on internalisation. Considering the main component of TIF-CDM is collagen I, we aimed to see whether EIPA treatment also diminished TIF-CDM internalisation. In fact, TIF-CDM uptake index was one third compared to the control in presence of the lower concentration (25 μ M). Outstandingly, 35 μ M EIPA completely abolished TIF-CDM internalisation ([Figure 3-15](#)). Overall, TIF-CDM internalisation partially relies on macropinocytosis, as well as dynamin.

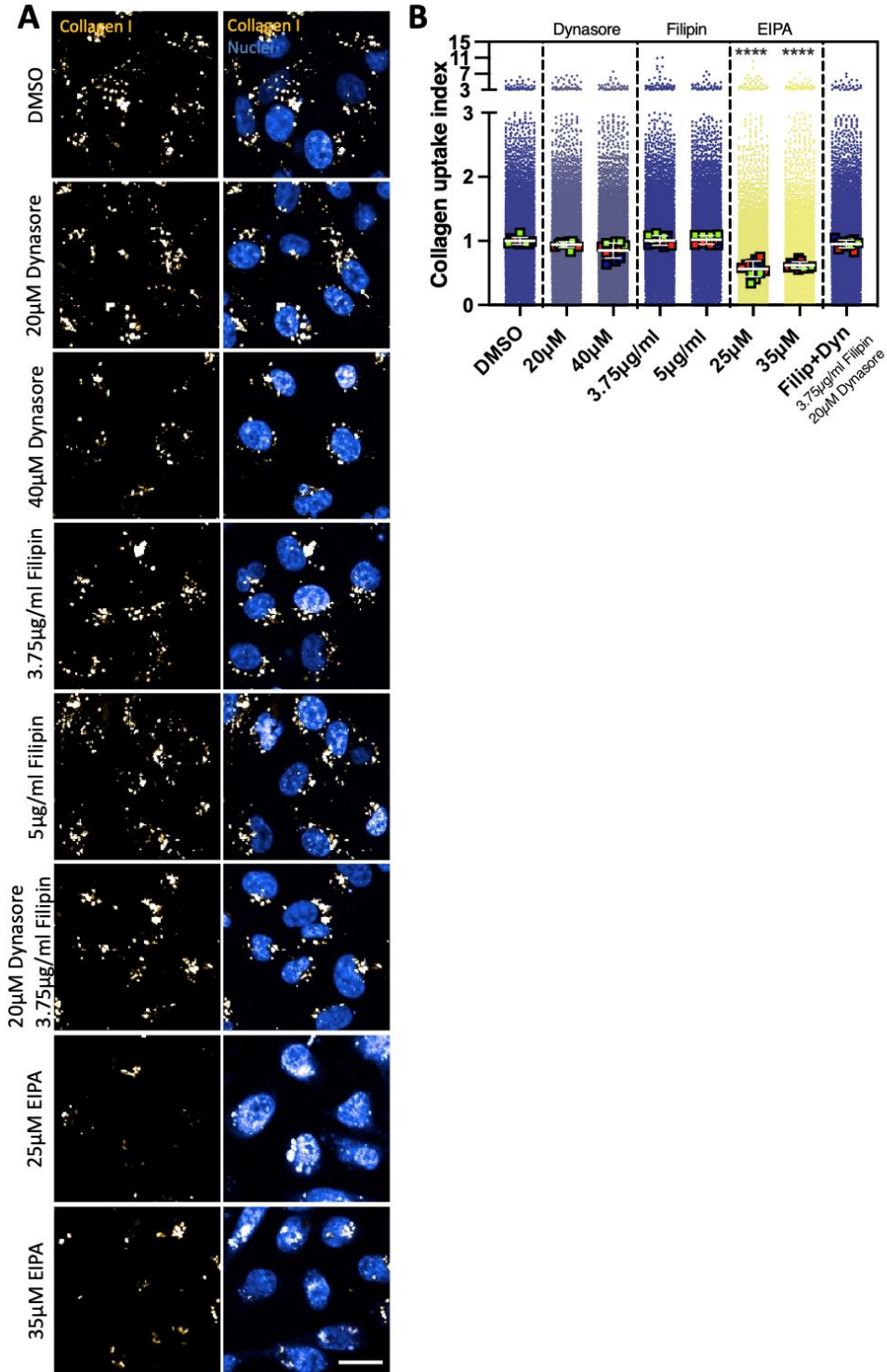


Figure 3-14. Collagen I uptake is inhibited by EIPA in MDA-MB-231 cells. 50 μ l ice cold PBS was added into each well. 15 μ l 0.5mg/ml collagen I (golden) was spiked in. Plates were centrifuged and kept at 4 $^{\circ}$ for 10min. Plates were then polymerised at 37 $^{\circ}$ C overnight and labelled with 20 μ g/ml pHrodo. Cells were cultured for 6h in the presence of the indicated inhibitors and stained with hoechst (blue; high intensity signal is white). Imaging was performed by a 40X water-immersion objective Opera Phenix microscope. Scale bar:20 μ m. Cell data analysis was performed with Columbus software. Values represented are cell data (dots) and well data (squares) + SD from N=3 independent experiments; well data was used for the statistical test; ****p<0.0001; Kruskal-Wallis test.

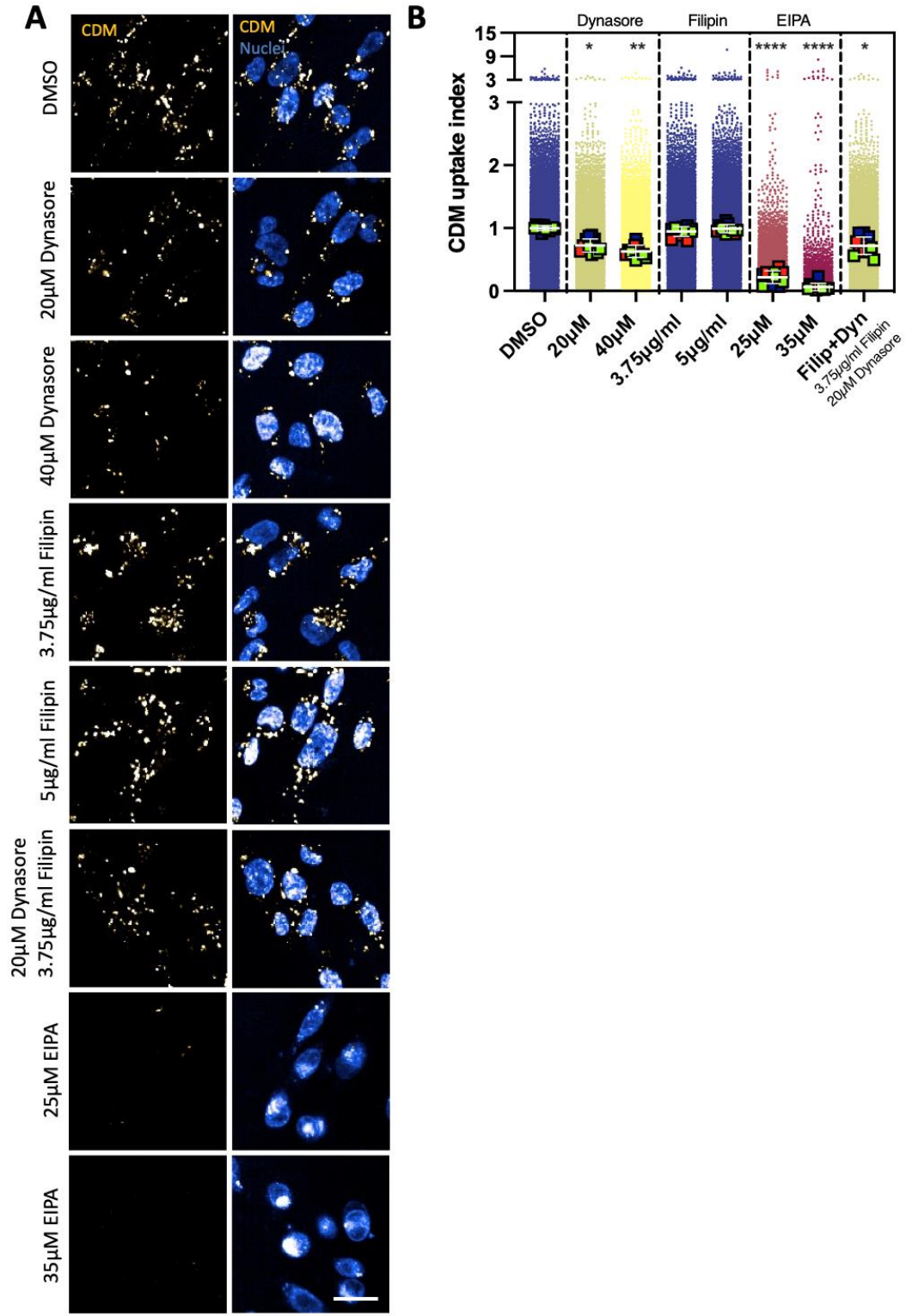


Figure 3-15. TIF-CDM uptake is inhibited by EIPA and Dynasore in MDA-MB-231 cells. CDMs (golden) were labelled with 20µg/ml pHrodo. 10.000 cells were cultured for 6h in the presence of the indicated inhibitors and labelled with hoechst (blue; high intensity signal is white). Imaging was performed by a 40X water-immersion objective Opera Phenix microscope. Scale bar:20µm. Cell data analysis was performed with Columbus software. Values represented are cell data (dots) and well data (squares) + SD from at least four independent experiments; well data was used for the statistical test; * $p \leq 0.0384$, ** $p = 0.0031$, **** $p < 0.0001$; Kruskal-Wallis test.

Taking everything into account, we conclude that inhibiting the GTPase activity of dynamin with dynasore impaired endocytosis of complex matrices, namely matrigel and TIF-CDM ([Figure 3-16](#)). 5 μ M filipin halved matrigel internalisation, however no effect on collagen I and TIF-CDM uptake was observed ([Figure 3-13](#) and [Figure 3-16](#)). The most striking effect on the three different matrices was EIPA treatment. This data demonstrates that breast cancer cells converge in macropinocytosis to internalise the diverse ECM components ([Figure 3-16](#)).

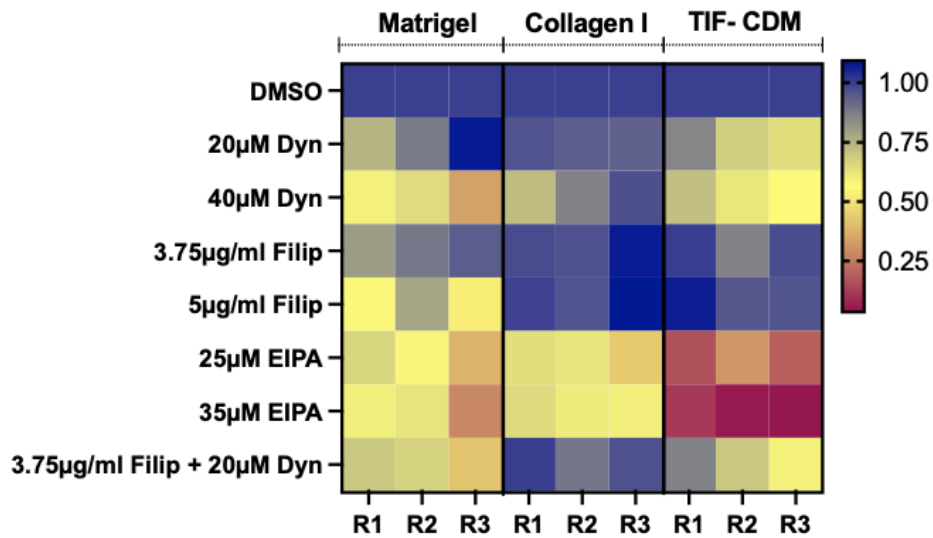


Figure 3-16. The invasive breast cancer cell line MDA-MB-231 converges in macropinocytosis to internalise ECM. For a detailed description see above: Figure 3-13, Figure 3-14 and Figure 3-15.

3.2.9. Optimisation of siRNA-mediated downregulation of target genes

To investigate modulators of ECM internalisation in the invasive breast cancer cell line MDA-MB-231, several endogenous proteins were depleted using siRNA in a 96-well plate format. Two main parameters were optimised to augment knockdown efficiency: seeding number and a non-toxic transfection reagent. We first tested downregulation of Polo-Like Kinase 1 (PLK1), which function is essential for initiating mitosis and it is upregulated in a diverse variety of tumours (de Cárcer *et al.*, 2018). In addition, PLK1 inhibition has been reported to induce apoptosis (Gao *et al.*, 2020), therefore it is a great candidate to easily assess knockdown efficiency in high content screenings. A range of different cell seeding and Dharmafect IV concentrations were assessed in presence of a non-targeting siRNA (siNT) and an siRNA targeting PLK1 (siPLK1). The effect of Dharmafect IV volume on cell number was minimal ([Figure 3-17A](#)). This preliminary optimisation enabled us to select 12.000 cells per well as a starting cell seeding number in a 96-well plate. Similarly, no significant differences in transfection efficiency were observed on the basis of the different cell seeding conditions. In fact, PLK1 down regulation resulted in significant changes in cell number, suggesting that transfection and DICER-mediated siRNA degradation effectively occurred ([Figure 3-17A](#)). Nevertheless, a relatively high proportion of cells remained after transfection with an siRNA against PLK1 compared to the effect observed in other cell lines (Y. C. Tang *et al.*, 2018).

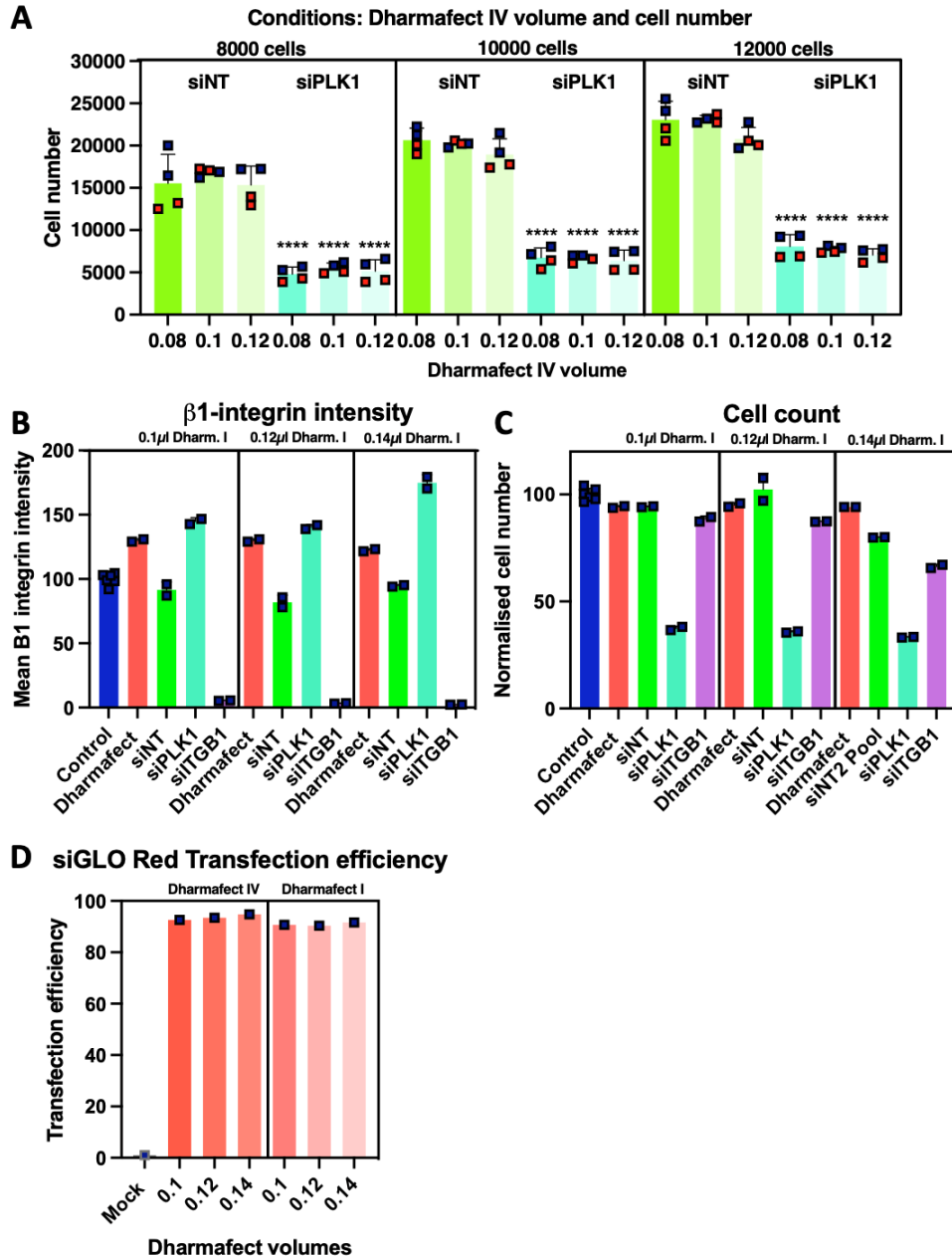


Figure 3-17. Dharmafect IV and I enable transfection and siRNA mediated downregulation of PLK1 and ITGB1 in MDA-MB-231 cells. (A) 5 μ l of 500nM siRNA (siNT and siPLK1) and 5 μ l OptiMEM were added into each well of a 96 well plate. Several volumes of Dharmafect IV 0.08 μ l, 0.1 μ l 0.12 μ l were respectively mixed with 9.92 μ l, 9.9 μ l and 9.88 μ l OptiMEM. These solutions were incubated for 5 minutes. Then 10 μ l was added on top of the 10 μ l siRNA-OptiMEM solution. The siRNA, Dharmafect and OptiMEM mix was incubated for 20min at room temperature in a shaker/rocker. 8000, 10000 and 12000 cells, contained in 80 μ l, were added into each well. Following 72h, cells were fixed and stained with hoechst for the nuclear count. Plots show the well data (squares) from two technical replicates per experiment; N=2 independent experiments; ****p<0.0001; Kruskal-Wallis test. (B-D) 5 μ l of 500nM siRNA (siNT, siPLK1, siITGB1) and 5 μ l OptiMEM were added into each well of a 96 well plate. Several volumes of Dharmafect I or IV 0.1 μ l, 0.12 μ l 0.14 μ l were respectively mixed with 9.9 μ l, 9.88 μ l and 9.86 μ l OptiMEM. These solutions were incubated for 5 minutes. Then 10 μ l was added on top of the 10 μ l siRNA-OptiMEM solution. The siRNA, Dharmafect and OptiMEM mix was incubated for 20min at room temperature in a shaker/rocker. 12000 cells, contained in 80 μ l, were added into each well. Following 72h, cells were fixed and stained with hoechst and ITGB1. All conditions (A-D) were imaged using a 20X (for nuclei counting) and 40X water immersion (for ITGB1 quantification) objective from Opera Phenix high content screening microscope. Plots show the well data (squares) from two technical replicates for B and C, one technical replicate for D; N=1 experiment.

Horizon discovery (Dharmacon) recommends using Dharmafect IV for MDA-MB-231 cells; however other transfection reagents, such as Dharmafect I, have been used to successfully downregulate protein expression in these cells. To assess whether Dharmafect I or Dharmafect IV showed better modulation of siRNA-mediated knockdown, three different Dharmafect I and Dharmafect IV volumes were tested ([Figure 3-17B-D](#) and [Figure 3-18](#)). MDA-MB-231 cells were transfected with an siRNA against PLK1 and β 1-integrin (ITGB1). No significant differences were observed regarding cell number (to assess cell toxicity) or the performance of siRNA-mediated downregulation of protein expression with either Dharmafect reagent ([Figure 3-17B-D](#) and [Figure 3-18](#)). In agreement with preliminary optimisation, PLK1 downregulation only reduced cell number by 50% ([Figure 3-17C](#) and [Figure 3-18C](#)). Nonetheless, cells displayed a clear phenotypic response. PLK1-transfected cells were enlarged and flat, characteristic traits of senescent cells. In agreement with these observations, PLK1 inhibition or downregulation was shown to induce senescence in a panel of cell lines (Driscoll *et al.*, 2014). Of note, siRNA-mediated downregulation of β 1-integrin resulted in around 97% knockdown efficiency using Dharmafect IV and 95% using Dharmafect I ([Figure 3-17B](#) and [Figure 3-18B](#)). Congruently, assessment of transfection efficiency with a fluorescent siRNA (siGLO Red) pointed that Dharmafect IV displayed an efficiency of 92.7% (0.1 μ l), 93.5 (0.12 μ l) and 94.8% (0.14) to transfect MDA-MB-231 cells ([Figure 3-17D](#)). For Dharmafect I, the efficiency for the different volumes was 90.7% (0.1 μ l), 90.4% (0.12 μ l) and 91.6% (0.14). Altogether, these experiments determined that the optimum conditions to transfect MDA-MB-231 cells were 0.1 μ l Dharmafect IV, in agreement with manufacturer recommendations (*DharmaFECT Cell Type Guide*, no date). Subsequent siRNA depletion experiments in high throughput were performed using these conditions.

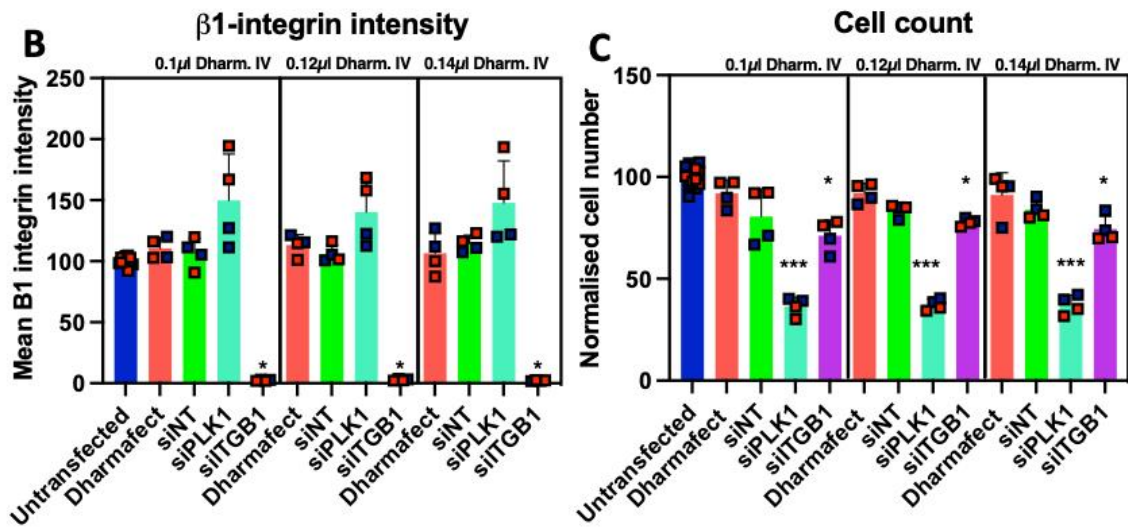
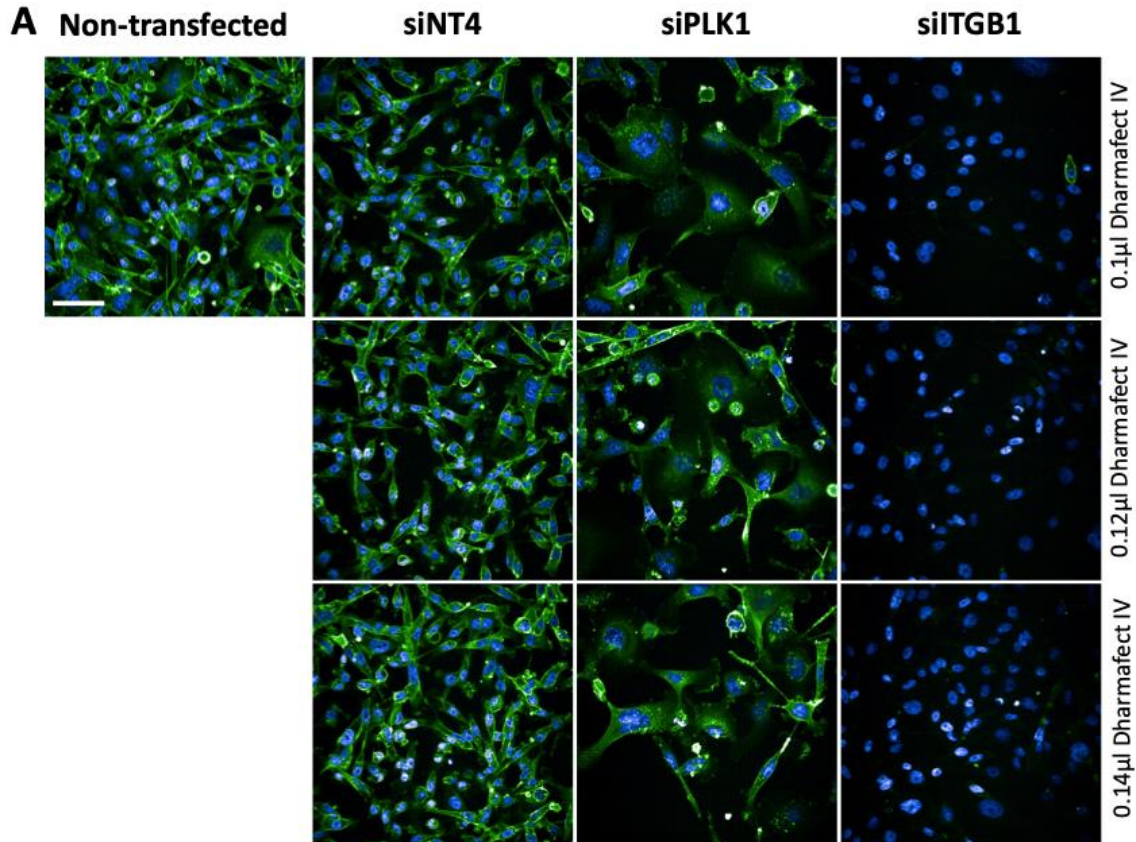


Figure 3-18. Dharmafect IV enables siRNA mediated downregulation of PLK1 and ITGB1 in MDA-MB-231 cells. (A-C) 5μl of 500nM siRNA (siNT, siPLK1, siITGB1) and 5μl OptiMEM were added into each well of a 96 well plate. Several volumes of Dharmafect IV 0.1μl, 0.12μl 0.14μl were respectively mixed with 9.9μl, 9.88μl and 9.86μl OptiMEM. These solutions were incubated for 5 minutes. Then 10μl was added on top of the 10μl siRNA-OptiMEM solution. The siRNA, Dharmafect and OptiMEM mix was incubated for 20min at room temperature in a shaker/rocker. 12000 cells, contained in 80μl, were added into each well. Following 72h, cells were fixed and stained for nuclei and ITGB1. Cell imaging: 20X (for nuclei imaging) and 40X water immersion (for ITGB1) objective from Opera Phenix high content screening microscope. Scale bar: 60μm. Plots show the well data (squares) from two technical replicates per experiment; N=2 independent experiments; *p≤0.0397 ***p≤0.0006; Kruskal-Wallis test.

3.2.10. Regulators of ECM internalisation: β 1-integrin is required for macropinocytosis of ECM

The design of biological experimental studies requires reproducible biological and technical replicates. Distinctive biological samples, also known as biological replicates, depict biological variation; while technical replicates are measurements of the same sample to assess noise or background associated with each sample. In the context of a high throughput screening, ensuring reproducibility, meaning minimal biological and technical variation is essential. To bypass this, samples are usually normalised to highly reproducible controls. In order to determine the optimal siRNA modulators of ECM internalisation in high throughput four different siRNA candidates were assessed: Integrins, tensins and subunits of the lysosomal v-ATPase.

Integrins are the foremost cell adhesion receptors. Integrin heterodimers containing β 1-integrin have been described to mediate internalisation of several ECM proteins (Rainero, 2016). In addition, integrins have been shown to cluster in nascent macropinosomes (Le *et al.*, 2021), further supporting that integrins may mediate ECM macropinocytosis. In order to validate whether β 1-integrin heterodimers regulated ECM internalisation, we knocked down β 1-integrin and assessed internalisation of matrigel and collagen I. Downregulation of β 1-integrin reduced matrigel and collagen I internalisation by 45% and 20%, respectively ([Figure 3-19](#) and [Figure 3-20](#)).

Tensins are scaffold proteins that localise in fibrillar adhesions and mediate fibronectin internalisation in the endometrioid ovarian cancer cell line A2780 overexpressing Rab25 (A2780-Rab25) (Rainero *et al.*, 2015). Tensin-3 is particularly overexpressed in 60% of all cancers and its downregulation impinges MDA-MB-231 invasion (Qian *et al.*, 2009; Shinchi *et al.*, 2015; Nizioł and Prczynicz, 2021). Moreover, ECM internalisation is upregulated in invasive breast cancer cells (Rainero, unpublished). Tensin-3 thus appears to be a potential candidate as a regulator of ECM internalisation in these cells. Congruently with previous reports (Rainero *et al.*, 2015), siRNA-mediated downregulation of tensin-3 showed a trend in diminishing matrigel (by 20%), but not collagen I, internalisation after 6h incubation ([Figure 3-19](#) and [Figure 3-20](#)). The observed reduction was not as significant as β 1-integrin, it was thus discarded as a potential control for the screening.

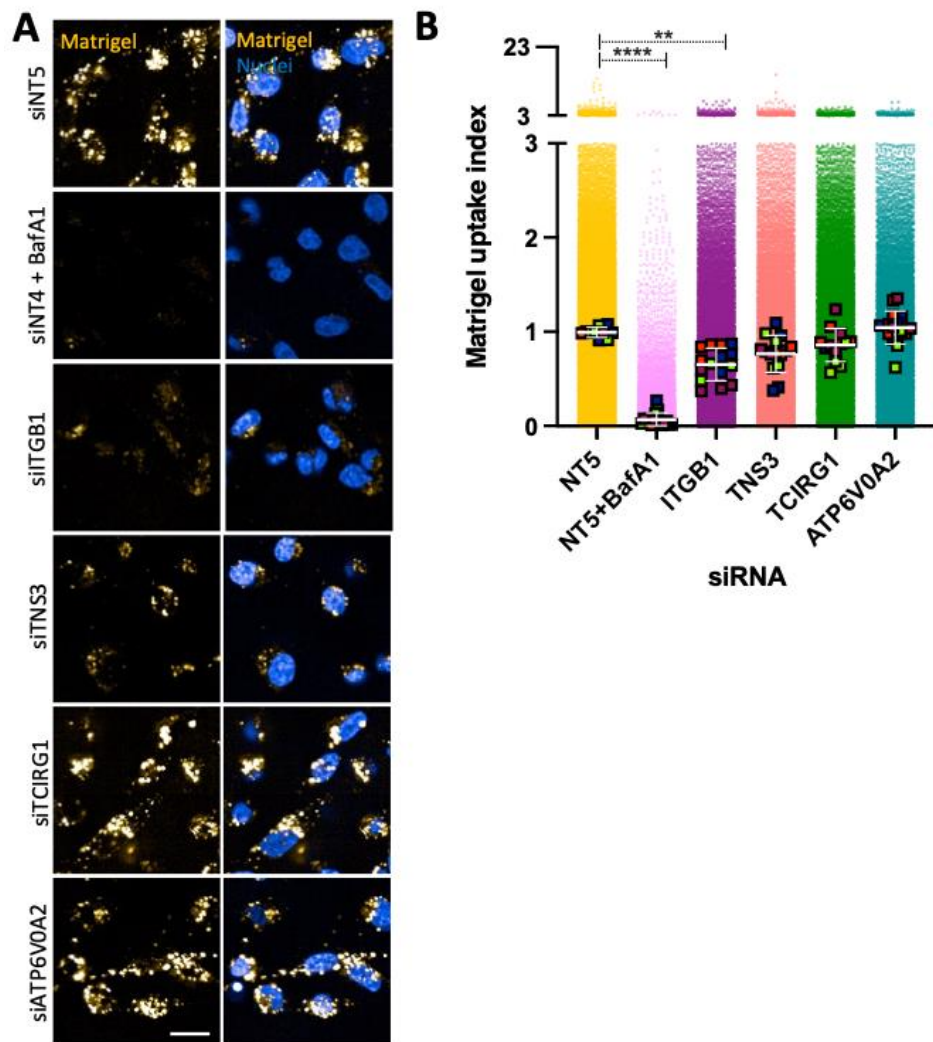


Figure 3-19. $\beta 1$ -integrin mediates matrigel internalisation in MDA-MB-231 cells. 2.5 μ l of 500nM siNT, siITGB1, siTNS3, siTCIRG1 or siATP6V0A2 and 2.5 μ l OptiMEM per well were mixed in a 384 well plate. 0.05 μ l Dharmafect IV was mixed with 4.95 μ l OptiMEM and incubated for 5min at room temperature. Then 5 μ l of this solution per well was added on top of the 5 μ l siRNA-OptiMEM solution. The siRNA, Dharmafect and OptiMEM mix was incubated for 20min at room temperature in a shaker/rocker. 3000 cells, contained in 40 μ l, were added into each well. Following 72h, cells were transferred to pHrodo matrigel (golden) plates using Integra ViaFlo 384 well head. After 6h, cells were stained with hoechst (blue) and imaged live with a 40X water immersion objective from Opera Phenix high content screening microscope. Columbus software was used for image analysis. Scale bar: 20 μ m. Values represented are cell data (dots) and well data (squares) + SD; N=3 independent experiments; well data was used for the statistical test; **p=0.034 ****p<0.0001; Kruskal-Wallis test.

We have previously shown that lysosomal acidification is key for this assay. T Cell immune regulator 1 (TCIRG1) constitutes the membrane-integral ATPase H⁺ transporting V0 subunit A3. TCIRG1 correlates with poor prognosis and overall survival of several cancers, including breast tumours (Hinton *et al.*, 2009; Qi *et al.*, 2021). Of note, MDA-MB-231 cells highly express TCIRG1 compared to the non-invasive breast cancer cell line MCF7 (Hinton *et al.*, 2009). Another membrane-integral subunit of the lysosomal ATPase is ATP6V0A2, which is also expressed in MDA-MB-231 cells (Hinton *et al.*, 2009). Downregulation of both subunit A3 and A2 has been shown to result in a slight alkalinisation of endosomes and lysosomes (Hinton *et al.*, 2009). However, knocking down either subunit did not affect the ECM uptake index. This suggests that either knockdown does not modify the lysosomal pH as strikingly as treatment with bafilomycin A ([Figure 3-19](#) and [Figure 3-20](#)). Taking everything into consideration, modulation of β 1-integrin using siRNA and blocking the lysosomal acidification using bafilomycin A1 may be adequate controls for ECM internalisation in high throughput.

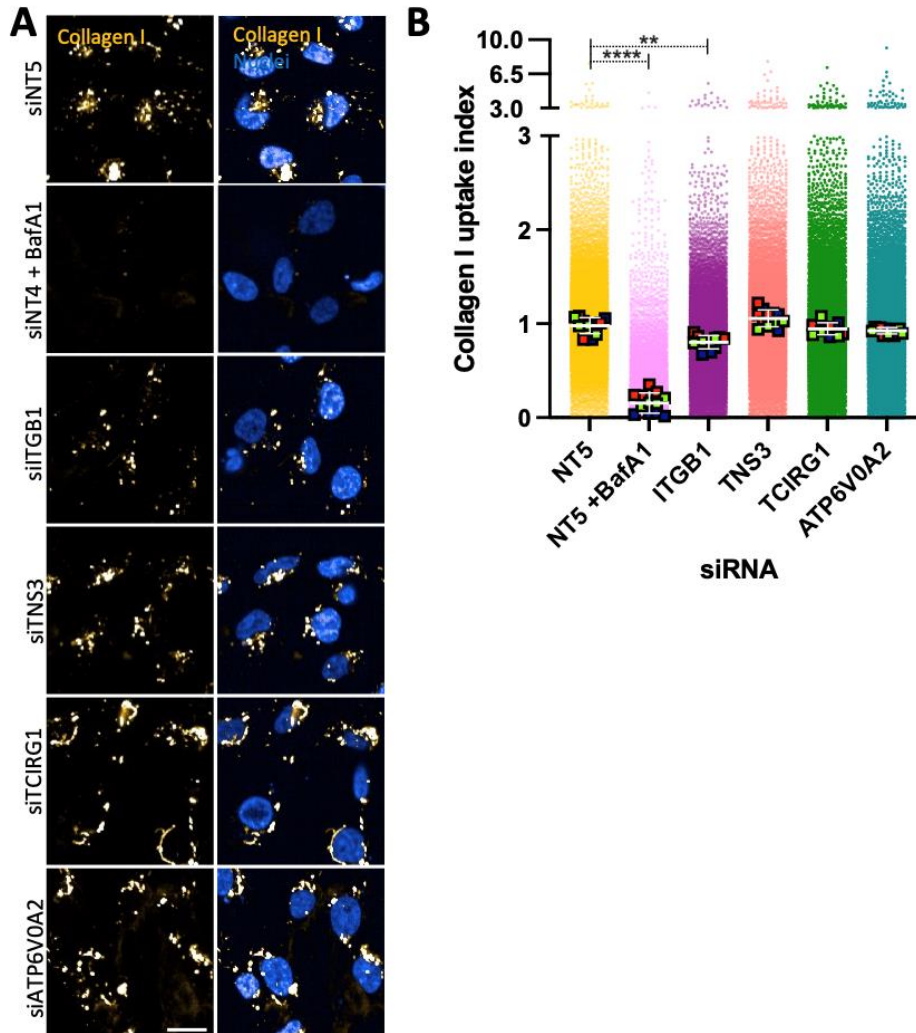


Figure 3-20. $\beta 1$ -integrin mediates internalisation of collagen I in MDA-MB-231 cells. 2.5 μ l of 500nM siNT, siITGB1, siTNS3, siTCIRG1 or siATP6V0A2 and 2.5 μ l OptiMEM per well were mixed in a 384 well plate. 0.05 μ l Dharmafect IV was mixed with 4.95 μ l OptiMEM and incubated for 5min at room temperature. Then 5 μ l of this solution per well was added on top of the 5 μ l siRNA-OptiMEM solution. The siRNA, Dharmafect and OptiMEM mix was incubated for 20min at room temperature in a shaker/rocker. 3000 cells, contained in 40 μ l, were added into each well. Following 72h, cells were transferred to pHrodo collagen I (golden) plates using Integra ViaFlo 384 well head. After 6h, cells were stained with hoechst (blue) and imaged with a 40X water immersion objective from Opera Phenix high content screening microscope. Columbus software was used for image analysis. Scale bar: 20 μ m. Values represented are cell data (dots) and well data (squares) + SD; N=3 independent experiments; well data was used for the statistical test; ** $p=0.034$ **** $p<0.0001$; Kruskal-Wallis test.

3.2.11. Optimisation of a high content screening ECM internalisation assay using pHrodo red

To assess whether this method was compatible with a high throughput screening assay, we sequentially tested the different core modules for this screening: knockdown, cell transfer, cell fixation and data acquisition/imaging. This assay is distinctively unique from other high

throughput screening assays since it requires transfer of cells from a source plate, where siRNA-mediated downregulation occurs, to a target plate, which is coated with ECM. Cell transfer is essential for various reasons. First and foremost, to avoid early internalisation and accumulation of ECM prior to efficient downregulation of target genes. Cell transfer would enable the evaluation of the full range of modulation of ECM uptake. In addition, assessing uptake for a shorter time (~6h) would allow to properly determine negative and positive regulators of ECM, that is to say hit genes that either promote/facilitate or prevent ECM uptake. Two different automation robots were successfully tested: Bravo liquid handling platform and Integra 384 well head. Following several rounds of optimisation, we determined that vortexing the plate every minute during 5 minutes significantly increased cell detachment and efficient cell transfer as depicted in the heatmap in [Figure 3-21A](#). More precisely, 40 to 80% of the cells were transferred in each row ([Figure 3-21B,C](#)). However, following siRNA-mediated downregulation, some conditions, including the control β 1-integrin, were highly adhesive to the glass-bottom-like substrate in the 384 well plates. TrypLE Express enzyme (TrypLE) is a c-terminal lysyl protease utilised for the detachment of cells in adherent cultures (*TrypLETM Express Enzyme (1X)*, phenol red, no date). Contrary to trypsin, TrypLE has been highly purified, which reduces cell damage and is highly specific. We therefore sought to determine whether TrypLE would improve the cell detachment. Indeed, using this trypsin substitute efficiently detached cells that previously did not (data not shown). TrypLE was thus used for following high throughput screening assays to boost trypsinization and cell transfer efficiency.

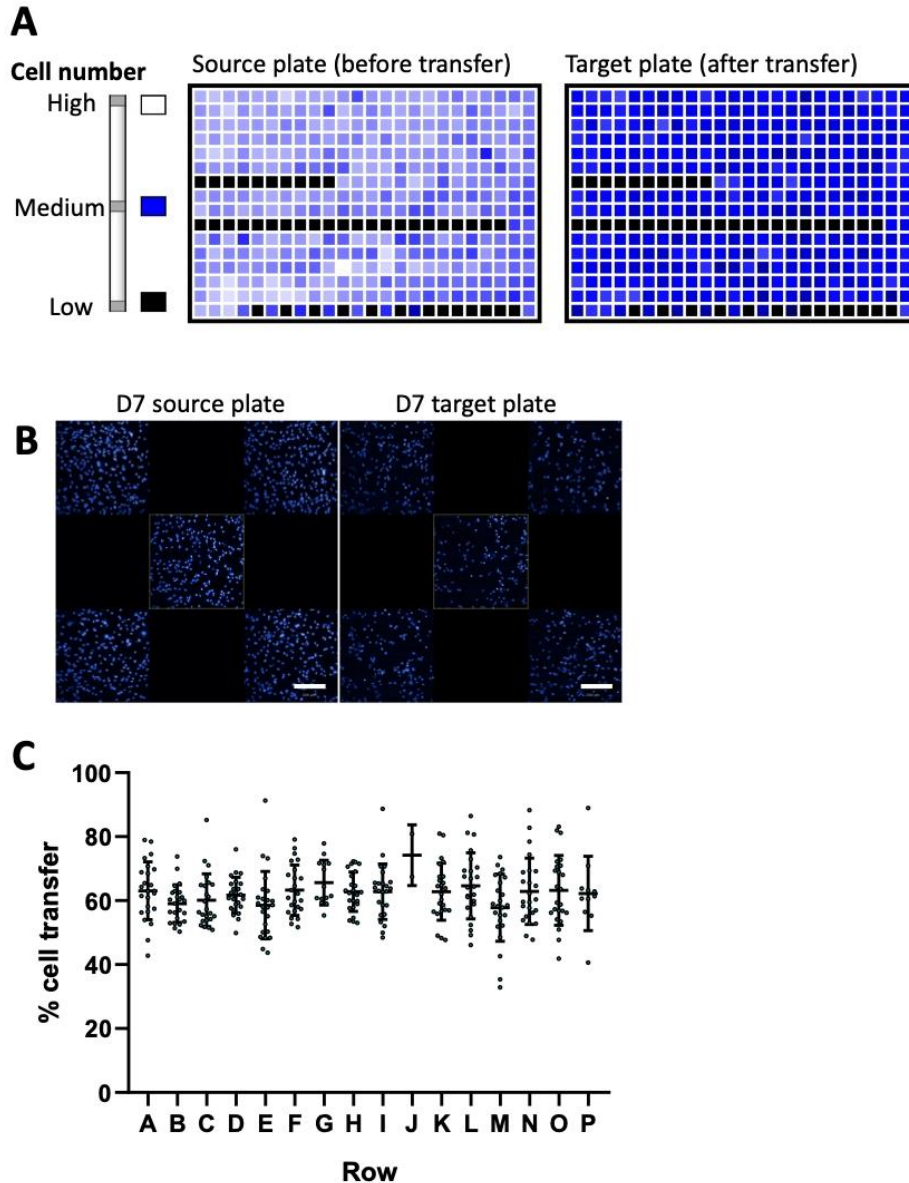


Figure 3-21. Optimisation of cell transfer. Confluent 384-well plates were stained with $1\mu\text{g/ml}$ hoechst (blue) and washed with $100\mu\text{l}$ PBS. $20\mu\text{l}$ trypsin enabled cell detachment. Cells were incubated for 5min at 37°C and later vortexed 4 times every minute. $100\mu\text{l}$ media was added into each well and $80\mu\text{l}$ of the cells were transferred to the target plate. Once cells adhered to the target plate, $5\times$ air objective opera phenix was used for cell imaging. Scale bar: $200\mu\text{m}$. Columbus software was used for nuclei count. (A) Columbus heat map of nuclei count before and after cell transfer. (B) Representative images from 5 fields of view in a 384 well plate. (C) Percentage of number of cells in target plate/cells in source plate. $N=1$ experiment. (Data collected together with Dr Xavier Le Guezennec).

Following the optimisation of high throughput trypsinization, MDA-MB-231 cells were transfected for 72h in presence of the possible regulators that were previously tested and several genes targeting established regulators of intracellular traffic. To ensure there was no variability in the processing of the plate, we tested the same conditions in the different quadrants of the

384-well plate (see plate layout in [Figure 3-22A](#)). Unexpectedly, variability within the technical replicates was extremely high as depicted in [Figure 3-22B,C](#). Notwithstanding that, variability within the same quadrant and row was minimal. In addition, there were some hits, including several proteins that belong to the family of clathrin Adaptor proteins: AP1M1, AP3B2, AP3D1, AP4E1, which clearly had a modulation in matrigel uptake index compared to the NT5. This was especially true for hits in the first and second quadrant. Transfection efficiency was assessed with siGLO green. Approximately 70% of the cells were transfected with the fluorescent siRNA ([Figure 3-22D](#)). This suggested to us that either the automated pipetting for pHrodo washing and cell transfer was tilted or that cell fixation led to changes in the intracellular pH over time. Changes in cell number were excluded after evaluating changes in cell number across the plate (data not shown). Changes in the laser acquisition setting were excluded once hoechst intensity of nuclear staining was analysed (data not shown). In addition, the plate was imaged again the following day and no difference in the signal intensity throughout the plate were observed. However, pHrodo signal intensity was extremely diminished compared to the imaging from the previous day (data not shown). This prompted us to consider that cell fixation was permeabilising the endosomal compartment as time passed, resulting in the shift in signal observed in [Figure 3-22B,C](#). Different fixative conditions were thus tested (see [Table 3-1](#)). Also several timings ranging from 10 minutes to half an hour were assessed. However, while some conditions diminished the observed shift, the results were not consistent within biological replicates (data not shown). For this reason, we tested whether live imaging could bypass the decrease in fluorescence observed following fixation. Actually, imaging the plate live showed less variability than using any fixation method [Figure 3-22E](#). Moreover, the slight and insignificant increase in uptake between columns within the 2h 30min of imaging was lower than using fixative conditions (displayed in [Figure 3-22E](#)). Taken together, despite identifying few hits that may have a regulatory role in ECM traffic, this data confirms that live imaging is the best alternative for unravelling novel regulators of ECM internalisation in high throughput systems. Applying this knowledge, Chapter 5 will describe the role of Adaptor proteins and further characterise the regulators of ECM traffic to lysosomes using live imaging.

A

	1	2	3	4	5	6	7	8	9	10	11	12	13	14	15	16	17	18	19	20	21	22	23	24
A																								
B																								
C		ITGB1	AP1S1	AP1M2	AP1B1	AP1AR	AP1G2	AP1S3	AP1G1	AP1M1	AP1S2	AP1M3	AP1S1	AP1M2	AP1B1	AP1AR	AP1G2	AP1S3	AP1G1	AP1M1	AP1S2	AP1M3	ITGB1	
D		NT5	AP2S1	AP2A1	AP2A2	AP3S1	AP3D1	AP3S2	AP3M2	AP3B2	AP4S1	AP4E1	AP2S1	AP2A1	AP2A2	AP3S1	AP3D1	AP3S2	AP3M2	AP3B2	AP4S1	AP4E1	NT5	
E		DNM1	AP4M1	AP4B1	AP5B1	AP5M1	AP5S1	AP5Z1	GGA1	GGA2	GGA3	RAB9A	AP4M1	AP4B1	AP5B1	AP5M1	AP5S1	AP5Z1	GGA1	GGA2	GGA3	RAB9A	DNM1	
F		PAK1	RAB9B	RAB6PK	RAB31	SORCS1	SORCS2	SORCS3	SORL1	IGF2R	M6PR	RAB7B	RAB9B	RAB6PK	RAB31	SORCS1	SORCS2	SORCS3	SORL1	IGF2R	M6PR	RAB7B	PAK1	
G		HGLO	RAB31	VPS26A	VPS26B	VPS29	SNX1	TSG101				RAB31	VPS26A	VPS26B	VPS29	SNX1	TSG101					HGLO		
H		Baf A1																						
I		ITGB1	AP1S1	AP1M2	AP1B1	AP1AR	AP1G2	AP1S3	AP1G1	AP1M1	AP1S2	AP1M3	AP1S1	AP1M2	AP1B1	AP1AR	AP1G2	AP1S3	AP1G1	AP1M1	AP1S2	AP1M3	ITGB1	
J		NT5	AP2S1	AP2A1	AP2A2	AP3S1	AP3D1	AP3S2	AP3M2	AP3B2	AP4S1	AP4E1	AP2S1	AP2A1	AP2A2	AP3S1	AP3D1	AP3S2	AP3M2	AP3B2	AP4S1	AP4E1	NT5	
K		DNM1	AP4M1	AP4B1	AP5B1	AP5M1	AP5S1	AP5Z1	GGA1	GGA2	GGA3	RAB9A	AP4M1	AP4B1	AP5B1	AP5M1	AP5S1	AP5Z1	GGA1	GGA2	GGA3	RAB9A	DNM1	
L		PAK1	RAB9B	RAB6PK	RAB31	SORCS1	SORCS2	SORCS3	SORL1	IGF2R	M6PR	RAB7B	RAB9B	RAB6PK	RAB31	SORCS1	SORCS2	SORCS3	SORL1	IGF2R	M6PR	RAB7B	PAK1	
M		HGLO	RAB31	VPS26A	VPS26B	VPS29	SNX1	TSG101				RAB31	VPS26A	VPS26B	VPS29	SNX1	TSG101					HGLO		
N		Baf A1																						
O																								
P																								

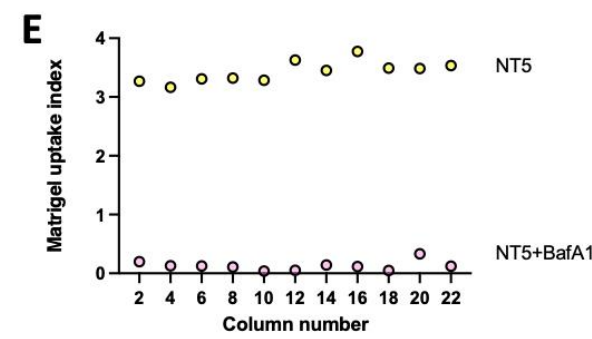
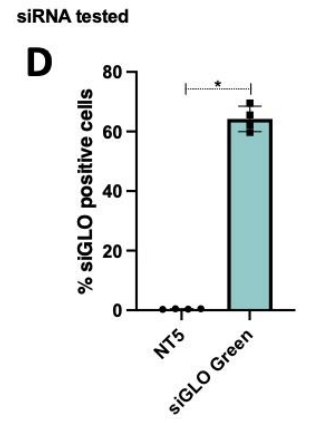
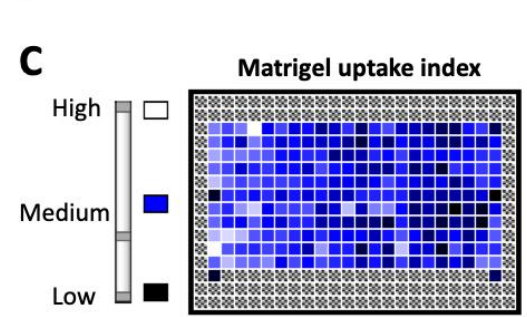
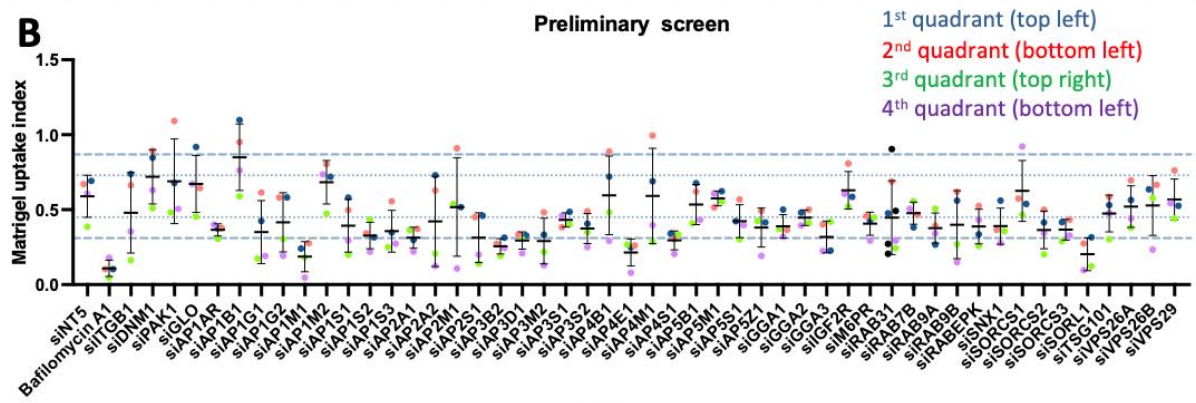


Figure 3-22. Optimisation of high throughput imaging for matrigel uptake. 3000 MDA-MB-231 cells were transfected as per protocol. Following 72h, cells were transferred into pH-rodo labelled matrices and incubated for 6h. (A-D) Cells were fixed and stained for hoehchst and ITGB1. 40X objective Opera phenix was used for cell imaging. (A) Plate layout of the siRNA tested. (B) Scatter plot from well data; 4 technical replicates. (C) Columbus software heatmap. (D) Transfection efficiency with siGLO Green. (E) Graph displaying the matrigel uptake index for NT5 and NT5+ Bafilomycin A1 per column.

Table 3-1. Fixative conditions tested. Cells were seeded on pHrodo labelled matrigel and seeded with different percentages of paraformaldehyde or glutaraldehyde. Cells were imaged at time 0h, 1h, 2h, 3h, 4h, 12h and 24h after fixation. pHrodo intensity was analysed with Columbus software.

Fixative conditions tested
4% paraformaldehyde
2.5% paraformaldehyde
1% paraformaldehyde
1% paraformaldehyde + 0.5% glutaraldehyde
1% paraformaldehyde + 0.25% glutaraldehyde
0.5% glutaraldehyde
0.25% glutaraldehyde

3.2.12. PAK1 regulates macropinocytosis of ECM components

To discern the discrete molecular mechanisms behind ECM internalisation, we performed a mini-screen targeting the most distinctive regulators of several well-known endocytic pathways. MDA-MB-231 cells were knocked down in high throughput and transferred into matrigel-coated 384 well plates in a semi-automated manner. Matrigel is a BM-like ECM, consisting of diverse core matrisome proteins. In agreement with its intricate nature, several endocytic pathways seemed to affect its internalisation. Simultaneous downregulation of caveolin 1 and 2 decreased matrigel uptake index by 66% ([Figure 3-23](#)), consistent with previous results showing that filipin treatment diminished matrigel internalisation ([Figure 3-13](#)). Similarly, knocking down both dynamin 2 and 3 resulted in a 56% decrease in matrigel uptake ([Figure 3-23](#)). Nonetheless, downregulation of clathrin heavy chain, flotillin 1 and 2 promoted a slight, but significant, increase (30%) in matrigel internalisation ([Figure 3-23](#)). We have previously shown that EIPA treatment blocked endocytosis of matrigel ([Figure 3-13](#) & [Figure 3-16](#)). Accordingly, siRNA mediated depletion of PAK1 occasioned a 35% reduction in matrigel internalisation ([Figure 3-23](#)).

In this chapter, we have hitherto established that breast cancer cells converge in macropinocytosis to internalise matrigel, collagen I and TIF-CDM ([Figure 3-16](#)). We thus aimed to validate the high throughput approach using high resolution confocal microscopy. In order to evaluate whether PAK1 modulated macropinocytosis of collagen I and exclude any effect on

lysosomal pH, a red non pH sensitive dye, NHS-Alexa fluor 555, was used instead. Indeed, siRNA against PAK1 halved collagen I internalisation ([Figure 3-24A,B](#) and [Figure S1-3](#)). Interestingly, PAK1 downregulation in MDA-MB-231 cells promoted mechanical rearrangement of collagen I fibres around the cells ([Figure 3-24B](#)). This suggests that prior to its internalisation, breast cancer cells may mechanically remodel the ECM. To assess whether a similar effect was observed in more complex matrices, we labelled CDMs derived from both TIFs and CAFs with pHrodo and siRNA downregulation of PAK1 strongly reduced the uptake index of TIF- and CAF-CDM by 70% and 60%, respectively ([Figure 3-24C-F](#) and [Figure S1-3](#)). Western Blot analysis confirmed that PAK1 protein expression (PAK1/GAPDH intensity) was decreased by 76%, verifying that the knockdown was efficient ([Figure 3-24](#) and [Figure S1-3](#)). Overall, this data substantiated previous results ([Figure 3-16](#)) and further evidenced that PAK1 regulates macropinocytosis of the different matrices.

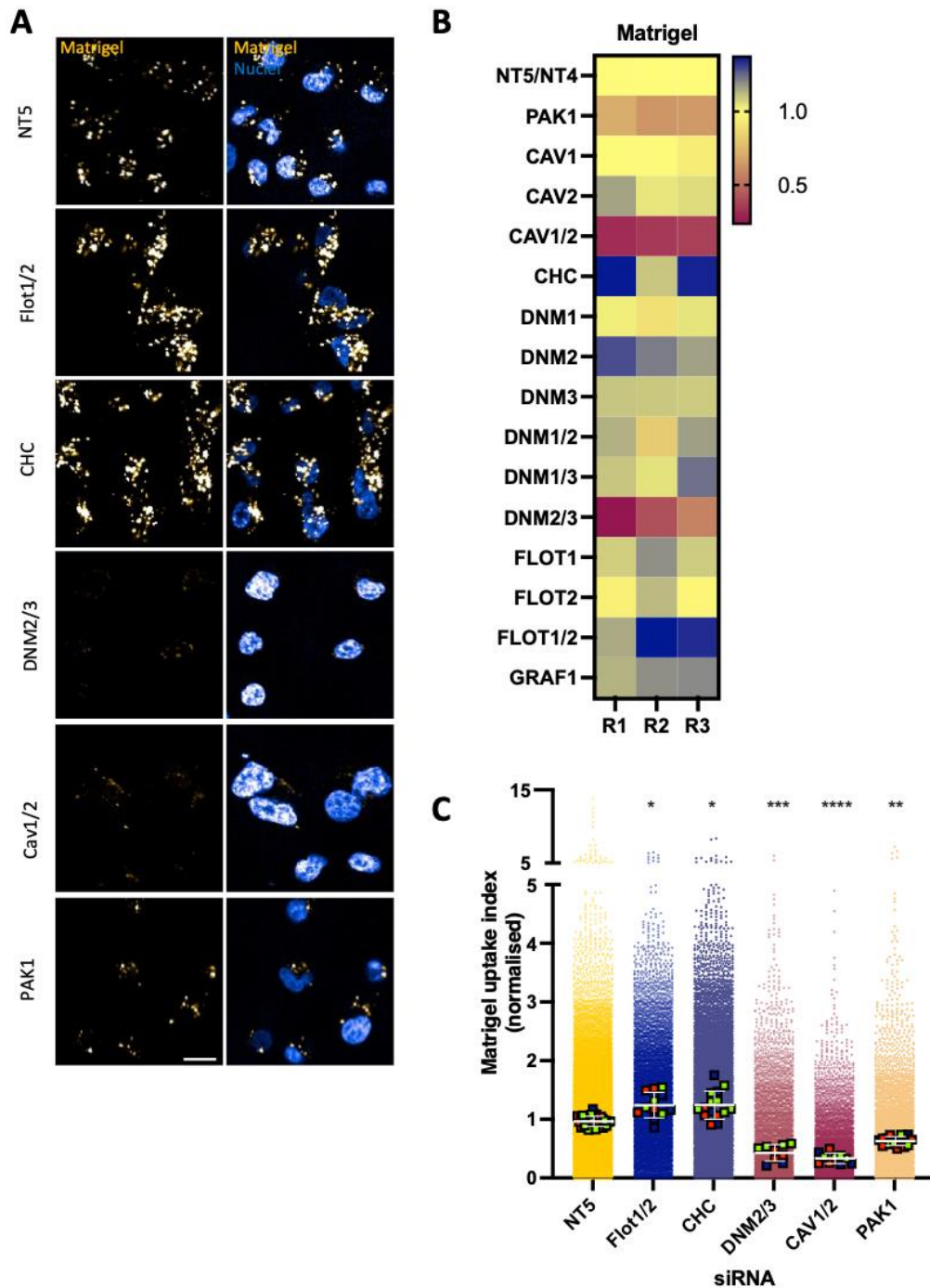


Figure 3-23. DNM2/3, CAV1/2 and PAK1 mediate matrigel internalisation in MDA-MB-231 cells. 2.5 μ l of 500nM siRNA per well and/or 2.5 μ l OptiMEM per well were mixed in a 384 well plate. 0.05 μ l Dharmafect IV was mixed and incubated with 4.95 μ l OptiMEM for 5min. Both siRNA and Dharmafect IV solutions were mixed in the well and incubated for 20min with gentle rocking. 3000 cells, contained in 40 μ l, were added into each well. Following 72h, cells were transferred to pHrodo-matrigel (golden) plates using Integra ViaFlo 384 well head. After 6h, cells were stained with hoechst (blue; high intensity signal is white) and imaged with a 40X water immersion objective from Opera Phenix high content screening microscope. Columbus software was used for image analysis. Scale bar: 20 μ m. Values represented are cell data (dots) and well data (squares) + SD; N=3 independent experiments; well data was used for the statistical test; * p ≤0.0411, ** p =0.0019, *** p =0.0002, **** p <0.0001; Kruskal-Wallis test.

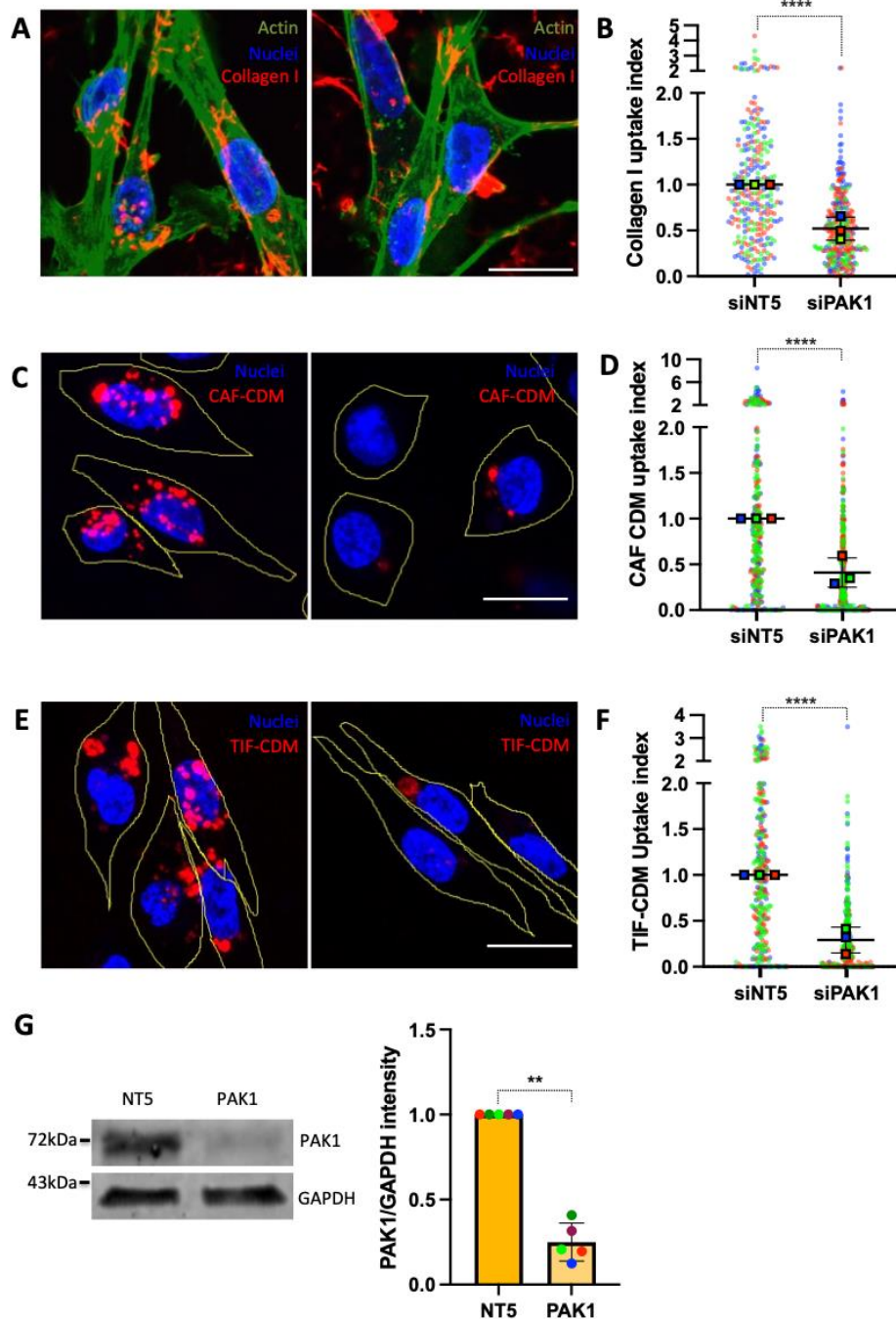


Figure 3-24. PAK1 mediates macropinocytosis of collagen-rich ECM in MDA-MB-231 cells. 10 μl of 5 μM siRNA and 190 μl OptiMEM per well were mixed in a 6 well plate. 1 μl Dharmafect I was mixed and incubated with 199 μl OptiMEM for 5 min. 200 μl of the solution was added on top of the siRNA and incubated for 20 min on a rocker. 4 × 10⁵ cells, contained in 1600 μl, were added into each well. Following 72 h, cells were trypsinised and counted. 3 × 10⁵ cells per condition were seeded onto 1 mg/ml NHS-Alexa Fluor 555 (red) labelled collagen I (A-B), or pHrodo (red) labelled TIF- (C-D) and CAF-CDM (E-F). Cells were incubated on top of the matrices for 6 h. For collagen I conditions, cells were fixed and stained for nuclei (blue) and Phalloidin Alexa fluor 488 (green). For CDMs, cells were stained with hoechst (blue) and imaged live. A 60X oil immersion objective from a Nikon A1 confocal microscope was used for imaging. Yellow lines show cell shape. Analysis was carried in ImageJ. Scale bar: 20 μm. Values represented are normalised cell data (dots) and normalised mean data (squares) + SD; N=3 independent experiments; ****p<0.0001; Mann Whitney test. (G) Western Blot and quantification of PAK1 and GAPDH. N=5 independent experiments; **p= 0.0079; Mann Whitney test.

3.2.13. Extracellular proteolysis by cysteine cathepsins and matrix metalloproteinases is partially required in ECM internalisation

Macropinocytosis is classically defined as internalisation of soluble ligands. To test whether extracellular cleavage of ECM was required in macropinocytosis of ECM, we measured ECM uptake index in the presence of a cell permeable cysteine cathepsin protease inhibitor (E64d), which also inhibits proteolytic degradation in the lysosomes, and a broad spectrum MMP inhibitor (GM6001). MMP inhibition resulted in a small but significant reduction of collagen I and CDM, 13% and 15% respectively ([Figure 3-25A-C,E](#)). Conversely, matrigel internalisation was not significantly impaired by GM6001 ([Figure 3-25D,F](#)). Of note, all 3 matrices moderately relied on cysteine cathepsins for their extracellular degradation and subsequent internalisation ([Figure 3-25](#)). Strikingly, E64d treatment led to a 35% reduction in matrigel uptake, while both collagen and CDM internalisation was diminished by about 20% ([Figure 3-25](#)). E64d is a cell permeable cysteine cathepsin inhibitor, which has been widely used to inhibit the degradation of proteins in the lysosomes. While treatment with GM6001 did not affect vesicle size or how vesicles distributed in the cytoplasm ([Figure 3-25A,C,D](#)), ECM accumulated in larger vesicles, resembling vacuoles, upon treatment with E64d, in accordance with the reported role of cysteine cathepsins in mediating intracellular degradation of ECM in the lysosomes ([Figure 3-11](#) and [Figure 5-2](#)). This data indicates that extracellular proteolysis prior to ECM internalisation is partially dispensable in MDA-MB-231 cells. Interestingly, cysteine cathepsins, rather than MMP, seem to be the main proteases mediating ECM internalisation. Nonetheless, MMP activity may concomitantly occur with cathepsins and enhance internalisation of collagen I-rich matrices.

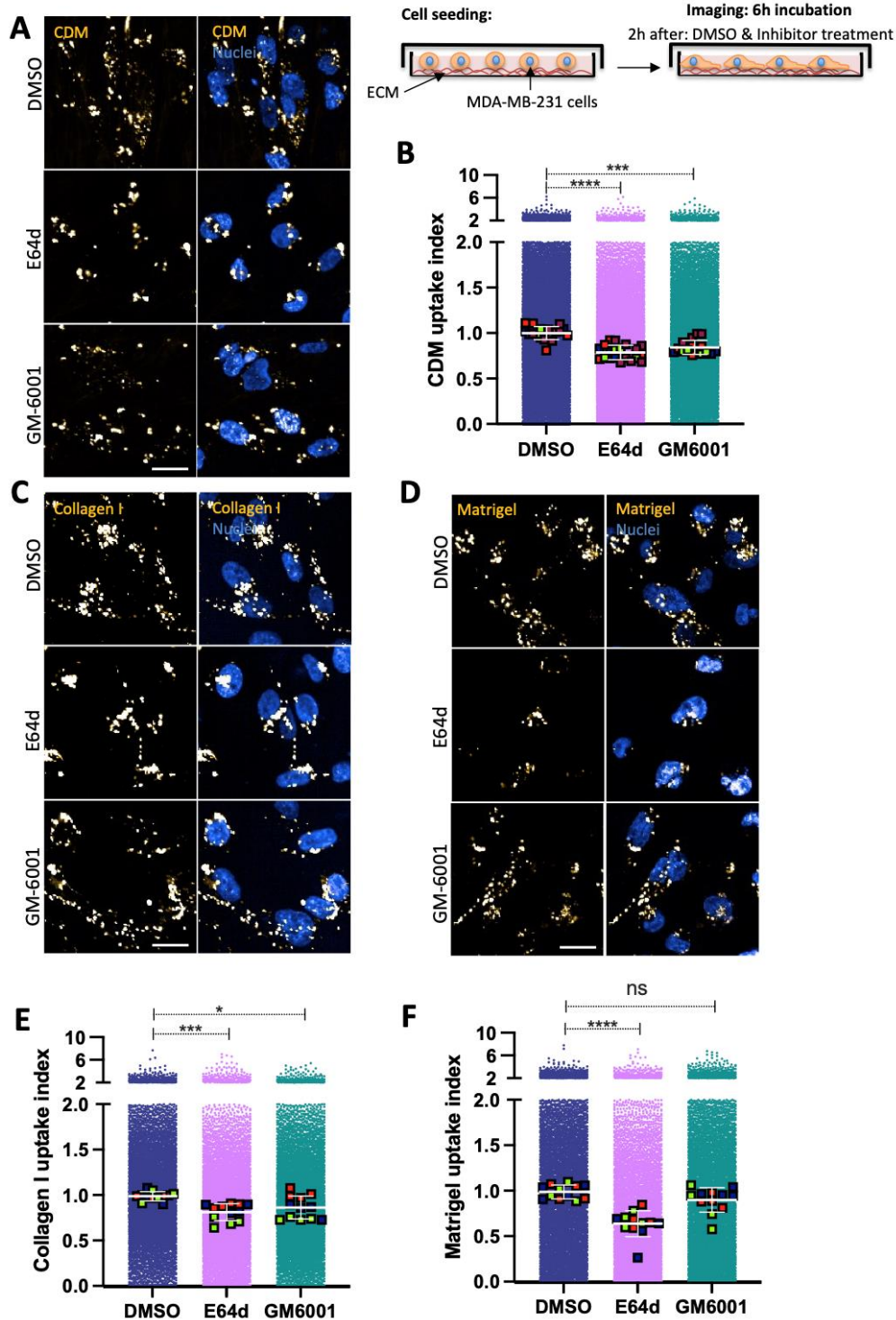


Figure 3-25. Inhibition of cysteine cathepsin reduces ECM uptake. TIF-CDMs were generated as per protocol (A-B). 50µl ice cold PBS was added per well. 2µl or 15µl 0.5mg/ml matrigel (D,F) or collagen I (C,E) was added and centrifuged. Matrigel was polymerised for 15min at room temperature; collagen I polymerised at 37°C. All matrices were labelled with 20µg/ml pHrodo (golden). Cells were cultured for 6h in presence of DMSO, E64d or GM6001. Cells were stained with hoechst (blue; high intensity signal is white) prior to live imaging with a 40X water-immersion objective from Opera Phenix microscope. Cell data was analysed with Columbus software. Scale bar: 20µm. Values represent cell data (dots) and well data (squares) + SD (N=3); well data used for the statistical test; ns (non-significant), *p=0.0105, ***p=0.0002, ****p<0.0001; Kruskal-Wallis test.

3.2.14. MDA-MB-231 breast cancer cells internalise extracellular matrix in 3D culture

In vivo, cancer cells dwell in a complex and restrictive environment. In physiopathological conditions, the tumour microenvironment is actually scarce of oxygen and nutrients. These characteristics highly differ from the classical 2D cultures. Cancer cells may upregulate mechanisms, e.g., changing the migratory behaviour, to bypass certain pharmacological treatments. Thus, studying this process using 3D spheroids may be a reliable approach to what we could observe *in vivo*. To evaluate whether invasive breast cancer cells internalise ECM in 3D culture, spheroids derived from MDA-MB-231 cells expressing GFP were embedded into pHrodo-labelled geltrex and collagen I gels. Live cell imaging revealed that breast cancer cells can internalise ECM in 3D systems. Our lab and others have shown that cancer cells and mammary cells under starvation internalise the ECM as a source of nutrients (Muranen *et al.*, 2017; Nazemi *et al.*, 2021). ECM internalisation promotes proliferation of breast cancer cells under amino acid starvation in 2.5D culture. Amino acid starvation has been shown to induce macropinocytosis (Lee *et al.*, 2019). We aimed to see whether we could recapitulate this phenomenon in 3D and determine whether there were any changes in ECM internalisation upon starvation. Cells showed significant levels of internalisation after 44h post-embedding (data not shown). Interestingly, amino acid starvation in 3D for 4h (see 48h in [Figure 3-26](#)) and 24h (see 72h in [Figure 3-26](#)) led to a small but significant increase in intracellular pHrodo-ECM. Collectively, our data indicates that breast cancer cells internalise ECM in 3D and upregulate this process under the nutrient-limiting conditions in the tumour microenvironment. Furthermore, this data supports previous reports that cancer cells increase ECM internalisation under amino acid starvation, suggesting that using a 2.5D model may aid in recapitulating *in vivo-like* features.

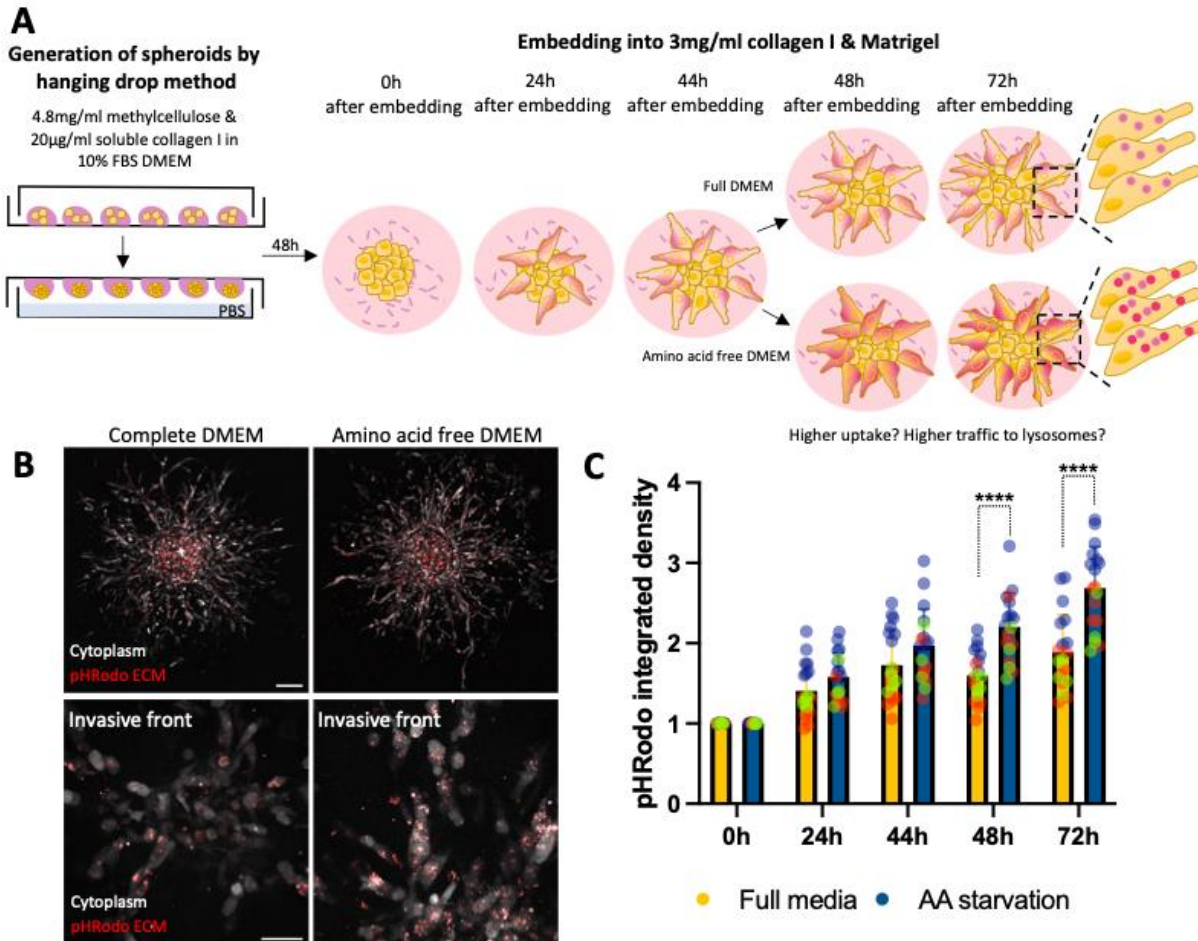


Figure 3-26. The invasive breast cancer cell line MDA-MB-231 internalises ECM in 3D. (A) Schematic representation. 3D spheroids were generated by the hanging drop method. 1000 cells per 20µl drop containing 4.8mg/ml methylcellulose and 20µg/ml soluble collagen I were pipetted on the lid of tissue culture dishes. Lids were turned and put on top of the bottom reservoir of the dish, which was filled with PBS to prevent evaporation. Following 48h, spheroids were embedded in 40µl of 3mg/ml rat tail collagen I and 3mg/ml geltrex. 1/5 of the matrix solution was labelled with 20µg/ml pHrodo (red) containing 0.1M NaHCO₃. Spheroids were polymerized at 37°C for 20min and then media was added into the dishes. Media was changed to 10% D-FBS DMEM and 10% D-FBS amino acid free DMEM after 44h of embedding. Cells (white) were imaged live every 24h until 72h post-embedding in the Nikon A1 confocal and Airyscan. (B) Representative images taken at 72h. Scale bar: 42µm for invasive front and 132µm for whole spheroids. (C) Analysis was performed in ImageJ and data was normalised to day 0. Values represent individual spheroids + SD (N=3); ****p<0.0001; 2way ANOVA.

3.3. DISCUSSION

Tumours have been compared and defined as complex organs or tissues (Egeblad, Nakasone and Werb, 2010). Tumours are not simply composed of cancer cells, but are surrounded by an intricate meshwork of proteins, known as the ECM, which not only acts as a scaffold but provides physico-mechanical and chemical cues that promote tumorigenesis (Egeblad, Nakasone and Werb, 2010; Elgundi *et al.*, 2019). In fact, high levels of ECM deposition and desmoplasia are associated with malignancies. However, the ECM is regarded as a double edge sword since it may

physically act as a barrier and impede or limit invasive migration or tumour growth. Notwithstanding that, cancer cells overcome the restrictive tumour microenvironment by upregulating certain mechanisms that enable ECM remodelling or degradation (Tsegaye *et al.*, 2021). Moreover, given the importance of the tumour microenvironment, including the ECM, in the raise or establishment of secondary metastatic sites, more effort should be put into studying cancer cell-ECM interactions. In the current study, we first presented a method to homogeneously coat matrigel and collagen I matrices in high throughput ([Figure 3-5](#) and [Figure 3-7](#)). In order to develop this methodology, we first optimised matrigel coating in a 96-well plate format (data not shown). Similar to the 384-well plate, no difference in the area of particles was observed and increasing the concentration led to a dose-dependent effect on the coefficient of variation. Nevertheless, matrigel particles did not increase in number as concentration augmented (data not shown). Matrigel internalisation in a 96-well plate more closely recapitulated data using the conventional method but simultaneously highly resembled the 384-well coating. In fact, increasing matrigel concentration (0.3mg/ml to 1mg/ml) showed a slight trend in increasing matrigel uptake index (data not shown). Increasing matrigel concentration between 3mg/ml to 5mg/ml generated matrigel gels that resulted in cells assembling into 3D culture-like structures (data not shown); the latter data is in agreement with the methods paper this protocol is based on (Ko, Tsai and Frampton, 2019). In addition, we successfully present that CDM production is compatible with high throughput imaging plates ([Figure 3-6B](#)). Moreover, the method described in this chapter enables the quantification of ECM uptake in high content screens ([Figure 3-9](#)) and may open new avenues for studying cell-ECM interactions in a high throughput fashion. Under those settings, matrigel uptake was reduced by dynasore, filipin and EIPA ([Figure 3-13](#)). To further unravel the molecular mechanisms behind matrigel internalisation, we performed a low throughput screen. Congruently with inhibitor data, dual downregulation of dynamin 2 and dynamin 3, as well as knocking down together caveolin 1 and caveolin 2 significantly diminished matrigel endocytosis ([Figure 3-23](#)). Matrigel is a BM-like ECM that is mainly composed of laminin, collagen IV, proteoglycans and the preparation contains traces of fibronectin as stated in its data sheet. Thus, the effect of filipin and dynamin on matrigel uptake may be on account of the fibronectin found in this ECM preparation since fibronectin

internalisation is $\alpha 5\beta 1$ and caveolin-dependent (Sottile and Chandler, 2005; Rainero, 2016). Nevertheless, the observed effect upon siRNA-mediated downregulation of CAV1/2 and DNM2/3 is striking considering laminin accounts for 60% of matrigel. In fact, dual downregulation of DNM2/3 and CAV1/2 respectively reduced matrigel internalisation in 56% and 66% ([Figure 3-23](#)). Caveolae, a plasma membrane region rich in caveolins, has been reported to sense and respond to low membrane tension at the rear of migrating cells (Hetmanski *et al.*, 2019). In addition, alterations in membrane tension promote changes in endocytosis (Dai, Ting-Beall and Sheetz, 1997; Raucher and Sheetz, 1999). Low membrane tension facilitates endocytosis, while high tension impinges upon the endocytic machinery, preventing internalisation (Raucher and Sheetz, 1999). Indeed, both caveolin-1 knockdown and osmotic shock, which increases membrane tension, were reported to stall RhoA activation at the rear of the cells (Hetmanski *et al.*, 2019). This suggests that downregulation of caveolin-1 may lead to high membrane tension. Therefore, changes in membrane tension, either by downregulation of caveolins or filipin-treatment, could impinge on matrigel endocytosis. Notwithstanding that, caveolin-1 alone does not block matrigel internalisation and, in addition, specifically matrigel, but not collagen nor TIF-CDM, endocytosis is reduced upon filipin treatment ([Figure 3-16](#) and [Figure 3-23](#)). Moreover, filipin treatment reduces proliferation of MDA-MB-231 under amino acid starvation on matrigel, but no effect was observed for collagen I (Rainero, unpublished). This implies that while collagen and TIF-CDM are not sensitive to changes in membrane tension, matrigel internalisation is. One possible explanation may be due to the different substrate stiffnesses. In addition, $\alpha 3\beta 1$ integrin was shown to induce Src-mediated CAV1 phosphorylation (Zhang *et al.*, 2003). CAV1 phosphorylation has been proposed to lead to endocytosis via activation of dynamin-dependent fission of caveolin pits (Sverdlov, Shajahan and Minshall, 2007). It could be also possible that laminin or certain matrix stiffness triggers caveolin-1 phosphorylation, which indirectly results in laminin internalisation. Recent reports suggested that downregulation of CAV1 promotes recycling of $\beta 1$ -integrin in a Rab4-dependent manner, rather than the “slow” Rab11-dependent recycling (Lolo *et al.*, 2022). CAV1 knockdown promotes higher adhesion to fibronectin and integrin activation at the PM (Lolo *et al.*, 2022). In this system, internalisation of $\beta 1$ -integrin relies on the CLIC-GEEC pathway (Lolo *et al.*, 2022). We tested GRAF1, a GTPase that has been shown to regulate the

CLIC-GEEC pathway ([Figure 3-23](#)). Our results suggest that GRAF1 is dispensable for internalisation of matrigel. Thus, changes in membrane tension by downregulating CAV1/2 may promote CLIC-GEEC dependent endocytosis of inactive integrins, instead of ECM-bound integrins. The shift in the endocytic pathways used (i.e. CLIC-GEEC, instead of macropinocytosis or caveolae/membrane tension-dependent endocytosis) would result in lower matrigel internalisation. Simultaneously, rapid recycling of integrins may be required for ECM internalisation; it may be possible that the effect seen is due to impaired recycling of β 1-integrin. The ECM is an intricate network of fibrillar proteins that interact with one another. Accordingly, one reasonable explanation would be that integrin recognition of a particular ECM protein may trigger internalisation of adjacent and closely interacting ECM molecules. That is to say, engagement of fibronectin to α 5 β 1 integrin, for instance, could trigger its endocytosis together with other ECM proteins via caveolin-mediated endocytosis. Interestingly, laminin internalisation has been described to be dystroglycan- and dynamin- dependent in normal mammary epithelial cells (Leonoudakis *et al.*, 2014). In the same study, the authors claim that the invasive breast cancer cell line MDA-MB-231 and the human glioma cell line LN18 were not able to internalise laminin since they lack dystroglycan glycosylation (Leonoudakis *et al.*, 2014). These results differ from ours (see [Chapter 5, Figure 5-2](#)) and other studies, which show that breast cancer cells are able to internalise laminin (Coopman *et al.*, 1996; Leonoudakis *et al.*, 2014). In fact, MDA-MB-231 were reported to phagocytose laminin in an α 3 β 1 integrin-dependent manner (Coopman *et al.*, 1996). The use of different techniques could give different results: it is noteworthy to mention that the former study used 10 μ g/ml soluble laminin-111, while the latter used gelatin or matrigel films, as well as gelatin-coated beads (Coopman *et al.*, 1996). This highlights the importance of using substrates that recapitulate *in vivo* features, rather than soluble ECM ligands. In addition, Coopman *et al.* pre-label matrigel with FITC, which could potentially affect the way matrigel polymerises since the free lysine side chains are required for self-aggregation of collagens (Tenni *et al.*, 2006; Harris and Reiber, 2007; Wilharm *et al.*, 2022). Secondly, the authors detach the cells with trypsin-EDTA and they use FACS to quantify the uptake; actually, trypsin could release cleaved FITC-matrigel peptides and alter the readout using FACS. Interestingly, the authors of this study claim MDA-MB-231 cells rely on phagocytosis to internalise laminin, however those

remarks are based on utilising gelatin-coated beads. While we used polymerised matrices, these studies have used soluble ligands or ECM-coated beads (Coopman *et al.*, 1996; Arora *et al.*, 2004; Leonoudakis *et al.*, 2014). In fact, inhibition of $\alpha 3\beta 1$ integrin does not decrease matrigel internalisation in MDA-MB-231 cells (Rainero, unpublished). Those different set ups could impact on the mechanical properties of cell-ECM interaction and the following signalling cascade that activates endocytosis of ECM. Gelatin is mainly denatured collagens; it thus seems unlikely that $\alpha 3\beta 1$ may recognise those beads. Actually, $\alpha 2\beta 1$ integrin, a well-known laminin and collagen receptor, has been described to mediate collagen I phagocytosis in fibroblasts (Arora *et al.*, 2004; Rainero, unpublished). Therefore, it may be possible that MDA-MB-231 cells phagocytosed gelatin-coated beads, while laminin internalisation relies on caveolin and dynamin.

While 20 μ M dynasore and 3.75 μ g/ml filipin alone did not impinge matrigel internalisation, the combinatory treatment diminished matrigel internalisation. This suggested that filipin and dynamin may be acting on separate endocytic pathways, most likely caveolin, clathrin or flotillin-dependent endocytosis. Nevertheless, downregulation of clathrin and flotillin resulted in a small increase in uptake. Interestingly, dynasore has been reported to have off-target effects and impinge on fluid-phase endocytosis, as well as membrane ruffling in a triple dynamin knockout cell line (Park *et al.*, 2013). Taking this into consideration, the observed combinatory effect may be on account of its effect on dynamin-dependent endocytosis and macropinocytosis. Congruently with this observation, as well as with EIPA data ([Figure 3-13](#)), PAK1 downregulation led to 35% decrease in matrigel uptake ([Figure 3-23](#)). Interestingly, collagen IV accounts for around 30% of matrigel (Corning Matrigel matrix datasheet). Altogether, laminin internalisation may be internalised in a caveolin- and dynamin- dependent manner; while collagen IV may follow a macropinocytic route. Actually, internalisation of collagen I was diminished upon EIPA treatment ([Figure 3-14](#)). However, dynamin inhibition had no effect on collagen I contrary to previous studies, which showed that soluble collagen fragments are internalised in a dynamin-dependent way through binding to Endo180 (Wienke, MacFadyen and Isacke, 2003). The observed differences in collagen internalisation could be cell type dependent. Dynasore and EIPA treatment significantly reduced internalisation of TIF-CDM ([Figure 3-15](#)). The decrease in TIF-CDM uptake in presence of dynasore could be on account of fibronectin internalisation in a

dynamamin- and caveolin-dependent manner (Sottile and Chandler, 2005; Rainero, 2016), however no effect was observed upon filipin treatment. CDMs contain complex and diverse ECM proteins, including thrombospondins. Alternatively, thrombospondin-1 internalisation is mediated by the low density lipoprotein receptor-related protein 1 (LRP1) (Mikhailenko *et al.*, 1997). Remarkably, LRP1 internalisation relies on dynamin-2 (Zemskov *et al.*, 2007). Overall, this data suggests that macropinocytosis is the main and common endocytic route invasive breast cancer cells use to internalise matrigel, collagen I and TIF-CDM (see [Figure 3-27](#)). More precisely, MDA-MB-231 cells rely on PAK1-mediated macropinocytosis to internalise stroma-like ECMs ([Figure 3-24](#)).

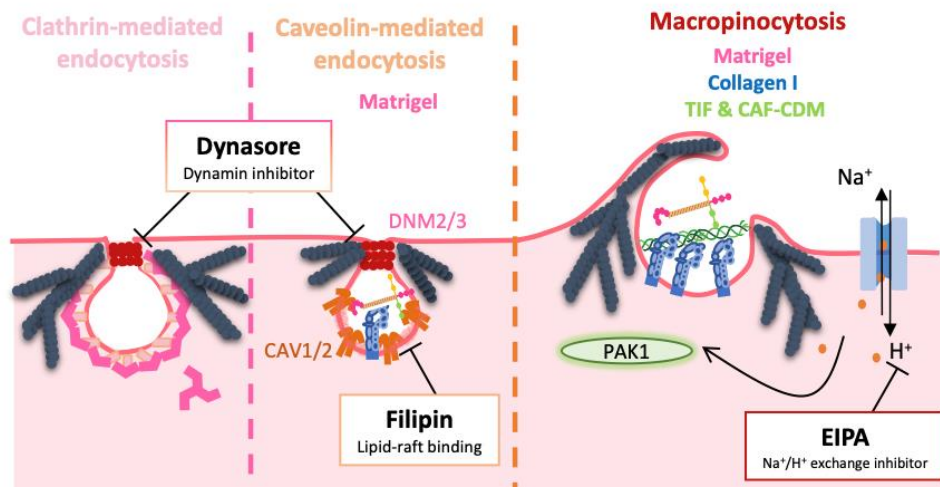


Figure 3-27. Schematic summary of the endocytic pathways regulating ECM internalisation. Invasive breast cancer cells converge on macropinocytosis to internalise matrigel, collagen I and CDM. In addition, matrigel internalisation is caveolin-mediated.

In this chapter we have established that breast cancer cells converge on macropinocytosis to internalise the different ECM components. Nonetheless, other studies pointed out that fibroblasts and breast cancer cells phagocytose collagens and laminin-111 (Coopman *et al.*, 1996; Arora *et al.*, 2004). Phagocytosis is defined as receptor-mediated engulfment of large particles. In fact, our results show that β 1-integrin is required for matrigel and collagen I uptake ([Figure 3-19](#) and [Figure 3-20](#)). Despite the use of different terminologies, it may be possible that the processes described are one and the same. In fact, PAK1 localises to phagocytic cups and it has been described to regulate phagocytosis (Dharmawardhane *et al.*, 1999; Chang *et al.*, 2020). Phagocytosis has been classically associated with professional phagocytic cells, including dendritic cells and macrophages, however non-professional phagocytic cells have been described

as well (Rabinovitch, 1995). For example, in early embryogenesis, cooperative epithelial phagocytosis in zebrafish and mouse embryos has a key role in scavenging apoptotic cells (Hojjman *et al.*, 2021). In pre-implantation embryos, embryonic stem cells rely on macropinocytosis of extracellular proteins and later lysosomal digestion as a source of nutrients (Todorova *et al.*, 2022). Similarly, pancreatic adenocarcinoma cells have been reported to uptake collagen fragments via macropinocytosis under starvation (Olivares *et al.*, 2017). In agreement with these results, amino acid starvation increased ECM internalisation in 3D culture ([Figure 3-26](#)). However, due to the pH sensitive nature of the dye, we cannot discard the fact that increased intracellular pHrodo signal may be on account of increased traffic to the lysosomes. Future studies may characterise whether amino acid starvation not only promotes ECM internalisation but ECM-integrin traffic to lysosomes. In addition, $\alpha 5\beta 1$ integrin clusters in nascent macropinocytic cups (Le *et al.*, 2021). The rising evidence on the different flavours of macropinocytosis suggests both terminologies may be possible (Lin, Mintern and Gleeson, 2020).

Following ECM endocytosis, the ECM components are trafficked and degraded in the lysosomes by cysteine cathepsins (Rainero, 2016). Interestingly, 24h E64d treatment led to accumulation of intracellular matrigel in MDA-MB-231 cells seeded on lower matrigel concentrations ([Figure 3-11](#) and [Figure 3-12](#)). However, no effect was observed at higher concentrations. We also validated this results in a 96-well plate format, E64d treatment on 0.5mg/ml significantly increased matrigel uptake, while the uptake was only slightly increased for MDA-MB-231 cells seeded on 1mg/ml matrigel when treated with the cysteine cathepsin inhibitor (data not shown). This data suggests that matrigel coating in a 384-well plate partially resembles the 96-well plate coating. These results differ from previous work in the lab (see [Chapter 5](#), Figure 5-2). E64d treatment has been shown to lead to loss of lysosomal acidification in the mouse mammary epithelial NMuMG cells and in the lung adenocarcinoma cell line A549 (Kern *et al.*, 2015). This suggests that the changes in pH induced by E64d may result in a decrease of signal using pHrodo labelled matrices and an increase in signal when matrices are labelled with NHS-fluorescein, since fluorescein loses fluorescence as acidity increases (Le Guern *et al.*, 2020). Another possible explanation is that in order to achieve homogeneous matrices, plates are centrifuged. This accumulates the matrix components at the bottom of the plate and, in addition, the forces

exhibited during centrifugation may have promoted the generation of stiffer matrices. In cancer, cysteine cathepsins are secreted to the extracellular space (Rainero, 2016; Vidak *et al.*, 2019), we thus hypothesised that low ECM concentrations or low stiffness substrates may not require extracellular proteolysis and under these conditions, matrigel accumulates inside the cells. However, higher concentrations or stiffnesses may rely on the extracellular proteolysis by cysteine cathepsins or matrix metalloproteinases. MMP inhibition only impinged collagen I and TIF-CDM internalisation by 13-15%, suggesting that extracellular degradation by MMPs is superfluous in ECM internalisation. However, inhibition of cysteine cathepsins resulted in 35% decrease in matrigel and only 20% decrease for collagen I and TIF-CDM ([Figure 3-25](#)); however, the current study did not include combinatory inhibition of MMPs and cysteine cathepsins.

Moreover, inhibition of ECM internalisation or siRNA-mediated downregulation of PAK1 results in accumulation of collagen I bundles around MDA-MB-231 cells. This suggests that breast cancer cells may mechanically remodel the surrounding ECM prior to its internalisation. This mechano-remodelling process may be coupled with extracellular degradation, thus an intermediate process between receptor-mediated macropinocytosis and phagocytosis may occur.

Altogether, in this chapter we have established a novel methodology to study internalisation of ECM in high throughput systems, with special focus on 384-well plates. However, these results are applicable to 96-well plate format as well. Despite fixation with 4% (w/v) paraformaldehyde significantly reduced the intracellular signal as time progressed, our data suggest that the quantified results do not strikingly differ between fixed and live imaged samples, probably because the loss of signal is equal in the few samples we compared right after fixation. Assessing internalisation of ECM requires live imaging for better and more reliable results.

However, the protocol could be applied to study integrin internalisation in high throughput systems or assessing a protein of interest whose expression changes in response to mechanotransduction or integrin engagement to ECM. Angiogenesis assays have been classically performed on matrigel matrices; therefore, this protocol could be adapted to assess regulators of angiogenesis in high throughput. In addition, we showed that increasing the concentration and volume of matrigel results in the formation of 3D-like structures, this protocol could thus be

useful to study regulators of mesenchymal transformation (i.e., EMT) or invasion in a high throughput fashion. Moreover, we presented the endocytic pathways regulating ECM internalisation, however the specific components internalised by cancer cells in complex matrices remain unexplored. The following chapter aims to characterise ECM proteins internalised by breast cancer cells in complex matrices.

Chapter 4 – Dissecting extracellular matrix internalisation using proteomics

Montserrat Llanses Martinez conceived, planned and performed most of the experiments. Dr Keqian Nan (former student in Elena Rainero lab) performed a replicate in [Figure 4-1](#), samples 1 to 3. The following results were written using the inclusive first-person plural.

4.1. INTRODUCTION

In vivo, once cancer cells breach through the BM, they encounter a complex network of secreted stromal proteins. The tumour microenvironment is a complex and miscellaneous *society* (Baghban *et al.*, 2020). In addition to the proteic and cellular constituents, there are lipid bilayers, known as extracellular vesicles (EVs) that are released by cancer and stromal cells (Verweij *et al.*, 2021). EVs are diverse, ranging from: multivesicular endosome-derived exosomes, ectosome and microvesicles that sprout from the PM, oncosomes, apoptotic bodies, migrasomes left at the trailing edge of migrating cells, among others (Verweij *et al.*, 2021). Of note, in addition to the traditional methods of cell-cell communication: signalling by direct contact, paracrine and autocrine signalling (Jin *et al.*, 2021), EVs are now regarded as a complementary mechanism for intracellular communication (Verweij *et al.*, 2021). EVs enable cells to receive proteins, lipids and genetic material from other cells (Verweij *et al.*, 2021). Cells in a complex environment require a certain degree of decision-making. To study better cancer cell-stromal interaction, we can take advantage of cell derived matrices derived from normal fibroblasts (or TIFs) or cancer-associated fibroblasts. The previous chapter identified that MDA-MB-231 cells internalise intricate cell derived matrices. While the main components of TIF-generated matrices are collagen I and fibronectin, other matrisome proteins are also present (Fitzpatrick and McDevitt, 2015). However, the approach used in the first chapter does not enable distinction between matrisome proteins. We thus sought to use an unbiased high throughput proteomic approach to identify core matrisome, as well as associated proteins, which are internalised by MDA-MB-231 when cultured on TIF-generated matrices.

Proteomics is the study of the proteome or, in other words, all the proteins expressed in the genome (Graham, Elliott and Van Eyk, 2005). Two major procedures for the study of proteomics

by mass spectrometry have been developed: bottom-up and top-down analysis (Feist and Hummon, 2015). While the latter analyses whole proteins, the former involves investigating peptides derived from digested proteins (Feist and Hummon, 2015). For bottom-up mass spectrometry, two main digestion approaches have been used: in-gel and in-solution digestion (Feist and Hummon, 2015). In-solution digestion requires denaturation, reduction, alkylation and digestion of proteins, which are contained in a liquid phase (Feist and Hummon, 2015). While samples of more complexity can be analysed following fractionation in a gel, in-solution digests require less proteins and sample loss is less acute (Feist and Hummon, 2015). A common approach to study a subcategory of proteins that participate in a biological function is through covalently tagging biotin to the proteins of interest through chemical modifications, including NHS esters (Schiapparelli *et al.*, 2014). Given the strong interaction between biotin and streptavidin (Fairhead and Howarth, 2015), biotinylated proteins can be enriched through their binding to streptavidin beads (Schiapparelli *et al.*, 2014). Biotinylated proteins are later eluted and digested so the sample can be analysed by mass spectrometry (Schiapparelli *et al.*, 2014).

In order to study how breast cancer cells interact with the non-cellular tumour microenvironment, we seeded MDA-MB-231 cells on biotinylated CDMs. Subsequent mass spectrometry revealed internalisation of several matrisome proteins associated with cancer progression. However, the utilised protocol did not enable characterisation of receptors that could mediate this process. Therefore, we aimed to establish a new proteomic approach for the detection of not only matrisome proteins, but also to determine the receptors or other interacting proteins, constituting the endo-adesome complex, that may mediate ECM endocytosis. This chapter includes preliminary data on the initial steps of developing this novel methodology.

4.2. RESULTS

4.2.1. Breast cancer cells internalise more ECM components from CDM than normal mammary epithelial cells

ECM internalisation is highly upregulated in invasive breast cancer cell lines compared to normal mammary epithelial cells (Rainero, unpublished). Therefore, we sought to recapitulate those

results by western blot. With these experiments, we first aimed to corroborate whether the biotinylation method enabled some degree of quantification between conditions. We cultured invasive MDA-MB-231 cells and non-transformed mammary epithelial MCF10A cells on biotinylated and/or non biotinylated CDMs. CDMs were labelled using Sulpho-NHS-SS-Biotin ([Figure 4-1A](#)). Interestingly, the molecule is thiol-cleavable, meaning that the disulfide bond can be reduced and only a small sulfhydryl group remains ([Figure 4-1A](#)). Taking advantage of this property, following 16h incubation the extracellular biotin was reduced using sodium 2-mercaptoethanesulfonate. In addition, iodoacetamide is later used to alkylate or *cap* reduced cysteines prior to protein extraction. Cell extracts derived from MDA-MB-231 and MCF10A cells seeded on biotinylated CDM, as well as cell extracts from MDA-MB-231 cultured on unlabelled CDM were assessed. Western blot analysis showed that two main bands were found in the non-biotinylated cell extracts ([Figure 4-1B](#)). Those bands correspond to endogenously expressed biotin-containing enzymes, most likely carboxylases. In addition to those bands, both MDA-MB-231 and MCF10A cells cultured on biotinylated CDM displayed multiple nicely defined bands of proteins. Interestingly, the band intensity, as well as the number of bands, was higher in MDA-MB-231 compared to MCF10A cells, confirming that invasive breast cancer cells internalise higher levels of ECM compared to normal mammary epithelial cells. Overall, our findings indicate that western blot analysis enables detection of internalised ECM in MDA-MB-231 cells, as well as MCF10A cells.

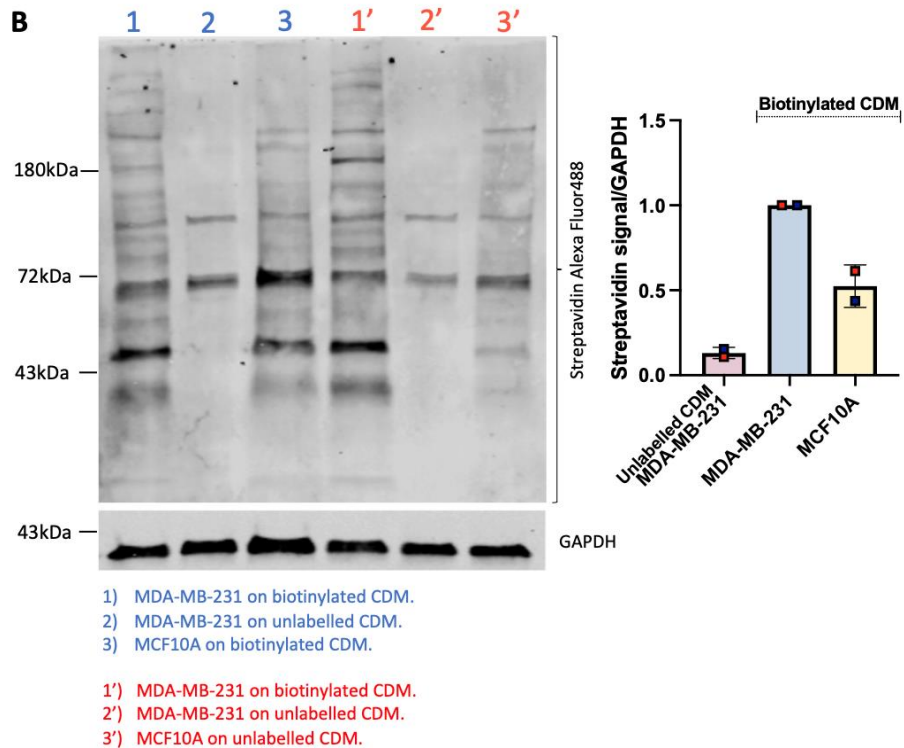
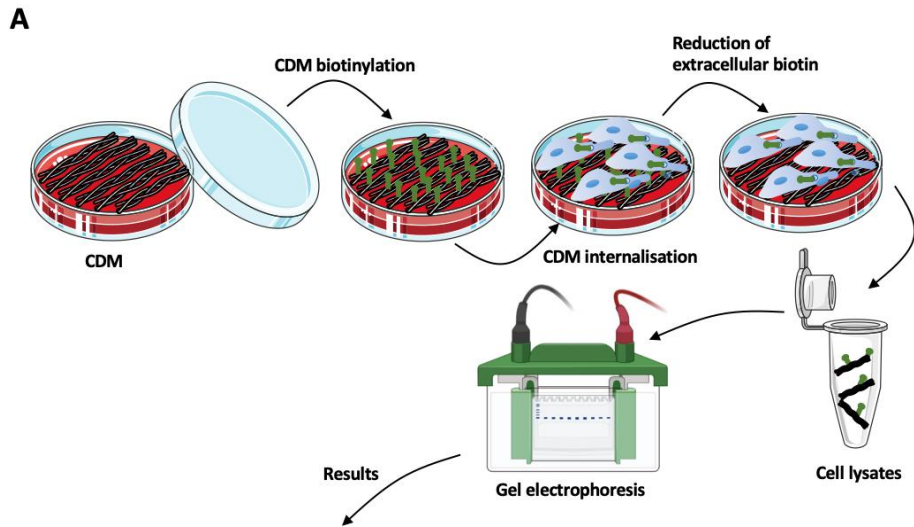


Figure 4-1. Invasive MDA-MB-231 cells internalise more CDM than normal mammary MCF10A cells by western blot analysis. CDMs were generated as per protocol in 10cm² dishes for nine days. The generated CDMs were labelled with 0.13mg/ml Sulpho-NHS-SS-Biotin for 30 minutes on gentle rocking at 4°C. MDA-MB-231 and MCF10A cells were cultured for 16h in presence of 20µM Aloxistatin (E64d). Extracellular biotin was reduced with 15mg/ml sodium 2-mercaptoethanesulfonate for 1h 30min at 4°C. Reduced cysteines were alkylated by adding 17mg/ml iodoacetamide for 10 minutes at 4°C. MDA-MB-231 and MCF10A cells were washed and extracted with ice-cold 20mM NH₄OH and 0.5% Triton X-100, containing a protease inhibitor cocktail. Cells were lysed on ice and gentle rocking for 15-20 minutes. Cell lysates were transferred into a Qia-shredder column and spun down at 13000 rpm for 10 minutes at 10°C. The supernatant was collected, mixed with NuPAGE buffer and heated up at 70°C for 5 minutes. Cell lysates were analysed by western blot (A). Data represents normalised mean ± SD from N=2 independent experiments (B). Replicates 1-3 (represented in blue) were performed by Keqian Nan, former PhD student in the Rainero lab. Image made using items from Servier medical Art.

4.2.2. Proteomic analysis identifies that breast cancer cells internalise pro-tumorigenic ECM-related proteins

To further investigate ECM internalisation in invasive breast cancer, we aimed to determine whether the methodology used above was compatible with mass spectrometry. In order to boost the amount of internalised peptides, cell seeding was increased from 1.2×10^6 cells per 10 cm^2 dish to 2.2×10^6 . MDA-MB-231 cells were plated on biotinylated and unlabelled CDMs for 16h. Similarly, extracellular biotin was reduced, sulfhydryl groups were alkylated and cells were extracted in presence of protease inhibitors. A fraction of the cell lysate was analysed by western blot. GAPDH enabled the assessment of cell extraction efficiency between conditions ([Figure 4-2](#)), while streptavidin allowed us to visualise that cell extracts contained biotinylated proteins. Western blot quantification confirmed that increasing cell number enabled a better quantification and visualisation of biotinylated proteins, as the Streptavidin/GAPDH signal was higher than in the previous replicates (data not shown). For mass spectrometry, the 3 biological replicates were run using the same standard or calibration curve to minimise technical variation. Mass spectrometry analysis was performed in Perseus, data was represented using a standard volcano plot (see [Figure 4-3](#)). 738 proteins were identified by mass spectrometry in three independent experiments. Potential contaminants were excluded, including human keratins and trypsin (used for sample digestion), but also proteins found in the FBS, such as bovine plasminogen, vitronectin and albumin, among others. Hits were narrowed down to 214 proteins in common between the three replicates (see [Figure 4-3](#) and [Table S1-4](#)). For the statistical analysis, two different S0 values were applied (0.1 and 1) coupled to a false discovery rate (FDR) of 0.05. S0 defines the artificial within groups variance or a minimal fold change. If a certain protein gives a good p-value but the fold change is below that value, it will not come up as significant. In other words, it regulates the relative significance of the resulting p-value and the difference between means (Perseus documentation, Jürgen Cox lab, Max Planck institute of biochemistry). Both S0 values allowed to determine proteins that MDA-MB-231 cells internalised. 81 proteins matched after selection between both S0 values (see [Figure 4-3D](#)).

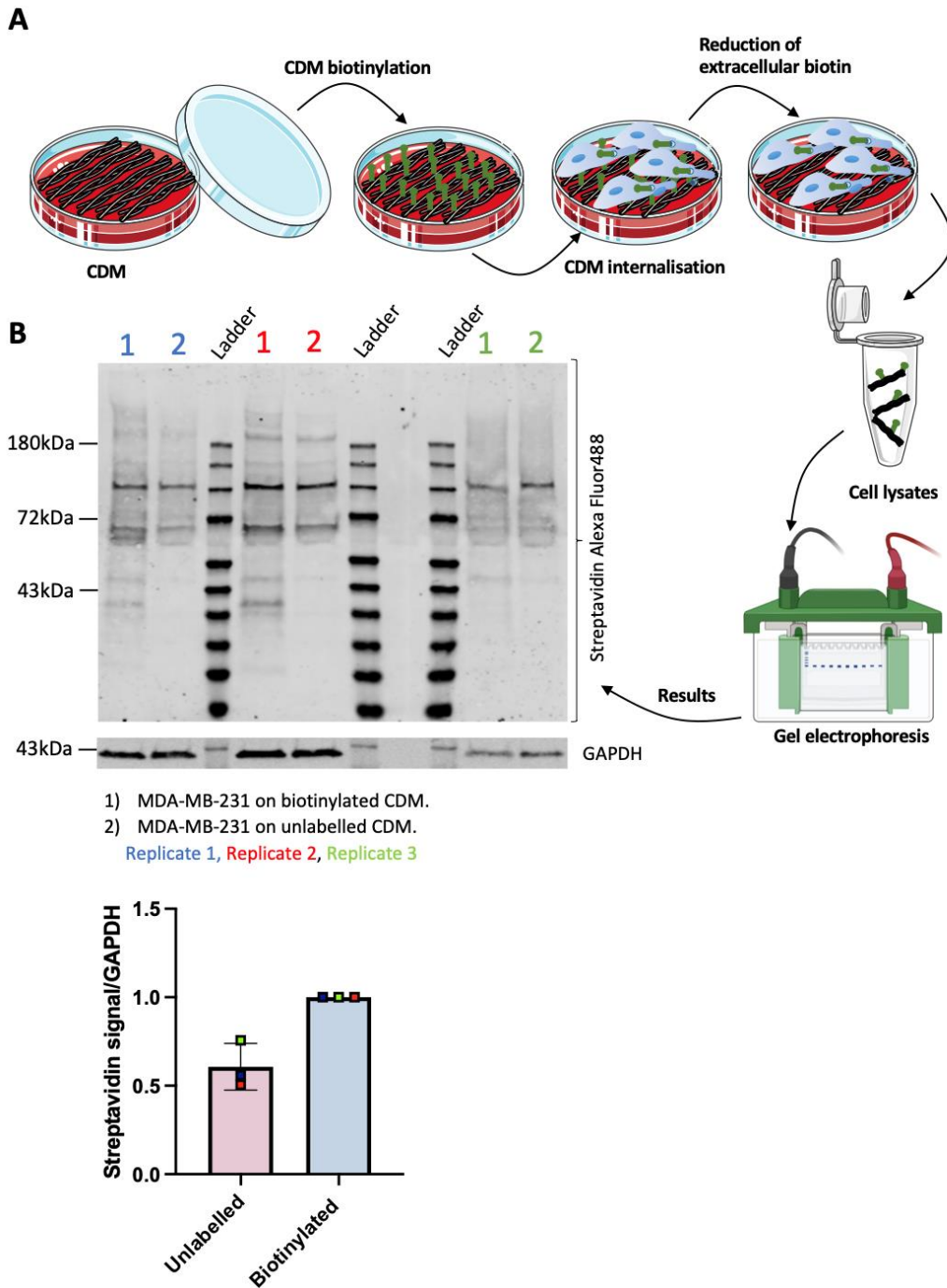


Figure 4-2. Western blot analysis of internalised CDM in MDA-MB-231 cells on unlabelled and biotinylated CDMs. CDMs were generated as per protocol in 10cm² dishes for nine days. The generated CDMs were labelled with 0.13mg/ml Sulpho-NHS-SS-Biotin for 30 minutes on gentle rocking at 4°C. 2,2x10⁶ MDA-MB-231 cells were cultured for 16h in presence of 20µM Aloxistatin (E64d). Extracellular biotin was reduced with 15mg/ml sodium 2-mercaptoethanesulfonate for 1h 30min at 4°C. Reduced cysteines were alkylated by adding 17mg/ml iodoacetamide for 10 minutes at 4°C. MDA-MB-231 cells were washed and extracted with ice-cold 20mM NH₄OH and 0.5% Triton X-100 (400µl/dish), containing a protease inhibitor cocktail. Cells were lysed on ice and gently rocking for 15-20 minutes. Cell lysates were transferred into a Qia-shredder column and spun down at 13000 rpm for 10 minutes at 10°C. 30µl of the supernatant was collected, mixed with NuPAGE buffer and heated up at 70°C for 5 minutes. Cell lysates were analysed by western blot (A). Data represents normalised mean ± SD from N=3 independent experiments; Colours represent biological replicates (B). Image made using items from Servier medical Art.

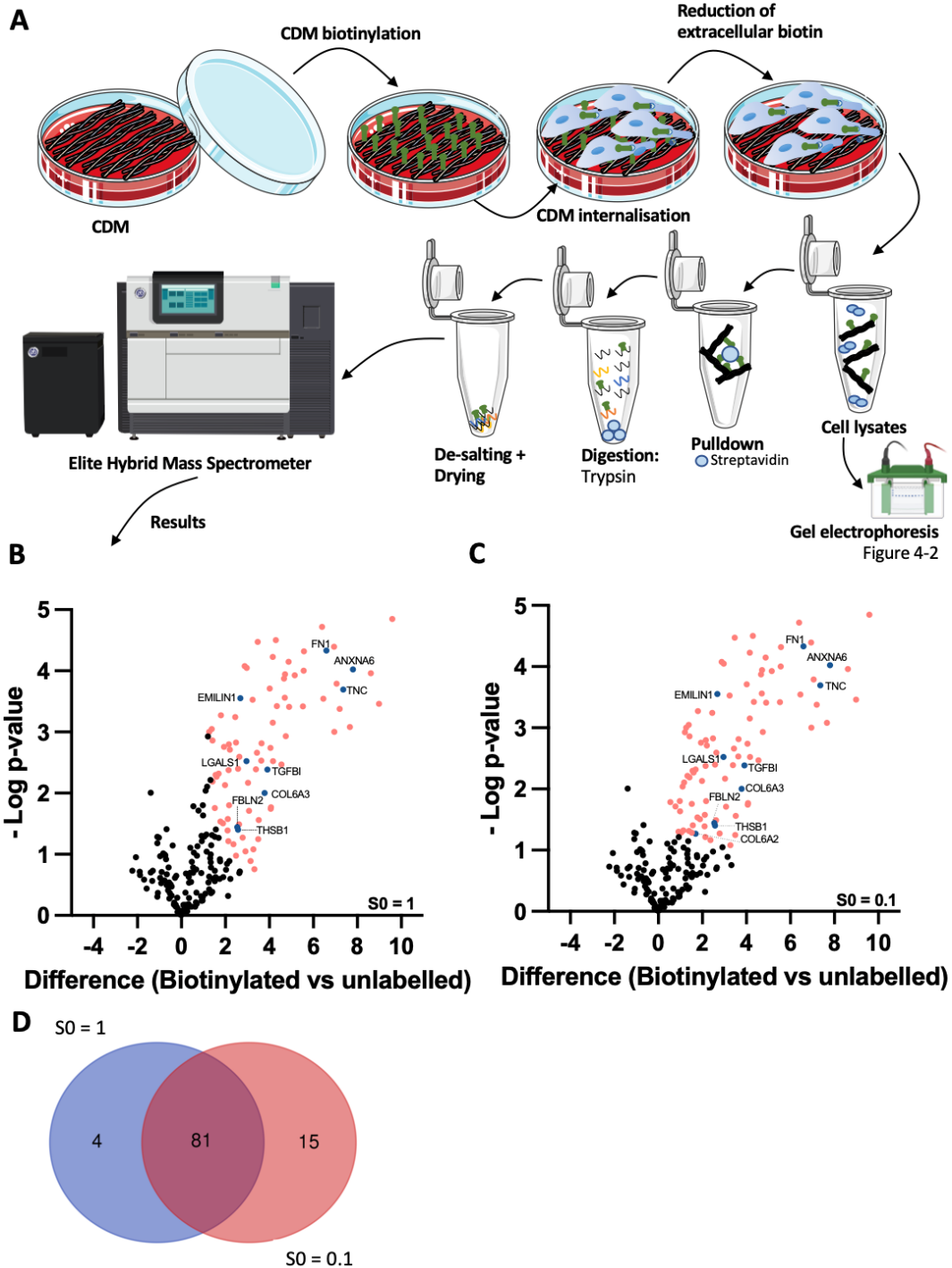


Figure 4-3. Mass spectrometry of internalised CDM in MDA-MB-231 cells. CDMs were generated, labelled and processed as in Figure 4-2. Cell number was increased to $2,2 \times 10^6$ cells per 10 cm^2 dish. Cell lysates were incubated with streptavidin beads overnight at 4°C . Beads were washed 3 times with (1) 2% SDS, (2) 2M urea + 50mM ammonium bicarbonate and (3) 50mM ammonium bicarbonate. Beads were collected in 50mM ammonium bicarbonate. TCEP was added to denature disulphide bonds, iodoacetamide quenched free cysteines. Beads were then trypsinised. Samples were collected, desalted and dried prior to mass spectrometry analysis (A). Volcano plot, threshold used $S_0 = 1$ (B). Volcano plot, threshold $S_0 = 0.1$ (C). Venn diagram of common hits between $S_0 = 1$ and $S_0 = 0.1$ (D). $N = 3$ independent experiments, 4 technical replicates per experiment. Mass spec samples were run and analysed by Dr Mark Collins. Image made using items from Servier medical Art.

In these experiments, we aimed to identify which ECM components MDA-MB-231 cells internalise in a complex matrix. The matrisome project is an open access platform to facilitate ECM research by enabling access to protocols, tools and data sets. MatrisomeDB (<http://matrisomeproject.mit.edu/proteins/>) is a searchable curated proteomic database from 17 studies on ECM of 15 normal tissue types, six cancer types and other diseases. We thus took advantage of this tool to see how many proteins matched in their database. From the 214 proteins that were in common in the 3 replicates, 14 proteins belong to either core matrisome or matrisome-associated proteins (see [Table 4-1](#) and [Figure 4-3](#)), while only 10 matrisome proteins were found in the statistically significant biotinylated group, including Annexin A6, Tenascin, Fibronectin, Collagen VI, among few others (see blue labelled proteins in [Table 4-1](#)). This data indicated that a high percentage (~70%) of matrisome proteins were preserved after statistical analysis. Outstandingly, many of these proteins have been reported in metastatic mammary carcinoma and melanoma xenografts, as well as on liver metastasis derived from colorectal carcinoma tumours (Naba *et al.*, 2012; Naba, Clauser, Lamar, *et al.*, 2014; Naba, Clauser, Whittaker, *et al.*, 2014).

Table 4-1. Core-matrisome and matrisome-associated proteins detected in the 214 common proteins in biotinylated CDM samples. Blue labelled proteins are statistically significantly upregulated, while black labelled proteins do not display a significant change. The table includes the matrisome division and category for each protein. In addition, annotations displaying in which tissue or tumours the proteins are expressed. Data from: <http://matrisomeproject.mit.edu/proteins/>.

Protein information	Experimental evidence (present in tissue)
<p>Annexin A6 (ANXA6) <u>Matrisome division:</u> matrisome-associated. <u>Category:</u> ECM-affiliated protein</p>	<p>Highly metastatic mammary carcinoma xenograft (MDA-MB-231-LM2) Poorly metastatic mammary carcinoma xenograft (MDA-MB-231) Human Colon Matrisome Human Liver Matrisome Human Liver Metastasis (from Primary Colorectal Tumour) Matrisome Human Metastatic Primary Colorectal Tumour Matrisome Poorly metastatic melanoma xenograft (A375) Glomerular basement membrane Retinal vascular basement membrane Lens capsule basement membrane</p>
<p>Annexin A5 (ANXA5) <u>Matrisome division:</u> matrisome-associated. <u>Category:</u> ECM-affiliated protein</p>	<p>Highly metastatic mammary carcinoma xenograft (MDA-MB-231-LM2) Poorly metastatic mammary carcinoma xenograft (MDA-MB-231) Poorly metastatic melanoma xenograft (A375) Human Colon Matrisome Human Liver Matrisome Human Liver Metastasis (from Primary Colorectal Tumour) Matrisome Human Metastatic Primary Colorectal Tumour Matrisome</p>

	Lens capsule basement membrane
<p>Annexin A1 (ANXA1) <u>Matrisome division:</u> matrisome-associated. Category: ECM-affiliated protein</p>	Highly metastatic mammary carcinoma xenograft (MDA-MB-231-LM2) Poorly metastatic mammary carcinoma xenograft (MDA-MB-231) Highly metastatic melanoma xenograft (MA2) Poorly metastatic melanoma xenograft (A375) Human Colon Matrisome Human Liver Matrisome Human Liver Metastasis (from Primary Colorectal Tumour) Matrisome Human Metastatic Primary Colorectal Tumour Matrisome Glomerular basement membrane Retinal vascular basement membrane Inner limiting membrane Lens capsule basement membrane
<p>Annexin A2 (fragment) (ANXA2) <u>Matrisome division:</u> matrisome-associated. Category: ECM-affiliated protein</p>	Highly metastatic mammary carcinoma xenograft (MDA-MB-231-LM2) Poorly metastatic mammary carcinoma xenograft (MDA-MB-231) Highly metastatic melanoma xenograft (MA2) Poorly metastatic melanoma xenograft (A375) Human Colon Matrisome Human Liver Matrisome Human Liver Metastasis (from Primary Colorectal Tumour) Matrisome Human Metastatic Primary Colorectal Tumour Matrisome Glomerular basement membrane Retinal vascular basement membrane Inner limiting membrane Lens capsule basement membrane
<p>Tenascin C (TNC) <u>Matrisome division:</u> Core matrisome. Category: ECM glycoprotein</p>	Highly metastatic mammary carcinoma xenograft (MDA-MB-231-LM2) Poorly metastatic mammary carcinoma xenograft (MDA-MB-231) Highly metastatic melanoma xenograft (MA2) Poorly metastatic melanoma xenograft (A375) Human Colon Matrisome Human Liver Matrisome Human Liver Metastasis (from Primary Colorectal Tumour) Matrisome Human Metastatic Primary Colorectal Tumour Matrisome Glomerular basement membrane Retinal vascular basement membrane Inner limiting membrane Lens capsule basement membrane
<p>Fibronectin (FN1) <u>Matrisome division:</u> Core matrisome. Category: ECM glycoprotein</p>	Highly metastatic mammary carcinoma xenograft (MDA-MB-231-LM2) Poorly metastatic mammary carcinoma xenograft (MDA-MB-231) Highly metastatic melanoma xenograft (MA2) Poorly metastatic melanoma xenograft (A375) Human Colon Matrisome Human Liver Matrisome Human Liver Metastasis (from Primary Colorectal Tumour) Matrisome Human Metastatic Primary Colorectal Tumour Matrisome Glomerular basement membrane Retinal vascular basement membrane Inner limiting membrane Lens capsule basement membrane
<p>Transforming growth factor-beta-induced protein ig-h3 (Fragment)</p>	Highly metastatic mammary carcinoma xenograft (MDA-MB-231-LM2) Highly metastatic melanoma xenograft (MA2) Human Colon Matrisome

<p>(TGFB1) <u>Matrisome division:</u> Core matrisome. Category: ECM glycoprotein</p>	<p>Human Liver Matrisome Human Liver Metastasis (from Primary Colorectal Tumour) Matrisome Human Metastatic Primary Colorectal Tumour Matrisome Poorly metastatic mammary carcinoma xenograft (MDA-MB-231) Poorly metastatic melanoma xenograft (A375) Glomerular basement membrane Retinal vascular basement membrane Inner limiting membrane Lens capsule basement membrane</p>
<p>Collagen alpha-3(VI) chain (COL6A3) <u>Matrisome division:</u> Core matrisome. Category: Collagens</p>	<p>Highly metastatic mammary carcinoma xenograft (LM2) Highly metastatic melanoma xenograft (MA2) Human Colon Matrisome Human Liver Matrisome Human Liver Metastasis (from Primary Colorectal Tumour) Matrisome Human Metastatic Primary Colorectal Tumour Matrisome Poorly metastatic mammary carcinoma xenograft (MDA-MB-231) Poorly metastatic melanoma xenograft (A375) Glomerular basement membrane Retinal vascular basement membrane Inner limiting membrane Lens capsule basement membrane</p>
<p>Collagen alpha-2(VI) chain (COL6A2) <u>Matrisome division:</u> Core matrisome. Category: Collagens</p>	<p>Highly metastatic mammary carcinoma xenograft (MDA-MB-231-LM2) Poorly metastatic mammary carcinoma xenograft (MDA-MB-231) Highly metastatic melanoma xenograft (MA2) Poorly metastatic melanoma xenograft (A375) Human Colon Matrisome Human Liver Matrisome Human Liver Metastasis (from Primary Colorectal Tumour) Matrisome Human Metastatic Primary Colorectal Tumour Matrisome Glomerular basement membrane Retinal vascular basement membrane Inner limiting membrane Lens capsule basement membrane</p>
<p>Collagen alpha-1(XII) chain (COL12A1) <u>Matrisome division:</u> Core matrisome. Category: Collagens</p>	<p>Highly metastatic mammary carcinoma xenograft (MDA-MB-231-LM2) Poorly metastatic mammary carcinoma xenograft (MDA-MB-231) Highly metastatic melanoma xenograft (MA2) Poorly metastatic melanoma xenograft (A375) Human Colon Matrisome Human Liver Matrisome Human Liver Metastasis (from Primary Colorectal Tumour) Matrisome Human Metastatic Primary Colorectal Tumour Matrisome Glomerular basement membrane Retinal vascular basement membrane Lens capsule basement membrane</p>
<p>Galectin-1 (LGALS1) <u>Matrisome division:</u> matrisome-associated. Category: ECM-affiliated protein</p>	<p>Highly metastatic mammary carcinoma xenograft (MDA-MB-231-LM2) Poorly metastatic mammary carcinoma xenograft (MDA-MB-231) Highly metastatic melanoma xenograft (MA2) Poorly metastatic melanoma xenograft (A375) Human Colon Matrisome Human Liver Matrisome Human Liver Metastasis (from Primary Colorectal Tumour) Matrisome Human Metastatic Primary Colorectal Tumour Matrisome Glomerular basement membrane</p>

<p>EMILIN-1 (EMILIN1) <u>Matrisome division:</u> Core matrisome. Category: ECM glycoprotein</p>	<p>Highly metastatic mammary carcinoma xenograft (MDA-MB-231-LM2) Poorly metastatic mammary carcinoma xenograft (MDA-MB-231) Highly metastatic melanoma xenograft (MA2) Poorly metastatic melanoma xenograft (A375) Human Colon Matrisome Human Liver Matrisome Human Liver Metastasis (from Primary Colorectal Tumour) Matrisome Human Metastatic Primary Colorectal Tumour Matrisome Glomerular basement membrane Retinal vascular basement membrane Inner limiting membrane Lens capsule basement membrane</p>
<p>Thrombospondin-1 (THBS1) <u>Matrisome division:</u> Core matrisome. Category: ECM glycoprotein</p>	<p>Highly metastatic mammary carcinoma xenograft (LM2) Poorly metastatic mammary carcinoma xenograft (MDA-MB-231) Highly metastatic melanoma xenograft (MA2) Poorly metastatic melanoma xenograft (A375) Human Liver Metastasis (from Primary Colorectal Tumour) Matrisome Human Metastatic Primary Colorectal Tumour Matrisome Glomerular basement membrane</p>
<p>Fibulin-2 (FBLN2) <u>Matrisome division:</u> Core matrisome. Category: ECM glycoprotein</p>	<p>Human Colon Matrisome Human Liver Matrisome Human Liver Metastasis (from Primary Colorectal Tumour) Matrisome Human Metastatic Primary Colorectal Tumour Matrisome</p>

Unexpectedly, in addition to matrisome proteins, we detected intracellular proteins, including β -actin, α -actinin (actin binding protein), vimentin (intermediate filaments), moesin (connect cortical actin to plasma membrane), talin-1 (focal adhesion protein) among others ([Table S1-4](#)). On the one hand, this data shows that CDM extraction is not 100% efficient and diverse cytoskeletal proteins remain. However, on the other hand, it may indicate that focal adhesion complexes remained on the CDMs even after extraction, showing the magnitude of focal adhesions in fibroblasts. Actually, other cell surface proteins were detected in these samples; including Prolyl endopeptidase FAP, type II-transmembrane serine protease highly expressed in arthritis, fibrosis and cancer. Interestingly, the raw data included $\alpha 2$, $\alpha 11$, $\beta 1$ and $\beta 6$ integrin subunits, which were likely excluded in previous steps because not all biological replicates displayed them (data not shown). This suggests that focal adhesion complexes or ECM remodelling structures, for example invadopodia, remain after CDM extraction. More strikingly, breast cancer cells not only internalise the gold-standard soluble ligands, such as transferrin and albumin, as well as ECM proteins but *scavenge* other molecules they encounter. Despite not

being statistically significant, another family of proteins found in the sample were heat shock chaperones, including Heat shock protein (HSP) 90 α , HSP90 β and HSPA8. Interestingly, these proteins are frequently integrated into exosomes. Exosomes carry molecules from diverse nature that denote their function, including metabolic enzymes and mitochondrial content. Interestingly, our samples also detected several mitochondrial proteins ([Table S1-4](#)). It has been reported that cancer cells internalise exosomes, MDA-MB-231 cells may internalise exosomes that may have remained on CDMs after extraction. Altogether, this data indicates that proteomic analysis of internalisation of ECM proteins is possible. Nonetheless, further optimisation is required to visualise biotinylated-CDM complexes together with other interactors, such as integrins or regulators of endocytic traffic.

4.2.3. Optimisation of protein extraction using phospholipase A2

We have shown that quantification of endocytosed TIF-CDM is possible, however the harsh alkaline extraction conditions and washes used impede to see protein complexes interacting with biotinylated extracellular proteins. While ammonium hydroxide and triton X-100 are conventionally used for CDM extraction, new protocols have emerged which are more gentle and better preserve the structure of some ECM proteins (Chaturvedi *et al.*, 2015; Keane, Swinehart and Badylak, 2015). We thus aimed to investigate whether the Phospholipase A2 (PLA2) method would suffice for extracting proteins in MDA-MB-231 cells. Two different time points (30 and 60 minutes) at 37°C were assessed based on previous optimisation (Chaturvedi *et al.*, 2015; Martin Humphries lab, personal communication). No difference in cell extraction was observed, however western blot assessment clearly showed a smear of proteins in 60-minute extraction, suggesting protein degradation occurred despite the presence of protease inhibitors (data not shown). Notwithstanding that, extraction for 30 minutes enabled visualisation of extracted proteins by western blot. The high pH in the ammonium hydroxide and triton X-100 buffer severely impinge on the detection of protein complexes. We then tested a panel of PLA2 buffer extraction conditions at pH 7 and pH8 to see which would be more suitable for mass spectroscopy ([Table 4-2](#)). In addition, we included an extraction condition missing the PLA2 to assess whether this enzyme was required. The latter condition very tightly recapitulates the RIPA buffer, previously used for purification of protein complexes (Immunoprecipitation protocol, Abcam).

Table 4-2. Extraction buffers used for optimisation of protein extraction. The table includes the volumes used to prepare the PLA2 extraction buffers from the stock solutions.

Conventional extraction buffer	PLA ⁺ pH7 (up to 10ml)		PLA ⁺ pH8 (up to 10ml)		PLA ⁻ pH8 (up to 10ml)
20mM NH ₄ OH 0.5% Triton X-100	1M Tris-HCl pH7	500µl	1M Tris-HCl pH8	500µl	500µl
	5M NaCl	300µl	5M NaCl	300µl	300µl
	0.1M MgCl ₂	100µl	0.1M MgCl ₂	100µl	100µl
	0.1M CaCl ₂	100µl	0.1M CaCl ₂	100µl	100µl
	627 U/ml PLA2	318.9µl	PLA2	318.9µl	N/A
	1% Sodium deoxycholate	5ml	1% Sodium deoxycholate	5ml	5ml
	H ₂ O	3.68ml	H ₂ O	3.68ml	4ml

While all the different conditions tested could extract proteins, the extraction buffer at pH 7 acquired colloid-like properties and was not as efficient at extracting proteins ([Figure 4-4](#), red colour). However, ammonium hydroxide, PLA₂⁺ and PLA₂⁻ extraction buffers at pH 8 enabled better extraction of proteins ([Figure 4-4](#), blue, green and orange colour). However, PLA₂⁺ outcompeted the other conditions in terms of Streptavidin signal/GAPDH ([Figure 4-4](#), green colour). In Chapter 3, we have shown that cysteine cathepsins may mediate the intracellular degradation. We thus compared whether E64d-treatment had an effect on streptavidin signal. No significant differences were observed by western blot analysis. However, all conditions displayed a trend in which DMSO had higher signal, further suggesting that cysteine cathepsins may partially mediate intracellular and extracellular ECM degradation. Altogether, these results show that PLA₂⁺ and PLA₂⁻ extraction buffers at pH 8 may be an alternative option to use in mass spectrometry.

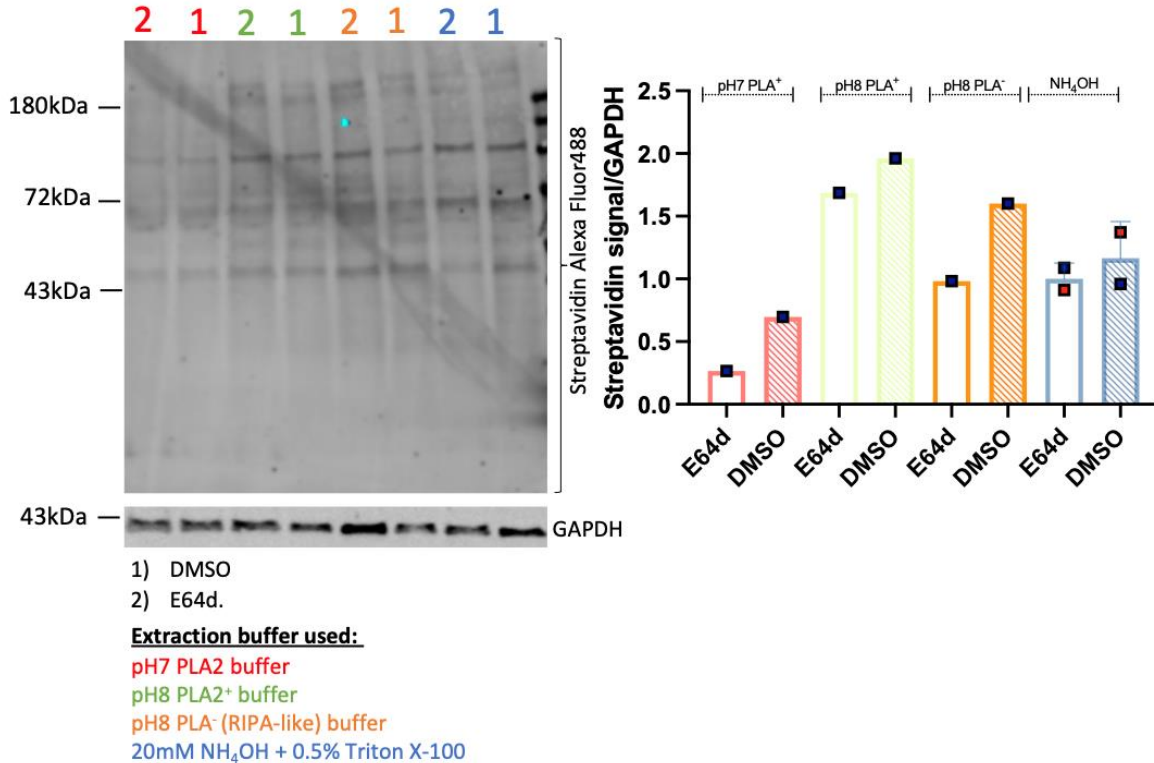


Figure 4-4. Western blot for optimisation of protein extraction. CDMs were generated as per protocol in 6 well plates. CDMs were labelled with 0.13mg/ml Sulpho-NHS-SS-Biotin for 30 minutes at 4°. MDA-MB-231 cells were cultured for 16h in the presence of DMSO or 20µM Aloxistatin (E64d). Extracellular biotin was reduced with sodium 2-mercaptoethanesulfonate. Reduced cysteines were alkylated by iodoacetamide. MDA-MB-231 cells were washed and extracted using 4 different extraction buffers (see Table 4-2), containing a protease inhibitor cocktail. Cells were lysed on ice and gently rocking for 15-20 minutes. Cell lysates were transferred into a Qia-shredder column and spun down at 13000 rpm for 10 minutes at 10°C. 30µl of the supernatant was collected, mixed with NuPAGE buffer and heated up at 70°C for 5 minutes. Cell lysates were analysed by western blot. Data represents normalised mean ± SD from at least N=1 experiment.

4.3. DISCUSSION

In this chapter we have presented that CDM biotinylation enables the detection and quantification of CDM internalisation by breast cancer cells. We have shown that several core matrisome and matrisome-associated proteins are significantly upregulated in the biotinylated CDM group. During metastatic growth, cancer cells undergo metabolic reprogramming (Faubert, Solmonson and DeBerardinis, 2020). In metastatic breast cancer cells mTORC1 signalling relies on pyruvate availability, which in turn promotes serine biosynthesis (Rinaldi *et al.*, 2021). Notwithstanding that, macropinocytosis of extracellular proteins has been reported in cancer cells (Commisso *et al.*, 2013; Kamphorst *et al.*, 2015; Palm *et al.*, 2015). Consequently, one could hypothesise that as tumours and metastases establish and grow, breast cancer cells utilise the

ECM as a nutrient source in the scarce and nutrient-limited conditions that the tumour core supposes. Indeed, our lab recently demonstrated that macropinocytosis-dependent ECM internalisation upregulates tyrosine/phenylalanine metabolism and production of fumarate (Nazemi *et al.*, 2021). Moreover, mTORC1 activity is restored, and localises into the lysosomes, in the presence of internalised extracellular matrix (Nazemi *et al.*, 2021). The results shown in this chapter indicate that breast cancer cells internalise TNC. Tenascin-C (TNC), for example, is highly upregulated in the tumour microenvironment and it correlates with poor prognosis and survival in several cancers, including breast cancer (Oskarsson *et al.*, 2011). While TNC is homogeneously expressed in lung and bone micrometastasis, in growing and established metastases, TNC localises into the invasive front (Oskarsson *et al.*, 2011). Moreover, TNC has been reported to promote an epithelial-to-mesenchymal transition-like switch mediated by the activation of Src and FAK kinase in breast cancer cell models of in situ carcinoma, e.g. MCF7 cells (Nagaharu *et al.*, 2011; Katoh *et al.*, 2013). This phenotype is mediated by $\alpha\beta 1$ integrin in the presence of TNC alone or $\alpha\beta 6$ in the presence of TGF β and TNC (Katoh *et al.*, 2013). In addition, TNC engagement to $\alpha 9\beta 1$ integrin was reported to inhibit YAP, by impinging on actin stress fibres, to promote amoeboid-like properties in vitro and metastasis *in vivo* using osteosarcoma models (Sun *et al.*, 2018). Simultaneously, TNC competes with syndecan-4 binding to fibronectin, which in turn impairs fibronectin binding to syndecan-4/ $\alpha 5\beta 1$ integrin (Sun *et al.*, 2018). While the role of TNC in mediating EMT-like changes is earlier on the tumorigenic process, it could be that in mesenchymal cells, such as MDA-MB-231 cells, TNC internalisation regulates the switch between the mesenchymal state to an amoeboid-like phenotype. In fact, inhibition of diverse extracellular proteolysis mechanisms (MMPs, cathepsins and serine proteases) in MDA-MB-231 cells and HT-1080 fibrosarcoma cells, which exhibit constitutively mesenchymal migration, results in conversion towards an amoeboid phenotype (Wolf *et al.*, 2003). In fact, cysteine cathepsin inhibition decreased ECM internalisation in MDA-MB-231 cells (see [Chapter 3](#), Figure 3-25) and it appears that streptavidin/GAPDH signal is slightly lower in E64d-treated conditions compared to DMSO (see Figure 4-4). Hence, it could be possible that inhibition of cysteine cathepsins results in a decrease of TNC endocytosis; higher levels of extracellular TNC may in turn promote an amoeboid-like phenotype.

Fibronectin has been extensively recognised as a driver of carcinogenesis (Lin *et al.*, 2019; Rick *et al.*, 2019). Fibronectin deposition is required for correctly assembling collagens into the ECM. Some studies have addressed the role of cancer-secreted fibronectin (from MDA-MB-231 cells) in bone metastasis. shRNA-mediated downregulation of fibronectin and chemical inhibition of fibronectin assembly by uPR4 severely affected collagen deposition and MDA-MB-231 metastatic ability, as well as proliferation in those tumours (Ghura *et al.*, 2021). Our mass spectrometry suggests that fibronectin is internalised by MDA-MB-231 cells. In fact, fibronectin internalisation has been reported to rely on caveolin- and $\alpha 5\beta 1$ integrin in fibroblasts (Shi and Sottile, 2008). Therefore, it may be possible that its internalisation promotes MDA-MB-231 cell proliferation and changes in the ECM architecture or the elastic properties of this, which may facilitate infiltration of cancer cells into the surrounding stroma or intravasation. ECM internalisation is enhanced in invasive breast cancer cells compared to normal mammary epithelial cells ([Figure 4-1](#); Rainero, unpublished). In the endometrioid ovarian cancer cell line A2780 overexpressing Rab25, $\alpha 5\beta 1$ integrin localises at fibrillar adhesions beneath the nucleus, from where fibronectin is internalised and trafficked to the lysosomes (Rainero *et al.*, 2015). Inhibition of fibrillar adhesions by downregulating tensin-1, tensin-2 and tensin-3 decreased invasive migration using inverted invasion assays (Rainero *et al.*, 2015). Interestingly, fibronectin internalisation links nutrient signalling via mTORC1 activation, which specifically senses nutrient availability, to invasive migration (Rainero *et al.*, 2015). Lysosomal traffic of ECM promotes mTORC1 activation in MDA-MB-231 cells (Nazemi *et al.*, 2021), suggesting that thus internalisation of fibronectin and other ECM components, may similarly promote invasive migration.

Transforming growth factor-beta-induced protein ig-h3 (TGFBI) is copiously expressed by the peritoneum (Ween *et al.*, 2011; Ween, Oehler and Ricciardelli, 2012), where it promotes serous ovarian cancer invasion, motility and adhesion to peritoneal cells (Ween *et al.*, 2011; Ween, Oehler and Ricciardelli, 2012). However, other reports suggest that it acts as a tumour suppressor. Ween and colleagues suggested that high TGFBI concentrations promote cell death, indicating that TGFBI could have an anti-tumorigenic role (Ween *et al.*, 2011). In lung, prostate and breast cancer cells, the TGFBI promoter is hypermethylated (Shao *et al.*, 2006). TGFBI overexpression has been shown to reduce metastasis of several cancers, including breast and

lung carcinomas, neuroblastoma and osteosarcomas (Wen *et al.*, 2011). Altogether, internalisation of TGFBI may regulate its pro-metastatic versus anti-tumorigenic roles. High levels of TGFBI endocytosis, and later degradation, may reduce its extracellular levels and potentiate its pro-metastatic effects. While it has been suggested that the methylation status of TGFBI promoter could be therapeutically targeted, modulation of ECM internalisation may open a similar avenue for modulating the levels of pro- and anti-tumorigenic ECM proteins. Future research may explore the role of ECM endocytosis in the regulation of pro- and anti-tumorigenic properties of the ECM components.

Increasing evidence points that collagen VI is a prognosis factor of tumorigenesis and tumour progression (Li *et al.*, 2022). High expression of collagen alpha-3 (VI) was reported to correlate with EMT in bladder carcinomas (Huang *et al.*, 2018). Similar to breast cancer, pancreatic carcinomas are characterised by desmoplasia or high levels of fibrotic tissue (Piersma, Hayward and Weaver, 2020). Our mass spec analysis identified collagen alpha-2 and alpha-3 (VI) chains in the biotinylated groups; both chains constitute two out of the three subunits of collagen VI. This suggests that both chains may be internalised together and that the collagen triple helix structure is partially conserved prior to its internalisation. A recent study showed that pancreatic cancer cells upregulate the expression of collagen VI, as well as fibronectin, but not collagen I to V in response to soft substrate hydrogels (Papalazarou *et al.*, 2022). Collagen VI secretion by cancer or stromal cells promotes invasion in inverted invasion assays, as well as migration in 3D wound healing assay (Papalazarou *et al.*, 2022). Remarkably, collagen VI expression determines the metastatic potential of pancreatic cancer cells *in vivo* (Papalazarou *et al.*, 2022). Of note, the authors of this study did not discard that on soft matrices, pancreatic cancer cells were unable to secrete collagen VI. In addition, it could also be that cancer cells internalise collagen VI and regulate its expression in a feedback loop. Endocytosis of EGFR has been shown to control proliferative signalling, as well as transcription of several genes. Many of the endocytosed proteins can indeed be transported to the nucleus via the ER or directly through nuclear envelope associated endosomes (Shah *et al.*, 2019). Nuclear interaction of EGFR and STAT-3 have been shown to regulate inducible nitric oxide synthase (iNOS2) (Lo *et al.*, 2005). In addition, EGFR downstream phosphorylation of the RNA-DNA binding protein fused in sarcoma (FUS) was

reported to regulate transcription of profibrotic collagen genes, namely collagen I, IV and X (Chiusa *et al.*, 2020). Growth factor receptors are internalised together with integrins, the main ECM receptors. Ligand-activated EGFR, Grb2, Src and β 5-integrin localise together in clathrin-coated plasma membrane regions (Alfonzo-Méndez *et al.*, 2022). Moreover, regulators of the endocytic machinery have been described to modulate transcription (Pyrzynska, Pilecka and Miaczynska, 2009); the recruitment of such proteins in the cytoplasm or the nucleoplasm may act as a switch in regulation of transcription. Alternatively, endosomal signalling has been described to suppress anoikis, promoting anchored-independent growth in metastatic cells (Alanko *et al.*, 2015). Secretion of collagen VI by either cancer or stromal cells and, later internalisation to the endosomal compartments may be a requisite by cancer cells to induce anchorage-independent survival, suppress anoikis and metastasis.

Galectins are carbohydrate-binding proteins or lectins that can be secreted or found in the intracellular and extracellular space. The results above show that Galectin-1 is internalised by MDA-MB-231 cells. The role of Galectin-1 in cancer is controversial. It was shown to be significantly upregulated in serum samples from breast cancer patients, as well as create an immunosuppressive tumour microenvironment (Dalotto-Moreno *et al.*, 2013; Gurel Cayir *et al.*, 2020). Other *in vitro* studies nevertheless reported that galectin-1 induces apoptosis and inhibits cell proliferation of MCF-7 cells in 2D and 3D cell culture models (Geiger *et al.*, 2016). The observed difference may be due to a concentration effect or a differential signalling in a 3D environment. MDA-MB-231 cells were reported to express high levels of Galectin-1. Galectin-1 secretion and later internalisation may be an advantage for invasive breast cancer cells. One possible mechanism could be inhibition of anoikis by promoting endosomal signalling. The tumour microenvironment is scarce of nutrients; considering its carbohydrate binding role, galectin-1 may promote an indirect internalisation of carbohydrates or glycosylated proteins. In the lysosomes the proteins and carbohydrates would be degraded and released into the cytoplasm. While both saccharides and proteins would result in increased proliferation, the derivative metabolites from saccharides may fuel the warburg effect. The warburg effect is defined as a preference of cancer cells to metabolise glucose towards lactate even in presence

of oxygen (Liberti and Locasale, 2016). This results in high acidosis in the tumour microenvironment, promoting invasion and immunosuppression (Liberti and Locasale, 2016).

Thrombospondin-1 (THBS1) is a negative regulator of angiogenesis in the tumour microenvironment. THBS1 was reported to have pro- and anti-metastatic effects (Yee *et al.*, 2009). To further study this, Yee and colleagues compared mouse tumours derived from PyMT to the corresponding THBS1- null tumours. Indeed, the latter displayed larger primary tumours and bigger blood vessels, however the metastasis burden to the lungs was significantly lower (Yee *et al.*, 2009). Under these conditions, THBS1 seems to promote migration and later metastasis (Yee *et al.*, 2009). THBS1 in addition increases adhesion of breast cancer cells to the endothelium and high serum levels appear to be a marker of invasive carcinoma (Byrne *et al.*, 2007). Internalisation of THBS1 could modulate the pro-angiogenic and pro-migratory phenotype, on the one hand, its internalisation in the primary tumour would promote angiogenesis. On the other hand, THBS1 endocytosis would reduce breast cancer cell adhesion to the endothelium and enable dissemination of breast cancer cells. THBS1-exosomes derived from MDA-MB-231 cells were shown to disrupt the integrity of endothelial cells (Cen *et al.*, 2019). THBS1 endocytosis could further contribute to this phenotype. THBS1 may be trafficked to MVB, once breast cancer cells reach the capillaries, THBS1⁺-MVB may be subsequently released and disrupt the endothelium.

Emilin-1 is important to maintain the skin homeostasis. It has been reported to inhibit proliferation of fibroblasts and keratinocytes upon its interaction with $\alpha 4\beta 1$ or $\alpha 9\beta 1$ integrins (Danussi *et al.*, 2011). Similarly, in colorectal tumorigenesis, it acts as a tumour suppressor through its interaction with $\beta 1$ -integrin (Capuano *et al.*, 2019). Emilin-1 interaction with tetraspanin 9 impairs invasive migration of gastric cancer cells (Qi *et al.*, 2019). Nevertheless, a recent study showed that cleaved Emilin-1 and its secretion in extracellular vesicles reduced its anti-tumorigenic properties (Amor López *et al.*, 2021). In fact, cleaved Emilin-1 reduces its interaction with $\alpha 4\beta 1$ or $\alpha 9\beta 1$ integrins, which regulate its anti-proliferative signalling (Maiorani *et al.*, 2017). It could thus be that highly invasive breast cancer cells cleave and internalise Emilin-1 to bypass its anti-proliferative properties.

Fibulin-2 is required for maintaining the integrity of the BM. Of note, fibulin-2 expression decreased in immunohistological samples where ductal carcinoma in situ (DCIS) tumours became invasive (Ibrahim *et al.*, 2018). Similarly, loss of Fibulin-2 in the perivasculature strongly correlates with vascular infiltration (Klingen *et al.*, 2021). Fibulin-2 degradation by ADAMTS5 and ADAMTS4 enhances invasion and migration of breast cancer cells and mammary fibroblasts, respectively (Fontanil *et al.*, 2017). Data from the Rainero lab suggests that internalisation of ECM is specifically upregulated in invasive breast cancer. Fibulin-2 internalisation could determine whether breast cancer cells may acquire invasive capabilities and be the first step in the metastatic cascade by disrupting the integrity of the BM.

Annexins are phospholipid/membrane binding proteins regulated by calcium (Mirsaeidi *et al.*, 2016). Twelve annexins have been described in humans, whose gene size ranges from 15kb (ANXA9) to 96kb (ANXA10) (Mirsaeidi *et al.*, 2016). Our mass spectrometry results identified ANXA6 as significantly upregulated in the biotinylated group. While it has been identified as an intracellular scaffold protein, ANXA6 is also detected in extracellular vesicles (Ochieng *et al.*, 2009; Korolkova *et al.*, 2020). Moreover, annexins were reported to be required for exosome uptake (Koumangoye *et al.*, 2011). Annexin A6 could facilitate exosome uptake by MDA-MB-231 cells. In accordance with this, our mass spectrometry included several proteins that have been previously detected in exosomes, such as HSP90 family proteins, which have been described in EVs (Figure 4-5). Fibroblast and CAFs promote metabolic reprogramming of endothelial cells and carry several integrin heterodimers (Santi *et al.*, 2023). In addition, preliminary studies have observed that MDA-MB-231 cells deposit EVs on collagen fibres, which can be later internalised by other cells (Frédéric Saltel lab, Bordeaux institute of oncology; personal communication). EV internalisation by MDA-MB-231 has been shown to promote cell migration by acquiring the DDR1 receptor (Frédéric Saltel, personal communication). It could thus be that fibroblast EVs, containing metabolic enzymes and integrin heterodimers, induce metabolic reprogramming but also induce signalling changes that enable internalisation of ECM. Considering the detected enzymes, mainly mitochondrial enzymes, it is likely that exosome internalisation leads to mitochondrial metabolic reprogramming in breast cancer cells. A recent study suggested that mitochondria can be laterally transferred from pro-tumorigenic M2-like macrophages to cancer

cells (Kidwell *et al.*, 2021). Interestingly, transfer of few mitochondria already results in increased reactive oxygen species and ERK signalling, which further promotes cell proliferation (Kidwell *et al.*, 2021). Transfer of mitochondrial enzymes by exosomes could similarly promote proliferation by activating ERK signalling. Alternatively, fibroblasts are highly contractile cells, it has been reported that the trailing edge ruptures and it is left behind upon retraction (Chen, 1981; Rigort *et al.*, 2004). It could thus be that fibroblast contraction during ECM remodelling leads to the deposition of detached membrane, in addition to EV secretion.

Collagen XII belongs to the classification of FACIT collagens, which are essential players in collagen I architecture (Papanicolaou *et al.*, 2022). A recent study reported that CAF-derived collagen XII impacts on the organisation of collagen I and its expression correlates with poor prognosis and metastatic relapse (Papanicolaou *et al.*, 2022). Its expression is a potential prognostic factor for gastric cancer (Jiang *et al.*, 2019). While the molecular mechanisms behind its pro-tumorigenic properties are not well understood, traces of collagen XII were detected in the current study. Similar to collagen VI, collagen XII internalisation may partially drive invasion and metastasis by inhibiting anoikis. Alternatively, its internalisation may alter the 3D ECM structure, making it more permissible to movement, and facilitate invasive migration. It is noteworthy to mention that the mass spectrometry results were carried out in presence of E64d, a cysteine cathepsin inhibitor, in order to block the lysosomal degradation of internalised ECM proteins. Similarly, previous results (see [Chapter 3](#)) show that MDA-MB-231 cells internalise collagen I, however collagen I was not enriched in biotinylated samples. It could thus be that collagen I and collagen XII internalisation is impaired upon E64d treatment ([Figure 4-5](#)). Future work aims to recapitulate these results in the absence of E64d to further investigate whether proteins with higher molecular weight are detected.

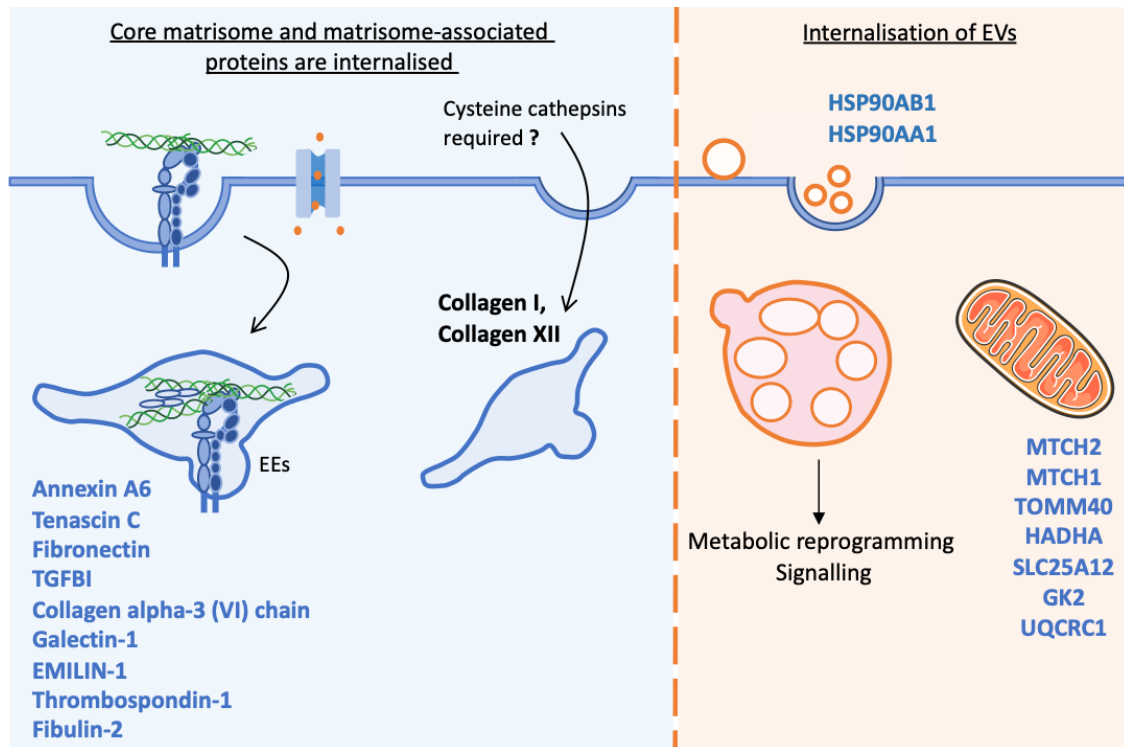


Figure 4-5. Schematic summary of the hits obtained by mass spectrometry. Proteins detected by mass spectrometry, which are statistically significant (labelled in blue) in the biotinylated group compared to the non-biotinylated. In black, matrisome proteins that were either detected but not statistically significant, such as collagen XII, or not detected, namely collagen I. The right diagram shows a schematic model displaying the EV markers found in the biotinylated group, as well as metabolic enzymes detected, which could induce metabolic reprogramming or changes in signalling pathways.

Furthermore, this chapter included preliminary data on the optimisation of a protein extraction buffer that would enable characterisation of protein complexes with integrin receptors and potentially intracellular binding partners, namely Rab proteins, adaptor proteins or signalling kinases. Future work will assess whether the extraction buffer is also efficient at 4°C instead of 37°C. In addition to the Sulpho-NHS-SS-Biotin, the generated CDM will be labelled with reductive dimethylation for stable isotope labelling (described in (Tolonen and Haas, 2014)); isotope labelling of the CDM will enable to differentiate between intracellular molecules remaining in the CDMs (remaining integrins, focal adhesion proteins, actin, cofilin, etc.) and intracellular regulators from MDA-MB-231 cells. Moreover, the binding time to streptavidin beads will be reduced to 2h (instead of overnight incubation) to avoid disrupting the complexes. Finally, peptides will be released from the streptavidin beads, in column tryptic digestion will be performed and peptides will be analysed by mass spectrometry (see [Figure 4-6](#) for changes in the workflow).

Taking everything into consideration, several tumorigenic matrisome proteins have been identified by mass spectrometry. These results suggest that mass spectrometry detection of internalised proteins is possible. However future work is required to further optimise and maximise the data generated by this protocol, detect interacting partners and differentiate between peptides from MDA-MB-231 cells and TIFs. In this study we have utilised an inhibitor against cysteine cathepsins to block lysosomal degradation of ECM. However, the molecular mechanisms regulating ECM traffic to lysosomes remain unexplored, the following chapter will explore trafficking regulators that participate in ECM delivery to lysosomes.

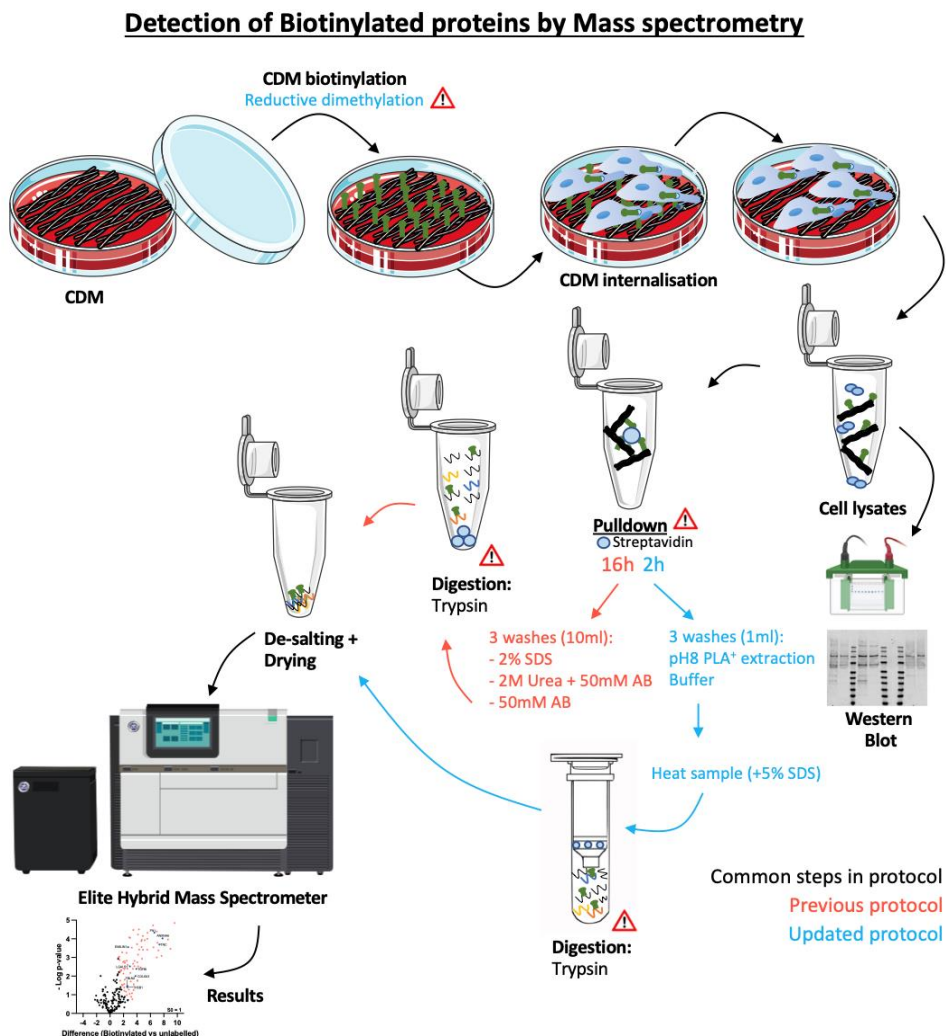


Figure 4-6. Schematic mass spectrometry protocol. Black arrows represent common steps in both versions of the protocol. Red arrows and headings represent the previous protocol, while blue arrows and writing represents the updated protocol. SDS, sodium dodecyl sulphate; AB, ammonium bicarbonate; PLA, phospholipase A2. Image made using items from Servier medical Art.

Chapter 5 – A trafficking screen identifies the AP3 complex as a novel regulator of ECM-bound integrin traffic to lysosomes

Montserrat Llanses Martinez conceived, planned, carried out and analysed all the experiments. Dr Xavier LeGuezennec (IMCB, Singapore) printed the siRNA plates for the screening (Figure 5-3). Dr Carl Harrison (Strutt lab, Sheffield) performed the imaging for Single-molecule localisation microscopy (Figure 5-9). Dr Elena Rainero set up the time-lapse microscope (Figure 5-9). This results chapter was written using inclusive first-person plural.

5.1. INTRODUCTION

Extracellular cargoes and receptors are endocytosed into endocytic vesicles. Once internalised, vesicles are carried toward the perinuclear region along microtubules via dynein and kinesin (York, Coyle and Arumugam, 2020). In the perinuclear region, the intracellular tails of receptors contained in vesicles interact with adaptor proteins and downstream effectors (York, Coyle and Arumugam, 2020). Receptors and/or recruited proteins are subject to modifications by phosphorylation and/or ubiquitination to determine the trafficking route or receptor fate, such as lysosomal degradation (Sorkin and von Zastrow, 2009; York, Coyle and Arumugam, 2020).

There are 5 types of adaptor protein (AP) complexes: AP1, AP2, AP3, AP4 and AP5 (Park and Guo, 2014). The AP2 complex is the most characterised and predominant adaptor of clathrin coated vesicles (Collins *et al.*, 2002). Clathrin interacts with the $\text{L}\phi\text{D}/\text{E}\phi\text{D}/\text{E}$ clathrin box motif that resides in the $\beta 2$ subunit of AP2 (Collins *et al.*, 2002). AP2 is required for initiating clathrin assembly into pits or lattices and it also regulates the dissociation of clathrin from coated vesicles (Collins *et al.*, 2002; Kovtun *et al.*, 2020). The function of the AP4 complex predominantly remains elusive (Davies *et al.*, 2018). Mutations affecting this complex are associated with neurological disorders and cerebral palsy (Abou Jamra *et al.*, 2011; Davies *et al.*, 2018). Recent studies suggest that AP4 mediates trafficking from the trans-Golgi network to the peripheral endosomal compartment. Specifically, it mediates ATG9A traffic, which regulates autophagosome biogenesis (Davies *et al.*, 2018). The AP3 complex is a heterotetramer constituted by one molecule each of δ (AP3D1), $\beta 3$ (AP3B1, AP3B2), $\mu 3$ (AP3M1, AP3M2) and $\sigma 3$ (AP3S1, AP3S2) adaptins (Dell'Angelica, 2009).

The AP3 complex localises in the tubular endosomal compartment, where it mediates the sorting of cargoes and lysosomal membrane proteins to lysosomes (see [Figure 5-1](#)) (Peden *et al.*, 2004). This mechanism is dependent on VAMP7-binding to δ -adaptin through hydrophobic residues (Ile702/Val704 and Leu709/Leu713) (Kent *et al.*, 2012). Specifically AP3 mediates VAMP7 transport when it is engaged in a cis-SNARE complex with STX7, STX8, VIT1B (Kent *et al.*, 2012). VAMP7 is involved in the fusion of early endosomes to lysosomes (Advani *et al.*, 1999). In addition, AP3 downregulation promotes re-localisation of lysosomal transmembrane protein I and II (LAMP1/2) to the PM suggesting AP3 is involved in trafficking LAMP1/2 from the PM to lysosomes. However, VAMP7 interaction with the δ -adaptin subunit is not required for trafficking LAMP1/2 to lysosomes (Kent *et al.*, 2012).

The μ -adaptin subunit specifically interacts with endosomal cargoes via tyrosine-based signals fitting the Yxx Φ motif (in which x represents any aminoacid and Φ is an amino acid with a bulky hydrophobic residue) (Ohno *et al.*, 1995; Zhuo *et al.*, 2021). The hemicomplex formed by the δ - and σ 3-adaptin subunits recognise the dileucine [D/E]XXXL[L/I] consensus motif (Janvier *et al.*, 2003). The [D/E]XXXL[L/I] sorting motif is required to mediate lysosomal delivery of the glucose transporter 8 (GLUT8) and lysosomal integral membrane protein II (LIMP2) (Sandoval *et al.*, 2000; Augustin, Riley and Moley, 2005). ADP-ribosylation factor 1 (Arf1) specifically mediates recruitment and facilitates the open conformation of the AP3 complex to endosomes (Ooi, Dell'Angelica and Bonifacino, 1998; Faundez and Kelly, 2000; Zhuo *et al.*, 2021). GTP-bound Arf1 associates with the δ - and σ 3-adaptin subunits (Lefrançois *et al.*, 2004). Simultaneously, ARF1 recruitment is regulated by the ears of the δ -adaptin (Lefrançois *et al.*, 2004). BIG1/ARFGEF1 and BIG2/ARFGEF2 promote Arf1 activation, while AGAP1-binding to δ - and σ 3-adaptin results in inactivation of Arf1 and dissociation of AP3 complex from the vesicular membrane (Nie *et al.*, 2003).

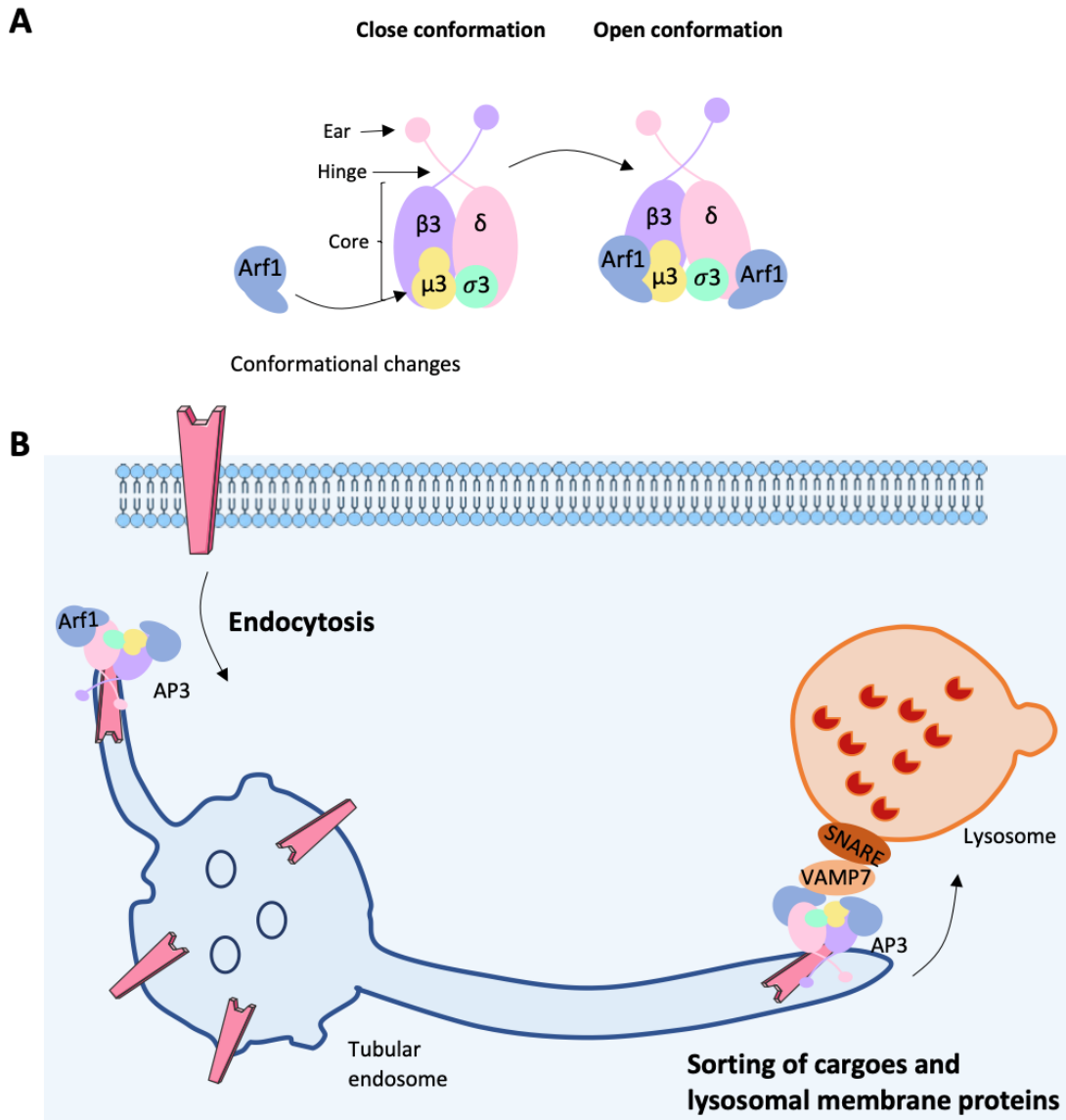


Figure 5-1. (A) Schematic representation of AP3 structure and (B) localization in tubular endosomes. AP3 mediates the sorting of cargoes and lysosomal proteins to lysosomes. VAMP7 has been involved in vesicle fusion of early endosomes with lysosomes. Adapted from (Bowman *et al.*, 2021). Image made using items from Servier medical Art.

Integrin endocytosis, recycling and targeting to lysosomes plays a key role in regulating its function. Integrin engagement to its ligand determines the trafficking route; unbound integrins are predominantly recycled to the PM, whereas ligand-engaged integrins are targeted to lysosomes (Arjonen *et al.*, 2012). $\alpha 5\beta 1$ engagement to fibronectin promotes its ubiquitination and delivery to lysosomes in a ESCRT-dependent manner in fibroblasts, while overexpression of Rab25 in endometrioid ovarian cancer cells A2780 drives traffic of $\alpha 5\beta 1$ to late endosomes/lysosomes (Lobert *et al.*, 2010; Dozynkiewicz *et al.*, 2012). Integrin delivery to

lysosomes is a requisite during 3D migration (Dozynkiewicz *et al.*, 2012; Rainero and Norman, 2013; Rainero *et al.*, 2015). Interestingly, integrins are not degraded but CLIC3 mediates their recycling back to the PM (Dozynkiewicz *et al.*, 2012). Integrin recycling or retrograde traffic from lysosomes is essential for the release of adhesions at the trailing edge of migrating and invading cancer cells (Rainero and Norman, 2013). Moreover, ligand-bound $\alpha 5\beta 1$ integrin has been described to link mTORC1 nutrient signalling to invasive migration (Rainero *et al.*, 2015). In spite of these findings, the mechanism by which other integrin heterodimers are targeted to lysosomes remains unclear.

This chapter aims to characterise the regulators controlling ECM-bound integrin traffic to lysosomes. We first show that the ECM components are degraded in the lysosomes. We then use a high content siRNA silencing approach to unravel novel modulators of ECM traffic. We perform a preliminary validation of a few hits on collagen I and matrigel matrices. The last sections include preliminary optimisation on super resolution microscopy to better understand how ECM-bound integrin is trafficked to lysosomes. Finally, we show that hindering ECM-integrin traffic to lysosomes leads to profound changes in cell migration in MDA-MB-231 cells.

5.2. RESULTS

5.2.1. The internalised ECM components are degraded in the lysosomes in MDA-MB-231 cells

Following receptor-mediated endocytosis, internalised ECM is targeted for lysosomal delivery and degradation (Rainero, 2016). To assess whether breast adenocarcinoma cells degrade endocytosed ECM as described in the literature, MDA-MB-231 cells were seeded on 1mg/ml collagen I, 1mg/ml matrigel and 2mg/ml laminin matrices in presence of E64d or the vehicle (DMSO). E64d is a PM-permeable and irreversible cysteine cathepsin inhibitor that blocks lysosomal degradation by forming a thioether bond with the active-site cysteine (Murray *et al.*, 1997). 24h-incubation on the different matrices in the presence of 20 μ M E64d considerably increased endocytosed ECM particles as shown in [Figure 5-2](#) which evidences that MDA-MB-231 cells degrade internalised ECM in the lysosomes as previously reported (Melcher and Chan, 1981; Kj oller *et al.*, 2004; Rainero, 2016). Interestingly, MDA-MB-231 cells seemed to uptake more

matrigel and laminin compared to collagen I when treated with E64d (see [Figure 5-2A,C,E](#)). Accordingly, the absolute values regarding ECM uptake were higher in laminin-rich matrices ([Figure S1-4 A,B,C](#) and [Table S1-5](#)). Quantification of the mean ECM uptake revealed that both laminin and collagen I showed approximately a ~2 fold increase, while matrigel uptake increased almost ~3 fold upon E64d treatment ([Figure 5-2B,D,F](#) and [Table S1-5](#)). Internalised matrigel and laminin vesicles were very similar in shape and in size. Endosomes containing laminin and matrigel were characteristically rounded or small-dotted in control cells, whereas E64d treated cells displayed big vesicles (see [Figure 5-2C,E](#)). Different from laminin and matrigel, collagen I was primarily in oval endosomes or elongated tubules upon E64d treatment. Similarly, some laminin-containing endosomes were also slightly oval in presence of the lysosomal inhibitor (see [Figure 5-2E](#)). Interestingly, matrigel tends to accumulate into irregular large endosomal structures, which resemble vacuoles, in cells treated with E64d ([Figure 5-2C](#)). Likewise, laminin and collagen I were also found in those vacuole-like compartments (see [Figure 5-A](#) for collagen I). Although ECM-containing endosomes could be visible across all the cytoplasm, large endosomes were considerably apparent near the perinuclear region. Notwithstanding lysosomes can be located across all cytoplasm (Pu *et al.*, 2016), lysosomes and trans Golgi network (TGN) vesicles commonly dwell in the perinuclear region (Jongsma *et al.*, 2016), which further supports that internalised ECM is degraded in the lysosomes in MDA-MB-231 cells.

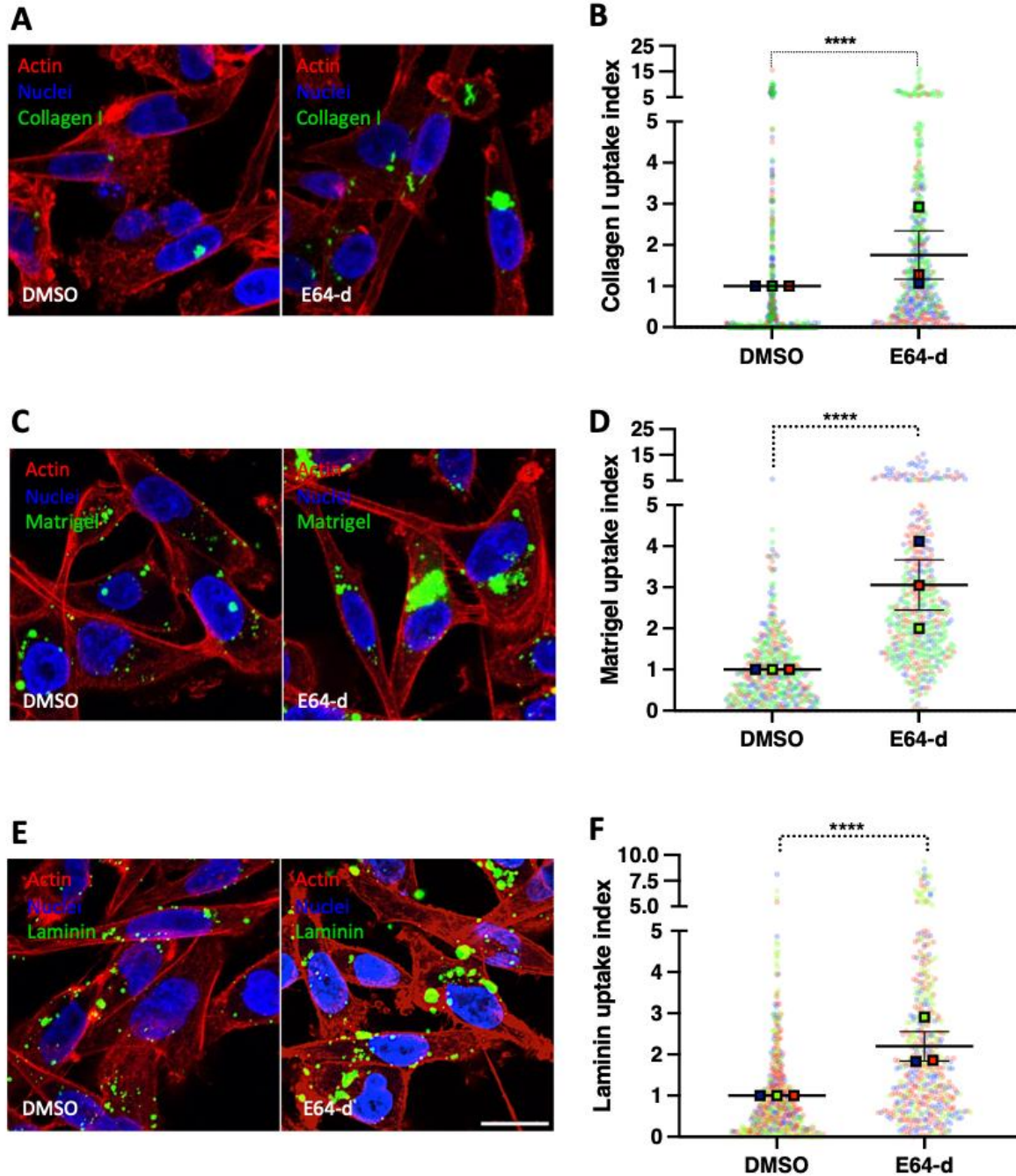


Figure 5-2. Endocytosed ECM is degraded in the lysosomes by cysteine cathepsins. 3×10^5 MDA-MB-231 cells were seeded on 35mm glass-bottom dishes coated with NHS-fluorescein (green)-labelled 1mg/ml collagen I (A,B), 1mg/ml matrigel (C,D) and 2mg/ml laminin-111 (E,F) for 24h in presence of DMSO (vehicle) or 20 μ M Aloxistatin (E64d). Cells were fixed and stained with Phalloidin Alexa 555 to label the actin cytoskeleton (red) and DAPI for the nucleus staining (blue). Scale bar represents 20 μ m. Cells were z-stacked imaged at 1 μ m intervals with a 60X objective of Nikon A1 confocal microscope. Image J software was used to analyse the ECM uptake index. The scatter plot shows the cell-level and mean values \pm standard error of the mean (SEM) from three independent experiments for collagen I (B), matrigel (D) and laminin-111 (F); each replicate is shown in a different colour (blue, red, green). **** $p < 0.0001$; Mann-Whitney test ($n > 400$ cells per condition).

5.2.2. An siRNA trafficking screen identifies regulators of ECM traffic to lysosomes

$\alpha 2\beta 1$ integrin promotes internalisation of matrigel, collagen I and CDM in MDA-MB-231 cells ([Chapter 6](#) and Rainero, unpublished). Internalised ECM colocalises with $\beta 1$ -integrin, suggesting that they are trafficked together (Rainero, unpublished). To identify the regulators and trafficking route that matrigel undergoes following its endocytosis, we first carried out a primary small interfering RNA (siRNA) screen. The screen targeted approximately 147 known regulators of lysosomal, Golgi and ER trafficking. Cell imaging was performed live. Matrigel uptake index was quantified as previously described (Commisso, Flinn and Bar-Sagi, 2014). Two separate analyses were performed. First, the Z-score (or standard score) for each value was calculated ([Table S1-6](#)). While the Z-score indicates the variability of a value within a dataset, it does not reflect the variability within technical replicates of the same condition. Therefore, data was normalised between the non-targeting NT5 (that is, negative) control and NT5 in presence of bafilomycin A1 (positive) control to better compare the modulation between technical replicates ([Figure 5-3A](#) and [Table S1-6](#)). Following data normalisation, we calculated the first derivative of the curve of mean values coming from 4 technical replicates to identify regulators that significantly impinged on ECM traffic ([Figure 5-3B](#)). We used a non-stringent cutoff for primary hit selection to capture true positive regulators, which would have been otherwise excluded by a more stringent cut-off. A total of 45 genes were scored as non-stringent positive regulators, while 7 genes scored as non-stringent negative regulators ([Figure 5-3B](#)). Consistent with previous data, the positive control $\beta 1$ -integrin showed a reduction in uptake between -0.36 and -0.23 between replicates compared to negative control 0 ([Figure 5-3A](#) and [Table S1-6](#)). To further delimit the positive regulators, we took values below -0.23 in all replicates as a criterion for identifying candidates regulating matrigel traffic. In addition, cell numbers were assessed to discard significant effects on cell toxicity (data not shown). To better understand the intracellular processes these hits regulated, we performed STRING analysis. Three main clusters were observed: Conserved oligomeric Golgi (COG) complex, SNARE complexes and AP complex proteins ([Figure S1-5](#)). The COG cluster was discarded due to general effects on intracellular trafficking and effects on protein secretion (Climer, Dobretsov and Lupashin, 2015). Cellular components (gene ontology) revealed that AP3 complex was a top hit. Four subunits of this complex were identified (AP3D1, AP3B2, AP3M2 and

AP3S1), while only one or two subunits were identified from the other AP complexes (AP1G1, AP2M1, AP2A2, AP4E1, AP5M1, AP5S1). Of note, the AP2 complex has a key role in clathrin-dependent endocytosis (Park and Guo, 2014), however downregulation of clathrin does not impair matrigel traffic ([Chapter 3](#)). This data supported the STRING results and suggested that the AP3 complex is an important regulator of matrigel traffic. Kyoto encyclopaedia of Genes and Genomes (KEGG) analysis confirmed STRING analysis results, being the top hits: *SNARE interactions in vesicular transport* and *lysosome* ([Figure S1-6](#) and [S1-7](#)). The SNARE cluster included several proteins; among them BET1, which mediates endoplasmic reticulum to Golgi traffic (Donkervoort *et al.*, 2021), BNIP1, which is involved in endoplasmic reticulum membrane fusion (Holling *et al.*, 2022), and STX12, which regulates membrane fusion at endosomal level (Ambrosio, Febvre and Di Pietro, 2022). In addition, literature research of the hits pointed towards a role of the AP3 complex in endosomal to lysosomal traffic (Peden *et al.*, 2004; Park and Guo, 2014). Cell data analysis confirmed that downregulation of AP3B2, AP3D1, AP3M2, AP3S1, VAMP7, ARF1 and ARFGEF2 impinged matrigel uptake in MDA-MB-231 cells ([Figure 5-3C, D and E](#)). All the hits significantly reduced the number of vesicles compared to the control and their effect was similar to the positive control β 1-integrin ([Figure 5-3C](#)). Of note, downregulation of the AP3 complex subunits resulted in a faint signal inside the cells. Taking into account the pH sensitive properties of pHrodo, the faint signal observed may be due to matrix accumulation in early endosomal compartments. Altogether, this data suggests that the AP3 complex, ARF1 and ARFGEF2, both established regulators of AP3 activation, mediate ECM traffic to acidic endosomal compartments or lysosomes.

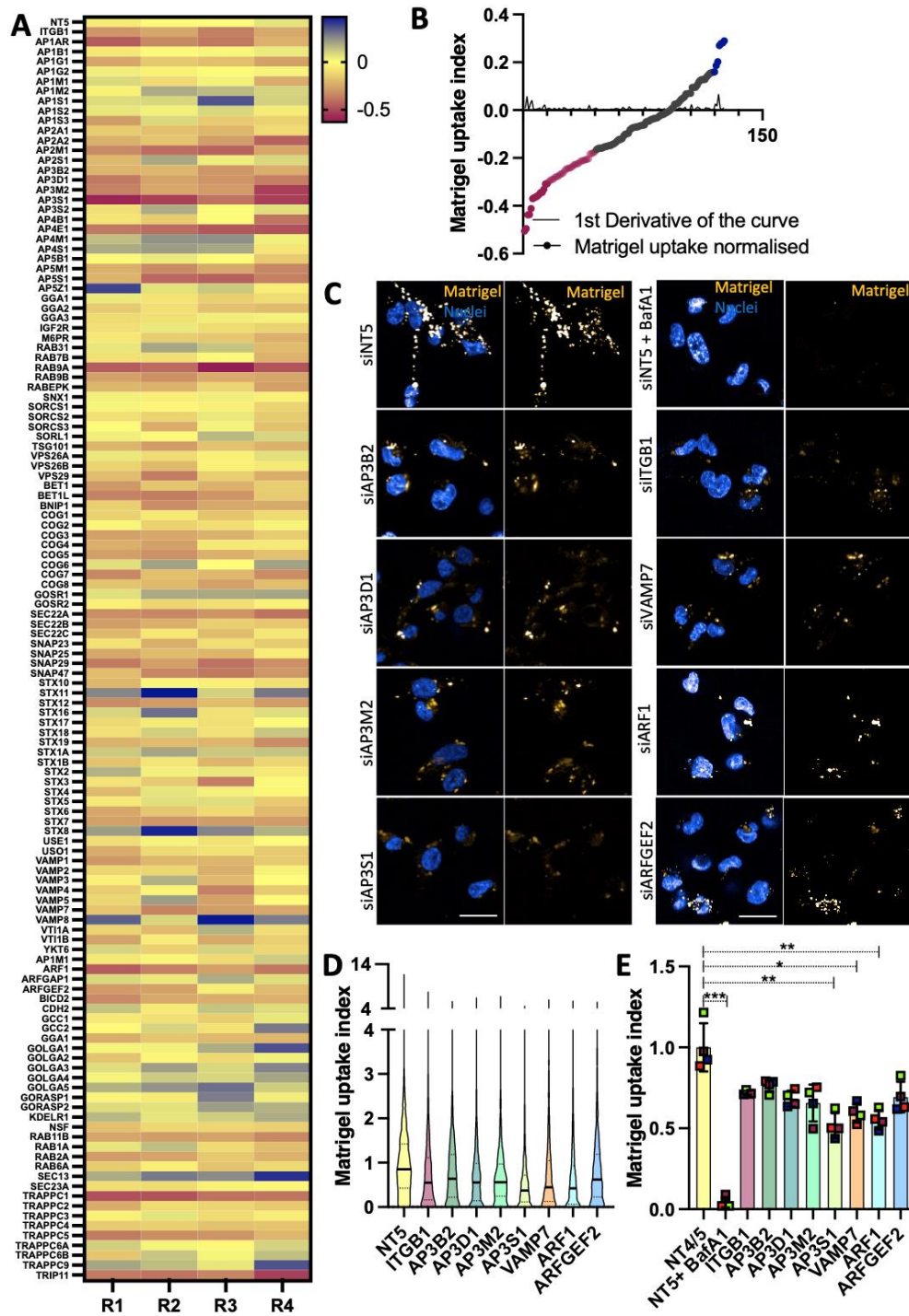


Figure 5-3. A trafficking screen identifies the AP3 complex, ARF1, ARFGF2 and VAMP7 to regulate matrigel traffic. 3000 MDA-MB-231 cells were transfected as per protocol. Following 72h, cells were transferred into pH-rodo labelled matrigel (0.5mg/ml; golden) and incubated for 6h. Cells were labelled with hoechst for nuclear staining (blue, high intensity signal is white). Cell imaging was carried out using a 40X objective in the Opera phenix microscope. Columbus software was used for image analysis. Scale bar: 20µm. (A) Heatmap of the genes tested; normalised data. (B) First derivative of the curve for hit selection. (C) Representative images of top hits and controls. (D) Violin plot of the top hits (values represented are cell data). (E) Values represented are well data + SD; 4 technical replicates; * $p=0.0366$, ** $p\leq 0.0098$, *** $p=0.0001$; Kruskal-Wallis test.

5.2.3. Preliminary hit validation confirmed AP3D1 reduced matrigel and collagen I uptake index

In order to validate the results above, we selected and assessed the effect of a few hits on two different matrices: matrigel and collagen. siRNA against AP3D1, AP4E1, ARFGEF2 and BET1 significantly reduced matrigel uptake, vesicles were smaller and displayed reduced brightness compared to the control ([Figure 5-4A](#)). Quantitative analysis showed that these genes indeed had the highest level of modulation across the 4 replicates as shown in [Figure 5-4B,D](#) and matrigel uptake index at cell level data also reflected the decrease in intracellular signal ([Figure 5-4C](#)). In addition, AP3B2 reduced matrigel uptake in two out of four replicates ([Figure 5-4B](#)) and cells displayed fewer vesicles compared to control ([Figure 5-4A](#)); however, no effect was observed at cell level data quantification ([Figure 5-4C](#)). The discrepancies between replicates may be owing to the fact that predominantly disruption of AP3D1 disables the AP3 complex (Kent *et al.*, 2012) and, in addition, the AP3B1 subunit could compensate for the lack of AP3B2. Alternatively, the differences observed between biological replicates may be due to changes in the endocytic rate and subsequent traffic to lysosomes. This data suggests that the AP3D1 complex mediates matrigel traffic and ARFGEF2 may additionally regulate this pathway.

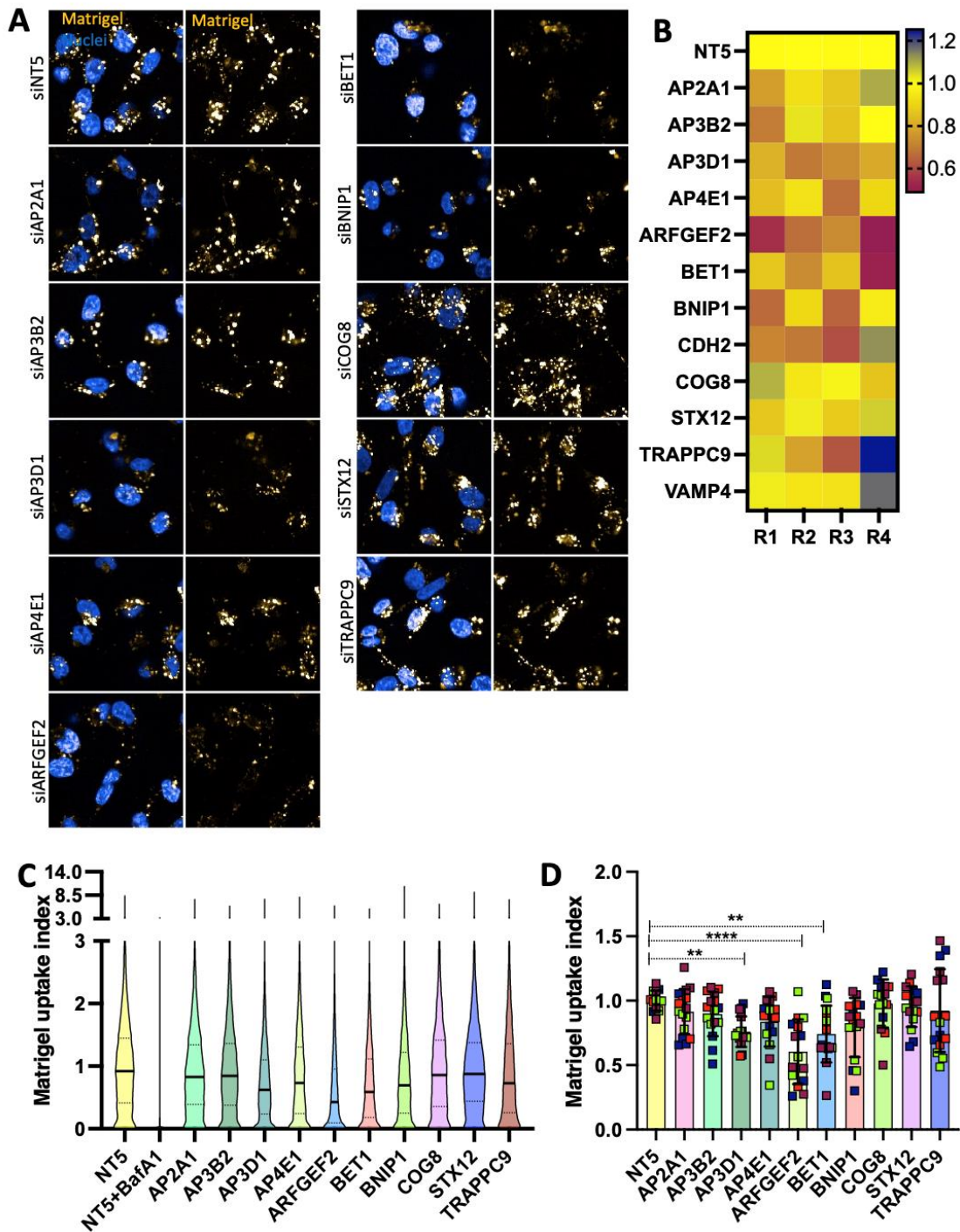


Figure 5-4. Preliminary validation confirms the role of AP3D1 and ARFGEF2 in matrigel traffic. (A) 3000 MDA-MB-231 cells were transfected as per protocol. Following 72h, cells were transferred into pH-rodo labelled matrigel (0.5mg/ml; golden) and incubated for 6h. Cells were labelled with hoechst (blue, high intensity signal is white). The 40X objective of an Opera phenix microscope was used for cell imaging. Columbus software was used for image analysis. Scale bar: 20 μ m. (B) Heatmap of well data. (C) Values represented are cell data. (D) Well data was used for statistical analysis; N=4 independent replicates; ** $p \leq 0.0059$, **** $p < 0.0001$; Kruskal-Wallis test. Kruskal-Wallis test.

Similarly, collagen uptake was predominantly affected by siRNA-mediated downregulation of AP2A1, AP3B2, AP3D1, AP4E1, BNIP1 and STX12 ([Figure 5-5A](#)). In agreement with the acquired images, quantification showed reduced collagen I uptake index in most of the replicates ([Figure 5-5B,D](#)) Cell data analysis confirmed that the uptake distribution (represented with a violin plot) varied compared to the control ([Figure 5-5C](#)). In addition, downregulation of STX12 led to a small decrease in intracellular collagen I signal ([Figure 5-5A,B,C](#)). Nonetheless, ARFGEF2 only impinged collagen I uptake index in two of the replicates, while BET1 strongly reduced the uptake index in one of the replicates ([Figure 5-5B](#)). On the one hand, the differences between replicates could be on account of the knockdown efficiency. On the other hand, it may be possible that under certain circumstances other proteins with redundant effects take over in the absence of the main effectors. Altogether, this data evidences that the AP3 complex, including AP3D1 and AP3B2 subunits, and ARFGEF2 are required for ECM traffic to lysosomes.

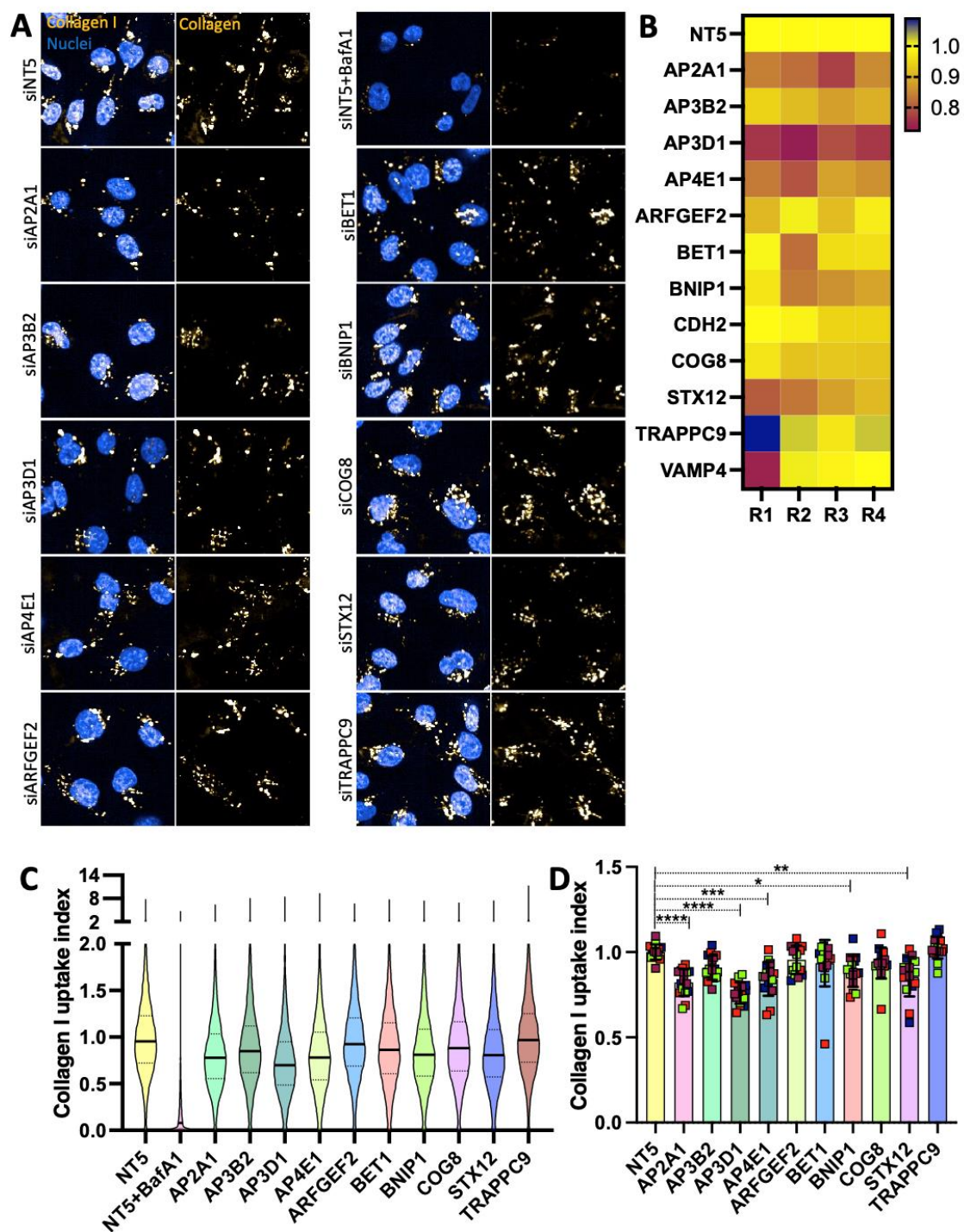


Figure 5-5. Preliminary validation confirms the role of AP3D1 and ARFGEF2 in collagen traffic. (A) 3000 MDA-MB-231 cells were transfected as per protocol. Following 72h, cells were transferred into pH-rodo labelled collagen (0.5mg/ml; golden) and incubated for 6h. Cells were labelled with hoechst (blue, high intensity signal is white). A 40X objective of an Opera phenix microscope was used for cell imaging. Columbus software was used for image analysis. Scale bar: 20µm. (B) Heatmap of well data. (C) Values represented are cell data; N=4 independent replicates; well data was used for statistical analysis; * $p=0.0107$, ** $p=0.0019$, *** $p=0.0003$ **** $p<0.0001$; Kruskal-Wallis test. Kruskal-Wallis test.

5.2.4. Downregulation of the AP3 complex promotes β 1-integrin endosomal accumulation in MDA-MB-231 cells

On account of the pH sensitive properties of pHrodo, the decrease in matrigel uptake index could either reflect defects in endocytosis or lysosomal traffic. To discern whether the AP3 complex mediates intracellular traffic of ECM-bound β 1-integrin or affects its internalisation, MDA-MB-231 cells were seeded on collagen I, labelled with a non pH sensitive dye (NHS-Alexa fluor 555) and stained for active β 1-integrin. No differences in collagen I uptake index were detected after 6h incubation in preliminary studies ([Figure 5-6A,B](#)); however, the internal pool of β 1-integrin was slightly higher in AP3D1 knockdown cells (p-value= 0.0595) ([Figure 5-6A,C](#)). Integrins have been described to regulate morphological changes and morphological differentiation in muscle (Martin-Bermudo, Dunin-Borkowski and Brown, 1998). Owing the small increase in the internal pool of β 1-integrin, we sought to determine whether downregulating AP3D1 had an impact on cell morphology. siRNA mediated downregulation of AP3D1 resulted in a small, but significant, reduction in the cellular aspect ratio (height/width ratio) ([Figure 5-6D](#)). That is to say, AP3D1 knockdown cells were less elongated than control cells, which may indicate that knocking down AP3D1 might result in defects in pseudopod extension in MDA-MB-231 cells. Overall, these results suggest that downregulating AP3D1 does not affect internalisation of collagen I, but rather impaired ECM-bound integrin traffic to acidic endosomes or lysosomes.

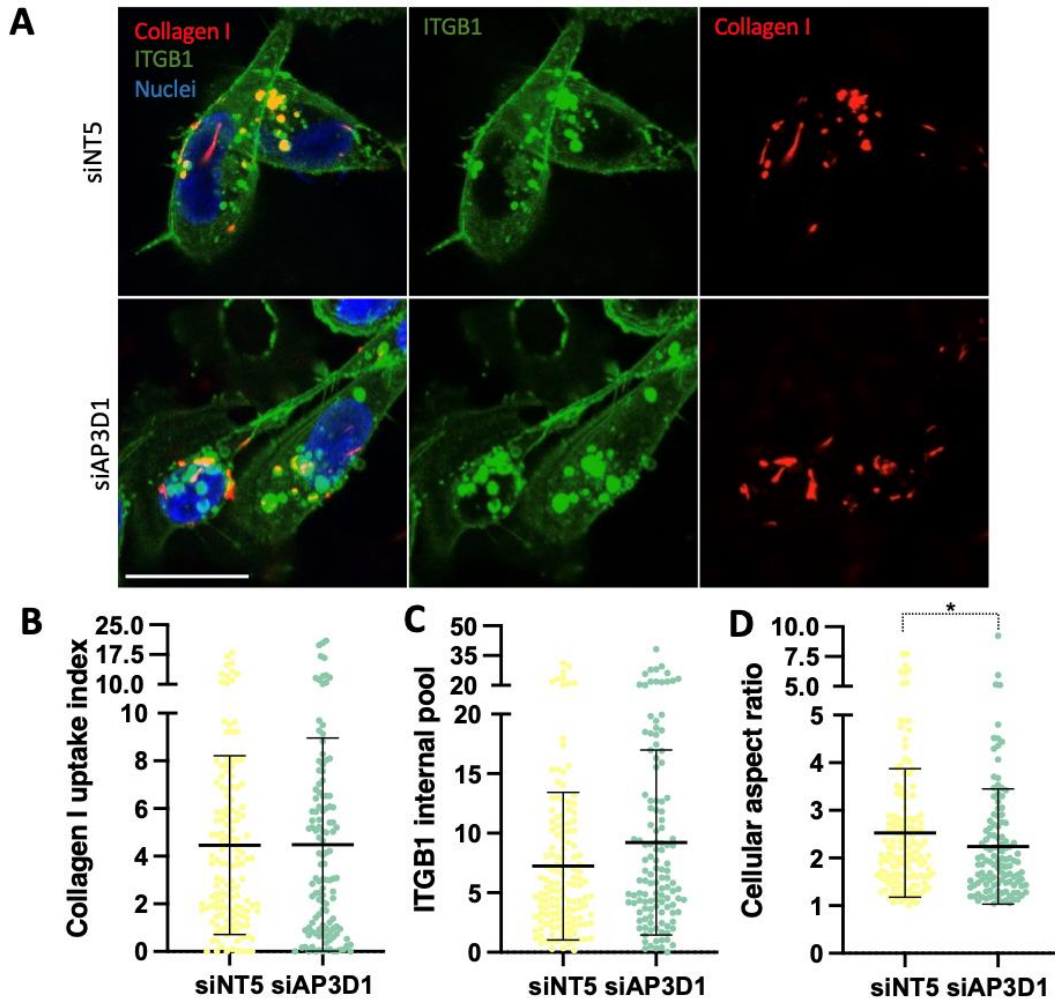


Figure 5-6. AP3D1 knockdown affects cell morphology and promotes a slight increase in the internal pool of ITGB1. 10 μ l of 5 μ M siNT5 or siAP3D1 and 190 μ l OptiMEM per well were mixed in a 6 well plate. 1 μ l Dharmafect I was mixed and incubated with 199 μ l OptiMEM for 5min. 200 μ l of the solution was added on top of the siRNA and incubated for 20min on a rocker. 4 \times 10⁵ cells, contained in 1600 μ l, were added into each well. Following 72h, cells were trypsinised and counted. 3 \times 10⁵ MDA-MB-231 cells were seeded on 35mm glass-bottom dishes coated with NHS-Alexa fluor 555 (red)-labelled 1mg/ml collagen I for 6h. Cells were fixed and stained with an antibody against active β 1-integrin (green) and DAPI for the nucleus staining (blue). Scale bar: 22 μ m. Cells were z-stacked imaged at 1 μ m intervals with a 60X objective of Nikon A1 confocal microscope. Image J software was used to analyse the morphology properties, matrigel and β 1-integrin uptake index. The scatter plot shows the cell-level values \pm SD from N=1 experiment * p <0.0382; Mann-Whitney test ($n \geq 121$ cells).

5.2.5. Downregulation of the AP3 complex promotes matrigel accumulation in early endosomes

To further investigate whether the AP3 complex mediates ECM-bound β 1-integrin traffic to lysosomes, MDA-MB-231 cells were seeded on matrigel, labelled with NHS-Alexa fluor 555. Cells were then fixed and stained for the early endosomal marker EEA1 and β 1-integrin to assess the colocalisation ratio between EEA1 and β 1-integrin or matrigel. The colocalisation correlation was calculated as previously described (Jaskolski, Mulle and Manzoni, 2005). siRNA-mediated downregulation of AP3D1 promoted accumulation of endocytosed matrigel in EEA1-positive early endosomes as shown and quantified in [Figure 5-7A](#) and [5-7B](#), respectively. Similarly, β 1-integrin displayed higher colocalisation levels with EEA1 in AP3D1 knockdown cells compared to control cells ([Figure 5-7C](#)). Western blot analysis showed that AP3D1 knockdown is effective in MDA-MB-231 cells ([Figure 5-7D](#)). This data shows that downregulating the adaptin subunit AP3D1 promotes matrigel and β 1-integrin accumulation in early endosomes, which indicates that the AP3 complex mediates ECM-bound integrin traffic to lysosomes.

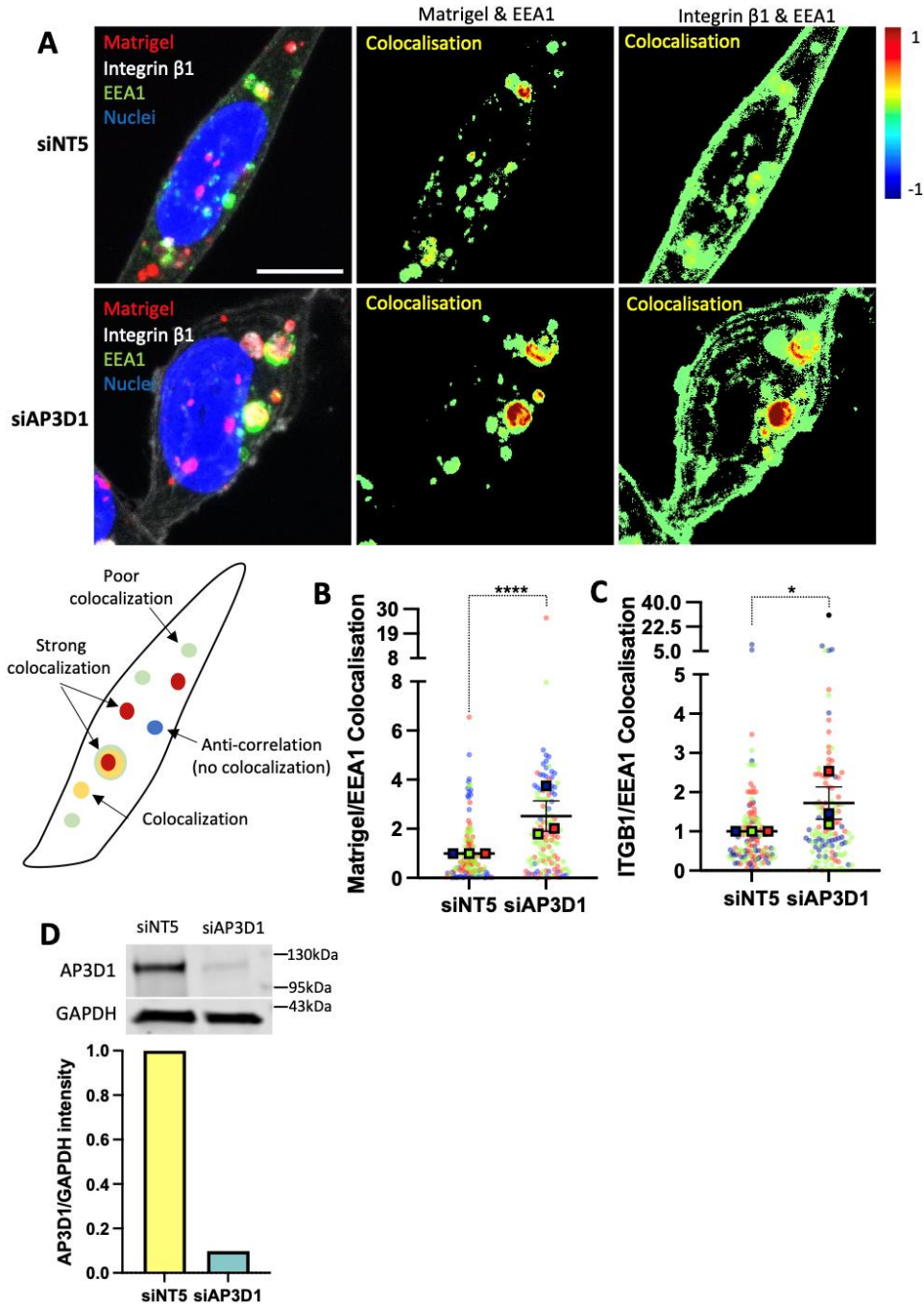


Figure 5-7. AP3D1 knockdown promotes accumulation of matrigel and ITGB1 in early endosomes. MDA-MB-231 cells were transfected as per protocol. Following 72h, cells were trypsinised and counted. 3×10^5 siNT5 or siAP3D1 MDA-MB-231 cells were seeded on 35mm glass-bottom dishes coated with NHS-Alexa fluor 555 (red)-labelled matrigel (1mg/ml) for 6h. Cells were fixed and stained for active $\beta 1$ -integrin (white), EEA1 (green) and DAPI for the nucleus staining (blue) (A). Scale bar: 10 μ m. Cells were z-stacked imaged at 1 μ m intervals with a 60X objective of Nikon A1 confocal microscope. The Colocalisation colormap (Gorlewicz et al., 2020) plugin (Fiji-ImageJ) was used for data analysis. (B) Matrigel and EEA1 co-localisation. (C) $\beta 1$ -integrin and EEA1 colocalisation. The SuperPlot shows the cell-level values (dots), mean data values (squares) \pm SEM from N=3 experiment * $p=0.0239$, **** $p<0.0001$; Mann-Whitney test. (D) Western blot analysis of protein expression upon siAP3D1 knockdown.

5.2.6. The AP3 complex is recruited to Rab5 and Arf1-positive early endosomes containing matrigel

We have previously shown that several AP3 adaptin subunits, ARFGEF2 and Arf1 are required for endocytic traffic of matrigel ([Figure 5-3](#)). We hypothesise that Arf1 activation results in recruitment of AP3 complex to early endosomes and promotes ECM traffic to lysosomes. To better characterise the role and recruitment of the AP3 complex to early endosomes, MDA-MB-231 cells were transiently transfected either with Arf1-mcherry or Rab5-mcherry. Following cell seeding, cells need a minimum of 2 to 3h to internalise ECM components. After 3h, internalised ECM strongly colocalises with early endosomal markers (Rainero, unpublished). Arf1 and Rab5 transfected cells were then cultured on NHS-Alexa fluor 647- labelled matrigel for 3h. Preliminary image visualisation confirmed that the AP3 δ subunit clustered around Arf1 and matrigel positive vesicles, suggesting that Arf1 might promote the recruitment of the AP3 complex to matrigel-containing endosomes ([Figure 5-8A](#)). To further confirm that the AP3 complex is recruited to early endosomes containing matrigel, MDA-MB-231 cells expressing Rab5-mcherry were used ([Figure 5-8B](#)). Indeed, the δ subunit of the AP3 complex is clustered in Rab5 and matrigel positive early endosomes. Strikingly, we could observe a strong colocalisation between matrigel vesicles, Arf1 and Rab5 ([Figure 5-8](#)). This data further confirmed that the AP3 complex is recruited to early endosomes that contain internalised matrigel.

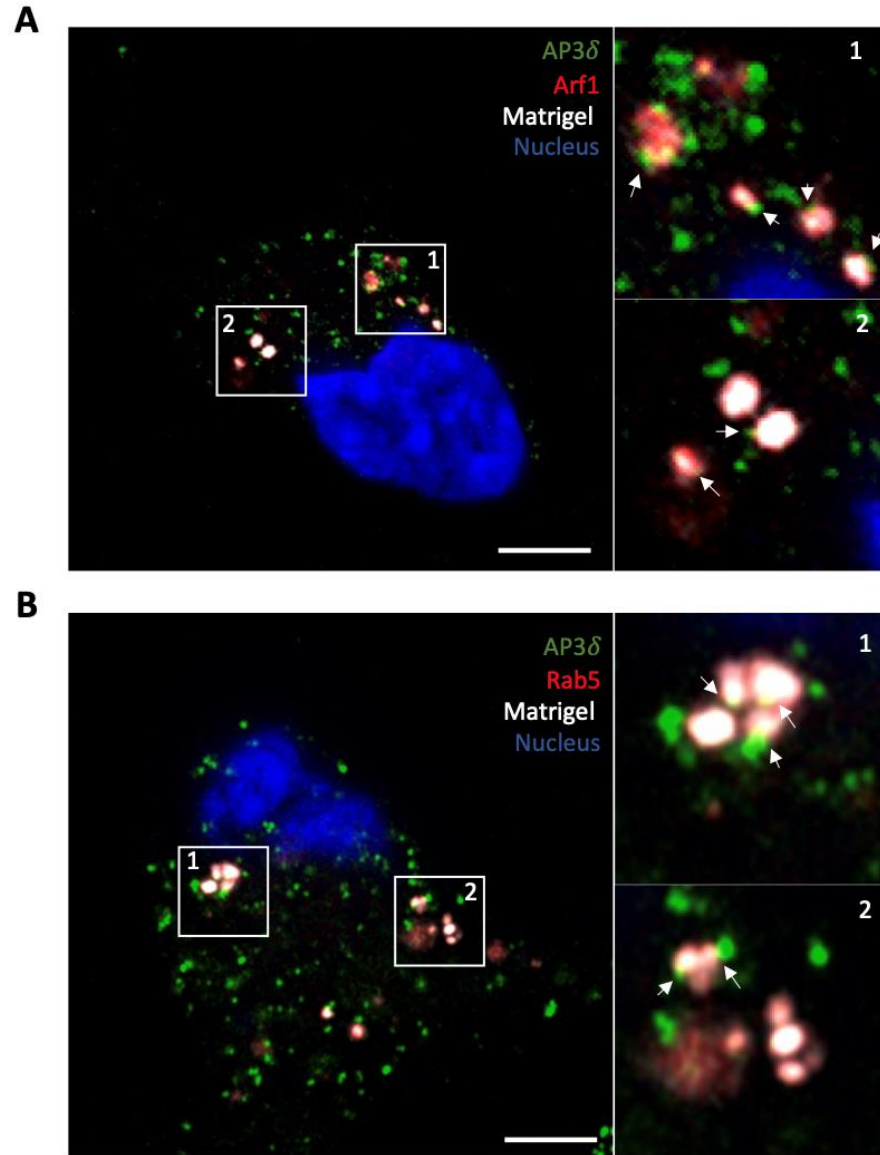


Figure 5-8. The AP3 complex is recruited to Arf1 and Rab5 positive early endosomes containing matrigel. MDA-MB-231 cells were transfected with lipofectamine 2000 and 2.5 μ g of either an mcherry-Rab5 or mcherry-Arf1 plasmid. The next day cells were trypsinised and counted. 3x10⁵ of Arf1- and Rab5-transfected (A and B respectively) MDA-MB-231 cells were seeded on 35mm glass-bottom dishes coated with NHS-Alexa fluor 647 (white)-labelled matrigel (1mg/ml) for 3h. Cells were fixed and stained for AP3D1 (green) and DAPI for the nucleus staining (blue). Scale bar: 5 μ m. Cells were z-stacked imaged with a 60X objective of an Zeiss AiryScan microscope. Representative images are single planes; arrows point colocalisation between endosomes and AP3D1.

5.2.7. Optimisation of single-molecule localisation microscopy

To better study the recruitment of the AP3 complex to early endosomes containing active β 1-integrin, we started optimising sample preparation for Single-molecule localisation microscopy (SMLM). SMLM englobes a family of imaging techniques that refines the spatial resolution compared to standard, diffraction-limited microscope techniques (Lelek *et al.*, 2021). This is achieved by localising individual fluorescent molecules provided the point spread function (PSF) do not overlap. In particular, photoswitching allows a spatio-temporal localisation of active molecules and non-overlapping PSFs (Lelek *et al.*, 2021). This enables imaging of subcellular structures or biological structures at molecular scale (Lelek *et al.*, 2021). For the preliminary optimisation, two fluorophores previously used in the literature were tested. Early endosomes were stained for EEA1 labelled by Alexa Fluor 488, while active β 1-integrin was stained with Alexa Fluor 647. ECM components, such as matrigel and collagen I, promote internalisation of α 2 β 1 integrin in MDA-MB-231 cells (Rainero, unpublished). To detect evident changes in the internal pool of β 1-integrin, MDA-MB-231 cells were seeded on a polymer substrate (Ibidi polymer coverslip) and 0.2mg/ml collagen I. No visual differences were observed regarding the early endosomes between both conditions ([Figure 5-9](#)). However, β 1-integrin strongly colocalised with early endosomes when cells were seeded on collagen I. While the ring shape characteristic of endosomes was not visible, β 1-integrin was distinctively around the EEA1 and displayed a ring-like shape. In particular, β 1-integrin was concretely recruited to certain regions of the endosomal membrane in other endosomes ([Figure 5-9B](#)). Moreover, MDA-MB-231 cells seeded on collagen I showed highly defined integrin containing patches that corresponded to focal adhesions. Altogether, these results suggest that SMLM microscopy is an adequate approach to study integrin traffic; specifically, β 1-integrin with the fluorophore Alexa fluor 647.

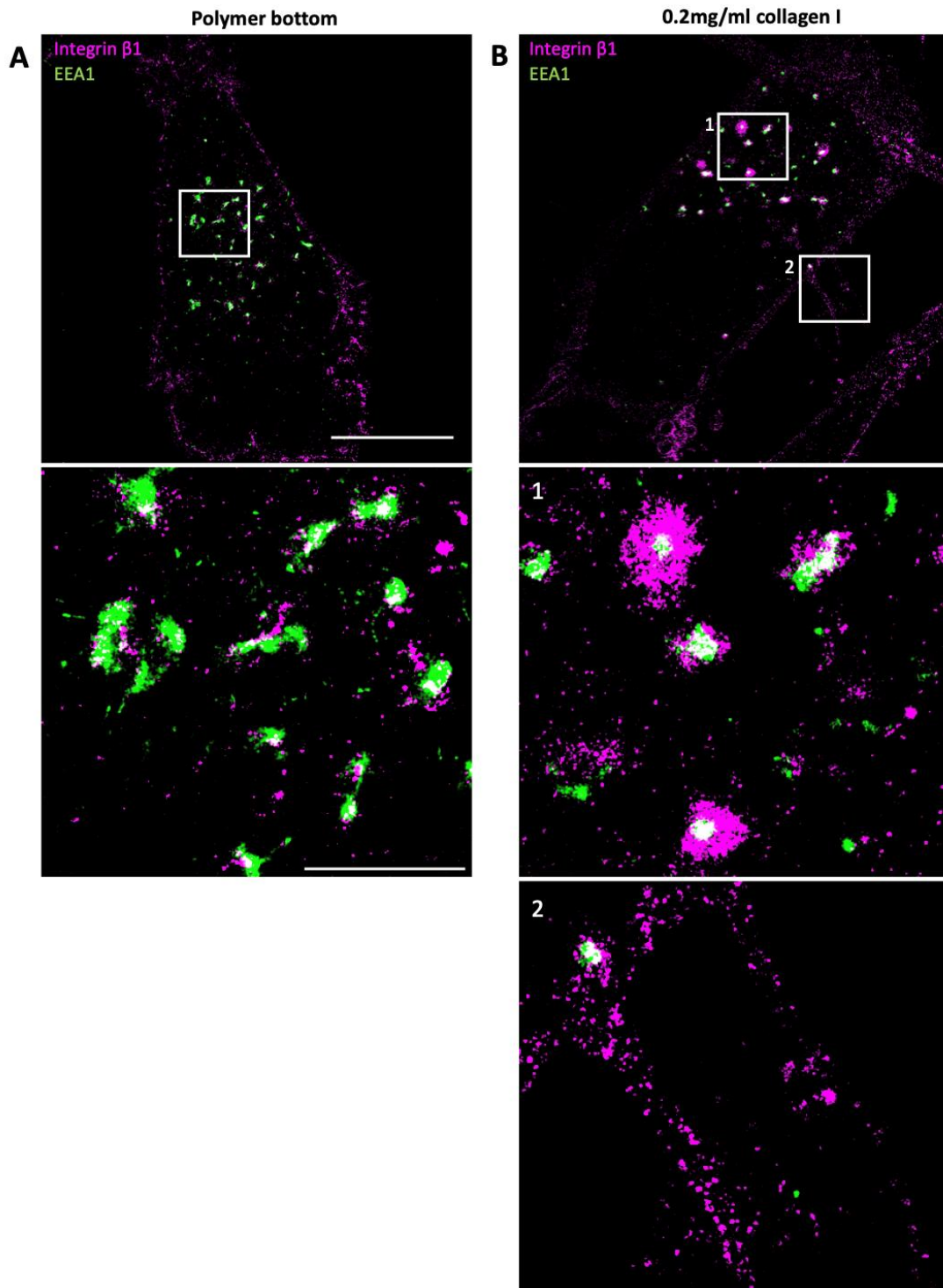


Figure 5-9. Optimisation of Single-molecule localisation microscopy: 0.2mg/ml collagen I drives integrin internalisation to early endosomes. 3×10^5 MDA-MB-231 cells were either seeded on glass-like plastic (A) or seeded on 0.2mg/ml collagen I (B) for 3h (SMLM-compatible Ibidi dishes). Cells were then fixed and stained for EEA1 (green) and active $\beta 1$ -integrin (magenta). Scale bar: $10 \mu\text{m}$ for top images and $2.5 \mu\text{m}$ for bottom (zoom-in) images. Images were acquired with an N-STORM microscope by Carl Harrison.

5.2.8. Disrupting ligand-bound integrin traffic to lysosomes impinges MDA-MB-231 cell migration on cell derived matrices and poor prognosis in breast cancer patients

Fibronectin-bound $\alpha 5\beta 1$ integrin internalisation has been shown to promote invasive migration (Rainero *et al.*, 2015). In addition, CLIC3-dependent integrin recycling from lysosomes in Rab25 overexpressing ovarian cancer cells is required for 3D migration (Dozynkiewicz *et al.*, 2012). In vivo, cancer cells utilise the fibres within the ECM as getaway tracks from the primary tumour (Rahman-Zaman, Shan and Reinhart-King, 2018). We thus sought to investigate whether the AP3 complex, which controls ECM-occupied $\beta 1$ -integrin traffic to lysosomes, was required for cell migration using CDMs, which present highly organised and oriented fibres. Migration was recorded overnight and images were acquired every 10 minutes. Indeed, knocking down AP3D1 resulted in profound changes in the ability of breast cancer cells to migrate in complex matrices. Visualisation of the time-lapse microscopy videos suggested that breast cancer cells were able to delve into the matrices (data not shown). However, AP3D1 downregulation impaired the ability of breast cancer cells to follow the directional ECM tracks; as depicted in the quantification in [Figure 5-10A,B](#), cell directionality was impaired. Moreover, AP3D1 knockdown cells exhibited decreased speed compared to the control group ([Figure 5-10C](#)). This data suggests that ECM-bound integrin traffic to lysosomes might be required for migration through CDMs.

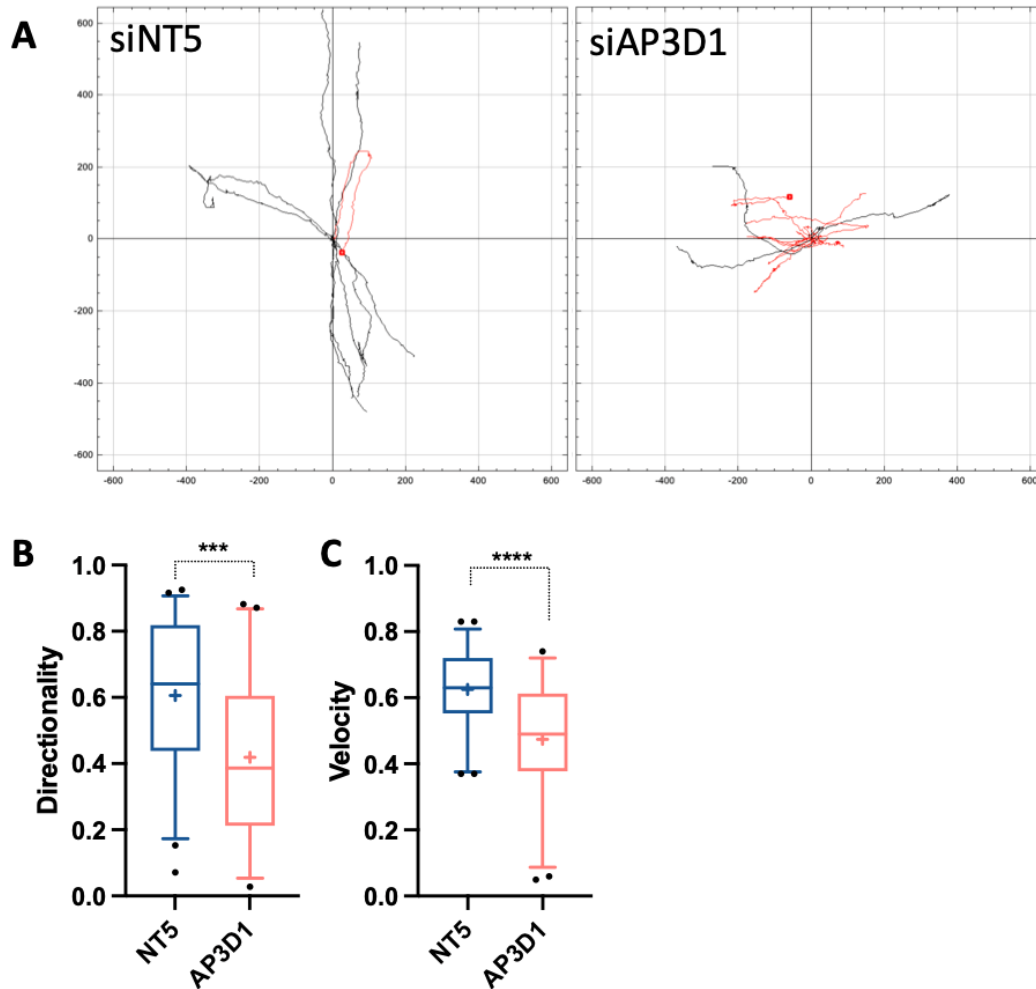


Figure 5-10. Disrupting the AP3 complex impinges on the directionality and average velocity of MDA-MB-231 cells on CDM. 10 μ l of 5 μ M siNT5 or siAP3D1 and 190 μ l OptiMEM per well were mixed in a 6 well plate. 1 μ l Dharmafect I was mixed and incubated with 199 μ l OptiMEM for 5 minutes. 200 μ l of the solution was added on top of the siRNA and incubated for 20 minutes on a rocker. 4 \times 10⁵ cells, contained in 1600 μ l, were added into each well. Following 72h, cells were trypsinised and counted. 0.5 \times 10⁵ cells were seeded per well in a 12-well plate containing TIF-generated CDM. Cells were let to adhere for 6h before imaging with a Nikon Widefield dual-camera microscope. Image acquisition was performed overnight and images were taken every 10 minutes. Time-lapses were analysed with Fiji-ImageJ. The Chemotaxis tool plugin was used to calculate the directionality and velocity. (A) Spider plots show the paths of manually tracked cells (directionality >0.5 is shown in black, directionality <0.5 is shown in red). (B) Cell directionality. (C) Cell velocity (μ m/min). N= 1 independent experiments. Box and whisker plots represent 5-95 percentile, + represents the mean, dots are <5% and >95%; ***p=0.0003; ****p<0.0001; Mann-Whitney test.

Directional persistence on CDM correlates with the invasive potential of breast cancer cells. Therefore, we aimed to investigate whether the expression of the AP3 complex is upregulated in breast cancer. To study this, we used a web tool (TNMplot.com) to compare the gene expression of normal tissue, tumours and metastases (Bartha and Gy rffy, 2021). RNA sequencing (RNAseq) in tumours and normal tissue showed that AP3D1 expression was upregulated in several cancers, including bladder, colon, oesophagus, prostate and breast cancer, among others ([Figure 5-11A](#)).

Specifically, breast tumours expressed higher levels of AP3D1 compared to normal tissues in RNAseq data and Gene chip data ([Figure 5-11B,C](#)). We thus aimed to examine whether AP3D1 upregulation translated to a clinical outcome. We took advantage of a freely available Kaplan-Meier plotter tool (kmplot.com) (Ósz, Lániczky and Gyórfy, 2021). We then selected the proteo-transcriptomics dataset that directly compared the proteomics and transcriptomics data from tumours from breast cancer patients and adjacent non-cancerous tissue (W. Tang *et al.*, 2018). Interestingly, AP3D1 expression correlated with poor prognosis and survival in breast cancer patients - despite the difference not being statistically significant, probably due to the small patient sample ([Figure 5-11D](#)). The median survival for the low expression cohort was 100 months, while it was only 48 months in the high expression cohort ([Figure 5-11E](#)). Altogether, this data suggests that ECM- bound integrin traffic to lysosomes may be required for invasive migration of breast cancer cells and it could correlate with poor survival in breast cancer patients.

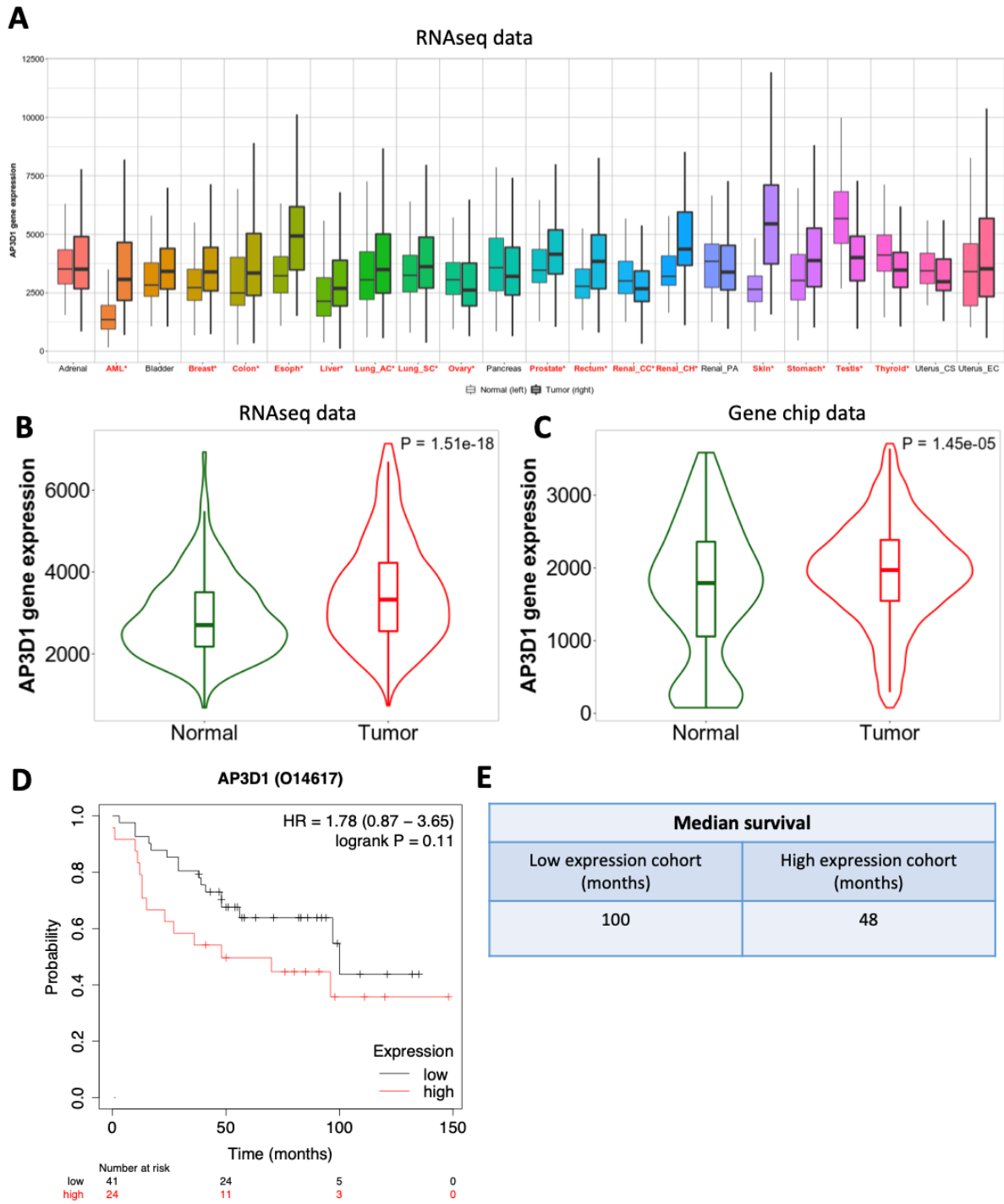


Figure 5-11. Comparison of AP3D1 RNA expression in tumour and normal tissues. (A) The web tool TNM Plot (TNMplot.com) was used to compare the gene expression of AP3D1 in several normal tissues and tumours (Bartha and Györfy, 2021). (B) Violin plot of AP3D1 expression in the mammary gland and breast tumours from RNAseq data. (C) Violin plot of AP3D1 expression in normal breast tissue and breast tumours using Gene chip data. (D-E) The Kaplan-Meier plotter tool (kmplot.com) was used to compare the survival curve and median survival of patients with tumours that exhibit low or high expression levels of AP3D1 (W. Tang et al., 2018; Ósz, Lánckzy and Györfy, 2021).

5.3. DISCUSSION

Integrin trafficking has been linked to cancer progression and metastasis (Ramsay, Marshall and Hart, 2007). While the endocytic pathways governing integrin endocytosis have been extensively studied, it is not fully understood how integrins are targeted for lysosomal delivery (Kharitidi *et al.*, 2015). The fibronectin-binding integrin $\alpha 5\beta 1$ is ubiquitinated, internalised and targeted to the lysosomes in a mechanism that relies on the formation of intraluminal vesicles by the ESCRT complex in fibroblasts (Kharitidi *et al.*, 2015). Nonetheless, it is not known how other integrins are delivered to lysosomes. Here we show that lysosomal cysteine cathepsins mediate the intracellular degradation of the ECM components ([Figure 5-2](#)). We show preliminary data on a novel mechanism that regulates ECM-bound integrin traffic to lysosomes. We find that several subunits of the AP3 complex, VAMP7, Arf1 and ARFGEF2 are required for matrigel traffic to acidic vesicles ([Figure 5-3](#)). Preliminary validation confirmed that AP3D1 diminished intracellular signal from matrigel and collagen endosomes ([Figure 5-4](#) and [5-5](#)). These results were further confirmed in an independent kinome and phosphatome screen, in which siAP3D1 was included as a control to modulate matrigel uptake ([Chapter 6, Table S1-7](#)). In addition to endosome-to-lysosome traffic, the AP3 complex is required for trafficking LAMP1/2 and LIMP2 from the TGN to lysosomes (Höning, Sandoval and von Figura, 1998; Le Borgne *et al.*, 1998; Peden *et al.*, 2004). LAMP2 participates in lysosomal biogenesis (Eskelinen *et al.*, 2002), one could therefore hypothesise that knocking down the AP3 complex results in defective lysosomes and matrigel uptake index is reduced when using a pH sensitive dye. Nevertheless, LAMP-2 deficiency does not affect the lysosomal pH (Tanaka *et al.*, 2000).

Internalised matrigel is trafficked together with $\beta 1$ -integrin (Rainero, unpublished). In particular, collagen I and matrigel endocytosis is dependent on $\alpha 2\beta 1$ integrin (Lee, Sodek and McCulloch, 1996; Arora *et al.*, 2000). The μ -adaptin subunits of the AP complexes interact with integrin α -chains through the Yxx Φ motif (De Franceschi *et al.*, 2016). Particularly, ten α -integrin subunits have been shown to contain the Yxx Φ motif, including $\alpha 2$, $\alpha 4$, $\alpha 9$, αM , αX , αD , αE , $\alpha 3$, $\alpha 6$ and $\alpha 7$ (De Franceschi *et al.*, 2016). This indicates that the AP3 complex might regulate ligand-occupied $\alpha 2\beta 1$ integrin delivery to lysosomes; as well as potentially other α -integrin subunits containing the Yxx Φ motif. Moreover, sequence alignment of the consensus motif ERAPLI of LIMP2 with $\alpha 2$ -

integrin (DTKNLI) and β 1-integrin (ELKNLI) revealed high percent identity or similarity between these sequences ([Figure S1-8](#)). This suggests that, in addition to being recognised by the Yxx Φ motif, the [D/E]XXXL[L/I] sorting motif could also participate in integrin sorting to lysosomes ([Figure 5-12A](#)). In agreement with this, knocking down AP3D1 results in slightly increased levels of internal β 1-integrin, however no effect on collagen I uptake index when using a non pH sensitive dye was observed ([Figure 5-6](#)). The small increase observed in the β 1-integrin internal pool may be because only a fraction of β 1-integrin heterodimers is responsible for ECM internalisation. On the one hand, internalisation of active β 1-integrin may not all be bound to labelled ECM. On the other hand, the observed difference between integrin accumulation and collagen I may be time-dependent. ECM internalised by MDA-MB-231 is not degraded in the lysosomes between 6 to 8 hours incubation, but its degradation seems more evident after 12 hours (based on optimisation data and Keqian Nan, former PhD Rainero lab). As a result, this may cause accumulation of β 1-integrin after an incubation period of 6 hours, but no differences in collagen I uptake index. Assessing collagen I uptake at later time points may show collagen I accumulation in AP3D1 knockdown cells. In fact, downregulation of AP3D1 led to accumulation of matrigel and β 1-integrin in early endosomes ([Figure 5-7](#)), suggesting that integrin traffic to lysosomes is impaired.

Moreover, preliminary validation also confirmed that siRNA against ARFGEF2 also resulted in decreased matrigel uptake index using pHrodo ([Figure 5-4](#)); however, no effect was seen for collagen uptake index ([Figure 5-5](#)). It has been proposed that ARFGEF1/2 and GBF1 activation downstream of integrin signalling leads to Arf1 activation and Golgi organisation (Singh, Erady and Balasubramanian, 2018). In fact, GBF1 has been found to co-localise with paxillin at focal adhesions (Busby *et al.*, 2017). Hence, it may be that Arf1 activation and subsequent traffic of collagen I to lysosomes is bypassed by other Arf1 GEFs, including ARFGEF1 and GBF1 (which were not present in our screening). In agreement with our results, the degradation rate of β 1-integrin is significantly slower in ARFGEF2 null in neuronal embryonic cells (Zhang *et al.*, 2012). However, we cannot discard the effect observed owing to a dysfunction in β 1-integrin trafficking. In fact, ARFGEF2 has been reported to coordinate actin cytoskeleton mechanics and recycling of β 1-integrin (Li *et al.*, 2012).

Moreover, Arf1 has been shown to regulate integrin endocytosis in a CLIC-GEEC dependent manner (Moreno-Layseca *et al.*, 2021). In addition, Arf1 has also been reported to regulate anterograde traffic (Gilbert, Sztul and Machamer, 2018), it could thus be that the effects observed upon siRNA depletion of Arf1 are on account of defects on integrin secretion. Furthermore, in MDA-MB-231 cells, Arf1 has been shown to regulate the recruitment of paxillin and focal adhesion kinase (FAK) to β 1-integrin containing focal adhesions (Schlienger, Ramirez and Claing, 2015). Nevertheless, airyscan microscopy confirmed that matrigel colocalises with Arf1 and Rab5 positive endosomes following 3h incubation. Strikingly, the AP3 complex is particularly recruited around those endosomes ([Figure 5-8A](#)). We thereby hypothesised that recruitment of an ARF1 GEF, such as ARFGEF2, to endosomal ECM-engaged integrins might trigger Arf1 activation. As a result, Arf1 activity promotes recruitment of the AP3 complex and VAMP7 to early endosomes, which subsequently promote lysosomal delivery of ECM- α 2 β 1 integrin complex ([Figure 5-12B](#)).

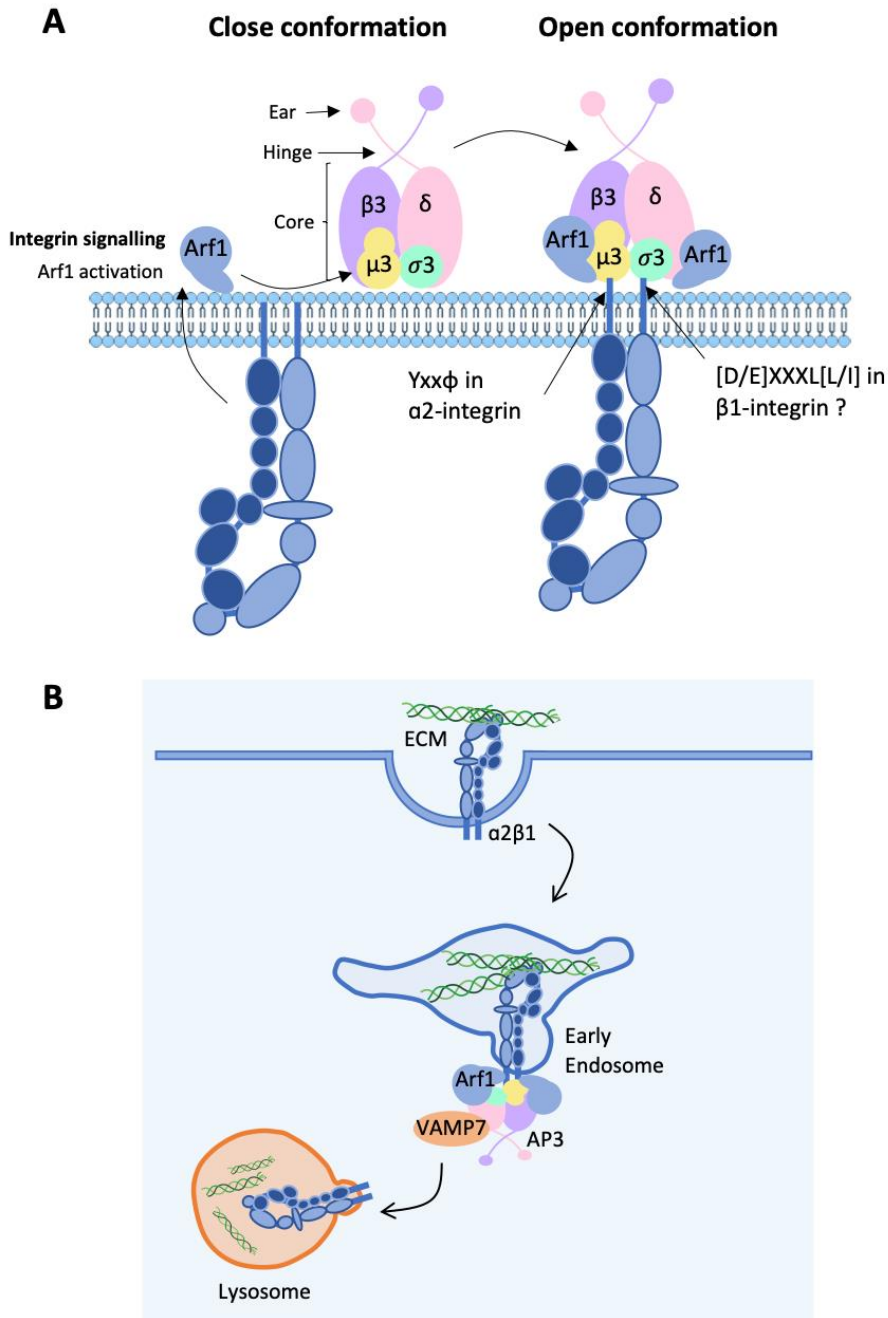


Figure 5-12. Schematic representation of the working model. (A) Proposed model: Arf1 activation downstream of integrin engagement to ECM promotes the open conformation of the AP3 complex, enabling the recognition of the YxxΦ motif in α2-integrin and maybe the [D/E]XXXL[L/I] motif in β1-integrin. (B) Proposed model: following ECM-integrin endocytosis, the AP3 complex and upstream activators, such as ARF1 and ARFGEF2, promote endosomal fusion to lysosomes via VAMP7.

Breast cancer cells use the ECM as a source of nutrients under amino acid starvation (Nazemi *et al.*, 2021). An independent proliferation screen on matrigel found that downregulation of AP3D1 reduced breast cancer cell proliferation under amino acid starvation (Rainero, unpublished). This data suggests that AP3-dependent ECM-bound integrin delivery to lysosomes could be required for ECM-dependent cell proliferation under nutrient limiting conditions. mTORC1 is recruited to lysosomes and activated under amino acid starvation in the presence of ECM (Nazemi *et al.*, 2021). Interestingly, integrin traffic to lysosomes has been shown to sustain mTORC1 activation and promote invasive migration (Rainero *et al.*, 2015). Similarly, our results show that the AP3 complex, which controls ECM-engaged integrin traffic to lysosomes, modulates directionality and migration speed in complex matrices. AP3D1 knockdown cells displayed a lower cellular aspect ratio, compared to control cells ([Figure 5-6D](#)), which may indicate defects in pseudopod extension and thus defects in cell migration ([Figure 5-10](#)). In agreement with our model, ARFGEF2 null mice display defects in the neurone migration during development (Zhang *et al.*, 2012). Rab25 and CLIC3 regulate integrin recycling from late endosomes or lysosomal compartments (Dozynkiewicz *et al.*, 2012). Of note, CLIC3-dependent recycling of integrins regulates migration of the cell line A2780-Rab25 (Dozynkiewicz *et al.*, 2012). Recent reports suggested that $\alpha 5\beta 1$ integrin can be recycled in intracellular nanovesicles that are positive for Rab11a and Rab25 (Larocque *et al.*, 2021). Interestingly, the SMLM images acquired also showed speckles of integrin clusters that did not colocalise with EEA1 ([Figure 5-9](#)), suggesting that these speckles may be intracellular nanovesicles that mediate integrin recycling. It is not clear whether the observed effects are due to impinged integrin recycling from lysosomes or owing to altered integrin endoadhesome signalling. On the one hand, mTORC1 activation in lysosomes may promote cell motility, invasion and subsequent metastasis (Zhou and Huang, 2011; Rainero *et al.*, 2015). Therefore, blocking ECM-integrin delivery to lysosomes may impair mTOR activation or integrin signalling in the lysosomes. On the other hand, accumulation of active integrin in early endosomes may lead to aberrant endoadhesome signalling, which has been reported to activate FAK, ERK-MAPK and PI3K-Akt pathways (Alanko and Ivaska, 2016). Basal signalling levels are required to suppress anoikis (Alanko and Ivaska, 2016). Nonetheless, it may be that basal levels also regulate cell migration of invasive breast cancer cells. During persistent migration, cells

establish different signalling pathways in the leading and trailing edge, which will respectively result in formation of membrane protrusion and retraction (Welf and Haugh, 2011). High integrin endoadesome signalling may lead to a disbalance in the tight regulation required for the spatial polarisation of signalling pathways, focal adhesion and actin cytoskeleton dynamics. In fact, cells display random changes in cell directionality in the absence of cues or in changes in the spatial organisation of intracellular signalling (Tranquillo, Lauffenburger and Zigmond, 1988; Arrieumerlou and Meyer, 2005; Bosgraaf and Van Haastert, 2009; Welf and Haugh, 2011). This suggests that the defects observed in migration could be due to changes in the spatial regulation of integrin signalling.

Several proteins involved in integrin endocytosis or recycling from lysosomes have been shown to correlate with poor prognosis (Dozynkiewicz *et al.*, 2012; Moreno-Layseca *et al.*, 2021). We thus checked RNAseq data (from TNMplot.com) from cancer patients (Bartha and Győrffy, 2021). RNAseq data confirmed that AP3D1 expression is upregulated in several carcinomas compared to the normal tissue, including breast cancer ([Figure 5-11](#)) (Bartha and Győrffy, 2021). Furthermore, AP3D1 could correlate with poor survival in breast cancer ([Figure 5-11](#)) (Ósz, Lánckzy and Győrffy, 2021). In agreement with this, high expression levels of AP3D1 are risk genes for ovarian cancer where it correlates with poor prognosis (H. Li *et al.*, 2021). In addition, patients with digestive organ carcinomas show high levels of antibodies against AP3D1 (S.-Y. Li *et al.*, 2021). In contrast, the AP3 complex was shown to be downregulated in cervical carcinomas (Petrenko *et al.*, 2006). This data suggests that the role of AP3D1 in cancer may be tumour specific. However, we cannot discard that the observed differences may be due to differences in the quantification of the mRNA or protein levels. Taken everything together, our results suggest that the AP3 complex is recruited to Arf1 positive early endosomes that contain active ECM-bound integrin. Recruitment of the AP3 complex to early endosomes promotes integrin traffic to lysosomes, which is required for directional migration in CDM. Future research will characterise the mechanism by which integrins are trafficked to lysosomes, as well as discern the role of integrin traffic to lysosomes or the intracellular integrin signalling in controlling directional migration.

Chapter 6 – A Kinase and Phosphatase functional screen unravels p38 mitogen-activated protein kinase pathway to promote macropinocytosis of integrin-bound extracellular matrix

Montserrat Llanses Martinez conceived, planned, carried out and analysed all the experiments. Dr Xavier LeGuezennec (IMCB, Singapore) printed the siRNA plates for the screening ([Figure 6-1](#) and [Figure 6-5](#)). Dr Elena Rainero set up the time-lapse microscope ([Figure 6-9](#), [6-23](#), [6-24](#)).

6.1. INTRODUCTION

p38 mitogen-protein activated kinase (MAPK) is a family of serine/threonine-specific protein kinases. Four p38 isoforms have been identified (p38 α or MAPK14, p38 β or MAPK11, p38 γ or MAPK12, and p38 δ or MAPK13) (Kudaravalli, den Hollander and Mani, 2022). p38 α and p38 β are ubiquitously found in tissues and share 75% amino acid sequence homology. Likewise, p38 γ and p38 δ share 70% sequence identity with each other and, respectively, 62% and 61% homology with p38 α (Kudaravalli, den Hollander and Mani, 2022). p38 MAPK plays an important role in cell proliferation, differentiation, stress responses, autophagy and cell migration, among other biological processes (Kudaravalli, den Hollander and Mani, 2022). The role of p38 in tumour development remains controversial. Knocking down Wip1, a p38 phosphatase, in mice showed reduced breast tumourigenesis and the p38 MAPK inhibitor SB203580 abolished Wip1-knockout effect (Bulavin and Fornace, 2004; Igea and Nebreda, 2015). Nevertheless, treatment with the p38 inhibitor LY2228820 reduced the growth of human breast cancer xenografts. Moreover, treatment with the p38 MAPK inhibitor PH797804 and cisplatin reduced the size of breast tumours using the MMTV-PyMT mouse model (Pereira *et al.*, 2013). While the role of p38 α in tumour progression has been extensively studied, recent evidence points that p38 γ and p38 δ may actively participate in cancer pathology. For instance, Ras-induced transformation required p38 γ , which was independent of its kinase activity (Tang *et al.*, 2005). Owing to the high sequence homology between p38 α and p38 β , little studies have focused on deciphering the role of p38 β in tumour progression. Nonetheless, recent evidence proposed that p38 β may have distinct and non-redundant functions (Arriazu *et al.*, 2020). In hepatic carcinoma, p38 β is a downstream effector of the proto-oncogenes *Pokemon* (Chen *et al.*, 2013). p38 β has been reported to

regulate lipocalin 2 expression, which correlates with increased invasion, tumour formation and metastasis (Basu *et al.*, 2018). p38 β , FAK and p90RSK1 have been found to associate with α -integrin, this results in c-myc translation and proliferation of keratinocytes (Duperret, Dahal and Ridky, 2015). Similarly, α 2 β 1 integrin has been reported to regulate collagen I transcription through p38 activation (Ivaska *et al.*, 1999). Integrins are a family of heterodimeric receptors for ECM ligands, which promote survival and migration of tumour cells (Lee and Juliano, 2000; Caswell *et al.*, 2008). β 1-integrin are endocytosed via clathrin (Pellinen *et al.*, 2008; Ezratty *et al.*, 2009; Teckchandani *et al.*, 2009), caveolin (Shi and Sottile, 2008), macropinocytosis (Gu *et al.*, 2011; Le *et al.*, 2021) and clathrin-independent carriers (Howes *et al.*, 2010; Moreno-Layseca *et al.*, 2021). Integrin conformation (active or inactive state) determines the endocytic route that cancer cells utilise. Inactive α 1 β 1, α 2 β 1 and α 3 β 1 are internalised in a Dab2 and clathrin-dependent manner (Teckchandani *et al.*, 2009, 2012), whilst active ligand-bound α 2 β 1 and α 3 β 1 have been reported to be phagocytosed in fibroblasts and cancer cells, respectively (Rainero, 2016). Notwithstanding that, these ECM endocytosis studies did not use matrices that recapitulate *in-vivo* like conditions, namely polymerised collagen I, matrigel or cell derived matrices. Moreover, the signalling regulators behind ECM-bound integrin endocytosis are poorly understood.

Here we identify that p38 MAPK, MAP3K1 and PPP2R1A regulate macropinocytosis of active ligand-occupied α 2 β 1 integrin. Invasive breast cancer cells internalise ECM as they migrate on CDM. In addition, blocking internalisation of ECM impinges on the velocity and directionality of migrating cells. This data suggests that ligand-bound integrin endocytosis is required during migration on cell derived matrices.

6.2. RESULTS

6.2.1. A kinase and phosphatase screen identifies EPH receptors and MAPK cascade as regulators of matrigel uptake

To define the signalling pathway that governs ECM internalisation, we carried out a kinase and phosphatase-wide siRNA screen (for the development of the assay, see [Chapter 3](#)). Invasive MDA-

MB-231 cells were knocked down for 72h prior to being seeded on pH-rodo-labelled matrigel, incubated for 6h, stained with hoechst and imaged live.

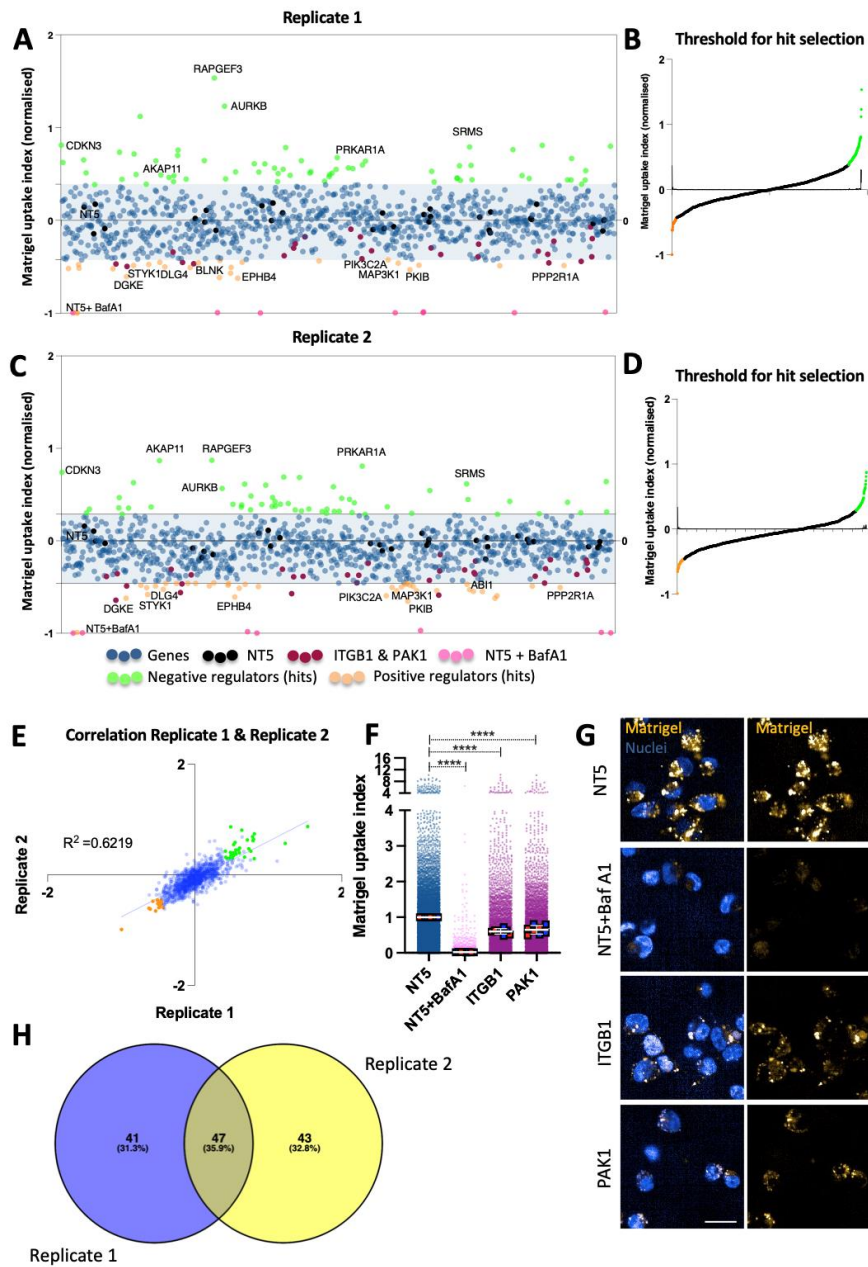


Figure 6-1. Kinome and phosphate-wide screen for regulators of matrigel internalisation in the invasive breast cancer cell line MDA-MB-231. 3000 MDA-MB-231 cells were transfected as per protocol. Following 72h, cells were transferred into pH-rodo labelled 0.5mg/ml matrigel (golden) and incubated for 6h. Cells were labelled with 1 μ g/ml hoechst (blue) for nuclear staining. Cell imaging was carried out using a 40X objective in the Opera phenix microscope. Columbus software was used for image analysis. Scale bar: 20 μ m. Cloud plot and first derivative of the curve from replicate 1 (A-B) and replicate 2 (C-D). Correlation between both replicates (E). Uptake index and representative images of NT5+Bafilomycin A1 (BafA1), ITGB1 and PAK1 KD; the SuperPlot shows the cell-level values (dots), mean data values (squares) \pm SD from 4 biological replicates from N=2 experiments * $p < 0.0469$, **** $p < 0.0001$; Kruskal-Wallis test (F-G). Venn diagram from selected hits in both replicates (H).

Using this pH sensitive system, we screened an siRNA library targeting 972 protein kinases and phosphatases. The screen was performed in duplicate; the same imaging and analysis threshold was applied for both replicates. Matrigel uptake index was similarly quantified as in (Commisso, Flinn and Bar-Sagi, 2014). Data was normalised between the average of the non-targeting NT5 control and NT5 in presence of bafilomycin A1 (positive) control to compare and assess the magnitude of modulation between technical replicates ([Table S1-7](#) and [Figure 6-1](#)). To identify the signalling modulators of ECM internalisation, we calculated the first derivative of the curve of normalised values within the population tested, excluding controls ([Figure 6-1B,D](#)). This enabled the identification of several novel positive and negative regulators of matrigel uptake. Positive regulators are defined as hits that led to a reduction in uptake upon siRNA knockdown, while negative regulators increased uptake. We identified 25 and 37 positive regulators for the first and second replicate, respectively, whereas 66 and 55 negative regulators passed the analysis threshold for the first and second replicate, respectively. To avoid quantifying effects related to apoptosis, survival and/or proliferation, we assessed the nuclei count ([Table S1-7](#)). The average nuclei number for hit genes and the total population (excluding the controls) was quantified. While the total population had an average nuclei count of 751 and 637 for replicate 1 and 2, respectively; the positive hits had an average of 579 and 511 for each replicate. The negative regulators displayed an average cell count of 704 and 543 per replicate. We thus followed a similar approach as in (Chia *et al.*, 2012); we considered that a nuclei count lower than 200 was due to cell toxicity. Of note, the only hit that had less than 200 nuclei was COPB2, which was discarded for later study. DGKE, STYK1, DLG4, BLNK, EPHB4, PIK3C2A, MAP3K1, PKIB, PPP2R1A and ABI1 were found among top positive regulator hits either in one replicate or both replicates together ([Figure 6-1A,C](#)). Whereas, CDKN3, AKAP11, AURKB, RAPGEF3, PRKAR1A, SRMS were common top negative regulator hits in the screen. To measure the reproducibility of the assay, we calculated the correlation parameter R^2 or coefficient of determination, which is defined as the proportion of variation in the dependent variable that can be explained to the independent variables. The parameter R^2 equaled 0.6219 ([Figure 6-1E](#)), indicating that 62.19% of the data fit the regression prediction, while the 37.81% may be attributed to unknown variability. In addition, it was reassuring that the controls β 1-integrin and PAK1 reduced matrigel uptake, an

indirect reporter of knockdown efficiency for the screen ([Figure 6-1F,G](#)). We utilised the online server ShinyGO (<http://bioinformatics.sdstate.edu/go/>) to assess enrichment for KEGG pathways. Significantly enriched pathways included: MAPK signalling pathway, PI3K-Akt signalling pathway, Fc gamma R-mediated phagocytosis, HIF1-signalling pathway, phospholipase D signalling pathway, phosphatidylinositol signalling system and choline metabolism in cancer (see [Figure S1-9](#), [S1-10](#), [S1-11](#)). To narrow down hit selection, common regulators between both replicates were considered strong modulators of uptake and were selected for further analysis ([Figure 6-1H](#)). Through the STRING database (<https://string-db.org/>), we obtained 27 protein-protein interactions out of 47 genes. Gene Ontology analysis in STRING of Biological process and Molecular function showed an enrichment of Ephrin Receptor activity, regulation of MAPK cascade, MAPK kinase activity and protein kinase (see [Figure S1-12](#)). In fact, Ephrin receptors had a strong interaction cluster in the STRING network map, suggesting an important role of ephrins in regulation of ECM internalisation. Cell data analysis of several common hits between both replicates, confirmed that the well/average quantification was reliable. Cell data was normalised to NT5 to better assess the modulation of the hits.

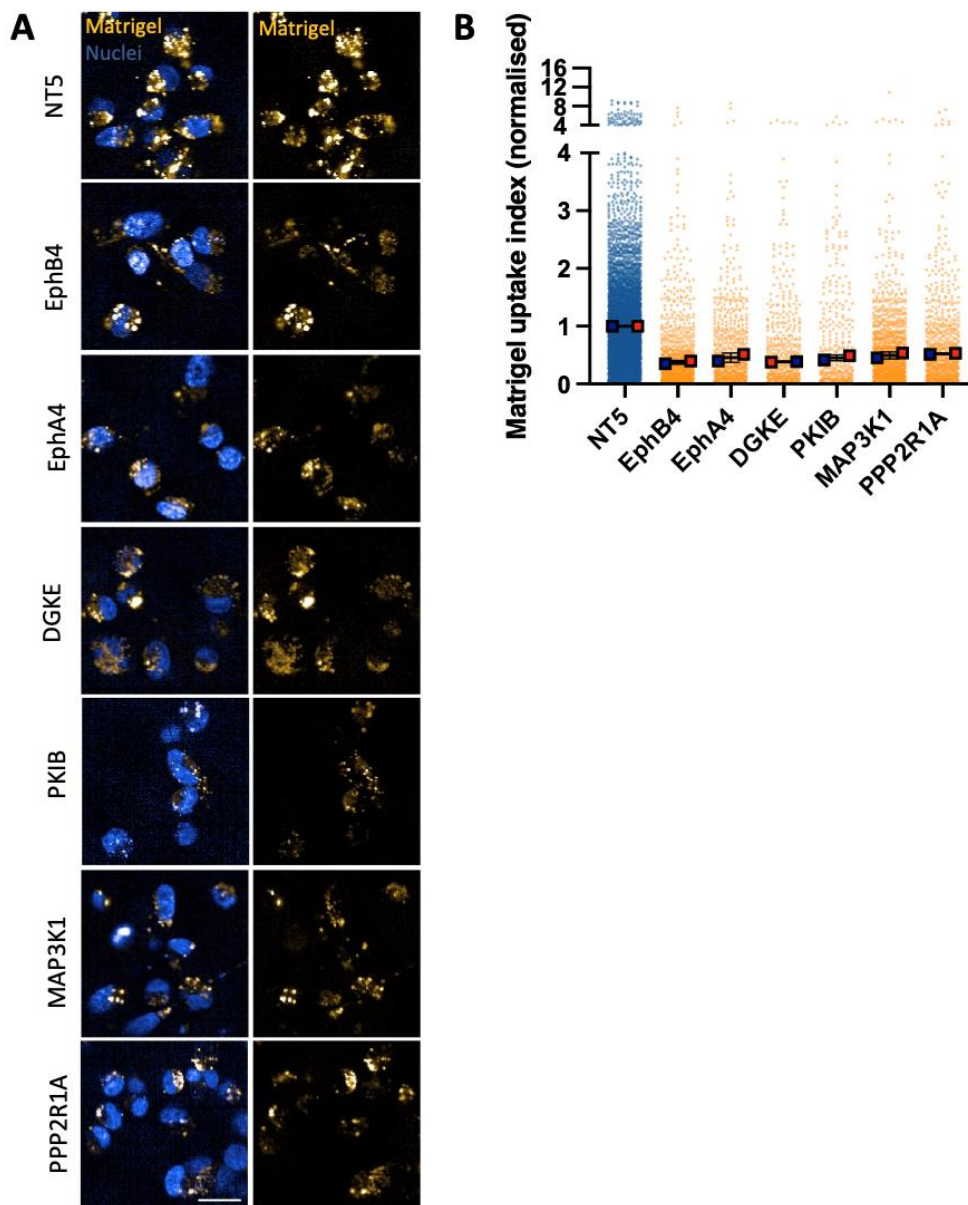


Figure 6-2. *siRNA-mediated downregulation of EphB4, EphA4, DGKE, PKIB, MAP3K1 and PPP2R1A impairs matrigel internalisation.* 3000 MDA-MB-231 cells were transfected as per protocol. Following 72h, cells were transferred into pH-rodolabelled 0.5mg/ml matrigel (golden) and incubated for 6h. Cells were labelled with 1µg/ml hoechst (blue) for nuclear staining. Cell imaging was carried out using a 40X objective in the Opera phenix microscope. Columbus software was used for image analysis. Scale bar: 20µm (A). Matrigel uptake index; the SuperPlot shows the cell-level values (dots), mean data values (squares) ± SD from two technical replicates (B).

EphB4, EphA4, DGKE, PKIB, MAP3K1 and PPP2R1A were found among the positive regulators and their knock down led to a 50% reduction in uptake ([Figure 6-2](#)). EphB4 belongs to class B ephrin receptors and it is involved in the formation of the cardiovascular system and neuronal guidance during development; in addition, it has been involved in brain malignancies (Piffko *et al.*, 2022).

EphA4, a class A ephrin receptor, activation is involved in motoneuron neurodegenerative diseases (Zhao *et al.*, 2021). Diacylglycerol kinase epsilon (DGKE) converts diacylglycerol into phosphatidic acid and has been involved in nephrotic syndrome. cAMP-dependent protein kinase inhibitor β (PKIB) overexpression is associated with aggressive prostate cancer and it promotes Akt phosphorylation, which results in cell growth and enhanced cell motility (Chung *et al.*, 2009). MAP3K1 is part of the MAPK signalling cascade. MAP3K1 promotes ERK1/2, JNK and p38 activation under distinct stimuli (Gallagher *et al.*, 2007; Yousaf *et al.*, 2015). Protein phosphatase 2 scaffold subunit α (PPP2R1A) is the regulatory subunit of protein phosphatase 2 A (PP2A) (Baker *et al.*, 2022). PPP2R1A has been involved in neurodevelopmental disorders (Baker *et al.*, 2022). In addition, we assessed the effect of hits that passed the threshold and scored high in one of the replicates; we considered them as moderate regulators. In the latter group, we specifically focused on hits that have been described to modulate endocytic-related processes. Indeed, knockdown of BLNK, DLG4, STYK1, PIK3C2A and ABI1 halved matrigel uptake index in MDA-MB-231 cells ([Figure 6-3](#)). B-Cell Linker Protein (BLNK) has been shown to regulate internalisation of B Cell receptors (BCR) and regulate B Cell differentiation (Lagresle-Peyrou *et al.*, 2014). Discs Large MAGUK Scaffold Protein 4 (DLG4) has been involved in cell polarisation via its interaction to the cell surface receptor CD46 (Ludford-Menting *et al.*, 2002). In addition, it has been identified in a screen as a regulator of macropinocytosis using a drugCIPHER, a whole-wide target prediction method (B. Zhang *et al.*, 2018). STYK1 was reported to promote EMT in hepatocellular carcinoma (Wang *et al.*, 2016) and, in addition, it promotes class I PI3K activation to promote autophagy (Zhou *et al.*, 2020). Phosphatidylinositol-4-phosphate 3-kinase catalytic subunit type 2 α (PIK3C2A) is involved in autophagy and maturation of endocytic vesicles (Merrill *et al.*, 2017). Abl interaction 1 (ABI1) recruits PI3K into signalling complexes (Innocenti *et al.*, 2003). ABI1 further promotes actin polymerisation as a regulator of Neural Wiskott–Aldrich syndrome protein (N-WASP) and the WAVE regulatory complex (Innocenti *et al.*, 2005). Altogether, few of these regulators may regulate ECM internalisation and/or trafficking through PI3K signalling and actin polymerisation.

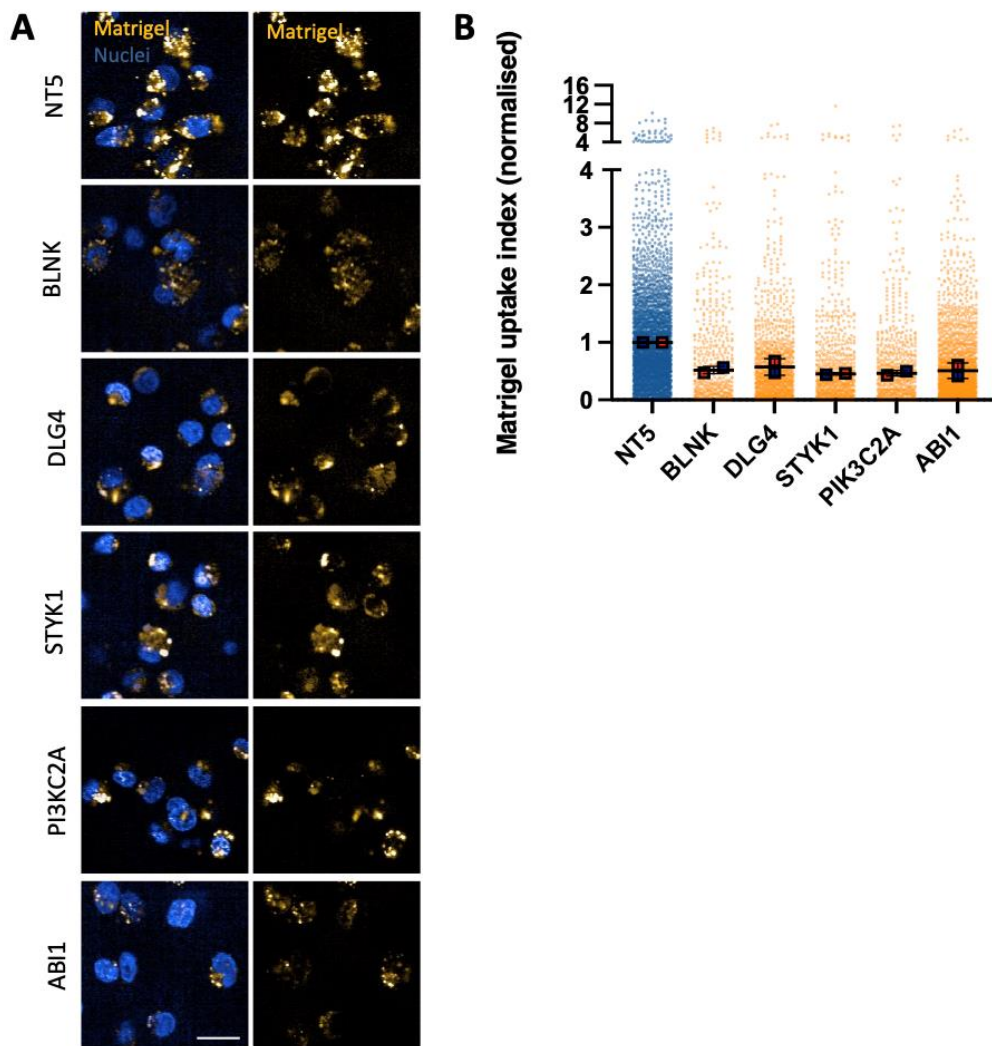


Figure 6-3. siRNA-mediated downregulation of BLNK, DLG4, STYK1, PI3KC2A, ABI1 reduce matrigel internalisation. 3000 MDA-MB-231 cells were transfected as per protocol. Following 72h, cells were transferred into pH-rodo labelled 0.5mg/ml matrigel (golden) and incubated for 6h. Cells were labelled with 1 μ g/ml hoechst (blue) for nuclear staining. Cell imaging was carried out using a 40X objective in the Opera phenix microscope. Columbus software was used for image analysis. Scale bar: 20 μ m (A). Matrigel uptake index; the SuperPlot shows the cell-level values (dots), mean data values (squares) \pm SD from two technical replicates (B).

Similarly, we assessed the modulation of negative regulators. Cell data analysis and image visualisation confirmed that the knockdown of AKAP11 (increased by 0.65 compared to normalised NT5), RAPGEF3 (~1 fold increase) and AURKB (increased by 0.83) led to a statistically significant upregulation of ECM internalisation ([Figure 6-4](#)), while the effect observed upon the downregulation of CDKN3 (increased by 0.53) and EphB2 (increased by 0.31) was smaller and not statistically significant ([Figure 6-4](#)). The effect of MPP2 knockdown was very low and it only increased the Matrigel uptake index by 0.18. This data highlights the importance of checking the

hits obtained at cell level in order to discard the study of false negative or positive regulators. In addition, this data suggests that the threshold applied is more stringent on detection of negative regulators than positive regulators, which may be due to the strong modulatory effect of bafilomycin A1.

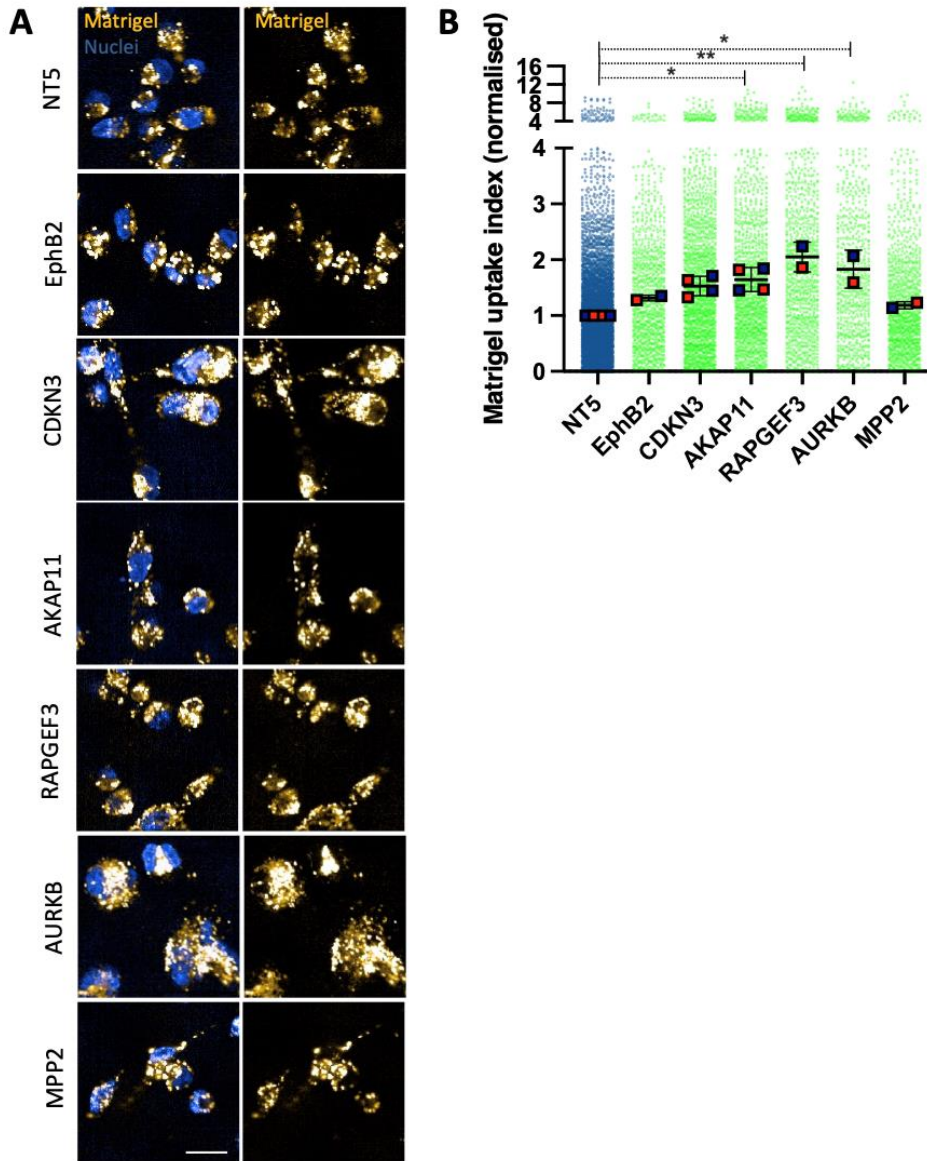


Figure 6-4. siRNA-mediated downregulation of AKAP11, RAPGEF3 and AURKB promotes matrigel internalisation. 3000 MDA-MB-231 cells were transfected as per protocol. Following 72h, cells were transferred into pH-rodo labelled 0.5mg/ml matrigel (golden) and incubated for 6h. Cells were labelled with 1µg/ml hoechst (blue) for nuclear staining. Cell imaging was carried out using a 40X objective in the Opera phenix microscope. Columbus software was used for image analysis. Scale bar: 20µm (A). Matrigel uptake index; the SuperPlot shows the cell-level values (dots), mean data values (squares) ± SD from N= 2 experiments; in addition, two biological replicates per experiment are shown for CDKN3 and AKAP11 since they were in duplicates in the screen; *p≤0.0490, **p=0.0074; Kruskal-Wallis test (B).

Altogether this data revealed novel signalling regulators of ECM endocytosis in MDA-MB-231 cells. Specifically, this data suggests an important role for lipid signalling, MAPK signalling and Ephrin receptor signalling in modulation of ECM internalisation.

6.2.2. A secondary screen confirms that MAP3K1 and PPP2R1A are required for the endocytosis of matrigel

We performed an orthogonal secondary validation screen for 45 common hits out of the 134 candidates obtained from the primary screen. The pooled siRNAs for each gene were deconvoluted into four individual siRNA. We adopted a similar approach as before and MDA-MB-231 cells were transferred to pHrodo-labelled matrigel. Cell count was assessed for each individual siRNA. However, no considerable differences were observed (data not shown). Data was normalised between NT5 (0) and NT5 cells treated with bafilomycin A1 (-1). We considered the hit was validated if 2 out of 4 siRNAs led to a reduction or increase in matrigel uptake. In addition, the criterion for hit selection was based on the modulation in matrigel uptake observed by downregulating β 1-integrin and PAK1. We took as a threshold a 0.3-fold change compared to NT5 (0) to confirm positive or negative regulators. According to this criterion 19 genes were validated. We confirmed the following positive regulators: EphB4, DGKE, PKIB, STK39, STYK1, EphA4, GRK1, PIK3C2A, MAP3K1, PPP2R1A, DUSP8 and STRADB ([Figure 6-5](#)). Moreover, we included in the validation the positive regulator COPB2 as a control of knockdown efficiency. Similar to the primary screen, knocking down COPB2 strongly reduced both matrigel uptake index and cell count. The effect of individual siRNAs of the selected negative regulators was not as accordant; in fact, some individual siRNAs (targeting the same gene) led to opposite outcomes, such as in UHMK1 or CDK20. Therefore, only consistent hits between at least two individual siRNAs were selected (EphB2, MARK3, SRMS, PRKAR1A, MPP3 and AURKB) ([Figure 6-5](#)). Taking into consideration that positive regulators of uptake were more consistent among individual siRNA, further assays will focus on the study of positive regulators in ECM uptake.

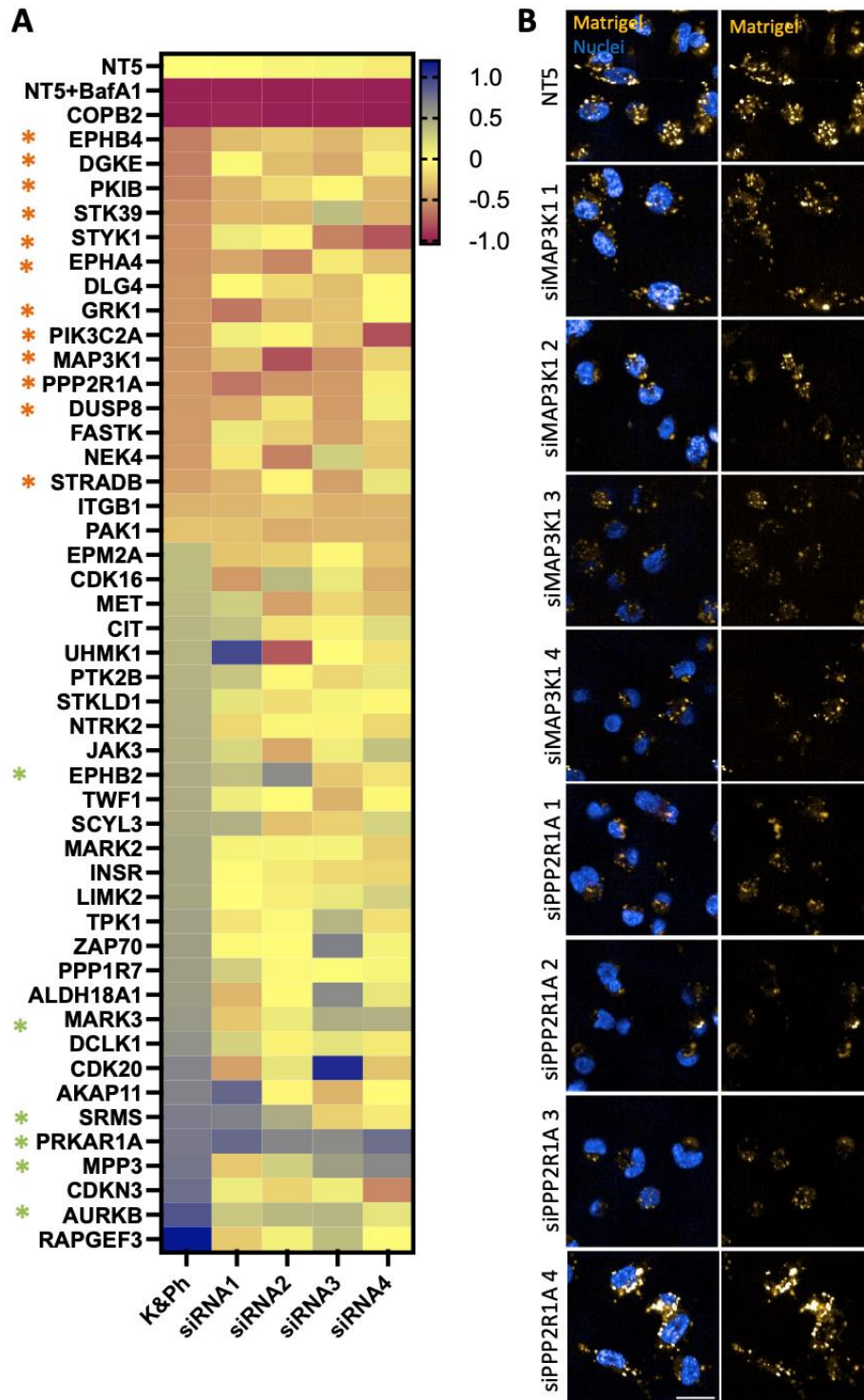


Figure 6-5. Secondary validation screen. 3000 MDA-MB-231 cells were transfected as per protocol. Following 72h, cells were transferred into pH-rodo labelled 0.5mg/ml matrigel (golden) and incubated for 6h. Cells were labelled with 1 μ g/ml hoechst (blue) for nuclear staining. Cell imaging was carried out using a 40X objective in the Opera phenix microscope. Columbus software was used for image analysis. Scale bar: 20 μ m. Heat map of the siRNA deconvolution of common hits. Orange stars (*) represent validated positive regulators, while green stars (*) are validated negative regulators according to the criterion established (A). Representative images of deconvoluted siRNAs for MAP3K1 and PPP2R1A (B).

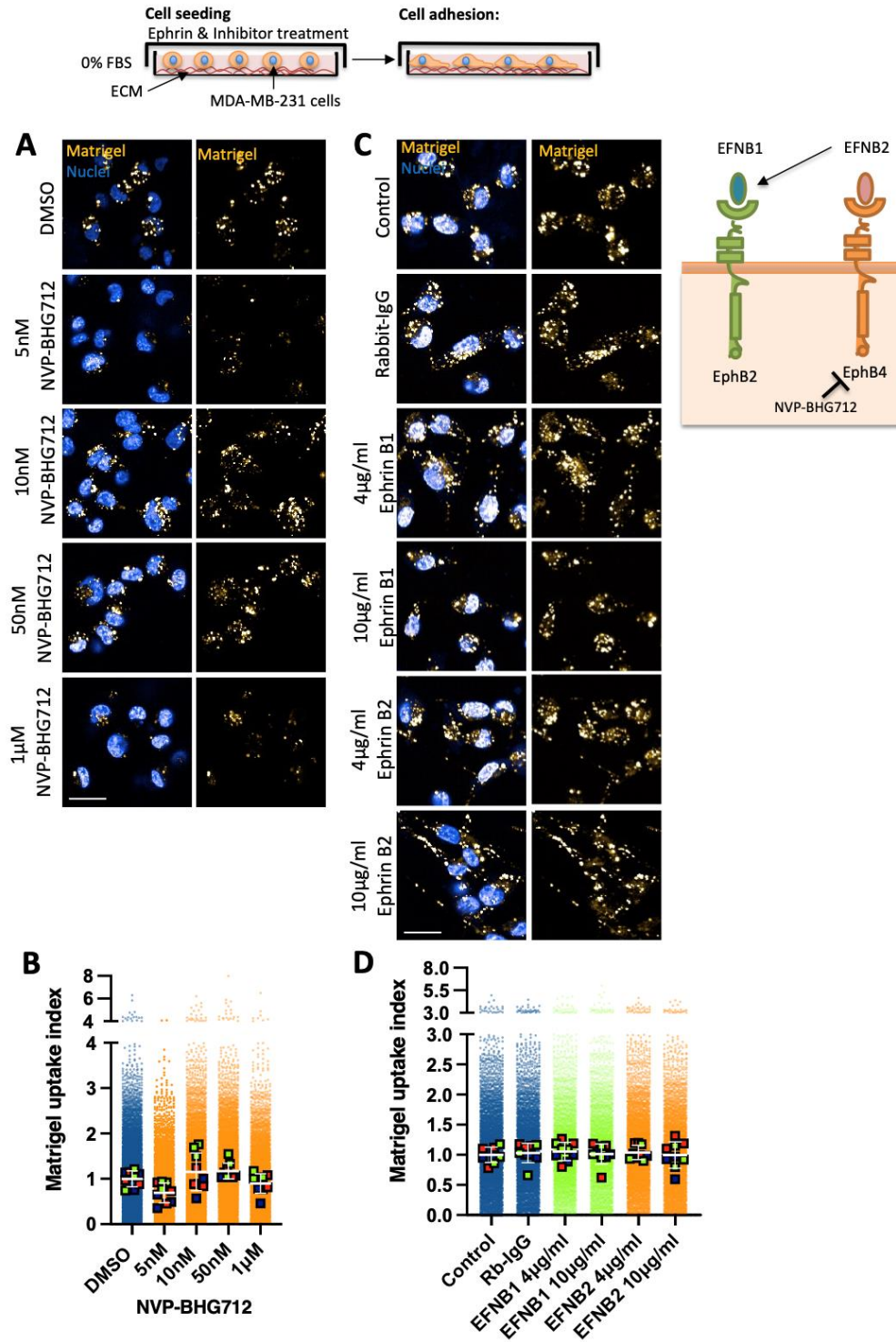


Figure 6-6. Effect of NVP-BHG712 treatment on matrigel internalisation. 10,000 cells were cultured on 0.5mg/ml matrigel (golden) for 6hr in presence of DMSO, 5nM, 10nM, 50nM and 1µM NVP-BHG712 or in presence of a Rabbit IgG (Rb-IgG), 4µg/ml or 10µg/ml ephrin B1 (EFNB1) or ephrin B2 (EFNB2). Cells were stained with 1µg/ml hoechst (blue, high intensity is white) and imaged live. 40X water-immersion objective Opera Phenix microscope was used for imaging. Scale bar, 20µm (A,C). Cell data analysis was performed with Columbus software. Values represented are cell data (dots) and well data (bigger squares) + SD from three independent experiments; well data was used for the statistical test (B). Superplot for matrigel uptake in presence of EFNB1 and EFNB2 (D).

6.2.3. Chemical inhibition of EphB4 slightly decreased internalisation of ECM in MDA-MB-231 cells

Ephrin receptors (EPHs) are receptor tyrosine kinases that are either transmembrane glycoproteins or attached to the PM through glycosylphosphatidylinositol. EPHs binding to their ligand ephrins (EFN) mediate cell-contact communication between cells, proliferation, cell morphology, adhesion and migration (Lisabeth, Falivelli and Pasquale, 2013). STRING analysis and later siRNA-mediated validation showed a strong Ephrin receptor cluster (EphB2, EphB4, EphA4) as regulators of matrigel internalisation. We thus thought to determine whether inhibition of EphB4 reduced specifically BM-like ECM internalisation or it was a broad-spectrum regulator of ECM internalisation. We tested a range of concentrations of NVP-BHG712, a specific EphB4 small molecule inhibitor (Buckens *et al.*, 2020; M. Zhu *et al.*, 2020; Su *et al.*, 2021), on matrigel, collagen I and CDM uptake. In disagreement with the primary screen and secondary screen validation, NVP-BHG712 treatment did not affect matrigel internalisation, as none of the concentrations used resulted in a statistically significant reduction of the matrigel uptake index ([Figure 6-6A,B](#)). In addition to ligand-dependent EPH-EFN signalling, EPHs can transduce signalling cues in a ligand-independent manner. Ephrin-B2 (EFNB2) is the ligand of EphB4, but also EphB2, which was found to be a negative regulator in the screen. In addition, EphB2 is also activated by Ephrin-B1 (EFNB1). We thus sought to determine the contribution of EFNs in ECM internalisation. MDA-MB-231 cells were treated with two different concentrations of EFNB1 and EFNB2, previously published (Wu *et al.*, 2012; M. Zhu *et al.*, 2020). No significant increase nor reduction in matrigel uptake was observed between the control (untreated) and control Rabbit-IgG. This data suggests that matrigel internalisation is not regulated by EphB4 and EphB2.

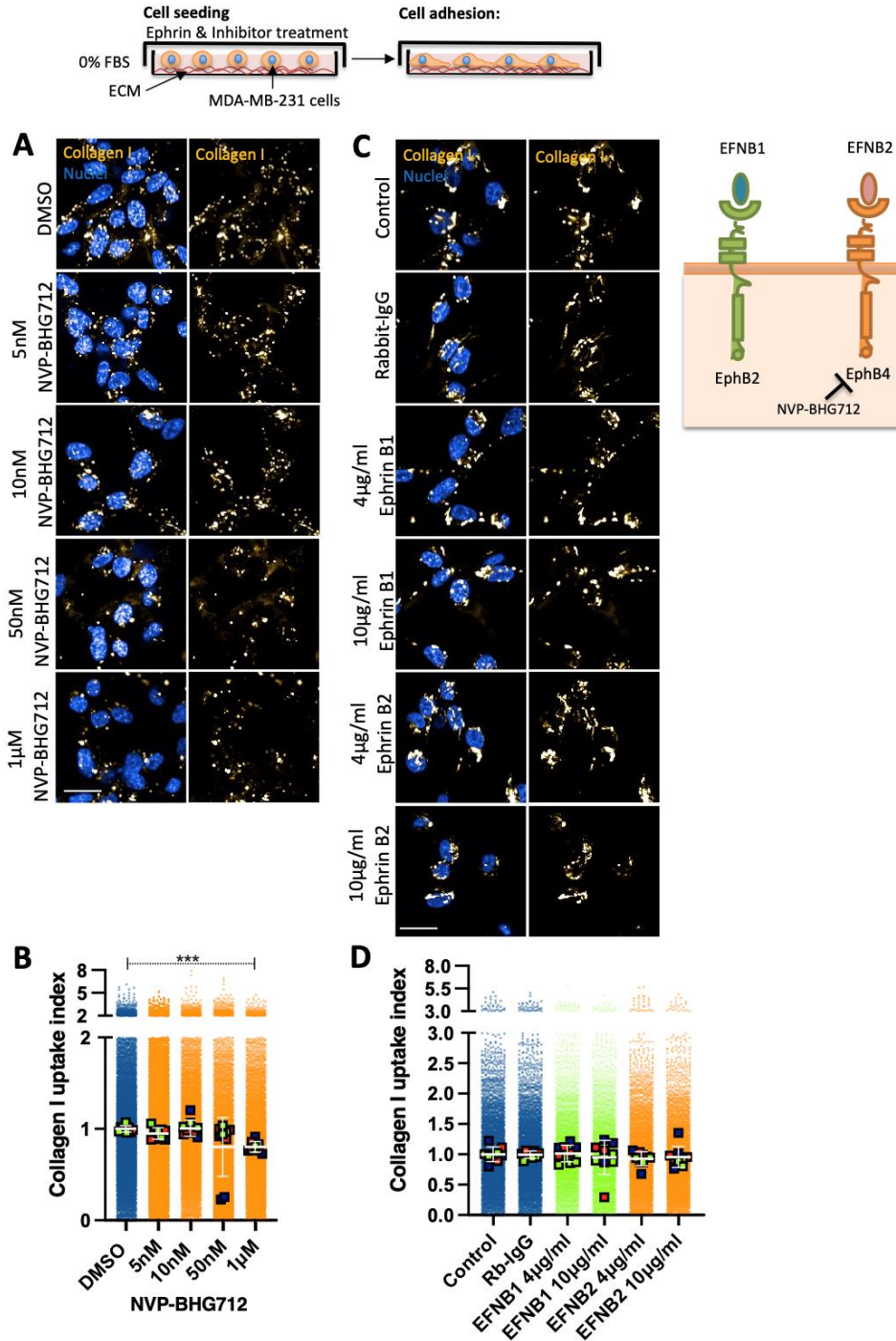


Figure 6-7. 1µM NVP-BHG712 slightly reduced collagen I internalisation. 10,000 cells were cultured on 0.5mg/ml collagen I (golden) for 6hr in presence of DMSO, 5nM, 10nM, 50nM and 1µM NVP-BHG712 or in presence of a Rabbit IgG (Rb-IgG), 4µg/ml or 10µg/ml EFNB1 or EFNB2. Cells were stained with 1µg/ml hoechst (blue, high intensity is white) and imaged live. 40X water-immersion objective Opera Phenix microscope was used for imaging. Scale bar, 20µm (A,C). Cell data analysis was performed with Columbus software. Values represented are cell data (dots) and well data (bigger squares) + SD from three independent experiments; well data was used for the statistical test; ***p=0.0002; Kruskal-Wallis test (B). Superplot for collagen I uptake in presence of EFNB1 and EFNB2 (D).

We next aimed to see whether collagen I internalisation was modulated by EphB4. 1 μ M NVP-BHG712 treatment significantly reduced endocytosis of collagen I and cells presented fewer vesicles, suggesting that EphB4 might be a regulator of ECM internalisation in MDA-MB-231 cells ([Figure 6-7](#)). Again, we aimed to study the effect of EFN ligand on collagen I uptake. No difference in uptake was observed between control (untreated) and Rabbit IgG treatment. Supplementing EFN1 and EFN2 to the cell culture did not affect collagen I uptake index; likewise, no changes in how collagen I-vesicles distributed in the cell were observed. This data indicates that EphB4 regulates collagen I uptake independently of its ligand EFN2.

In vivo, cells encounter a complex environment with multiple ECM components. We took advantage of TIF-CDM to confirm whether in a complex environment with several matrisome proteins, EphB4 mediated internalisation of stromal ECM. Similar to collagen I results, TIF-CDM was statistically significantly diminished upon 1 μ M NVP-BHG712 treatment, confirming that EphB4 regulates internalisation of collagen I-rich ECM ([Figure 6-8](#)). Collagen I is the most abundant component of TIF-CDM (Fitzpatrick and McDevitt, 2015). We thus aimed to evaluate whether the effect observed by EphB2 and EphB4 would be similarly ligand independent. No differences were quantified upon EFN1 and EFN2 treatment. Taking everything into account, this data suggests that EphB4 might primarily regulate collagen I and CDM internalisation, but not matrigel, however more studies are required to further elucidate the role of EFNs in mediating ECM uptake or endosomal trafficking.

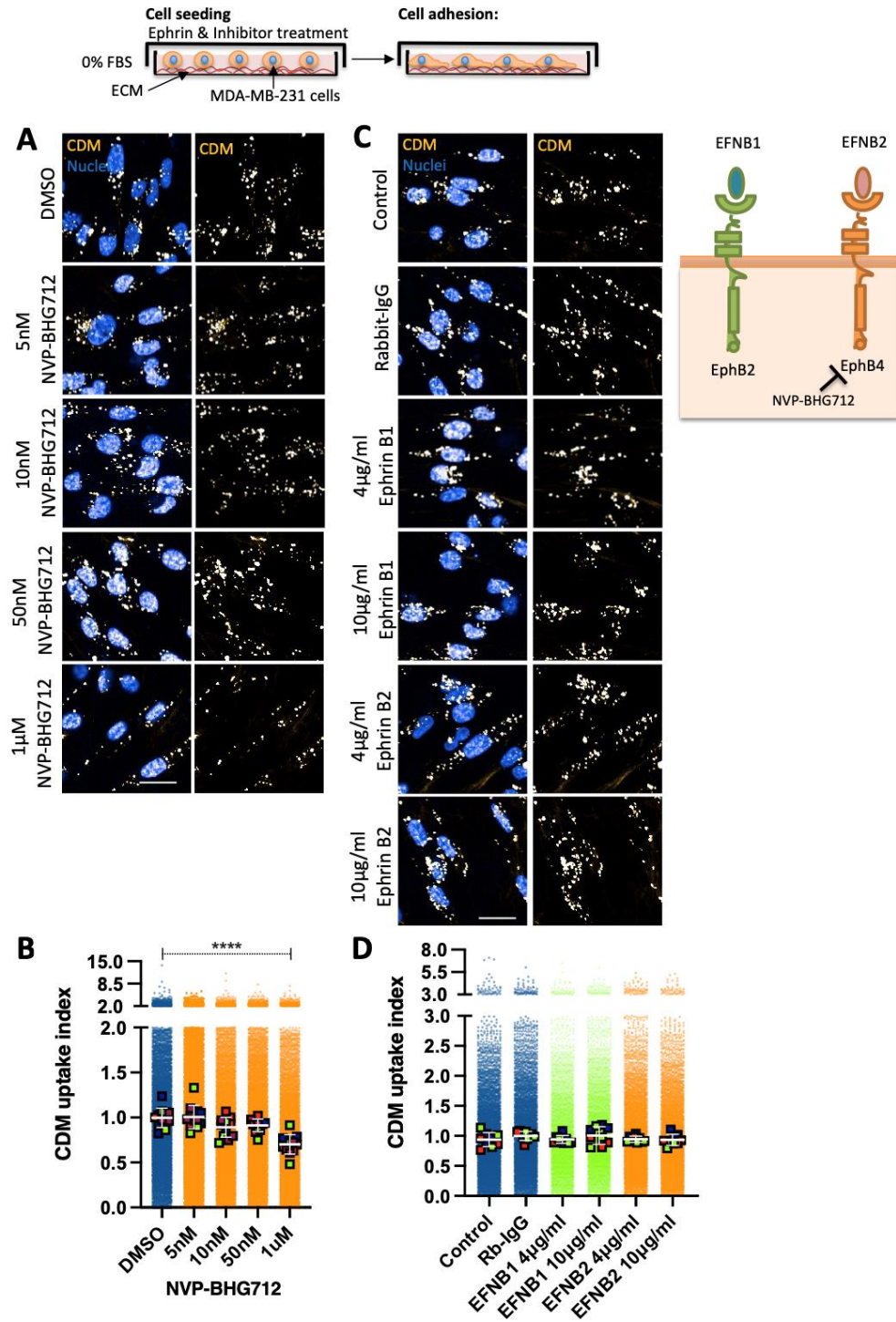


Figure 6-8. 1µM NVP-BHG712 slightly reduced CDM internalisation. TIF-CDMs were generated as per protocol and labeled with 20µg/ml pHrodo (golden) for 1h at room temperature. 10,000 cells were cultured for 6hr in presence of DMSO, 5nM, 10nM, 50nM and 1µM NVP-BHG712 or in presence of a Rabbit IgG (Rb-IgG), 4µg/ml or 10µg/ml EFNB1 and EFNB2. Cells were stained with 1µg/ml hoechst (blue, high intensity is white) and imaged live. 40X water-immersion objective Opera Phenix microscope was used for imaging. Scale bar, 20µm (A,C). Cell data analysis was performed with Columbus software. Values represented are cell data (dots) and well data (bigger squares) + SD from three independent experiments; well data was used for the statistical test; **** $p < 0.0001$; Kruskal-Wallis test (B). Superplot for CDM uptake in presence of EFNB1 and EFNB2 (D).

6.2.4. Pharmacological inhibition of EphB4 impairs MDA-MB-231 cell migration

Ephrin signalling is involved in cell migration during embryonic development (Santiago and Erickson, 2002). In addition, EphB4 signalling has been shown to promote endothelial cell migration during angiogenesis via the PI3K signalling pathway (Steinle *et al.*, 2002). We thus aimed to discern whether EphB4 inhibition would affect MDA-MB-231 cell migration on CDM. MDA-MB-231 cells were seeded in the presence of DMSO or 1 μ M NVP-BHG712 for a period of 6h before time-lapse imaging was performed for an additional period of 7h. Preliminary data indicated that NVP-BHG712 treatment statistically significantly reduced the velocity of cell migration (Figure 6-9). In addition, directionality of migrating cells was slightly, but significantly, diminished upon treatment (Figure 6-9). This data suggests that EphB4 may regulate migration of MDA-MB-231 cells on CDM.

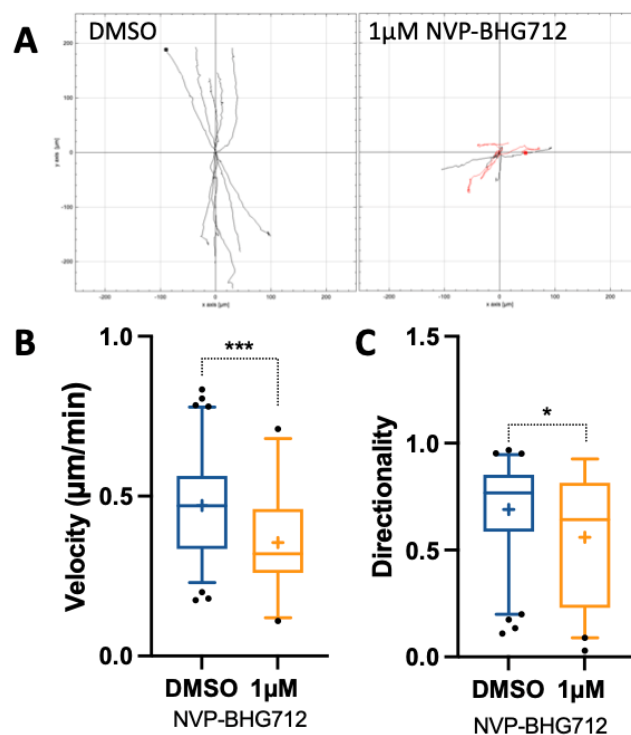


Figure 6-9. 1 μ M NVP-BHG712 reduced velocity and directionality of MDA-MB-231 cells migrating on CDMs. TIF-CDMs were generated as per protocol. 5×10^4 MDA-MB-231 cells were cultured for 6hr in presence of DMSO and 1 μ M NVP-BHG712. After this time, cells were imaged with a 10X Nikon dual cam whitefield microscope for a period of 7h. (A) Spider plots show the migration paths of manually tracked cells (directionality >0.5 in black, directionality <0.5 in red). (B) Average velocity (μ m/min). (C) Directionality. $N=1$ independent experiments. Box and whisker plots represent 5-95 percentile, + represents the mean, dots are $<5\%$ and $>95\%$; * $p=0.0316$, *** $p=0.0002$; Mann-Whitney test.

6.2.5. p38 MAPK is required for ECM macropinocytosis in MDA-MB-231 cells

KEGG pathway and STRING analysis pointed towards regulation of MAPK signalling cascade as a modulator of ECM internalisation. Nevertheless, the primary screen did not select any of the major kinases involved in signalling, including ERK1/2, JNK1-3 nor the p38 family. We thus checked the modulation on matrigel uptake upon ERK, JNK and p38 knockdown in the original primary screen. Strikingly, only p38 β (MAPK11) showed a trend towards a reduction (45%) in matrigel internalisation (p-value = 0.3109, well data) compared to the other kinases (p-value > 0.9999) ([Figure 6-10](#)).

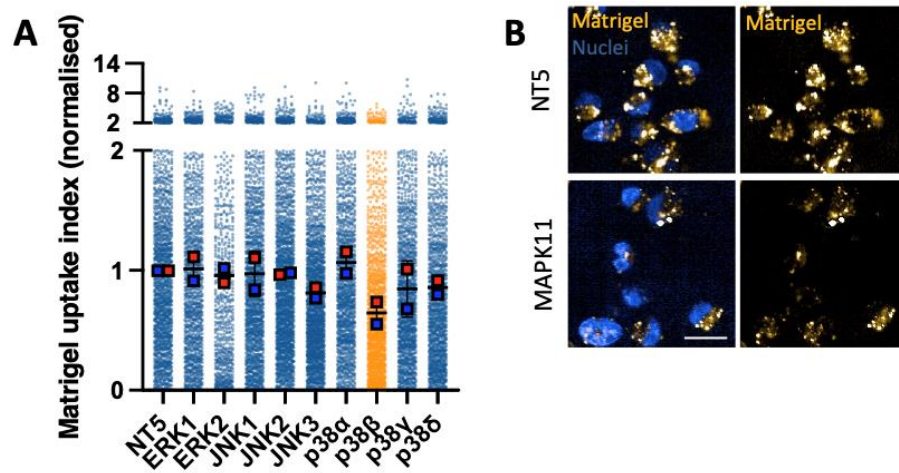


Figure 6-10. p38 β showed a trend towards reduced matrigel uptake index in the kinome and phosphate screen. 3000 MDA-MB-231 cells were transfected as per protocol. Following 72h, cells were transferred into pH-rodo labelled 0.5mg/ml matrigel and incubated for 6h. Cells were labelled with 1 μ g/ml hoechst for nuclear staining. Cell imaging was carried out using a 40X objective in the Opera phenix microscope. Columbus software was used for image analysis. Scale bar: 20 μ m. (A) Uptake index of ERK, JNK and p38 MAPKs; the SuperPlot shows the cell-level values (dots), mean data values (squares) \pm SD from 2 technical replicates; p-value for p38 β (MAPK11) is 0.3109; Kruskal-Wallis test test. (B) Representative images of NT5 and MAPK11.

To determine the role of MAPK signalling, four different inhibitors against p38 α/β , ERK1/2 and MEK1/2 were tested. Three different concentrations were used 2 μ M, 10 μ M and 50 μ M based on previous studies (Hu *et al.*, 2012; Düzgün *et al.*, 2017; Huth *et al.*, 2017; Zhao *et al.*, 2017; Xiao, Mohanakrishnan and Schmid, 2018).

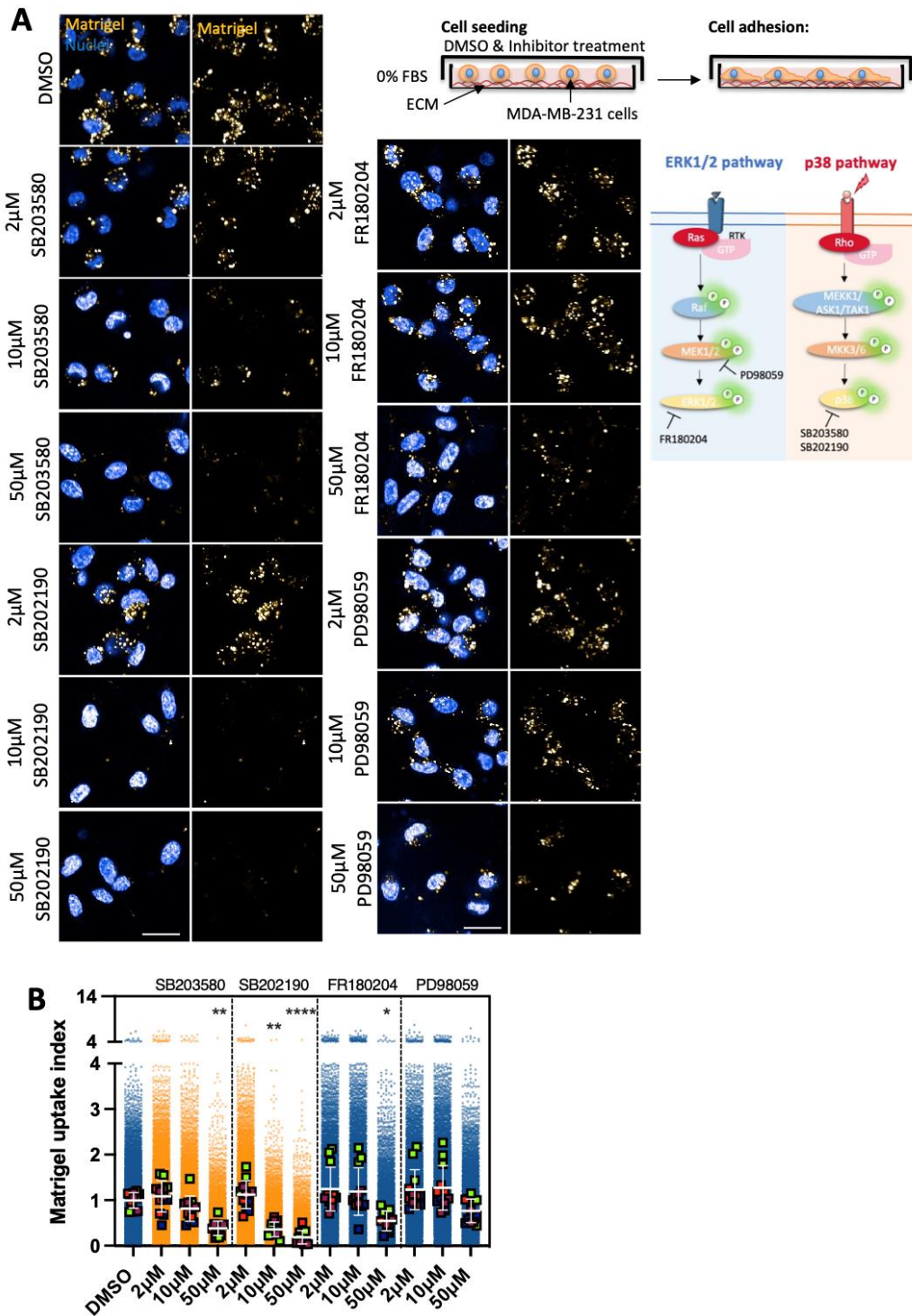


Figure 6-11. Effect of MAPK inhibition on matrigel internalisation. 10.000 cells were cultured on 0.5mg/ml pHrodo-labelled matrigel (golden) for 6hr in presence of DMSO, and three concentrations (2 μ M, 10 μ M and 50 μ M) of SB203580, SB202190, FR180204 and PD98059. Cells were stained with 1 μ g/ml hoechst (blue, high intensity is white) and imaged live. 40X water-immersion objective Opera Phenix microscope was used for imaging. Scale bar, 20 μ m (A). Cell data analysis was performed with Columbus software. Values represented are cell data (dots) and well data (bigger squares) + SD from three independent experiments; well data was used for the statistical test; * p =0.0434, ** p ≤0.0013, **** p <0.0001; Kruskal-Wallis test (B). Image made using items from Servier medical Art.

To specifically study MAPK signalling stimulated by the ECM, experiments were performed in the absence of serum. In addition, cells were treated with MAPK inhibitors at the moment of cell seeding, before adhesion occurred. p38 inhibition with 10 μ M and 50 μ M SB203580 respectively reduced the internalisation of matrigel by 20% and 60%, indicating a dose-dependent inhibition ([Figure 6-11](#)). To ensure the effect observed was not off-target, we tested another p38 MAPK inhibitor, SB202190. Similarly, matrigel internalisation decreased by 45% and 80% upon treatment with 10 μ M and 50 μ M SB202190, respectively. Furthermore, we aimed to assess the significance and specificity of p38 MAPK. Integrins have been reported to promote EGFR activation, resulting in ERK1/2 activation (Bill *et al.*, 2004). In addition, aberrant K-Ras has been reported to induce macropinocytosis in cancer cells (Commisso *et al.*, 2013), as well as hyperactivation of ERK signalling (Huang *et al.*, 2021). We thus tested whether ERK1/2 could contribute to matrigel internalisation. ERK1/2 inhibition with FR180204 did not show a dose-dependent reduction of matrigel internalisation; in fact, only 50 μ M FR180204 resulted in a small, but significant reduction in uptake. This effect may be explained since higher concentrations (>10 μ M) of FR180204 has been reported to inhibit p38 MAPK (FR180204 (CAS 865362-74-9), no date). To exclude off-target effects, we tested another inhibitor against MEK1/2, upstream activator of ERK1/2. MEK1/2 inhibition by PD98059 did not significantly reduce matrigel internalisation, although 50 μ M PD98059 had a small, but not significant, decrease in matrigel uptake. Altogether, taking into consideration the dose-dependent effect of p38 inhibition on matrigel internalisation, this data supports the role of p38, rather than ERK1/2, in mediating matrigel uptake.

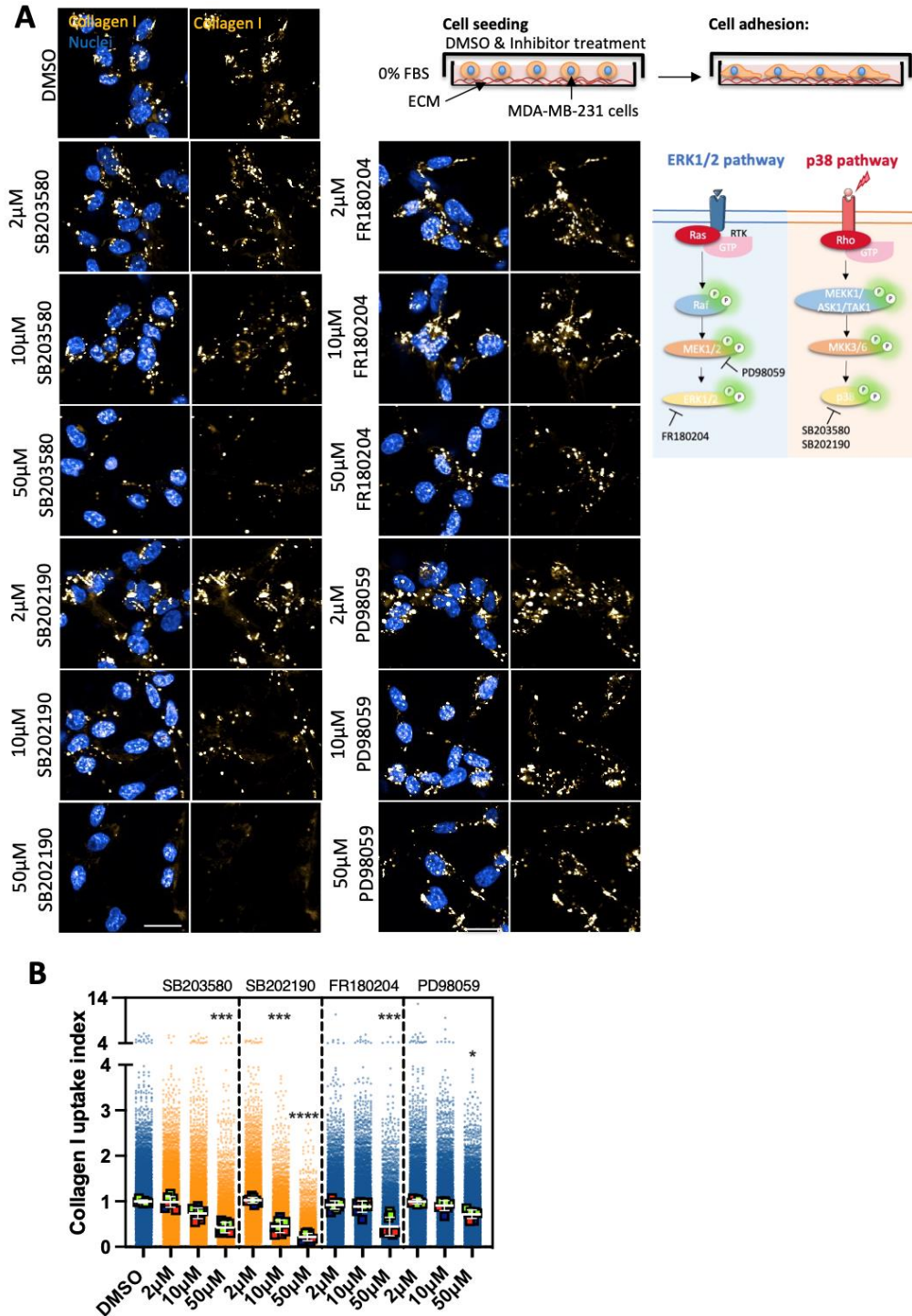


Figure 6-12. Effect of MAPK inhibition on collagen I internalisation. 10.000 cells were cultured for 6hr on 0.5mg/ml pHrodo-labelled collagen I (golden) in presence of DMSO, and three concentrations (2 μ M, 10 μ M and 50 μ M) of SB203580, SB202190, FR180204 and PD98059. Cells were stained with 1 μ g/ml hoechst (blue, high intensity is white) and imaged live. 40X water-immersion objective Opera Phenix microscope was used for imaging. Scale bar, 20 μ m (A). Cell data analysis was performed with Columbus software. Values represented are cell data (dots) and well data (bigger squares) + SD from three independent experiments; well data was used for the statistical test; * $p=0.0434$, ** $p<0.0013$, *** $p<0.0001$; Kruskal-Wallis test (B). Image made using items from Servier medical Art.

To assess whether different MAPKs regulated internalisation of distinct ECM components, we tested the panel of inhibitors on collagen I uptake. Similar to matrigel, collagen I internalisation was reduced by 30% and 60% upon treatment with 10 μ M and 50 μ M SB203580, respectively ([Figure 6-12](#)). Likewise, p38 inhibition with 10 μ M and 50 μ M SB202190 respectively diminished collagen I uptake by 60% and 80%. We further tested the specificity of p38 by testing FR180204, an inhibitor of ERK1/2. Endocytic uptake of collagen I was significantly reduced upon treatment with 50 μ M FR180204 (by ~55%), however lower concentrations had no effect on uptake. To further confirm the effect observed upon p38 and ERK1/2 inhibition, MDA-MB-231 cells were treated with PD98059, a MEK1/2 inhibitor. MEK1/2 inhibition did not affect internalisation of collagen I in a dose-dependent manner; however, 50 μ M treatment led to a small, but statistically significant, decrease in collagen I uptake index. This data suggests that mainly p38, and not ERK1/2, regulates collagen I uptake.

Collagen I may be used as a substitute of stromal ECM, however *in vivo*, stromal ECM is a complex protein structure. To assess the effect of MAPK activation on ECM internalisation, we used CDM to better recapitulate the *in vivo* stroma. Treatment with 10 μ M and 50 μ M SB203580 reduced by 35% and 65% internalisation of CDM ([Figure 6-13](#)). While, 10 μ M and 50 μ M SB202190 diminished uptake by 62% and 92%, respectively. Again, to test the specificity of p38 in CDM internalisation, we treated MDA-MB-231 cells with FR180204 and PD98059. 50 μ M FR180204 significantly reduced CDM uptake (50%), however inhibiting the upstream activator of ERK1/2 had no effect on CDM internalisation. This data is in agreement with collagen I and matrigel internalisation, suggesting that p38 MAPK mediates ECM internalisation.

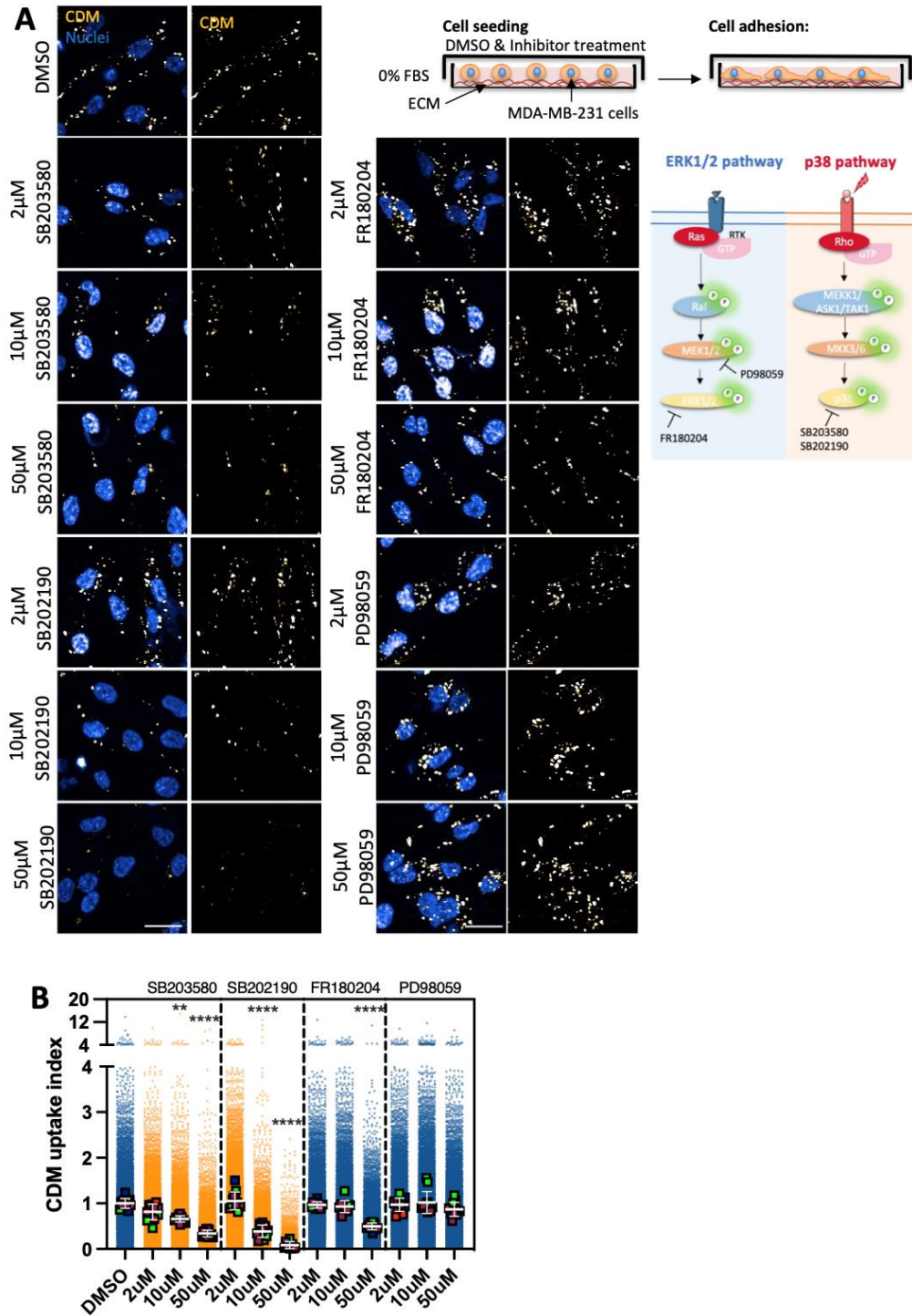


Figure 6-13. Effect of MAPK inhibition on TIF-CDM internalisation. CDMs were generated as per protocol and labelled with 20μg/ml pHrodo (golden) for 1h at room temperature. 10.000 cells were cultured for 6hr in presence of DMSO, and three concentrations (2μM, 10μM and 50μM) of SB203580, SB202190, FR180204 and PD98059. Cells were stained with 1μg/ml hoechst (blue, high intensity is white) and imaged live. 40X water-immersion objective Opera Phenix microscope was used for imaging. Scale bar, 20μm (A). Cell data analysis was performed with Columbus software. Values represented are cell data (dots) and well data (bigger squares) + SD from three independent experiments; well data was used for the statistical test; **p=0.0002, ****p<0.0001; Kruskal-Wallis test (B). Image made using items from Servier medical Art.

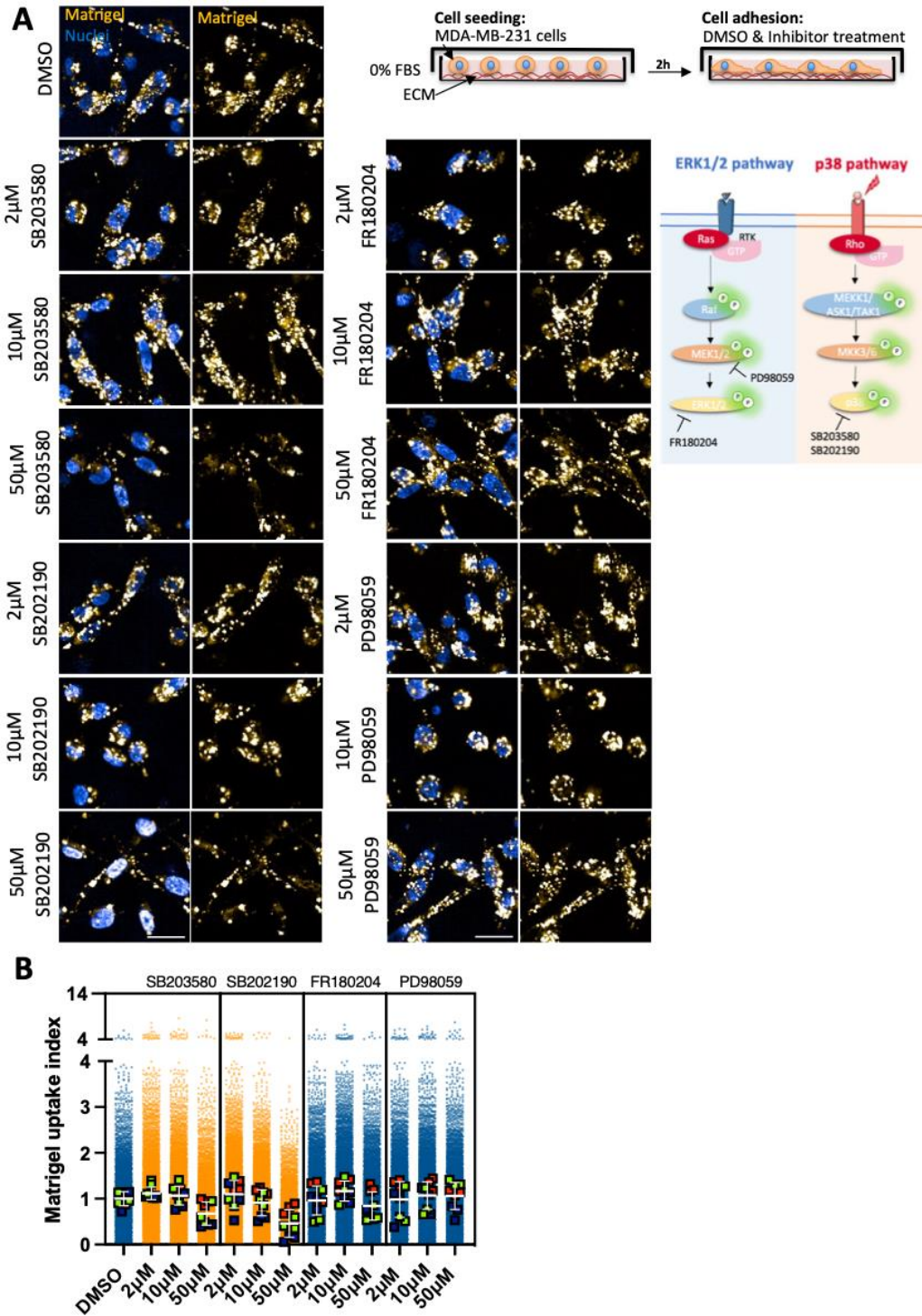


Figure 6-14. Effect of MAPK inhibition on matrigel internalisation. 10.000 cells were cultured on 0.5mg/ml pHrodo (golden)-labelled matrigel for 6hr in presence of DMSO, and three concentrations (2 μ M, 10 μ M and 50 μ M) of SB203580, SB202190, FR180204 and PD98059. Inhibitors were added 2h after seeding the cells. Cells were stained with 1 μ g/ml hoechst (blue, high intensity is in white) and imaged live. 40X water-immersion objective Opera Phenix microscope was used for imaging. Scale bar, 20 μ m (A). Cell data analysis was performed with Columbus software. Values represented are cell data (dots) and well data (bigger squares) + SD from three independent experiments; well data was used for the statistical test; * p =0.0434, ** p ≤0.0013, *** p <0.0001; Kruskal-Wallis test (B). Image made using items from Servier medical Art.

$\alpha 2\beta 1$ integrin has been shown to activate p38 MAPK signalling upon adhesion to ECM (Ivaska *et al.*, 1999). In addition, $\alpha 2\beta 1$ integrin promotes ECM internalisation in MDA-MB-231 cells (Rainero, unpublished). To better understand the spatiotemporal signalling regulation of ECM uptake, we cultured cells on ECM for 2h, enabling cell adhesion and spreading, prior to inhibiting MAPK signalling. In addition, we chose a 2h time-point to add inhibitors since ECM is not yet internalised in MDA-MB-231 cells (Rainero, unpublished). Matrigel internalisation was not affected by any of the MAPK inhibitors tested. Strikingly, only treatment with 50 μ M SB203580 (30%) and SB202190 (50%) led to a small, but insignificant, decrease in matrigel uptake index in MDA-MB-231 cells ([Figure 6-14](#)). Likewise, MAPK inhibition after 2h did not modulate collagen I uptake as MAPK inhibition during cell seeding. In fact, 50 μ M SB202190 and SB203580 significantly reduced collagen I internalisation by only 30% and 40%, respectively ([Figure 6-15](#)). While 50 μ M FR180204 treatment resulted in a small (20%), but statistically significant, decrease. Similar results were observed for CDM uptake. While 10 μ M and 50 μ M SB202190 and SB203580 significantly reduced CDM internalisation by 50 to 60%, the effect observed was not as striking as p38 inhibition before cell adhesion and spreading ([Figure 6-16](#)). This data suggested that ECM-integrin signalling upon cell adhesion is required for ECM internalisation.

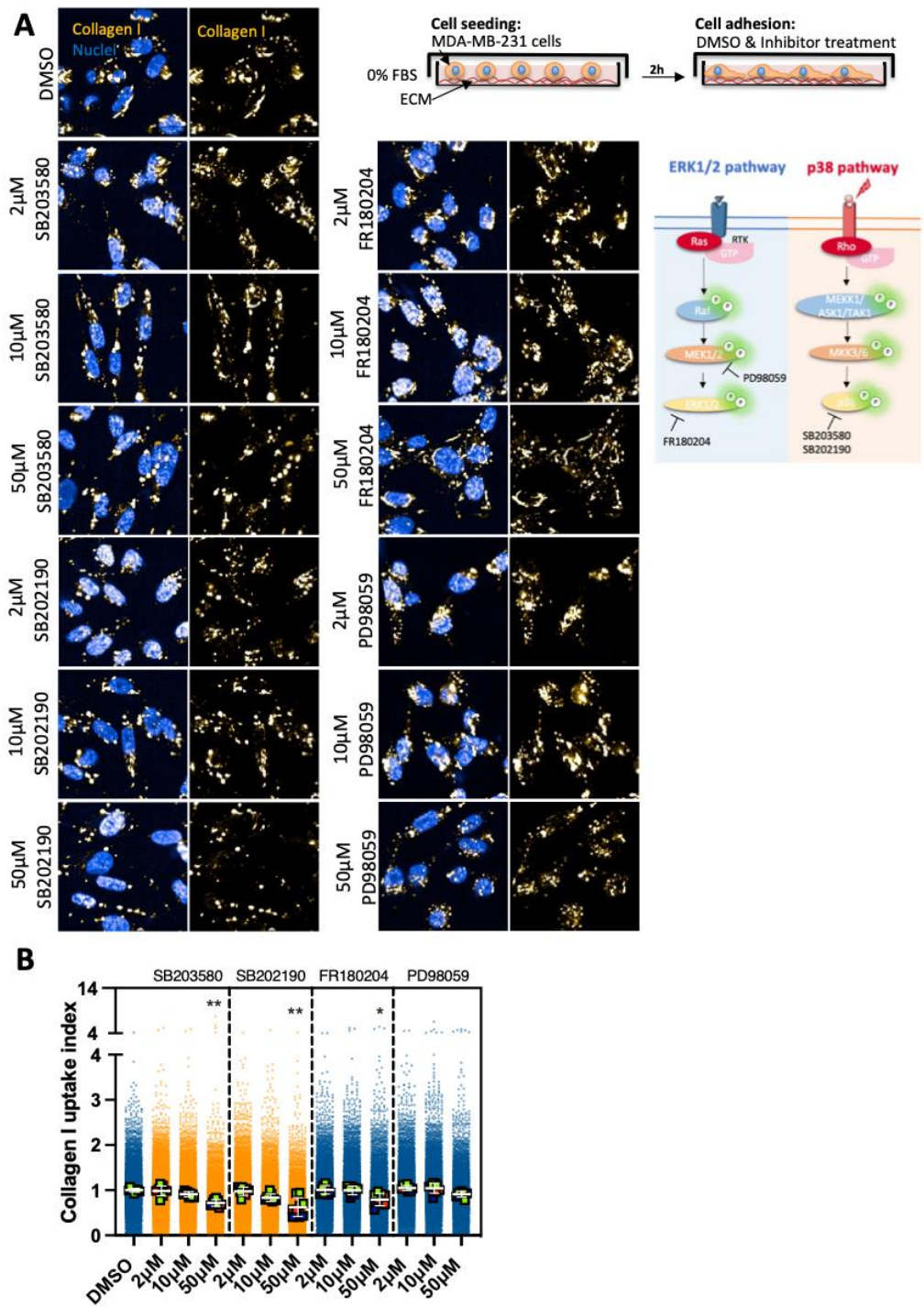


Figure 6-15. Effect of MAPK inhibition on collagen I internalisation. 10.000 cells were cultured on 0.5mg/ml pHrodo-labelled 0.5mg/ml collagen I (golden) for 6hr in presence of DMSO, and three concentrations (2μM, 10μM and 50μM) of SB203580, SB202190, FR180204 and PD98059. Inhibitors were added 2h after cell seeding. Cells were stained with 1μg/ml hoechst (blue, high intensity is white) and imaged live. 40X water-immersion objective Opera Phenix microscope was used for imaging. Scale bar, 20μm (A). Cell data analysis was performed with Columbus software. Values represented are cell data (dots) and well data (bigger squares) + SD from three independent experiments; well data was used for the statistical test; *p=0.0256, **p<0.0012; Kruskal-Wallis test (B). Image made using items from Servier medical Art.

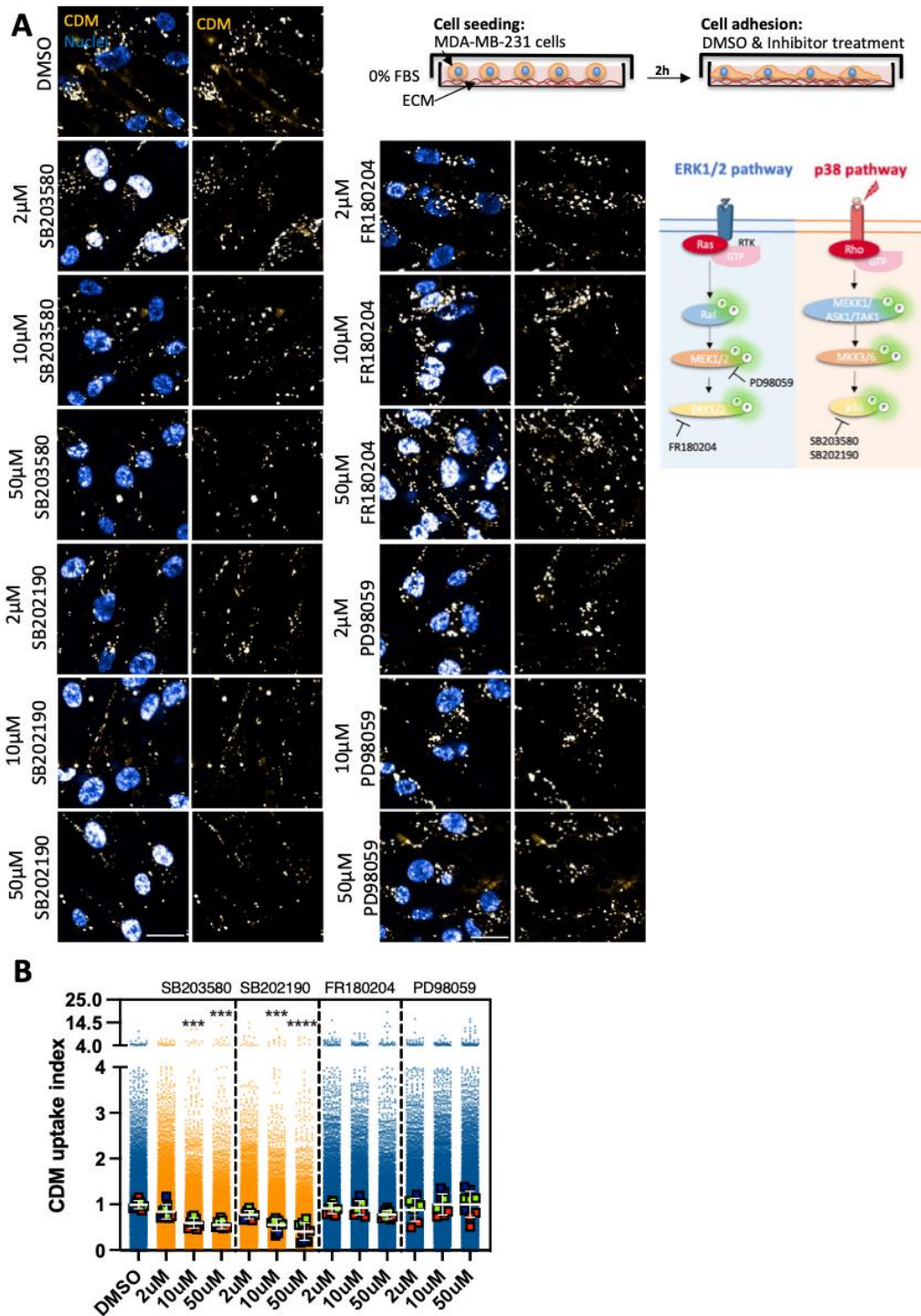


Figure 6-16. Effect of MAPK inhibition on TIF-CDM internalisation. 10.000 cells were cultured on pHrodo-labelled CDM (golden) for 6hr in presence of DMSO, and three concentrations (2μM, 10μM and 50μM) of SB203580, SB202190, FR180204 and PD98059. Inhibitors were added 2h after cell seeding. Cells were stained with 1μg/ml hoechst (blue, high intensity is white) and imaged live. 40X water-immersion objective Opera Phenix microscope was used for imaging. Scale bar, 20μm (A). Cell data analysis was performed with Columbus software. Values represented are cell data (dots) and well data (bigger squares) + SD from three independent experiments; well data was used for the statistical test; *** $p < 0.0007$, **** $p < 0.0001$; Kruskal-Wallis test (B). Image made using items from Servier medical Art.

Data from our lab indicate that $\alpha 2\beta 1$ is trafficked together with endocytosed ECM in MDA-MB-231 cells (Rainero, unpublished). In addition, $\alpha 2\beta 1$ integrin has been shown to induce p38 activation on 3D collagen I matrices (Ivaska *et al.*, 1999). We thus hypothesised that in MDA-MB-231 cells, $\alpha 2\beta 1$ integrin may lead to p38 activation, which results in ECM- $\alpha 2\beta 1$ internalisation. Similar to prior experiments, MDA-MB-231 cells were serum starved overnight to block MAPK signalling. However, cells were seeded on 5% FBS to validate that p38 inhibition decreased collagen I uptake also in the presence of serum. Moreover, collagen I was labelled using a non-pH sensitive dye, NHS-Alexa fluor 555, to confirm that the observed effect was not due to changes in pH. Based on previous modulation of ECM uptake, two different concentrations (10 μ M and 50 μ M) of SB203580 and SB202190 were selected. MDA-MB-231 cells were seeded on collagen I matrices in the presence of DMSO and the two concentrations of SB203580 and SB202190 ([Figure 6-17](#)). Preliminary data indicated that p38 MAPK inhibition significantly affected collagen I internalisation, suggesting that the observed effect was not due to changes in pH. Moreover, we assessed whether $\alpha 2$ -integrin internal pool was also reduced upon p38 inhibition. Indeed, 10 μ M and 50 μ M SB203580 and SB202190 statistically significantly reduced the internal pool of $\alpha 2$ -integrin ([Figure 6-17](#)). This preliminary data suggests that p38 may promote internalisation of ligand-bound $\alpha 2\beta 1$ integrin. Integrin signalling modulates cell morphology (Boudreau and Jones, 1999). To characterise whether p38 inhibition had an effect on cell morphology, the cellular aspect ratio was calculated. 50 μ M SB202190 resulted in a slight, but significant, increase in the cellular aspect ratio, suggesting that cells might be slightly more elongated in the presence of p38 inhibition.

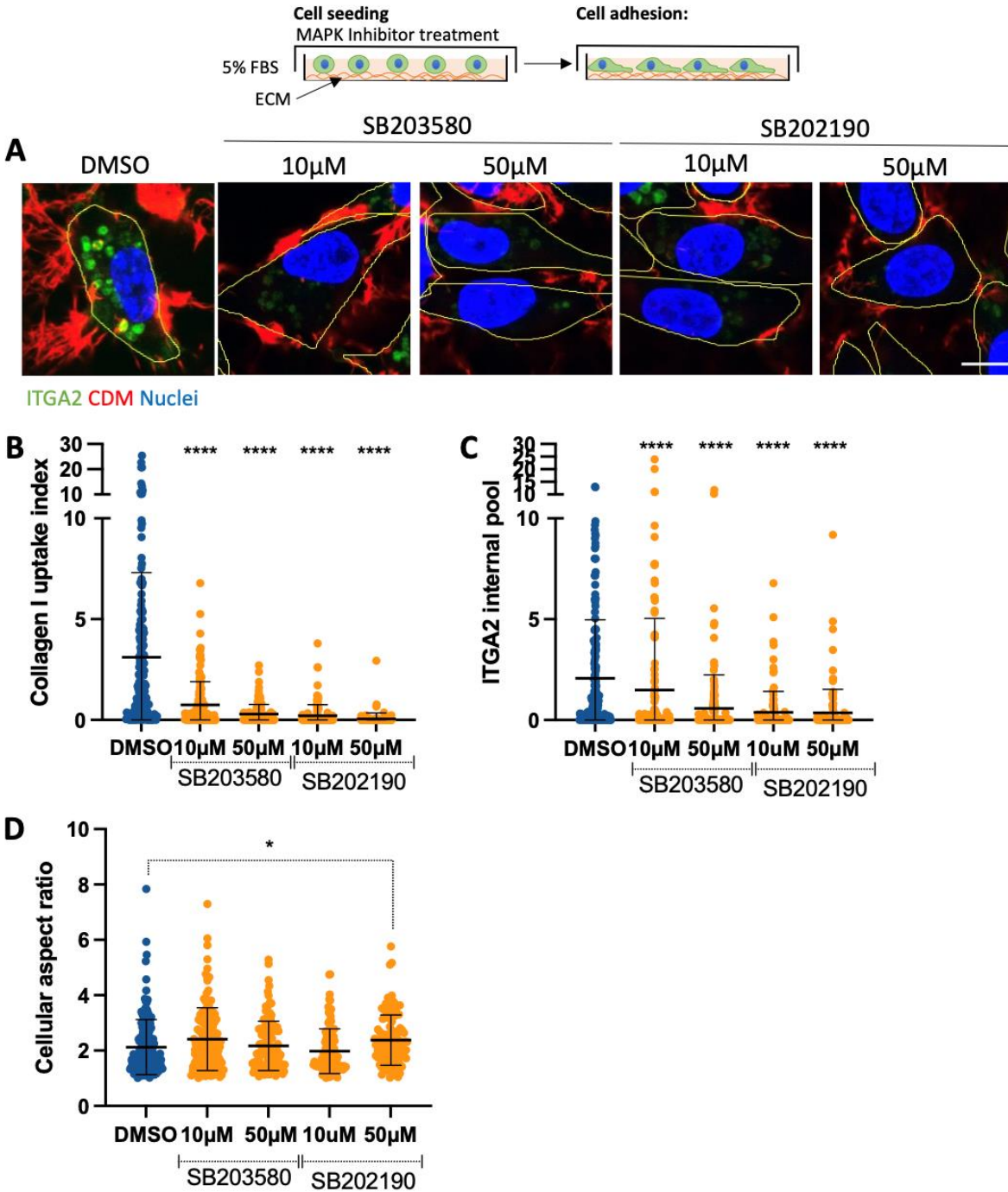


Figure 6-17. p38 MAPK inhibition on reduced collagen I internalisation. MDA-MB-231 cells were serum starved for 16 to 18h. 3×10^5 cells were cultured on 1mg/ml collagen I, labelled with NHS-Alexa fluor 555 (red), for 6hr in presence of DMSO, and two concentrations (10µM and 50µM) of SB203580 and SB202190 in 5%FBS. Cells were fixed and stained with $\alpha 2$ -integrin (green) and DAPI (blue). 60X oil-immersion objective from Nikon A1 confocal microscope was used for imaging. Scale bar, 10µm. Yellow lines show cell morphology (A). Cell data analysis was performed with ImageJ. (B-D) Values represented are cell data + SD from N=1 experiment; * $p=0.0106$, **** $p<0.0001$; Kruskal-Wallis test.

To confirm that these results were reproducible in complex matrices, we replicated these experiments on CDMs. Similarly, 10 μ M and 50 μ M SB203580 and SB202190 treatment significantly reduced CDM internalisation in MDA-MB-231 cells ([Figure 6-18](#)). Again, the cellular aspect ratio significantly increased upon p38 MAPK inhibition, suggesting that cells were elongated. To assess whether these results were specific to invasive breast cancer cells, we studied how 10 μ M and 50 μ M SB202190 treatment affected CDM uptake in the endometrioid ovarian cancer cell line A2780-Rab25 cells, which has been reported to endocytose fibronectin (Rainero *et al.*, 2015). Similar to MDA-MB-231 cells, preliminary data indicated that p38 inhibition significantly decreased CDM uptake index in A2780-Rab25 cells, however the cellular aspect ratio significantly decreased upon treatment ([Figure 6-18](#)). Altogether, these results suggest that p38 promotes ECM endocytosis in the invasive breast cancer cell line MDA-MB-231 and the ovarian cancer cell line A2780-Rab25, which may indicate that p38-mediated ECM internalisation is not specific for breast cancer.

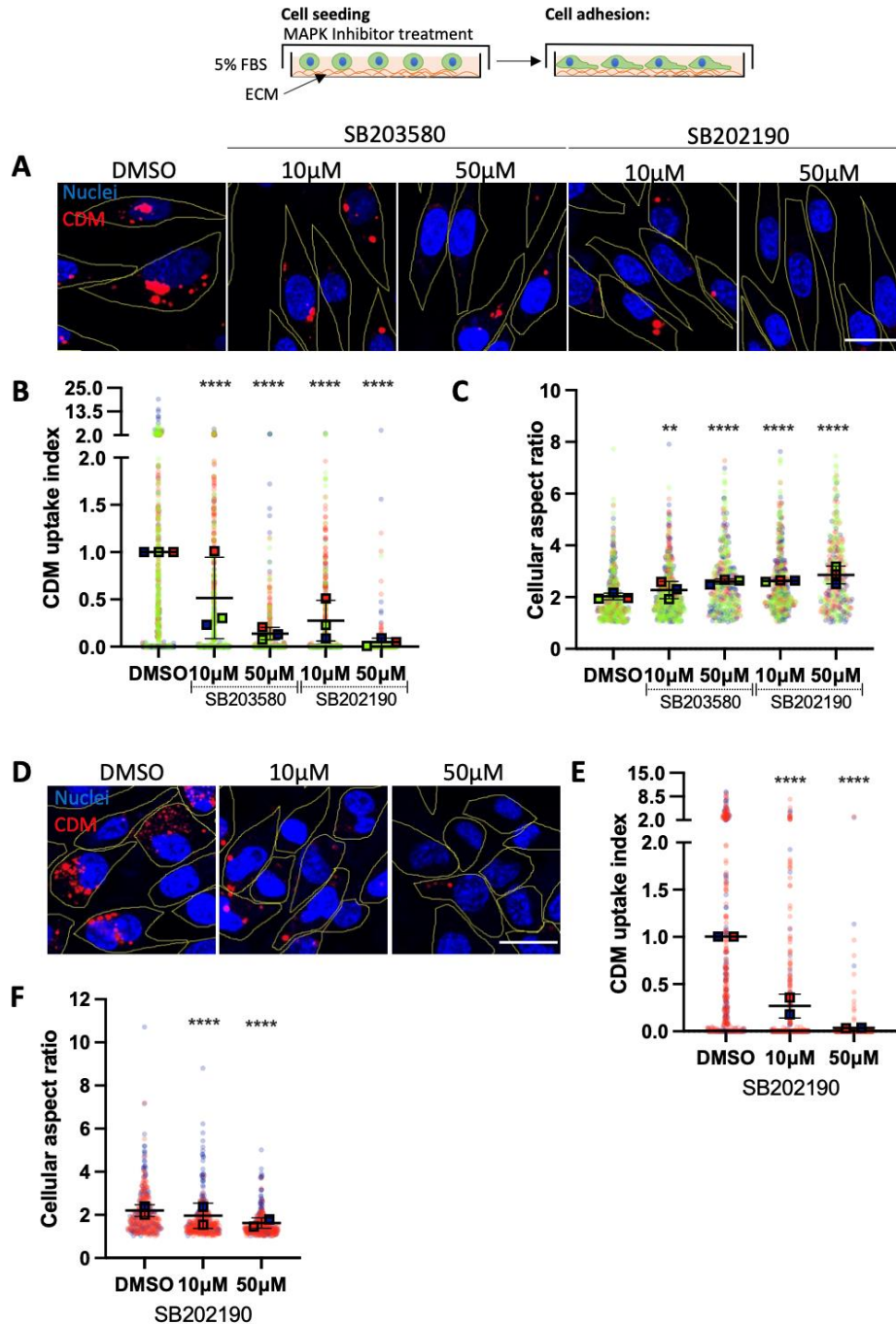


Figure 6-18. Effect of p38 MAPK inhibition on TIF-CDM internalisation. MDA-MB-231 (A-C) and A2780-Rab25 (D-F) cells were serum starved for 16 to 18h. 3×10^5 cells were cultured on TIF-CDM, labelled with pHrodo (red), for 6hr in presence of DMSO, and two concentrations (10 μ M and 50 μ M) of SB203580 and SB202190 in 5%FBS for MDA-MB-231 cells. A2780-Rab25 were treated with 10 μ M and 50 μ M SB202190. Cells were stained with 1 μ g/ml hoechst (blue) and image live with a 60X oil-immersion objective from Nikon A1 confocal microscope was used for imaging. Scale bar, 22 μ m. Yellow lines show cell morphology (A,D). Cell data analysis was performed with ImageJ. Values represented are cell data (dots) and mean data (squares) + SD from N=3 experiment for MDA-MB-231 (B-C) and N=2 for A2780-Rab25 (E-F); cell data was used for statistical test; **p=0.0026, ****p<0.0001; Kruskal-Wallis test.

6.2.6. p38 is required for macropinocytosis of dextran

Macropinocytosis is regarded as a non-specific endocytic mechanism, characterised by internalisation of extracellular fluid and solutes contained in it (Palm, 2019). We thus aimed to discern whether p38 MAPK is a specific regulator of ECM macropinocytosis or a general macropinocytosis regulator. ECM internalisation is upregulated in invasive breast cancer cells ([Chapter 4](#) and Rainero, unpublished). Therefore, we aimed to see whether the effect observed was specific to cancer cells. In the previous section, 50 μ M SB202190 showed the highest modulation of matrigel, collagen I and TIF-CDM uptake. We hence tested the effect of 50 μ M SB202190 on the non-transformed mammary epithelial cell line MCF10A, the invasive breast cancer cell line MCF10CA1a and the mesenchymal and metastatic breast cancer cell line MDA-MB-231. Interestingly, preliminary data showed that p38 inhibition led to a 50% reduction in dextran uptake index in the 3 different cell lines tested, suggesting a general effect on macropinocytosis ([Figure 6-19](#)). Furthermore, the modulation was similar across cell lines indicating that the effects were not cancer-specific. These experiments were performed on 0.1mg/ml collagen I, integrin engagement to the ECM triggers integrin endocytosis. Mesenchymal cells, such as MDA-MB-231 cells, internalise high levels of active β 1-integrin. Dextran partially co-localised with internalised β 1-integrin in MDA-MB-231 cells, suggesting that partial permeabilization of MDA-MB-231 cells during fixation may cause a reduction of dextran uptake index. Ras-induced transformation in cancer promotes macropinocytosis of extracellular molecules (Zwartkuis and Burgering, 2013). In agreement with this, MCF10CA1a, which are H-Ras transformed (Kadota *et al.*, 2010), internalised higher levels of dextran compared to MCF10A. K-Ras mutations similarly promote macropinocytosis (Kadota *et al.*, 2010). MDA-MB-231 cells are K-Ras mutant, however dextran uptake was lower compared to MCF10CA1 cells. Altogether, this data suggests that p38 MAPK might be required for endocytosis of dextran in non-transformed mammary epithelial cells and breast cancer cells.

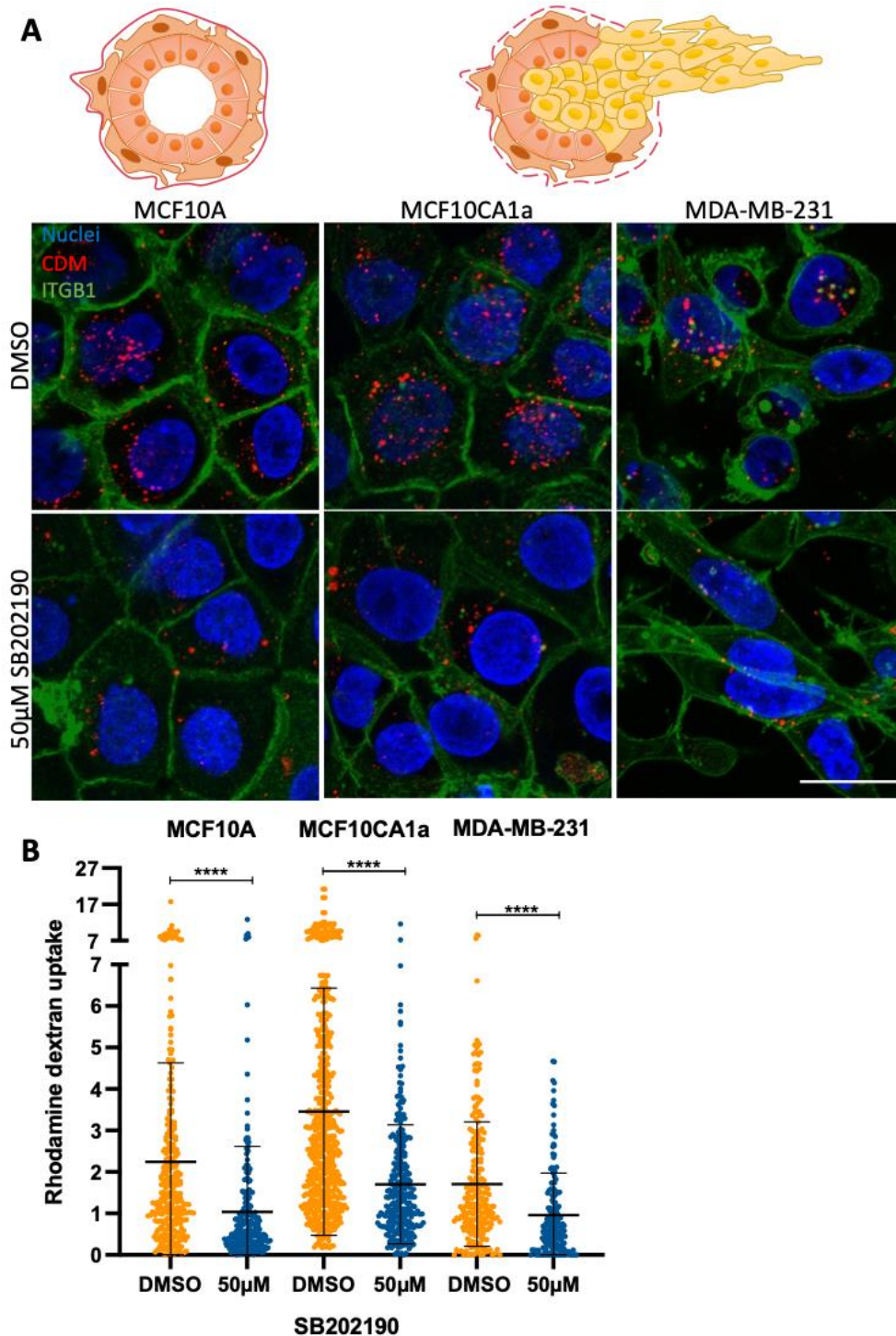


Figure 6-19. SB202190 blocks Rhodamine-dextran internalisation in MDA-MB-231 cells. 3×10^5 MCF10A, MCF10CA1 and MDA-MB-231 cells were seeded on 35mm glass-bottom dishes coated with 0.1mg/ml collagen I for 6h. Cells were then pre-treated with DMSO (vehicle) and 50µM SB202190 for 30 minutes. Following pre-treatment, cells were incubated in the presence of 0.2mg/ml Rhodamine-dextran (red) for another 60 minutes. Cells were then fixed and stained with an antibody against active $\beta 1$ -integrin (green) and the nuclei (blue). Cell imaging was carried out with a 60x objective Nikon A1 confocal microscope (A). Image J was used to analyse the dextran uptake index. Scale bar, 22µm. The scatter plot shows the cell-level data and mean values \pm SD from N=1 independent experiments; **** $p < 0.0001$; One-way ANOVA (B).

6.2.7. MAP3K1, MAPK11, PPP2R1A and α 2-integrin promote macropinocytosis of ECM

α 2 β 1 is trafficked in ECM-positive endosomes and siRNA downregulation of α 2-integrin (also ITGA2) impairs ECM internalisation in MDA-MB-231 cells (Rainero, unpublished). In addition, we have previously shown in section [6.2.5. p38 MAPK is required for ECM macropinocytosis in MDA-MB-231 cells](#) that pharmacological inhibition of p38 leads to reduced collagen uptake and internal pool of α 2-integrin. We thus aimed to characterise whether MAP3K1, MAPK11 and PPP2R1A knockdown impaired internalisation of collagen I in MDA-MB-231 and A2780-Rab25 cells. In addition, α 2-integrin was knocked down to compare its effect together with the positive regulators obtained in the screen. In MDA-MB-231 cells, preliminary data indicates that siRNA against MAP3K1, MAPK11 and PPP2R1A reduced collagen I and β 1-integrin internal pool ([Figure 6-20](#)). In particular, downregulation of MAP3K1 diminished by 50% collagen I uptake index and α 2-integrin internal pool, while MAPK11 and PPP2R1A reduced α 2-integrin internal pool by 90% and 80% respectively. Similarly, α 2-integrin knockdown significantly reduced collagen I uptake (80%) and β 1- integrin internal pool (50%) ([Figure 6-20](#)). Furthermore, α 2-integrin internal pool signal was abolished by 97%, suggesting that α 2-integrin was effectively knocked down ([Figure 6-20](#)). Altogether, this data suggests that MAP3K1, MAPK11, PPP2R1A and α 2-integrin promote ECM endocytosis in MDA-MB-231 cells. To confirm that the observed effects were not on account of off-target effects, we optimised an alternative methodology, namely clustered regularly interspaced short palindromic repeats interference (CRISPRi), which consists of a deactivated Cas9 nuclease (dCas9) that is fused to two repressor proteins, such as SALL1 and SDS3. The guide RNA (sgRNA) directs the dCas9-SALL1-SDS3 fusion protein to the promoter of a gene of interest, which results in genetic repression of the specific gene. This enables high specificity and reduces off-target effects (CRISPRi, Horizon discovery). Of note, preliminary studies suggested that reducing gene expression of PPP2R1A lead to a small, but significant reduction in matrigel internalisation ([Figure 6-21](#)). This data confirms that CRISPRi may be an alternative methodology to confirm the effect of the positive regulators that were found in the screen.

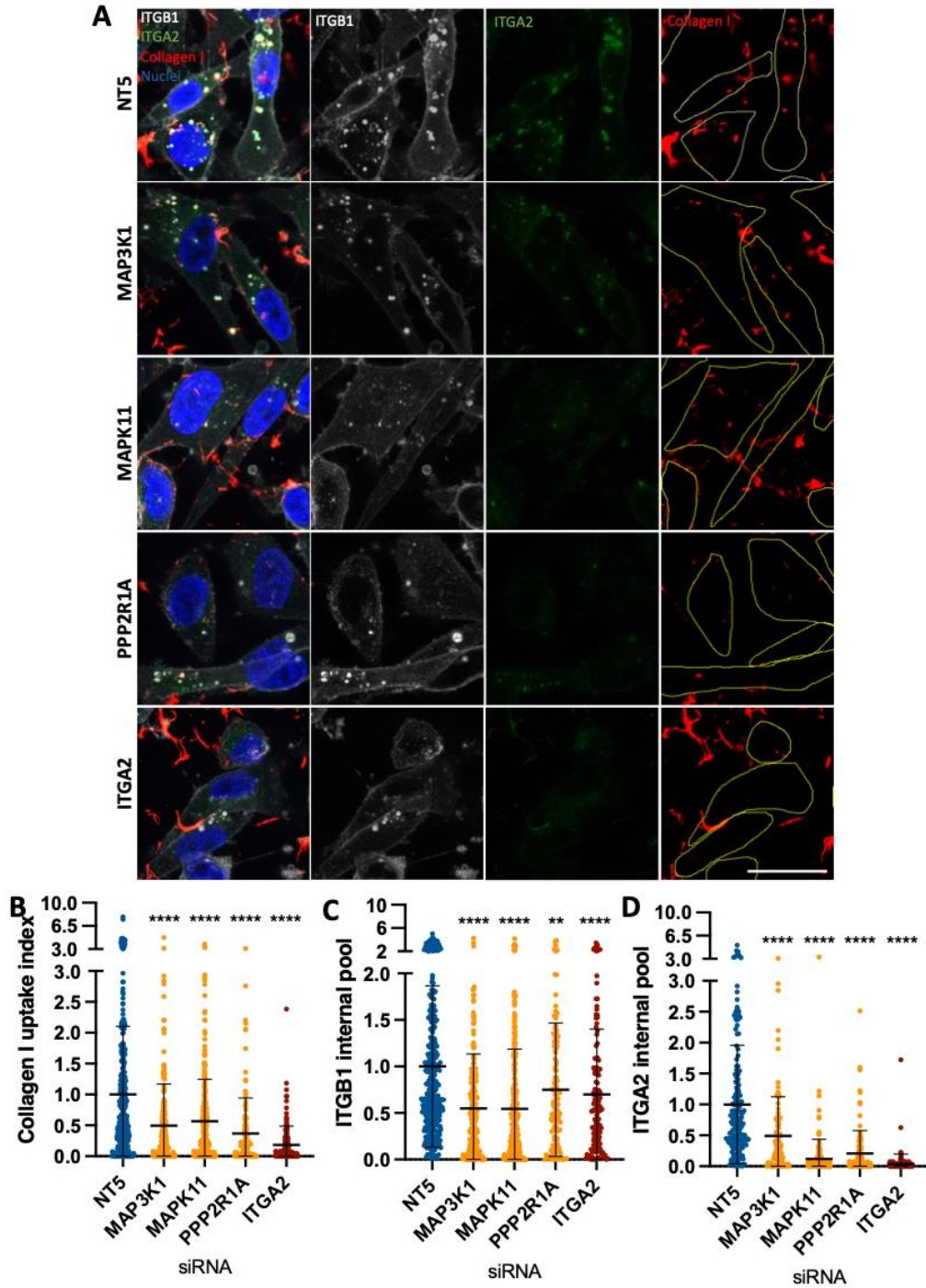


Figure 6-20. MAP3K1, MAPK11, PPP2R1A and α 2-integrin (ITGA2) are required for collagen I internalisation. MDA-MB-231 cells were transfected with the corresponding siRNA. After 3 days, 3×10^5 cells were seeded on 1mg/ml collagen I, labelled with NHS-Alexa fluor 555 (red), for 6 hours. Cells were fixed and stained with β 1-integrin (white), α 2-integrin (green) and DAPI (blue). 60X oil-immersion objective from Nikon A1 confocal microscope was used for imaging. Scale bar, 22 μ m. Yellow lines show cell morphology (A). Cell data analysis was performed with ImageJ. Values represented are cell data + SD from N=2 experiment for MAP3K1, MAPK11 and N=1 experiment for PPP2R1A and α 2-integrin; ** $p=0.0056$, *** $p<0.0001$; Kruskal-Wallis test (B-D).

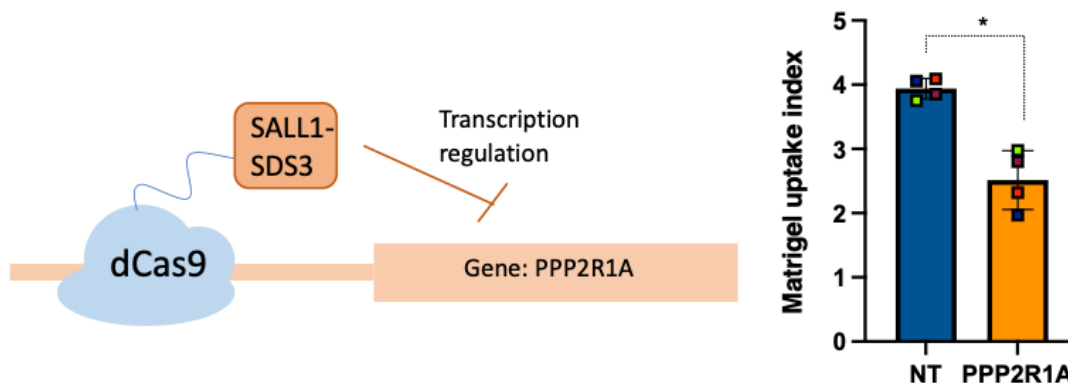


Figure 6-21. sgRNA against PPP2R1A reduced matrigel uptake index in MDA-MB-231 cells. 3000 MDA-MB-231 cells were transfected as per protocol. Following 72h, cells were transferred in an automated way into pH-rodo labelled 0.5mg/ml matrigel and incubated for 6h. Cells were labelled with 1 μ g/ml hoechst for nuclear staining. Cell imaging was carried out using a 40X objective in the Opera phenix microscope. Columbus software was used for image analysis. Well data values (squares) \pm SD from 4 technical replicates; * $p= 0.0286$; Mann-Whitney test.

To study whether these results were specific to breast cancer cells, we assessed how MAP3K1, MAPK11, PPP2R1A and α 2-integrin affected collagen I internalisation in A2780-Rab25 cells. Preliminary results show that MAP3K1 knockdown reduced collagen I internalisation by 70% and, in addition, it reduced by 95% the internal pool of β 1-integrin ([Figure 6-22](#)). MAPK11 and PPP2R1A impaired collagen I uptake index by 50%, while β 1-integrin internal pool was significantly diminished by 75% and 40%, respectively ([Figure 6-22](#)). Similar to MDA-MB-231 cells, downregulation of α 2-integrin resulted in a significant decrease (90%) in collagen I uptake and it reduced by 50% the internal pool of β 1-integrin ([Figure 6-22](#)). Altogether these results indicate that MAP3K1, MAPK11, PPP2R1A and α 2-integrin regulate ECM internalisation in A2780-Rab25 and MDA-MB-231 cells.

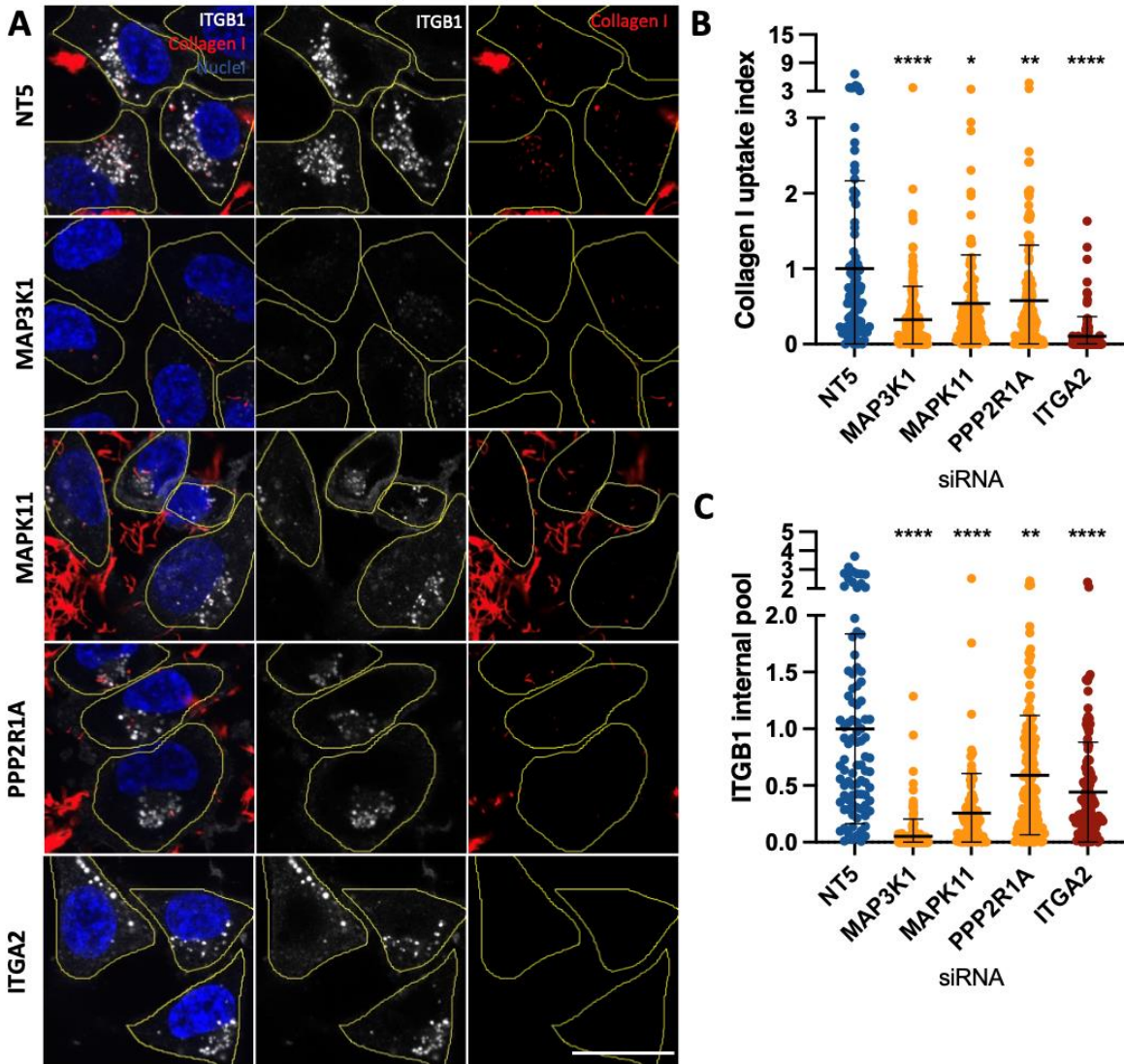
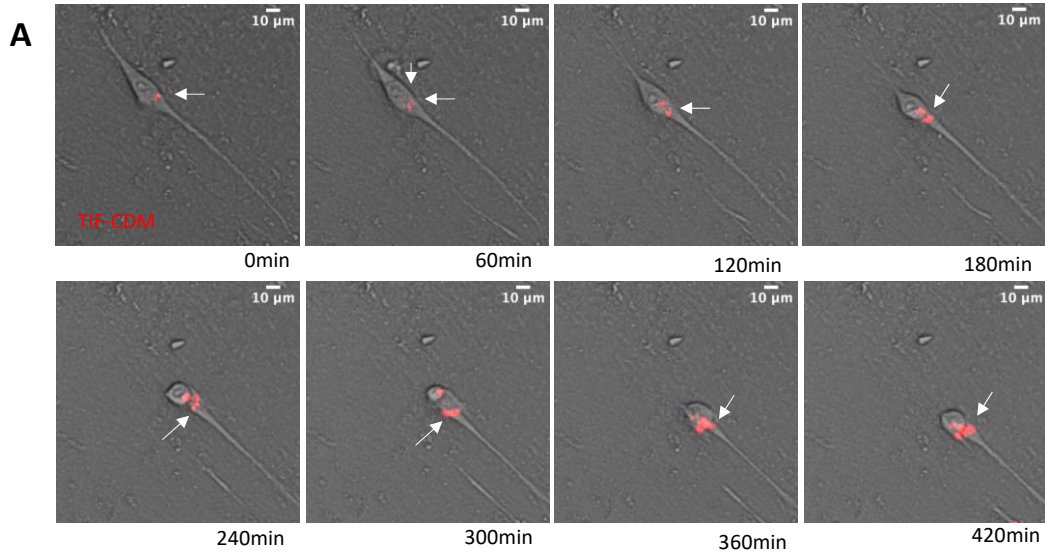


Figure 6-22. MAP3K1, MAPK11, PPP2R1A and α 2-integrin (ITGA2) are required for collagen I internalisation. A2780-Rab25 cells were transfected with the corresponding siRNA. After 3 days, 3×10^5 cells were seeded on 1mg/ml collagen I, labelled with NHS-Alexa fluor 555 (red), for 6 hours. Cells were fixed and stained with β 1-integrin (white) and DAPI (blue). 60X oil-immersion objective from Nikon A1 confocal microscope was used for imaging. Scale bar, 22 μ m. Yellow lines show cell morphology (A). Cell data analysis was performed with ImageJ. Values represented are cell data + SD from N=1 experiment; * $p=0.0365$, ** $p \leq 0.0027$, **** $p < 0.0001$; Kruskal-Wallis test (B-C).

6.2.8. Inhibition of p38 MAPK impairs migration of MDA-MB-231 cells

Internalisation of ligand-occupied $\alpha 5\beta 1$ integrin is required for invasive migration in A2780-Rab25 cells (Rainero *et al.*, 2015). In addition, $\alpha 2\beta 1$ integrin has been shown to be required in melanoma cell migration (Etoh *et al.*, 1993). ECM internalisation is upregulated in invasive and metastatic breast cancer cells, suggesting that it may confer an advantage during invasion and metastatic dissemination. To characterise whether MDA-MB-231 cells internalise ECM during cell migration, CDMs were labelled with the pH sensitive dye, pHrodo and cell imaging was performed every 10 minutes. Time-lapse visualisation indicated that MDA-MB-231 cells were able to internalise CDM as they migrated through ([Figure 6-23A](#)). To assess whether ECM internalisation contributed to cell migration, we inhibited ECM-bound $\alpha 2\beta 1$ internalisation in MDA-MB-231 cells using p38 MAPK inhibitors and an inhibitor of $\alpha 2$ -integrin, BTT-3033. Preliminary data indicated that 10 μ M and 50 μ M SB203580 and SB202190 significantly reduced the velocity of MDA-MB-231 cells migrating on CDMs ([Figure 6-23](#)), while only 50 μ M SB203580 and SB202190 significantly affected directionality of migrating cells. Similarly, inhibition of $\alpha 2$ -integrin using the inhibitor BTT-3033 impaired velocity and directionality of MDA-MB-231 cells ([Figure 6-23](#)). Altogether, this data indicates that there is a correlation between the regulators of ECM internalisation and cell migration in MDA-MB-231 cells, which may suggest that ECM internalisation may facilitate cell migration on CDMs.



QR code link:
MDA-MB-231 cells
internalising CDM (red)

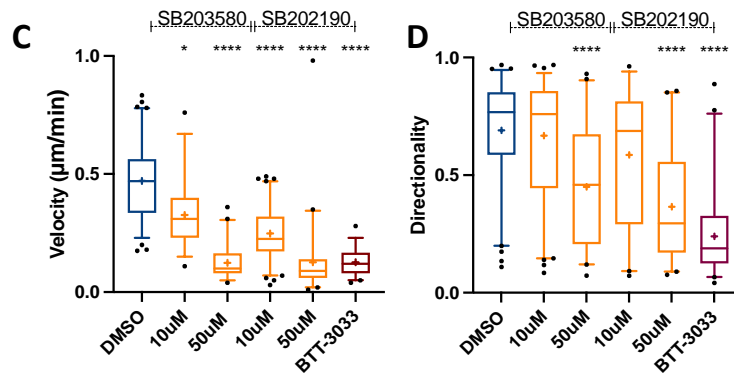
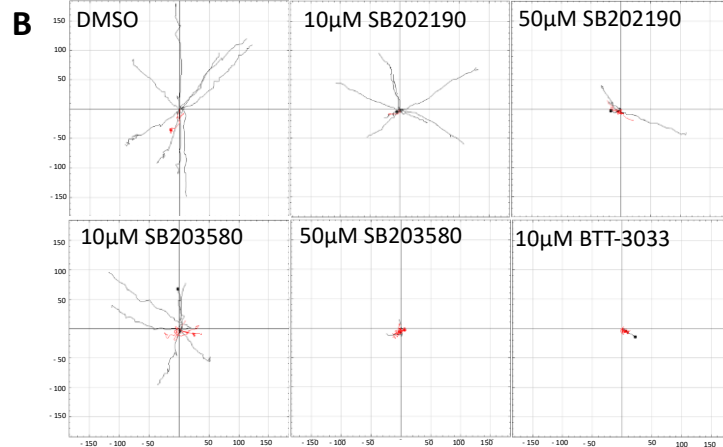


Figure 6-23. p38 inhibition reduces velocity and directionality in MDA-MB-231 cells migrating on CDMs. TIF-CDMs were generated as per protocol. 5×10^4 MDA-MB-231 cells were seeded per well in a 12-well plate. (A) Representative images of MDA-MB-231 cells migrating and internalising CDM (see QR code for a video; DOI: 10.15131/shef.data.23553003). (B) For inhibitor treatment, cells were cultured for 6hr in presence of DMSO, 10 μM and 50 μM SB203580 and SB202190. MDA-MB-231 cells were allowed to adhere for 4 hours before adding 10 μM BTT-3033. After this time, cells were imaged with a 10X Nikon dual cam white field microscope for a period of 7h. (B) Spider plots show the migration paths of manually tracked cells (directionality > 0.5 in black, directionality < 0.5 in red). (C) Average velocity ($\mu\text{m}/\text{min}$). (D) Directionality. $N = 1$ independent experiments. Box and whisker plots represent 5-95 percentile, + represents the mean, dots are $< 5\%$ and $> 95\%$; * $p = 0.0153$, **** $p < 0.0001$; Kruskal Wallis test.

To confirm the findings observed with pharmacological inhibition of p38, MAP3K1 and MAPK11 were downregulated by siRNA. In agreement with the observed results upon treatment with SB203580 and SB202190, preliminary data showed that MAP3K1 and MAPK11 knockdown significantly reduced velocity and directionality of MDA-MB-231 cells migrating on CDM (Figure 6-24). Taken together, this data suggests that MAP3K1 and MAPK11, positive regulators of ECM uptake, may be required for directional cell migration on CDM.

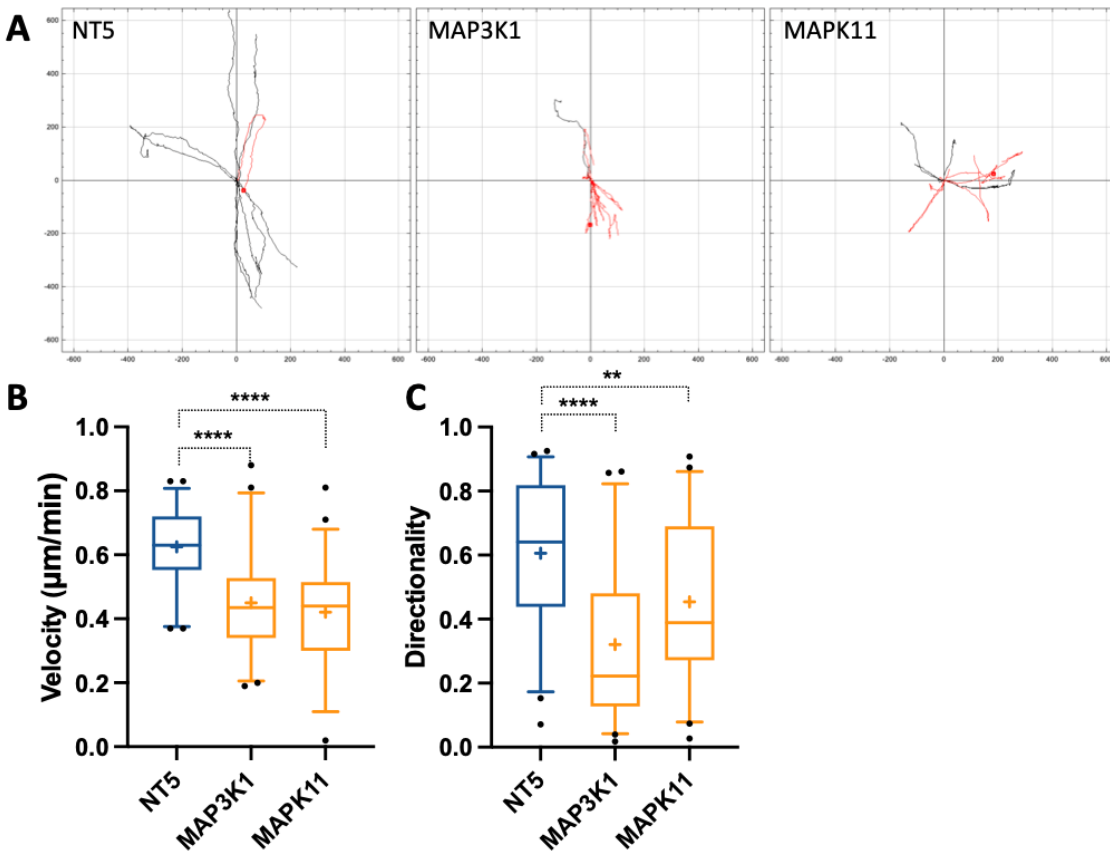


Figure 6-24. siRNA downregulation of MAP3K1 and MAPK11 reduces velocity and directionality in MDA-MB-231 cells migrating on CDMs. TIF-CDMs were generated as per protocol. MDA-MB-231 cells were transfected and after 72h, 5×10^4 MDA-MB-231 cells were seeded per well in a 12-well plate. Knockdown cells were cultured for 6hr before imaging with a 10X Nikon dual cam whitefield microscope for a period of 7h, images were taken every 10 minutes. (A) Spider plots show the migration paths of manually tracked cells (directionality >0.5 in black, directionality <0.5 in red). (B) Average velocity ($\mu\text{m}/\text{min}$). (C) Directionality. $N=1$ independent experiments. Box and whisker plots represent 5-95 percentile, + represents the mean, dots are <5% and >95%; ** $p=0.0094$, **** $p<0.0001$; Kruskal Wallis test.

6.3. DISCUSSION

Integrins signalling has mainly been associated with Src , FAK and EGFR activation, resulting in cell adhesion, proliferation and migration (Bill *et al.*, 2004; Shattil, 2005; Guan, 2010). Notwithstanding this, the signalling regulators downstream integrin engagement to the ECM that promote its internalisation have remained unexplored. In this chapter, we used a high content imaging approach to identify regulators of ECM endocytosis ([Figure 6-1](#)). To further narrow down hit selection, we assessed changes in nuclei count. In high content screenings, nuclei count enables the assessment of cell toxicity mediated by siRNA knockdown. No significant differences were observed, except for COPB2 knockdown. However, owing to the nature of the screen and the need to detach and transfer cells in a semi-automated manner, cell numbers displayed high levels of variability as observed for the cell count for the controls (NT4, NT5, ITGB1 and PAK1) in [Table S1-7](#). Therefore, assessing cell number is not a reliable analysis to assess cell toxicity in this type of screen. Common hits between the two biological replicates were considered strong hits and selected for future validation. siRNA deconvolution confirmed 18 out of the 45 candidates tested ([Figure 6-5](#)). STRING analysis determined two main gene ontology groups: MAPK signalling cascade and Ephrin receptors. The latter cluster included EphB4 and EphA4, as positive regulators, while EphB2 was categorised into negative regulators. In agreement with this, EphB2 receptors negatively regulate integrin activity and promote loss of cell-ECM adhesion (Zou *et al.*, 1999). It could thus be that its role in impeding integrin activity and cell-ECM contact sites negatively influences ECM internalisation. 1 μ M NVP-BHG712, a highly specific pharmacological inhibitor of EphB4, significantly reduced collagen I and CDM internalisation. Matrigel internalisation showed a small, but not significant, decrease (20% to 30%) in presence of 5nM and 1 μ M NVP-BHG712. However, no effect was observed at 10nM and 50nM. Considering the strong Ephrin receptor cluster in the screen with pro- and anti-internalisation effects, the discrepancies observed between the different matrices may be due to their distinct composition. EphB4 may regulate collagen internalisation since its inhibition results in a significant reduction of collagen I and CDM, which is highly enriched in collagen I (Fitzpatrick and McDevitt, 2015). Collagen IV accounts for 30% of matrigel composition (Matrigel, Corning, Certificate of analysis). Taking into consideration this, the small, but not significant, reduction in the matrigel uptake

index may be through EphB4 signalling in regulating collagen IV endocytosis. However, we could not discard that NVP-BHG712 may have off-target effects on other Ephrin receptors. Despite, 1 μ M NVP-BHG712 has been extensively used for studying EphB4 (Martiny-Baron *et al.*, 2010; Su *et al.*, 2021), another study showed that NVP-BHG712 has high affinity for the majority of Ephrin receptors, ranging from EphA3 (0.3nM) and EphA1 (303nM) (Tröster *et al.*, 2018). It could thus be that the simultaneous inhibitory role on a wide range of Ephrin receptors may lead to discrepancies between concentrations. EphA4 is regarded as a promiscuous Ephrin receptor. EphA4 undergoes conformational changes, which resemble class A Ephrin receptors, in the presence of its ligand EFNA2 (Bowden *et al.*, 2009). However, EphA4 can additionally bind to EFNB2 promoting a conformational change closer to class B Ephrin receptors (Bowden *et al.*, 2009). We tested two different ligands EFNB1, which binds to EphB2, and EFNB2 that classically binds to EphB2 and EphB4 (Wu *et al.*, 2012; M. Zhu *et al.*, 2020). Addition of EFNB1 and EFNB2 to the media had no significant effect on ECM uptake index ([Figure 6-6](#), [6-7](#), [6-8](#)). This data suggests that EphB4 regulates ECM internalisation independently of EFNB2. Other reports have otherwise suggested that high ligand concentrations may act as a competitive inhibitor with the endogenous ligands expressed by cancer cells (Bossart *et al.*, 2008). In addition, it has also been suggested that Ephrin ligands from different sources may display different activity, which may determine the effective concentration needed (Zheng *et al.*, 2017).

On account of the pH sensitive nature of the assay, we cannot discern whether the EphB4 may regulate collagen internalisation or collagen trafficking towards acidic compartments, such as lysosomes. While no studies shed light into the role of EFN-EPH signalling in lysosomal traffic or organelle organisation, EFN-EPH signalling is known to regulate cell migration during development and in axonal guidance (Santiago and Erickson, 2002; Xu and Henkemeyer, 2012). Integrin traffic has been extensively studied in the context of cell migration; in addition, the ECM provides specific integrin binding sites that regulate axonal outgrowth (Myers, Santiago-Medina and Gomez, 2011). Some studies have investigated the cross-talk between integrins and Ephrin signalling. In T lymphocytes, forward EphA and EFNA promote integrin-mediated adhesion (Sharfe *et al.*, 2008). Similarly, EFNA1 promotes migration in CD4⁺ lymphocytes by inducing changes in EphA1 and PYK2 phosphorylation (Aasheim, Delabie and Finne, 2005), while EphA2-

EFNA1 signalling was reported to suppress integrin function and dephosphorylate FAK (Miao *et al.*, 2000). EFNB1 has been shown to induce membrane ruffling and promote assembly of focal adhesions (Nagashima *et al.*, 2002). Moreover, EphB1-EFNB1 positively regulates cell attachment through $\alpha\beta3$ (vitronectin) and $\alpha5\beta1$ (fibronectin) activation (Huynh-Do *et al.*, 1999). Matrigel contains traces of fibronectin (Matrigel, Corning, Certificate of analysis), while both fibronectin and vitronectin are secreted and deposited by fibroblasts during CDM generation (Fitzpatrick and McDevitt, 2015). It may be possible that the observed effect is partially mediated by controlling fibronectin and vitronectin traffic as a result of $\alpha\beta3$ and $\alpha5\beta1$ activation. In addition, given the role of Eph-EFN in cell migration we assess whether EphB4 inhibition affected cell migration. Preliminary data suggested that 1 μ M NVP-BHG712 reduced directional migration and velocity in MDA-MB-231 cells ([Figure 6-9](#)). Although the effects observed upon NVP-BHG712 treatment may be due to the known role of ephrins in controlling cell migration, this data indicates that there may be a correlation between regulators of ECM internalisation and migration in invasive breast cancer cells, such as MDA-MB-231 cells. Taking everything into account, the quantification results suggest that EFNB1 and EFNB2 do not mediate ECM internalisation through Eph signalling. Nevertheless, this assay cannot discern whether the observed effect was due to changes in intracellular trafficking to lysosomes, rather than endocytosis.

In addition to Ephrin receptors, BLNK, DGKE, MAP3K1 and PPP2R1A were found among the top positive regulators in both kinome and phosphatome replicates. DGKE is the only isoform among diacylglycerol kinases that specifically phosphorylates a specific diacylglycerol, stearyl-2-arachidonyl glycerol (Epanand *et al.*, 2016). In addition, it has a predicted transmembrane helix domain, making it the only diacylglycerol kinase that is bound to membranes (Decaffmeyer *et al.*, 2008). It is found at the PM and endoplasmic reticulum (Kobayashi *et al.*, 2007; Epanand *et al.*, 2016). Interestingly, a previous high throughput screening found Sec22A as a regulator of matrigel internalisation ([Chapter 5](#)). Sec22A is tether protein that has been shown to regulate endoplasmic reticulum to PM contact sites (C. Li *et al.*, 2021), while Sec22B has been reported to negatively regulate endoplasmic reticulum-mediated phagocytosis (Hatsuzawa *et al.*, 2009). This suggested that endoplasmic reticulum contact sites may be required during ECM macropinocytosis. Indeed, phosphatidic acid is required for constitutive ruffling and

macropinocytosis in phagocytes (Bohdanowicz *et al.*, 2013). It could thus be that DGKE activity in endoplasmic reticulum-PM contact sites promotes changes in the lipid composition of the PM, membrane ruffling and subsequent macropinocytosis. In fact, a recent preprint study has shown that the endoplasmic reticulum - PM contact sites, in particular on FAs, mediated by the tether protein VAPA regulate FA maturation and turnover (Siegfried *et al.*, 2022). One could hypothesise that these endoplasmic reticulum contact sites at FA may facilitate macropinocytosis of ECM.

BLNK is predominantly expressed in macrophages and B cells (Pathmanathan *et al.*, 2022). BLNK has mainly been studied in the context of B cell activation (Lagresle-Peyrou *et al.*, 2014). Interestingly, epithelial cells show low expression levels of BLNK, however TNMplot analysis showed that BLNK expression is upregulated in certain tumours, including breast, renal, pancreatic, prostate and lung carcinomas (Bartha and Gyórfy, 2021). This may suggest that BLNK expression in those carcinomas may confer an advantage for tumour development. Integrin endoathesome signalling has been shown to suppress anoikis (Alanko *et al.*, 2015). We could hypothesise that in breast cancer, BLNK-mediated ECM internalisation may similarly block anoikis. However, a recent study has shown that BLNK expression is downregulated in MCF10A cells overexpressing HER2 (Liu *et al.*, 2022). In these cells, HER2-induced downregulation of BLNK blocks apoptosis and anoikis by inactivating p38, a downstream effector of BLNK (Liu *et al.*, 2022). The authors of this study did not address whether BLNK expression has a similar effect on other cancer subtypes, it could thus be that BLNK has distinct roles in HER2-positive breast cancer and TNBC subtypes, namely MDA-MB-231 cells. Future work will characterise how BLNK affects ECM internalisation in MDA-MB-231 cells and discern its apoptotic role in TNBC. It may be possible that BLNK-mediated activation of a specific p38 isoform results in distinct outcomes.

Our data suggests that p38, more specifically MAPK11/p38 β ([Figure 6-10](#)), may regulate ECM macropinocytosis in cancer. To better characterise the contribution of p38 in this process, we took advantage of specific inhibitors targeting well known regulators of MAPK signalling pathways, including p38 α/β , ERK1/2 and MEK1/2. Pharmacological inhibition of p38 using 10 μ M and 50 μ M SB203580 and SB202190 seem to reduce ECM internalisation in a dose-dependent manner in MDA-MB-231 cells ([Figure 6-11](#), [6-12](#), [6-13](#)). Nevertheless, addition of the inhibitors 2h after cell seeding, once cells adhered, did not result in the same level of ECM uptake

modulation. This suggested that cells *sensed* the ECM upon adhesion and triggered p38-dependent ECM internalisation. In addition to integrins, other receptors could mediate adhesion-dependent signalling, including the DDR family. No significant effect of DDR1 downregulation was observed on matrigel internalisation in the kinome and phosphatome screen, while DDR2 knockdown increased matrigel uptake by 30% in both replicates. This suggested that DDRs are not responsible for ECM internalisation in MDA-MB-231 cells. Our lab has shown that $\alpha 2\beta 1$ integrin mediates matrigel, collagen and CDM internalisation in MDA-MB-231 cells (Rainero, unpublished). In pancreatic cancer, $\alpha 2$ -integrin expression correlates with poor overall survival and resistance to gemcitabine in high stiffness matrices (Gregori *et al.*, 2023). In addition, 3D collagen I has been shown to lead to p38 activation in mesenchymal cells, such as fibroblasts (Ivaska *et al.*, 1999). We thus hypothesised that p38 activation downstream of $\alpha 2\beta 1$ integrin promotes ECM internalisation in breast cancer. Surprisingly, despite no effect on matrigel uptake upon siRNA-mediated knockdown of ERK1/2 in the kinome and phosphatome screen ([Figure 6-10](#)), ERK1/2 inhibition slightly, but significantly, reduced matrigel uptake. In addition, the effect appeared more pronounced in collagen I and CDM. This data may have suggested that ERK1/2 may additionally regulate ECM internalisation, specifically of collagen I and complex matrices, such as CDMs. However, high FR180204 concentrations have been shown to inhibit p38 isoforms (FR180204 (CAS 865362-74-9), no date).

Interestingly, p38 inhibition at cell seeding seemed to have a stronger effect on CDM uptake, compared to collagen I and matrigel. This data may suggest that p38 may have a more prominent role in regulating ECM internalisation of highly aligned collagen I and fibronectin matrices. In addition, preliminary studies showed that p38 inhibition reduced dextran uptake in MDA-MB-231 cells ([Figure 6-19](#)). While PAK1-mediated macropinocytosis regulates matrigel internalisation, this is also highly reduced upon CAV1/2 knockdown, suggesting that macropinocytosis is not the only pathway driving matrigel uptake in MDA-MB-231 cells (see [Chapter 3](#) for a more detailed discussion). Taking this into consideration, a possibly reasonable explanation could be that p38 more prominently regulates macropinocytosis of *in vivo-like* collagen I. This would result in a stronger effect on internalisation of CDMs compared to matrigel and disorganised collagen fibres, such as the ones found in collagen I preparations. While $\alpha 2\beta 1$

integrin is a laminin and collagen receptor (Languino *et al.*, 1989; Staatz *et al.*, 1990), it may be possible that $\alpha 2\beta 1$ integrin preferentially bind to fibrillar and aligned collagens to effectively trigger downstream signalling pathways, such as p38. In agreement with the effect of p38 inhibition on CDM uptake, preliminary quantification of the cellular aspect ratio indicates that MDA-MB-231 cells were more elongated on CDMs compared to collagen I matrices. However, A2780-Rab25 were shorter upon treatment with SB202190. In agreement with this, preliminary studies using live cell imaging suggest that MDA-MB-231 cells treated with p38 inhibitors highly align with the collagen fibres and spread/elongate along that axis, leading to more elongated cells. Time-lapse visualisation indicates that following elongation, cells rapidly retract one of the cell protrusions, which may enable cells to move (*migrate*) forward. This results in a combination of long and short cells, which may be difficult to quantify in fixed cells. More detailed examination of time-lapse migration movies may allow a better characterization of the role of p38 MAPK in controlling cell morphology during cell migration. Moreover, preliminary time-lapse visualisation suggests that MDA-MB-231 cells are able to internalise CDM while migrating. This differs for other studies that have shown that blocking macropinocytosis increases cell surface expression of integrins and promotes cell migration (Le *et al.*, 2021). Notwithstanding that, it is not clear whether MDA-MB-231 cells internalise ECM as they are migrating or rather ECM internalisation facilitates cell migration in 3D complex environments. This prompted us to assess whether p38-mediated ECM internalisation would affect migration of invasive breast cancer cells on CDMs. In fact, preliminary data showed that 10 μ M SB203580 and SB202190 significantly reduced the average speed/velocity of cell migration, while higher concentrations of these inhibitors (50 μ M) led to a significant effect on cell velocity and directionality of migrating cells. This suggests that at least there is a correlation between ECM internalisation and cell migration. To further investigate this correlation, we knockdown MAP3K1, which was validated as a positive regulator of matrigel uptake, and MAPK11. MAP3K1 (also known as MEK1) has been reported to lead to activation of p38 and JNK signalling cascades. Literature research of the hits and analysis of the modulation of ERK1/2, p38 isoforms and JNK1/2/3 ([Figure 6-10](#)) suggested that p38, specifically p38 β (MAPK11), may regulate ECM internalisation. We have previously shown that PAK1 modulates macropinocytosis of matrigel, collagen I, TIF- and CAF-CDM ([Chapter 3](#)). Interestingly,

PAK1 has been shown to phosphorylate MAP3K1 on serine 67, which inhibits its binding to JNK kinases (Gallagher *et al.*, 2002). Moreover, PAK1 is recruited to the p38 kinase complex in a phosphorylation-dependent manner (Chan, Lim and Manser, 2008). In this system, PI3K and Cdc42 upstream of PAK1 lead to its activation (Chan, Lim and Manser, 2008). Interestingly, we identified PIK3C2A, the catalytic subunit of class II PI3K, as a positive regulator of matrigel internalisation ([Figure 6-1](#) and [6-3](#)). However, Cdc42 and Rac1 do not seem to affect ECM internalisation in MDA-MB-231 cells (Rainero, unpublished). However, PI3K has been shown to directly activate PAK1 (Papakonstanti and Stournaras, 2002) and data from our lab indicate that PI3K is required for matrigel uptake (Zhe Bao, Rainero lab, unpublished). It could thus be that direct interaction between PI3K and PAK1 promotes activation of the latter and ECM macropinocytosis. We thus hypothesised that active PAK1 in turn promotes MAP3K1 phosphorylation and activation of p38 MAPK pathway ([Figure 6-25](#)).

Protein phosphatases have been commonly studied in the context of negative regulation of MAPK signalling pathways. Interestingly, knocking down the regulatory subunit of PP2A, PPP2R1A, resulted in a decrease in matrigel uptake, which may indicate that it regulates ECM endocytosis. PP2A has been shown to negatively regulate p38 MAPK pathway (L. Zhang *et al.*, 2018). Despite the negative regulation of protein phosphatases, such as PP2A, on MAPK, our results may indicate that protein kinases (MAP3K1 and MAPK11) may cooperate with PPP2R1A and promote ECM internalisation. In fact, PP2A activity downstream of p38 activation has been shown to negatively regulate ERK1/2 in cardiomyocytes. Under these settings p38 leads to a dual activation of apoptosis, as well as, pro-survival signalling via ERK1/2 (Liu and Hofmann, 2004). In fact, p38 activation promotes cell survival in response to DNA damage (Liu and Hofmann, 2004; Phong *et al.*, 2010). Similarly, p38 activation has been shown to upregulate proliferation and migration of MDA-MB-231 cells (Huth *et al.*, 2017). In addition, MEK2-dependent activation of p38 has been shown to promote prosurvival effects on MDA-MB-231 cells (Huth *et al.*, 2016). This may partially explain why 50µM PD98059, which has been shown to inhibit MEK2 (Inhibitor data sheet, MedChem express), leads to a small but significant reduction of collagen I uptake. Altogether this suggests that in addition to promoting apoptosis, p38 also mediates pro-survival events. Interestingly, PP2A is found in integrin adhesion complexes (Chastney *et al.*, 2020). PP2A

has been shown to promote FA maturation and cell migration of the fibrosarcoma cell line HT1080 (Janssens *et al.*, 2016). Moreover, PP2A has been shown to dephosphorylate paxillin (Ito *et al.*, 2000). We thus hypothesised that MAP3K1 activation downstream of $\alpha 2\beta 1$ integrin promotes p38 activation, which subsequently activates PP2A ([Figure 6-25](#)). Taken together, it may be possible that PP2A activity on FA may be required for FA disassembly (or turnover) to enable internalisation of ECM ([Figure 6-25](#)). Nevertheless, a biorxiv study has identified that PPP2R1A associates with ABI1, a subunit of the WAVE complex (Wang *et al.*, 2022). Particularly, PPP2R1A associates with the WAVE shell complex, which contains NHSL1 instead of the subunit WAVE (which constitutes the canonical WAVE regulatory complex) (Wang *et al.*, 2022). PPP2R1A and the WAVE shell complex would regulate actin polymerisation and persistence of cell migration (Wang *et al.*, 2022). It could thus be that the PPP2R1A knockdown leads to a decrease in ECM uptake due to defects in actin polymerization ([Figure 6-25](#)).

Collectively, p38 MAPK seems to be required for ECM internalisation in the breast cancer cell line MDA-MB-231 cells and in the endometrioid ovarian cancer cell line A2780-Rab25. Future work will further characterise the signalling pathways upstream and downstream of p38 activation and how it regulates ECM macropinocytosis and migration in breast and ovarian cancer.

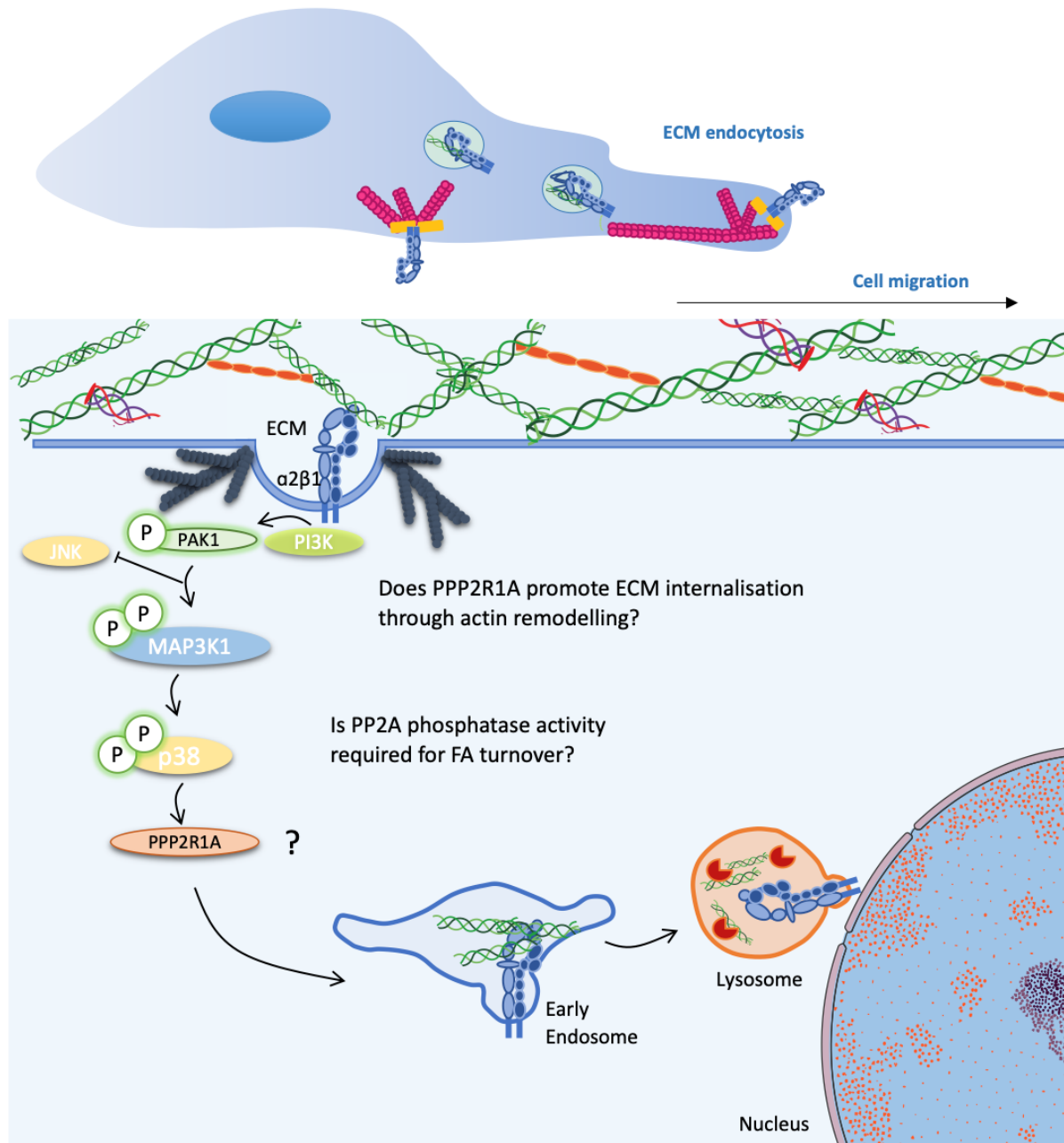


Figure 6-25. Schematic representation of the proposed mechanism promoting ECM internalisation. PAK1 activation downstream of $\alpha 2\beta 1$ integrin activation promotes MAP3K1 (MEKK1) phosphorylation, which in turn leads to p38 activation. We propose that PPP2R1A is downstream of p38. PPP2R1A may be regulating ECM internalisation through actin polymerisation or remodelling via the WAVE shell complex. Alternatively, PPP2R1A, as part of the PP2A complex, may be involved in dephosphorylation of FA proteins, which in turn may promote FA disassembly or turnover. This may enable ECM internalisation and ultimately migration of cancer cells. Image made using items from Servier medical Art.

Chapter 7 – Final Discussion

7.1. SUMMARY: PUTTING KEY FINDINGS INTO PERSPECTIVE

Increasing levels of endocytosis and intracellular trafficking, as well as dysregulations in endocytic proteins, is regarded as a paramount feature of tumour progression that culminates in metastasis (Khan and Steeg, 2021). Swiprosin 1, which is upregulated in HER2⁺ and triple negative breast cancer tumours, has been identified as a specific cargo adaptor that couples Rab21-associated β 1-integrin to components of the CLIC-GEEC pathway (Moreno-Layseca *et al.*, 2021). More recently, there is some evidence that suggests that flat clathrin lattices, rather than classical clathrin coated pits, correlate with the metastatic potential of colorectal cancer cell lines (Cresens *et al.*, 2023). In this study, we developed a high throughput ECM coating assay to characterise regulators of ECM internalisation. Using this novel methodology, we identified the endocytic pathways responsible for internalisation of matrigel, collagen I, TIF-CDM and CAF-CDM. While matrigel endocytosis may partially depend on changes in membrane tension due to the effect observed upon Cav1/2 downregulation, all the matrices tested strongly relied on PAK1-mediated macropinocytosis for their internalisation ([Chapter 3](#)). To delve into the signalling pathways behind ECM macropinocytosis, we screened for 972 kinases and phosphatases. Gene ontology and STRING analysis pointed to upregulation of MAPK signalling. siRNA downregulation of p38 β (MAPK11), MAP3K1, PPP2R1A strongly correlated with reduced ECM uptake index in MDA-MB-231 ([Chapter 6](#)). We confirmed these results using chemical inhibitors. Inhibiting p38 activity before cell adhesion reduced ECM internalisation in a dose-dependent manner, however inhibition after cells adhered and spread on the ECM had a small effect on uptake ([Chapter 6](#)). This data suggested to us that upon cell adhesion, ECM receptors activate p38 to promote macropinocytosis of ECM. α 2 β 1 integrin mediates internalisation of ECM in MDA-MB-231 cells ([Chapter 6](#) and Rainero data, unpublished). In addition, ECM endocytosis is upregulated in invasive breast cancer cells ([Chapter 4](#) and Rainero, unpublished). We therefore tested whether ECM-bound integrin internalisation conferred any advantage on cell migration on CDMs. We observed that MDA-MB-231 cells internalise ECM as they migrate through the matrix pores and, furthermore, blocking ECM macropinocytosis significantly reduced velocity and directionality

during cell migration. Future work is required to examine whether the effect on cell migration is due to impaired integrin traffic or endosomal signalling ([Figure 7-1](#)).

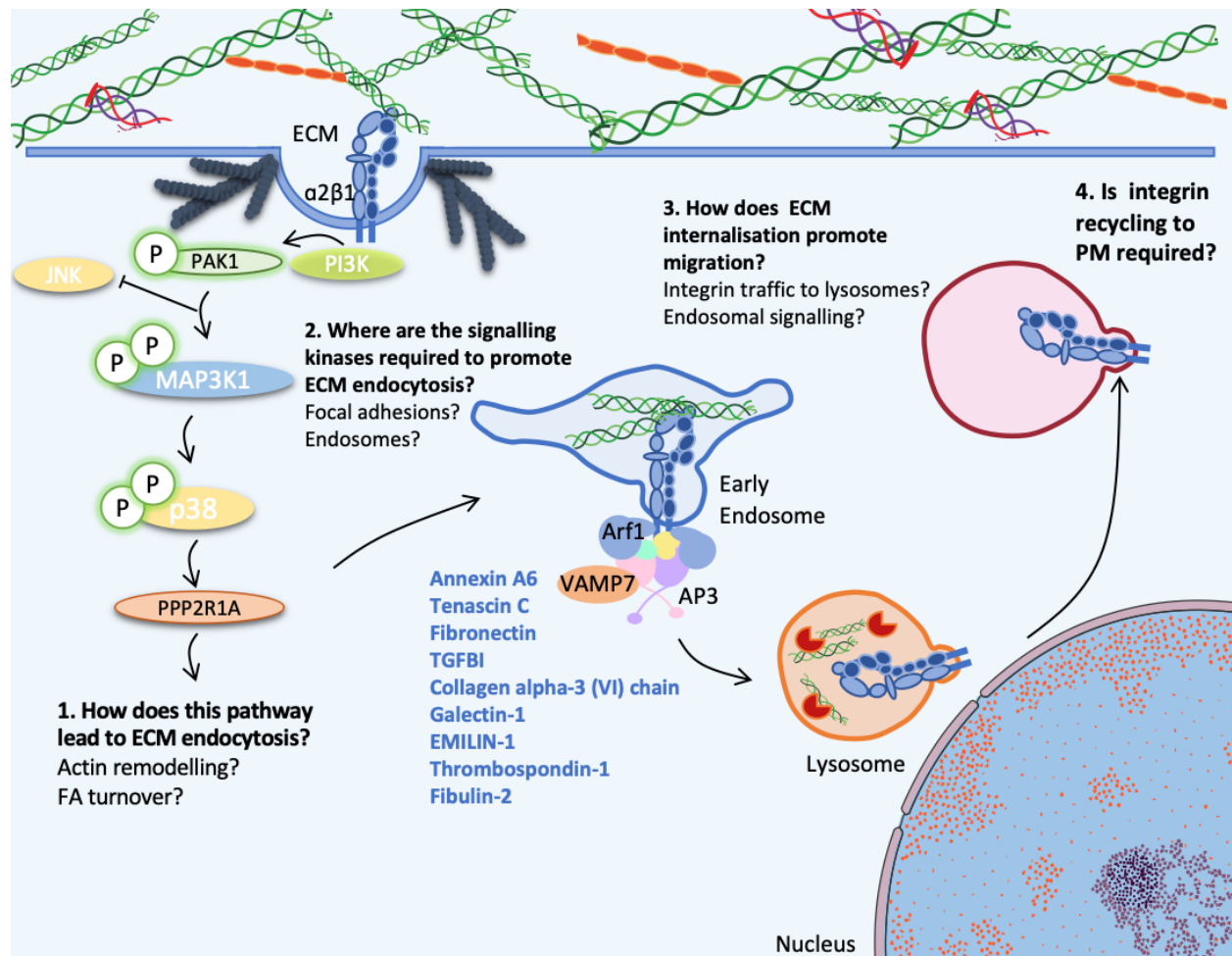


Figure 7-1. Schematic summary on the mechanism behind ECM internalisation. *p38* MAPK signalling is required for internalisation of collagen I, matrigel and CDM. Delivery of endocytosed ECM to lysosomes requires the AP3 complex. Blocking ECM internalisation, as well as its trafficking to lysosomes, leads to profound changes in migration. Image made using items from Servier medical Art.

ECM proteins have been shown to regulate intracellular signalling. Proteomics data showed that Tenascin C was internalised by MDA-MB-231 cells ([Chapter 4](#)). Interestingly, Tenascin C upregulates angiogenesis via Ephrin B2-EphB4 signalling axis (Tiosano *et al.*, 2019). EphB4 downregulation resulted in a decrease in matrigel internalisation, while inhibitor treatment indicated that the effect was collagen I-specific ([Chapter 6](#)). It could thus be that tenascin C could further drive internalisation of collagen I through Ephb4 signalling. Fibronectin-bound $\alpha 5 \beta 1$ has been shown to promote recruitment of mTORC1 to late endosomes in A2780-Rab25 cells, linking

nutrient signalling to invasive migration (Rainero *et al.*, 2015). Similarly, MDA-MB-231 cells under amino acid starvation are able to internalise ECM components, rescue mTORC1 activation and promote cancer cell proliferation (Nazemi *et al.*, 2021). Accordingly, 3D internalisation assay using spheroids indicated that amino acid starvation promotes ECM internalisation or ECM trafficking to acidic compartments ([Chapter 3](#)). In addition, the presented data in this thesis suggests that internalised ECM is trafficked and degraded by cysteine cathepsins in the lysosomes ([Chapter 5](#)). We identified the AP3 complex, its regulators, Arf1 and ARFGEF2, and VAMP7 as candidates to mediate ECM-bound integrin delivery to lysosomes. In addition, siRNA downregulation of Vti1b and STX7 slightly reduced matrigel uptake index ([Chapter 5](#)). It has been reported that VAMP7 participates in a complex with Vti1b, STX7 and STX8 to mediate lysosomal delivery (Kent *et al.*, 2012). Hence, we hypothesised that ARFGEF2 activation by $\alpha 2\beta 1$ integrin promotes Arf1 activation ([Chapter 5](#)). This results in recruitment of the AP3 complex and VAMP7 to early endosomes, which subsequently escorts ECM-bound $\alpha 2\beta 1$ integrin to lysosomes. siRNA-mediated downregulation of the δ -adaptin (AP3D1) led to accumulation of matrigel and $\beta 1$ -integrin in early endosomes ([Chapter 5](#)). Moreover, high resolution microscopy confirmed that the AP3 complex accumulated around endosomes positive for both matrigel and Arf1 ([Chapter 5](#)). Downregulation of the δ -adaptin (AP3D1) subunit significantly impaired directionality and velocity of MDA-MB-231 cells on CDM, suggesting ECM delivery to lysosomes is required for cancer cells migration in MDA-MB-231 cells. It is not clear whether the effect on cell migration upon blocking lysosomal delivery of ECM are due to impaired integrin recycling or changes in endosomal signalling. Further studies are needed to characterise how ECM endocytosis and its delivery to lysosomes regulate cancer cell migration ([Figure 7-1](#)).

7.2. ARE INTEGRINS NOVEL REGULATORS OF MACROPINOCYTOSIS?

Macropinocytosis is a non-specific type of endocytosis, which has been distinctively characterised by engulfing large amounts of extracellular fluid and solutes. Notwithstanding that, a recent publication has shed light on integrins, specifically $\alpha 5\beta 1$, to accumulate in macropinocytic cups (Le *et al.*, 2021). Furthermore, the results presented in Chapter 6 suggest that integrin signalling activates not only ECM uptake, but Dextran macropinocytosis. p38 inhibition by SB202190

reduced (by 50%) dextran internalisation ([Chapter 6](#)). In fact, dextran endocytosis is upregulated when cells are seeded on increasing collagen I concentration, suggesting that $\alpha 2\beta 1$ integrin may promote macropinocytosis (Rainero, unpublished). Phorbol 12-myristate 13-acetate (PMA), an analogue of diacylglycerol, has been shown to activate macropinocytosis upstream of Ras (Yoshida *et al.*, 2015). Interestingly, PMA was shown to mediate $\beta 1$ -integrin adhesion to fibronectin (Rock *et al.*, 2000), suggesting an interplay of integrin-mediated adhesion and macropinocytosis. PIK3C2A, a positive regulator/hit of matrigel uptake, is a class II member of PI3K family (Tiosano *et al.*, 2019). Similarly, inhibition of PIK3C2A reduced not only ECM internalisation but dextran internalisation on collagen I, but not matrigel (Rainero, unpublished). This data suggests that collagen I specifically promotes macropinocytosis. In fact, our data suggests that laminin, 60% of matrigel, internalisation is dependent on Cav 1/2. Our results with MDA-MB-231 showed some levels of colocalisation between dextran and $\beta 1$ -integrin, likely due to partial permabilisation of the PM ([Chapter 6](#)). This suggested that dextran and integrins may be internalised and/or trafficked together. Accordingly, dextran has been shown to be internalised and colocalise with collagen I in MDA-MB-231 cells (Rainero, unpublished). The fact that dextran, integrins and collagen I seem to accumulate in the same early endosomes suggest that they may have been internalised together. Along these lines, our mass spectrometry data showed that actin binding proteins are internalised by MDA-MB-231 ([Chapter 4](#)); it could thus be that ECM internalisation triggered non-specific internalisation of ECM-bound proteins. However, it could also be that ECM-integrin signalling promotes dextran macropinocytosis and dextran vesicles fuse to ECM “macropino-phagosomes”. Recent reports have shown that macropinosomes gather around phagosomes and fuse with them (Jason King, The University of Sheffield, personal communication). In addition, downregulation of tensin-3, modulator of ECM internalisation, does not inhibit dextran macropinocytosis (Rainero, unpublished). This data indicates that specifically MAPK activation (likely downstream of integrins), but not coupling of integrin to cytoskeleton dynamics, promotes dextran macropinocytosis independently of ECM internalisation. PAK1 inhibition or siRNA-mediated downregulation, specifically reduced ECM-dependent proliferation of MDA-MB-231 cells under starvation (Nazemi *et al.*, 2021). Interestingly, pharmacological inhibition of Rac1 alone or in combination with a Cdc42 inhibitor,

did not affect cell proliferation of MDA-MB-231 cells under starvation (Rainero, unpublished). PIP2, a substrate of PI3K, has been shown to induce direct activation of PAK1 (Strochlic *et al.*, 2010), actually PAK1 activation mediates resistance to PI3K inhibition in lymphomas (Walsh *et al.*, 2013). PI3K has been reported to be activated downstream of FAK and Src (Wu *et al.*, 2016). However, FAK inhibition does not affect ECM-dependent cell proliferation under amino acid starvation (Nazemi *et al.*, 2021). Interestingly, β 1-integrin can induce PI3K activation independently of FAK and Src (Velling *et al.*, 2004). We thus hypothesised that PI3K activation downstream of β 1-integrin, rather than Rac1 and Cdc42, promotes PAK1 activation and subsequent ECM macropinocytosis. Blocking ECM macropinocytosis impaired the migration velocity and directionality of MDA-MB-231 cells on CDM. Similarly, inhibiting α 2 β 1 integrin using BTT-3033 significantly affected migration of A2780-Rab25 cells (data not shown). These results differ from other studies. CYRI-A has been identified as a novel suppressor of Rac1 activity, Rac1 inhibition promotes closure of the macropinocytic cup (Le *et al.*, 2021). Of note, double knockdown of CYRI-A and CYRI-B increased cell surface expression of α 5 β 1 internalisation, which in turn enhanced cell migration (Le *et al.*, 2021). Increasing evidence suggests that regulators of macropinocytosis are cell type specific, in addition to coexisting with subtypes of macropinocytosis (Lin, Mintern and Gleeson, 2020). It could thus be that the different effects observed regarding migration may be cell type specific.

7.3. EXTRACELLULAR AND INTRACELLULAR DEGRADATION IN ECM INTERNALISATION

Extracellular ECM degradation is a hallmark of cancer (Brassart-Pasco *et al.*, 2020). Our results suggest that MMPs are majorly dispensable for ECM internalisation in MDA-MB-231 cells. MMP inhibition slightly reduced internalisation of collagen I-rich matrices, including CDM ([Chapter 3](#)). Contrarily, MMP inhibition increased matrigel internalisation under amino acid starvation conditions, without affecting collagen I uptake (Nazemi *et al.*, 2021). Expression and localisation of Tks5 and MT1-MMP to invadopodia structures are upregulated in G1 (Bayarmagnai *et al.*, 2019). We thus aimed to examine whether the cell cycle had an effect on ECM uptake. Indeed, internalisation of laminin-rich matrices was upregulated in G1 ([Figure S1-13](#) and [S1-14](#)). We thus

hypothesised that differential signalling between the G1 and G2 phase of the cell cycle may result in these changes. Surprisingly, our kinome and phosphatome data showed that siRNA downregulation of Aurora Kinase B (AURKB), which activity is required in mitosis during chromosome segregation (Krenn and Musacchio, 2015), highly upregulated matrigel internalisation. During mitosis, classical adhesion complexes are disassembled, but cells remain adhered to the substrate through integrins (Dix *et al.*, 2018). It could thus be that AURKB may block internalisation of laminin as cell cycle progresses to G2 and mitosis by inducing changes in focal adhesion dynamics.

Highly dynamic podosome-like structures in nascent phagocytic cups have been shown to tightly adhere to the target for endocytosis (Ostrowski *et al.*, 2019). Simultaneously, frustrated phagocytosis resembles actin rosettes, present in invadopodia (Herron *et al.*, 2022). In addition to regulating macropinocytosis, PAK1 promotes cortactin phosphorylation, actin assembly and invadopodia formation (Nicholas *et al.*, 2019). Moreover, at later stages, invadopodia maturation requires PAK4 (Nicholas *et al.*, 2019). Our kinome and phosphatome screen identified PAK4 downregulation to increase internalisation of matrigel to 0.64 and 0.68 (normalised data) compared to NT5 (which is normalised to 0) in both technical replicates (Chapter 6). On matrigel or basement membrane, one could therefore hypothesise that the initial stages of macropinocytosis (and phagocytosis) highly resemble initial stages of invadopodia formation. This inverse correlation between invadopodia assembly at later stages (by siRNA-mediated downregulation of PAK4 together with upregulation of ECM uptake under certain conditions upon MMP inhibition) could indicate that MDA-MB-231 cells either promote macropinocytosis of ECM or invadopodia formation. Alternatively, we could also hypothesise that frustrated/aborted invadopodia events are resolved by switching those incipient invadosomes towards macropinocytic events. This may differ in other cell lines, as preliminary data on the pancreatic cancer line PANC1 suggested that MMP activity is actually required for internalisation of matrigel and collagen I (data not shown).

In addition to extracellular degradation by MMPs, cancer cells secrete cysteine cathepsins, resulting in cancer progression and metastasis (Rudzińska *et al.*, 2019). Our results suggest that

cysteine cathepsin inhibition reduces internalisation of matrigel, collagen I and TIF-CDM (Chapter 3). E64d was shown to inhibit calpains, a calcium activated protease (Murray *et al.*, 1997; Tsubokawa *et al.*, 2006). A biochemical study showed that calpains cleave the cytoplasmic domain of β 3- and β 1-integrin (Pfaff, Du and Ginsberg, 1999). In fact, clustered α 2 β 1 integrin is degraded by active calpain 1 in multivesicular bodies, promoting non-recycling turnover of α 2 β 1 integrin (Rintanen *et al.*, 2012). It may be possible that both cathepsins and calpains aid in the intracellular degradation process. Nevertheless, β 1-integrin engaged to fibronectin surfaces has been shown to promote outside-in signalling events that promote calpain activation in focal adhesions (Rock *et al.*, 2000). Calpain cleaves protein tyrosine phosphatase 1B (PTP-1B), which results in T cell adhesion and changes in cell shape (Rock *et al.*, 2000). The effects observed upon E64d treatment could partially be explained by changes in integrin adhesion by inhibiting calpains. However, at the same time cysteine cathepsins mediate intracellular degradation of ECM ([Chapter 5](#)). Increasing matrigel and collagen I concentration leads to higher elastic moduli/stiffness (Application note from Corning). As the methodology used in this study involved centrifuging the plates, we hypothesise that this approach led to the generation of stiff matrices. However, we noticed that lowering the concentration of matrigel to 0.1mg/ml and 0.3mg/ml (in [Chapter 3](#)) resulted in a similar output as using the conventional matrigel coating method (in [Chapter 5](#)). Interestingly, E64d treatment did not increase collagen I (1mg/ml) internalisation as strikingly as for laminin and matrigel (2mg/ml and 1mg/ml, respectively). This suggested that 1mg/ml collagen I may be stiffer and thus cysteine cathepsins are required. Indeed, E64d treatment on 0.5mg/ml collagen had no effect on uptake (labelled with NHS-fluorescein), but internalisation of 1mg/ml was decreased (Rainero, unpublished). These results suggest that cysteine cathepsins display a dual role in ECM internalisation, on the one hand they are involved in degradation of internalised matrix. On the other hand, cysteine cathepsin activity seems required extracellularly to promote ECM macropinocytosis. In addition, for collagen I-rich matrices, cysteine cathepsins may cooperate with MMPs. Future studies will unravel the implications and requirements of extracellular degradation on ECM uptake.

7.4. INVASIVE AND ANCHORAGE INDEPENDENT GROWTH

Anchorage independent cell growth is a hallmark of metastasis. This is achieved through integrin signalling in the endosomal compartments (also known as integrin endosomal signalling) (Alanko *et al.*, 2015). ECM-bound to active integrins promotes ERK, AKT and FAK activation in early endosomes, which in turn suppresses anoikis (Alanko *et al.*, 2015). ECM internalisation in invasive breast cancer cells and the pancreatic cancer cell line PANC-1 promotes cell proliferation under starvation (Nazemi *et al.*, 2021). Arf1 has been involved in regulating FAK signalling and it regulates MAPK signalling in cancer (Casalou, Faustino and Barral, 2016; Davis *et al.*, 2016). Our results show Arf1 in matrigel positive endosomes ([Chapter 5](#)). Arf1 activity may promote conformational changes in the AP3 complex that enable recognition of ECM-occupied $\alpha 2\beta 1$ integrin ([Chapter 5](#)). In addition, we showed that the p38 MAPK signalling pathway is required for ECM internalisation. Nevertheless, we have not yet established the spatio-temporal regulation of p38, whether p38 MAPK signalling is required at conventional focal adhesions or p38 endosomal signalling promotes ECM internalisation in a positive-feedback loop.

p38-dependent ECM internalisation and AP3 complex-mediated ECM traffic to lysosomes promotes cancer cell migration. p38-induced cell migration seems to be required for velocity and directional persistence. Visual observation of time-lapse microscopy videos suggested that MAP3K1 and p38 MAPK may be necessary to migrate into CDMs. Similarly, blocking ECM-traffic to lysosomes only impaired on velocity and directionality of cancer cells; conversely, no effect was seen in the ability of MDA-MB-231 cells to delve (migrate) into the CDMs upon siRNA knockdown of AP3D1 when observing time-lapses. This suggests that the implications of blocking ECM internalisation or its trafficking differ. Nevertheless, it is not clear whether lysosomal $\alpha 2\beta 1$ integrin may additionally trigger activation of other signalling cascades, which differ from integrin endosomal signalling.

7.5. THERAPEUTIC OPPORTUNITIES

The ECM is the major component of the tumour microenvironment. During malignant progression, the ECM becomes fibrotic and desmoplastic (Cox *et al.*, 2013). This is partially because of increased collagen crosslinking (Cox *et al.*, 2013). To target this feature of cancer, inhibitors against LOX have been developed (Barker, Cox and Erler, 2012). MMP-mediated extracellular proteolysis has been regarded as the major contributor in ECM remodelling (Bonnans, Chou and Werb, 2014). Therefore, selective therapeutic targeting of MMPs has been considered for some cancers. Particularly, breast cancer tumours display high levels of MT1-MMP (MMP14) (Devy *et al.*, 2009). Accordingly, preclinical models of murine breast cancer have tested a selective inhibitor of MT1-MMP, DX-2400 (Devy *et al.*, 2009). MT1-MMP inhibition blocked tumour growth, angiogenesis and formation of metastatic lesions (Devy *et al.*, 2009). However, broad spectrum inhibition of MMPs failed in clinical trials probably due to the dual tumour-promoting and -suppressive role of different MMPs (Vandenbroucke and Libert, 2014). In this thesis we have highlighted the potential role of ECM endocytosis in breast cancer cell migration. Cysteine cathepsins seem to be required for its extracellular degradation and subsequent internalisation. In addition, cysteine cathepsins mediate ECM degradation in the lysosomes. Inhibition of cysteine cathepsins have been used in mouse models (Tsubokawa *et al.*, 2006). Similarly, E64d treatment reduced the cleavage of the precursor of amyloid- β , in turn ameliorating Alzheimer's disease in mice models (Hook, Hook and Kindy, 2011). ECM internalisation promotes cell proliferation under nutrient limiting sources (Nazemi *et al.*, 2021). Cysteine cathepsin inhibition could similarly benefit breast cancer patients by inhibiting the extracellular and intracellular degradation of ECM components. ECM is internalised together with integrins ([Chapter 6](#) and Rainero, unpublished), therapeutically targeting integrins or their delivery to lysosomes may similarly benefit breast and endometrioid ovarian cancer patients. Interestingly, Arf1 inhibition by demethylzeylasteral reduced breast cancer proliferation *in vitro* and *in vivo* (Chang *et al.*, 2022). ATN-161, a non-RGD peptide, is an $\alpha 5\beta 1$ integrin antagonist, which has been shown to block breast cancer growth and metastasis in mice (Khalili *et al.*, 2006). Additionally, ATN-161 blocked angiogenesis and metastasis of solid tumours in Phase 1 clinical trials (Cianfrocca *et al.*, 2006). Our mass spectrometry identified that fibronectin is internalised

by MDA-MB-231 cells ([Chapter 4](#)). Fibronectin is internalised in an $\alpha 5\beta 1$ integrin dependent manner by ovarian cancer cells (Rainero *et al.*, 2015). Future work may elucidate whether $\alpha 5\beta 1$ integrin mediated fibronectin internalisation in invasive breast cancer. Likewise, a monoclonal antibody against anti- αv integrin (intetumumab) in a phase II clinical study reported a nonsignificant trend in improved overall survival in advanced melanoma (Cianfrocca *et al.*, 2006; O'Day *et al.*, 2011).

$\alpha 2\beta 1$ integrin has been linked to bone metastasis in breast cancer patients (Moritz *et al.*, 2021). Moreover, ECM endocytosis relies on $\alpha 2\beta 1$ integrin, nevertheless no pharmacological inhibitors have been developed for its use in clinical trials. $\alpha 2\beta 1$ integrin has been shown to activate p38 MAPK signalling (Ivaska *et al.*, 1999). A selective p38 MAPK inhibitor, dilmapiomod, has been tested in 50 patients with neuropathic pain (Anand *et al.*, 2011). In this study, p38 inhibition did not display clinically relevant adverse effects. Therefore, in the future, triple negative breast cancer patients may benefit from p38 inhibition by reducing velocity and directionality of migrating cells.

7.6. CONCLUSIONS AND FUTURE DIRECTIONS

The current study revealed a role of ECM internalisation in driving breast cancer cell migration, as well as preliminary data suggesting that collagen I signalling regulates macropinocytosis of soluble molecules, such as dextran. Simultaneously, this work has raised several questions on how ECM internalisation, traffic to lysosomes and signalling regulates cell migration ([Figure 7-1](#)). The following points include an outline of aspects that remain to be addressed:

- Fully understand how $\alpha 2\beta 1$ integrin and the identified signalling regulators (specifically MAP3K1, MAPK11 and PPP2R1A) interplay to promote ECM macropinocytosis. To characterise how these proteins sequentially act in the signalling cascade, MAP3K1 or PPP2R1A knockdown cells will be cultured in the presence or absence of sorbitol or anisomycin, which strongly induce p38 activation.

- Identify whether PP2A phosphatase activity (using the inhibitor Okadaic acid) is required in ECM internalisation or whether the effects observed are due to its role in actin polymerisation through the WAVE Shell complex.
- In this study, we have performed migration assays using cell derived matrices. To further investigate the effect of p38 and $\alpha 2\beta 1$ on directional migration, a microfluidic device will be used. In addition, wound healing assay on plastic will determine whether the effects observed are matrix specific.
- ECM internalisation promotes proliferation in 2D and 3D (Nazemi *et al.*, 2021). 3D spheroid models, as well as patient-derived xenograft models, may be utilised to discern the role of p38 and $\alpha 2\beta 1$ integrin on invasive growth in breast and ovarian cancer. In addition, additional experiments will define how MAP3K1, MAPK11 and PPP2R1A contribute to ECM-mediated proliferation of invasive MDA-MB-231, MCF10CA1a and MCF10A cells under amino acid starvation. This will identify whether any of the hits may represent a novel cancer-specific therapeutic target.
- ECM internalisation is upregulated in invasive breast cancer ([Chapter 4](#) and Rainero, unpublished). We thus aim to utilise murine normal tissue and tumour samples at different stages of tumour development to study whether expression of MAP3K1, MAPK11 and PPP2R1A increases as tumours progress.
- Determine localisation of p38 MAPK activation: focal adhesion complexes or endosomal.
- Characterise how the AP3 complex promotes ECM-occupied integrin delivery to lysosomes.
- Assess the contribution of extracellular degradation in ECM endocytosis.
- Elucidate the mechanisms by which integrin signalling contributes to macropinocytosis of soluble ligands, namely dextran and albumin.

Altogether, these findings suggest that breast cancer cells converge into macropinocytosis to internalise the different ECM components. We show that MAP3K1, PPP2R1A and MAPK11 promote ECM internalisation. In addition, p38 MAPK activation is required for ECM and dextran macropinocytosis. Following its internalisation, the ECM is trafficked to lysosomes in an AP3-complex dependent pathway. Blocking macropinocytosis or lysosomal delivery leads to profound

changes in mesenchymal cell migration in MDA-MB-231 cells. In addition, inhibition of $\alpha 2\beta 1$ integrin significantly affects migration of A2780-Rab25 cells. Considering the importance of the tumour microenvironment and integrin traffic in breast cancer, having a deep understanding of the regulators and signalling pathways behind internalisation of ECM-bound integrins may open new avenues for treatment of breast and ovarian cancer. Thus, the signalling and trafficking regulators identified in this thesis may assist in the development of such targeted therapies.

Chapter 8 – References

- Aasheim, H.-C., Delabie, J. and Finne, E.F. (2005) 'Ephrin-A1 binding to CD4+ T lymphocytes stimulates migration and induces tyrosine phosphorylation of PYK2', *Blood*, 105(7), pp. 2869–2876.
- Abou Jamra, R. *et al.* (2011) 'Adaptor protein complex 4 deficiency causes severe autosomal-recessive intellectual disability, progressive spastic paraplegia, shy character, and short stature', *American journal of human genetics*, 88(6), pp. 788–795.
- Abraham, L.C. *et al.* (2007) 'Phagocytosis and remodeling of collagen matrices', *Experimental cell research*, 313(5), pp. 1045–1055.
- Adams, J.C. and Lawler, J. (2004) 'The thrombospondins', *The international journal of biochemistry & cell biology*, 36(6), pp. 961–968.
- Adams, J. and Lawler, J. (1993) 'Extracellular matrix: the thrombospondin family', *Current biology: CB*, 3(3), pp. 188–190.
- Advani, R.J. *et al.* (1999) 'VAMP-7 mediates vesicular transport from endosomes to lysosomes', *The Journal of cell biology*, 146(4), pp. 765–776.
- Afratis, N.A. *et al.* (2017) 'Syndecans - key regulators of cell signaling and biological functions', *The FEBS journal*, 284(1), pp. 27–41.
- Alanko, J. *et al.* (2015) 'Integrin endosomal signalling suppresses anoikis', *Nature cell biology*, 17(11), pp. 1412–1421.
- Alanko, J. and Ivaska, J. (2016) 'Integrin "endoadhesome" signaling suppresses anoikis', *Cell cycle*, 15(5), pp. 605–606.
- Alečković, M. *et al.* (2017) 'Identification of Nidogen 1 as a lung metastasis protein through secretome analysis', *Genes & development*, 31(14), pp. 1439–1455.
- Alfonzo-Méndez, M.A. *et al.* (2022) 'Dual clathrin and integrin signaling systems regulate growth factor receptor activation', *Nature communications*, 13(1), p. 905.
- Alves, F. *et al.* (2001) 'Identification of two novel, kinase-deficient variants of discoidin domain receptor 1: differential expression in human colon cancer cell lines', *FASEB journal: official publication of the Federation of American Societies for Experimental Biology*, 15(7), pp. 1321–1323.
- Ambrosio, A.L., Febvre, H.P. and Di Pietro, S.M. (2022) 'Syntaxin 12 and COMMD3 are new factors that function with VPS33B in the biogenesis of platelet α -granules', *Blood*, 139(6), pp. 922–935.
- Amor López, A. *et al.* (2021) 'Inactivation of EMILIN-1 by Proteolysis and Secretion in Small Extracellular Vesicles Favors Melanoma Progression and Metastasis', *International journal of molecular sciences*, 22(14). Available at: <https://doi.org/10.3390/ijms22147406>.
- Anand, P. *et al.* (2011) 'Clinical trial of the p38 MAP kinase inhibitor diltapimod in neuropathic pain following nerve injury', *European journal of pain*, 15(10), pp. 1040–1048.
- Anttonen, A. *et al.* (1999) 'Syndecan-1 expression has prognostic significance in head and neck carcinoma', *British journal of cancer*, 79(3-4), pp. 558–564.
- Anttonen, A. *et al.* (2001) 'High syndecan-1 expression is associated with favourable outcome in squamous cell lung carcinoma treated with radical surgery', *Lung cancer*, 32(3), pp. 297–305.
- Aprile, G. *et al.* (2013) 'Biglycan expression and clinical outcome in patients with pancreatic adenocarcinoma', *Tumour biology: the journal of the International Society for Oncodevelopmental Biology*

and Medicine, 34(1), pp. 131–137.

Arafat, H.A. *et al.* (2011) 'Tumor-specific Expression And Alternative Splicing Of The COL6A3 Gene in Pancreatic Cancer', *Journal of Surgical Research*, p. 176. Available at: <https://doi.org/10.1016/j.jss.2010.11.782>.

Arjonen, A. *et al.* (2012) 'Distinct recycling of active and inactive β 1 integrins', *Traffic*, 13(4), pp. 610–625.

Armony, G. *et al.* (2016) 'Cross-linking reveals laminin coiled-coil architecture', *Proceedings of the National Academy of Sciences of the United States of America*, 113(47), pp. 13384–13389.

Arora, P.D. *et al.* (2000) 'A novel model system for characterization of phagosomal maturation, acidification, and intracellular collagen degradation in fibroblasts', *The Journal of biological chemistry*, 275(45), pp. 35432–35441.

Arora, P.D. *et al.* (2004) 'Gelsolin mediates collagen phagocytosis through a rac-dependent step', *Molecular biology of the cell*, 15(2), pp. 588–599.

Arora, P.D. *et al.* (2013) 'Collagen remodeling by phagocytosis is determined by collagen substrate topology and calcium-dependent interactions of gelsolin with nonmuscle myosin IIA in cell adhesions', *Molecular biology of the cell*, 24(6), pp. 734–747.

Arora, P.D., Marignani, P.A. and McCulloch, C.A. (2008) 'Collagen phagocytosis is regulated by the guanine nucleotide exchange factor Vav2', *American journal of physiology. Cell physiology*, 295(1), pp. C130–7.

Arpino, G. *et al.* (2022) 'Clathrin-mediated endocytosis cooperates with bulk endocytosis to generate vesicles', *iScience*, 25(2), p. 103809.

Arriazu, E. *et al.* (2020) 'A new regulatory mechanism of protein phosphatase 2A activity via SET in acute myeloid leukemia', *Blood cancer journal*, 10(1), p. 3.

Arriemerlou, C. and Meyer, T. (2005) 'A local coupling model and compass parameter for eukaryotic chemotaxis', *Developmental cell*, 8(2), pp. 215–227.

Atri, C., Guerfali, F.Z. and Laouini, D. (2018) 'Role of Human Macrophage Polarization in Inflammation during Infectious Diseases', *International journal of molecular sciences*, 19(6). Available at: <https://doi.org/10.3390/ijms19061801>.

Attieh, Y. *et al.* (2017) 'Cancer-associated fibroblasts lead tumor invasion through integrin- β 3-dependent fibronectin assembly', *The Journal of cell biology*, 216(11), pp. 3509–3520.

Augustin, R., Riley, J. and Moley, K.H. (2005) 'GLUT8 contains a [DE]XXXL[LI] sorting motif and localizes to a late endosomal/lysosomal compartment', *Traffic*, 6(12), pp. 1196–1212.

Babuke, T. *et al.* (2009) 'Hetero-oligomerization of reggie-1/flotillin-2 and reggie-2/flotillin-1 is required for their endocytosis', *Cellular signalling*, 21(8), pp. 1287–1297.

Bachmann, A. *et al.* (2005) 'Collagen triple-helix formation in all-trans chains proceeds by a nucleation/growth mechanism with a purely entropic barrier', *Proceedings of the National Academy of Sciences of the United States of America*, 102(39), pp. 13897–13902.

Bachmann, M. *et al.* (2020) 'Induction of ligand promiscuity of α V β 3 integrin by mechanical force', *Journal of cell science*, 133(9). Available at: <https://doi.org/10.1242/jcs.242404>.

Baghban, R. *et al.* (2020) 'Tumor microenvironment complexity and therapeutic implications at a glance', *Cell communication and signaling: CCS*, 18(1), p. 59.

Baker, E.K. *et al.* (2022) 'PPP2R1A neurodevelopmental disorder is associated with congenital heart defects', *American journal of medical genetics. Part A*, 188(11), pp. 3262–3277.

- Balderhaar, H.J.K. *et al.* (2013) 'The CORVET complex promotes tethering and fusion of Rab5/Vps21-positive membranes', *Proceedings of the National Academy of Sciences of the United States of America*, 110(10), pp. 3823–3828.
- Baneyx, G., Baugh, L. and Vogel, V. (2002) 'Fibronectin extension and unfolding within cell matrix fibrils controlled by cytoskeletal tension', *Proceedings of the National Academy of Sciences of the United States of America*, 99(8), pp. 5139–5143.
- Barbazan, J. *et al.* (2021) 'Cancer-associated fibroblasts actively compress cancer cells and modulate mechanotransduction', *bioRxiv*. bioRxiv. Available at: <https://doi.org/10.1101/2021.04.05.438443>.
- Barbieri, E., Di Fiore, P.P. and Sigismund, S. (2016) 'Endocytic control of signaling at the plasma membrane', *Current opinion in cell biology*, 39, pp. 21–27.
- del Barco Barrantes, I. and Nebreda, A.R. (2012) 'Roles of p38 MAPKs in invasion and metastasis', *Biochemical Society transactions*, 40(1), pp. 79–84.
- Bardwell, L. (2006) 'Mechanisms of MAPK signalling specificity', *Biochemical Society transactions*, 34(Pt 5), pp. 837–841.
- Barker, H.E. *et al.* (2011) 'LOXL2-mediated matrix remodeling in metastasis and mammary gland involution', *Cancer research*, 71(5), pp. 1561–1572.
- Barker, H.E., Cox, T.R. and Erler, J.T. (2012) 'The rationale for targeting the LOX family in cancer', *Nature reviews. Cancer*, 12(8), pp. 540–552.
- Bartels, A.-K. *et al.* (2019) 'KDEL Receptor 1 Contributes to Cell Surface Association of Protein Disulfide Isomerases', *Cellular physiology and biochemistry: international journal of experimental cellular physiology, biochemistry, and pharmacology*, 52(4), pp. 850–868.
- Bartha, Á. and Gyórfy, B. (2021) 'TNMplot.com: A Web Tool for the Comparison of Gene Expression in Normal, Tumor and Metastatic Tissues', *International journal of molecular sciences*, 22(5). Available at: <https://doi.org/10.3390/ijms22052622>.
- Barth, D., Musiol, H.-J., *et al.* (2003) 'The role of cystine knots in collagen folding and stability, part I. Conformational properties of (Pro-Hyp-Gly)₅ and (Pro-(4S)-FPro-Gly)₅ model trimers with an artificial cystine knot', *Chemistry*, 9(15), pp. 3692–3702.
- Barth, D., Kyrieleis, O., *et al.* (2003) 'The role of cystine knots in collagen folding and stability, part II. Conformational properties of (Pro-Hyp-Gly)_n model trimers with N- and C-terminal collagen type III cystine knots', *Chemistry*, 9(15), pp. 3703–3714.
- Bartoschek, M. *et al.* (2018) 'Spatially and functionally distinct subclasses of breast cancer-associated fibroblasts revealed by single cell RNA sequencing', *Nature communications*, 9(1), p. 5150.
- Basu, S. *et al.* (2018) 'Plakophilin3 loss leads to an increase in lipocalin2 expression, which is required for tumour formation', *Experimental cell research*, 369(2), pp. 251–265.
- Battaglia, C. *et al.* (1992) 'Basement-membrane heparan sulfate proteoglycan binds to laminin by its heparan sulfate chains and to nidogen by sites in the protein core', *European journal of biochemistry / FEBS*, 208(2), pp. 359–366.
- Bayarmagnai, B. *et al.* (2019) 'Invadopodia-mediated ECM degradation is enhanced in the G1 phase of the cell cycle', *Journal of cell science*, 132(20). Available at: <https://doi.org/10.1242/jcs.227116>.
- Bayer-Garner, I.B. *et al.* (2001) 'Syndecan-1 (CD138) immunoreactivity in bone marrow biopsies of multiple myeloma: shed syndecan-1 accumulates in fibrotic regions', *Modern pathology: an official journal of the United States and Canadian Academy of Pathology, Inc*, 14(10), pp. 1052–1058.

- Beaty, B.T. *et al.* (2013) 'β1 integrin regulates Arg to promote invadopodial maturation and matrix degradation', *Molecular biology of the cell*, 24(11), pp. 1661–75, S1–11.
- Beauvais, D.M. *et al.* (2009) 'Syndecan-1 regulates alphavbeta3 and alphavbeta5 integrin activation during angiogenesis and is blocked by synstatin, a novel peptide inhibitor', *The Journal of experimental medicine*, 206(3), pp. 691–705.
- Beecher, N. *et al.* (2011) 'Collagen VI, conformation of A-domain arrays and microfibril architecture', *The Journal of biological chemistry*, 286(46), pp. 40266–40275.
- Behrendt, N. *et al.* (2000) 'A urokinase receptor-associated protein with specific collagen binding properties', *The Journal of biological chemistry*, 275(3), pp. 1993–2002.
- Bejarano, P.A. *et al.* (1988) 'Degradation of basement membranes by human matrix metalloproteinase 3 (stromelysin)', *Biochemical Journal*, 256(2), pp. 413–419.
- Berg, R.A. and Prockop, D.J. (1973) 'The thermal transition of a non-hydroxylated form of collagen. Evidence for a role for hydroxyproline in stabilizing the triple-helix of collagen', *Biochemical and biophysical research communications*, 52(1), pp. 115–120.
- Betts, M.J. *et al.* (2017) 'Systematic identification of phosphorylation-mediated protein interaction switches', *PLoS computational biology*, 13(3), p. e1005462.
- Bickel, P.E. *et al.* (1997) 'Flotillin and epidermal surface antigen define a new family of caveolae-associated integral membrane proteins', *The Journal of biological chemistry*, 272(21), pp. 13793–13802.
- Bidanset, D.J. *et al.* (1992) 'Binding of the proteoglycan decorin to collagen type VI', *The Journal of biological chemistry*, 267(8), pp. 5250–5256.
- Bill, H.M. *et al.* (2004) 'Epidermal growth factor receptor-dependent regulation of integrin-mediated signaling and cell cycle entry in epithelial cells', *Molecular and cellular biology*, 24(19), pp. 8586–8599.
- Bohdanowicz, M. *et al.* (2013) 'Phosphatidic acid is required for the constitutive ruffling and macropinocytosis of phagocytes', *Molecular biology of the cell*, 24(11), pp. 1700–12, S1–7.
- Bonaldo, P. *et al.* (1990) 'Structural and functional features of the .alpha.3 chain indicate a bridging role for chicken collagen VI in connective tissues', *Biochemistry*, pp. 1245–1254. Available at: <https://doi.org/10.1021/bi00457a021>.
- Bonnans, C., Chou, J. and Werb, Z. (2014) 'Remodelling the extracellular matrix in development and disease', *Nature reviews. Molecular cell biology*, 15(12), pp. 786–801.
- Boon, L. *et al.* (2021) 'Citrullination as a novel posttranslational modification of matrix metalloproteinases', *Matrix biology: journal of the International Society for Matrix Biology*, 95, pp. 68–83.
- Boraschi-Diaz, I. (2017) *Regulation of Osteoclasts by Collagen Type I Degradation Fragments: The Implications for Bone Destruction and Whole Body Metabolism in Osteogenesis Imperfecta*.
- Bordignon, P. *et al.* (2019) 'Dualism of FGF and TGF-β Signaling in Heterogeneous Cancer-Associated Fibroblast Activation with ETV1 as a Critical Determinant', *Cell reports*, 28(9), pp. 2358–2372.e6.
- Bosgraaf, L. and Van Haastert, P.J.M. (2009) 'The ordered extension of pseudopodia by amoeboid cells in the absence of external cues', *PLoS one*, 4(4), p. e5253.
- Bošnjak, I. *et al.* (2014) 'Occurrence of protein disulfide bonds in different domains of life: a comparison of proteins from the Protein Data Bank', *Protein engineering, design & selection: PEDS*, 27(3), pp. 65–72.
- Bossart, K.N. *et al.* (2008) 'Functional studies of host-specific ephrin-B ligands as Henipavirus receptors', *Virology*, 372(2), pp. 357–371.

- Boudreau, N.J. and Jones, P.L. (1999) 'Extracellular matrix and integrin signalling: the shape of things to come', *Biochemical Journal*, 339 (Pt 3)(Pt 3), pp. 481–488.
- Boutillier, A.J. and Elsawa, S.F. (2021) 'Macrophage Polarization States in the Tumor Microenvironment', *International journal of molecular sciences*, 22(13). Available at: <https://doi.org/10.3390/ijms22136995>.
- Bowden, T.A. *et al.* (2009) 'Structural plasticity of eph receptor A4 facilitates cross-class ephrin signaling', *Structure*, 17(10), pp. 1386–1397.
- Bowman, S.L. *et al.* (2021) 'A BLOC-1-AP-3 super-complex sorts a cis-SNARE complex into endosome-derived tubular transport carriers', *The Journal of cell biology*, 220(7). Available at: <https://doi.org/10.1083/jcb.202005173>.
- Brafman, D.A. *et al.* (2013) 'Regulation of endodermal differentiation of human embryonic stem cells through integrin-ECM interactions', *Cell death and differentiation*, 20(3), pp. 369–381.
- Brassart-Pasco, S. *et al.* (2020) 'Tumor Microenvironment: Extracellular Matrix Alterations Influence Tumor Progression', *Frontiers in oncology*, 10, p. 397.
- Bravo-Cordero, J.J. *et al.* (2007) 'MT1-MMP proinvasive activity is regulated by a novel Rab8-dependent exocytic pathway', *The EMBO journal*, 26(6), pp. 1499–1510.
- Bray, F. *et al.* (2018) 'Global cancer statistics 2018: GLOBOCAN estimates of incidence and mortality worldwide for 36 cancers in 185 countries', *CA: a cancer journal for clinicians*, 68(6), pp. 394–424.
- Brazel, D. *et al.* (1988) 'Human basement membrane collagen (type IV). The amino acid sequence of the alpha2(IV) chain and its comparison with the alpha1(IV) chain reveals deletions in the alpha1(IV) chain', *European Journal of Biochemistry*, pp. 35–42. Available at: <https://doi.org/10.1111/j.1432-1033.1988.tb13852.x>.
- Breast cancer statistics, CRUK 2015* (2015) *Cancer Research UK*. Available at: <https://www.cancerresearchuk.org/health-professional/cancer-statistics/statistics-by-cancer-type/breast-cancer/incidence-invasive> (Accessed: 6 July 2022).
- Briggs, D.C. *et al.* (2016) 'Structural basis of laminin binding to the LARGE glycans on dystroglycan', *Nature chemical biology*, 12(10), pp. 810–814.
- Brittingham, R., Uitto, J. and Fertala, A. (2006) 'High-affinity binding of the NC1 domain of collagen VII to laminin 5 and collagen IV', *Biochemical and biophysical research communications*, 343(3), pp. 692–699.
- Buckens, O.J. *et al.* (2020) 'The role of Eph receptors in cancer and how to target them: novel approaches in cancer treatment', *Expert opinion on investigational drugs*, 29(6), pp. 567–582.
- Bulavin, D.V. and Fornace, A.J. (2004) 'p38 MAP Kinase's Emerging Role as a Tumor Suppressor', *Advances in Cancer Research*, pp. 95–118. Available at: [https://doi.org/10.1016/s0065-230x\(04\)92005-2](https://doi.org/10.1016/s0065-230x(04)92005-2).
- Bulleid, N.J., Wilson, R. and Lees, J.F. (1996) 'Type-III procollagen assembly in semi-intact cells: chain association, nucleation and triple-helix folding do not require formation of inter-chain disulphide bonds but triple-helix nucleation does require hydroxylation', *Biochemical Journal*, pp. 195–202. Available at: <https://doi.org/10.1042/bj3170195>.
- Bunk, J. *et al.* (2021) 'Cathepsin D Variants Associated With Neurodegenerative Diseases Show Dysregulated Functionality and Modified α -Synuclein Degradation Properties', *Frontiers in cell and developmental biology*, 9, p. 581805.
- Burgdorf, S., Lukacs-Kornek, V. and Kurts, C. (2006) 'The Mannose Receptor Mediates Uptake of Soluble but Not of Cell-Associated Antigen for Cross-Presentation', *The Journal of Immunology*, 176(11), pp. 6770–6776.

- Burgeson, R.E. *et al.* (1994) 'A new nomenclature for the laminins', *Matrix biology: journal of the International Society for Matrix Biology*, 14(3), pp. 209–211.
- Busby, T. *et al.* (2017) 'The Arf activator GBF1 localizes to plasma membrane sites involved in cell adhesion and motility', *Cellular logistics*, 7(2), p. e1308900.
- Byrne, G.J. *et al.* (2007) 'Angiogenic characteristics of circulating and tumoural thrombospondin-1 in breast cancer', *International journal of oncology*, 31(5), pp. 1127–1132.
- Calderwood, D.A., Shattil, S.J. and Ginsberg, M.H. (2000) 'Integrins and actin filaments: reciprocal regulation of cell adhesion and signaling', *The Journal of biological chemistry*, 275(30), pp. 22607–22610.
- Callewaert, B. *et al.* (2011) 'New insights into the pathogenesis of autosomal-dominant cutis laxa with report of five ELN mutations', *Human mutation*, 32(4), pp. 445–455.
- Cancer today, GLOBOCAN 2020* (no date) *World Health organization*. Available at: <https://gco.iarc.fr/today/home> (Accessed: 6 July 2022).
- Capuano, A. *et al.* (2019) 'Abrogation of EMILIN1- β 1 integrin interaction promotes experimental colitis and colon carcinogenesis', *Matrix biology: journal of the International Society for Matrix Biology*, 83, pp. 97–115.
- de Cárcer, G. *et al.* (2018) 'Plk1 overexpression induces chromosomal instability and suppresses tumor development', *Nature communications*, 9(1), p. 3012.
- Cardelli, J. (2001) 'Phagocytosis and macropinocytosis in Dictyostelium: phosphoinositide-based processes, biochemically distinct', *Traffic*, 2(5), pp. 311–320.
- Cargnello, M. and Roux, P.P. (2011) 'Activation and function of the MAPKs and their substrates, the MAPK-activated protein kinases', *Microbiology and molecular biology reviews: MMBR*, 75(1), pp. 50–83.
- Carlsen, S., Nandakumar, K.S. and Holmdahl, R. (2006) 'Type IX collagen deficiency enhances the binding of cartilage-specific antibodies and arthritis severity', *Arthritis research & therapy*, 8(4), p. R102.
- Carmeliet, P. and Jain, R.K. (2000) 'Angiogenesis in cancer and other diseases', *Nature*, 407(6801), pp. 249–257.
- Casalou, C., Faustino, A. and Barral, D.C. (2016) 'Arf proteins in cancer cell migration', *Small GTPases*, 7(4), pp. 270–282.
- Castellano, E. and Downward, J. (2011) 'RAS Interaction with PI3K: More Than Just Another Effector Pathway', *Genes & cancer*, 2(3), pp. 261–274.
- Castelló-Cros, R. *et al.* (2009) 'Staged stromal extracellular 3D matrices differentially regulate breast cancer cell responses through PI3K and beta1-integrins', *BMC cancer*, 9, p. 94.
- Caswell, P.T. *et al.* (2007) 'Rab25 associates with alpha5beta1 integrin to promote invasive migration in 3D microenvironments', *Developmental cell*, 13(4), pp. 496–510.
- Caswell, P.T. *et al.* (2008) 'Rab-coupling protein coordinates recycling of alpha5beta1 integrin and EGFR1 to promote cell migration in 3D microenvironments', *The Journal of cell biology*, 183(1), pp. 143–155.
- Cen, J. *et al.* (2019) 'Exosomal Thrombospondin-1 Disrupts the Integrity of Endothelial Intercellular Junctions to Facilitate Breast Cancer Cell Metastasis', *Cancers*, 11(12). Available at: <https://doi.org/10.3390/cancers11121946>.
- Cerqueira, O.L.D. *et al.* (2015) 'CIP4 promotes metastasis in triple-negative breast cancer and is associated with poor patient prognosis', *Oncotarget*, 6(11), pp. 9397–9408.
- Chaffer, C.L. and Weinberg, R.A. (2011) 'A perspective on cancer cell metastasis', *Science*, 331(6024), pp.

1559–1564.

Chakravarthi, S. *et al.* (2007) 'Intracellular catalysis of disulfide bond formation by the human sulphhydryl oxidase, QSOX1', *Biochemical Journal*, 404(3), pp. 403–411.

Chang, H. *et al.* (2020) 'P21 activated kinase-1 (PAK1) in macrophages is required for promotion of Th17 cell response during helminth infection', *Journal of cellular and molecular medicine*, 24(24), pp. 14325–14338.

Chang, J. *et al.* (2022) 'Discovery of ARF1-targeting inhibitor demethylzeylasteral as a potential agent against breast cancer', *Acta pharmaceutica Sinica. B*, 12(5), pp. 2619–2622.

Chan, K.T., Cortesio, C.L. and Huttenlocher, A. (2009) 'FAK alters invadopodia and focal adhesion composition and dynamics to regulate breast cancer invasion', *The Journal of cell biology*, 185(2), pp. 357–370.

Chan, P.M., Lim, L. and Manser, E. (2008) 'PAK is regulated by PI3K, PIX, CDC42, and PP2Calpha and mediates focal adhesion turnover in the hyperosmotic stress-induced p38 pathway', *The Journal of biological chemistry*, 283(36), pp. 24949–24961.

Chastney, M.R. *et al.* (2020) 'Topological features of integrin adhesion complexes revealed by multiplexed proximity biotinylation', *The Journal of cell biology*, 219(8). Available at: <https://doi.org/10.1083/jcb.202003038>.

Chaturvedi, V. *et al.* (2015) 'Interactions between Skeletal Muscle Myoblasts and their Extracellular Matrix Revealed by a Serum Free Culture System', *PloS one*, 10(6), p. e0127675.

Chaudhuri, O. *et al.* (2014) 'Extracellular matrix stiffness and composition jointly regulate the induction of malignant phenotypes in mammary epithelium', *Nature materials*, 13(10), pp. 970–978.

Chellaiah, M. *et al.* (1998) 'c-Src is required for stimulation of gelsolin-associated phosphatidylinositol 3-kinase', *The Journal of biological chemistry*, 273(19), pp. 11908–11916.

Chen, C. *et al.* (2018) 'The biology and role of CD44 in cancer progression: therapeutic implications', *Journal of hematology & oncology*, 11(1), p. 64.

Cheng, I.H. *et al.* (2011) 'Collagen VI protects against neuronal apoptosis elicited by ultraviolet irradiation via an Akt/phosphatidylinositol 3-kinase signaling pathway', *Neuroscience*, 183, pp. 178–188.

Cheng, K.W. *et al.* (2004) 'The RAB25 small GTPase determines aggressiveness of ovarian and breast cancers', *Nature medicine*, 10(11), pp. 1251–1256.

Chen, J.-W.E. *et al.* (2018) 'Influence of Hyaluronic Acid Transitions in Tumor Microenvironment on Glioblastoma Malignancy and Invasive Behavior', *Frontiers of materials science*, 5. Available at: <https://doi.org/10.3389/fmats.2018.00039>.

Chen, K. and Williams, K.J. (2013) 'Molecular mediators for raft-dependent endocytosis of syndecan-1, a highly conserved, multifunctional receptor', *The Journal of biological chemistry*, 288(20), pp. 13988–13999.

Chen, P.-H. *et al.* (2017) 'Crosstalk between CLCb/Dyn1-Mediated Adaptive Clathrin-Mediated Endocytosis and Epidermal Growth Factor Receptor Signaling Increases Metastasis', *Developmental cell*, 40(3), pp. 278–288.e5.

Chen, W.T. (1981) 'Mechanism of retraction of the trailing edge during fibroblast movement', *The Journal of cell biology*, 90(1), pp. 187–200.

Chen, W.T. (1989) 'Proteolytic activity of specialized surface protrusions formed at rosette contact sites

- of transformed cells', *The Journal of experimental zoology*, 251(2), pp. 167–185.
- Chen, X.-D. *et al.* (2004) 'The small leucine-rich proteoglycan biglycan modulates BMP-4-induced osteoblast differentiation', *FASEB journal: official publication of the Federation of American Societies for Experimental Biology*, 18(9), pp. 948–958.
- Chen, Y. *et al.* (2015) 'Lysyl hydroxylase 2 induces a collagen cross-link switch in tumor stroma', *The Journal of clinical investigation*, 125(3), pp. 1147–1162.
- Chen, Z. *et al.* (2013) 'p38 β , A novel regulatory target of Pokemon in hepatic cells', *International journal of molecular sciences*, 14(7), pp. 13511–13524.
- Chia, J. *et al.* (2012) 'RNAi screening reveals a large signaling network controlling the Golgi apparatus in human cells', *Molecular systems biology*, 8, p. 629.
- Chia, J. *et al.* (2020) 'Src activates retrograde membrane traffic through phosphorylation of GBF1', *Cold Spring Harbor Laboratory*. Available at: <https://doi.org/10.1101/2020.08.02.233353>.
- Chiquet-Ehrismann, R. *et al.* (1986) 'Tenascin: an extracellular matrix protein involved in tissue interactions during fetal development and oncogenesis', *Cell*, 47(1), pp. 131–139.
- Chiquet, M. (2020) 'Tenascin-C: From Discovery to Structure-Function Relationships', *Frontiers in immunology*, 11, p. 611789.
- Chiusa, M. *et al.* (2020) 'EGF receptor-mediated FUS phosphorylation promotes its nuclear translocation and fibrotic signaling', *The Journal of cell biology*, 219(9). Available at: <https://doi.org/10.1083/jcb.202001120>.
- Chow, C.R. *et al.* (2016) 'Cancer Cell Invasion in Three-dimensional Collagen Is Regulated Differentially by α 13 Protein and Discoidin Domain Receptor 1-Par3 Protein Signaling', *The Journal of biological chemistry*, 291(4), pp. 1605–1618.
- Chuma, M. *et al.* (2004) 'Overexpression of cortactin is involved in motility and metastasis of hepatocellular carcinoma', *Journal of hepatology*, 41(4), pp. 629–636.
- Chu, M.L. *et al.* (1989) 'Sequence analysis of alpha 1(VI) and alpha 2(VI) chains of human type VI collagen reveals internal triplication of globular domains similar to the A domains of von Willebrand factor and two alpha 2(VI) chain variants that differ in the carboxy terminus', *The EMBO journal*, 8(7), pp. 1939–1946.
- Chung, S. *et al.* (2009) 'Overexpressing PKIB in prostate cancer promotes its aggressiveness by linking between PKA and Akt pathways', *Oncogene*, 28(32), pp. 2849–2859.
- Chun, T.-H. *et al.* (2006) 'A pericellular collagenase directs the 3-dimensional development of white adipose tissue', *Cell*, 125(3), pp. 577–591.
- Chute, C. *et al.* (2018) 'Syndecan-1 induction in lung microenvironment supports the establishment of breast tumor metastases', *Breast cancer research: BCR*, 20(1), p. 66.
- Cianfrocca, M.E. *et al.* (2006) 'Phase 1 trial of the antiangiogenic peptide ATN-161 (Ac-PHSCN-NH(2)), a beta integrin antagonist, in patients with solid tumours', *British journal of cancer*, 94(11), pp. 1621–1626.
- Climer, L.K., Dobretsov, M. and Lupashin, V. (2015) 'Defects in the COG complex and COG-related trafficking regulators affect neuronal Golgi function', *Frontiers in neuroscience*, 9, p. 405.
- Codriansky, K.A. *et al.* (2009) 'Intracellular degradation of elastin by cathepsin K in skin fibroblasts--a possible role in photoaging', *Photochemistry and photobiology*, 85(6), pp. 1356–1363.
- Colak, S. and Ten Dijke, P. (2017) 'Targeting TGF- β Signaling in Cancer', *Trends in cancer research*, 3(1), pp. 56–71.

- Collins, B.M. *et al.* (2002) 'Molecular architecture and functional model of the endocytic AP2 complex', *Cell*, 109(4), pp. 523–535.
- Colombo, M. *et al.* (2003) 'Procollagen VII Self-Assembly Depends on Site-Specific Interactions and Is Promoted by Cleavage of the NC2 Domain with Procollagen C-Proteinase⁺', *Biochemistry*, pp. 11434–11442. Available at: <https://doi.org/10.1021/bi034925d>.
- Commisso, C. *et al.* (2013) 'Macropinocytosis of protein is an amino acid supply route in Ras-transformed cells', *Nature*, 497(7451), pp. 633–637.
- Commisso, C., Flinn, R.J. and Bar-Sagi, D. (2014) 'Determining the macropinocytic index of cells through a quantitative image-based assay', *Nature protocols*, 9(1), pp. 182–192.
- Coopman, P.J. *et al.* (1996) 'Integrin alpha 3 beta 1 participates in the phagocytosis of extracellular matrix molecules by human breast cancer cells', *Molecular biology of the cell*, 7(11), pp. 1789–1804.
- Coppock, D. *et al.* (2000) 'Regulation of the quiescence-induced genes: quiescin Q6, decorin, and ribosomal protein S29', *Biochemical and biophysical research communications*, 269(2), pp. 604–610.
- Corning® Matrigel® Matrix (no date) Corning® Matrigel® Matrix datasheet. Available at: <https://www.corning.com/catalog/cls/documents/faqs/CLS-DL-CC-026.pdf> (Accessed: 27 June 2023).
- da Costa, A.C. *et al.* (2020) 'Cathepsin S as a target in gastric cancer', *Molecular and clinical oncology*, 12(2), pp. 99–103.
- Couchman, J.R. (2003) 'Syndecans: proteoglycan regulators of cell-surface microdomains?', *Nature reviews. Molecular cell biology*, 4(12), pp. 926–937.
- Cox, R.F. and Morgan, M.P. (2013) 'Microcalcifications in breast cancer: Lessons from physiological mineralization', *Bone*, 53(2), pp. 437–450.
- Cox, T.R. *et al.* (2013) 'LOX-mediated collagen crosslinking is responsible for fibrosis-enhanced metastasis', *Cancer research*, 73(6), pp. 1721–1732.
- Cresens, C. *et al.* (2023) 'Flat clathrin lattices are linked to metastatic potential in colorectal cancer'. Available at: <https://doi.org/10.1101/2023.01.12.520576>.
- Curino, A.C. *et al.* (2005) 'Intracellular collagen degradation mediated by uPARAP/Endo180 is a major pathway of extracellular matrix turnover during malignancy', *The Journal of cell biology*, 169(6), pp. 977–985.
- Curry, J.M. *et al.* (2013) 'Cancer metabolism, stemness and tumor recurrence: MCT1 and MCT4 are functional biomarkers of metabolic symbiosis in head and neck cancer', *Cell cycle*, 12(9), pp. 1371–1384.
- Dai, J., Ting-Beall, H.P. and Sheetz, M.P. (1997) 'The secretion-coupled endocytosis correlates with membrane tension changes in RBL 2H3 cells', *The Journal of general physiology*, 110(1), pp. 1–10.
- Dalaka, E. *et al.* (2020) 'Direct measurement of vertical forces shows correlation between mechanical activity and proteolytic ability of invadopodia', *Science advances*, 6(11), p. eaax6912.
- Dalotto-Moreno, T. *et al.* (2013) 'Targeting galectin-1 overcomes breast cancer-associated immunosuppression and prevents metastatic disease', *Cancer research*, 73(3), pp. 1107–1117.
- Danussi, C. *et al.* (2011) 'EMILIN1- α 4/ α 9 integrin interaction inhibits dermal fibroblast and keratinocyte proliferation', *The Journal of cell biology*, 195(1), pp. 131–145.
- Davies, A.K. *et al.* (2018) 'AP-4 vesicles contribute to spatial control of autophagy via RUSC-dependent peripheral delivery of ATG9A', *Nature communications*, 9(1), p. 3958.
- Davies, H. *et al.* (2002) 'Mutations of the BRAF gene in human cancer', *Nature*, 417(6892), pp. 949–954.

- Davies, M.A. and Samuels, Y. (2010) 'Analysis of the genome to personalize therapy for melanoma', *Oncogene*, 29(41), pp. 5545–5555.
- Davis, G.E. (1992) 'Affinity of integrins for damaged extracellular matrix: alpha v beta 3 binds to denatured collagen type I through RGD sites', *Biochemical and biophysical research communications*, 182(3), pp. 1025–1031.
- Davis, J.E. *et al.* (2016) 'ARF1 promotes prostate tumorigenesis via targeting oncogenic MAPK signaling', *Oncotarget*, 7(26), pp. 39834–39845.
- Dawson, P.J. *et al.* (1996) 'MCF10AT: a model for the evolution of cancer from proliferative breast disease', *The American journal of pathology*, 148(1), pp. 313–319.
- Decaffmeyer, M. *et al.* (2008) 'Determination of the topology of the hydrophobic segment of mammalian diacylglycerol kinase epsilon in a cell membrane and its relationship to predictions from modeling', *Journal of molecular biology*, 383(4), pp. 797–809.
- De Franceschi, N. *et al.* (2016) 'Selective integrin endocytosis is driven by interactions between the integrin α -chain and AP2', *Nature structural & molecular biology*, 23(2), pp. 172–179.
- De Laporte, L. *et al.* (2013) 'Tenascin C promiscuously binds growth factors via its fifth fibronectin type III-like domain', *PloS one*, 8(4), p. e62076.
- Delarue, M. *et al.* (2014) 'Compressive stress inhibits proliferation in tumor spheroids through a volume limitation', *Biophysical journal*, 107(8), pp. 1821–1828.
- Dell'Angelica, E.C. (2009) 'AP-3-dependent trafficking and disease: the first decade', *Current opinion in cell biology*, 21(4), pp. 552–559.
- De Oliveira, T. *et al.* (2012) 'Syndecan-2 promotes perineural invasion and cooperates with K-ras to induce an invasive pancreatic cancer cell phenotype', *Molecular cancer*, 11, p. 19.
- Devy, L. *et al.* (2009) 'Selective inhibition of matrix metalloproteinase-14 blocks tumor growth, invasion, and angiogenesis', *Cancer research*, 69(4), pp. 1517–1526.
- DharmaFECT Cell Type Guide* (no date). Available at: <https://horizondiscovery.com/en/transfection-and-ancillary-reagents/dharmafect-cell-type-guide> (Accessed: 14 December 2022).
- Dharmawardhane, S. *et al.* (1999) 'Localization of p21-activated kinase 1 (PAK1) to pseudopodia, membrane ruffles, and phagocytic cups in activated human neutrophils', *Journal of leukocyte biology*, 66(3), pp. 521–527.
- Dharmawardhane, S. *et al.* (2000) 'Regulation of macropinocytosis by p21-activated kinase-1', *Molecular biology of the cell*, 11(10), pp. 3341–3352.
- Diab, M., Wu, J.J. and Eyre, D.R. (1996) 'Collagen type IX from human cartilage: a structural profile of intermolecular cross-linking sites', *Biochemical Journal*, 314 (Pt 1), pp. 327–332.
- Diamantopoulou, Z. *et al.* (2012) 'Loss of receptor protein tyrosine phosphatase β/ζ (RPTP β/ζ) promotes prostate cancer metastasis', *The Journal of biological chemistry*, 287(48), pp. 40339–40349.
- Dix, C.L. *et al.* (2018) 'The Role of Mitotic Cell-Substrate Adhesion Re-modeling in Animal Cell Division', *Developmental cell*, 45(1), pp. 132–145.e3.
- Dong, Z. *et al.* (2013) 'Leptin-mediated regulation of MT1-MMP localization is KIF1B dependent and enhances gastric cancer cell invasion', *Carcinogenesis*, 34(5), pp. 974–983.
- Donkervoort, S. *et al.* (2021) 'BET1 variants establish impaired vesicular transport as a cause for muscular dystrophy with epilepsy', *EMBO molecular medicine*, 13(12), p. e13787.

- Dornier, E. *et al.* (2017) 'Glutaminolysis drives membrane trafficking to promote invasiveness of breast cancer cells', *Nature communications*, 8(1), p. 2255.
- Dozynkiewicz, M.A. *et al.* (2012) 'Rab25 and CLIC3 collaborate to promote integrin recycling from late endosomes/lysosomes and drive cancer progression', *Developmental cell*, 22(1), pp. 131–145.
- Driscoll, D.L. *et al.* (2014) 'Plk1 inhibition causes post-mitotic DNA damage and senescence in a range of human tumor cell lines', *PloS one*, 9(11), p. e111060.
- D'Souza, R.S. *et al.* (2020) 'Calcium-stimulated disassembly of focal adhesions mediated by an ORP3/IQSec1 complex', *eLife*, 9. Available at: <https://doi.org/10.7554/eLife.54113>.
- Duan, Q. *et al.* (2019) 'High glucose promotes pancreatic cancer cells to escape from immune surveillance via AMPK-Bmi1-GATA2-MICA/B pathway', *Journal of experimental & clinical cancer research: CR*, 38(1). Available at: <https://doi.org/10.1186/s13046-019-1209-9>.
- Dufour, A. and Overall, C.M. (2013) 'Missing the target: matrix metalloproteinase antitargets in inflammation and cancer', *Trends in pharmacological sciences*, 34(4), pp. 233–242.
- Duperret, E.K., Dahal, A. and Ridky, T.W. (2015) 'Focal-adhesion-independent integrin- α regulation of FAK and c-Myc is necessary for 3D skin formation and tumor invasion', *Journal of cell science*, 128(21), pp. 3997–4013.
- Düzgün, Ş.A. *et al.* (2017) 'Differential effects of p38 MAP kinase inhibitors SB203580 and SB202190 on growth and migration of human MDA-MB-231 cancer cell line', *Cytotechnology*, 69(4), pp. 711–724.
- Dzamba, B.J. *et al.* (1993) 'Fibronectin binding site in type I collagen regulates fibronectin fibril formation', *The Journal of cell biology*, 121(5), pp. 1165–1172.
- Eagle, H. and Harris, T.N. (1937) 'STUDIES IN BLOOD COAGULATION : V. THE COAGULATION OF BLOOD BY PROTEOLYTIC ENZYMES (TRYPSIN, PAPAINE)', *The Journal of general physiology*, 20(4), pp. 543–560.
- Eckert, M.A. *et al.* (2011) 'Twist1-induced invadopodia formation promotes tumor metastasis', *Cancer cell*, 19(3), pp. 372–386.
- Edwards, D.R. *et al.* (1987) 'Transforming growth factor beta modulates the expression of collagenase and metalloproteinase inhibitor', *The EMBO journal*, 6(7), pp. 1899–1904.
- Egeblad, M., Nakasone, E.S. and Werb, Z. (2010) 'Tumors as organs: complex tissues that interface with the entire organism', *Developmental cell*, 18(6), pp. 884–901.
- Egging, D. *et al.* (2007) 'Interactions of human tenascin-X domains with dermal extracellular matrix molecules', *Archives for dermatological research. Archiv fur dermatologische Forschung*, 298(8), pp. 389–396.
- El Azreq, M.-A. *et al.* (2016) 'Discoidin domain receptor 1 promotes Th17 cell migration by activating the RhoA/ROCK/MAPK/ERK signaling pathway', *Oncotarget*, 7(29), pp. 44975–44990.
- Egundi, Z. *et al.* (2019) 'Cancer Metastasis: The Role of the Extracellular Matrix and the Heparan Sulfate Proteoglycan Perlecan', *Frontiers in oncology*, 9, p. 1482.
- Elkin, S.R., Lakoduk, A.M. and Schmid, S.L. (2016) 'Endocytic pathways and endosomal trafficking: a primer', *Wiener medizinische Wochenschrift*, 166(7-8), pp. 196–204.
- Engelholm, L.H. *et al.* (2001) 'The urokinase receptor associated protein (uPARAP/endo180): a novel internalization receptor connected to the plasminogen activation system', *Trends in cardiovascular medicine*, 11(1), pp. 7–13.
- Engel, J. *et al.* (1981) 'Shapes, domain organizations and flexibility of laminin and fibronectin, two

multifunctional proteins of the extracellular matrix', *Journal of molecular biology*, 150(1), pp. 97–120.

Engel, J. *et al.* (1985) 'Structure and macromolecular organization of type VI collagen', *Annals of the New York Academy of Sciences*, 460, pp. 25–37.

Epanand, R.M. *et al.* (2016) 'Diacylglycerol Kinase- ϵ : Properties and Biological Roles', *Frontiers in cell and developmental biology*, 4, p. 112.

Eppinga, R.D. *et al.* (2012) 'Increased expression of the large GTPase dynamin 2 potentiates metastatic migration and invasion of pancreatic ductal carcinoma', *Oncogene*, 31(10), pp. 1228–1241.

Erhard Hohenester, P.D.Y. (2013) 'Laminins in basement membrane assembly', *Cell adhesion & migration*, 7(1), p. 56.

Eskelinen, E.-L. *et al.* (2002) 'Role of LAMP-2 in lysosome biogenesis and autophagy', *Molecular biology of the cell*, 13(9), pp. 3355–3368.

Esser, S. *et al.* (1998) 'Vascular endothelial growth factor induces endothelial fenestrations in vitro', *The Journal of cell biology*, 140(4), pp. 947–959.

Etoh, T. *et al.* (1993) 'Role of integrin alpha 2 beta 1 (VLA-2) in the migration of human melanoma cells on laminin and type IV collagen', *The Journal of investigative dermatology*, 100(5), pp. 640–647.

Ezratty, E.J. *et al.* (2009) 'Clathrin mediates integrin endocytosis for focal adhesion disassembly in migrating cells', *The Journal of cell biology*, 187(5), pp. 733–747.

Fairhead, M. and Howarth, M. (2015) 'Site-specific biotinylation of purified proteins using BirA', *Methods in molecular biology*, 1266, pp. 171–184.

Fan, M.-H. *et al.* (2016) 'Fibroblast Activation Protein (FAP) Accelerates Collagen Degradation and Clearance from Lungs in Mice', *The Journal of biological chemistry*, 291(15), pp. 8070–8089.

Farnedi, A. *et al.* (2015) 'Proteoglycan-based diversification of disease outcome in head and neck cancer patients identifies NG2/CSPG4 and syndecan-2 as unique relapse and overall survival predicting factors', *BMC cancer*, 15, p. 352.

Faubert, B., Solmonson, A. and DeBerardinis, R.J. (2020) 'Metabolic reprogramming and cancer progression', *Science*, 368(6487). Available at: <https://doi.org/10.1126/science.aaw5473>.

Faundez, V.V. and Kelly, R.B. (2000) 'The AP-3 complex required for endosomal synaptic vesicle biogenesis is associated with a casein kinase I α -like isoform', *Molecular biology of the cell*, 11(8), pp. 2591–2604.

Feist, P. and Hummon, A.B. (2015) 'Proteomic challenges: sample preparation techniques for microgram-quantity protein analysis from biological samples', *International journal of molecular sciences*, 16(2), pp. 3537–3563.

Feldman, T. *et al.* (2020) 'Inhibition of fibroblast secreted QSOX1 perturbs extracellular matrix in the tumor microenvironment and decreases tumor growth and metastasis in murine cancer models', *Oncotarget*, 11(4), pp. 386–398.

Fernandez-Zapico, M.E. *et al.* (2005) 'Ectopic expression of VAV1 reveals an unexpected role in pancreatic cancer tumorigenesis', *Cancer cell*, 7(1), pp. 39–49.

Fernow, I., Icking, A. and Tikkanen, R. (2007) 'Reggie-1 and reggie-2 localize in non-caveolar rafts in epithelial cells: cellular localization is not dependent on the expression of caveolin proteins', *European journal of cell biology*, 86(6), pp. 345–352.

Fidler, A.L. *et al.* (2017) 'Collagen IV and basement membrane at the evolutionary dawn of metazoan tissues', *eLife*, 6. Available at: <https://doi.org/10.7554/eLife.24176>.

Fischer, H. *et al.* (2001) 'Colorectal carcinogenesis is associated with stromal expression of COL11A1 and COL5A2', *Carcinogenesis*, 22(6), pp. 875–878.

Fitzgerald, J. *et al.* (2001) 'The N-terminal N5 Subdomain of the $\alpha 3$ (VI) Chain Is Important for Collagen VI Microfibril Formation', *Journal of Biological Chemistry*, pp. 187–193. Available at: <https://doi.org/10.1074/jbc.m008173200>.

Fitzpatrick, L.E. and McDevitt, T.C. (2015) 'Cell-derived matrices for tissue engineering and regenerative medicine applications', *Biomaterials science*, 3(1), pp. 12–24.

Fonović, M. and Turk, B. (2014) 'Cysteine cathepsins and extracellular matrix degradation', *Biochimica et Biophysica Acta (BBA) - General Subjects*, pp. 2560–2570. Available at: <https://doi.org/10.1016/j.bbagen.2014.03.017>.

Fontanil, T. *et al.* (2017) 'Cleavage of Fibulin-2 by the aggrecanases ADAMTS-4 and ADAMTS-5 contributes to the tumorigenic potential of breast cancer cells', *Oncotarget*, 8(8), pp. 13716–13729.

Fox, J.W. *et al.* (1991) 'Recombinant nidogen consists of three globular domains and mediates binding of laminin to collagen type IV', *The EMBO journal*, 10(11), pp. 3137–3146.

FR180204 (CAS 865362-74-9) (no date). Available at: <https://www.caymanchem.com/product/15544> (Accessed: 12 January 2023).

Frantz, C., Stewart, K.M. and Weaver, V.M. (2010) 'The extracellular matrix at a glance', *Journal of cell science*, 123(Pt 24), pp. 4195–4200.

Frenette, G.P. *et al.* (1988) 'Biosynthesis and secretion of laminin and laminin-associated glycoproteins by nonmalignant and malignant human keratinocytes: comparison of cell lines from primary and secondary tumors in the same patient', *Cancer research*, 48(18), pp. 5193–5202.

Frittoli, E. *et al.* (2014) 'A RAB5/RAB4 recycling circuitry induces a proteolytic invasive program and promotes tumor dissemination', *The Journal of cell biology*, 206(2), pp. 307–328.

Frolova, E.G. *et al.* (2012) 'Thrombospondin-4 regulates fibrosis and remodeling of the myocardium in response to pressure overload', *FASEB journal: official publication of the Federation of American Societies for Experimental Biology*, 26(6), pp. 2363–2373.

Frosch, B.A. *et al.* (1999) 'Molecular regulation, membrane association and secretion of tumor cathepsin B', *APMIS*, pp. 28–37. Available at: <https://doi.org/10.1111/j.1699-0463.1999.tb01523.x>.

Fuchs, R., Mâle, P. and Mellman, I. (1989) 'Acidification and ion permeabilities of highly purified rat liver endosomes', *The Journal of biological chemistry*, 264(4), pp. 2212–2220.

Fu, H.-L. *et al.* (2013) 'Discoidin domain receptors: unique receptor tyrosine kinases in collagen-mediated signaling', *The Journal of biological chemistry*, 288(11), pp. 7430–7437.

Fu, M.X. *et al.* (1994) 'Glycation, glycoxidation, and cross-linking of collagen by glucose. Kinetics, mechanisms, and inhibition of late stages of the Maillard reaction', *Diabetes*, 43(5), pp. 676–683.

Fuster, M.M. and Esko, J.D. (2005) 'The sweet and sour of cancer: glycans as novel therapeutic targets', *Nature reviews. Cancer*, 5(7), pp. 526–542.

Futter, C.E. *et al.* (2001) 'Human VPS34 is required for internal vesicle formation within multivesicular endosomes', *The Journal of cell biology*, 155(7), pp. 1251–1264.

Gallagher, E. *et al.* (2007) 'Kinase MEKK1 is required for CD40-dependent activation of the kinases Jnk and p38, germinal center formation, B cell proliferation and antibody production', *Nature immunology*, 8(1), pp. 57–63.

- Gallagher, E.D. *et al.* (2002) 'Binding of JNK/SAPK to MEKK1 is regulated by phosphorylation', *The Journal of biological chemistry*, 277(48), pp. 45785–45792.
- Gao, Z. *et al.* (2020) 'PLK1 promotes proliferation and suppresses apoptosis of renal cell carcinoma cells by phosphorylating MCM3', *Cancer gene therapy*, 27(6), pp. 412–423.
- Garrett, W.S. *et al.* (2000) 'Developmental control of endocytosis in dendritic cells by Cdc42', *Cell*, 102(3), pp. 325–334.
- Garrett, W.S. and Mellman, I. (2001) 'Studies of endocytosis', in *Dendritic Cells*. Elsevier, pp. 213–cp1.
- Gauthier-Rouvière, C. *et al.* (2020) 'Flotillin membrane domains in cancer', *Cancer metastasis reviews*, 39(2), pp. 361–374.
- Gebb, C. *et al.* (1986) 'Interaction of vitronectin with collagen', *The Journal of biological chemistry*, 261(35), pp. 16698–16703.
- Geiger, P. *et al.* (2016) 'Binding of galectin-1 to breast cancer cells MCF7 induces apoptosis and inhibition of proliferation in vitro in a 2D- and 3D- cell culture model', *BMC cancer*, 16(1), p. 870.
- Genna, A. *et al.* (2018) 'Pyk2 and FAK differentially regulate invadopodia formation and function in breast cancer cells', *The Journal of cell biology*, 217(1), pp. 375–395.
- Gerl, M. *et al.* (1991) 'Localization of a major nidogen-binding site to domain III of laminin B2 chain', *European journal of biochemistry / FEBS*, 202(1), pp. 167–174.
- Ghura, H. *et al.* (2021) 'Inhibition of fibronectin accumulation suppresses tumor growth', *Neoplasia*, 23(9), pp. 837–850.
- Giatromanolaki, A. *et al.* (2012) 'The metabolic interactions between tumor cells and tumor-associated stroma (TAS) in prostatic cancer', *Cancer biology & therapy*, 13(13), pp. 1284–1289.
- Gilbert, C.E., Sztul, E. and Machamer, C.E. (2018) 'Commonly used trafficking blocks disrupt ARF1 activation and the localization and function of specific Golgi proteins', *Molecular biology of the cell*, 29(8), pp. 937–947.
- Glebov, O.O., Bright, N.A. and Nichols, B.J. (2006) 'Flotillin-1 defines a clathrin-independent endocytic pathway in mammalian cells', *Nature cell biology*, 8(1), pp. 46–54.
- Goetz, J.G. *et al.* (2008) 'Caveolin-1 in tumor progression: the good, the bad and the ugly', *Cancer metastasis reviews*, 27(4), pp. 715–735.
- Goicoechea, S. *et al.* (2000) 'Thrombospondin mediates focal adhesion disassembly through interactions with cell surface calreticulin', *The Journal of biological chemistry*, 275(46), pp. 36358–36368.
- Gomez, D.E. *et al.* (1997) 'Tissue inhibitors of metalloproteinases: structure, regulation and biological functions', *European journal of cell biology*, 74(2), pp. 111–122.
- Gonzalo, P. *et al.* (2010) 'MT1-MMP is required for myeloid cell fusion via regulation of Rac1 signaling', *Developmental cell*, 18(1), pp. 77–89.
- Gopalakrishna, R. *et al.* (2018) 'Laminin-1 induces endocytosis of 67KDa laminin receptor and protects Neuroscreen-1 cells against death induced by serum withdrawal', *Biochemical and biophysical research communications*, 495(1), pp. 230–237.
- Gopinathan, A. *et al.* (2012) 'Cathepsin B promotes the progression of pancreatic ductal adenocarcinoma in mice', *Gut*, 61(6), pp. 877–884.
- Gordon, S. (2016) 'Phagocytosis: An Immunobiologic Process', *Immunity*, 44(3), pp. 463–475.

- Gorlewicz, A. *et al.* (2020) 'Colocalization Colormap -an ImageJ Plugin for the Quantification and Visualization of Colocalized Signals', *Neuroinformatics*, 18(4), pp. 661–664.
- Grafinger, O.R. *et al.* (2020) 'β1 integrin-mediated signaling regulates MT1-MMP phosphorylation to promote tumor cell invasion', *Journal of cell science*, 133(9). Available at: <https://doi.org/10.1242/jcs.239152>.
- Graham, D.R.M., Elliott, S.T. and Van Eyk, J.E. (2005) 'Broad-based proteomic strategies: a practical guide to proteomics and functional screening', *The Journal of physiology*, 563(Pt 1), pp. 1–9.
- Gramann, M. *et al.* (2009) 'Prominent collagen type VI expression in juvenile angiofibromas', *Histochemistry and cell biology*, 131(1), pp. 155–164.
- Greco, M.R. *et al.* (2021) 'Integrin-Linked Kinase Links Integrin Activation to Invadopodia Function and Invasion via the p(T567)-Ezrin/NHERF1/NHE1 Pathway', *International journal of molecular sciences*, 22(4). Available at: <https://doi.org/10.3390/ijms22042162>.
- Gregori, A. *et al.* (2023) 'Prognostic significance of integrin subunit alpha 2 (ITGA2) and role of mechanical cues in resistance to gemcitabine in pancreatic ductal adenocarcinoma (PDAC)', *Cancers*, 15(3), p. 628.
- Gress, T.M. *et al.* (1995) 'Expression and in-situ localization of genes coding for extracellular matrix proteins and extracellular matrix degrading proteases in pancreatic cancer', *International journal of cancer. Journal international du cancer*, 62(4), pp. 407–413.
- Greyner, H.J. *et al.* (2010) 'Inducible macropinocytosis of hyaluronan in B16-F10 melanoma cells', *Matrix biology: journal of the International Society for Matrix Biology*, 29(6), pp. 503–510.
- Grinnell, F., Billingham, R.E. and Burgess, L. (1981) 'Distribution of fibronectin during wound healing in vivo', *The Journal of investigative dermatology*, 76(3), pp. 181–189.
- Gross, J. and Kirk, D. (1958) 'The heat precipitation of collagen from neutral salt solutions: some rate-regulating factors', *The Journal of biological chemistry*, 233(2), pp. 355–360.
- Grumati, P. *et al.* (2010) 'Autophagy is defective in collagen VI muscular dystrophies, and its reactivation rescues myofiber degeneration', *Nature medicine*, 16(11), pp. 1313–1320.
- Guan, J.-L. (2010) 'Integrin signaling through FAK in the regulation of mammary stem cells and breast cancer', *IUBMB life*, 62(4), pp. 268–276.
- Guarino, M. (2010) 'Src signaling in cancer invasion', *Journal of cellular physiology*, 223(1), pp. 14–26.
- Guinec, N., Dalet-Fumeron, V. and Pagano, M. (1993) "'In vitro" study of basement membrane degradation by the cysteine proteinases, cathepsins B, B-like and L. Digestion of collagen IV, laminin, fibronectin, and release of gelatinase activities from basement membrane fibronectin', *Biological chemistry Hoppe-Seyler*, 374(12), pp. 1135–1146.
- Gunaydin, G. (2021) 'CAFs Interacting With TAMs in Tumor Microenvironment to Enhance Tumorigenesis and Immune Evasion', *Frontiers in oncology*, 11, p. 668349.
- Guo, Q., Yang, C. and Gao, F. (2021) 'The state of CD44 activation in cancer progression and therapeutic targeting', *The FEBS journal* [Preprint]. Available at: <https://doi.org/10.1111/febs.16179>.
- Gupta, R., Woodley, D.T. and Chen, M. (2012) 'Epidermolysis bullosa acquisita', *Clinics in dermatology*, 30(1), pp. 60–69.
- Gurel Cayir, E. *et al.* (2020) 'Preliminary study of serum Galectin-1 in breast cancer carcinogenesis [Izmir Oncology Group (IZOG) study]', *Journal of B.U.ON.: official journal of the Balkan Union of Oncology*, 25(2), pp. 675–680.

- Gu, Z. *et al.* (2011) 'Integrins traffic rapidly via circular dorsal ruffles and macropinocytosis during stimulated cell migration', *The Journal of cell biology*, 193(1), pp. 61–70.
- Hamadi, A. *et al.* (2005) 'Regulation of focal adhesion dynamics and disassembly by phosphorylation of FAK at tyrosine 397', *Journal of cell science*, 118(Pt 19), pp. 4415–4425.
- Hanahan, D. (2022) 'Hallmarks of Cancer: New Dimensions', *Cancer discovery*, 12(1), pp. 31–46.
- Hanahan, D. and Weinberg, R.A. (2000) 'The hallmarks of cancer', *Cell*, 100(1), pp. 57–70.
- Hanahan, D. and Weinberg, R.A. (2011) 'Hallmarks of cancer: the next generation', *Cell*, 144(5), pp. 646–674.
- Hanayama, R. *et al.* (2002) 'Identification of a factor that links apoptotic cells to phagocytes', *Nature*, 417(6885), pp. 182–187.
- Harris, J.R. and Reiber, A. (2007) 'Influence of saline and pH on collagen type I fibrillogenesis in vitro: fibril polymorphism and colloidal gold labelling', *Micron*, 38(5), pp. 513–521.
- Harvey, S.J. and Thorner, P.S. (2005) 'Type IV collagen: A network for development, differentiation, and disease', in *Extracellular Matrix in Development and Disease*. Elsevier (Advances in developmental biology (Amsterdam, Netherlands)), pp. 1–64.
- Hatsuzawa, K. *et al.* (2009) 'Sec22b is a negative regulator of phagocytosis in macrophages', *Molecular biology of the cell*, 20(20), pp. 4435–4443.
- Henley, J.R. *et al.* (1998) 'Dynamin-mediated internalization of caveolae', *The Journal of cell biology*, 141(1), pp. 85–99.
- Henneke, I. *et al.* (2010) 'Inhibition of urokinase activity reduces primary tumor growth and metastasis formation in a murine lung carcinoma model', *American journal of respiratory and critical care medicine*, 181(6), pp. 611–619.
- Henne, W.M. *et al.* (2010) 'FCHo proteins are nucleators of clathrin-mediated endocytosis', *Science*, 328(5983), pp. 1281–1284.
- Herron, J.C. *et al.* (2022) 'Spatial models of pattern formation during phagocytosis', *PLoS computational biology*, 18(10), p. e1010092.
- Hetmanski, J.H.R. *et al.* (2019) 'Membrane Tension Orchestrates Rear Retraction in Matrix-Directed Cell Migration', *Developmental cell*, 51(4), pp. 460–475.e10.
- Heuser, J. (1980) 'Three-dimensional visualization of coated vesicle formation in fibroblasts', *The Journal of cell biology*, 84(3), pp. 560–583.
- Hinton, A. *et al.* (2009) 'Function of a subunit isoforms of the V-ATPase in pH homeostasis and in vitro invasion of MDA-MB231 human breast cancer cells', *The Journal of biological chemistry*, 284(24), pp. 16400–16408.
- Hohendahl, A. *et al.* (2017) 'Structural inhibition of dynamin-mediated membrane fission by endophilin', *eLife*, 6. Available at: <https://doi.org/10.7554/eLife.26856>.
- Hohenester, E. *et al.* (1999) 'The crystal structure of a laminin G-like module reveals the molecular basis of alpha-dystroglycan binding to laminins, perlecan, and agrin', *Molecular cell*, 4(5), pp. 783–792.
- Hohenester, E. (2019) 'Structural biology of laminins', *Essays in Biochemistry*, pp. 285–295. Available at: <https://doi.org/10.1042/ebc20180075>.
- Hoijman, E. *et al.* (2021) 'Cooperative epithelial phagocytosis enables error correction in the early embryo', *Nature*, 590(7847), pp. 618–623.

- Holling, T. *et al.* (2022) 'A homozygous hypomorphic BNIP1 variant causes an increase in autophagosomes and reduced autophagic flux and results in a spondylo-epiphyseal dysplasia', *Human mutation*, 43(5), pp. 625–642.
- Holstein, E. *et al.* (2021) 'The Burden of Post-Translational Modification (PTM)—Disrupting Mutations in the Tumor Matrisome', *Cancers*, 13(5), p. 1081.
- Höning, S., Sandoval, I.V. and von Figura, K. (1998) 'A di-leucine-based motif in the cytoplasmic tail of LIMP-II and tyrosinase mediates selective binding of AP-3', *The EMBO journal*, 17(5), pp. 1304–1314.
- Hook, G., Hook, V. and Kindy, M. (2011) 'The cysteine protease inhibitor, E64d, reduces brain amyloid- β and improves memory deficits in Alzheimer's disease animal models by inhibiting cathepsin B, but not BACE1, β -secretase activity', *Journal of Alzheimer's disease: JAD*, 26(2), pp. 387–408.
- Hotary, K. *et al.* (2006) 'A cancer cell metalloprotease triad regulates the basement membrane transmigration program', *Genes & development*, 20(19), pp. 2673–2686.
- Hou, S. *et al.* (2016) 'Distinct effects of β 1 integrin on cell proliferation and cellular signaling in MDA-MB-231 breast cancer cells', *Scientific reports*, 6, p. 18430.
- Howes, M.T. *et al.* (2010) 'Clathrin-independent carriers form a high capacity endocytic sorting system at the leading edge of migrating cells', *The Journal of cell biology*, 190(4), pp. 675–691.
- Huang, L. *et al.* (2021) 'KRAS mutation: from undruggable to druggable in cancer', *Signal transduction and targeted therapy*, 6(1), p. 386.
- Huang, W. *et al.* (2001) 'Interference of tenascin-C with syndecan-4 binding to fibronectin blocks cell adhesion and stimulates tumor cell proliferation', *Cancer research*, 61(23), pp. 8586–8594.
- Huang, Y. *et al.* (2018) 'Collagen Type VI Alpha 3 Chain Promotes Epithelial-Mesenchymal Transition in Bladder Cancer Cells via Transforming Growth Factor β (TGF- β)/Smad Pathway', *Medical science monitor: international medical journal of experimental and clinical research*, 24, pp. 5346–5354.
- Hu, C. *et al.* (2012) 'Opposite regulation by PI3K/Akt and MAPK/ERK pathways of tissue factor expression, cell-associated procoagulant activity and invasiveness in MDA-MB-231 cells', *Journal of hematology & oncology*, 5, p. 16.
- Hughes, P.E. *et al.* (1997) 'Suppression of integrin activation: a novel function of a Ras/Raf-initiated MAP kinase pathway', *Cell*, 88(4), pp. 521–530.
- Hu, J. *et al.* (2011) 'Cdc42-interacting protein 4 is a Src substrate that regulates invadopodia and invasiveness of breast tumors by promoting MT1-MMP endocytosis', *Journal of cell science*, 124(Pt 10), pp. 1739–1751.
- Hu, K. *et al.* (2007) 'Differential transmission of actin motion within focal adhesions', *Science*, 315(5808), pp. 111–115.
- Hu, L. *et al.* (2014) 'Biglycan enhances gastric cancer invasion by activating FAK signaling pathway', *Oncotarget*, 5(7), pp. 1885–1896.
- Humphries, J.D., Byron, A. and Humphries, M.J. (2006) 'Integrin ligands at a glance', *Journal of cell science*, 119(Pt 19), pp. 3901–3903.
- Huth, H.W. *et al.* (2016) 'MEK2 controls the activation of MKK3/MKK6-p38 axis involved in the MDA-MB-231 breast cancer cell survival: Correlation with cyclin D1 expression', *Cellular signalling*, 28(9), pp. 1283–1291.
- Huth, H.W. *et al.* (2017) 'Upregulation of p38 pathway accelerates proliferation and migration of MDA-

- MB-231 breast cancer cells', *Oncology reports*, 37(4), pp. 2497–2505.
- Huynh-Do, U. *et al.* (1999) 'Surface densities of ephrin-B1 determine EphB1-coupled activation of cell attachment through alphavbeta3 and alpha5beta1 integrins', *The EMBO journal*, 18(8), pp. 2165–2173.
- Hynes, R.O. (2002) 'Integrins: bidirectional, allosteric signaling machines', *Cell*, 110(6), pp. 673–687.
- Hynes, R.O. and Naba, A. (2012) 'Overview of the matrisome--an inventory of extracellular matrix constituents and functions', *Cold Spring Harbor perspectives in biology*, 4(1), p. a004903.
- Hynes, R.O. and Yamada, K.M. (1982) 'Fibronectins: multifunctional modular glycoproteins', *The Journal of cell biology*, 95(2 Pt 1), pp. 369–377.
- Ibrahim, A.M. *et al.* (2018) 'Fibulin-2 is required for basement membrane integrity of mammary epithelium', *Scientific reports*, 8(1), p. 14139.
- Igea, A. and Nebreda, A.R. (2015) 'The Stress Kinase p38 α as a Target for Cancer Therapy', *Cancer research*, 75(19), pp. 3997–4002.
- Ilani, T. *et al.* (2013) 'A secreted disulfide catalyst controls extracellular matrix composition and function', *Science*, 341(6141), pp. 74–76.
- Imai, K. *et al.* (1994) 'Susceptibility of tenascin to degradation by matrix metalloproteinases and serine proteinases', *FEBS letters*, 352(2), pp. 216–218.
- Imai, K. *et al.* (1997) 'Degradation of decorin by matrix metalloproteinases: identification of the cleavage sites, kinetic analyses and transforming growth factor-beta1 release', *Biochemical Journal*, 322 (Pt 3), pp. 809–814.
- Infante, E. *et al.* (2018) 'LINC complex-Lis1 interplay controls MT1-MMP matrix digest-on-demand response for confined tumor cell migration', *Nature communications*, 9(1), p. 2443.
- Innocenti, M. *et al.* (2003) 'Phosphoinositide 3-kinase activates Rac by entering in a complex with Eps8, Abi1, and Sos-1', *The Journal of cell biology*, 160(1), pp. 17–23.
- Innocenti, M. *et al.* (2005) 'Abi1 regulates the activity of N-WASP and WAVE in distinct actin-based processes', *Nature cell biology*, 7(10), pp. 969–976.
- Ishikawa, T. *et al.* (2014) 'Laminins 411 and 421 differentially promote tumor cell migration via $\alpha 6\beta 1$ integrin and MCAM (CD146)', *Matrix biology: journal of the International Society for Matrix Biology*, 38, pp. 69–83.
- Ito, A. *et al.* (2000) 'A truncated isoform of the PP2A B56 subunit promotes cell motility through paxillin phosphorylation', *The EMBO journal*, 19(4), pp. 562–571.
- Ivanov, A.I. (2008) 'Pharmacological inhibition of endocytic pathways: is it specific enough to be useful?', *Methods in molecular biology*, 440, pp. 15–33.
- Ivaska, J. *et al.* (1999) 'Integrin alpha2beta1 mediates isoform-specific activation of p38 and upregulation of collagen gene transcription by a mechanism involving the alpha2 cytoplasmic tail', *The Journal of cell biology*, 147(2), pp. 401–416.
- Ivaska, J. and Heino, J. (2010) 'Interplay between cell adhesion and growth factor receptors: from the plasma membrane to the endosomes', *Cell and tissue research*, 339(1), pp. 111–120.
- Izzi, V., Davis, M.N. and Naba, A. (2020) 'Pan-Cancer Analysis of the Genomic Alterations and Mutations of the Matrisome', *Cancers*, 12(8). Available at: <https://doi.org/10.3390/cancers12082046>.
- Jabłońska-Trypuć, A., Matejczyk, M. and Rosochacki, S. (2016) 'Matrix metalloproteinases (MMPs), the main extracellular matrix (ECM) enzymes in collagen degradation, as a target for anticancer drugs', *Journal*

of enzyme inhibition and medicinal chemistry, 31(sup1), pp. 177–183.

Jacob, A. *et al.* (2013) 'Rab40b regulates trafficking of MMP2 and MMP9 during invadopodia formation and invasion of breast cancer cells', *Journal of cell science*, 126(Pt 20), pp. 4647–4658.

Jacobsen, F. *et al.* (2017) 'Up-regulation of Biglycan is Associated with Poor Prognosis and PTEN Deletion in Patients with Prostate Cancer', *Neoplasia*, 19(9), pp. 707–715.

Janssens, V. *et al.* (2016) 'PP2A binds to the LIM domains of lipoma-preferred partner through its PR130/B" subunit to regulate cell adhesion and migration', *Journal of cell science*, 129(8), pp. 1605–1618.

Janvier, K. *et al.* (2003) 'Recognition of dileucine-based sorting signals from HIV-1 Nef and LIMP-II by the AP-1 gamma-sigma1 and AP-3 delta-sigma3 hemicomplexes', *The Journal of cell biology*, 163(6), pp. 1281–1290.

Jaskolski, F., Mulle, C. and Manzoni, O.J. (2005) 'An automated method to quantify and visualize colocalized fluorescent signals', *Journal of neuroscience methods*, 146(1), pp. 42–49.

Javitt, G. *et al.* (2019) 'cis-Proline mutants of quiescin sulfhydryl oxidase 1 with altered redox properties undermine extracellular matrix integrity and cell adhesion in fibroblast cultures', *Protein science: a publication of the Protein Society*, 28(1), pp. 228–238.

Jenne, D. and Stanley, K.K. (1987) 'Nucleotide sequence and organization of the human S-protein gene: repeating peptide motifs in the "pexin" family and a model for their evolution', *Biochemistry*, 26(21), pp. 6735–6742.

Jessop, C.E. and Bulleid, N.J. (2004) 'Glutathione directly reduces an oxidoreductase in the endoplasmic reticulum of mammalian cells', *The Journal of biological chemistry*, 279(53), pp. 55341–55347.

Jiang, X. *et al.* (2019) 'COL12A1, a novel potential prognostic factor and therapeutic target in gastric cancer', *Molecular medicine reports*, 20(4), pp. 3103–3112.

Jin, S. *et al.* (2021) 'Inference and analysis of cell-cell communication using CellChat', *Nature communications*, 12(1), p. 1088.

John, W.G. and Lamb, E.J. (1993) 'The Maillard or browning reaction in diabetes', *Eye*, 7 (Pt 2), pp. 230–237.

Jones, P.L. and Jones, F.S. (2000) 'Tenascin-C in development and disease: gene regulation and cell function', *Matrix biology: journal of the International Society for Matrix Biology*, 19(7), pp. 581–596.

Jongsma, M.L.M. *et al.* (2016) 'An ER-Associated Pathway Defines Endosomal Architecture for Controlled Cargo Transport', *Cell*, 166(1), pp. 152–166.

Joshi, B. *et al.* (2008) 'Phosphorylated caveolin-1 regulates Rho/ROCK-dependent focal adhesion dynamics and tumor cell migration and invasion', *Cancer research*, 68(20), pp. 8210–8220.

Joyce, J.A. *et al.* (2004) 'Cathepsin cysteine proteases are effectors of invasive growth and angiogenesis during multistage tumorigenesis', *Cancer cell*, 5(5), pp. 443–453.

Juin, A. *et al.* (2014) 'Discoidin domain receptor 1 controls linear invadosome formation via a Cdc42-Tuba pathway', *The Journal of cell biology*, 207(4), pp. 517–533.

Jürgensen, H.J. *et al.* (2011) 'A novel functional role of collagen glycosylation: interaction with the endocytic collagen receptor uparap/ENDO180', *The Journal of biological chemistry*, 286(37), pp. 32736–32748.

Jürgensen, H.J. *et al.* (2019) 'CCL2/MCP-1 signaling drives extracellular matrix turnover by diverse macrophage subsets', *Matrix biology plus*, 1, p. 100003.

- Kadlecova, Z. *et al.* (2017) 'Regulation of clathrin-mediated endocytosis by hierarchical allosteric activation of AP2', *The Journal of cell biology*, 216(1), pp. 167–179.
- Kadler, K.E. *et al.* (1990) 'Assembly of Type I Collagen Fibrils de Novo by the Specific Enzymic Cleavage of pC Collagen', *Annals of the New York Academy of Sciences*, pp. 214–224. Available at: <https://doi.org/10.1111/j.1749-6632.1990.tb17930.x>.
- Kadler, K.E., Hill, A. and Canty-Laird, E.G. (2008) 'Collagen fibrillogenesis: fibronectin, integrins, and minor collagens as organizers and nucleators', *Current opinion in cell biology*, 20(5), pp. 495–501.
- Kadota, M. *et al.* (2010) 'Delineating genetic alterations for tumor progression in the MCF10A series of breast cancer cell lines', *PloS one*, 5(2), p. e9201.
- Kajiho, H. *et al.* (2016) 'RAB2A controls MT1-MMP endocytic and E-cadherin polarized Golgi trafficking to promote invasive breast cancer programs', *EMBO reports*, 17(7), pp. 1061–1080.
- Kaksonen, M. and Roux, A. (2018) 'Mechanisms of clathrin-mediated endocytosis', *Nature reviews. Molecular cell biology*, 19(5), pp. 313–326.
- Kamikubo, Y.-I., Okumura, Y. and Loskutoff, D.J. (2002) 'Identification of the disulfide bonds in the recombinant somatomedin B domain of human vitronectin', *The Journal of biological chemistry*, 277(30), pp. 27109–27119.
- Kammerer, R.A. *et al.* (1995) 'Selective Chain Recognition in the C-terminal α -Helical Coiled-coil Region of Laminin', *Journal of Molecular Biology*, pp. 64–73. Available at: <https://doi.org/10.1006/jmbi.1995.0358>.
- Kamphorst, J.J. *et al.* (2015) 'Human pancreatic cancer tumors are nutrient poor and tumor cells actively scavenge extracellular protein', *Cancer research*, 75(3), pp. 544–553.
- Kao, R.T., Wong, M. and Stern, R. (1982) 'Elastin degradation by proteases from cultured human breast cancer cells', *Biochemical and biophysical research communications*, 105(1), pp. 383–389.
- Karami Fath, M. *et al.* (2022) 'PI3K/Akt/mTOR signaling pathway in cancer stem cells', *Pathology, research and practice*, 237, p. 154010.
- Karimi, M. *et al.* (2016) 'Reactivity of disulfide bonds is markedly affected by structure and environment: implications for protein modification and stability', *Scientific reports*, 6, p. 38572.
- Kar, L. *et al.* (1993) '1H NMR-based determination of the three-dimensional structure of the human plasma fibronectin fragment containing inter-chain disulfide bonds', *The Journal of biological chemistry*, 268(12), pp. 8580–8589.
- Karpatová, M. *et al.* (1996) 'Shedding of the 67-kD laminin receptor by human cancer cells', *Journal of cellular biochemistry*, 60(2), pp. 226–234.
- Katoh, D. *et al.* (2013) 'Binding of $\alpha v \beta 1$ and $\alpha v \beta 6$ integrins to tenascin-C induces epithelial-mesenchymal transition-like change of breast cancer cells', *Oncogenesis*, 2(8), p. e65.
- Kaufman, C.S. and Butler, M.G. (2016) 'Mutation in gene causes moderate to severe Ehlers-Danlos syndrome', *World journal of medical genetics*, 6(2), pp. 17–21.
- Kaukonen, R. *et al.* (2017) 'Cell-derived matrices for studying cell proliferation and directional migration in a complex 3D microenvironment', *Nature protocols*, 12(11), pp. 2376–2390.
- Kay, E.J. *et al.* (2022) 'Cancer-associated fibroblasts require proline synthesis by PYCR1 for the deposition of pro-tumorigenic extracellular matrix', *Nature metabolism*, 4(6), pp. 693–710.
- Kciuk, M. *et al.* (2022) 'Metastasis and MAPK Pathways', *International journal of molecular sciences*, 23(7). Available at: <https://doi.org/10.3390/ijms23073847>.

- Keane, T.J., Swinehart, I.T. and Badylak, S.F. (2015) 'Methods of tissue decellularization used for preparation of biologic scaffolds and in vivo relevance', *Methods*, 84, pp. 25–34.
- Keene, D.R. *et al.* (1987) 'Type VII collagen forms an extended network of anchoring fibrils', *The Journal of cell biology*, 104(3), pp. 611–621.
- Kelley, L.C. *et al.* (2019) 'Adaptive F-Actin Polymerization and Localized ATP Production Drive Basement Membrane Invasion in the Absence of MMPs', *Developmental cell*, 48(3), pp. 313–328.e8.
- Kennecke, H. *et al.* (2010) 'Metastatic behavior of breast cancer subtypes', *Journal of clinical oncology: official journal of the American Society of Clinical Oncology*, 28(20), pp. 3271–3277.
- Kenny, H.A. *et al.* (2014) 'Mesothelial cells promote early ovarian cancer metastasis through fibronectin secretion', *The Journal of clinical investigation*, 124(10), pp. 4614–4628.
- Kent, H.M. *et al.* (2012) 'Structural basis of the intracellular sorting of the SNARE VAMP7 by the AP3 adaptor complex', *Developmental cell*, 22(5), pp. 979–988.
- Kern, U. *et al.* (2015) 'Lysosomal protein turnover contributes to the acquisition of TGF β -1 induced invasive properties of mammary cancer cells', *Molecular cancer*, 14, p. 39.
- Kessler, E. *et al.* (1996) 'Bone morphogenetic protein-1: the type I procollagen C-proteinase', *Science*, 271(5247), pp. 360–362.
- Ke, X. *et al.* (2019) 'Hypoxia modifies the polarization of macrophages and their inflammatory microenvironment, and inhibits malignant behavior in cancer cells', *Oncology letters*, 18(6), pp. 5871–5878.
- Khalili, P. *et al.* (2006) 'A non-RGD-based integrin binding peptide (ATN-161) blocks breast cancer growth and metastasis in vivo', *Molecular cancer therapeutics*, 5(9), pp. 2271–2280.
- Khamis, Z.I., Sahab, Z.J. and Sang, Q.-X.A. (2012) 'Active roles of tumor stroma in breast cancer metastasis', *International journal of breast cancer*, 2012, p. 574025.
- Khan, I. and Steeg, P.S. (2021) 'Endocytosis: a pivotal pathway for regulating metastasis', *British journal of cancer*, 124(1), pp. 66–75.
- Khan, M.M.G. *et al.* (2012) 'Protein disulfide isomerase-mediated disulfide bonds regulate the gelatinolytic activity and secretion of matrix metalloproteinase-9', *Experimental cell research*, 318(8), pp. 904–914.
- Kharitidi, D. *et al.* (2015) 'Interplay of Endosomal pH and Ligand Occupancy in Integrin α 5 β 1 Ubiquitination, Endocytic Sorting, and Cell Migration', *Cell reports*, 13(3), pp. 599–609.
- Khoo, A.S. *et al.* (2019) 'Breast Cancer Cells Transition from Mesenchymal to Amoeboid Migration in Tunable Three-Dimensional Silk-Collagen Hydrogels', *ACS biomaterials science & engineering*, 5(9), pp. 4341–4354.
- Kidwell, C.U. *et al.* (2021) 'Laterally transferred macrophage mitochondria act as a signaling source promoting cancer cell proliferation', *bioRxiv*. bioRxiv. Available at: <https://doi.org/10.1101/2021.08.10.455713>.
- Kiss, A.L. and Botos, E. (2009) 'Endocytosis via caveolae: alternative pathway with distinct cellular compartments to avoid lysosomal degradation?', *Journal of cellular and molecular medicine*, 13(7), pp. 1228–1237.
- Kjøller, L. *et al.* (2004) 'uPARAP/endo180 directs lysosomal delivery and degradation of collagen IV', *Experimental cell research*, 293(1), pp. 106–116.

- Klingen, T.A. *et al.* (2021) 'Fibulin-2 expression associates with vascular invasion and patient survival in breast cancer', *PloS one*, 16(4), p. e0249767.
- Knott, L. and Bailey, A.J. (1998) 'Collagen cross-links in mineralizing tissues: a review of their chemistry, function, and clinical relevance', *Bone*, 22(3), pp. 181–187.
- Kobayashi, N. *et al.* (2007) 'Differential subcellular targeting and activity-dependent subcellular localization of diacylglycerol kinase isozymes in transfected cells', *European journal of cell biology*, 86(8), pp. 433–444.
- Kocbek, V. *et al.* (2014) 'Increased levels of biglycan in endometriomas and peritoneal fluid samples from ovarian endometriosis patients', *Gynecological endocrinology: the official journal of the International Society of Gynecological Endocrinology*, 30(7), pp. 520–524.
- Kockx, M. *et al.* (2014) 'Pharmacological inhibition of dynamin II reduces constitutive protein secretion from primary human macrophages', *PloS one*, 9(10), p. e111186.
- Koh, M. *et al.* (2016) 'A novel role for flotillin-1 in H-Ras-regulated breast cancer aggressiveness', *International journal of cancer. Journal international du cancer*, 138(5), pp. 1232–1245.
- Koivu, J. (1987) 'Identification of disulfide bonds in carboxy-terminal propeptides of human type I procollagen', *FEBS letters*, 212(2), pp. 229–232.
- Koivusalo, M. *et al.* (2010) 'Amiloride inhibits macropinocytosis by lowering submembranous pH and preventing Rac1 and Cdc42 signaling', *The Journal of cell biology*, 188(4), pp. 547–563.
- Ko, K.R., Tsai, M.-C. and Frampton, J.P. (2019) 'Fabrication of thin-layer matrigel-based constructs for three-dimensional cell culture', *Biotechnology progress*, 35(1), p. e2733.
- Kolli-Bouhafs, K. *et al.* (2014) 'FAK competes for Src to promote migration against invasion in melanoma cells', *Cell death & disease*, 5, p. e1379.
- Konstantinopoulos, P.A. *et al.* (2008) 'Matrix metalloproteinase inhibitors as anticancer agents', *The international journal of biochemistry & cell biology*, 40(6-7), pp. 1156–1168.
- Korolkova, O.Y. *et al.* (2020) 'Diverse Roles of Annexin A6 in Triple-Negative Breast Cancer Diagnosis, Prognosis and EGFR-Targeted Therapies', *Cells*, 9(8). Available at: <https://doi.org/10.3390/cells9081855>.
- Koul, H.K., Pal, M. and Koul, S. (2013) 'Role of p38 MAP kinase signal transduction in solid tumors', *Genes & cancer*, 4(9-10), pp. 342–359.
- Koumangoye, R.B. *et al.* (2011) 'Detachment of breast tumor cells induces rapid secretion of exosomes which subsequently mediate cellular adhesion and spreading', *PloS one*, 6(9), p. e24234.
- Kovtun, O. *et al.* (2020) 'Architecture of the AP2/clathrin coat on the membranes of clathrin-coated vesicles', *Science advances*, 6(30), p. eaba8381.
- Krenn, V. and Musacchio, A. (2015) 'The Aurora B Kinase in Chromosome Bi-Orientation and Spindle Checkpoint Signaling', *Frontiers in oncology*, 5, p. 225.
- Kudaravalli, S., den Hollander, P. and Mani, S.A. (2022) 'Role of p38 MAP kinase in cancer stem cells and metastasis', *Oncogene*, 41(23), pp. 3177–3185.
- Kumagai, C., Kadowaki, T. and Kitagawa, Y. (1997) 'Disulfide-bonding between Drosophila laminin β and γ chains is essential for α chain to form $\alpha\beta\gamma$ trimer', *FEBS Letters*, pp. 211–216. Available at: [https://doi.org/10.1016/s0014-5793\(97\)00780-1](https://doi.org/10.1016/s0014-5793(97)00780-1).
- Kumari, S. and Mayor, S. (2008) 'ARF1 is directly involved in dynamin-independent endocytosis', *Nature cell biology*, 10(1), pp. 30–41.

- Kuo, H.J. *et al.* (1997) 'Type VI collagen anchors endothelial basement membranes by interacting with type IV collagen', *The Journal of biological chemistry*, 272(42), pp. 26522–26529.
- Lagresle-Peyrou, C. *et al.* (2014) 'The BLNK adaptor protein has a nonredundant role in human B-cell differentiation', *The Journal of allergy and clinical immunology*, 134(1), pp. 145–154.
- Lamandé, S.R. *et al.* (2006) 'The C5 Domain of the Collagen VI α 3(VI) Chain Is Critical for Extracellular Microfibril Formation and Is Present in the Extracellular Matrix of Cultured Cells', *Journal of Biological Chemistry*, pp. 16607–16614. Available at: <https://doi.org/10.1074/jbc.m510192200>.
- Lambrechts, D. *et al.* (2018) 'Phenotype molding of stromal cells in the lung tumor microenvironment', *Nature medicine*, 24(8), pp. 1277–1289.
- Langenbach, K.J. and Sottile, J. (1999) 'Identification of protein-disulfide isomerase activity in fibronectin', *The Journal of biological chemistry*, 274(11), pp. 7032–7038.
- Languino, L.R. *et al.* (1989) 'Endothelial cells use alpha 2 beta 1 integrin as a laminin receptor', *The Journal of cell biology*, 109(5), pp. 2455–2462.
- Lanzetti, L. and Di Fiore, P.P. (2017) 'Behind the Scenes: Endo/Exocytosis in the Acquisition of Metastatic Traits', *Cancer research*, 77(8), pp. 1813–1817.
- Larionova, I. *et al.* (2020) 'Tumor-Associated Macrophages in Human Breast, Colorectal, Lung, Ovarian and Prostate Cancers', *Frontiers in oncology*, 10, p. 566511.
- Larocque, G. *et al.* (2021) 'Intracellular nanovesicles mediate α 5 β 1 integrin trafficking during cell migration', *The Journal of cell biology*, 220(10). Available at: <https://doi.org/10.1083/jcb.202009028>.
- Le, A.H. *et al.* (2021) 'CYRI-A limits invasive migration through macropinosome formation and integrin uptake regulation', *The Journal of cell biology*, 220(9). Available at: <https://doi.org/10.1083/jcb.202012114>.
- Le Borgne, R. *et al.* (1998) 'The mammalian AP-3 adaptor-like complex mediates the intracellular transport of lysosomal membrane glycoproteins', *The Journal of biological chemistry*, 273(45), pp. 29451–29461.
- Lee, H. *et al.* (2000) 'Constitutive and growth factor-regulated phosphorylation of caveolin-1 occurs at the same site (Tyr-14) in vivo: identification of a c-Src/Cav-1/Grb7 signaling cassette', *Molecular endocrinology*, 14(11), pp. 1750–1775.
- Lee, H. *et al.* (2002) 'Src-induced phosphorylation of caveolin-2 on tyrosine 19. Phospho-caveolin-2 (Tyr(P)19) is localized near focal adhesions, remains associated with lipid rafts/caveolae, but no longer forms a high molecular mass hetero-oligomer with caveolin-1', *The Journal of biological chemistry*, 277(37), pp. 34556–34567.
- Lee, J.W. and Juliano, R.L. (2000) 'alpha5beta1 integrin protects intestinal epithelial cells from apoptosis through a phosphatidylinositol 3-kinase and protein kinase B-dependent pathway', *Molecular biology of the cell*, 11(6), pp. 1973–1987.
- Leeming, D.J. *et al.* (2011) 'Post-translational modifications of the extracellular matrix are key events in cancer progression: opportunities for biochemical marker development', *Biomarkers: biochemical indicators of exposure, response, and susceptibility to chemicals*, 16(3), pp. 193–205.
- Lees, J.F., Tasab, M. and Bulleid, N.J. (1997) 'Identification of the molecular recognition sequence which determines the type-specific assembly of procollagen', *The EMBO journal*, 16(5), pp. 908–916.
- Lee, S.-W. *et al.* (2019) 'EGFR-Pak Signaling Selectively Regulates Glutamine Deprivation-Induced Macropinocytosis', *Developmental cell*, 50(3), pp. 381–392.e5.

- Lee, V.S. *et al.* (2016) 'Loss of function mutation in LOX causes thoracic aortic aneurysm and dissection in humans', *Proceedings of the National Academy of Sciences of the United States of America*, 113(31), pp. 8759–8764.
- Lee, W., Sodek, J. and McCulloch, C.A. (1996) 'Role of integrins in regulation of collagen phagocytosis by human fibroblasts', *Journal of cellular physiology*, 168(3), pp. 695–704.
- Lefrançois, S. *et al.* (2004) 'An ear-core interaction regulates the recruitment of the AP-3 complex to membranes', *Developmental cell*, 7(4), pp. 619–625.
- Le Guern, F. *et al.* (2020) 'Fluorescein Derivatives as Fluorescent Probes for pH Monitoring along Recent Biological Applications', *International journal of molecular sciences*, 21(23). Available at: <https://doi.org/10.3390/ijms21239217>.
- Leitinger, B. (2014) 'Discoidin domain receptor functions in physiological and pathological conditions', *International review of cell and molecular biology*, 310, pp. 39–87.
- Lelek, M. *et al.* (2021) 'Single-molecule localization microscopy', *Nature reviews. Methods primers*, 1. Available at: <https://doi.org/10.1038/s43586-021-00038-x>.
- Lendorf, M.E. *et al.* (2011) 'Syndecan-1 and syndecan-4 are independent indicators in breast carcinoma', *The journal of histochemistry and cytochemistry: official journal of the Histochemistry Society*, 59(6), pp. 615–629.
- Leonoudakis, D. *et al.* (2014) 'Endocytic trafficking of laminin is controlled by dystroglycan and is disrupted in cancers', *Journal of cell science*, 127(Pt 22), pp. 4894–4903.
- Lethias, C. *et al.* (2006) 'A model of tenascin-X integration within the collagenous network', *FEBS letters*, 580(26), pp. 6281–6285.
- Levental, K.R. *et al.* (2009) 'Matrix crosslinking forces tumor progression by enhancing integrin signaling', *Cell*, 139(5), pp. 891–906.
- Levin, R., Grinstein, S. and Schlam, D. (2015) 'Phosphoinositides in phagocytosis and macropinocytosis', *Biochimica et biophysica acta*, 1851(6), pp. 805–823.
- Liberti, M.V. and Locasale, J.W. (2016) 'The Warburg Effect: How Does it Benefit Cancer Cells?', *Trends in biochemical sciences*, 41(3), pp. 211–218.
- Li, C. *et al.* (2021) 'Endoplasmic Reticulum-Plasma Membrane Contact Sites: Regulators, Mechanisms, and Physiological Functions', *Frontiers in cell and developmental biology*, 9, p. 627700.
- Li, C.-C. *et al.* (2012) 'BIG2, an ARF guanine nucleotide-exchange protein, regulates cell migration via effects integrin β 1 cycling and actin cytoskeleton remodeling', *FASEB journal: official publication of the Federation of American Societies for Experimental Biology*, 26(S1). Available at: https://doi.org/10.1096/fasebj.26.1_supplement.782.7.
- Li, H. *et al.* (2017) 'Reference component analysis of single-cell transcriptomes elucidates cellular heterogeneity in human colorectal tumors', *Nature genetics*, 49(5), pp. 708–718.
- Li, H. *et al.* (2021) 'Screening and prognostic value of potential biomarkers for ovarian cancer', *Annals of translational medicine*, 9(12), p. 1007.
- Li, J. *et al.* (2020) 'Elastin is a key factor of tumor development in colorectal cancer', *BMC cancer*, 20(1), p. 217.
- Li, L. *et al.* (2015) 'Nidogen-1: a candidate biomarker for ovarian serous cancer', *Japanese journal of clinical oncology*, 45(2), pp. 176–182.

- Lim, H.C. and Couchman, J.R. (2014) 'Syndecan-2 regulation of morphology in breast carcinoma cells is dependent on RhoGTPases', *Biochimica et biophysica acta*, 1840(8), pp. 2482–2490.
- Lindner, B., Burkard, T. and Schuler, M. (2020) 'Phagocytosis assays with different pH-sensitive fluorescent particles and various readouts', *BioTechniques*, 68(5), pp. 245–250.
- Ling, G. *et al.* (2016) 'Epithelial-mesenchymal transition regulated by p38/MAPK signaling pathways participates in vasculogenic mimicry formation in SHG44 cells transfected with TGF- β cDNA loaded lentivirus in vitro and in vivo', *International journal of oncology*, 49(6), pp. 2387–2398.
- Lin, T.-C. *et al.* (2019) 'Fibronectin in Cancer: Friend or Foe', *Cells*, 9(1). Available at: <https://doi.org/10.3390/cells9010027>.
- Lin, X.P., Mintern, J.D. and Gleeson, P.A. (2020) 'Macropinocytosis in Different Cell Types: Similarities and Differences', *Membranes*, 10(8). Available at: <https://doi.org/10.3390/membranes10080177>.
- Lin, Y. *et al.* (2016) 'p38 MAPK mediates epithelial-mesenchymal transition by regulating p38IP and Snail in head and neck squamous cell carcinoma', *Oral oncology*, 60, pp. 81–89.
- Liot, S. *et al.* (2020) 'Loss of Tenascin-X expression during tumor progression: A new pan-cancer marker', *Matrix biology plus*, 6-7, p. 100021.
- Liotta, L.A., Goldfarb, R.H. and Terranova, V.P. (1981) 'Cleavage of laminin by thrombin and plasmin: alpha thrombin selectively cleaves the beta chain of laminin', *Thrombosis research*, 21(6), pp. 663–673.
- Li, S. *et al.* (2003) 'Vascular smooth muscle cells orchestrate the assembly of type I collagen via alpha2beta1 integrin, RhoA, and fibronectin polymerization', *The American journal of pathology*, 163(3), pp. 1045–1056.
- Lisabeth, E.M., Falivelli, G. and Pasquale, E.B. (2013) 'Eph receptor signaling and ephrins', *Cold Spring Harbor perspectives in biology*, 5(9). Available at: <https://doi.org/10.1101/cshperspect.a009159>.
- Li, S., Seitz, R. and Lisanti, M.P. (1996) 'Phosphorylation of caveolin by src tyrosine kinases. The alpha-isoform of caveolin is selectively phosphorylated by v-Src in vivo', *The Journal of biological chemistry*, 271(7), pp. 3863–3868.
- Li, S.-Y. *et al.* (2021) 'Serum anti-AP3D1 antibodies are risk factors for acute ischemic stroke related with atherosclerosis', *Scientific reports*, 11(1), p. 13450.
- Liu, C.-C. *et al.* (2018) 'Collagen XVII/laminin-5 activates epithelial-to-mesenchymal transition and is associated with poor prognosis in lung cancer', *Oncotarget*, 9(2), pp. 1656–1672.
- Liu, C.-L. *et al.* (2018) 'Cysteine protease cathepsins in cardiovascular disease: from basic research to clinical trials', *Nature reviews. Cardiology*, 15(6), pp. 351–370.
- Liu, Q. and Hofmann, P.A. (2004) 'Protein phosphatase 2A-mediated cross-talk between p38 MAPK and ERK in apoptosis of cardiac myocytes', *American journal of physiology. Heart and circulatory physiology*, 286(6), pp. H2204–12.
- Liu, Q.-P. *et al.* (2020) 'Stiffer Matrix Accelerates Migration of Hepatocellular Carcinoma Cells through Enhanced Aerobic Glycolysis Via the MAPK-YAP Signaling', *Cancers*, 12(2). Available at: <https://doi.org/10.3390/cancers12020490>.
- Liu, S. *et al.* (2010) 'Laminin-332-beta1 integrin interactions negatively regulate invadopodia', *Journal of cellular physiology*, 223(1), pp. 134–142.
- Liu, S., Liao, G. and Li, G. (2017) 'Regulatory effects of COL1A1 on apoptosis induced by radiation in cervical cancer cells', *Cancer cell international*, 17(1), p. 73.

- Liu, T. *et al.* (2019) 'Cancer-associated fibroblasts: an emerging target of anti-cancer immunotherapy', *Journal of hematology & oncology*, 12(1), p. 86.
- Liu, X. *et al.* (2022) 'ErbB2/Her2-dependent downregulation of a cell death-promoting protein BLNK in breast cancer cells is required for 3D breast tumor growth', *Cell death & disease*, 13(8), p. 687.
- Li, X. *et al.* (2022) 'A pan-cancer analysis of collagen VI family on prognosis, tumor microenvironment, and its potential therapeutic effect', *BMC bioinformatics*, 23(1), p. 390.
- Li, Z. *et al.* (2010) 'High-resolution melting analysis of ADAMTS18 methylation levels in gastric, colorectal and pancreatic cancers', *Medical oncology*, 27(3), pp. 998–1004.
- Llanses Martinez, M. and Rainero, E. (2019) 'Membrane dynamics in cell migration', *Essays in biochemistry*, 63(5), pp. 469–482.
- Lober, V.H. *et al.* (2010) 'Ubiquitination of alpha 5 beta 1 integrin controls fibroblast migration through lysosomal degradation of fibronectin-integrin complexes', *Developmental cell*, 19(1), pp. 148–159.
- Löffek, S., Schilling, O. and Franzke, C.-W. (2011) 'Series "matrix metalloproteinases in lung health and disease": Biological role of matrix metalloproteinases: a critical balance', *The European respiratory journal: official journal of the European Society for Clinical Respiratory Physiology*, 38(1), pp. 191–208.
- Lo, H.-W. *et al.* (2005) 'Nuclear interaction of EGFR and STAT3 in the activation of the iNOS/NO pathway', *Cancer cell*, 7(6), pp. 575–589.
- Lolo, F.-N. *et al.* (2022) 'Caveolae couple mechanical stress to integrin recycling and activation', *eLife*, 11. Available at: <https://doi.org/10.7554/eLife.82348>.
- Lord, S.J. *et al.* (2020) 'SuperPlots: Communicating reproducibility and variability in cell biology', *The Journal of cell biology*, 219(6). Available at: <https://doi.org/10.1083/jcb.202001064>.
- Lössl, P. *et al.* (2014) 'Analysis of nidogen-1/laminin γ 1 interaction by cross-linking, mass spectrometry, and computational modeling reveals multiple binding modes', *PLoS one*, 9(11), p. e112886.
- Lowry, J.R. and Klegeris, A. (2018) 'Emerging roles of microglial cathepsins in neurodegenerative disease', *Brain research bulletin*, 139, pp. 144–156.
- Lucas, J.T., Jr *et al.* (2010) 'Regulation of invasive behavior by vascular endothelial growth factor is HEF1-dependent', *Oncogene*, 29(31), pp. 4449–4459.
- Lucio-Eterovic, A.K., Piao, Y. and de Groot, J.F. (2009) 'Mediators of glioblastoma resistance and invasion during anti-vascular endothelial growth factor therapy', *Clinical cancer research: an official journal of the American Association for Cancer Research*, 15(14), pp. 4589–4599.
- Ludford-Menting, M.J. *et al.* (2002) 'A functional interaction between CD46 and DLG4: a role for DLG4 in epithelial polarization', *The Journal of biological chemistry*, 277(6), pp. 4477–4484.
- Lundmark, R. *et al.* (2008) 'The GTPase-activating protein GRAF1 regulates the CLIC/GEEC endocytic pathway', *Current biology: CB*, 18(22), pp. 1802–1808.
- Luo, M.-L. *et al.* (2015) 'The Rab2A GTPase promotes breast cancer stem cells and tumorigenesis via Erk signaling activation', *Cell reports*, 11(1), pp. 111–124.
- Macpherson, I.R. *et al.* (2014) 'CLIC3 controls recycling of late endosomal MT1-MMP and dictates invasion and metastasis in breast cancer', *Journal of cell science*, 127(Pt 18), pp. 3893–3901.
- Mader, C.C. *et al.* (2011) 'An EGFR-Src-Arg-cortactin pathway mediates functional maturation of invadopodia and breast cancer cell invasion', *Cancer research*, 71(5), pp. 1730–1741.
- Madsen, D.H. *et al.* (2011) 'The non-phagocytic route of collagen uptake: a distinct degradation pathway',

The Journal of biological chemistry, 286(30), pp. 26996–27010.

Madsen, D.H. *et al.* (2017) 'Tumor-Associated Macrophages Derived from Circulating Inflammatory Monocytes Degrade Collagen through Cellular Uptake', *Cell reports*, 21(13), pp. 3662–3671.

Magalhaes, M.A.O. *et al.* (2011) 'Cortactin phosphorylation regulates cell invasion through a pH-dependent pathway', *The Journal of cell biology*, 195(5), pp. 903–920.

Mai, J. *et al.* (2002) 'Degradation of extracellular matrix protein tenascin-C by cathepsin B: an interaction involved in the progression of gliomas', *Biological chemistry*, 383(9), pp. 1407–1413.

Maiorani, O. *et al.* (2017) 'Neutrophil elastase cleavage of the gC1q domain impairs the EMILIN1- α 4 β 1 integrin interaction, cell adhesion and anti-proliferative activity', *Scientific reports*, 7, p. 39974.

Majeed, S.R. *et al.* (2014) 'Clathrin light chains are required for the gyrating-clathrin recycling pathway and thereby promote cell migration', *Nature communications*, 5, p. 3891.

Ma, L. *et al.* (2016) 'Transient Fcho1/2·Eps15/R·AP-2 Nanoclusters Prime the AP-2 Clathrin Adaptor for Cargo Binding', *Developmental cell*, 37(5), pp. 428–443.

Mandal, S., Johnson, K.R. and Wheelock, M.J. (2008) 'TGF-beta induces formation of F-actin cores and matrix degradation in human breast cancer cells via distinct signaling pathways', *Experimental cell research*, 314(19), pp. 3478–3493.

Mann, K., Deutzmann, R. and Timpl, R. (1988) 'Characterization of proteolytic fragments of the laminin-nidogen complex and their activity in ligand-binding assays', *European journal of biochemistry / FEBS*, 178(1), pp. 71–80.

Marchesin, V. *et al.* (2015) 'ARF6-JIP3/4 regulate endosomal tubules for MT1-MMP exocytosis in cancer invasion', *The Journal of cell biology*, 211(2), pp. 339–358.

Martin-Bermudo, M.D., Dunin-Borkowski, O.M. and Brown, N.H. (1998) 'Modulation of integrin activity is vital for morphogenesis', *The Journal of cell biology*, 141(4), pp. 1073–1081.

Martino-Echarri, E. *et al.* (2013) 'Contribution of ADAMTS1 as a tumor suppressor gene in human breast carcinoma. Linking its tumor inhibitory properties to its proteolytic activity on nidogen-1 and nidogen-2', *International journal of cancer. Journal international du cancer*, 133(10), pp. 2315–2324.

Martiny-Baron, G. *et al.* (2010) 'The small molecule specific EphB4 kinase inhibitor NVP-BHG712 inhibits VEGF driven angiogenesis', *Angiogenesis*, 13(3), pp. 259–267.

Masucci, M.T., Minopoli, M. and Carriero, M.V. (2019) 'Tumor Associated Neutrophils. Their Role in Tumorigenesis, Metastasis, Prognosis and Therapy', *Frontiers in oncology*, 9, p. 1146.

Matthaeus, C. and Taraska, J.W. (2020) 'Energy and Dynamics of Caveolae Trafficking', *Frontiers in cell and developmental biology*, 8, p. 614472.

Matulka, M. *et al.* (2019) 'Expression and Concentration of Matrix Metalloproteinase 9 and Tissue Inhibitor of Matrix Metalloproteinases 1 in Laryngeal Squamous Cell Carcinoma', *Disease markers*, 2019, p. 3136792.

Ma, Y. *et al.* (2017) 'Introducing Membrane Charge and Membrane Potential to T Cell Signaling', *Frontiers in immunology*, 8, p. 1513.

Mayer, U. *et al.* (1993) 'Sites of nidogen cleavage by proteases involved in tissue homeostasis and remodelling', *European journal of biochemistry / FEBS*, 217(3), pp. 877–884.

Mayne, R. *et al.* (1993) 'Isolation and characterization of the chains of type V/type XI collagen present in bovine vitreous', *The Journal of biological chemistry*, 268(13), pp. 9381–9386.

- Mayor, S. and Pagano, R.E. (2007) 'Pathways of clathrin-independent endocytosis', *Nature reviews. Molecular cell biology*, 8(8), pp. 603–612.
- McBride, O.W., Wesley McBride, O. and Harrington, W.F. (1967) 'Ascaris Cuticle Collagen: on the Disulfide Cross-Linkages and the Molecular Properties of the Subunits*', *Biochemistry*, pp. 1484–1498. Available at: <https://doi.org/10.1021/bi00857a035>.
- McCawley, L.J. *et al.* (2004) 'A protective role for matrix metalloproteinase-3 in squamous cell carcinoma', *Cancer research*, 64(19), pp. 6965–6972.
- McDonald, J.A., Kelley, D.G. and Broekelmann, T.J. (1982) 'Role of fibronectin in collagen deposition: Fab' to the gelatin-binding domain of fibronectin inhibits both fibronectin and collagen organization in fibroblast extracellular matrix', *The Journal of cell biology*, 92(2), pp. 485–492.
- McKeown-Longo, P.J. and Mosher, D.F. (1983) 'Binding of plasma fibronectin to cell layers of human skin fibroblasts', *The Journal of cell biology*, 97(2), pp. 466–472.
- Melcher, A.H. and Chan, J. (1981) 'Phagocytosis and digestion of collagen by gingival fibroblasts in vivo: a study of serial sections', *Journal of ultrastructure research*, 77(1), pp. 1–36.
- Mellman, I., Fuchs, R. and Helenius, A. (1986) 'Acidification of the endocytic and exocytic pathways', *Annual review of biochemistry*, 55, pp. 663–700.
- Mendler, M. *et al.* (1989) 'Cartilage contains mixed fibrils of collagen types II, IX, and XI', *The Journal of cell biology*, 108(1), pp. 191–197.
- Merceron, T.K. and Murphy, S.V. (2015) 'Hydrogels for 3D Bioprinting Applications', in *Essentials of 3D Biofabrication and Translation*. Elsevier, pp. 249–270.
- Merrifield, C.J. *et al.* (2002) 'Imaging actin and dynamin recruitment during invagination of single clathrin-coated pits', *Nature cell biology*, 4(9), pp. 691–698.
- Merrill, N.M. *et al.* (2017) 'PI3K-C2 α knockdown decreases autophagy and maturation of endocytic vesicles', *PloS one*, 12(9), p. e0184909.
- Miao, H. *et al.* (2000) 'Activation of EphA2 kinase suppresses integrin function and causes focal-adhesion-kinase dephosphorylation', *Nature cell biology*, 2(2), pp. 62–69.
- Middleton, R.B. and Bulleid, N.J. (1993) 'Reconstitution of the folding pathway of collagen in a cell-free system: formation of correctly aligned and hydroxylated triple helices', *Biochemical Journal*, pp. 511–517. Available at: <https://doi.org/10.1042/bj2960511>.
- Midwood, K.S. *et al.* (2016) 'Tenascin-C at a glance', *Journal of cell science*, 129(23), pp. 4321–4327.
- Mikhailenko, I. *et al.* (1997) 'Cellular internalization and degradation of thrombospondin-1 is mediated by the amino-terminal heparin binding domain (HBD). High affinity interaction of dimeric HBD with the low density lipoprotein receptor-related protein', *The Journal of biological chemistry*, 272(10), pp. 6784–6791.
- Miranti, C.K. and Brugge, J.S. (2002) 'Sensing the environment: a historical perspective on integrin signal transduction', *Nature cell biology*, 4(4), pp. E83–90.
- Mirsaeidi, M. *et al.* (2016) 'Annexins family: insights into their functions and potential role in pathogenesis of sarcoidosis', *Journal of translational medicine*, 14, p. 89.
- Mitrović, A., Pečar Fonović, U. and Kos, J. (2017) 'Cysteine cathepsins B and X promote epithelial-mesenchymal transition of tumor cells', *European journal of cell biology*, 96(6), pp. 622–631.
- Mohamed, M.M. and Sloane, B.F. (2006) 'Cysteine cathepsins: multifunctional enzymes in cancer', *Nature reviews. Cancer*, 6(10), pp. 764–775.

- Molnar, J. *et al.* (1979) 'Purification of opsonically active human and rat cold-insoluble globulin (plasma fibronectin)', *Biochemistry*, 18(18), pp. 3909–3916.
- Montel, V. *et al.* (2004) 'Altered metastatic behavior of human breast cancer cells after experimental manipulation of matrix metalloproteinase 8 gene expression', *Cancer research*, 64(5), pp. 1687–1694.
- Montuori, N. *et al.* (2016) '67 kDa laminin receptor (67LR) in normal and neoplastic hematopoietic cells: is its targeting a feasible approach?', *Translational medicine @ UniSa*, 15, pp. 8–14.
- Moreau, H.D. *et al.* (2018) 'Macropinocytosis overcomes directional bias due to hydraulic resistance to enhance space exploration by dendritic cells', *SSRN Electronic Journal* [Preprint]. Available at: <https://doi.org/10.2139/ssrn.3155703>.
- Moreno-Layseca, P. *et al.* (2019) 'Integrin trafficking in cells and tissues', *Nature cell biology*, 21(2), pp. 122–132.
- Moreno-Layseca, P. *et al.* (2021) 'Cargo-specific recruitment in clathrin- and dynamin-independent endocytosis', *Nature cell biology*, 23(10), pp. 1073–1084.
- Moritz, M.N.O. *et al.* (2021) 'Biphasic $\alpha 2\beta 1$ Integrin Expression in Breast Cancer Metastasis to Bone', *International journal of molecular sciences*, 22(13). Available at: <https://doi.org/10.3390/ijms22136906>.
- Moriya, K. *et al.* (2011) 'A fibronectin-independent mechanism of collagen fibrillogenesis in adult liver remodeling', *Gastroenterology*, 140(5), pp. 1653–1663.
- Mortazavi, M. *et al.* (2022) 'Prospects of targeting PI3K/AKT/mTOR pathway in pancreatic cancer', *Critical reviews in oncology/hematology*, 176, p. 103749.
- Mostafavi-Pour, Z. *et al.* (2003) 'Integrin-specific signaling pathways controlling focal adhesion formation and cell migration', *The Journal of cell biology*, 161(1), pp. 155–167.
- Mousavi, S.A. *et al.* (2004) 'Clathrin-dependent endocytosis', *Biochemical Journal*, 377(Pt 1), pp. 1–16.
- Mueller, S.C. *et al.* (1999) 'A novel protease-docking function of integrin at invadopodia', *The Journal of biological chemistry*, 274(35), pp. 24947–24952.
- Müllenbach, E., Walter, L. and Dressel, R. (2006) 'A novel discoidin domain receptor 1 (Ddr1) transcript is expressed in postmeiotic germ cells of the rat testis depending on the major histocompatibility complex haplotype', *Gene*, 372, pp. 53–61.
- Muller, P.A.J. *et al.* (2009) 'Mutant p53 drives invasion by promoting integrin recycling', *Cell*, 139(7), pp. 1327–1341.
- Mundy, D.I. *et al.* (2002) 'Dual control of caveolar membrane traffic by microtubules and the actin cytoskeleton', *Journal of cell science*, 115(Pt 22), pp. 4327–4339.
- Muranen, T. *et al.* (2017) 'Starved epithelial cells uptake extracellular matrix for survival', *Nature communications*, 8, p. 13989.
- Murphy, D.A. and Courtneidge, S.A. (2011) 'The “ins” and “outs” of podosomes and invadopodia: characteristics, formation and function', *Nature reviews. Molecular cell biology*, 12(7), pp. 413–426.
- Murray, E.J. *et al.* (1997) 'E64d, a membrane-permeable cysteine protease inhibitor, attenuates the effects of parathyroid hormone on osteoblasts in vitro', *Metabolism: clinical and experimental*, 46(9), pp. 1090–1094.
- Murray, G.I. *et al.* (1996) 'Matrix metalloproteinase-1 is associated with poor prognosis in colorectal cancer', *Nature medicine*, 2(4), pp. 461–462.
- Myers, J.P., Santiago-Medina, M. and Gomez, T.M. (2011) 'Regulation of axonal outgrowth and

- pathfinding by integrin-ECM interactions', *Developmental neurobiology*, 71(11), pp. 901–923.
- Naba, A. *et al.* (2012) 'The matrisome: in silico definition and in vivo characterization by proteomics of normal and tumor extracellular matrices', *Molecular & cellular proteomics: MCP*, 11(4), p. M111.014647.
- Naba, A., Clauser, K.R., Lamar, J.M., *et al.* (2014) 'Extracellular matrix signatures of human mammary carcinoma identify novel metastasis promoters', *eLife*, 3, p. e01308.
- Naba, A., Clauser, K.R., Whittaker, C.A., *et al.* (2014) 'Extracellular matrix signatures of human primary metastatic colon cancers and their metastases to liver', *BMC cancer*, 14, p. 518.
- Nagaharu, K. *et al.* (2011) 'Tenascin C induces epithelial-mesenchymal transition-like change accompanied by SRC activation and focal adhesion kinase phosphorylation in human breast cancer cells', *The American journal of pathology*, 178(2), pp. 754–763.
- Nagashima, K.-I. *et al.* (2002) 'Adaptor protein Crk is required for ephrin-B1-induced membrane ruffling and focal complex assembly of human aortic endothelial cells', *Molecular biology of the cell*, 13(12), pp. 4231–4242.
- Nagato, S. *et al.* (2005) 'Downregulation of laminin alpha4 chain expression inhibits glioma invasion in vitro and in vivo', *International journal of cancer. Journal international du cancer*, 117(1), pp. 41–50.
- Nagl, L. *et al.* (2020) 'Tumor Endothelial Cells (TECs) as Potential Immune Directors of the Tumor Microenvironment - New Findings and Future Perspectives', *Frontiers in cell and developmental biology*, 8, p. 766.
- Nanda, J.S. and Lorsch, J.R. (2014) 'Labeling a protein with fluorophores using NHS ester derivitization', *Methods in enzymology*, 536, pp. 87–94.
- Nazemi, M. *et al.* (2021) 'The extracellular matrix promotes breast cancer cell growth under amino acid starvation by promoting tyrosine catabolism', *bioRxiv*. bioRxiv. Available at: <https://doi.org/10.1101/2021.06.09.447520>.
- Neumann-Giesen, C. *et al.* (2004) 'Membrane and raft association of reggie-1/flotillin-2: role of myristoylation, palmitoylation and oligomerization and induction of filopodia by overexpression', *Biochemical Journal*, 378(Pt 2), pp. 509–518.
- Nicholas, N.S. *et al.* (2019) 'Differential role for PAK1 and PAK4 during the invadopodia lifecycle', *Small GTPases*, 10(4), pp. 289–295.
- Nie, Z. *et al.* (2003) 'Specific regulation of the adaptor protein complex AP-3 by the Arf GAP AGAP1', *Developmental cell*, 5(3), pp. 513–521.
- Nikolov, A. and Popovski, N. (2021) 'Role of Gelatinases MMP-2 and MMP-9 in Healthy and Complicated Pregnancy and Their Future Potential as Preeclampsia Biomarkers', *Diagnostics (Basel, Switzerland)*, 11(3). Available at: <https://doi.org/10.3390/diagnostics11030480>.
- Niland, S., Riscanevo, A.X. and Eble, J.A. (2021) 'Matrix Metalloproteinases Shape the Tumor Microenvironment in Cancer Progression', *International journal of molecular sciences*, 23(1). Available at: <https://doi.org/10.3390/ijms23010146>.
- Nizioł, M. and Pryczynicz, A. (2021) 'The role of tensins in malignant neoplasms', *Archives of medical science: AMS* [Preprint]. Available at: <https://doi.org/10.5114/aoms/127085>.
- Noh, H., Hong, S. and Huang, S. (2013) 'Role of urokinase receptor in tumor progression and development', *Theranostics*, 3(7), pp. 487–495.
- Nomizu, M. *et al.* (1994) 'Assembly of synthetic laminin peptides into a triple-stranded coiled-coil

- structure', *The Journal of biological chemistry*, 269(48), pp. 30386–30392.
- Nørregaard, K.S. *et al.* (2022) 'The endocytic receptor uPARAP is a regulator of extracellular thrombospondin-1', *Matrix biology: journal of the International Society for Matrix Biology*, 111, pp. 307–328.
- Nossal, R. (2001) 'Energetics of clathrin basket assembly', *Traffic*, 2(2), pp. 138–147.
- Nwosu, Z.C. *et al.* (2016) 'Caveolin-1 in the regulation of cell metabolism: a cancer perspective', *Molecular cancer*, 15(1), p. 71.
- Nyalendo, C. *et al.* (2007) 'Src-dependent phosphorylation of membrane type I matrix metalloproteinase on cytoplasmic tyrosine 573: role in endothelial and tumor cell migration', *The Journal of biological chemistry*, 282(21), pp. 15690–15699.
- Nyalendo, C. *et al.* (2008) 'Impaired tyrosine phosphorylation of membrane type 1-matrix metalloproteinase reduces tumor cell proliferation in three-dimensional matrices and abrogates tumor growth in mice', *Carcinogenesis*, 29(8), pp. 1655–1664.
- Ochieng, J. *et al.* (2009) 'Anchorage-independent growth of breast carcinoma cells is mediated by serum exosomes', *Experimental cell research*, 315(11), pp. 1875–1888.
- O'Day, S. *et al.* (2011) 'A randomised, phase II study of intetumumab, an anti- α -v-integrin mAb, alone and with dacarbazine in stage IV melanoma', *British journal of cancer*, 105(3), pp. 346–352.
- Öhlund, D. *et al.* (2013) 'Type IV collagen stimulates pancreatic cancer cell proliferation, migration, and inhibits apoptosis through an autocrine loop', *BMC cancer*, 13(1), p. 154.
- Ohno, H. *et al.* (1995) 'Interaction of tyrosine-based sorting signals with clathrin-associated proteins', *Science*, 269(5232), pp. 1872–1875.
- Oh, P., McIntosh, D.P. and Schnitzer, J.E. (1998) 'Dynamin at the neck of caveolae mediates their budding to form transport vesicles by GTP-driven fission from the plasma membrane of endothelium', *The Journal of cell biology*, 141(1), pp. 101–114.
- Olivares, O. *et al.* (2017) 'Collagen-derived proline promotes pancreatic ductal adenocarcinoma cell survival under nutrient limited conditions', *Nature communications*, 8(1), p. 16031.
- Oliver, J.D. *et al.* (1999) 'ERp57 functions as a subunit of specific complexes formed with the ER lectins calreticulin and calnexin', *Molecular biology of the cell*, 10(8), pp. 2573–2582.
- Ooi, C.E., Dell'Angelica, E.C. and Bonifacino, J.S. (1998) 'ADP-Ribosylation factor 1 (ARF1) regulates recruitment of the AP-3 adaptor complex to membranes', *The Journal of cell biology*, 142(2), pp. 391–402.
- Ortega, N. and Werb, Z. (2002) 'New functional roles for non-collagenous domains of basement membrane collagens', *Journal of cell science*, 115(Pt 22), pp. 4201–4214.
- Ortiz-Urda, S. *et al.* (2005) 'Type VII collagen is required for Ras-driven human epidermal tumorigenesis', *Science*, 307(5716), pp. 1773–1776.
- Oser, M. *et al.* (2009) 'Cortactin regulates cofilin and N-WASp activities to control the stages of invadopodium assembly and maturation', *The Journal of cell biology*, 186(4), pp. 571–587.
- Oskarsson, T. *et al.* (2011) 'Breast cancer cells produce tenascin C as a metastatic niche component to colonize the lungs', *Nature medicine*, 17(7), pp. 867–874.
- Ostrowski, P.P. *et al.* (2019) 'Dynamic Podosome-Like Structures in Nascent Phagosomes Are Coordinated by Phosphoinositides', *Developmental cell*, 50(4), pp. 397–410.e3.
- Ósz, Á., Lánczky, A. and Gyórfy, B. (2021) 'Survival analysis in breast cancer using proteomic data from

four independent datasets', *Scientific reports*, 11(1), p. 16787.

Ott, U. *et al.* (1982) 'Protease resistance and conformation of laminin', *European journal of biochemistry / FEBS*, 123(1), pp. 63–72.

Owusu-Ansah, K.G. *et al.* (2019) 'COL6A1 promotes metastasis and predicts poor prognosis in patients with pancreatic cancer', *International journal of oncology*, 55(2), pp. 391–404.

Palamidessi, A. *et al.* (2008) 'Endocytic trafficking of Rac is required for the spatial restriction of signaling in cell migration', *Cell*, 134(1), pp. 135–147.

Palm, W. *et al.* (2015) 'The Utilization of Extracellular Proteins as Nutrients Is Suppressed by mTORC1', *Cell*, 162(2), pp. 259–270.

Palm, W. (2019) 'Metabolic functions of macropinocytosis', *Philosophical transactions of the Royal Society of London. Series B, Biological sciences*, 374(1765), p. 20180285.

Panetti, T.S. and McKeown-Longo, P.J. (1993) 'The alpha v beta 5 integrin receptor regulates receptor-mediated endocytosis of vitronectin', *The Journal of biological chemistry*, 268(16), pp. 11492–11495.

Pankov, R. and Yamada, K.M. (2002) 'Fibronectin at a glance', *Journal of cell science*, 115(Pt 20), pp. 3861–3863.

Pan, S. *et al.* (2014) 'Quantitative glycoproteomics analysis reveals changes in N-glycosylation level associated with pancreatic ductal adenocarcinoma', *Journal of proteome research*, 13(3), pp. 1293–1306.

Papakonstanti, E.A. and Stournaras, C. (2002) 'Association of PI-3 kinase with PAK1 leads to actin phosphorylation and cytoskeletal reorganization', *Molecular biology of the cell*, 13(8), pp. 2946–2962.

Papalazarou, V. *et al.* (2022) 'Collagen VI expression is negatively mechanosensitive in pancreatic cancer cells and supports the metastatic niche', *Journal of cell science*, 135(24). Available at: <https://doi.org/10.1242/jcs.259978>.

Papanicolaou, M. *et al.* (2022) 'Temporal profiling of the breast tumour microenvironment reveals collagen XII as a driver of metastasis', *Nature communications*, 13(1), p. 4587.

Park, H.-J. and Helfman, D.M. (2019) 'Up-regulated fibronectin in 3D culture facilitates spreading of triple negative breast cancer cells on 2D through integrin β -5 and Src', *Scientific reports*, 9(1), p. 19950.

Park, J. and Scherer, P.E. (2012) 'Adipocyte-derived endotrophin promotes malignant tumor progression', *The Journal of clinical investigation*, 122(11), pp. 4243–4256.

Park, R.J. *et al.* (2013) 'Dynamin triple knockout cells reveal off target effects of commonly used dynamin inhibitors', *Journal of cell science*, 126(Pt 22), pp. 5305–5312.

Park, S.Y. and Guo, X. (2014) 'Adaptor protein complexes and intracellular transport', *Bioscience reports*, 34(4). Available at: <https://doi.org/10.1042/BSR20140069>.

Parton, R.G., Kozlov, M.M. and Ariotti, N. (2020) 'Caveolae and lipid sorting: Shaping the cellular response to stress', *The Journal of cell biology*, 219(4). Available at: <https://doi.org/10.1083/jcb.201905071>.

Patel, R.S. *et al.* (1987) 'Organization of the fibronectin gene provides evidence for exon shuffling during evolution', *The EMBO journal*, 6(9), pp. 2565–2572.

Patel, S. *et al.* (2018) 'Cathepsins: Proteases that are vital for survival but can also be fatal', *Biomedicine & pharmacotherapy = Biomedecine & pharmacotherapie*, 105, pp. 526–532.

Pathmanathan, S. *et al.* (2022) 'B cell linker protein (BLNK) is a regulator of Met receptor signaling and trafficking in non-small cell lung cancer', *iScience*, 25(11), p. 105419.

- Paulsson, M. *et al.* (1985) 'Evidence for coiled-coil alpha-helical regions in the long arm of laminin', *The EMBO journal*, 4(2), pp. 309–316.
- Payne, S.N. *et al.* (2015) 'PIK3CA mutations can initiate pancreatic tumorigenesis and are targetable with PI3K inhibitors', *Oncogenesis*, 4, p. e169.
- Peden, A.A. *et al.* (2004) 'Localization of the AP-3 adaptor complex defines a novel endosomal exit site for lysosomal membrane proteins', *The Journal of cell biology*, 164(7), pp. 1065–1076.
- Pellinen, T. *et al.* (2006) 'Small GTPase Rab21 regulates cell adhesion and controls endosomal traffic of beta1-integrins', *The Journal of cell biology*, 173(5), pp. 767–780.
- Pellinen, T. *et al.* (2008) 'Integrin trafficking regulated by Rab21 is necessary for cytokinesis', *Developmental cell*, 15(3), pp. 371–385.
- Pereira, L. *et al.* (2013) 'Inhibition of p38 MAPK sensitizes tumour cells to cisplatin-induced apoptosis mediated by reactive oxygen species and JNK', *EMBO molecular medicine*, 5(11), pp. 1759–1774.
- Petrenko, A.A. *et al.* (2006) 'Downregulation of genes encoding for subunits of adaptor complex-3 in cervical carcinomas', *Biochemistry. Biokhimiia*, 71(10), pp. 1153–1160.
- Pfaff, M., Du, X. and Ginsberg, M.H. (1999) 'Calpain cleavage of integrin beta cytoplasmic domains', *FEBS letters*, 460(1), pp. 17–22.
- Phan, H.-P. *et al.* (2008) 'Expression and chain assembly of human laminin-332 in an insect cell-free translation system', *Bioscience, biotechnology, and biochemistry*, 72(7), pp. 1847–1852.
- Phong, M.S. *et al.* (2010) 'p38 mitogen-activated protein kinase promotes cell survival in response to DNA damage but is not required for the G(2) DNA damage checkpoint in human cancer cells', *Molecular and cellular biology*, 30(15), pp. 3816–3826.
- Piccard, H., Muschel, R.J. and Opdenakker, G. (2012) 'On the dual roles and polarized phenotypes of neutrophils in tumor development and progression', *Critical reviews in oncology/hematology*, 82(3), pp. 296–309.
- Piccard, H., Van den Steen, P.E. and Opdenakker, G. (2007) 'Hemopexin domains as multifunctional liganding modules in matrix metalloproteinases and other proteins', *Journal of leukocyte biology*, 81(4), pp. 870–892.
- Pickup, M.W., Mouw, J.K. and Weaver, V.M. (2014) 'The extracellular matrix modulates the hallmarks of cancer', *EMBO reports*, 15(12), pp. 1243–1253.
- Piersma, B., Hayward, M.-K. and Weaver, V.M. (2020) 'Fibrosis and cancer: A strained relationship', *Biochimica et Biophysica Acta, Reviews on Cancer*, 1873(2), p. 188356.
- Piffko, A. *et al.* (2022) 'EphrinB2-EphB4 Signaling in Neurooncological Disease', *International journal of molecular sciences*, 23(3). Available at: <https://doi.org/10.3390/ijms23031679>.
- Pihlajaniemi, T., Myllylä, R. and Kivirikko, K.I. (1991) 'Prolyl 4-hydroxylase and its role in collagen synthesis', *Journal of Hepatology*, pp. S2–S7. Available at: [https://doi.org/10.1016/0168-8278\(91\)90002-s](https://doi.org/10.1016/0168-8278(91)90002-s).
- Pinnell, S.R. and Martin, G.R. (1968) 'The cross-linking of collagen and elastin: enzymatic conversion of lysine in peptide linkage to alpha-amino adipic-delta-semialdehyde (allysine) by an extract from bone', *Proceedings of the National Academy of Sciences of the United States of America*, 61(2), pp. 708–716.
- Planchon, D. *et al.* (2018) 'MT1-MMP targeting to endolysosomes is mediated by upregulation of flotillins', *Journal of cell science*, 131(17). Available at: <https://doi.org/10.1242/jcs.218925>.

- Porter, S. *et al.* (2006) 'ADAMTS8 and ADAMTS15 expression predicts survival in human breast carcinoma', *International journal of cancer. Journal international du cancer*, 118(5), pp. 1241–1247.
- Porter, N. and Barbieri, M.A. (2015) 'The role of endocytic Rab GTPases in regulation of growth factor signaling and the migration and invasion of tumor cells', *Small GTPases*, 6(3), pp. 135–144.
- Pöschl, E. *et al.* (2004) 'Collagen IV is essential for basement membrane stability but dispensable for initiation of its assembly during early development', *Development*, 131(7), pp. 1619–1628.
- Pourfarhangi, K.E., Bergman, A. and Gligorijevic, B. (2018) 'ECM Cross-Linking Regulates Invadopodia Dynamics', *Biophysical journal*, 114(6), pp. 1455–1466.
- del Pozo, M.A. *et al.* (2005) 'Phospho-caveolin-1 mediates integrin-regulated membrane domain internalization', *Nature cell biology*, 7(9), pp. 901–908.
- Preta, G., Cronin, J.G. and Sheldon, I.M. (2015) 'Dynasore - not just a dynamin inhibitor', *Cell communication and signaling: CCS*, 13, p. 24.
- Provenzano, P.P. *et al.* (2006) 'Collagen reorganization at the tumor-stromal interface facilitates local invasion', *BMC medicine*, 4(1), p. 38.
- Przemyslaw, L. *et al.* (2013) 'ADAM and ADAMTS family proteins and their role in the colorectal cancer etiopathogenesis', *BMB reports*, 46(3), pp. 139–150.
- Pucci, B., Kasten, M. and Giordano, A. (2000) 'Cell cycle and apoptosis', *Neoplasia*, 2(4), pp. 291–299.
- Pu, J. *et al.* (2016) 'Mechanisms and functions of lysosome positioning', *Journal of cell science*, 129(23), pp. 4329–4339.
- Pyrzynska, B., Pilecka, I. and Miaczynska, M. (2009) 'Endocytic proteins in the regulation of nuclear signaling, transcription and tumorigenesis', *Molecular oncology*, 3(4), pp. 321–338.
- Qian, X. *et al.* (2009) 'The Tensin-3 protein, including its SH2 domain, is phosphorylated by Src and contributes to tumorigenesis and metastasis', *Cancer cell*, 16(3), pp. 246–258.
- Qi, C. *et al.* (2021) 'T cell immune regulator 1 is a prognostic marker associated with immune infiltration in glioblastoma multiforme', *Oncology letters*, 21(4), p. 252.
- Qi, Y. *et al.* (2019) 'TSPAN9 and EMILIN1 synergistically inhibit the migration and invasion of gastric cancer cells by increasing TSPAN9 expression', *BMC cancer*, 19(1), p. 630.
- Quan, A. *et al.* (2007) 'Myristyl trimethyl ammonium bromide and octadecyl trimethyl ammonium bromide are surface-active small molecule dynamin inhibitors that block endocytosis mediated by dynamin I or dynamin II', *Molecular pharmacology*, 72(6), pp. 1425–1439.
- Rabinovitch, M. (1995) 'Professional and non-professional phagocytes: an introduction', *Trends in cell biology*, 5(3), pp. 85–87.
- Rädler, P.D. *et al.* (2021) 'Highly metastatic claudin-low mammary cancers can originate from luminal epithelial cells', *Nature communications*, 12(1), p. 3742.
- Rahman-Zaman, A., Shan, S. and Reinhart-King, C.A. (2018) 'Cell Migration in Microfabricated 3D Collagen Microtracks is Mediated through the Prometastatic Protein Girdin', *Cellular and molecular bioengineering*, 11(1), pp. 1–10.
- Raiborg, C. and Stenmark, H. (2009) 'The ESCRT machinery in endosomal sorting of ubiquitylated membrane proteins', *Nature*, 458(7237), pp. 445–452.
- Rainero, E. *et al.* (2012) 'Diacylglycerol kinase α controls RCP-dependent integrin trafficking to promote invasive migration', *The Journal of cell biology*, 196(2), pp. 277–295.

- Rainero, E. *et al.* (2015) 'Ligand-Occupied Integrin Internalization Links Nutrient Signaling to Invasive Migration', *Cell reports*, 10(3), pp. 398–413.
- Rainero, E. (2016) 'Extracellular matrix endocytosis in controlling matrix turnover and beyond: emerging roles in cancer', *Biochemical Society transactions*, 44(5), pp. 1347–1354.
- Rainero, E. and Norman, J.C. (2013) 'Late endosomal and lysosomal trafficking during integrin-mediated cell migration and invasion: cell matrix receptors are trafficked through the late endosomal pathway in a way that dictates how cells migrate', *BioEssays: news and reviews in molecular, cellular and developmental biology*, 35(6), pp. 523–532.
- Rajadurai, C.V. *et al.* (2012) 'Met receptor tyrosine kinase signals through a cortactin-Gab1 scaffold complex, to mediate invadopodia', *Journal of cell science*, 125(Pt 12), pp. 2940–2953.
- Rakash, S. (2012) 'Role of proteases in cancer: A review', *Biotechnology and Molecular Biology Reviews*, 7(4), pp. 90–101.
- Ramsay, A.G., Marshall, J.F. and Hart, I.R. (2007) 'Integrin trafficking and its role in cancer metastasis', *Cancer metastasis reviews*, 26(3-4), pp. 567–578.
- Rath, N. *et al.* (2017) 'ROCK signaling promotes collagen remodeling to facilitate invasive pancreatic ductal adenocarcinoma tumor cell growth', *EMBO molecular medicine*, 9(2), pp. 198–218.
- Raucher, D. and Sheetz, M.P. (1999) 'Membrane expansion increases endocytosis rate during mitosis', *The Journal of cell biology*, 144(3), pp. 497–506.
- Razidlo, G.L. *et al.* (2013) 'Dynamin 2 potentiates invasive migration of pancreatic tumor cells through stabilization of the Rac1 GEF Vav1', *Developmental cell*, 24(6), pp. 573–585.
- Reinhardt, D. *et al.* (1993) 'Mapping of nidogen binding sites for collagen type IV, heparan sulfate proteoglycan, and zinc', *The Journal of biological chemistry*, 268(15), pp. 10881–10887.
- Reis, C.R. *et al.* (2015) 'Crosstalk between Akt/GSK3 β signaling and dynamin-1 regulates clathrin-mediated endocytosis', *The EMBO journal*, 34(16), pp. 2132–2146.
- Rejman, J., Bragonzi, A. and Conese, M. (2005) 'Role of clathrin- and caveolae-mediated endocytosis in gene transfer mediated by lipo- and polyplexes', *Molecular therapy: the journal of the American Society of Gene Therapy*, 12(3), pp. 468–474.
- Remacle, A., Murphy, G. and Roghi, C. (2003) 'Membrane type I-matrix metalloproteinase (MT1-MMP) is internalised by two different pathways and is recycled to the cell surface', *Journal of cell science*, 116(Pt 19), pp. 3905–3916.
- Rennick, J.J., Johnston, A.P.R. and Parton, R.G. (2021) 'Key principles and methods for studying the endocytosis of biological and nanoparticle therapeutics', *Nature nanotechnology*, 16(3), pp. 266–276.
- Rhee, D.K., Park, S.H. and Jang, Y.K. (2008) 'Molecular signatures associated with transformation and progression to breast cancer in the isogenic MCF10 model', *Genomics*, 92(6), pp. 419–428.
- Ricard-Blum, S. (2011) 'The Collagen Family', *Cold Spring Harbor Perspectives in Biology*, pp. a004978–a004978. Available at: <https://doi.org/10.1101/cshperspect.a004978>.
- Rice, A.J. *et al.* (2017) 'Matrix stiffness induces epithelial-mesenchymal transition and promotes chemoresistance in pancreatic cancer cells', *Oncogenesis*, 6(7), p. e352.
- Rick, J.W. *et al.* (2019) 'Fibronectin in malignancy: Cancer-specific alterations, protumoral effects, and therapeutic implications', *Seminars in oncology*, 46(3), pp. 284–290.
- Riento, K. *et al.* (2009) 'Endocytosis of flotillin-1 and flotillin-2 is regulated by Fyn kinase', *Journal of cell*

science, 122(Pt 7), pp. 912–918.

Rigort, A. *et al.* (2004) 'Release of integrin macroaggregates as a mechanism of rear detachment during keratinocyte migration', *European journal of cell biology*, 83(11-12), pp. 725–733.

Rinaldi, G. *et al.* (2021) 'In Vivo Evidence for Serine Biosynthesis-Defined Sensitivity of Lung Metastasis, but Not of Primary Breast Tumors, to mTORC1 Inhibition', *Molecular cell*, 81(2), pp. 386–397.e7.

Rintanen, N. *et al.* (2012) 'Calpains promote $\alpha 2\beta 1$ integrin turnover in nonrecycling integrin pathway', *Molecular biology of the cell*, 23(3), pp. 448–463.

Roberts, M. *et al.* (2001) 'PDGF-regulated rab4-dependent recycling of $\alpha v\beta 3$ integrin from early endosomes is necessary for cell adhesion and spreading', *Current biology: CB*, 11(18), pp. 1392–1402.

Rock, M.T. *et al.* (2000) 'Beta1 integrin-mediated T cell adhesion and cell spreading are regulated by calpain', *Experimental cell research*, 261(1), pp. 260–270.

Rodrigues, L.R. *et al.* (2007) 'The role of osteopontin in tumor progression and metastasis in breast cancer', *Cancer epidemiology, biomarkers & prevention: a publication of the American Association for Cancer Research, cosponsored by the American Society of Preventive Oncology*, 16(6), pp. 1087–1097.

Rodriguez, R.R. *et al.* (2004) 'A type XI collagen mutation leads to increased degradation of type II collagen in articular cartilage', *Osteoarthritis and cartilage / OARS, Osteoarthritis Research Society*, 12(4), pp. 314–320.

Rodriguez-Teja, M. *et al.* (2015) 'AGE-modified basement membrane cooperates with Endo180 to promote epithelial cell invasiveness and decrease prostate cancer survival', *The Journal of pathology*, 235(4), pp. 581–592.

Rolland, Y. *et al.* (2014) 'The CDC42-interacting protein 4 controls epithelial cell cohesion and tumor dissemination', *Developmental cell*, 30(5), pp. 553–568.

Rosenbloom, J., Harsch, M. and Jimenez, S. (1973) 'Hydroxyproline content determines the denaturation temperature of chick tendon collagen', *Archives of biochemistry and biophysics*, 158(2), pp. 478–484.

Roshy, S., Sloane, B.F. and Moin, K. (2003) 'Pericellular cathepsin B and malignant progression', *Cancer metastasis reviews*, 22(2-3), pp. 271–286.

Ros, M. *et al.* (2020) 'ER-resident oxidoreductases are glycosylated and trafficked to the cell surface to promote matrix degradation by tumour cells', *Nature cell biology* [Preprint]. Available at: <https://doi.org/10.1038/s41556-020-00590-w>.

Rottiers, P. *et al.* (2009) 'TGFbeta-induced endothelial podosomes mediate basement membrane collagen degradation in arterial vessels', *Journal of cell science*, 122(Pt 23), pp. 4311–4318.

Rowe, R.G. and Weiss, S.J. (2008) 'Breaching the basement membrane: who, when and how?', *Trends in cell biology*, 18(11), pp. 560–574.

Rozhin, J. *et al.* (1994) 'Pericellular pH affects distribution and secretion of cathepsin B in malignant cells', *Cancer research*, 54(24), pp. 6517–6525.

Rubí-Sans, G. *et al.* (2021) 'Development of Cell-Derived Matrices for Three-Dimensional Cancer Cell Models', *ACS applied materials & interfaces*, 13(37), pp. 44108–44123.

Rudzińska, M. *et al.* (2019) 'The Role of Cysteine Cathepsins in Cancer Progression and Drug Resistance', *International journal of molecular sciences*, 20(14). Available at: <https://doi.org/10.3390/ijms20143602>.

Sabharanjak, S. *et al.* (2002) 'GPI-anchored proteins are delivered to recycling endosomes via a distinct cdc42-regulated, clathrin-independent pinocytic pathway', *Developmental cell*, 2(4), pp. 411–423.

Saisana, M. (2014) 'Standard Scores', in *Encyclopedia of Quality of Life and Well-Being Research*. Dordrecht: Springer Netherlands, pp. 6321–6322.

Sakamoto, T. and Seiki, M. (2010) 'A membrane protease regulates energy production in macrophages by activating hypoxia-inducible factor-1 via a non-proteolytic mechanism', *The Journal of biological chemistry*, 285(39), pp. 29951–29964.

Sallusto, F. *et al.* (1995) 'Dendritic cells use macropinocytosis and the mannose receptor to concentrate macromolecules in the major histocompatibility complex class II compartment: downregulation by cytokines and bacterial products', *The Journal of experimental medicine*, 182(2), pp. 389–400.

Sandoval, I.V. *et al.* (2000) 'Distinct reading of different structural determinants modulates the dileucine-mediated transport steps of the lysosomal membrane protein LIMP2 and the insulin-sensitive glucose transporter GLUT4', *The Journal of biological chemistry*, 275(51), pp. 39874–39885.

Sandri, C. *et al.* (2012) 'The R-Ras/RIN2/Rab5 complex controls endothelial cell adhesion and morphogenesis via active integrin endocytosis and Rac signaling', *Cell research*, 22(10), pp. 1479–1501.

Santamaría, P.G. *et al.* (2018) 'Lysyl oxidase-like 3 is required for melanoma cell survival by maintaining genomic stability', *Cell death and differentiation*, 25(5), pp. 935–950.

Santi, A. *et al.* (2023) 'Cancer-associated fibroblasts produce matrix-bound vesicles that influence endothelial cell function', *bioRxiv*. Available at: <https://doi.org/10.1101/2023.01.13.523951>.

Santiago, A. and Erickson, C.A. (2002) 'Ephrin-B ligands play a dual role in the control of neural crest cell migration', *Development*, 129(15), pp. 3621–3632.

Santibanez, J.F. (2013) 'Transforming growth factor-Beta and urokinase-type plasminogen activator: dangerous partners in tumorigenesis-implications in skin cancer', *ISRN dermatology*, 2013, p. 597927.

Sanz-Moreno, V. *et al.* (2022) 'AMPK is a mechano-metabolic sensor linking cell adhesion and mitochondrial dynamics to Myosin II dependent cell migration', *Research Square*. Available at: <https://doi.org/10.21203/rs.3.rs-1653312/v1>.

Sathe, M. *et al.* (2018) 'Small GTPases and BAR domain proteins regulate branched actin polymerisation for clathrin and dynamin-independent endocytosis', *Nature communications*, 9(1), p. 1835.

Schiapparelli, L.M. *et al.* (2014) 'Direct detection of biotinylated proteins by mass spectrometry', *Journal of proteome research*, 13(9), pp. 3966–3978.

Schjoldager, K.T. *et al.* (2020) 'Global view of human protein glycosylation pathways and functions', *Nature reviews. Molecular cell biology*, 21(12), pp. 729–749.

Schlaepfer, D.D. and Hunter, T. (1997) 'Focal adhesion kinase overexpression enhances ras-dependent integrin signaling to ERK2/mitogen-activated protein kinase through interactions with and activation of c-Src', *The Journal of biological chemistry*, 272(20), pp. 13189–13195.

Schlienger, S., Ramirez, R.A.M. and Claing, A. (2015) 'ARF1 regulates adhesion of MDA-MB-231 invasive breast cancer cells through formation of focal adhesions', *Cellular signalling*, 27(3), pp. 403–415.

Schnaeker, E.-M. *et al.* (2004) 'Microtubule-dependent matrix metalloproteinase-2/matrix metalloproteinase-9 exocytosis: prerequisite in human melanoma cell invasion', *Cancer research*, 64(24), pp. 8924–8931.

Schreij, A.M.A., Fon, E.A. and McPherson, P.S. (2016) 'Endocytic membrane trafficking and neurodegenerative disease', *Cellular and molecular life sciences: CMLS*, 73(8), pp. 1529–1545.

Schulte, J.D., Aghi, M.K. and Taylor, J.W. (2021) 'Anti-angiogenic therapies in the management of

glioblastoma', *Chinese clinical oncology*, 10(4), p. 37.

Schu, P.V. *et al.* (1993) 'Phosphatidylinositol 3-kinase encoded by yeast VPS34 gene essential for protein sorting', *Science*, 260(5104), pp. 88–91.

Schwartz, I., Seger, D. and Shaltiel, S. (1999) 'Vitronectin', *The international journal of biochemistry & cell biology*, 31(5), pp. 539–544.

Scott, P.G. *et al.* (2004) 'Crystal structure of the dimeric protein core of decorin, the archetypal small leucine-rich repeat proteoglycan', *Proceedings of the National Academy of Sciences of the United States of America*, 101(44), pp. 15633–15638.

Scully, O.J. *et al.* (2012) 'Breast cancer metastasis', *Cancer genomics & proteomics*, 9(5), pp. 311–320.

Seiffert, D. and Smith, J.W. (1997) 'The cell adhesion domain in plasma vitronectin is cryptic', *The Journal of biological chemistry*, 272(21), pp. 13705–13710.

Semenza, G.L. (1998) 'Hypoxia-inducible factor 1: master regulator of O₂ homeostasis', *Current opinion in genetics & development*, 8(5), pp. 588–594.

Setargew, Y.F.I. *et al.* (2021) 'Targeting Lysyl Oxidase Family Mediated Matrix Cross-Linking as an Anti-Stromal Therapy in Solid Tumours', *Cancers*, 13(3). Available at: <https://doi.org/10.3390/cancers13030491>.

Shah, P. *et al.* (2019) 'The NAE Pathway: Autobahn to the Nucleus for Cell Surface Receptors', *Cells*, 8(8). Available at: <https://doi.org/10.3390/cells8080915>.

Shang, M. *et al.* (2001) 'The LG3 Module of Laminin-5 Harbors a Binding Site for Integrin $\alpha 3\beta 1$ That Promotes Cell Adhesion, Spreading, and Migration', *Journal of Biological Chemistry*, pp. 33045–33053. Available at: <https://doi.org/10.1074/jbc.m100798200>.

Shao, G. *et al.* (2006) 'Epigenetic inactivation of Betaig-h3 gene in human cancer cells', *Cancer research*, 66(9), pp. 4566–4573.

Sharfe, N. *et al.* (2008) 'EphA and ephrin-A proteins regulate integrin-mediated T lymphocyte interactions', *Molecular immunology*, 45(5), pp. 1208–1220.

Shattil, S.J. (2005) 'Integrins and Src: dynamic duo of adhesion signaling', *Trends in cell biology*, 15(8), pp. 399–403.

Sheikh, H. *et al.* (2000) 'Endo180, an endocytic recycling glycoprotein related to the macrophage mannose receptor is expressed on fibroblasts, endothelial cells and macrophages and functions as a lectin receptor', *Journal of cell science*, 113 (Pt 6), pp. 1021–1032.

Shi, F. and Sottile, J. (2008) 'Caveolin-1-dependent beta1 integrin endocytosis is a critical regulator of fibronectin turnover', *Journal of cell science*, 121(Pt 14), pp. 2360–2371.

Shi, J.-Y. *et al.* (2020) 'Expression of ectopic trypsin in atherosclerotic plaques and the effects of aprotinin on plaque stability', *Archives of biochemistry and biophysics*, 690, p. 108460.

Shinchi, Y. *et al.* (2015) 'SUV420H2 suppresses breast cancer cell invasion through down regulation of the SH2 domain-containing focal adhesion protein tensin-3', *Experimental cell research*, 334(1), pp. 90–99.

Shiroto, T. *et al.* (2014) 'Caveolin-1 is a critical determinant of autophagy, metabolic switching, and oxidative stress in vascular endothelium', *PloS one*, 9(2), p. e87871.

Shi, Y.-B. *et al.* (2020) 'Multifaceted Roles of Caveolin-1 in Lung Cancer: A New Investigation Focused on Tumor Occurrence, Development and Therapy', *Cancers*, 12(2). Available at: <https://doi.org/10.3390/cancers12020291>.

- Siegfried, H. *et al.* (2022) 'The ER tether VAPA is required for proper cell motility and anchors ER-PM contact sites to focal adhesions', *bioRxiv*. Available at: <https://doi.org/10.1101/2022.10.17.512434>.
- Singh, V., Erady, C. and Balasubramanian, N. (2018) 'Cell-matrix adhesion controls Golgi organization and function through Arf1 activation in anchorage-dependent cells', *Journal of cell science*, 131(16). Available at: <https://doi.org/10.1242/jcs.215855>.
- Sinha, S. *et al.* (2016) 'Cortactin promotes exosome secretion by controlling branched actin dynamics', *The Journal of cell biology*, 214(2), pp. 197–213.
- Siri, A. *et al.* (1995) 'Different susceptibility of small and large human tenascin-C isoforms to degradation by matrix metalloproteinases', *The Journal of biological chemistry*, 270(15), pp. 8650–8654.
- Snellman, A. *et al.* (2000) 'Type XIII collagen forms homotrimers with three triple helical collagenous domains and its association into disulfide-bonded trimers is enhanced by prolyl 4-hydroxylase', *The Journal of biological chemistry*, 275(12), pp. 8936–8944.
- Snellman, A. *et al.* (2007) 'The Role of Disulfide Bonds and α -Helical Coiled-coils in the Biosynthesis of Type XIII Collagen and Other Collagenous Transmembrane Proteins', *Journal of Biological Chemistry*, pp. 14898–14905. Available at: <https://doi.org/10.1074/jbc.m609605200>.
- Sok, J.C. *et al.* (2013) 'Collagen type XI α 1 facilitates head and neck squamous cell cancer growth and invasion', *British journal of cancer*, 109(12), pp. 3049–3056.
- Soliman, N.A. and Yussif, S.M. (2016) 'Ki-67 as a prognostic marker according to breast cancer molecular subtype', *Cancer biology & medicine*, 13(4), pp. 496–504.
- Solis, G.P. *et al.* (2007) 'Reggie/flotillin proteins are organized into stable tetramers in membrane microdomains', *Biochemical Journal*, 403(2), pp. 313–322.
- Soreide, K. *et al.* (2006) 'Trypsin in colorectal cancer: molecular biological mechanisms of proliferation, invasion, and metastasis', *The Journal of pathology*, 209(2), pp. 147–156.
- Sorkin, A. and von Zastrow, M. (2009) 'Endocytosis and signalling: intertwining molecular networks', *Nature reviews. Molecular cell biology*, 10(9), pp. 609–622.
- Sottile, J. and Chandler, J. (2005) 'Fibronectin matrix turnover occurs through a caveolin-1-dependent process', *Molecular biology of the cell*, 16(2), pp. 757–768.
- Soussi, T. and Wiman, K.G. (2015) 'TP53: an oncogene in disguise', *Cell death and differentiation*, 22(8), pp. 1239–1249.
- Sowa, G. *et al.* (2003) 'The phosphorylation of caveolin-2 on serines 23 and 36 modulates caveolin-1-dependent caveolae formation', *Proceedings of the National Academy of Sciences of the United States of America*, 100(11), pp. 6511–6516.
- Specks, U. *et al.* (1992) 'Structure of recombinant N-terminal globule of type VI collagen alpha 3 chain and its binding to heparin and hyaluronan', *The EMBO journal*, 11(12), pp. 4281–4290.
- Spuul, P. *et al.* (2014) 'Importance of RhoGTPases in formation, characteristics, and functions of invadosomes', *Small GTPases*, 5, p. e28195.
- Staatz, W.D. *et al.* (1990) 'The alpha 2 beta 1 integrin cell surface collagen receptor binds to the alpha 1 (I)-CB3 peptide of collagen', *The Journal of biological chemistry*, 265(9), pp. 4778–4781.
- Steentoft, C. *et al.* (2013) 'Precision mapping of the human O-GalNAc glycoproteome through SimpleCell technology', *The EMBO journal*, 32(10), pp. 1478–1488.
- Steffensen, B. *et al.* (2002) 'Human fibronectin and MMP-2 collagen binding domains compete for collagen

binding sites and modify cellular activation of MMP-2', *Matrix biology: journal of the International Society for Matrix Biology*, 21(5), pp. 399–414.

Steinle, J.J. *et al.* (2002) 'Eph B4 receptor signaling mediates endothelial cell migration and proliferation via the phosphatidylinositol 3-kinase pathway', *The Journal of biological chemistry*, 277(46), pp. 43830–43835.

Stenmark, H. (2009) 'Rab GTPases as coordinators of vesicle traffic', *Nature reviews. Molecular cell biology*, 10(8), pp. 513–525.

Stephens, D.C. *et al.* (2019) 'Spatiotemporal organization and protein dynamics involved in regulated exocytosis of MMP-9 in breast cancer cells', *The Journal of general physiology*, 151(12), pp. 1386–1403.

Stockwell, B.R. (2004) 'Exploring biology with small organic molecules', *Nature*, 432(7019), pp. 846–854.

Stricker, T.P. *et al.* (2001) 'Structural analysis of the alpha(2) integrin I domain/procollagenase-1 (matrix metalloproteinase-1) interaction', *The Journal of biological chemistry*, 276(31), pp. 29375–29381.

Strochlic, T.I. *et al.* (2010) 'Phosphoinositides are essential coactivators for p21-activated kinase 1', *Molecular cell*, 40(3), pp. 493–500.

Strzyz, P. (2019) 'Forcing through barriers', *Nature reviews. Molecular cell biology*, p. 136.

Subramanian, A. and Schilling, T.F. (2014) 'Thrombospondin-4 controls matrix assembly during development and repair of myotendinous junctions', *eLife*, 3. Available at: <https://doi.org/10.7554/eLife.02372>.

Sugahara, K.N. *et al.* (2006) 'Tumor cells enhance their own CD44 cleavage and motility by generating hyaluronan fragments', *The Journal of biological chemistry*, 281(9), pp. 5861–5868.

Sung, B.H. *et al.* (2011) 'Cortactin controls cell motility and lamellipodial dynamics by regulating ECM secretion', *Current biology: CB*, 21(17), pp. 1460–1469.

Sun, T. *et al.* (2019) 'Blockade of a laminin-411 - Notch axis with CRISPR/Cas9 or a nanobioconjugate inhibits glioblastoma growth through tumor-microenvironment crosstalk', *Cancer research*, 79(6), p. 1239.

Sun, Y. *et al.* (2008) 'Role of siRNA silencing of MMP-2 gene on invasion and growth of laryngeal squamous cell carcinoma', *European archives of oto-rhino-laryngology: official journal of the European Federation of Oto-Rhino-Laryngological Societies : affiliated with the German Society for Oto-Rhino-Laryngology - Head and Neck Surgery*, 265(11), pp. 1385–1391.

Sun, Z. *et al.* (2018) 'Tenascin-C Promotes Tumor Cell Migration and Metastasis through Integrin $\alpha 9\beta 1$ -Mediated YAP Inhibition', *Cancer research*, 78(4), pp. 950–961.

Su, Q. *et al.* (2021) 'Sanguinarine combats hypoxia-induced activation of EphB4 and HIF-1 α pathways in breast cancer', *Phytomedicine: international journal of phytotherapy and phytopharmacology*, 84, p. 153503.

Sverdlov, M., Shajahan, A.N. and Minshall, R.D. (2007) 'Tyrosine phosphorylation-dependence of caveolae-mediated endocytosis', *Journal of cellular and molecular medicine*, 11(6), pp. 1239–1250.

Svoboda, K.K. (1991) 'Intracellular localization of types I and II collagen mRNA and endoplasmic reticulum in embryonic corneal epithelia', *Journal of cell science*, 100 (Pt 1), pp. 23–33.

Szabova, L. *et al.* (2008) 'MT1-MMP is required for efficient tumor dissemination in experimental metastatic disease', *Oncogene*, 27(23), pp. 3274–3281.

Takahashi, N., Takahashi, Y. and Putnam, F.W. (1985) 'Complete amino acid sequence of human hemopexin, the heme-binding protein of serum', *Proceedings of the National Academy of Sciences of the*

United States of America, 82(1), pp. 73–77.

Takahashi, S. *et al.* (2011) 'Downregulation of uPARAP mediates cytoskeletal rearrangements and decreases invasion and migration properties in glioma cells', *Journal of neuro-oncology*, 103(2), pp. 267–276.

Tam, E.M. *et al.* (2002) 'Collagen binding properties of the membrane type-1 matrix metalloproteinase (MT1-MMP) hemopexin C domain. The ectodomain of the 44-kDa autocatalytic product of MT1-MMP inhibits cell invasion by disrupting native type I collagen cleavage', *The Journal of biological chemistry*, 277(41), pp. 39005–39014.

Tam, E.M. *et al.* (2004) 'Characterization of the distinct collagen binding, helicase and cleavage mechanisms of matrix metalloproteinase 2 and 14 (gelatinase A and MT1-MMP): the differential roles of the MMP hemopexin c domains and the MMP-2 fibronectin type II modules in collagen triple helicase activities', *The Journal of biological chemistry*, 279(41), pp. 43336–43344.

Tanaka, K. *et al.* (2004) 'Tenascin-C regulates angiogenesis in tumor through the regulation of vascular endothelial growth factor expression', *International journal of cancer. Journal international du cancer*, 108(1), pp. 31–40.

Tanaka, Y. *et al.* (2000) 'Accumulation of autophagic vacuoles and cardiomyopathy in LAMP-2-deficient mice', *Nature*, 406(6798), pp. 902–906.

Tanase, C.P. *et al.* (2009) 'Caveolin-1 overexpression correlates with tumour progression markers in pancreatic ductal adenocarcinoma', *Journal of molecular histology*, 40(1), pp. 23–29.

Tang, J. *et al.* (2005) 'Essential role of p38gamma in K-Ras transformation independent of phosphorylation', *The Journal of biological chemistry*, 280(25), pp. 23910–23917.

Tang, W. *et al.* (2018) 'Integrated proteotranscriptomics of breast cancer reveals globally increased protein-mRNA concordance associated with subtypes and survival', *Genome medicine*, 10(1), p. 94.

Tang, Y.C. *et al.* (2018) 'Functional genomics identifies specific vulnerabilities in PTEN-deficient breast cancer', *Breast cancer research: BCR*, 20(1), p. 22.

Tan, K. and Lawler, J. (2009) 'The interaction of Thrombospondins with extracellular matrix proteins', *Journal of Cell Communication and Signaling*, pp. 177–187. Available at: <https://doi.org/10.1007/s12079-009-0074-2>.

Tarabozetti, G. *et al.* (1993) 'Enhancement of metastatic potential of murine and human melanoma cells by laminin receptor peptide G: attachment of cancer cells to subendothelial matrix as a pathway for hematogenous metastasis', *Journal of the National Cancer Institute*, 85(3), pp. 235–240.

Taylor, M.J., Perrais, D. and Merrifield, C.J. (2011) 'A high precision survey of the molecular dynamics of mammalian clathrin-mediated endocytosis', *PLoS biology*, 9(3), p. e1000604.

Teckchandani, A. *et al.* (2009) 'Quantitative proteomics identifies a Dab2/integrin module regulating cell migration', *The Journal of cell biology*, 186(1), pp. 99–111.

Teckchandani, A. *et al.* (2012) 'The clathrin adaptor Dab2 recruits EH domain scaffold proteins to regulate integrin β 1 endocytosis', *Molecular biology of the cell*, 23(15), pp. 2905–2916.

Tenni, R. *et al.* (2006) 'Self-aggregation of fibrillar collagens I and II involves lysine side chains', *Micron*, pp. 640–647. Available at: <https://doi.org/10.1016/j.micron.2006.01.011>.

Thodeti, C.K. *et al.* (2003) 'ADAM12/syndecan-4 signaling promotes beta 1 integrin-dependent cell spreading through protein kinase Calpha and RhoA', *The Journal of biological chemistry*, 278(11), pp. 9576–9584.

- Thomas, J.D. *et al.* (2014) 'Rab1A is an mTORC1 activator and a colorectal oncogene', *Cancer cell*, 26(5), pp. 754–769.
- Tian, E., Hoffman, M.P. and Ten Hagen, K.G. (2012) 'O-glycosylation modulates integrin and FGF signalling by influencing the secretion of basement membrane components', *Nature communications*, 3, p. 869.
- Timp, W. and Feinberg, A.P. (2013) 'Cancer as a dysregulated epigenome allowing cellular growth advantage at the expense of the host', *Nature reviews. Cancer*, 13(7), pp. 497–510.
- Tiosano, D. *et al.* (2019) 'Mutations in PIK3C2A cause syndromic short stature, skeletal abnormalities, and cataracts associated with ciliary dysfunction', *PLoS genetics*, 15(4), p. e1008088.
- Todorova, P.K. *et al.* (2022) 'Amino acid intake strategies define pluripotent cell states'. Available at: <https://doi.org/10.1101/2022.11.16.516803>.
- Tolonen, A.C. and Haas, W. (2014) 'Quantitative proteomics using reductive dimethylation for stable isotope labeling', *Journal of visualized experiments: JoVE* [Preprint], (89). Available at: <https://doi.org/10.3791/51416>.
- Tranquillo, R.T., Lauffenburger, D.A. and Zigmond, S.H. (1988) 'A stochastic model for leukocyte random motility and chemotaxis based on receptor binding fluctuations', *The Journal of cell biology*, 106(2), pp. 303–309.
- Tröster, A. *et al.* (2018) 'NVP-BHG712: Effects of Regioisomers on the Affinity and Selectivity toward the Ephrin Family', *ChemMedChem*, 13(16), pp. 1629–1633.
- TrypLE™ Express Enzyme (1X), phenol red (no date). Available at: <https://www.thermofisher.com/order/catalog/product/12605010> (Accessed: 14 December 2022).
- Tsai, Y.-L. *et al.* (2018) 'Endoplasmic reticulum stress activates SRC, relocating chaperones to the cell surface where GRP78/CD109 blocks TGF- β signaling', *Proceedings of the National Academy of Sciences of the United States of America*, 115(18), pp. E4245–E4254.
- Tsegaye, S. *et al.* (2021) 'Cysteine Cathepsins and Matrix Metalloproteases Among Breast Cancer Patients', *Breast cancer*, 13, pp. 271–283.
- Tsubokawa, T. *et al.* (2006) 'Cathepsin and calpain inhibitor E64d attenuates matrix metalloproteinase-9 activity after focal cerebral ischemia in rats', *Stroke; a journal of cerebral circulation*, 37(7), pp. 1888–1894.
- Turtoi, A. *et al.* (2014) 'Accessibilome of human glioblastoma: collagen-VI-alpha-1 is a new target and a marker of poor outcome', *Journal of proteome research*, 13(12), pp. 5660–5669.
- Ubersax, J.A. and Ferrell, J.E., Jr (2007) 'Mechanisms of specificity in protein phosphorylation', *Nature reviews. Molecular cell biology*, 8(7), pp. 530–541.
- Ueno, H. *et al.* (1997) 'Expression and tissue localization of membrane-types 1, 2, and 3 matrix metalloproteinases in human invasive breast carcinomas', *Cancer research*, 57(10), pp. 2055–2060.
- Ulazzi, L. *et al.* (2007) 'Nidogen 1 and 2 gene promoters are aberrantly methylated in human gastrointestinal cancer', *Molecular cancer*, 6, p. 17.
- Umasankar, P.K. *et al.* (2012) 'Distinct and separable activities of the endocytic clathrin-coat components Fcho1/2 and AP-2 in developmental patterning', *Nature cell biology*, 14(5), pp. 488–501.
- Urra, H. *et al.* (2012) 'Caveolin-1-enhanced motility and focal adhesion turnover require tyrosine-14 but not accumulation to the rear in metastatic cancer cells', *PloS one*, 7(4), p. e33085.
- Vachon, E. *et al.* (2006) 'CD44 is a phagocytic receptor', *Blood*, 107(10), pp. 4149–4158.

- Valtavaara, M. *et al.* (1997) 'Cloning and characterization of a novel human lysyl hydroxylase isoform highly expressed in pancreas and muscle', *The Journal of biological chemistry*, 272(11), pp. 6831–6834.
- Valtavaara, M. *et al.* (1998) 'Primary Structure, Tissue Distribution, and Chromosomal Localization of a Novel Isoform of Lysyl Hydroxylase (Lysyl Hydroxylase 3)', *Journal of Biological Chemistry*, pp. 12881–12886. Available at: <https://doi.org/10.1074/jbc.273.21.12881>.
- Vandenbroucke, R.E. and Libert, C. (2014) 'Is there new hope for therapeutic matrix metalloproteinase inhibition?', *Nature reviews. Drug discovery*, 13(12), pp. 904–927.
- Vargas, A.C. *et al.* (2012) 'Gene expression profiling of tumour epithelial and stromal compartments during breast cancer progression', *Breast cancer research and treatment*, 135(1), pp. 153–165.
- Veit, G. *et al.* (2006) 'Collagen XII interacts with avian tenascin-X through its NC3 domain', *The Journal of biological chemistry*, 281(37), pp. 27461–27470.
- Velling, T. *et al.* (2004) 'beta1-Integrins induce phosphorylation of Akt on serine 473 independently of focal adhesion kinase and Src family kinases', *EMBO reports*, 5(9), pp. 901–905.
- Veltman, D.M. *et al.* (2016) 'A plasma membrane template for macropinocytic cups', *eLife*, 5. Available at: <https://doi.org/10.7554/eLife.20085>.
- Vercauteren, D. *et al.* (2010) 'The use of inhibitors to study endocytic pathways of gene carriers: optimization and pitfalls', *Molecular therapy: the journal of the American Society of Gene Therapy*, 18(3), pp. 561–569.
- Verweij, F.J. *et al.* (2021) 'The power of imaging to understand extracellular vesicle biology in vivo', *Nature methods*, 18(9), pp. 1013–1026.
- Verzijl, N. *et al.* (2002) 'Crosslinking by advanced glycation end products increases the stiffness of the collagen network in human articular cartilage: a possible mechanism through which age is a risk factor for osteoarthritis', *Arthritis and rheumatism*, 46(1), pp. 114–123.
- Vicente, C.M. *et al.* (2013) 'Syndecan-2 is upregulated in colorectal cancer cells through interactions with extracellular matrix produced by stromal fibroblasts', *BMC cell biology*, 14, p. 25.
- Vidak, E. *et al.* (2019) 'Cysteine Cathepsins and their Extracellular Roles: Shaping the Microenvironment', *Cells*, 8(3). Available at: <https://doi.org/10.3390/cells8030264>.
- Vindin, H., Mithieux, S.M. and Weiss, A.S. (2019) 'Elastin architecture', *Matrix biology: journal of the International Society for Matrix Biology*, 84, pp. 4–16.
- Vizovišek, M., Fonović, M. and Turk, B. (2019) 'Cysteine cathepsins in extracellular matrix remodeling: Extracellular matrix degradation and beyond', *Matrix biology: journal of the International Society for Matrix Biology*, 75-76, pp. 141–159.
- Vogel, W. *et al.* (1997) 'The discoidin domain receptor tyrosine kinases are activated by collagen', *Molecular cell*, 1(1), pp. 13–23.
- Völker, W., Schön, P. and Vischer, P. (1991) 'Binding and endocytosis of thrombospondin and thrombospondin fragments in endothelial cell cultures analyzed by cuproinic blue staining, colloidal gold labeling, and silver enhancement techniques', *The journal of histochemistry and cytochemistry: official journal of the Histochemistry Society*, 39(10), pp. 1385–1394.
- Vranka, J.A., Sakai, L.Y. and Bächinger, H.P. (2004) 'Prolyl 3-hydroxylase 1, enzyme characterization and identification of a novel family of enzymes', *The Journal of biological chemistry*, 279(22), pp. 23615–23621.

Walsh, K. *et al.* (2013) 'PAK1 mediates resistance to PI3K inhibition in lymphomas', *Clinical cancer research: an official journal of the American Association for Cancer Research*, 19(5), pp. 1106–1115.

Wang, F.-T. *et al.* (2019) 'Cancer-associated fibroblast regulation of tumor neo-angiogenesis as a therapeutic target in cancer', *Oncology letters*, 17(3), pp. 3055–3065.

Wang, J. *et al.* (2009) 'GIT1 mediates VEGF-induced podosome formation in endothelial cells: critical role for PLCgamma', *Arteriosclerosis, thrombosis, and vascular biology*, 29(2), pp. 202–208.

Wang, T. and Hong, W. (2006) 'RILP interacts with VPS22 and VPS36 of ESCRT-II and regulates their membrane recruitment', *Biochemical and biophysical research communications*, 350(2), pp. 413–423.

Wang, Y. *et al.* (2022) 'PPP2R1A regulates migration persistence through the WAVE Shell Complex', *bioRxiv*. Available at: <https://doi.org/10.1101/2022.06.02.494622>.

Wang, Z. *et al.* (2016) 'STYK1 promotes epithelial-mesenchymal transition and tumor metastasis in human hepatocellular carcinoma through MEK/ERK and PI3K/AKT signaling', *Scientific reports*, 6, p. 33205.

Wang, Z. *et al.* (2017) 'Binding of PLD2-Generated Phosphatidic Acid to KIF5B Promotes MT1-MMP Surface Trafficking and Lung Metastasis of Mouse Breast Cancer Cells', *Developmental cell*, 43(2), pp. 186–197.e7.

Wang, Z. *et al.* (2021) 'Cancer-Associated Fibroblasts Suppress Cancer Development: The Other Side of the Coin', *Frontiers in cell and developmental biology*, 9, p. 613534.

Weber, C.K. *et al.* (2001) 'Biglycan is overexpressed in pancreatic cancer and induces G1-arrest in pancreatic cancer cell lines', *Gastroenterology*, 121(3), pp. 657–667.

Ween, M.P. *et al.* (2011) 'Transforming growth factor-beta-induced protein secreted by peritoneal cells increases the metastatic potential of ovarian cancer cells', *International journal of cancer. Journal international du cancer*, 128(7), pp. 1570–1584.

Ween, M.P., Oehler, M.K. and Ricciardelli, C. (2012) 'Transforming growth Factor-Beta-Induced Protein (TGFB1)/(β ig-H3): a matrix protein with dual functions in ovarian cancer', *International journal of molecular sciences*, 13(8), pp. 10461–10477.

Wegener, H., Paulsen, H. and Seeger, K. (2014) 'The cysteine-rich region of type VII collagen is a cystine knot with a new topology', *The Journal of biological chemistry*, 289(8), pp. 4861–4869.

Wei, H.-T. *et al.* (2015) 'Prognostic and clinical significance of syndecan-1 in colorectal cancer: a meta-analysis', *BMC gastroenterology*, 15, p. 152.

Wei, P.-L. *et al.* (2011) 'Nicotine enhances colon cancer cell migration by induction of fibronectin', *Annals of surgical oncology*, 18(6), pp. 1782–1790.

Welf, E.S. and Haugh, J.M. (2011) 'Signaling pathways that control cell migration: models and analysis', *Wiley interdisciplinary reviews. Systems biology and medicine*, 3(2), pp. 231–240.

Wen, G. *et al.* (2011) 'TGFB1 expression reduces in vitro and in vivo metastatic potential of lung and breast tumor cells', *Cancer letters*, 308(1), pp. 23–32.

Wenstrup, R.J. *et al.* (2004) 'Type V collagen controls the initiation of collagen fibril assembly', *The Journal of biological chemistry*, 279(51), pp. 53331–53337.

Werb, Z., Bainton, D.F. and Jones, P.A. (1980) 'Degradation of connective tissue matrices by macrophages. III. Morphological and biochemical studies on extracellular, pericellular, and intracellular events in matrix proteolysis by macrophages in culture', *The Journal of experimental medicine*, 152(6), pp. 1537–1553.

West, M.A. *et al.* (2000) 'Rac is required for constitutive macropinocytosis by dendritic cells but does not control its downregulation', *Current biology: CB*, 10(14), pp. 839–848.

- Wiberg, C. *et al.* (2003) 'Complexes of matrilin-1 and biglycan or decorin connect collagen VI microfibrils to both collagen II and aggrecan', *The Journal of biological chemistry*, 278(39), pp. 37698–37704.
- Wienke, D., MacFadyen, J.R. and Isacke, C.M. (2003) 'Identification and characterization of the endocytic transmembrane glycoprotein Endo180 as a novel collagen receptor', *Molecular biology of the cell*, 14(9), pp. 3592–3604.
- Wiesner, C. *et al.* (2010) 'KIF5B and KIF3A/KIF3B kinesins drive MT1-MMP surface exposure, CD44 shedding, and extracellular matrix degradation in primary macrophages', *Blood*, 116(9), pp. 1559–1569.
- Wilharm, N. *et al.* (2022) 'Biomimetic crosslinking of collagen gels by energetic electrons: The role of L-lysine', *Acta biomaterialia*, 140, pp. 219–232.
- Wilkins-Port, C.E. and McKeown-Longo, P.J. (1998) 'Degradation of distinct forms of multimeric vitronectin by human fibroblasts', *Biochimica et biophysica acta*, 1404(3), pp. 353–366.
- Williams, K.C. and Coppelino, M.G. (2011) 'Phosphorylation of membrane type 1-matrix metalloproteinase (MT1-MMP) and its vesicle-associated membrane protein 7 (VAMP7)-dependent trafficking facilitate cell invasion and migration', *The Journal of biological chemistry*, 286(50), pp. 43405–43416.
- Willumsen, N. *et al.* (2017) 'Nidogen-1 Degraded by Cathepsin S can be Quantified in Serum and is Associated with Non-Small Cell Lung Cancer', *Neoplasia*, 19(4), pp. 271–278.
- Winkler, J. *et al.* (2020) 'Concepts of extracellular matrix remodelling in tumour progression and metastasis', *Nature communications*, 11(1), p. 5120.
- Winter, A.D., McCormack, G. and Page, A.P. (2007) 'Protein disulfide isomerase activity is essential for viability and extracellular matrix formation in the nematode *Caenorhabditis elegans*', *Developmental biology*, 308(2), pp. 449–461.
- Wisdom, K.M. *et al.* (2020) 'Covalent cross-linking of basement membrane-like matrices physically restricts invasive protrusions in breast cancer cells', *Matrix biology: journal of the International Society for Matrix Biology*, 85–86, pp. 94–111.
- Wishart, A.L. *et al.* (2020) 'Decellularized extracellular matrix scaffolds identify full-length collagen VI as a driver of breast cancer cell invasion in obesity and metastasis', *Science advances*, 6(43). Available at: <https://doi.org/10.1126/sciadv.abc3175>.
- Witkiewicz, A.K. *et al.* (2012) 'Using the “reverse Warburg effect” to identify high-risk breast cancer patients: stromal MCT4 predicts poor clinical outcome in triple-negative breast cancers', *Cell cycle*, 11(6), pp. 1108–1117.
- Wolf, K. *et al.* (2003) 'Compensation mechanism in tumor cell migration: mesenchymal-amoeboid transition after blocking of pericellular proteolysis', *The Journal of cell biology*, 160(2), pp. 267–277.
- Wu, C. *et al.* (2016) 'Phosphatidylinositol 3-Kinase/Akt Mediates Integrin Signaling To Control RNA Polymerase I Transcriptional Activity', *Molecular and cellular biology*, 36(10), pp. 1555–1568.
- Wu, J.J. *et al.* (1991) 'Sites of stromelysin cleavage in collagen types II, IX, X, and XI of cartilage', *The Journal of biological chemistry*, 266(9), pp. 5625–5628.
- Wu, J.J. and Eyre, D.R. (1995) 'Structural analysis of cross-linking domains in cartilage type XI collagen. Insights on polymeric assembly', *The Journal of biological chemistry*, 270(32), pp. 18865–18870.
- Wu, J.J. and Eyre, D.R. (1998) 'Matrilin-3 forms disulfide-linked oligomers with matrilin-1 in bovine epiphyseal cartilage', *The Journal of biological chemistry*, 273(28), pp. 17433–17438.

- Wu, W. *et al.* (2020) 'Hyaluronic acid predicts poor prognosis in breast cancer patients: A protocol for systematic review and meta analysis', *Medicine*, 99(22), p. e20438.
- Wu, X. *et al.* (2005) 'FAK-mediated src phosphorylation of endophilin A2 inhibits endocytosis of MT1-MMP and promotes ECM degradation', *Developmental cell*, 9(2), pp. 185–196.
- Wu, Y.-H. *et al.* (2014) 'COL11A1 promotes tumor progression and predicts poor clinical outcome in ovarian cancer', *Oncogene*, 33(26), pp. 3432–3440.
- Wu, Z. *et al.* (2012) 'Possible role of Efnb1 protein, a ligand of Eph receptor tyrosine kinases, in modulating blood pressure', *The Journal of biological chemistry*, 287(19), pp. 15557–15569.
- Xiao, G.-Y., Mohanakrishnan, A. and Schmid, S.L. (2018) 'Role for ERK1/2-dependent activation of FCHSD2 in cancer cell-selective regulation of clathrin-mediated endocytosis', *Proceedings of the National Academy of Sciences of the United States of America*, 115(41), pp. E9570–E9579.
- Xing, X. *et al.* (2015) 'Biglycan up-regulated vascular endothelial growth factor (VEGF) expression and promoted angiogenesis in colon cancer', *Tumour biology: the journal of the International Society for Oncodevelopmental Biology and Medicine*, 36(3), pp. 1773–1780.
- Xu, H. *et al.* (2011) 'Collagen binding specificity of the discoidin domain receptors: binding sites on collagens II and III and molecular determinants for collagen IV recognition by DDR1', *Matrix biology: journal of the International Society for Matrix Biology*, 30(1), pp. 16–26.
- Xu, N.-J. and Henkemeyer, M. (2012) 'Ephrin reverse signaling in axon guidance and synaptogenesis', *Seminars in cell & developmental biology*, 23(1), pp. 58–64.
- Yadati, T. *et al.* (2020) 'Physiological Function and Role in Disease Management', *Cells*, 9(7). Available at: <https://doi.org/10.3390/cells9071679>.
- Yamaguchi, H. *et al.* (2011) 'Phosphoinositide 3-kinase signaling pathway mediated by p110 α regulates invadopodia formation', *The Journal of cell biology*, 193(7), pp. 1275–1288.
- Yamamoto, K., Miyazaki, K. and Higashi, S. (2010) 'Cholesterol sulfate alters substrate preference of matrix metalloproteinase-7 and promotes degradations of pericellular laminin-332 and fibronectin', *The Journal of biological chemistry*, 285(37), pp. 28862–28873.
- Yamashiro, Y. *et al.* (2020) 'Matrix mechanotransduction mediated by thrombospondin-1/integrin/YAP in the vascular remodeling', *Proceedings of the National Academy of Sciences of the United States of America*, 117(18), pp. 9896–9905.
- Yamauchi, M. and Sricholpech, M. (2012) 'Lysine post-translational modifications of collagen', *Essays in Biochemistry*, pp. 113–133. Available at: <https://doi.org/10.1042/bse0520113>.
- Yamazaki, S. *et al.* (2020) 'Uptake of collagen type I via macropinocytosis cause mTOR activation and anti-cancer drug resistance', *Biochemical and biophysical research communications*, 526(1), pp. 191–198.
- Yano, S. *et al.* (2014) 'Invading cancer cells are predominantly in G0/G1 resulting in chemoresistance demonstrated by real-time FUCCI imaging', *Cell cycle*, 13(6), pp. 953–960.
- Yan, S. *et al.* (2016) 'MMP inhibitor Ilomastat induced amoeboid-like motility via activation of the Rho signaling pathway in glioblastoma cells', *Tumour biology: the journal of the International Society for Oncodevelopmental Biology and Medicine* [Preprint]. Available at: <https://doi.org/10.1007/s13277-016-5464-5>.
- Yan, S. *et al.* (2019) 'LncRNA LINC01305 silencing inhibits cell epithelial-mesenchymal transition in cervical cancer by inhibiting TNXB-mediated PI3K/Akt signalling pathway', *Journal of Cellular and Molecular Medicine*, pp. 2656–2666. Available at: <https://doi.org/10.1111/jcmm.14161>.

- Yao, J. *et al.* (2014) 'Midkine promotes perineural invasion in human pancreatic cancer', *World journal of gastroenterology: WJG*, 20(11), pp. 3018–3024.
- Yasuda, Y. *et al.* (2004) 'Cathepsin V, a Novel and Potent Elastolytic Activity Expressed in Activated Macrophages', *Journal of Biological Chemistry*, pp. 36761–36770. Available at: <https://doi.org/10.1074/jbc.m403986200>.
- Yee, K.O. *et al.* (2009) 'The effect of thrombospondin-1 on breast cancer metastasis', *Breast cancer research and treatment*, 114(1), pp. 85–96.
- Yeowell, H.N. and Walker, L.C. (1999) 'Tissue specificity of a new splice form of the human lysyl hydroxylase 2 gene', *Matrix biology: journal of the International Society for Matrix Biology*, 18(2), pp. 179–187.
- Yersal, O. and Barutca, S. (2014) 'Biological subtypes of breast cancer: Prognostic and therapeutic implications', *World journal of clinical oncology*, 5(3), pp. 412–424.
- Ying Chow, W. *et al.* (2015) 'Hydroxyproline Ring Pucker Causes Frustration of Helix Parameters in the Collagen Triple Helix', *Scientific reports*, 5(1), pp. 1–11.
- Yoneda, A. *et al.* (1998) 'Characterization of the ligand binding activities of vitronectin: interaction of vitronectin with lipids and identification of the binding domains for various ligands using recombinant domains', *Biochemistry*, 37(18), pp. 6351–6360.
- York, H.M., Coyle, J. and Arumugam, S. (2020) 'To be more precise: the role of intracellular trafficking in development and pattern formation', *Biochemical Society transactions*, 48(5), pp. 2051–2066.
- Yoshida, S. *et al.* (2015) 'Differential signaling during macropinocytosis in response to M-CSF and PMA in macrophages', *Frontiers in physiology*, 6, p. 8.
- Yousaf, R. *et al.* (2015) 'MAP3K1 function is essential for cytoarchitecture of the mouse organ of Corti and survival of auditory hair cells', *Disease models & mechanisms*, 8(12), pp. 1543–1553.
- Yu, C.-H. *et al.* (2015) 'Integrin-beta3 clusters recruit clathrin-mediated endocytic machinery in the absence of traction force', *Nature communications*, 6, p. 8672.
- Yu, Q. and Stamenkovic, I. (2000) 'Cell surface-localized matrix metalloproteinase-9 proteolytically activates TGF- β and promotes tumor invasion and angiogenesis', *Genes & development*, 14(2), pp. 163–176.
- Yurchenco, P.D. and Ruben, G.C. (1987) 'Basement membrane structure in situ: evidence for lateral associations in the type IV collagen network', *The Journal of cell biology*, 105(6 Pt 1), pp. 2559–2568.
- Yu, S. *et al.* (2017) 'Development and clinical application of anti-HER2 monoclonal and bispecific antibodies for cancer treatment', *Experimental hematology & oncology*, 6, p. 31.
- Zanussi, S. *et al.* (1992) 'The human type VI collagen gene. mRNA and protein variants of the alpha 3 chain generated by alternative splicing of an additional 5-end exon', *The Journal of biological chemistry*, 267(33), pp. 24082–24089.
- Zanuttin, F. *et al.* (2004) 'Folding of epidermal growth factor-like repeats from human tenascin studied through a sequence frame-shift approach', *European journal of biochemistry / FEBS*, 271(21), pp. 4229–4240.
- Zemskov, E.A. *et al.* (2007) 'Cell-surface transglutaminase undergoes internalization and lysosomal degradation: an essential role for LRP1', *Journal of cell science*, 120(Pt 18), pp. 3188–3199.
- Zeng, Z.S., Cohen, A.M. and Guillem, J.G. (1999) 'Loss of basement membrane type IV collagen is

associated with increased expression of metalloproteinases 2 and 9 (MMP-2 and MMP-9) during human colorectal tumorigenesis', *Carcinogenesis*, 20(5), pp. 749–755.

Zhang, B. *et al.* (2008) 'Tumor-derived matrix metalloproteinase-13 (MMP-13) correlates with poor prognoses of invasive breast cancer', *BMC cancer*, 8, p. 83.

Zhang, B. *et al.* (2018) 'Matrine Is Identified as a Novel Macropinocytosis Inducer by a Network Target Approach', *Frontiers in pharmacology*, 9, p. 10.

Zhang, F. *et al.* (2003) 'Distinct ligand binding sites in integrin alpha3beta1 regulate matrix adhesion and cell-cell contact', *The Journal of cell biology*, 163(1), pp. 177–188.

Zhang, H. *et al.* (2018) 'Membrane associated collagen XIII promotes cancer metastasis and enhances anoikis resistance', *Breast cancer research: BCR*, 20(1), p. 116.

Zhang, J. *et al.* (2012) 'Brefeldin A-inhibited guanine exchange factor 2 regulates filamin A phosphorylation and neuronal migration', *The Journal of neuroscience: the official journal of the Society for Neuroscience*, 32(36), pp. 12619–12629.

Zhang, L. *et al.* (2018) 'Protein phosphatase 2A regulates the p38 signaling pathway to affect the migration of astrocytes', *Molecular medicine reports*, 18(5), pp. 4328–4334.

Zhang, M.S. *et al.* (2022) 'Hypoxia-induced macropinocytosis represents a metabolic route for liver cancer', *Nature communications*, 13(1), p. 954.

Zhang, Z. *et al.* (2018) 'COL1A1 promotes metastasis in colorectal cancer by regulating the WNT/PCP pathway', *Molecular medicine reports*, 17(4), pp. 5037–5042.

Zhao, B. *et al.* (2007) 'Inactivation of YAP oncoprotein by the Hippo pathway is involved in cell contact inhibition and tissue growth control', *Genes & development*, 21(21), pp. 2747–2761.

Zhao, J. *et al.* (2021) 'Role of EphA4 in Mediating Motor Neuron Death in MND', *International journal of molecular sciences*, 22(17). Available at: <https://doi.org/10.3390/ijms22179430>.

Zhao, Y. *et al.* (2017) 'MEK inhibitor, PD98059, promotes breast cancer cell migration by inducing β -catenin nuclear accumulation', *Oncology reports*, 38(5), pp. 3055–3063.

Zheng, L.-C. *et al.* (2017) 'Ephrin-B2/Fc promotes proliferation and migration, and suppresses apoptosis in human umbilical vein endothelial cells', *Oncotarget*, 8(25), pp. 41348–41363.

Zhou, C. *et al.* (2020) 'STYK1 promotes autophagy through enhancing the assembly of autophagy-specific class III phosphatidylinositol 3-kinase complex I', *Autophagy*, 16(10), pp. 1786–1806.

Zhou, H. and Huang, S. (2011) 'Role of mTOR signaling in tumor cell motility, invasion and metastasis', *Current protein & peptide science*, 12(1), pp. 30–42.

Zhu, M. *et al.* (2020) 'Homoharringtonine suppresses tumor proliferation and migration by regulating EphB4-mediated β -catenin loss in hepatocellular carcinoma', *Cell death & disease*, 11(8), p. 632.

Zhuo, M. *et al.* (2021) 'AP-3 adaptor complex-mediated vesicle trafficking', *Biophysics reports*, 7(2), pp. 91–100.

Zhu, Z. *et al.* (2020) 'Tumour-reprogrammed stromal BCAT1 fuels branched-chain ketoacid dependency in stromal-rich PDAC tumours', *Nature metabolism*, 2(8), pp. 775–792.

Zigrino, P. *et al.* (2016) 'Fibroblast-Derived MMP-14 Regulates Collagen Homeostasis in Adult Skin', *The Journal of investigative dermatology*, 136(8), pp. 1575–1583.

Zijlstra, A. *et al.* (2004) 'Collagenolysis-dependent angiogenesis mediated by matrix metalloproteinase-13 (collagenase-3)', *The Journal of biological chemistry*, 279(26), pp. 27633–27645.

Zoratti, G.L. *et al.* (2015) 'Targeting matriptase in breast cancer abrogates tumour progression via impairment of stromal-epithelial growth factor signalling', *Nature communications*, 6, p. 6776.

Zou, J.X. *et al.* (1999) 'An Eph receptor regulates integrin activity through R-Ras', *Proceedings of the National Academy of Sciences of the United States of America*, 96(24), pp. 13813–13818.

Zwartkruis, F.J.T. and Burgering, B.M.T. (2013) 'Ras and macropinocytosis: trick and treat', *Cell research*, 23(8), pp. 982–983.

Zweckstetter, M. *et al.* (1996) 'Structure and multiple conformations of the Kunitz-type domain from human type VI collagen $\alpha 3(VI)$ chain in solution', *Structure*, pp. 195–209. Available at: [https://doi.org/10.1016/s0969-2126\(96\)00022-6](https://doi.org/10.1016/s0969-2126(96)00022-6).

Chapter 9 – Appendix

9.1. Supplementary figures

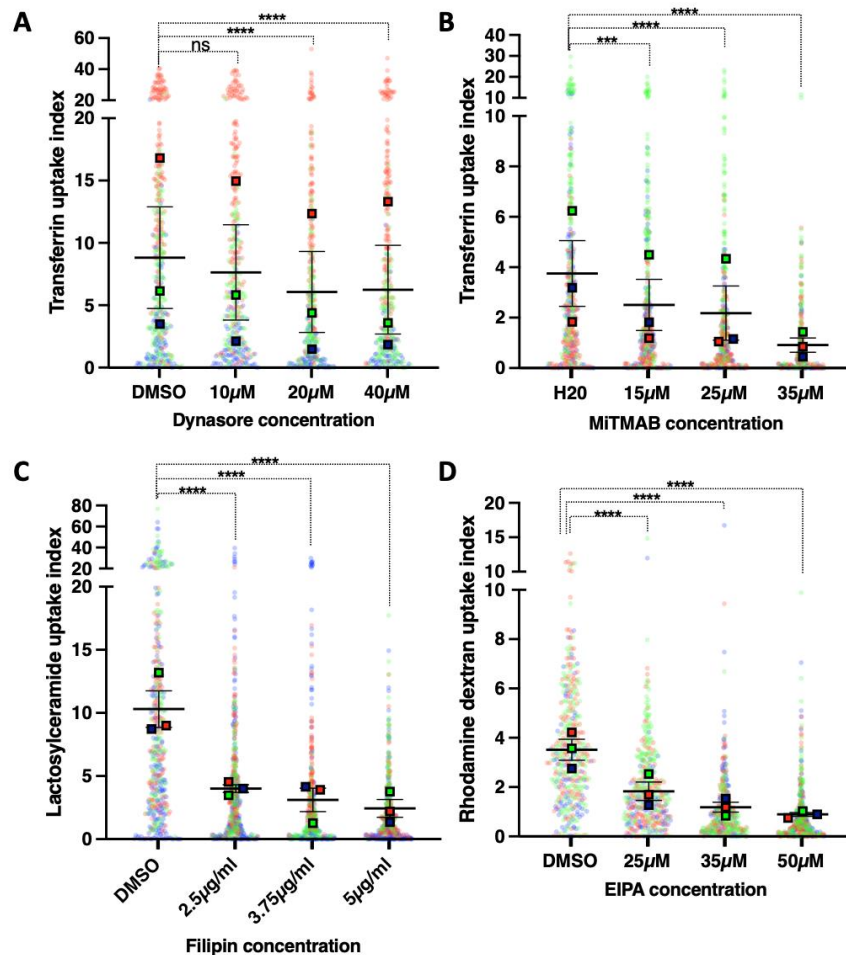


Figure S1-1. Transferrin, Lactosylceramide and Rhodamine-dextran uptake (non-normalised data related to [Figure 3-2](#), [3-3](#) and [3-4](#)). 3×10^5 MDA-MB-231 cells were seeded on 35mm glass-bottom dishes coated with 0.1mg/ml collagen I for 6h. (A-B) Afterwards, cells were pre-treated with the indicated concentrations of the dynamin inhibitors (10 μ M, 20 μ M, 40 μ M Dynasore in 2% FBS; 15 μ M, 25 μ M, 35 μ M MiTMAB) and the corresponding vehicle controls (DMSO or H₂O respectively) for 30min. Following pre-treatment, cells were incubated in the presence of 5 μ g/ml Transferrin for another 30 min and then fixed and stained with Phalloidin Alexa Fluor 647 and DAPI to visualise F-actin and the nuclei. Cell imaging was carried out with a 60X objective Nikon A1 confocal microscope. Image J was used to analyse the TF uptake index. (C) Cells were then pre-treated with DMSO (vehicle), 2.5 μ g/ml, 3.75 μ g/ml and 5 μ g/ml Filipin for 30min; media was then aspirated and cells were further incubated for 10min on ice with ice-cold 0.5 μ M Lactosylceramide media, which additionally contained either DMSO (vehicle), 2.5 μ g/ml, 3.75 μ g/ml or 5 μ g/ml Filipin. The dishes were later incubated for 90 seconds at 37 $^{\circ}$ C. Phalloidin Alexa 555 was used to label the actin cytoskeleton and Vectashield mounting medium with DAPI for the nuclei staining. Imaging with a 60X objective Nikon A1 confocal microscope was followed by Image J analysis. (D) Cells were then pre-treated with DMSO (vehicle), 25 μ M, 35 μ M and 50 μ M EIPA for 30min. Following pre-treatment, cells were incubated in the presence of 0.2mg/ml Rhodamine-dextran (red) for another 60min. Cells were then fixed and stained with an antibody against β 1-integrin to visualise the PM (green) and the nuclei (blue). Cell imaging was carried out with a 60X objective Nikon A1 confocal microscope. Image J was used to analyse the dextran uptake index. The SuperPlot shows the normalised cell-level data and mean values \pm SEM from N=3 independent experiments; ns (not significant), *** $p=0.0002$, **** $p<0.0001$; Kruskal-Wallis test.

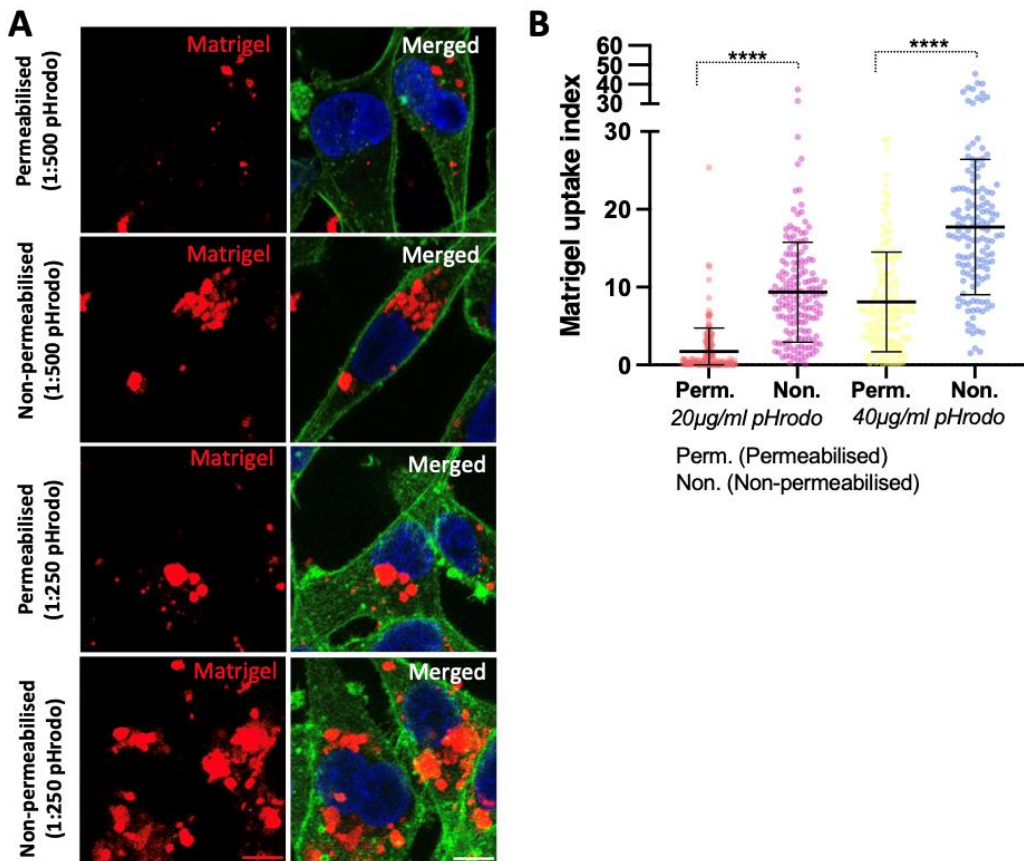


Figure S1-2. Cell permeabilization decreases the fluorescence intensity of endocytosed pH-rodo labelled matrigel in MDA-MB-231 cells. MDA-MB-231 cells were serum starved for 24h and seeded on 35mm glass-bottom dishes coated with pHrodo red-labelled 1mg/ml matrigel in presence of 20µM Aloxistatin (E64d) for 24h. Two different pHrodo dilutions (20µg/ml and 40µg/ml) were used. Cells were either fixed and permeabilized with 0.25% Triton X-100 and later stained with Phalloidin Alexa 488 to label the actin cytoskeleton (green) or fixed and stained for β1-integrin (to delimit the cell membrane). Vectashield mounting media containing DAPI was used for the nucleus staining (blue). Scale bar, 20µm. Cells were z-stacked imaged at 1µm intervals with a 60X objective of Nikon A1 confocal microscope. Image J software was used to analyse the ECM uptake index. The scatter plot shows the normalised mean and SD from N=1 experiment; * $p=0.0117$; **** $p<0.0001$; Kruskal-Wallis test.

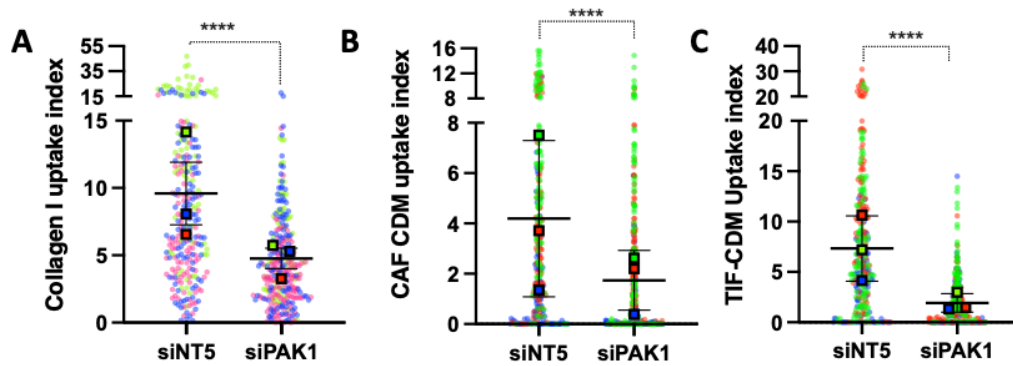


Figure S1-3. PAK1 mediates macropinocytosis of collagen-rich ECM in MDA-MB-231 cells (non-normalised data related to Figure 3-24). 10 μ l of 5 μ M siRNA and 190 μ l OptiMEM per well were mixed in a 6 well plate. 1 μ l Dharmafect I was mixed and incubated with 199 μ l OptiMEM for 5min. 200 μ l of the solution was added on top of the siRNA and incubated for 20min on a rocker. 4 \times 10⁵ cells, contained in 1600 μ l, were added into each well. Following 72h, cells were trypsinized and counted. 3 \times 10⁵ cells per condition were seeded onto 1mg/ml collagen I (NHS-Alexa fluor 555; A), CAF- (pHrodo; B) and TIF-CDM (pHrodo; C). Cells were incubated on top of the matrices for 6h. In (A), cells were fixed and stained with hoechst and Phalloidin Alexa fluor 488. In (B-C), cells were stained with hoechst and imaged live. A 60X oil immersion objective from a Nikon A1 confocal microscope was used for imaging. Analysis was carried in ImageJ. Values represented are cell data (dots) and mean data (squares) + SD; N=3 independent experiments; **** p <0.0001; Mann-Whitney test.

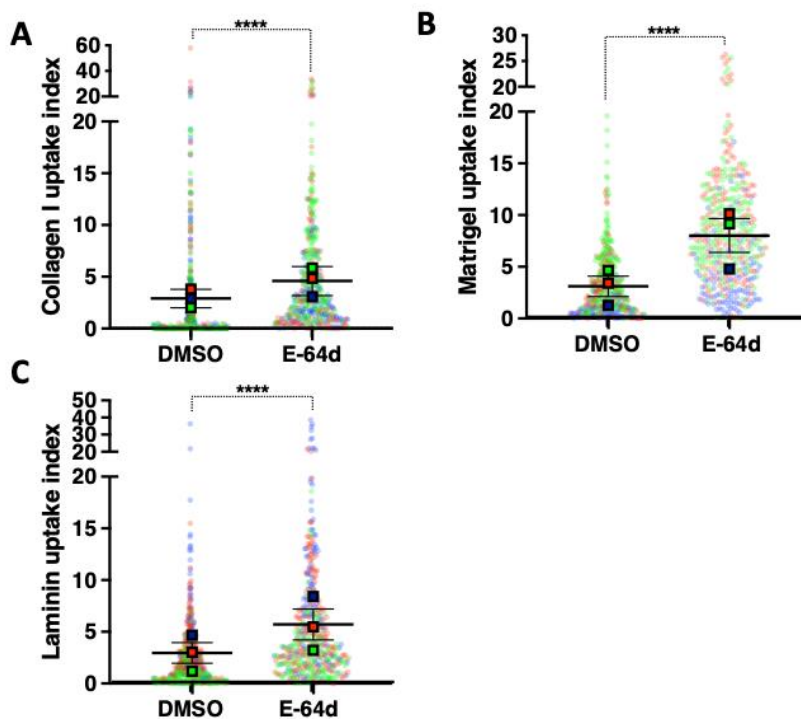


Figure S1-4. Endocytosed ECM is degraded in the lysosomes by cysteine cathepsins (non-normalised data related to Figure 5-2). 3 \times 10⁵ MDA-MB-231 cells were seeded on 35mm glass-bottom dishes coated with NHS-fluorescein (green)-labelled 1mg/ml collagen I (A), 1mg/ml matrigel (B) and 2mg/ml laminin-111 (C) for 24h in presence of DMSO (vehicle) or 20 μ M Aloxistatin (E64d). Cells were fixed and stained with Phalloidin Alexa 555 to label the actin cytoskeleton (red) and DAPI for the nucleus staining (blue). Scale bar represents 20 μ m. Cells were z-stacked imaged at 1 μ m intervals with a 60X objective of Nikon A1 confocal microscope. Image J software was used to analyse the ECM uptake index. The scatter plot shows the cell-level and mean values \pm standard error of the mean (SEM) from three independent experiments; each replicate is shown in a different colour (blue, red, green). **** p <0.0001; Mann-Whitney test ($n > 400$ cells per condition).

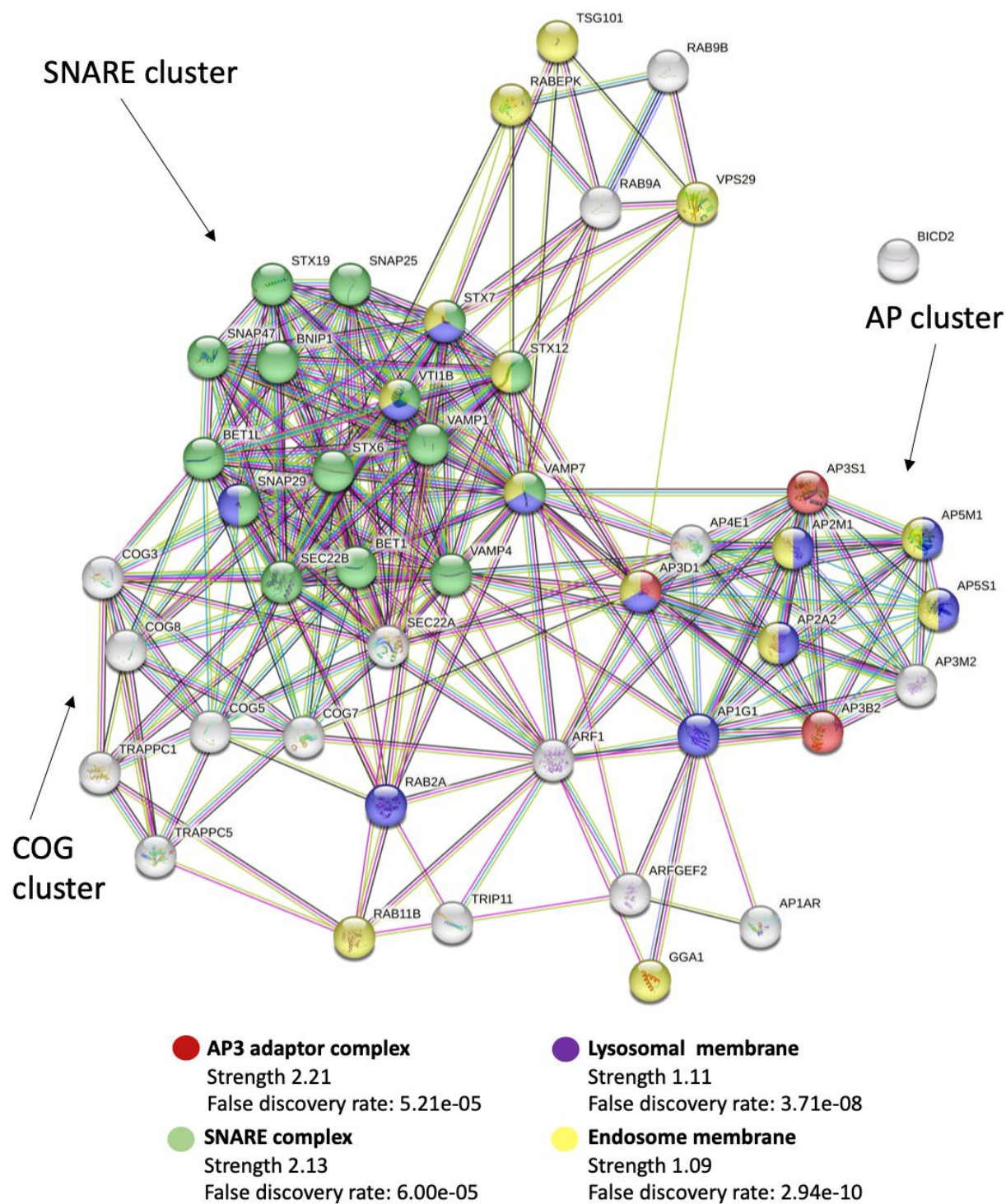


Figure S1-5. STRING Analysis: Trafficking screen. The online server *STRING: Protein-Protein Interaction networks & functional enrichment analysis* (<https://string-db.org/>) is a biological database of known and predicted protein interactions. 45 non-stringent hits were analysed using this online platform. Three main clusters were observed: COG, SNARE and AP proteins. Gene ontology analysis by cellular component showed a strong cluster of AP3 adaptor complex (red) and SNARE complex (green). Proteins were categorised into lysosomal (purple) and endosomal (yellow) membranes.

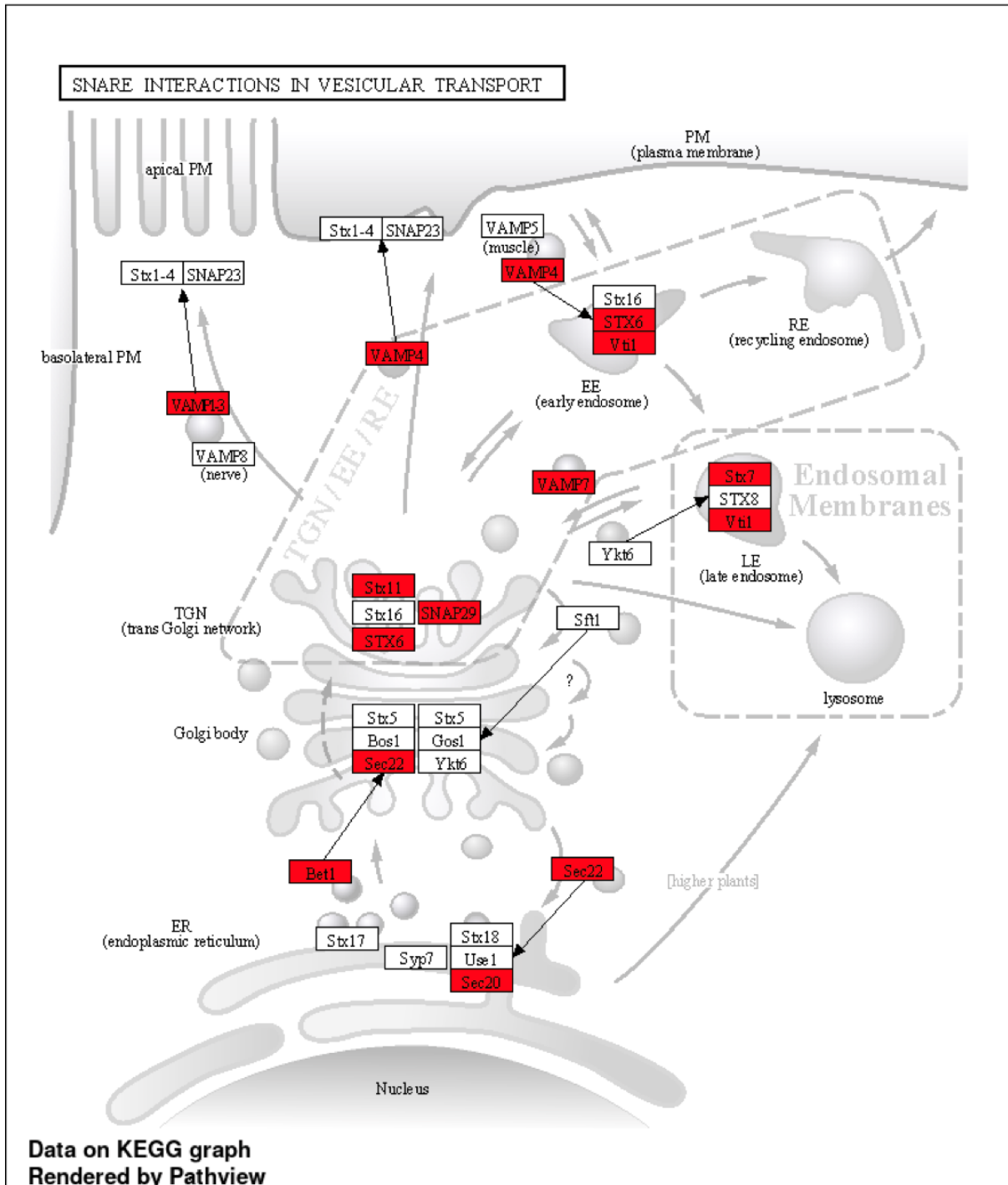


Figure S1-6. KEGG analysis- SNARE interactions in vesicular transport. Enrichment analysis displayed by the e graphical bioinformatics tool ShinyGO (<http://bioinformatics.sdstate.edu/go/>).

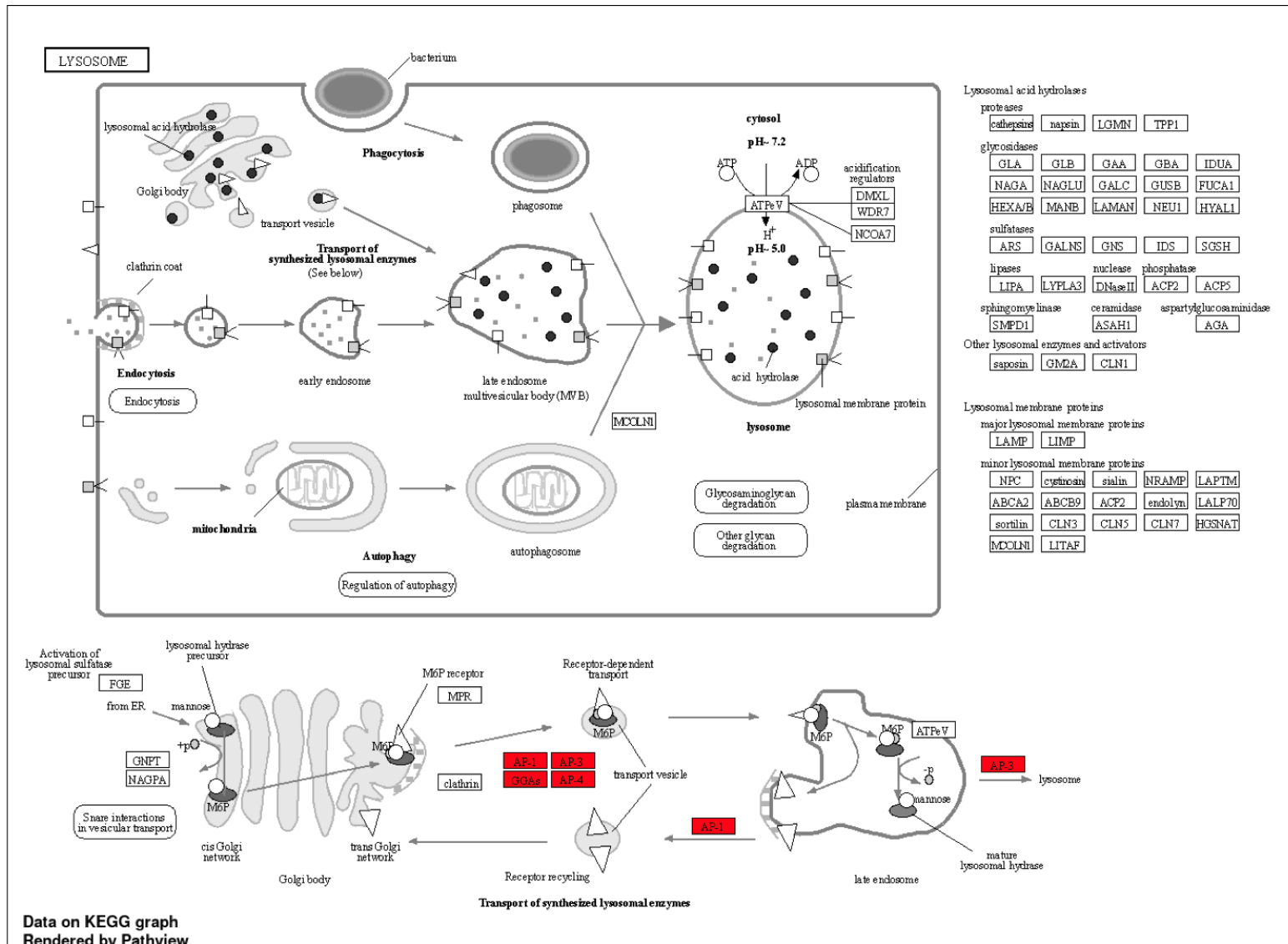


Figure S1-7. KEGG analysis- Lysosome. Enrichment analysis displayed by the e graphical bioinformatics tool ShinyGO (<http://bioinformatics.sdstate.edu/go/>).

A > P05556 (UniProt ID) – ITGB1
 MNLQPIFWIG LISSVCCVFA QTDENRCLKA NAKSCGECIQ AGPNCGWCTN STFLQEGMPT
 SARCCDDLEAL KKKGCPPDDI ENPRGSKDIK KNKNVNTNRSK GTAELKLPED ITQIQPQQLV
 LRLRSGEPQT FTLKFKRAED YPIDLYYLM DLSYSMKDDLE NVKSLGTDLM NEMRRITSDF
 RIGFGSFVEK TVMPYISTTP AKLRNPCTSE QNCTSPFSYK NVLSLTNKG VFNELVKGQR
 ISGNLDSPEG GFDAIMQVAV CGSLIGWRNV TRLLVFSTDA GFHFAGDGLK GGIVLPNDGQ
 CHLENNMYTM SHYYDYPISA HLVQKLENN IQTIFAVTEE **FQPVYKELKN LIPKSAVGLT**
 SANSSNVQL IIDAYNSLSS EVILENGKLS EGVTSYKSY CKNGVNGTGE NGRKCSNISI
 GDEVQFEISI TSNKCPK KDS DSKIRPLGF TEEVEVILQY ICECECQSEG IPESPKCHEG
 NGTFECGACR CNEGRVGRHC ECSTDEVNSE DMDAYCRKEN SSEICSNNGE CVCGQCVCRK
 RDNTNEIYSG KFCECDNFNC DRNGLICGG NGVCKCRVCE CNPNYTGSA C DCSLDTSTCE
 ASNGQICNQR GICEGCVCK TDPKFGQTC EMCQTC LGVC AEHKECVQCR AFNKGEK KDT
 CTQECYSFNI TKVESRDKLP QPVQDPVSH CEKDVDDCW FYFTYSVNGN NEVMVHVVEN
 PECPTGPDII PIVAGVVAGI VLIGLALLI WKLLMIHDR REFAKFEKEK MNAKWDTGEN
 PIYKSAVTV VNPKEGK

> P17301 (UniProt ID) – ITGA2
 MGPERTGAAP LPLLLVLALS QGILNCCLAY NVGLPEAKIF SGPSEQFGY AVQQFINPKG
 NWLLVGGSPWS GFPENRMGDV YKCPVDLSTA TCEKLNLTQS TSIPNVTEMK TNMSLGLILT
 RNMGTGGFLT CGPLWAQQCG NQYTTGVCS DISPDFQLSA SFSPATQPCP SLIDVVVCD
 ESNISYPWDA VKNFLEKLVQ GLDIGPTKTQ VGLIQYANNP RVVFNLTNYK TKEEMIVATS
 QTSQYGGDLT NTFGAIQYAR KYAYSAASGG RRSATKVMVV VTDGESH DGS MLKAVIDQCEN
 HDNLRFGIA VLYGLNRNAL **DTKNLKEIK** AIASIPTEY FFNVSDEAAL LEKAGTLGEQ
 IFSIEGTVQG GDNFQMEMSQ VGFSA DYSSQ NDILMLGAVG AFGWSGTIVQ KTSHGHLIFP
 KQAFDQILQD RNHSSYLGYS VAAISTGEST HFVAGAPRAN YTGQIVLYSV NENGNITVIQ
 AHRGDQIGSY FGSVLCSDV DKTITDVL VLGAPMYMSDL KKEEGRVYLF TIKEGILGQH
 QFLEGPEGIE NTRFGSAIAA LSDINMDGFN DVIVGSPLEN QNSGAVYIN GHQGTIRTKY
 SQKILGSDGA FRSHLQYFGR SLDGYGDLNG DSITDV SIGA FGQVVLWSQ SIADVAIEAS
 FTPEKITLVN KNAQIILKLC FSAKFRPTKQ NNQVAIVYNI TLDADGFSSR VTSRGLFKEN
 NERCLQKNMV VNAQSQCEPH IYIQEPSDV VNSLDRVDI SLENPGTSPA LEAYSETAKV
 FSIPFHKDCG EDGLCISDLV LDVRQIPAAQ EQPFIVSNQN KRLTFSVTLK NKRESAYNTG
 IVVDFSENLF FASFLPVDG TEVTCQVAAS QKSVACDVGY PALKREQQVT FTINDFNLQ
 NLQNQASLSF QALSESQ EEN KADNLVNLKI PLYDAEIH LTRSTNINFYE ISSDGNVPSI
 VHSFEDVGPK FIFSLKVTG SVPVSMATVI IHIPQYKKEK NPLMYLTGVQ TDKAGDISCN
 ADINPLKIGQ TSSSVFSKSE NFRHTKELNC RTASC SNVTC WLKDVHMKGE YFVNVTTRIV
 NGTFASSTFQ TVQLTAAAEI NTYNPEIYVI EDNTVTIPLM IMKPDEKAEV PTGVIIGSII
 AGILLLLALV AILWKLGF FFK RYKEMTKNP DEIDETTELS S

> Q14108 (UniProt ID) – LIMP2
 MGRCCFYTAG TSLLLLLVTS VTLVARVFQ KAVDQSIEKK IVLRNGTEAF DSWEKPLPV
 YTQFYFNVN NPEEILRGET PRVEEVGPY YRELNRKANI QFGDNGTTIS AVSNKAYVFE
 RDQSVGDPKI DLIRTLNIPV LTVIEWSQVH FLREIEAML KAYQKLFVT HTVDELLWGY
 KDEILSLIH FRPDISPYFG LFYEKNGTND GDYVLTGED SYLNF TKIVE WNGKTSLDWW
 ITDKCNMING TDGDSFHPLI TKDEVLYVFP SDFCRSVYIT FSDYESVQGL PAFRYKVP AE
 ILANTSDNAG FCIPEGNCLG SGVLNVSICK NGAPIIMSFP HFYQADERFV SAIEGMHPNQ
 EDHETFVDIN PLTGILKAA KRFQINIYVK KLDDFVETGD IRTMVFPVMY LNESVHIDKE
 TASRLKSMIN TTLITNIPY IIMALGVFFG LVFTWLACKG **QGSMDDEGTAD ERAPLIRT**

B

```

CLUSTAL O(1.2.4) multiple sequence alignment

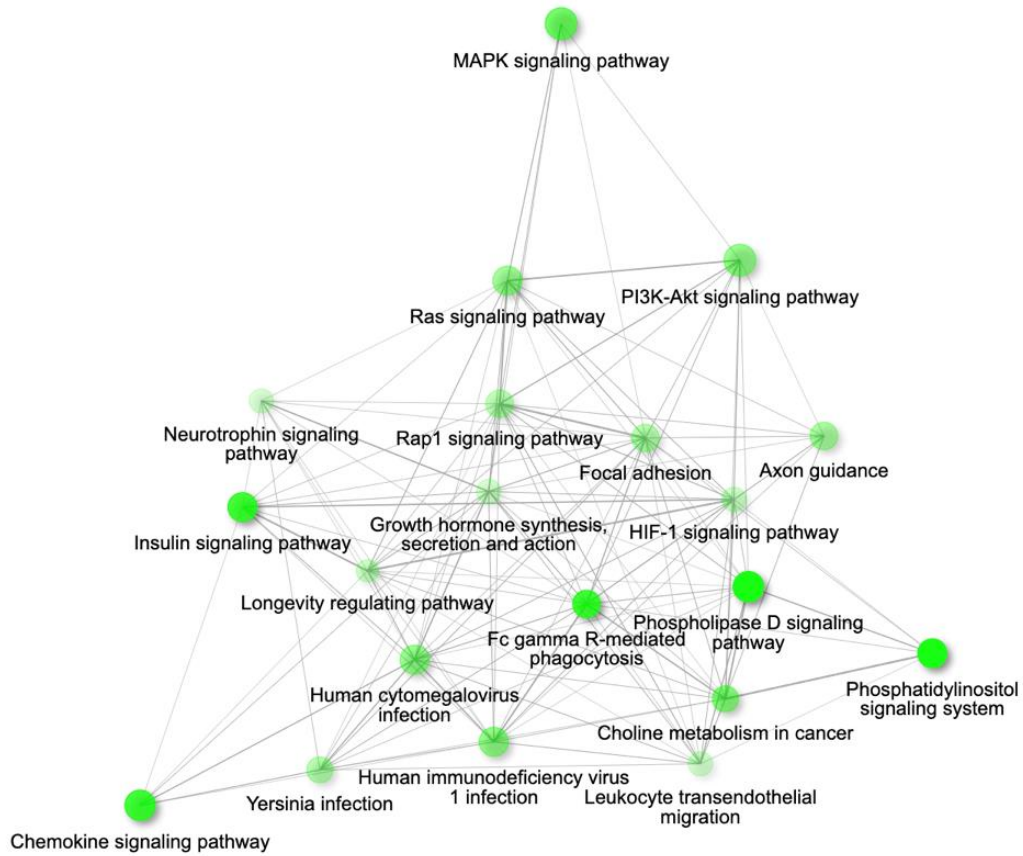
ITGB1      FQ-PVYKELKNLIPKS      15
ITGA2      LN-RNALDTKNLIKEI      15
LIMP2      MDEGTADERAPLIRT-      15
          ::      :      **
  
```

C Percent Identity Matrix

ITGB1	100.00%	26.67%	21.43%
ITGA2	26.67%	100.00%	21.43%
LIMP2	21.43%	21.43%	100.00%

Figure S1-8. Sequence analysis of ITGB1, ITGA2 and LIMP2. (A) The online database UniProt (<https://www.uniprot.org/>) was used for freely accessing the protein sequences of ITGB1, ITGA2 and LIMP2. (B) Sequence alignment of a protein fragment from potential [D/E]XXXL[L/I] motives in ITGB1 and ITGA2 against the [D/E]XXXL[L/I] motif from LIMP2. (C) Percent identity matrix from the sequence alignment in B.

A



B

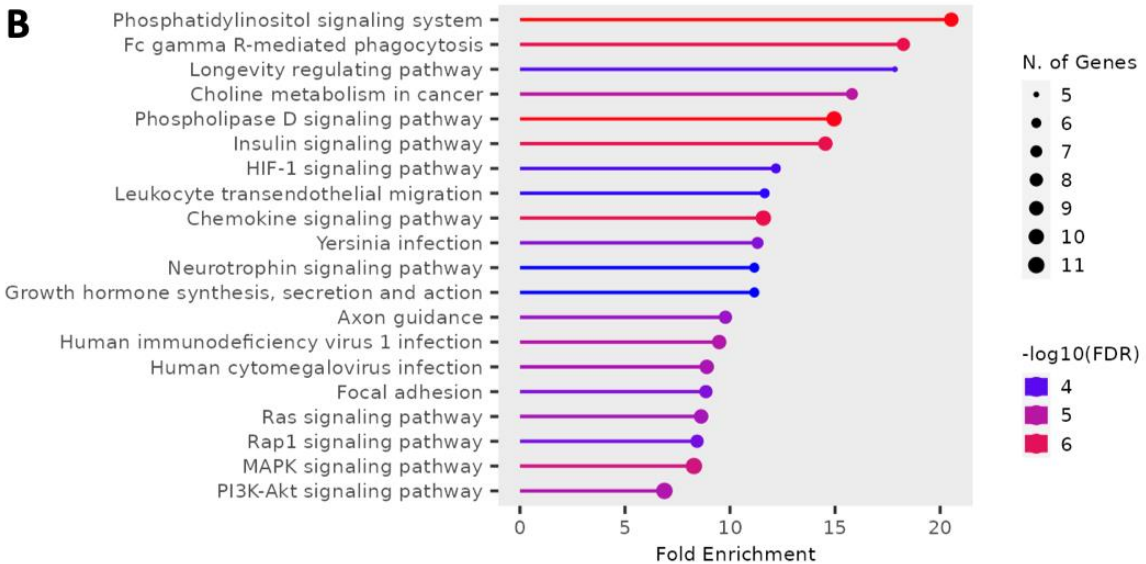
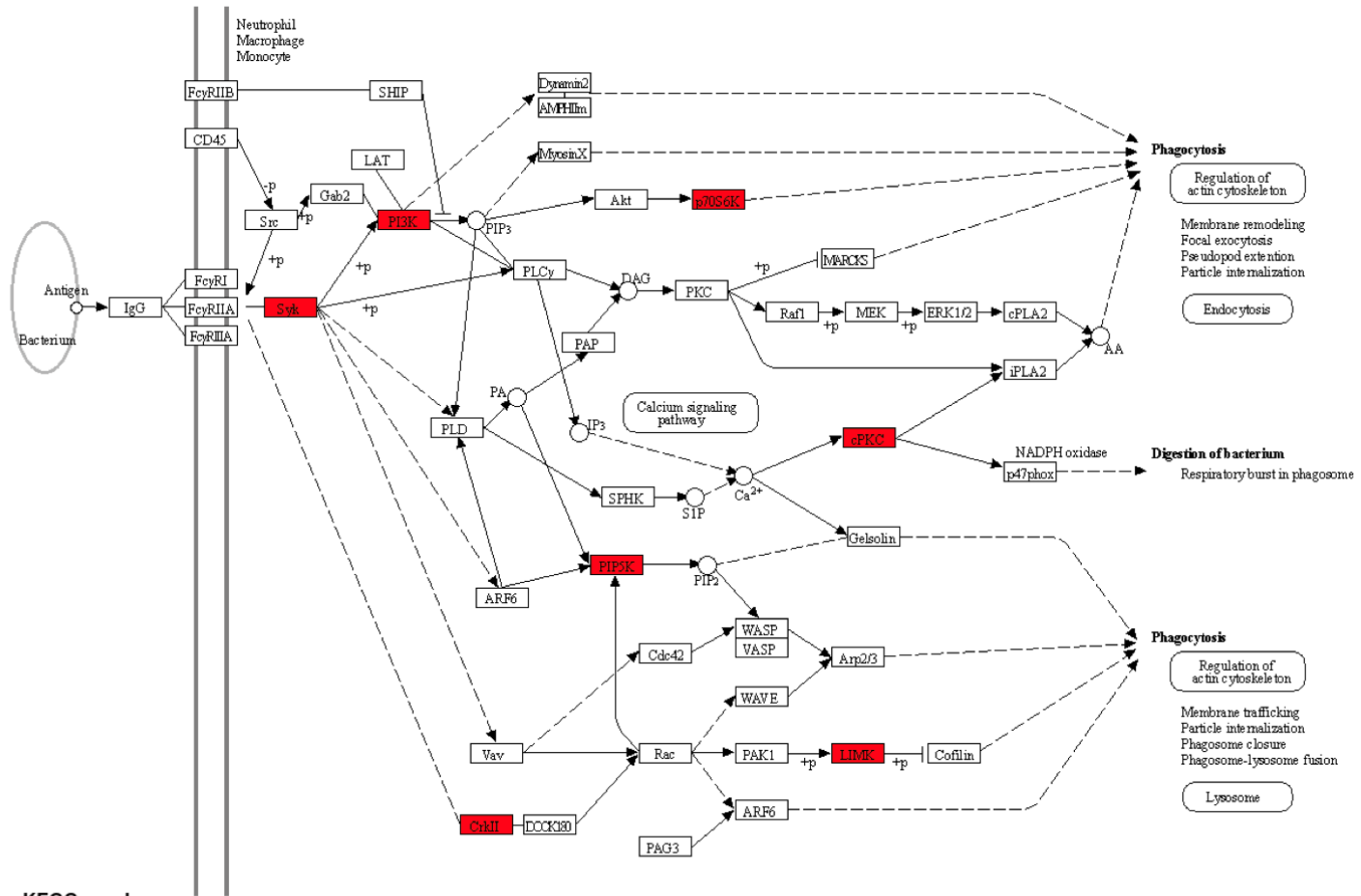


Figure S1-9. KEGG pathways enriched in the primary screen. Enrichment analysis was performed using the online server ShinyGO (<http://bioinformatics.sdstate.edu/go/>). Significantly enriched pathways included: MAPK signalling pathway, PI3K-Akt signalling pathway, Fc gamma R-mediated phagocytosis, HIF1-signalling pathway, phospholipase D signalling pathway, phosphatidylinositol signalling system and choline metabolism in cancer.

FcγR-MEDIATED PHAGOCYTOSIS



Data on KEGG graph
Rendered by Pathview

Figure S1-10. KEGG pathway: FcR-mediated phagocytosis. Enrichment analysis displayed by the e graphical bioinformatics tool ShinyGO (<http://bioinformatics.sdstate.edu/go/>).

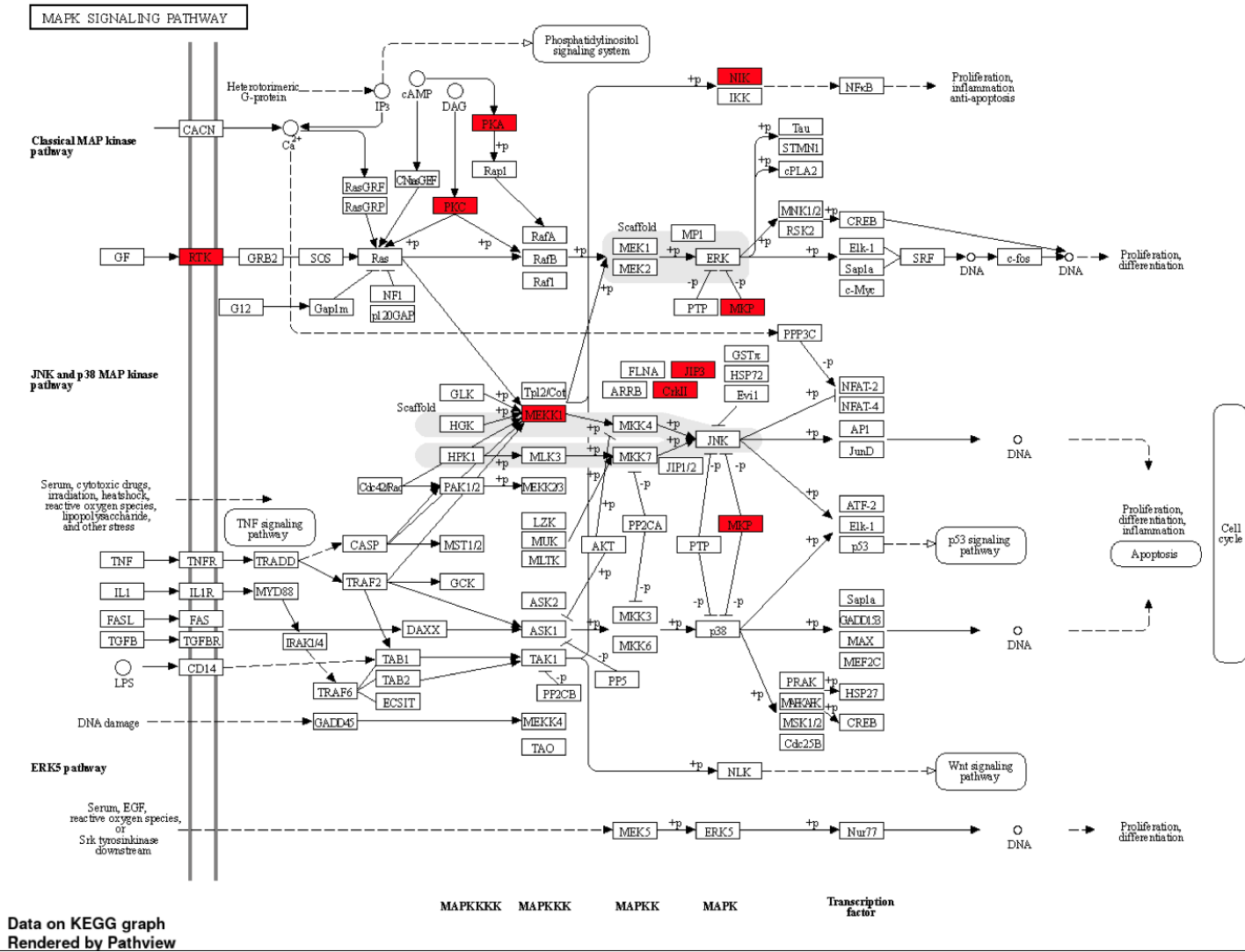
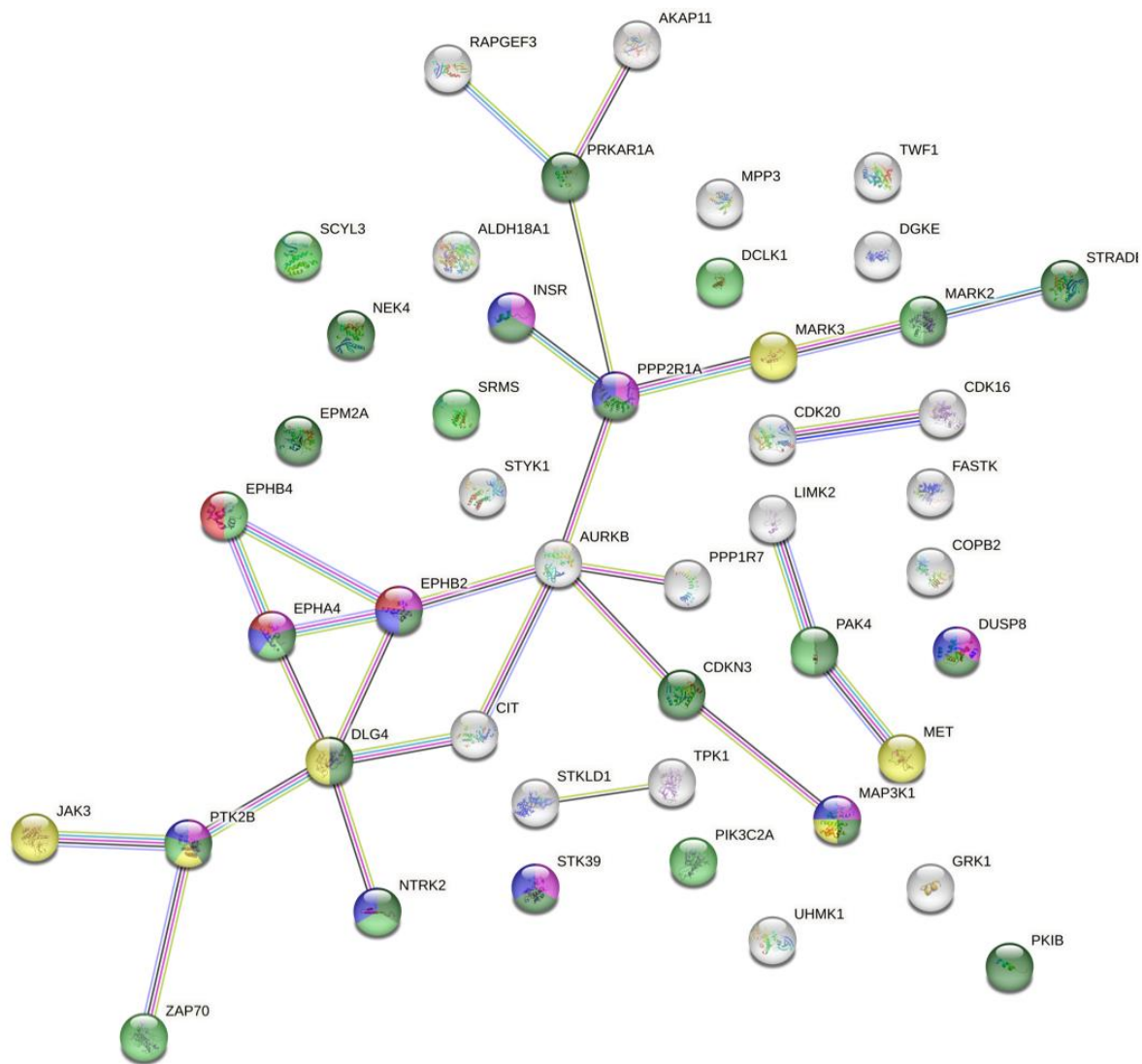


Figure S1-11. KEGG pathways: MAPK Signalling pathway. Enrichment analysis displayed by the e graphical bioinformatics tool ShinyGO (<http://bioinformatics.sdstate.edu/go/>).



- **Ephrin Receptor activity**
 Strength 1.83
 False discovery rate: 0.0021

● **Cell migration**
 Strength 0.72
 False discovery rate: 0.0012

● **Regulation of protein kinase activity**
 Strength 0.97
 False discovery rate: 1.10e-10
- **Regulation of MAPK Cascade**
 Strength 0.72
 False discovery rate: 0.0064

● **MAPK Cascade**
 Strength 0.84
 False discovery rate: 0.0246

● **Regulation of MAPK activity**
 Strength 1
 False discovery rate: 0.00033

Figure S1-12. STRING Analysis: Kinome and Phosphatome. The online server STRING: Protein-Protein Interaction networks & functional enrichment analysis (<https://string-db.org/>) is a biological database of known and predicted protein interactions. 47 hits were analysed using this online platform. Gene ontology analysis by Biological process and Molecular function showed a strong cluster of Ephrin Receptor activity (red), Cell migration (light green), Regulation of protein kinase activity (dark green), Regulation of MAPK Cascade (purple), MAPK Cascade (yellow) and Regulation of MAPK activity (pink).

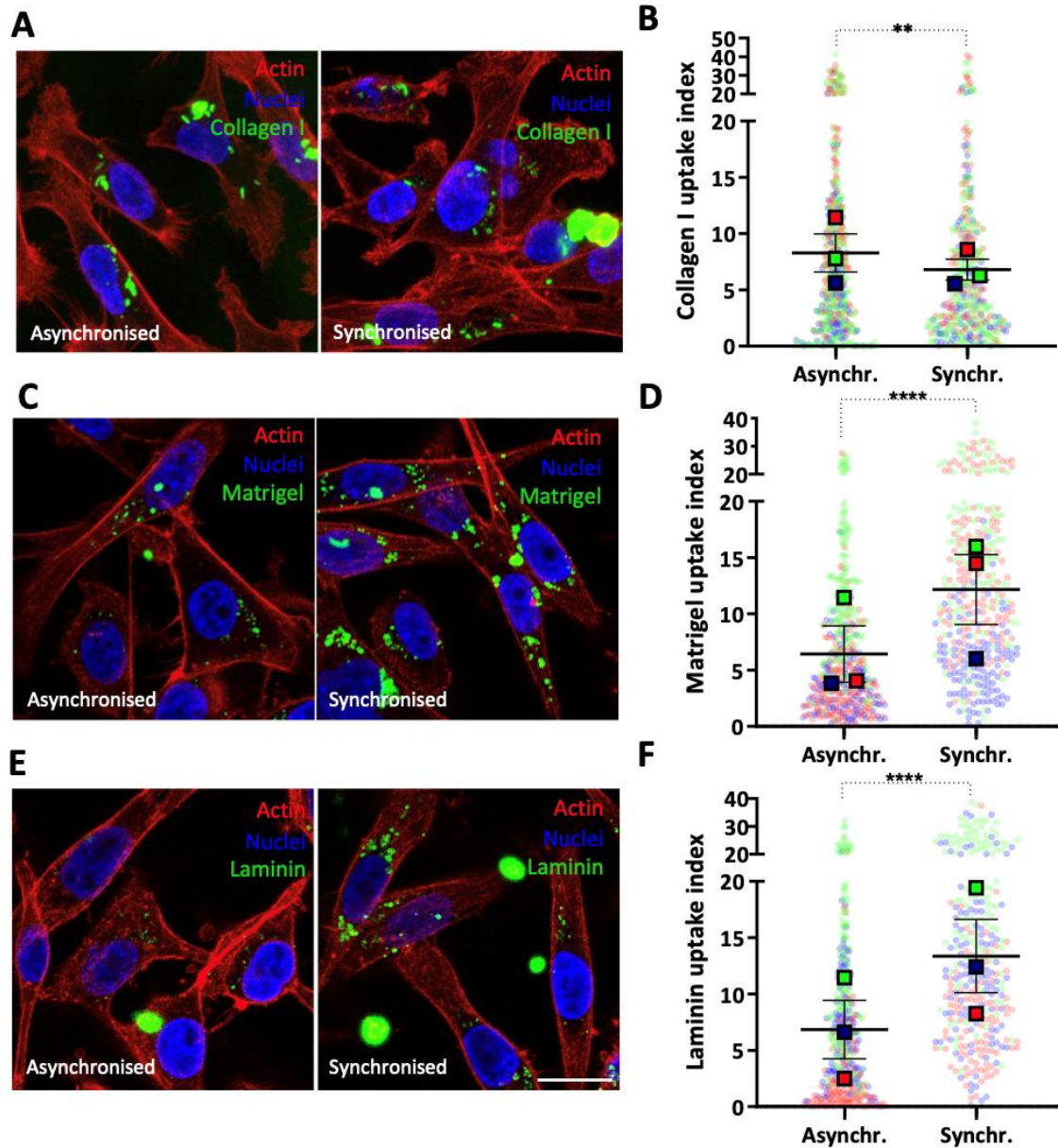


Figure S1-13. Effect of synchronisation by serum starvation on ECM uptake. 40% confluent MDA-MB-231 cells were serum-starved for 24h in order to synchronise them at G0/G1 phase (as described previously on Langan and Chou, 2011), referred to as serum-synchronisation. Asynchronous and synchronous MDA-MB-231 cells were plated on NHS-fluorescein labelled (green) 1mg/ml collagen I (A,B), 1mg/ml matrigel (C,D) and 2mg/ml laminin (E,F) as described in Figure 3-2. Cells were incubated for 24h in presence of 20 μ M E64d and were later fixed and stained with Phalloidin Alexa 555 to label the actin cytoskeleton (red). Vectashield mounting agent containing DAPI was used to visualise the nuclei (blue). Z-stacked images were taken with 60X objective of Nikon A1 confocal microscope. ECM uptake index was analysed with ImageJ. Scale bar, 20 μ m. The scatter plot shows the cell level data and mean \pm SEM from N=3 independent experiments, each replicate is shown in a different colour (blue, red, green); **** p <0.0001, ** p =0.0082; Mann-Whitney test.

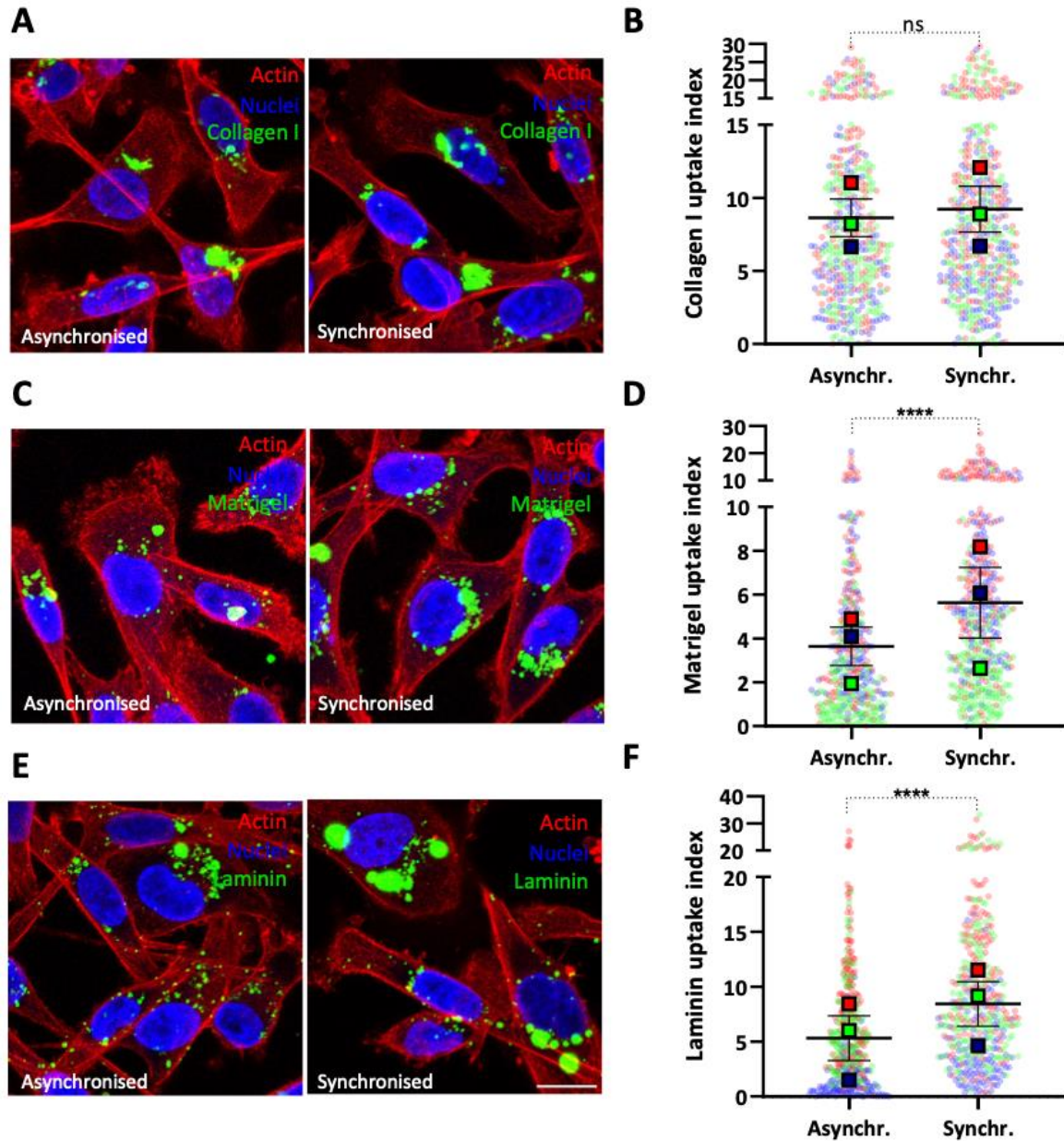


Figure S1-14. Effect of double thymidine block synchronisation on ECM uptake. Double thymidine block (thoroughly described in Chen and Deng, 2018) was used to stop cell cycle in the G1/S phase boundary. 2×10^6 to 3×10^6 MDA-MB-231 cells were plated overnight in a 10cm dish. The following day, MDA-MB-231 cells were cultured in DMEM media supplemented with 2mM thymidine for 18h. Cells were then washed twice with 1X PBS and incubated in thymidine-free media for 9h. A second 18h- incubation round of 2mM thymidine was performed to stop cell cycle in the G1/S phase boundary. Asynchronised and synchronised cells were seeded on NHS-labelled 1mg/ml collagen I (A,B), 1mg/ml matrigel (C,D) and 2mg/ml laminin (E,F) for 24h in presence of $20 \mu\text{M}$ E64d to enhance endocytosed ECM levels. Following fixation, Phalloidin Alexa 555 and DAPI were utilised to stain the actin cytoskeleton and the nuclei. Cells were z-stacked imaged with a 60X objective of Nikon A1 confocal microscope. Scale bar represents $20 \mu\text{m}$. Image J was utilised to analyse ECM uptake index. The scatter plot shows the cell level data and mean \pm SEM from three independent experiments, each replicate is in a different colour (blue, red, green); **** $p < 0.0001$, ns (not significant); Mann-Whitney test.

9.2. Supplementary tables

Table S1-1. Heat map table that shows the median and arithmetic mean values for TF uptake index upon dynasore treatment.

	Dynasore concentration	Median	Arithmetic mean
Absolute values	DMSO	7.245	9.575
	10 μ M	5.941	8.823
	20 μ M	3.814	6.285
	40 μ M	4.469	7.202
Normalised values	DMSO	0.8737	1
	10 μ M	0.7009	0.8385
	20 μ M	0.4743	0.6339
	40 μ M	0.5024	0.6584

Table S1-2. Heat map table with the median and arithmetic mean values for TF uptake upon MiTMAB treatment.

	MiTMAB concentration	Median	Arithmetic mean
Absolute values	H2O	2.349	3.721
	15 μ M	1.388	2.653
	25 μ M	0.9922	2.213
	35 μ M	0.3491	0.9571
Normalised values	H2O	0.7524	1
	15 μ M	0.4422	0.6525
	25 μ M	0.3093	0.5637
	35 μ M	0.09918	0.2951

Table S1-3. Heat map table with the median and arithmetic mean values for lactosylceramide uptake upon Filipin treatment.

	Filipin concentration	Median	Arithmetic mean
Absolute values	DMSO	6.964	10.11
	2.5 μ g/ml	2.535	4.035
	3.75 μ g/ml	1.501	3.265
	5 μ g/ml	1.187	2.196
Normalised values	DMSO	0.7088	1
	2.5 μ g/ml	0.2453	0.4242
	3.75 μ g/ml	0.1433	0.3558
	5 μ g/ml	0.1199	0.2159

Table S1-4. List of 214 proteins identified by mass spectrometry and differentially regulated between biotinylated and unlabelled CDMs. Positive hits are highlighted in blue.

Protein name	Gene name	Student's T-test Difference +biotin_- biotin S0=0.1	Student's T-test Difference +biotin_- biotin S0=1
Voltage-dependent anion-selective channel protein 3	VDAC3	10.53955	10.53955
Voltage-dependent anion-selective channel protein 2 (Fragment)	VDAC2	9.584098	9.584098
MICOS complex subunit MIC60	IMMT	8.986141	8.986141
Acyl-CoA 6-desaturase	FADS2	8.612524	8.612524
Annexin A6	ANXA6	7.805672	7.805672
Mitochondrial carrier homolog 2	MTCH2	7.667495	7.667495
Tenascin C	TNC	7.359021	7.359021
Caveolin (Fragment)	CAV1	7.203031	7.203031
Voltage-dependent anion-selective channel protein 1	VDAC1	7.063192	7.063192
Acyl-CoA (8-3)-desaturase	FADS1	6.956679	6.956679
Mitochondrial carrier homolog 1	MTCH1	6.940424	6.940424
Fibronectin	FN1	6.593774	6.593774
Mitochondrial import receptor subunit TOM40 homolog	TOMM40	6.448902	6.448902
Cytochrome b-c1 complex subunit 2, mitochondrial	UQCRC2	6.393945	6.393945
Surfeit 4	SURF4	5.655561	5.655561
Erythrocyte band 7 integral membrane protein	STOM	5.5763	5.5763
DnaJ homolog subfamily C member 11	DNAJC11	5.56075	5.56075
Glycerol kinase 3	GK3P	5.525429	5.525429
NADH dehydrogenase [ubiquinone] 1 beta subcomplex subunit 9	NDUFB9	5.148815	5.148815
Trifunctional enzyme subunit alpha, mitochondrial	HADHA	4.90379	4.90379
Myosin light polypeptide 6	MYL6	4.878547	4.878547
Microsomal glutathione S-transferase 1	MGST1	4.745102	4.745102
Prolyl endopeptidase FAP	FAP	4.71572	4.71572
Calcium-binding mitochondrial carrier protein Aralar1	SLC25A12	4.70651	4.70651
Sorting and assembly machinery component 50 homolog	SAMM50	4.660712	4.660712
Glycerol kinase 2	GK2	4.544693	4.544693
Eukaryotic initiation factor 4A-I	EIF4A1	4.340341	4.340341
Guanine nucleotide-binding protein G(I)/G(S)/G(T) subunit beta-1	GNB1	4.295762	4.295762
Dolichyl-diphosphooligosaccharide--protein glycosyltransferase subunit 1	RPN1	4.172052	4.172052
Importin-5	IPO5	4.152826	4.152826
Transportin-1	TNPO1	4.149689	4.149689
Microsomal glutathione S-transferase 3	MGST3	4.076183	4.076183

Transmembrane protein 43	TMEM43	4.063311	4.063311
Myosin regulatory light polypeptide 9	MYL9	4.053379	4.053379
Aminopeptidase N	ANPEP	4.01174	4.01174
Transforming growth factor-beta-induced protein ig-h3 (Fragment)	TGFBI	3.910111	3.910111
Collagen alpha-3(VI) chain	COL6A3	3.788417	3.788417
Serine/threonine-protein phosphatase 2A 65 kDa regulatory subunit A alpha isoform	PPP2R1A	3.644986	3.644986
Copine-3 (Fragment)	CPNE3	3.631011	3.631011
Importin subunit beta-1	KPNB1	3.518541	3.518541
Cullin-associated NEDD8-dissociated protein 1	CAND1	3.488196	3.488196
Hexokinase-1	HK1	3.468447	3.468447
Myosin-9	MYH9	3.439954	3.439954
Clathrin heavy chain 1	CLTC	3.388367	3.388367
Cytoskeleton-associated protein 4	CKAP4	3.276732	3.276732
6-phosphogluconate dehydrogenase, decarboxylating (Fragment)	PGD	3.242708	3.242708
Sidoreflexin	SFXN3	3.076559	3.076559
Dipeptidyl peptidase 4	DPP4	3.034134	3.034134
Lysophospholipid acyltransferase 7	MBOAT7	2.966705	2.966705
Galectin-1	LGALS1	2.95992	2.95992
T-complex protein 1 subunit epsilon	CCT5	2.875503	2.875503
Importin-7	IPO7	2.779784	2.779784
EMILIN-1	EMILIN1	2.682018	2.682018
ATP synthase subunit beta, mitochondrial	ATP5F1B	2.637112	2.637112
Farnesyl pyrophosphate synthase	FDPS	2.627485	2.627485
Thrombospondin-1	THBS1	2.581849	2.581849
Coatmer subunit beta	COPB1	2.577916	2.577916
Fibulin-2	FBLN2	2.537358	2.537358
Prolow-density lipoprotein receptor-related protein 1	LRP1	2.480196	2.480196
Coatmer subunit beta	COPB2	2.451904	2.451904
Alpha-actinin-1	ACTN1	2.370201	2.370201
HLA class I histocompatibility antigen, C alpha chain	HLA-C	2.209668	2.209668
Calcium-binding mitochondrial carrier protein Aralar2	SLC25A13	2.171592	2.171592
NAD(P) transhydrogenase, mitochondrial	NNT	2.163708	2.163708
Transitional endoplasmic reticulum ATPase	VCP	2.147847	2.147847
Leucine--tRNA ligase, cytoplasmic	LARS1	2.130969	2.130969
2,4-dienoyl-CoA reductase, mitochondrial	DECR1	2.115036	2.115036
Tumour suppressor candidate 3	TUSC3	2.102768	2.102768
Microtubule-actin cross-linking factor 1, isoforms 1/2/3/5	MACF1	1.980353	1.980353

Neprilysin	MME	1.94029	1.94029
NADH dehydrogenase [ubiquinone] 1 alpha subcomplex subunit 9, mitochondrial	NDUFA9	1.895071	1.895071
Tubulin alpha-1B chain	TUBA1B	1.79408	1.79408
Exportin-1	XPO1	1.769611	1.769611
Sarcoplasmic/endoplasmic reticulum calcium ATPase 2	ATP2A2	1.694986	1.694986
Collagen alpha-2(VI) chain	COL6A2	1.690508	1.690508
Coatomer subunit gamma-1	COPG1	1.604673	1.604673
Methionine--tRNA ligase, cytoplasmic	MARS1	1.571301	1.571301
Ribonuclease inhibitor	RNH1	1.560175	1.560175
Importin-9	IPO9	1.522964	1.522964
Baculoviral IAP repeat-containing protein 6 (Fragment)	BIRC6	1.522399	1.522399
Tubulin beta chain	TUBB	1.413542	1.413542
Sodium/potassium-transporting ATPase subunit alpha-1	ATP1A1	1.410324	1.410324
Actin, cytoplasmic 1	ACTB	1.392959	1.392959
Cytochrome b-c1 complex subunit 1, mitochondrial	UQCRC1	1.379265	1.379265
Heat shock protein HSP 90-beta	HSP90AB1	1.326962	1.326962
Dolichyl-diphosphooligosaccharide--protein glycosyltransferase subunit STT3A	STT3A	1.264541	1.264541
Proteasome adapter and scaffold protein ECM29	ECPAS	1.203898	1.203898
Dolichyl-diphosphooligosaccharide--protein glycosyltransferase subunit 2	RPN2	1.175294	1.175294
Alpha-actinin-4	ACTN4	1.130663	1.130663
Heat shock protein HSP 90-alpha	HSP90AA1	1.104583	1.104583
Cytoplasmic dynein 1 heavy chain 1	DYNC1H1	1.038802	1.038802
Myoferlin	MYOF	0.984436	0.984436
DNA-dependent protein kinase catalytic subunit	PRKDC	0.974013	0.974013
Unconventional myosin-Ic	MYO1C	0.919033	0.919033
AT-rich interactive domain-containing protein 1A	ARID1A	0.77146	0.77146
Nicotinamide phosphoribosyltransferase	NAMPT	0.5422	0.5422
Mitochondrial import inner membrane translocase subunit TIM16	PAM16	-1.02793	-1.02793
U2 snRNP-associated SURP motif-containing protein	U2SURP	-1.09021	-1.09021
Flap endonuclease 1	FEN1	-1.39297	-1.39297
T-complex protein 1 subunit alpha	TCP1	3.313509	3.313509
Poly(rC)-binding protein 1	PCBP1	3.143188	3.143188
E3 ubiquitin-protein ligase HUWE1	HUWE1	2.911989	2.911989
GTP-binding nuclear protein Ran	RAN	2.655588	2.655588
60S ribosomal protein L22	RPL22	2.632071	2.632071
40S ribosomal protein S3	RPS3	2.487611	2.487611

Probable ATP-dependent RNA helicase DDX5	DDX5	2.226161	2.226161
Very-long-chain (3R)-3-hydroxyacyl-CoA dehydratase	HACD3	2.182128	2.182128
Probable ubiquitin carboxyl-terminal hydrolase FAF-X	USP9X	2.128172	2.128172
Poly [ADP-ribose] polymerase 1	PARP1	2.072164	2.072164
PDZ and LIM domain protein 5	PDLIM5	2.028032	2.028032
CAD protein	CAD	1.903346	1.903346
Ubiquitin-like modifier-activating enzyme 1	UBA1	1.763551	1.763551
60S ribosomal protein L18a	RPL18A	1.756282	1.756282
Spectrin beta chain	SPTBN1	1.738635	1.738635
Programmed cell death 6-interacting protein	PDCD6IP	1.554228	1.554228
Annexin	ANXA5	1.51995	1.51995
Stress-70 protein, mitochondrial	HSPA9	1.516541	1.516541
T-complex protein 1 subunit delta	CCT4	1.435966	1.435966
Moesin	MSN	1.398618	1.398618
Major vault protein	MVP	1.35244	1.35244
eIF-2-alpha kinase activator GCN1	GCN1	1.346489	1.346489
Prelamin-A/C	LMNA	1.342836	1.342836
E3 ubiquitin-protein ligase UBR4	UBR4	1.336523	1.336523
T-complex protein 1 subunit eta	CCT7	1.333531	1.333531
Elongation factor 1-gamma	EEF1G	1.309979	1.309979
Heterogeneous nuclear ribonucleoprotein U (Fragment)	HNRNPU	1.266208	1.266208
Long-chain-fatty-acid--CoA ligase 3	ACSL3	1.264521	1.264521
E3 SUMO-protein ligase RanBP2	RANBP2	1.229135	1.229135
Fatty acid synthase	FASN	1.148679	1.148679
Plectin	PLEC	1.091163	1.091163
40S ribosomal protein S8	RPS8	0.973627	0.973627
Splicing factor 3B subunit 1	SF3B1	0.958629	0.958629
Tricarboxylate transport protein, mitochondrial	SLC25A1	0.927721	0.927721
Heterogeneous nuclear ribonucleoprotein H	HNRNPH1	0.916849	0.916849
Filamin-B	FLNB	0.904206	0.904206
40S ribosomal protein S15a	RPS15A	0.895604	0.895604
Peroxiredoxin-1	PRDX1	0.727538	0.727538
Phosphate carrier protein, mitochondrial	SLC25A3	0.703355	0.703355
Splicing factor, proline- and glutamine-rich	SFPQ	0.69678	0.69678
Far upstream element-binding protein 2	KHSRP	0.686493	0.686493
Filamin-A	FLNA	0.6665	0.6665
Ubiquitin-associated protein 2-like	UBAP2L	0.657174	0.657174
Polypyrimidine tract binding protein 1, isoform CRA_b	PTBP1	0.622721	0.622721

ATP synthase subunit alpha, mitochondrial	ATP5F1A	0.569159	0.569159
Talin-1	TLN1	0.529904	0.529904
Coatomer subunit alpha	COPA	0.52831	0.52831
Heat shock cognate 71 kDa protein	HSPA8	0.470204	0.470204
Vimentin	VIM	0.453211	0.453211
Endoplasmic reticulum chaperone BiP	HSPA5	0.441403	0.441403
ATP-dependent 6-phosphofructokinase, platelet type	PFKP	0.40758	0.40758
Elongation factor 2	EEF2	0.404927	0.404927
Annexin A1	ANXA1	0.348703	0.348703
Filamin-C	FLNC	0.346548	0.346548
Heterogeneous nuclear ribonucleoprotein L	HNRNPL	0.334883	0.334883
T-complex protein 1 subunit zeta	CCT6A	0.330362	0.330362
Cytoskeleton-associated protein 5	CKAP5	0.323185	0.323185
Nucleolin	NCL	0.265728	0.265728
C-1-tetrahydrofolate synthase, cytoplasmic	MTHFD1	0.202294	0.202294
Collagen alpha-1(XII) chain	COL12A1	0.184996	0.184996
Long-chain-fatty-acid--CoA ligase 4	ACSL4	0.181208	0.181208
Dihydropyrimidinase-related protein 2	DPYSL2	0.135102	0.135102
N-alpha-acetyltransferase 15, NatA auxiliary subunit	NAA15	0.114388	0.114388
Acetyl-CoA carboxylase 2	ACACB	0.100238	0.100238
Microtubule-associated protein 1B	MAP1B	0.090682	0.090682
Ras GTPase-activating-like protein IQGAP1	IQGAP1	0.066053	0.066053
Dermcidin	DCD	0.051314	0.051314
Phosphoglycerate mutase 1	PGAM1	0.047954	0.047954
Alpha-enolase	ENO1	-0.01295	-0.01295
Pyruvate kinase PKM	PKM	-0.06169	-0.06169
Desmoplakin	DSP	-0.06232	-0.06232
Neuroblast differentiation-associated protein AHNAK	AHNAK	-0.08599	-0.08599
RNA-binding protein 14	RBM14	-0.1725	-0.1725
Calnexin	CANX	-0.18808	-0.18808
Eukaryotic translation initiation factor 3 subunit C-like protein	EIF3CL	-0.18862	-0.18862
ATP-dependent RNA helicase A	DHX9	-0.23	-0.23
60S ribosomal protein L11	RPL11	-0.25503	-0.25503
Acetyl-CoA carboxylase 1	ACACA	-0.26087	-0.26087
ADP/ATP translocase 2	SLC25A5	-0.28915	-0.28915
Peptidyl-prolyl cis-trans isomerase A	PPIA	-0.32747	-0.32747
RNA-binding protein FUS	FUS	-0.33543	-0.33543

G patch domain-containing protein 1	GPATCH1	-0.39481	-0.39481
Methylcrotonoyl-CoA carboxylase subunit alpha, mitochondrial	MCCC1	-0.43842	-0.43842
ADP/ATP translocase 1	SLC25A4	-0.44584	-0.44584
RNA-binding protein 25	RBM25	-0.49237	-0.49237
Glyceraldehyde-3-phosphate dehydrogenase	GAPDH	-0.52262	-0.52262
Malectin (Fragment)	MLEC	-0.54562	-0.54562
Trinucleotide repeat-containing gene 6B protein	TNRC6B	-0.55311	-0.55311
Desmoglein-1	DSG1	-0.58559	-0.58559
Propionyl-CoA carboxylase alpha chain, mitochondrial	PCCA	-0.60522	-0.60522
CD44 antigen	CD44	-0.65023	-0.65023
Pyruvate carboxylase, mitochondrial	PC	-0.66467	-0.66467
40S ribosomal protein S17	RPS17	-0.66621	-0.66621
Eukaryotic translation initiation factor 4 gamma 1	EIF4G1	-0.67307	-0.67307
Putative elongation factor 1-alpha-like 3	EEF1A1P5	-0.69731	-0.69731
Calcium homeostasis endoplasmic reticulum protein	CHERP	-0.72792	-0.72792
40S ribosomal protein S5 (Fragment)	RPS5	-0.76122	-0.76122
Armadillo repeat-containing X-linked protein 3	ARMCX3	-0.7685	-0.7685
Calcium-binding mitochondrial carrier protein SCaMC-1	SLC25A24	-0.83136	-0.83136
Abasic site processing protein HMCES (Fragment)	HMCES	-0.89299	-0.89299
Probable ATP-dependent RNA helicase DDX46	DDX46	-0.91335	-0.91335
Brain acid soluble protein 1	BASP1	-0.96105	-0.96105
RNA-binding protein 39	RBM39	-0.96663	-0.96663
Fatty acid-binding protein 5	FABP5	-1.06463	-1.06463
Pre-mRNA-processing factor 40 homolog A	PRPF40A	-1.09097	-1.09097
Annexin A2 (Fragment)	ANXA2	-1.09652	-1.09652
Splicing factor, suppressor of white-apricot homolog	SFSWAP	-1.29642	-1.29642
LIM and senescent cell antigen-like-containing domain protein 1	LIMS1	-1.33061	-1.33061
Putative RNA-binding protein Luc7-like 2	LUC7L2	-1.3931	-1.3931
Profilin-1	PFN1	-1.58242	-1.58242
Cysteine and glycine-rich protein 1	CSRP1	-1.69512	-1.69512
Luc7-like protein 3	LUC7L3	-1.88806	-1.88806
Splicing regulatory glutamine/lysine-rich protein 1	SREK1	-1.8913	-1.8913
Eukaryotic translation initiation factor 5B	EIF5B	-2.06781	-2.06781
Calmodulin-like protein 5	CALML5	-2.23045	-2.23045

Table S1-5. Heat map table showing the differences in the median and arithmetic mean values for ECM uptake.

Conditions		Collagen		Matrigel		Laminin	
		Median	Arithmetic mean	Median	Arithmetic mean	Median	Arithmetic mean
Absolute values	DMSO	0.2192	2.694	2.322	3.177	1.674	2.655
	E64d	2.734	4.554	7.34	8.125	3.562	5.414
Normalised values	DMSO	0.07895	1	0.8347	1	0.6759	1
	E64d	1.082	1.847	2.32	2.906	1.644	2.18

Table S1-6. Raw data values (related to [Figure 5-3](#)) for matrigel uptake index (of at least 4 technical replicates), normalisation between NT5+BafA1 and Z-score calculated for data value. Hits are in blue; controls are in green.

Gene name	Matrigel uptake index				Normalisation between NT5+BafA1 and NT5 (0 to -1)				Z-score			
AP1AR	2.32973	2.77457	2.61015	3.21813	-0.4554245	-0.3428442	-0.3844557	-0.2305879	-1.4074482	-0.8995115	-1.0872531	-0.3930364
AP1B1	3.87184	4.15219	4.18398	4.29611	-0.0651467	0.0058044	0.01384983	0.04222773	0.35339674	0.67351196	0.70981109	0.83784576
AP1G1	3.08921	3.48873	3.38563	3.04278	-0.263215	-0.1621043	-0.1881969	-0.2749655	-0.5402426	-0.0840541	-0.2017779	-0.5932582
AP1G2	4.26308	3.9762	4.15772	4.20864	0.03386849	-0.0387352	0.00720393	0.02009079	0.80013074	0.4725593	0.67982634	0.7379689
AP1M1	4.45077	3.69797	4.229	3.16441	0.08136915	-0.1091498	0.02524351	-0.2441834	1.01444294	0.15486478	0.76121679	-0.4543761
	3.33179	3.61921	3.19055	3.95219	-0.0676718	0.01513125	-0.1083618	0.11105976	-0.0553826	0.34223276	-0.2507733	0.8028756
AP1M2	3.96948	4.84244	4.71359	4.49899	-0.0404359	0.18049315	0.14788374	0.09357268	0.46488612	1.46166794	1.31454168	1.06950253
AP1S1	4.42214	4.47629	5.52381	4.52807	0.07412345	0.08782776	0.35293455	0.10093226	0.98175203	1.04358273	2.23968437	1.10270728
AP1S2	4.32587	4.23424	4.46926	3.90669	0.0497594	0.02656965	0.0860486	-0.0563268	0.87182696	0.76720004	1.03555559	0.39318991
AP1S3	3.00536	4.45085	3.52281	3.60125	-0.2844358	0.08138939	-0.1534793	-0.1336277	-0.6359859	1.01453429	-0.0451401	0.04442589
AP2A1	3.538	3.38313	3.26721	3.71814	-0.1496351	-0.1888296	-0.2181667	-0.1040452	-0.0277956	-0.2046325	-0.3369948	0.17789572
AP2A2	3.22479	3.44661	3.01551	2.38625	-0.2289024	-0.1727641	-0.281867	-0.4411204	-0.3854317	-0.1321485	-0.6243963	-1.3429113
AP2M1	2.79431	2.50535	2.3844	3.09606	-0.3378484	-0.4109785	-0.4415886	-0.2614814	-0.8769716	-1.206918	-1.3450237	-0.5324209
AP2S1	3.31165	4.86621	4.25586	4.46989	-0.2069198	0.18650887	0.03204124	0.08620804	-0.2862514	1.48880951	0.79188665	1.03627495
AP3B2	3.25328	3.26859	2.9138	3.17915	-0.2216921	-0.2178174	-0.3076078	-0.240453	-0.3529006	-0.3354191	-0.7405329	-0.4375453
AP3D1	2.6233	3.07027	2.90701	2.68266	-0.3811277	-0.2680084	-0.3093263	-0.3661049	-1.0722378	-0.561869	-0.748286	-1.0044581
AP3M2	2.69981	3.11051	2.97893	2.05241	-0.3617645	-0.2578244	-0.2911247	-0.5256088	-0.9848756	-0.5159213	-0.6661648	-1.7241037
AP3S1	1.807	2.07465	2.57389	2.06468	-0.5877172	-0.5199803	-0.3936324	-0.5225035	-2.0043229	-1.6987091	-1.1286562	-1.7100933
AP3S2	3.74651	4.84736	4.10026	4.39614	-0.0968653	0.18173831	-0.0073381	0.06754336	0.21028976	1.4672858	0.61421614	0.95206415
AP4B1	3.8281	3.53394	4.14106	2.58548	-0.0762164	-0.1506626	0.00298761	-0.3906992	0.3034526	-0.0324315	0.66080326	-1.1154223
AP4E1	2.60288	2.49561	2.28561	2.23072	-0.3862956	-0.4134435	-0.4665904	-0.480482	-1.0955543	-1.2180396	-1.4578263	-1.5205019
AP4M1	4.6843	5.04287	5.07046	4.24862	0.14047101	0.23121806	0.23820054	0.03020894	1.28109715	1.6905272	1.7220306	0.78361972
AP4S1	4.85648	4.95796	4.87693	3.8389	0.1840464	0.209729	0.18922189	-0.0734832	1.47769939	1.59357345	1.50105005	0.31578448
AP5B1	4.07105	4.3176	4.10744	3.50443	-0.0147305	0.04766643	-0.0055209	-0.158131	0.58086295	0.86238393	0.62241456	-0.0661272

AP5M1	3.208	2.80206	3.11405	2.7525	-0.2331516	-0.335887	-0.2569285	-0.3484297	-0.4046032	-0.8681223	-0.5118792	-0.9247119
AP5S1	3.24809	2.43268	2.36788	2.68501	-0.2230056	-0.4293699	-0.4457695	-0.3655101	-0.3588268	-1.2898956	-1.363887	-1.0017748
AP5Z1	5.63323	4.375	4.59707	3.92918	0.3806266	0.06219324	0.11839481	-0.0506351	2.36462465	0.92792562	1.18149433	0.41886992
ARF1	2.00169	2.30131	2.59804	2.22986	-0.4508615	-0.3645437	-0.2790585	-0.3851278	-1.8954362	-1.4809434	-1.0704486	-1.579787
ARFGAP1	3.85395	3.72258	4.18919	3.81696	0.08275771	0.04491121	0.1793373	0.07210123	0.66697088	0.48523429	1.1307402	0.6157991
ARFGEF2	2.55323	2.60679	3.40473	2.87698	-0.2919679	-0.2765377	-0.0466585	-0.1986984	-1.1324386	-1.0583439	0.04552221	-0.6845645
BET1	2.33361	2.77072	2.58556	2.84024	-0.3036582	-0.1698439	-0.2265277	-0.1485615	-0.8016314	-0.1739953	-0.4398622	-0.0741731
BET1L	2.14265	2.10283	2.31615	2.80767	-0.3621176	-0.3743078	-0.3090033	-0.1585323	-1.0758265	-1.1330031	-0.8267018	-0.1209396
BICD2	2.38758	2.69872	2.73737	2.77666	-0.3396901	-0.2500535	-0.2389188	-0.2275997	-1.3615979	-0.9311684	-0.8777002	-0.8233466
BNIP1	2.86311	2.24588	2.4966	2.51625	-0.1415602	-0.3305153	-0.2537614	-0.2477459	-0.0413346	-0.9276009	-0.5675978	-0.5393829
CDH2	4.01669	3.34062	4.02059	3.82337	0.12964162	-0.065128	0.13076517	0.07394789	0.89210457	-0.0431672	0.89749981	0.62466667
COG1	2.88592	3.12087	2.76902	2.97149	-0.1345773	-0.0626511	-0.1703644	-0.1083814	-0.0085823	0.328777	-0.1764363	0.11428572
COG2	3.37099	2.89382	3.0091	3.39074	0.01391915	-0.1321588	-0.0968677	0.0199653	0.68791852	0.00276116	0.16828904	0.71627709
COG3	2.41567	2.48491	2.58811	2.83568	-0.2785368	-0.2573401	-0.2257471	-0.1499575	-0.6838034	-0.5843832	-0.4362008	-0.0807207
COG4	2.55638	2.4174	3.13058	3.11473	-0.2354607	-0.2780072	-0.0596785	-0.0645308	-0.4817611	-0.6813193	0.34271936	0.31996072
COG5	2.40825	2.29049	2.56792	2.71403	-0.2808084	-0.3168587	-0.2319279	-0.1871987	-0.6944576	-0.8635464	-0.4651911	-0.2553951
COG6	3.54633	3.97946	3.32133	3.98207	0.0675967	0.20019254	-0.0012835	0.20099155	0.93968517	1.56160651	0.61661287	1.56535414
COG7	2.1941	2.70994	2.63566	2.24164	-0.346367	-0.1884508	-0.2111904	-0.3318133	-1.0019506	-0.2612679	-0.3679248	-0.933689
COG8	2.7525	2.65083	2.40673	2.70278	-0.1754217	-0.2065464	-0.2812737	-0.1906427	-0.200157	-0.3461426	-0.6966401	-0.2715488
DNM1	3.77567	3.34926	3.81199	4.25559	-0.0894854	-0.1974015	-0.0802936	0.03197291	0.24358585	-0.2433067	0.28505753	0.79157835
	2.42646	2.91064	2.06379	3.06122	-0.2752337	-0.1270097	-0.3862593	-0.080912	-0.6683102	0.02691261	-1.1890597	0.24312695
	3.38473	4.08555	3.56922	3.68551	-0.0524203	0.14947956	0.00072959	0.03423168	0.01785431	0.98736515	0.27307684	0.43395184
GCC1	3.34317	3.24673	3.05274	3.74845	-0.0643934	-0.0921768	-0.1480636	0.05236412	-0.0396396	-0.1730542	-0.441419	0.52102272
GCC2	3.54418	3.88908	3.26699	4.53902	-0.0064842	0.09287834	-0.0863401	0.28012013	0.23843664	0.71556955	-0.1450266	1.61469325
GGA1	4.30144	3.81125	3.56063	3.72263	0.04357665	-0.0804808	-0.1439078	-0.1029088	0.84393178	0.28421257	-0.0019557	0.18302259
GGA1	2.73441	2.98628	2.84386	2.83102	-0.2397716	-0.1672101	-0.20824	-0.2119391	-0.8817951	-0.5333594	-0.7303825	-0.7481453
GGA2	3.5108	3.76295	3.41373	3.33916	-0.1565188	-0.0927046	-0.1810854	-0.1999576	-0.0588537	0.22906163	-0.1696922	-0.2548393

GGA3	3.70926	3.76376	4.26458	4.22506	-0.1062925	-0.0924996	0.03424811	0.02424637	0.16775617	0.22998652	0.8018435	0.75671793
GOLGA1	3.64118	3.66815	4.18548	4.80271	0.02146061	0.02923042	0.17826848	0.35608682	0.37262594	0.40993611	1.1256078	1.97948066
GOLGA2	2.95311	3.47294	3.16861	3.66304	-0.1767661	-0.0270078	-0.1146825	0.02775828	-0.5792466	0.13988358	-0.281125	0.40286696
GOLGA3	3.81603	4.27924	3.86349	4.4763	0.0718333	0.20527988	0.08550609	0.26205107	0.61451255	1.25531491	0.68016847	1.52792672
GOLGA4	3.64276	3.96263	3.87208	4.23217	0.02191579	0.11406743	0.0879808	0.19171944	0.37481171	0.81731824	0.69205183	1.19019851
GOLGA5	4.15023	4.37395	4.62143	3.9329	0.16811328	0.23256497	0.3038617	0.10550248	1.07684313	1.38633625	1.72869882	0.77618991
GORASP1	3.62765	3.36432	4.52519	3.68382	0.01756274	-0.0583002	0.27613583	0.03374481	0.35390861	-0.0103808	1.5955609	0.4316139
GORASP2	3.82886	3.77888	4.29643	4.15305	0.07552951	0.06113073	0.21023216	0.16892569	0.6322615	0.56311943	1.27909547	1.08074431
GOSR1	3.53312	3.93042	3.93558	3.9657	0.06355266	0.18517973	0.18675938	0.19598014	0.92071723	1.49119111	1.49860023	1.54184884
GOSR2	3.18121	2.92398	3.00635	3.19446	-0.044179	-0.1229258	-0.0977096	-0.0401227	0.41541781	0.04606721	0.16434038	0.43444318
IGF2R	3.76626	4.314	3.71071	3.60961	-0.0918669	0.04675534	-0.1059255	-0.131512	0.23284113	0.8582733	0.16941184	0.05397168
ITGB1	2.93029	2.94174	3.045	2.9521	-0.3034345	-0.3005368	-0.2744037	-0.2979149	-0.721704	-0.7086299	-0.5907234	-0.6968004
	1.9081	2.15066	1.48493	2.64893	-0.4339213	-0.3596654	-0.563468	-0.207128	-1.4126114	-1.0643251	-2.0202314	-0.3488707
	2.94018	3.10971	2.64589	2.66348	-0.1804911	-0.1316511	-0.2652734	-0.2602058	-0.5971339	-0.362607	-1.0042532	-0.9799193
KDELR1	4.10334	3.75437	3.94681	4.19143	0.15460469	0.05406962	0.10950983	0.17998262	1.01197574	0.52921242	0.79543294	1.133839
M6PR	3.86162	3.54778	3.4756	3.21539	-0.0677332	-0.1471599	-0.1654273	-0.2312813	0.34172712	-0.0166284	-0.0990465	-0.396165
NSF	2.92062	3.16194	3.15392	3.07223	-0.1861262	-0.1166041	-0.1189146	-0.1424487	-0.6241931	-0.2903522	-0.3014471	-0.4144566
NT4	3.59742	3.83177	3.99827	3.89267	-0.134597	-0.0752876	-0.0331497	-0.059875	0.04005264	0.30764315	0.49775974	0.37718129
	3.20408	3.30113	2.7746	3.08848	-0.0371777	-0.0074674	-0.1686561	-0.0725668	0.44825631	0.58760816	-0.1684241	0.28226895
	3.35157	4.1659	4.35593	3.63878	-0.0619734	0.17262766	0.22737357	0.02076919	-0.0280191	1.09852093	1.36140747	0.3693058
NT5	3.81716	3.65362	5.02052	4.02572	-0.0789851	-0.1203739	0.22556171	-0.0262027	0.29096085	0.10422412	1.66500705	0.52910328
	2.93563	3.6072	3.12797	3.63129	-0.1193594	0.08623108	-0.0604775	0.09360585	0.06279517	1.02708699	0.33897173	1.06167726
	3.04684	3.60363	3.68199	3.93429	-0.1497633	0.0106428	0.0332176	0.10590293	-0.449581	0.32067946	0.42908229	0.77811283
NT5 + BafA1	0.044572	0.0817989	0.0715905	0.0379574	-1.0044107	-0.9930143	-0.9961394	-1.0064356	-4.0884081	-4.0349548	-4.0496128	-4.0979058
	0.0997028	0.0586629	0.13508	0.088797	-0.9988067	-1.0106299	-0.9886148	-1.0019486	-4.5266357	-4.58341	-4.477695	-4.5417227
	0.16355	0.0876592	0.0877132	0.372844	-1.0036422	-1.0228487	-1.022835	-0.950674	-3.8808821	-3.9675373	-3.9674757	-3.6419015
PAK1	2.88637	2.75347	3.16423	2.8998	-0.3145498	-0.3481842	-0.2442289	-0.311151	-0.7718536	-0.9236044	-0.4545816	-0.7565187

	1.86961	2.24127	1.80831	2.31419	-0.4457044	-0.3319266	-0.4644704	-0.3096033	-1.4678783	-0.9342203	-1.5558975	-0.8295161
	2.05299	2.72294	2.11238	2.23717	-0.4360825	-0.243076	-0.4189727	-0.3830219	-1.8244681	-0.8976626	-1.7423082	-1.5696744
RAB11B	2.65381	2.57766	2.63825	2.37656	-0.2629917	-0.2849298	-0.2674744	-0.3428649	-0.9932967	-1.0986422	-1.0148223	-1.376843
RAB1A	3.75334	4.05885	3.19654	2.88241	0.05377288	0.14178753	-0.1066361	-0.1971341	0.52778752	0.9504285	-0.2424868	-0.6770526
RAB2A	2.5694	2.64676	3.01053	2.7762	-0.2873094	-0.2650227	-0.1602239	-0.2277322	-1.1100691	-1.0030496	-0.4998121	-0.823983
RAB31	4.32966	4.9034	4.64363	3.33623	0.05071858	0.19592093	0.13017823	-0.2006991	0.87615454	1.53127459	1.23465846	-0.2581849
	4.69897	3.38673	4.62767	4.84132	0.1441837	-0.1879185	0.12613907	0.1802097	1.29784796	-0.2005219	1.21643468	1.46038908
RAB6A	3.04363	3.4113	2.93318	3.17636	-0.1506881	-0.0447657	-0.1825077	-0.1124498	-0.4540217	0.05461112	-0.6068177	-0.2704037
RAB7B	3.77545	3.7529	4.16239	3.22842	-0.0895411	-0.0952481	0.00838582	-0.2279837	0.24333465	0.21758613	0.68515874	-0.3812868
RAB9A	2.32628	2.46886	1.63828	2.24785	-0.4562976	-0.4202134	-0.630417	-0.4761467	-1.4113876	-1.2485838	-2.1969744	-1.5009422
RAB9B	3.03159	2.86161	3.16019	3.08545	-0.2777975	-0.3208161	-0.2452514	-0.2641666	-0.6060354	-0.8001256	-0.4591947	-0.5445359
RABEPK	3.26971	3.24017	3.63609	3.03874	-0.217534	-0.22501	-0.1248104	-0.275988	-0.3341402	-0.3678702	0.08420764	-0.5978713
SEC13	4.18919	4.5491	4.42548	5.00182	0.1793373	0.28302409	0.24741029	0.41344859	1.1307402	1.62863787	1.45762259	2.25492842
SEC22A	2.26731	2.20158	2.3127	2.02436	-0.3239549	-0.3440771	-0.3100595	-0.3983302	-0.89683	-0.9912102	-0.8316556	-1.2456763
SEC22B	2.39605	2.56131	2.8576	2.79196	-0.2845432	-0.2339515	-0.143247	-0.1633417	-0.7119753	-0.4746823	-0.0492463	-0.1434973
SEC22C	2.65348	3.1047	2.68089	3.09499	-0.2057351	-0.0676013	-0.197344	-0.0705738	-0.3423375	0.30555887	-0.3029801	0.29161651
SEC23A	3.23871	3.20431	3.44028	3.48665	-0.0944873	-0.1043977	-0.0364168	-0.0230581	-0.184149	-0.2317378	0.0947019	0.15884993
SNAP23	3.04737	2.54447	3.01788	2.82621	-0.085152	-0.2391068	-0.0941798	-0.1528566	0.22324005	-0.4988624	0.18089604	-0.0943185
SNAP25	2.48	2.67307	2.62754	3.14834	-0.2588432	-0.1997379	-0.2136762	-0.0542416	-0.5914334	-0.3142087	-0.3795841	0.36822054
SNAP29	2.08492	2.41185	2.01041	2.28591	-0.3797907	-0.2797063	-0.4026007	-0.3182608	-1.1587196	-0.6892884	-1.2657068	-0.8701227
SNAP47	2.68776	2.18914	2.07693	2.3232	-0.1952408	-0.3478854	-0.3822367	-0.3068451	-0.2931156	-1.0090725	-1.1701923	-0.8165789
SNX1	4.24275	3.94142	4.26542	3.97696	0.02872336	-0.0475374	0.03446069	-0.0385429	0.77691711	0.43284606	0.80280265	0.4734271
SORCS1	4.21006	4.02348	3.95278	3.61305	0.02045016	-0.0267696	-0.0446624	-0.1306414	0.73959031	0.52654556	0.44581737	0.05789962
SORCS2	3.76234	3.61834	4.31233	3.52104	-0.092859	-0.1293026	0.0463327	-0.1539273	0.22836511	0.06393996	0.85636643	-0.0471612
SORCS3	4.14017	3.18914	4.21983	3.39461	0.00276237	-0.2379247	0.02292276	-0.1859243	0.65978702	-0.4261383	0.7507461	-0.1915242
SORL1	4.26069	4.15175	4.73021	4.48869	0.03326362	0.00569304	0.15208994	0.09096596	0.79740174	0.67300955	1.33351909	1.05774157
STX10	2.62448	3.21358	3.18756	3.01106	-0.214613	-0.0342694	-0.042235	-0.0962677	-0.3839779	0.46189714	0.42453563	0.17110336

STX11	4.1633	4.86018	3.6542	4.26025	0.25647223	0.46981093	0.10061938	0.28615192	1.82557811	2.82621197	1.0945732	1.96478637
STX12	2.23556	2.37486	2.68632	2.38123	-0.3336746	-0.2910302	-0.1956817	-0.2890801	-0.9424191	-0.7424015	-0.2951833	-0.733255
STX16	3.62615	4.3178	3.02771	3.56471	0.09203232	0.30376994	-0.0911705	0.07322344	1.05429686	2.04742108	0.19501071	0.96607658
STX17	2.95927	3.12378	3.01322	3.29976	-0.1121224	-0.0617603	-0.0956064	-0.0078868	0.0967393	0.3329554	0.17420486	0.58564101
STX18	3.02484	3.65965	3.03269	3.73045	-0.0920492	0.10228781	-0.089646	0.1239621	0.19088975	1.10239873	0.20216138	1.20405881
STX19	2.59012	2.67429	2.6219	2.23636	-0.2251318	-0.1993644	-0.2154028	-0.3334297	-0.4333146	-0.3124569	-0.3876825	-0.9412704
STX1A	3.69906	3.95813	3.70969	3.74846	0.11435255	0.1936627	0.11760676	0.12947557	1.15898664	1.53097925	1.17425001	1.22991895
STX1B	2.74922	3.07733	2.61314	2.93327	-0.1764258	-0.0759802	-0.2180845	-0.1200818	-0.2048666	0.26625892	-0.4002608	0.0594065
STX2	3.87569	3.42554	3.47231	3.10961	0.16842501	0.03061876	0.04493665	-0.0660982	1.41260557	0.7662456	0.83340156	0.31260903
STX3	3.06513	2.80775	2.10976	3.35594	-0.079715	-0.1585078	-0.3721863	0.00931183	0.24874122	-0.1208248	-1.1230524	0.66630857
STX4	2.6433	3.50067	3.40405	3.25854	-0.2088515	0.05361861	0.02403994	-0.0205056	-0.3569547	0.87412303	0.73538861	0.52645417
STX5	3.12713	3.54755	3.56408	2.80783	-0.0607347	0.06797018	0.07303058	-0.1584833	0.33776559	0.94143694	0.96517198	-0.1207099
STX6	2.48016	2.7869	2.98527	2.66325	-0.2587943	-0.1648907	-0.1041629	-0.2027442	-0.5912037	-0.1507628	0.1340721	-0.328309
STX7	2.41947	2.32858	2.396	2.38414	-0.2773735	-0.3051981	-0.2845585	-0.2881892	-0.678347	-0.8088539	-0.7120471	-0.7290766
STX8	4.01393	4.75637	4.17922	3.87652	0.21074498	0.43803115	0.26134588	0.1686791	1.61110118	2.67715359	1.84843727	1.41379734
TNS3	4.16716	3.63522	3.72221	3.42657	0.00959301	-0.1250306	-0.1030151	-0.1778358	0.69060532	0.08321424	0.18254302	-0.155031
	2.94776	2.87397	2.55247	2.42301	-0.115646	-0.1382356	-0.2366577	-0.2762898	0.08021236	-0.025741	-0.4873754	-0.673264
	2.73262	3.49978	3.14744	3.37699	-0.2402872	-0.0192754	-0.1207814	-0.0546501	-0.8842714	0.1770139	-0.3104115	0.00714684
TRAPPC1	1.88706	1.91679	2.17451	2.20492	-0.4838854	-0.4753204	-0.4010736	-0.3923128	-2.0540148	-2.0128864	-1.6563579	-1.6142889
TRAPPC2	2.7169	3.2007	3.12242	3.01431	-0.244816	-0.1054377	-0.1279894	-0.1591349	-0.9060183	-0.2367319	-0.345024	-0.4945828
TRAPPC3	3.42783	3.76806	3.20536	3.39421	-0.0400036	0.05801358	-0.1040952	-0.0496892	0.07747864	0.54815109	-0.2302852	0.0309689
TRAPPC4	3.034	3.08339	2.9442	2.97697	-0.1534624	-0.1392336	-0.179333	-0.1698922	-0.4673438	-0.3990179	-0.5915727	-0.5462388
TRAPPC5	2.25495	2.42781	2.48889	2.81809	-0.3778996	-0.3281002	-0.3105036	-0.2156641	-1.5450776	-1.305944	-1.2214462	-0.7660326
TRAPPC6A	3.92042	3.64174	3.50069	3.89534	0.10190711	0.02162194	-0.0190133	0.09468179	0.75892514	0.37340065	0.17827279	0.7242296
TRAPPC6B	2.9841	4.00707	3.63554	4.04295	-0.1678381	0.12687018	0.01983578	0.13720689	-0.5363752	0.87879632	0.3648236	0.92843253
TRAPPC9	4.24542	4.06359	3.74794	4.78969	0.19553665	0.14315308	0.05221719	0.35233587	1.2085285	0.9569858	0.52031719	1.96146886
TRIP11	2.25999	2.19171	2.35548	1.74778	-0.3764476	-0.3961185	-0.3489378	-0.5240107	-1.5381053	-1.6325635	-1.4060049	-2.246694

TSG101	3.26464	2.99288	3.4347	3.23124	-0.2188171	-0.2875942	-0.1757783	-0.22727	-0.3399293	-0.6502361	-0.1457478	-0.3780668
USE1	2.99176	3.39411	3.05888	3.33157	-0.1021761	0.02099697	-0.0816284	0.00185135	0.14339094	0.72111599	0.23976699	0.63131625
USO1	2.53354	2.97117	3.04815	2.80872	-0.2424528	-0.1084794	-0.0849132	-0.1582108	-0.5145566	0.11382624	0.22436004	-0.119432
VAMP1	2.33419	2.62721	2.60757	2.81624	-0.3034806	-0.2137772	-0.2197897	-0.1559087	-0.8007986	-0.380058	-0.4082586	-0.1086342
VAMP2	2.9332	2.93594	2.5386	3.21106	-0.1201033	-0.1192645	-0.2409038	-0.0350409	0.05930599	0.06324029	-0.507291	0.45827873
VAMP3	3.18392	3.87793	2.64222	3.31943	-0.0433493	0.16911075	-0.2091822	-0.0018651	0.41930904	1.41582193	-0.3585055	0.61388471
VAMP4	2.84461	3.23246	2.14264	2.81606	-0.1472237	-0.0284896	-0.3621206	-0.1559638	-0.0678983	0.4890065	-1.0758408	-0.1088926
VAMP5	2.93351	4.01616	2.44033	3.29767	-0.1200084	0.21142766	-0.2709876	-0.0085266	0.05975111	1.61430319	-0.6483946	0.58264003
VAMP7	2.76351	2.16553	2.39577	2.50366	-0.1720512	-0.3551132	-0.2846289	-0.2516001	-0.184348	-1.0429736	-0.7123773	-0.5574606
VAMP8	4.40593	3.62031	4.83106	4.22559	0.33074953	0.09024449	0.4608963	0.27554132	2.17396491	1.04591133	2.78439923	1.91501888
VPS26A	4.30973	3.71137	3.95364	4.38777	0.04567469	-0.1057585	-0.0444447	0.06542508	0.85339764	0.17016546	0.44679936	0.94250694
VPS26B	3.61969	3.32776	3.98631	3.8853	-0.1289609	-0.2028427	-0.0361766	-0.0617402	0.06548144	-0.2678563	0.48410331	0.36876592
VPS29	3.35587	2.64645	3.56118	3.16893	-0.1957286	-0.3752689	-0.1437687	-0.2430394	-0.2357591	-1.0458042	-0.0013277	-0.449215
VTI1A	2.90324	2.6611	3.87052	3.00805	-0.1292751	-0.2034024	0.1668423	-0.0971891	0.01628712	-0.3313961	1.40518208	0.16678137
VTI1B	2.44811	3.16616	2.5067	2.85025	-0.2686058	-0.0487863	-0.2506695	-0.1454971	-0.6372235	0.39380786	-0.5530955	-0.0598
YKT6	3.62472	2.86911	3.63827	2.93197	0.09159454	-0.1397234	0.09574266	-0.1204798	1.05224355	-0.0327194	1.07169968	0.05753986

Table S1-7. Raw data values (related to [Figure 6-1](#)) for matrigel uptake index and normalisation between NT5+BafA1 (-1) and NT5 (0). Hits are in light blue, controls are in green.

Gene name	Replicate 1			Replicate 2		
	Nuclei count	Matrigel uptake index	Normalisation between NT5+BafA1 and NT5 (0 to -1)	Nuclei count	Matrigel uptake index	Normalisation between NT5+BafA1 and NT5 (0 to -1)
AAK1	405	4.66916	0.62435	327	5.03695	0.18806388
AATK	402	1.72755	-0.4096	369	2.98478	-0.3044519
ABI1	1090	2.68874	-0.4145226	990	2.05092	-0.5271942
ABL1	818	2.74667	-0.05139	628	3.81675	-0.1047811
ABL2	584	2.9599	0.023562	587	4.4287	0.04208537
ACP1	510	5.65018	0.32827134	499	4.38178	0.01720747
ACP2	528	4.47383	0.04502796	469	4.55745	0.05888022
ACP5	388	2.90331	-0.3331243	360	3.53039	-0.1847608
ACP6	495	4.0038	-0.0681466	590	4.45142	0.0337276
ACPP	646	4.68763	0.09650705	807	3.39387	-0.2171463
ACPT	968	3.20534	-0.260401	674	3.23933	-0.2538065
ACVR1	615	3.07912	0.065467	654	4.19818	-0.0132389
ACVR1B	750	2.98193	0.031305	590	3.36901	-0.2122376
ACVR1C	581	2.86897	-0.0084	492	3.94555	-0.0738694
ACVR2	674	2.34914	-0.19111	764	4.23314	-0.0048486
ACVR2B	645	2.84425	-0.01709	468	4.05882	-0.0466849
ACVRL1	861	2.49876	-0.13852	729	3.32368	-0.2231167
ACYP1	714	3.38908	-0.2161598	577	3.94624	-0.0861121
ACYP2	795	4.30148	0.00352926	846	3.31821	-0.2350945
ADAM9	751	3.10536	0.07469	565	4.02044	-0.055896
ADCK1	699	2.61341	-0.09823	690	4.34903	0.02296477
ADCK2	432	3.14909	0.090061	374	4.28807	0.00833452
ADCK4	743	2.60678	-0.10056	623	3.73799	-0.1236833
ADCK5	718	1.50772	-0.48686	545	3.64527	-0.1459359
ADK	976	3.04267	0.052655	666	3.98847	-0.0635688
ADRA1A	837	1.87379	-0.35819	674	2.42016	-0.4399593
ADRA1B	720	2.6247	-0.09426	632	3.8172	-0.1046731
ADRB2	609	1.70567	-0.41729	467	3.21642	-0.2488589
ADRBK1	498	2.84448	-0.01701	384	4.64073	0.09297205
ADRBK2	753	1.89601	-0.35038	659	3.23682	-0.2439629
AGTR2	850	2.63361	-0.09113	568	3.43171	-0.1971898
AK1	842	3.15002	0.090387	647	4.42911	0.04218377
AK2	998	3.08873	0.068845	749	3.61384	-0.153479
AK3	901	4.71905	0.641886	700	4.92259	0.16061776
AK3L1	877	1.97083	-0.32409	618	2.21785	-0.4885132
AK5	443	3.44263	0.193237	451	3.44387	-0.1942714
AK7	1088	2.5087	-0.13503	789	3.42338	-0.199189
AKAP1	713	1.6077	-0.45172	476	2.47146	-0.4276474
AKAP11	345	7.45169	0.76204172	493	6.11144	0.42752048

	290	4.28538	0.489455	196	7.87002	0.86799376
AKAP13	1077	4.26469	0.482183	917	4.73249	0.11499423
AKAP3	853	3.30207	0.143832	803	4.43883	0.04451655
AKAP4	975	2.58899	-0.10681	702	3.57897	-0.1618478
AKAP5	617	2.32598	-0.19925	680	2.70613	-0.3713272
AKAP6	697	5.04888	0.757818	514	5.35642	0.2647359
AKAP7	384	2.79881	-0.03306	451	4.0004	-0.0607056
AKAP8	599	3.29249	0.140464	518	4.80793	0.13309964
AKT1	728	1.72324	-0.41111	549	2.67215	-0.3794823
AKT2	712	3.76784	0.307545	602	4.73408	0.11537582
AKT3	717	3.20674	0.110324	516	3.25777	-0.238935
ALK	848	2.7371	-0.05475	887	3.76311	-0.1176546
ALPI	643	3.29012	-0.2399876	812	3.32686	-0.2330425
ALPL	641	6.28979	0.48227763	820	4.86058	0.13078926
ALPP	1027	4.24127	-0.0109682	1125	4.62609	0.07516312
ALPPL2	915	4.41501	0.03086519	770	4.55737	0.05886124
ALS2CR2	750	1.59443	-0.45639	577	2.3329	-0.4609015
ALS2CR7	841	2.90529	0.004367	666	4.47828	0.05398445
AMHR2	696	3.62368	0.256874	553	4.48821	0.05636763
ANGPT4	686	2.7293	-0.05749	587	3.43674	-0.1959826
ANKK1	678	2.29693	-0.20947	551	3.37064	-0.2118464
ANKRD3	594	2.40156	-0.17269	456	3.55243	-0.1682173
ANP32E	1110	4.28324	-0.0008626	946	4.2083	-0.0239458
AP3D1	781	1.54614	-0.47336	519	2.1913	-0.4948852
	801	1.60775	-0.45171	480	2.11376	-0.5134946
	814	2.4497	-0.4030511	523	2.33315	-0.4745526
	658	2.75063	-0.4002757	648	2.01122	-0.5367834
	827	2.68012	-0.3868643	539	1.86219	-0.5804941
	964	2.80905	-0.3868276	520	2.79856	-0.3466067
	762	2.82493	-0.3831721	624	1.97634	-0.5452085
	816	1.807	-0.38167	545	2.66509	-0.3811767
	956	2.54149	-0.3799631	163	2.91838	-0.3368922
	984	2.71456	-0.3785718	704	2.54193	-0.419245
	851	2.79562	-0.3590541	485	2.26358	-0.4852757
	801	1.90744	-0.34637	576	2.39419	-0.4461921
	985	3.01432	-0.3395751	650	2.84012	-0.3365682
	707	2.91512	-0.3302807	495	2.04482	-0.5371703
848	3.13381	-0.2309771	609	2.45651	-0.4455353	
1012	3.13754	-0.2300389	638	2.66314	-0.3969309	
APEG1	745	4.72415	0.643679	670	4.75783	0.12107577
APPL	424	1.71964	-0.41238	417	4.11594	-0.0329763
ARAF1	422	2.69857	-0.06829	431	3.47452	-0.1869155
ARK5	904	1.13669	-0.61728	892	2.72246	-0.3674081
ASK	720	1.73178	-0.40811	597	2.62879	-0.3898886
ASP	472	2.55076	-0.12025	361	4.58741	0.08017538

ATM	262	2.22653	-0.23421	394	4.22688	-0.0063509
ATR	610	3.2667	0.131399	493	4.39255	0.03340946
AURKB	413	6.39378	1.230538	294	6.61559	0.56693362
AURKC	489	4.16564	0.447368	629	4.94031	0.16487052
AVPR1A	432	2.95364	0.021362	490	3.74239	-0.1226274
AVPR1B	315	3.12169	0.08043	371	3.6105	-0.1542806
AXL	651	2.53156	-0.127	610	3.01276	-0.2977368
AZU1	180	3.74622	0.299946	226	4.33898	0.02055279
BCKDK	551	2.17338	-0.25289	404	3.3789	-0.2098641
BCR	451	2.63263	-0.09147	370	3.17993	-0.2576164
BDKRB2	778	2.44742	-0.15657	499	3.6317	-0.1491927
BLK	838	2.49932	-0.13833	871	3.0121	-0.2978952
BLNK	259	1.66605	-0.43121	335	2.89757	-0.3253821
BMP2K	535	2.80197	-0.03195	829	3.63309	-0.1488591
BMPR1A	912	1.75865	-0.39867	574	4.09134	-0.0388802
BMPR1B	692	2.84198	-0.01789	651	4.15984	-0.0224404
BMPR2	830	3.03834	0.051133	693	3.66655	-0.1408288
BMX	595	2.06435	-0.29121	632	2.8845	-0.3285189
BPNT1	1062	4.26858	-0.0043925	1000	3.19811	-0.2635848
BRAF	502	2.57515	-0.11167	508	3.37461	-0.2108937
BRD2	745	2.42192	-0.16553	701	3.327	-0.2223199
BRDT	542	2.17484	-0.25238	534	2.73176	-0.3651761
BTK	657	2.16373	-0.25628	700	2.98932	-0.3033623
BUB1	792	1.95071	-0.33116	721	3.17839	-0.257986
BUB1B	826	2.56133	-0.11653	775	3.00202	-0.3003143
C14ORF20	627	2.59528	-0.1046	684	3.2075	-0.2509996
C14ORF24	609	3.85163	-0.1047863	622	4.0974	-0.0502537
C21ORF6	1156	3.68306	-0.1453749	999	3.76607	-0.1288523
C6ORF199	770	2.01829	-0.3074	592	3.33622	-0.2201072
C7ORF16	743	3.5431	0.228551	675	4.61369	0.08648252
C7ORF16	613	6.16267	0.45166948	629	5.04668	0.17493623
C9ORF12	625	4.88027	0.698554	650	4.57301	0.07671942
C9ORF96	725	6.14473	0.52635841	587	5.81608	0.34471809
C9ORF98	708	3.31778	0.149353	634	3.53695	-0.1719324
CALM3	629	3.40903	0.181427	581	4.11357	-0.0335451
CAMK1	659	3.16271	0.094848	605	4.26427	0.00262257
CAMK1D	778	2.3816	-0.1797	730	3.63815	-0.1476447
CAMK1G	1199	4.08243	0.418121	860	3.72939	-0.1257473
CAMK2A	705	1.81668	-0.37827	774	2.76283	-0.3577194
CAMK2B	857	1.94743	-0.33231	638	2.71781	-0.368524
CAMK2D	1100	2.51429	-0.13307	767	3.2425	-0.2425997
CAMK2G	730	2.44363	-0.1579	662	2.46521	-0.4291474
CAMK4	715	3.77885	0.311415	542	4.25252	-0.0001974
CAMKK1	801	3.81433	0.323886	629	3.96491	-0.0692231
CAMKK2	1027	2.6882	-0.07194	858	3.27223	-0.2354646

CARD10	778	3.27683	0.13496	562	4.08056	-0.0414674
CARD14	517	2.57959	-0.11011	398	5.78071	0.36656446
CARKL	658	2.50313	-0.13699	551	3.71458	-0.1293017
CASK	758	3.21103	0.111832	501	4.50577	0.06058198
CCL2	740	4.29914	0.494292	639	5.37574	0.26937266
CCL4	572	3.3642	0.16567	525	4.49315	0.05755321
CCRK	689	4.92654	0.714817	506	6.87269	0.62863699
CD3E	810	3.10457	0.074412	175	4.95197	0.16766889
CD4	679	3.52169	0.221026	610	4.19401	-0.0142397
CD7	683	2.79678	-0.03377	650	4.76296	0.12230695
CDADC1	557	2.23906	-0.22981	423	4.4913	0.05710922
CDC14A	636	5.11144	0.19855268	821	3.79161	-0.1227937
CDC14B	974	5.07722	0.19031314	897	4.80589	0.1178156
CDC2	362	3.75797	0.304076	345	5.73031	0.35446859
CDC25A	1183	4.50072	0.05150257	998	4.54385	0.05565401
CDC25B	801	4.21585	-0.0170889	689	4.25791	-0.0121772
CDC25C	965	5.01688	0.17578438	1055	4.34974	0.00960689
CDC2L1	307	3.58316	0.242632	540	3.82978	-0.101654
CDC2L2	533	1.74844	-0.40225	641	2.88778	-0.3277317
CDC2L5	864	1.99921	-0.31411	790	3.74007	-0.1231841
CDC42BPA	361	1.40905	-0.52155	259	2.73524	-0.3643409
CDC42BPB	1010	1.73626	-0.40654	998	3.38249	-0.2090025
CDC7	521	2.31158	-0.20432	429	4.22199	-0.0075245
CDK10	720	2.20894	-0.24039	566	3.97354	-0.0671519
CDK11	663	2.18459	-0.24895	538	3.72401	-0.1270385
CDK2	872	3.51975	0.220344	793	4.68633	0.10391594
CDK3	937	2.2872	-0.21289	694	3.74418	-0.1221978
CDK4	415	3.74499	0.299514	523	5.01493	0.18277914
CDK5	798	3.49393	0.211269	585	4.17769	-0.0181564
CDK5R1	582	2.73062	-0.05703	492	4.4504	0.04729332
CDK5R2	795	2.72754	-0.05811	674	3.83111	-0.1013348
CDK5RAP1	462	3.62056	0.255778	465	4.67873	0.10209196
CDK5RAP3	596	2.7234	-0.05957	420	4.01013	-0.0583704
CDK6	643	3.04014	0.051766	684	5.13526	0.21165804
CDK7	842	2.7508	-0.04993	471	4.28867	0.00847851
CDK8	750	3.95603	0.373692	786	5.3447	0.26192313
CDK9	834	3.37041	0.167852	714	4.62062	0.0881457
CDKL1	361	4.74802	0.652069	521	5.31416	0.25459361
CDKL2	402	2.18052	-0.25038	471	3.98509	-0.0643799
CDKL3	838	3.00225	0.038448	683	4.27675	0.00561774
CDKL5	434	1.41418	-0.51974	366	3.14577	-0.2658147
CDKN1A	773	3.0927	0.07024	585	4.26803	0.00352496
CDKN1B	721	2.67614	-0.07618	723	3.82713	-0.10229
CDKN1C	577	2.48496	-0.14337	423	4.06452	-0.0453169
CDKN2B	501	3.02926	0.047942	491	4.7032	0.1079647

CDKN2C	660	3.51022	0.216994	455	4.35328	0.02398476
CDKN2D	399	3.47803	0.20568	377	4.36711	0.02730392
CDKN3	540	7.64454	0.80847645	610	5.53919	0.29177032
	238	5.1998	0.810865	304	7.34072	0.74096305
CERK	564	3.54082	0.22775	454	4.62704	0.08968649
CHEK1	364	1.77108	-0.3943	488	4.21553	-0.0090749
CHEK2	451	2.62758	-0.09325	560	3.46089	-0.1901867
CHKA	444	3.33526	0.155498	410	4.67352	0.10084157
CHKB	559	2.51844	-0.13161	563	3.75465	-0.119685
CHRM1	523	3.76216	0.305549	426	5.05519	0.19244144
CHUK	527	3.18244	0.101783	274	3.91248	-0.0818062
CILP	936	3.97919	-0.0740722	1000	3.06922	-0.2941603
CINP	758	1.80114	-0.38373	850	4.4432	0.04556534
CIT	497	4.35135	0.512643	464	5.51112	0.30186352
CKB	634	3.09059	0.069498	500	4.77588	0.12540772
CKM	657	2.12773	-0.26894	542	3.3857	-0.2082321
CKMT1	590	3.27259	0.13347	407	5.68115	0.34267031
CKMT2	692	2.74877	-0.05065	662	4.22099	-0.0077645
CKS1B	765	2.67654	-0.07604	702	4.25388	0.000129
CKS2	914	2.95755	0.022736	613	4.16625	-0.020902
CLK1	848	1.93235	-0.33761	585	3.41092	-0.2021793
CLK2	651	2.33771	-0.19513	580	2.87191	-0.3315404
CLK3	787	1.78112	-0.39077	538	3.29748	-0.2294047
CLK4	749	2.38993	-0.17678	775	3.37417	-0.2109992
CNKS1A1	403	1.94348	-0.3337	287	2.70898	-0.3706432
COASY	430	4.37987	0.08244386	482	4.05947	-0.0684798
COL4A3BP	700	2.35115	-0.19041	580	3.1478	-0.2653275
COPB2	168	0.058428	-0.99628	178	0.12353	-0.9911449
CRK7	634	2.61144	-0.09892	545	4.54358	0.06965629
CRKL	373	1.42477	-0.51602	292	3.12553	-0.2706722
CSF1R	552	3.71548	0.289141	521	4.95617	0.16867688
CSK	934	2.2207	-0.23626	646	3.19432	-0.2541628
CSNK1A1	745	2.66785	-0.07909	578	3.50705	-0.1791084
CSNK1A1L	573	4.46642	0.10421375	469	2.97959	-0.3224941
CSNK1D	656	2.99775	0.036866	630	3.74765	-0.121365
CSNK1E	718	3.68591	0.278748	569	4.25931	0.00143219
CSNK1G1	754	1.91146	-0.34495	540	2.54613	-0.4097268
CSNK1G2	712	2.86498	-0.0098	550	4.23931	-0.0033678
CSNK1G3	908	2.89089	-0.00069	743	4.25345	2.58E-05
CSNK2A1	751	3.73617	0.296414	563	4.12625	-0.0305019
CSNK2A2	462	3.32138	0.150619	438	5.11317	0.2063565
CSNK2B	658	2.14726	-0.26207	590	3.80817	-0.1068403
CTDP1	835	4.2854	-0.0003425	746	5.00809	0.16578184
CXCL10	805	2.41705	-0.16724	800	4.21387	-0.0094733
DAPK1	503	2.039	-0.30013	428	2.68209	-0.3770968

DAPK2	896	2.42494	-0.16447	562	3.84016	-0.0991628
DAPK3	745	2.13742	-0.26553	701	3.4246	-0.1988962
DCAMKL1	788	4.98247	0.734476	477	6.20231	0.46774743
DCK	426	3.91485	0.359218	378	5.0382	0.18836388
DDR1	867	2.2448	-0.22779	705	4.1742	-0.018994
DDR2	713	3.88862	0.349998	565	5.45507	0.28841166
DGKA	673	3.18451	0.10251	730	4.22681	-0.0063677
DGKB	754	2.22712	-0.234	647	3.61143	-0.1540574
DGKD	1110	2.4311	-0.16231	890	2.84498	-0.3380036
DGKE	377	1.17069	-0.60533	368	1.66415	-0.6213999
DGKG	608	3.558	0.233788	776	3.47617	-0.1865195
DGKI	814	2.43406	-0.16127	674	3.53821	-0.1716301
DGKQ	735	2.03395	-0.3019	660	2.24735	-0.4814333
DGKZ	733	2.37715	-0.18127	499	3.67691	-0.1383424
DGUOK	791	2.51805	-0.13174	677	3.17376	-0.2590972
DKFZP434C131	1039	2.31782	-0.20212	1068	2.50587	-0.4193891
DKFZP586B1621	889	2.22747	-0.23388	651	3.38742	-0.2078193
DKFZP761G058	1046	4.74183	0.10955741	833	4.56307	0.06021341
DKFZP761P0423	652	1.77483	-0.39298	646	2.14341	-0.5063786
DLG1	585	2.12741	-0.26905	469	2.89774	-0.3253413
DLG2	611	3.08473	0.067439	541	4.56376	0.07449944
DLG3	781	3.53892	0.227082	593	4.6519	0.09565283
DLG4	917	1.46716	-0.50112	625	2.07027	-0.5239321
DMPK	595	2.55131	-0.12005	525	2.96219	-0.3098734
DNAJC3	886	3.27827	0.135466	558	4.50682	0.06083398
DNAJC6	930	4.29105	0.0010179	603	3.59027	-0.1705559
DOK1	604	3.48003	0.206383	545	5.03947	0.18866868
DTYMK	892	4.20836	0.462384	699	4.5931	0.08154097
DUSP1	826	2.21158	-0.23947	689	2.93835	-0.315595
DUSP1	977	4.51256	0.05435343	832	3.97868	-0.0784166
DUSP10	747	3.04424	0.053207	630	2.80485	-0.3476347
DUSP10	852	4.42288	0.03276014	812	3.7514	-0.1323324
DUSP11	1237	5.22807	0.22663504	1033	4.69673	0.09192047
DUSP12	1211	4.28618	-0.0001547	829	4.25757	-0.0122578
DUSP13	958	4.48739	0.04829295	763	4.21913	-0.0213766
DUSP14	885	5.37091	0.26102828	772	5.01596	0.16764877
DUSP15	1174	5.16039	0.21033894	1001	3.6553	-0.1551294
DUSP18	934	3.76909	-0.1246604	823	2.96509	-0.3188622
DUSP19	901	4.08511	-0.0485686	773	4.14166	-0.0397542
DUSP2	653	3.04875	0.054792	656	4.09204	-0.0387122
DUSP2	933	5.27186	0.23717886	779	4.43219	0.02916582
DUSP21	985	4.08291	-0.0490984	1010	4.18269	-0.030021
DUSP22	719	2.12228	-0.27085	567	3.10808	-0.2748602
DUSP22	812	3.97862	-0.0742095	795	3.96007	-0.0828313
DUSP23	946	4.25391	-0.0079247	977	3.9591	-0.0830614

DUSP3	1101	4.14846	-0.0333151	813	3.69961	-0.1446181
DUSP4	822	4.15647	0.444145	671	4.63934	0.09263846
	819	6.09777	0.43604276	741	5.15056	0.19957882
DUSP5	939	2.76627	-0.0445	766	3.59931	-0.1569662
DUSP5	1238	4.55815	0.06533066	845	4.60374	0.06986122
DUSP6	801	2.04535	-0.29789	736	2.68429	-0.3765688
DUSP6	1102	3.69414	-0.142707	904	2.9464	-0.3232959
DUSP7	1243	4.17813	-0.0261711	1009	4.69288	0.09100717
DUSP8	938	1.4462	-0.50849	567	2.3379	-0.4597015
DUSP8	1033	4.09922	-0.0451712	928	3.48736	-0.1949684
DUT	1067	4.28673	-2.227E-05	861	3.5714	-0.1750323
DYRK1A	854	2.31602	-0.20276	579	3.16226	-0.2618571
DYRK1B	563	2.86915	-0.00834	483	3.8713	-0.0916893
DYRK2	790	2.42409	-0.16477	728	3.35049	-0.2166824
DYRK3	620	2.81876	-0.02605	551	4.59192	0.08125777
DYRK4	391	2.15713	-0.2586	585	3.01428	-0.297372
EDN2	513	2.24464	-0.22784	347	3.25915	-0.2386038
EEF2K	427	3.04106	0.052089	415	3.84458	-0.098102
EGFR	692	2.92699	0.011995	524	3.95311	-0.0720551
EIF2AK3	656	3.1676	0.096567	580	3.02786	-0.2941128
EIF2AK4	688	2.90681	0.004902	724	3.2563	-0.2392878
EK11	708	3.41012	0.18181	603	4.51202	0.06208197
ENPP1	950	5.28694	0.24080985	859	3.81983	-0.1160993
ENPP2	971	4.37017	0.02006854	885	3.40773	-0.2138584
ENPP3	885	4.32717	0.00971493	816	4.57318	0.06261172
ENPP4	1180	4.07529	-0.0509331	828	4.30507	-0.0009898
ENPP5	1204	3.41587	-0.2097093	1094	3.94029	-0.0875236
ENPP6	1111	4.23505	-0.0124659	826	4.22181	-0.0207409
ENPP7	898	6.09598	0.43561176	932	4.18428	-0.0296438
EPHA1	769	2.41286	-0.16872	659	3.63234	-0.1490391
EPHA2	820	2.2929	-0.21088	714	2.35424	-0.45578
EPHA3	384	2.49532	-0.13973	459	3.16695	-0.2607315
EPHA4	356	1.27037	-0.57029	453	2.25263	-0.4801661
EPHA5	720	2.19526	-0.2452	515	3.0564	-0.2872633
EPHA6	516	3.53011	0.223985	343	5.33518	0.25963835
EPHA7	383	2.21016	-0.23996	330	2.8087	-0.3467107
EPHA8	372	2.32124	-0.20092	434	2.93264	-0.3169654
EPHB1	528	2.05965	-0.29287	354	2.98352	-0.3047543
EPHB2	572	4.37918	0.522425	386	5.89966	0.39511217
EPHB3	243	2.23511	-0.23119	300	3.57167	-0.1635997
EPHB4	642	1.11905	-0.62348	571	1.72596	-0.6065656
EPHB6	519	1.9519	-0.33074	440	2.71715	-0.3686824
EPM2A	953	6.09373	0.43507	782	5.58794	0.30333488
ERBB2	413	2.85453	-0.01347	443	3.4785	-0.1859603
ERBB3	419	2.35298	-0.18976	475	3.67316	-0.1392424

ERBB4	335	2.42549	-0.16428	637	3.87468	-0.0908781
ERK8	369	2.49958	-0.13824	354	3.49314	-0.1824467
ERN1	305	2.6724	-0.07749	372	3.4709	-0.1877843
EVI1	444	3.35123	0.161111	370	2.91772	-0.3205461
EXOSC10	467	4.33398	0.07090117	333	5.03619	0.16126879
FASTK	651	1.45158	-0.5066	641	2.3311	-0.4613335
FBP1	1067	5.28901	0.24130827	730	4.06924	-0.0569338
FBP2	1221	3.99045	-0.071361	921	3.53096	-0.1846256
FER	498	3.06165	0.059326	481	2.98841	-0.3035807
FES	465	1.91784	-0.34271	265	2.59008	-0.3991789
FGFR1	658	2.62297	-0.09487	552	3.35182	-0.2163632
FGFR2	660	2.35431	-0.1893	481	4.30123	0.01149288
FGFR3	598	3.05057	0.055432	515	3.69853	-0.1331536
FGFR4	679	2.28458	-0.21381	646	3.08301	-0.2808769
FGR	345	2.85311	-0.01397	296	2.22251	-0.4873948
FHIT	991	5.61954	0.32089379	786	4.03754	-0.0644537
FLJ10074	879	3.29668	0.141937	728	4.38914	0.03259107
FLJ10761	569	2.57181	-0.11285	576	3.51863	-0.1763292
FLJ10842	554	3.28454	0.13767	527	5.06752	0.19540061
FLJ12476	617	2.84767	-0.01589	471	3.63414	-0.1486071
FLJ13052	714	2.50227	-0.13729	714	3.48879	-0.1834907
FLJ23074	817	1.93375	-0.33712	702	3.02967	-0.2936784
FLJ23356	549	2.77741	-0.04058	420	3.93411	-0.076615
FLJ23751	713	4.13967	-0.0354316	806	3.30959	-0.2371393
FLJ25006	713	3.63528	0.260952	565	4.29121	0.00908811
FLJ32685	979	2.45525	-0.15382	718	3.8019	-0.1083451
FLJ34389	373	3.55681	0.23337	450	4.07805	-0.0420698
FLJ40125	580	5.01125	0.17442878	590	4.519	0.04975904
FLT1	817	2.66249	-0.08097	735	3.25155	-0.2404278
FLT3	587	3.05552	0.057172	490	4.10962	-0.034493
FLT4	613	1.8374	-0.37099	461	2.33732	-0.4598407
FN3K	825	3.31711	0.149118	820	4.26786	0.00348416
FN3KRP	391	3.87658	0.345766	308	4.23858	-0.003543
FRAP1	744	2.61574	-0.09741	647	3.79444	-0.1101355
FRDA	731	2.1088	-0.27559	795	2.67194	-0.3795327
FRK	939	2.13406	-0.26671	774	3.18815	-0.2556436
FRMPD2	532	4.09193	-0.0469265	337	3.45366	-0.2029628
FUK	435	3.57968	0.241409	504	3.96045	-0.0702935
FYB	824	2.39306	-0.17568	681	3.50125	-0.1805004
FYN	784	2.51707	-0.13209	679	3.34836	-0.2171936
GAK	812	4.00159	0.389706	607	5.164	0.21855557
GALK1	711	3.14465	0.0885	520	3.77706	-0.1143066
GALK2	552	3.13692	0.085783	421	4.70897	0.10934949
GAP43	803	1.89309	-0.35141	670	2.95534	-0.3115174
GCK	900	2.58692	-0.10754	790	4.45545	0.04850531

GFRA2	884	3.61065	0.252294	718	5.05458	0.19229504
GK	847	6.08042	1.120395	847	5.27291	0.24469371
GK2	688	1.95638	-0.32917	646	3.71646	-0.1288505
GMFB	975	2.53054	-0.12735	853	2.91113	-0.3221277
GMFG	734	2.15258	-0.2602	667	3.56708	-0.1647013
GNE	1039	1.8309	-0.37327	998	2.93538	-0.3163078
GRK1	726	2.39071	-0.4831281	715	1.9942	-0.5408945
GRK4	433	1.7962	-0.38547	345	3.49142	-0.1828595
GRK5	881	4.14928	0.441618	669	5.2672	0.24332332
GRK6	696	3.63422	0.260579	557	4.69609	0.10625832
GRK7	647	3.03119	0.04862	458	3.84244	-0.0986156
GSG2	607	3.78244	0.312677	556	5.74232	0.35735096
GSK3A	618	3.44816	0.195181	605	4.68333	0.10319595
GSK3B	811	2.49438	-0.14006	640	3.02996	-0.2936088
GTF2H1	797	2.74196	-0.05304	616	3.83365	-0.1007252
GUCY2C	757	2.55059	-0.12031	593	3.8209	-0.1037851
GUCY2D	657	2.78232	-0.03886	668	3.5997	-0.1568726
GUCY2F	799	3.37248	0.16858	785	4.38321	0.03116788
GUK1	770	3.0433	0.052876	632	3.5989	-0.1570646
HAK	715	3.15586	0.09244	560	4.04896	-0.0490513
HCK	722	3.02334	0.045861	658	4.93398	0.16335134
HIPK1	789	2.11941	-0.27186	642	4.36292	0.02629833
HIPK2	557	3.98716	0.384634	575	5.22565	0.23335142
HIPK3	654	1.68026	-0.42622	561	3.00822	-0.2988264
HIPK4	728	1.85577	-0.36453	579	3.21997	-0.2480069
HK1	616	2.59534	-0.10458	607	3.25659	-0.2392182
HK2	473	1.53403	-0.47762	361	2.75408	-0.3598193
HK3	669	2.42662	-0.16388	422	3.21568	-0.2490365
HRI	546	1.90207	-0.34825	436	3.1845	-0.2565196
HSMDPKIN	839	3.62816	0.258449	541	4.47394	0.05294286
HSPB8	918	1.99519	-0.31552	675	3.72482	-0.1268441
HSPC129	785	4.33416	0.011398	815	4.39002	0.01916218
HUNK	370	2.34314	-0.19322	450	3.97065	-0.0678455
I-4	768	3.96791	-0.0767882	738	4.09014	-0.0519759
ICK	617	3.81501	-0.0596352	472	4.15769	-0.045376
IGBP1	826	3.76394	-0.1259005	740	4.61875	0.07342192
IGF1R	491	3.49561	-0.1399737	590	4.50567	0.03647745
IHPK1	715	3.36125	-0.1737692	546	4.52317	0.04059388
IHPK2	322	3.72401	-0.0825244	548	3.79018	-0.1318234
IHPK3	500	5.38212	0.33453942	731	6.0009	0.3881923
IKBKAP	483	3.8773	-0.0439674	415	4.59643	0.05782643
IKBKB	443	4.42035	0.09262578	457	4.25814	-0.0217477
IKBKE	437	5.12791	0.27059807	535	6.95883	0.61352097
IL2	593	3.79057	-0.0657825	574	4.25355	-0.0228274
ILK	613	4.47675	0.10681205	462	4.35424	0.00085739

ILKAP	1399	4.20888	-0.0187671	1041	4.23709	-0.0171161
ILKAP	1093	4.46532	0.10393707	907	4.69324	0.08059853
IMPA1	1030	4.19698	-0.0216324	973	4.25659	-0.0124903
IMPA2	893	4.44085	0.03708698	739	3.8802	-0.1017782
INPP1	1214	4.22247	-0.0154949	958	3.26058	-0.2487656
INPP4B	998	3.77303	-0.1237118	1106	3.39325	-0.2172934
INPP5B	793	4.94964	0.15959423	917	4.13296	-0.041818
INPP5D	931	4.00018	-0.0690182	836	3.78953	-0.1232871
INSR	450	6.46977	0.6081156	442	6.02548	0.39397412
INSRR	797	3.74386	-0.0775315	519	3.92106	-0.1010372
IPMK	688	4.2123	0.04029504	660	4.88174	0.12493836
IRAK1	592	3.59813	-0.1141869	526	3.25746	-0.2571322
IRAK2	837	3.25812	-0.1997095	809	2.90651	-0.3396843
IRAK3	592	4.84898	0.20043892	633	6.9094	0.60189382
IRS1	449	4.40868	0.08969043	449	4.32526	-0.0059594
ITGB1	500	1.55494	-0.47027	345	1.57414	-0.643002
	368	1.5624	-0.46765	469	2.72102	-0.3677537
	514	2.40574	-0.4141083	469	2.77177	-0.3713784
	570	2.65778	-0.3922434	553	3.29372	-0.240904
	562	2.78762	-0.3917607	479	2.74599	-0.3593047
	537	2.53952	-0.3804587	420	3.04601	-0.3068705
	532	2.89268	-0.3675763	469	1.80097	-0.5875679
	592	2.76875	-0.3655239	498	2.38413	-0.4566786
	401	1.91389	-0.3441	550	2.30973	-0.4664622
	361	1.9278	-0.33921	482	2.64698	-0.3855231
	598	2.90752	-0.3321106	548	2.69305	-0.383396
	595	2.75082	-0.3273105	311	3.32091	-0.2422072
	496	2.8679	-0.2978614	406	1.9206	-0.5715945
	710	3.20171	-0.2964386	480	2.46152	-0.4280165
	487	3.374	-0.256778	446	3.32427	-0.219625
495	3.47058	-0.1965361	384	2.97905	-0.3155506	
ITGB1BP1	366	2.49115	-0.1412	427	3.07239	-0.2834257
ITK	940	4.81203	0.1911449	698	4.63921	0.06788934
ITPK1	489	3.77502	-0.0696938	387	3.55799	-0.1864402
ITPKA	941	5.26811	0.30586252	813	4.91663	0.13314534
ITPKB	765	3.94664	-0.0265263	700	3.84118	-0.1198269
ITPKC	933	4.05078	-0.000332	754	4.62785	0.06521719
JAK1	1038	3.9798	-0.0181856	820	4.2005	-0.035306
JAK2	833	3.76945	-0.0710948	639	4.00306	-0.0817488
JAK3	803	5.98051	0.48505222	557	6.06994	0.4044322
JIK	1034	2.97739	-0.2703214	899	3.47139	-0.2068106
KALRN	609	2.8816	-0.3701268	558	2.29019	-0.4694001
KDR	742	3.16773	-0.2224452	615	3.03564	-0.3093097
KHK	456	5.21403	0.2922598	379	4.64067	0.06823277
KIAA0999	788	4.32692	0.06912537	687	3.77481	-0.1354388

KIAA1361	744	3.79173	-0.0654908	94	4.07977	-0.0637047
KIAA1639	820	4.0813	0.00734466	669	3.6602	-0.1623979
KIAA1765	1063	2.69033	-0.3425255	906	2.87209	-0.3477807
KIAA1804	901	3.54627	-0.1272312	817	3.84267	-0.1194764
KIAA1811	554	4.88625	0.20981343	313	4.23922	-0.0261981
KIF13B	916	4.14542	0.02347274	630	4.685	0.07866027
KIT	664	4.08483	0.00823256	668	3.89236	-0.1077881
KSR2	659	3.49925	-0.1390581	727	4.34301	-0.0017842
LAK	648	5.15372	0.27709005	575	4.57448	0.05266325
LATS1	819	3.38915	-0.1667516	768	3.10618	-0.292717
LATS2	852	3.99636	-0.0140203	715	4.08267	-0.0630225
LCK	814	3.05168	-0.2516353	579	3.49373	-0.2015557
LCP2	774	4.41227	0.09059342	570	4.14816	-0.0476177
LIM	843	3.13434	-0.2308438	775	2.78949	-0.3672103
LIMK1	894	4.75754	0.17743905	711	4.55218	0.04741775
LIMK2	643	6.27173	0.55830267	482	6.25815	0.44870382
LMTK2	1119	3.27592	-0.1952323	754	3.74377	-0.1427402
LMTK3	648	2.82162	-0.3095022	689	2.70743	-0.3865128
LOC115704	1113	4.39099	0.08524087	827	4.08209	-0.063159
LOC151242	1051	4.78973	0.12109085	824	4.71013	0.09509924
LOC388445	725	2.62272	-0.09495	663	2.98912	-0.3034103
LPPR4	627	3.71416	-0.1378866	551	3.96007	-0.0828313
LRRK1	959	2.34156	-0.19378	703	3.512	-0.1779204
LTK	567	3.89607	-0.0392462	516	3.20969	-0.2683689
LYK5	1007	4.59362	0.13620832	751	3.87205	-0.1125655
LYN	688	2.95867	-0.27503	524	2.43002	-0.4517664
MAGI-3	977	3.24036	-0.2041766	814	2.75068	-0.3763393
MAK	780	3.63612	-0.1046313	632	2.70279	-0.3876042
MALT1	852	4.34972	0.07486024	841	3.92347	-0.1004703
MAP2K1	926	3.72319	-0.0827306	851	3.50826	-0.1981379
MAP2K1IP1	897	4.44706	0.09934414	592	4.21046	-0.0329632
MAP2K2	1043	3.7496	-0.0760877	852	3.18895	-0.2732475
MAP2K3	878	3.92128	-0.0329051	781	3.83415	-0.1214806
MAP2K4	884	3.80918	-0.0611016	728	3.73397	-0.1450454
MAP2K5	830	3.56648	-0.1221478	669	3.26804	-0.2546435
MAP2K6	767	3.14319	-0.2286178	479	3.21468	-0.2671951
MAP2K7	928	3.67864	-0.0939362	693	5.18766	0.19689826
MAP3K1	672	2.22194	-0.4603394	590	2.0526	-0.5405449
MAP3K10	1050	3.77414	-0.0699152	514	4.45614	0.02482678
MAP3K11	397	4.3125	0.06549831	308	3.65865	-0.1627625
MAP3K12	835	4.01545	-0.0092186	521	4.03036	-0.0753271
MAP3K13	378	5.24385	0.29976042	332	4.48194	0.03089557
MAP3K14	986	2.60825	-0.363171	530	2.23137	-0.4984938
MAP3K2	739	3.5771	-0.1194766	551	4.33158	-0.0044728
MAP3K3	552	4.36238	0.07804461	390	3.01679	-0.3137437

MAP3K4	956	2.96671	-0.2730077	670	2.80207	-0.3642511
MAP3K5	819	4.01273	-0.0099027	578	4.12553	-0.0529408
MAP3K6	551	3.33085	-0.1814157	456	2.57791	-0.4169791
MAP3K7	779	4.66475	0.15409962	646	4.5816	0.05433805
MAP3K7IP1	538	2.64889	-0.3943839	405	2.92967	-0.3272646
MAP3K8	379	2.57733	-0.3709483	280	2.93049	-0.3340436
MAP3K9	665	3.53433	-0.1302345	372	2.75853	-0.3744928
MAP4K1	852	4.64574	0.14931804	626	5.44184	0.25668764
MAP4K2	1086	3.64245	-0.1030391	709	4.08018	-0.0636083
MAP4K3	1110	3.50343	-0.1380068	709	3.45248	-0.2112587
MAP4K4	1101	3.44015	-0.1539235	684	3.52471	-0.1942684
MAP4K5	502	3.55878	-0.1240846	577	3.15881	-0.2803371
MAPK1	494	3.59287	-0.1155099	327	4.39621	0.01072977
MAPK10	1085	3.62977	-0.1062285	865	3.53808	-0.1911235
MAPK11	850	3.05081	-0.2518541	690	2.65581	-0.3986551
MAPK12	839	4.12696	0.01882951	733	3.05523	-0.3047017
MAPK13	764	3.77951	-0.0685645	776	3.69176	-0.1549742
MAPK14	732	4.81328	0.19145931	678	4.6083	0.06061855
MAPK3	675	4.62534	0.14418684	634	4.25838	-0.0216912
MAPK4	989	5.04074	0.24867224	737	5.16426	0.19139401
MAPK6	1044	4.15155	0.02501462	710	3.70521	-0.1518104
MAPK7	1199	4.16272	0.02782421	898	3.48497	-0.2036163
MAPK8	830	4.66271	0.1535865	796	3.97495	-0.0883609
MAPK8IP1	840	5.19953	0.28861262	681	4.24295	-0.0253207
MAPK8IP2	663	4.41743	0.09189131	624	3.92547	-0.0999998
MAPK8IP3	838	5.55651	0.37840366	727	5.65538	0.3069175
MAPK9	1159	4.11854	0.01671163	833	4.55317	0.04765062
MAPKAPK2	885	4.22412	0.04326812	712	3.57958	-0.1813617
MAPKAPK3	1028	4.43422	0.0961145	777	4.82708	0.11208098
MAPKAPK5	806	5.46799	0.35613826	611	4.05031	-0.0706344
MARCH4	874	5.28992	0.31134839	800	4.47785	0.0299335
MARK1	768	5.17295	0.28192697	657	3.27843	-0.2521996
MARK2	541	6.74557	0.67748747	583	5.70398	0.31834941
MARK3	643	6.23229	0.54838235	580	6.83316	0.5839603
MARK4	533	5.17673	0.28287775	370	4.26715	-0.0196283
MAST2	422	4.26847	0.05442346	402	3.43534	-0.2152905
MAST3	959	5.12661	0.27027108	650	4.71829	0.0864909
MASTL	773	3.41722	0.184306	561	4.42919	0.04220297
MATK	916	5.14918	0.27594811	811	4.05564	-0.0693807
MBIP	923	6.07535	0.50890729	753	5.22204	0.20498528
MELK	879	4.06449	0.00311645	758	4.24516	-0.0248009
MERTK	1015	3.4345	-0.1553447	755	3.98228	-0.0866367
MET	795	5.92514	0.47112503	573	5.61749	0.29800484
MGC1136	743	3.75325	-0.1284744	660	3.85623	-0.1074644
MGC16169	826	5.20128	0.2890528	686	5.28007	0.21863536

MGC26484	784	7.60768	0.79960124	830	7.01079	0.64086587
MGC26597	974	3.55064	-0.126132	760	3.97639	-0.0880222
MGC42105	1151	2.77731	-0.3206474	774	3.39115	-0.225685
MGC45428	717	6.0772	0.50937262	537	5.29829	0.22292116
MGC4796	821	3.69501	-0.0898187	577	4.02132	-0.0774536
MGC5601	1023	4.12868	0.01926214	744	4.11804	-0.0547027
MGC8407	619	4.88206	0.20875952	521	4.46202	0.0262099
MIDORI	882	4.21709	0.04149987	755	4.32917	-0.0050397
MINK	594	3.5603	-0.1237023	533	3.90044	-0.1058875
MINPP1	784	4.75534	0.11281037	819	4.18307	-0.0299309
MK-STYX	814	4.60507	0.07662813	693	3.91478	-0.0935751
MKNK1	756	3.55599	-0.1247864	751	3.94918	-0.0944227
MKNK2	690	5.11976	0.26854811	543	4.50097	0.0353719
MLCK	862	5.57087	0.38201563	712	6.09829	0.41110082
MOS	868	4.72632	0.1695863	646	4.69881	0.08190873
MPP1	886	4.13625	0.02116622	706	4.75283	0.09461556
MPP2	602	4.94212	0.22386639	510	5.12959	0.18323877
MPP3	573	7.17342	0.78510441	527	7.28155	0.68943265
MPZL1	968	4.95744	0.22771982	617	4.07615	-0.0645562
MRC2	791	4.31768	0.06680123	628	3.68636	-0.1562444
MST1R	593	4.76511	0.17934313	591	4.433	0.01938368
MTM1	528	5.86065	0.37894863	689	4.55294	0.05781035
MTMR1	647	5.32577	0.2501594	606	4.2787	-0.0072453
MTMR2	969	3.69009	-0.1436822	963	3.89191	-0.0990004
MTMR3	826	4.42532	0.03334764	873	4.55523	0.05835359
MTMR4	791	4.40551	0.02857776	973	3.90912	-0.0949178
MTMR7	687	4.93025	0.15492547	494	5.62402	0.31189384
MUSK	662	4.55032	0.12531708	664	4.22175	-0.0303075
MVD	480	4.89101	0.21101071	386	5.20316	0.20054424
MVK	1065	3.45695	-0.1496978	794	3.7663	-0.1374405
MYLK	986	2.92764	-0.282835	967	3.55022	-0.1882679
MYLK2	592	4.08831	0.00910789	577	5.2568	0.21316169
MYO3A	663	4.8716	0.20612852	525	5.01343	0.15591508
MYO3B	972	4.90707	0.21505027	189	4.5636	0.05010401
NAGK	661	2.51645	-0.3862615	471	2.2468	-0.4948643
NBEA	540	2.6621	-0.3496262	543	2.3461	-0.4715065
NEK1	362	2.37802	-0.4210807	249	3.06634	-0.3020883
NEK11	330	4.75825	0.17761764	448	5.11074	0.17880479
NEK2	340	5.3916	0.33692392	230	5.9025	0.3650462
NEK3	376	5.16955	0.28107177	410	5.42068	0.25171029
NEK4	352	2.26214	-0.4502279	372	2.17235	-0.5123768
NEK6	456	4.01814	-0.0085419	549	4.22058	-0.0305827
NEK7	735	2.85319	-0.3015614	558	2.60071	-0.411616
NEK8	345	4.64513	0.14916461	307	5.17548	0.19403323
NEK9	883	5.07184	0.25649481	857	4.98301	0.14875955

NLK	520	3.14572	-0.2279814	595	3.21055	-0.2681666
NME1	606	4.96624	0.22993328	699	5.77885	0.33596068
NME2	545	4.50196	0.11315311	628	5.15376	0.18892415
NME3	206	4.37334	0.08080137	229	4.4667	0.02731075
NME4	796	3.99236	-0.0150264	778	3.99498	-0.0836494
NME5	633	3.84523	-0.0520339	755	3.64375	-0.1662673
NME6	794	6.1243	0.52121966	701	5.46763	0.26275409
NME7	675	3.80511	-0.0621253	759	4.03508	-0.0742169
NPR1	535	5.42828	0.34615002	449	4.85421	0.11846263
NPR2	1189	3.65518	-0.0998371	1029	3.16855	-0.278046
NRBP	796	5.27533	0.30767857	633	6.34503	0.46914013
NRBP2	837	2.65587	-0.3511932	606	2.5251	-0.4294013
NRG3	730	3.98536	-0.0167871	539	4.46955	0.02798114
NT4	974	3.82082	-0.1122048	869	3.99024	-0.0756743
	1003	4.02462	-0.1070075	866	3.41337	-0.1981035
	1069	3.65679	-0.0994322	749	4.22841	-0.0287409
	910	2.6446	-0.08726	794	4.13539	-0.0283083
	1315	4.14755	-0.0335342	1193	4.04193	-0.0634123
	870	2.83901	-0.01893	793	3.49051	-0.1830779
	1246	4.33091	0.01061546	1016	4.22779	-0.0193223
	925	2.95215	0.020838	897	3.91907	-0.0802246
	1031	4.64288	0.03531389	834	4.25086	0.00418655
	869	4.66884	0.04128979	842	4.29552	0.01497387
	1012	4.36459	0.07860049	816	4.16641	-0.0433248
	965	4.37667	0.08163897	799	4.49091	0.03300554
	1035	5.02172	0.12252158	1015	4.12996	-0.025016
	956	3.38904	0.174401	814	4.24308	-0.002463
	929	5.01248	0.17472494	917	4.2823	-0.0063913
1182	4.79653	0.18724619	1004	4.10906	-0.056815	
NT5	840	2.48253	-0.14423	699	4.91403	0.15856338
	1059	3.90387	-0.1348037	845	4.03295	-0.0484481
	652	2.5867	-0.10761	728	3.77669	-0.1143954
	1123	3.70653	-0.0869211	750	4.83244	0.11334179
	829	3.77884	-0.068733	921	3.89109	-0.1080869
	870	4.41617	-0.016874	706	3.97813	-0.0876129
	861	4.04259	-0.002392	697	3.6363	-0.1480887
	1090	4.28113	-0.0013706	894	4.37577	0.01578177
	757	4.311	0.0058215	761	4.05947	-0.0592515
	966	4.37082	0.02022505	745	3.96728	-0.0643103
	808	4.87943	0.0897669	828	4.36545	0.03186499
	931	3.1997	0.10785	578	4.68635	0.10392074
	1132	4.18434	-0.0246759	1067	4.53113	0.05263654
	876	4.75842	0.06191081	755	4.56843	0.08089345
	858	3.30253	0.143993	787	4.2706	-0.0091668
923	4.68044	0.15804612	803	4.70072	0.08235801	

NT5+BafA1	815	0.11633	-1.0066827	294	0.0598799	-1.0081165
	814	0.0617671	-1.0036869	564	0.171	-0.9831435
	994	0.0929374	-0.9958466	598	0.0587482	-1.0095478
	889	0.153119	-0.9953196	703	0.0928576	-1.0002183
	623	0.061169	-0.99531	530	0.0925639	-0.9985767
	860	0.170282	-0.9942631	561	0.219345	-0.9695988
	705	0.065018	-0.99396	677	0.0850033	-1.0003912
	928	0.178159	-0.9892904	583	0.136479	-0.9898703
	760	0.0824499	-1.0123354	657	0.0354664	-1.0138327
	662	0.046491	-1.00047	570	0.105843	-0.9953897
	603	0.0824757	-0.9984781	600	0.107328	-0.9981207
	783	0.205873	-0.9860702	448	0.0384797	-1.0132856
	800	0.0889559	-1.0129841	575	0.0562257	-1.0089991
	538	0.018666	-1.01025	517	0.0631233	-1.0056424
	617	0.120994	-1.0030547	562	0.110308	-0.9960787
758	0.0685197	-1.0019884	630	0.060278	-1.009188	
NTRK1	1019	5.14388	0.274615	894	5.32017	0.22806787
NTRK2	833	6.05945	0.50490797	749	5.95209	0.37671098
NTRK3	850	3.99636	-0.0140203	674	4.50942	0.03735954
NYD-SP25	710	3.8093	-0.0610714	749	3.73469	-0.144876
OCRL	1068	4.1814	-0.0253838	741	4.19113	-0.0280189
OSR1	828	4.29972	0.06228376	923	4.66294	0.07347122
P15RS	974	5.25857	0.30346293	859	4.82649	0.1119422
PACE-1	581	6.23756	0.54970791	499	6.0386	0.39706026
PACSIN1	1071	4.1893	0.03450986	891	4.30695	-0.0102664
PAG	802	3.24441	-0.203158	790	3.22397	-0.2650099
PAK1	740	3.83254	-0.0552258	598	3.96725	-0.0901722
PAK1	664	1.48089	-0.4963	511	2.21622	-0.4889044
	719	2.38113	-0.4588556	734	3.03552	-0.3021547
	469	1.60431	-0.45291	532	1.9209	-0.5597805
	735	2.45288	-0.4415795	711	2.77814	-0.3632108
	706	1.92194	-0.34127	575	2.96571	-0.3090287
	563	2.05657	-0.29395	403	2.77188	-0.3555474
	598	3.04748	-0.2526917	375	2.69421	-0.3896225
	677	3.35149	-0.2252108	493	3.44895	-0.2040801
	697	3.71652	-0.1779311	501	3.61598	-0.1491644
	761	3.34558	-0.1777107	578	2.71388	-0.3849956
	668	3.71823	-0.1775374	462	2.80737	-0.3444787
	670	3.34773	-0.1771699	433	2.42039	-0.4540317
	683	3.72764	-0.1753713	626	2.88327	-0.3261456
	744	3.67337	-0.0952618	678	2.77836	-0.3698283
	752	4.13428	-0.0817641	596	2.92812	-0.3153124
598	3.99159	-0.0710865	527	3.43849	-0.2065614	
PAK2	780	5.14643	0.2752564	621	5.05772	0.16633318
PAK3	996	3.43512	-0.1551887	682	4.21303	-0.0323587

PAK4	609	6.60854	0.64302036	449	7.26001	0.68436591
PAK6	1076	4.86319	0.20401315	836	4.66453	0.07384523
PAK7	768	5.44876	0.35130135	686	5.72164	0.32250348
PANK1	791	4.92177	0.21874776	874	5.11267	0.17925877
PANK3	599	3.3548	-0.1753916	455	3.27696	-0.2525453
PANK4	386	4.55785	0.1272111	307	4.44945	0.02325313
PAPSS1	776	4.28666	0.05899879	677	3.61484	-0.1730677
PAPSS2	878	3.81835	-0.058795	574	4.77	0.09865436
PASK	772	4.36116	0.07773774	620	4.32848	-0.005202
PCK1	756	4.467	0.10435964	668	3.34609	-0.2362843
PCK2	636	3.78606	-0.0669169	477	3.24932	-0.2590469
PCTK1	869	5.72835	0.42162651	774	5.69826	0.31700393
PCTK2	779	5.57176	0.38223949	659	4.30747	-0.0101441
PCTK3	1028	4.47625	0.10668629	733	4.79661	0.10491369
PDGFRA	724	3.7814	-0.0680891	473	2.97119	-0.32447
PDGFRB	682	3.74867	-0.0763216	488	4.14791	-0.0476765
PDIK1L	849	3.99886	-0.0133914	777	3.25829	-0.256937
PDK1	1047	3.06454	-0.2484006	783	2.40911	-0.456685
PDK2	808	5.08408	0.25957353	679	3.79932	-0.1296734
PDK3	955	3.15634	-0.2253102	735	3.62101	-0.1716163
PDK4	798	5.45575	0.35305954	560	6.30627	0.46002282
PDP2	906	4.35781	0.01709248	832	4.37825	0.01637008
PDPK1	924	3.84083	-0.0531407	750	4.57874	0.05366531
PDXK	675	5.22064	0.29392241	622	4.50299	0.03584705
PFKFB1	620	4.33095	0.07013903	352	3.71301	-0.1499757
PFKFB1	822	4.57594	0.06961416	804	4.73114	0.10008327
PFKFB2	726	3.9316	-0.0303093	444	4.03444	-0.0743674
PFKFB2	881	4.00362	-0.0681899	790	4.73402	0.10076647
PFKFB3	713	4.29916	0.06214291	762	3.43592	-0.215154
PFKFB3	1016	4.20352	-0.0200577	706	3.94403	-0.0866364
PFKFB4	1078	3.00696	-0.2628837	769	3.60097	-0.1763302
PFKFB4	701	4.36822	0.01959902	733	4.48542	0.04179314
PFKL	797	3.65745	-0.0992662	662	3.60717	-0.1748718
PFKM	1175	4.31865	0.06704522	892	4.32019	-0.007152
PFKP	794	4.58343	0.13364523	618	4.5317	0.04260035
PFTK1	855	3.96432	-0.0220793	581	2.42597	-0.4527191
PGK1	901	3.83013	-0.055832	654	3.72745	-0.146579
PGK2	882	4.38105	0.08274067	676	4.86305	0.12054201
PHKA1	708	5.50876	0.36639313	599	5.41517	0.2504142
PHKA2	998	4.13766	0.02152087	846	3.59263	-0.178292
PHKG1	923	3.66487	-0.0973998	543	3.48909	-0.2026471
PHKG2	376	5.4812	0.35946097	247	3.71996	-0.1483409
PHPT1	731	5.37256	0.26142556	794	4.17072	-0.0328606
PI4K2B	650	4.23835	0.04684739	519	5.10878	0.17834375
PI4KII	802	2.78599	-0.3184642	737	2.54429	-0.4248873

PIB5PA	957	4.19591	-0.0218901	748	3.68954	-0.1470069
PIK3C2A	435	2.35713	-0.4263351	285	1.82244	-0.5946842
PIK3C2B	880	4.30833	0.06444943	640	5.91673	0.36839344
PIK3C2G	1138	2.97552	-0.2707918	676	2.57854	-0.4168309
PIK3CA	622	3.86492	-0.0470813	446	4.33427	-0.00384
PIK3CB	747	3.23695	-0.2050344	666	3.53321	-0.192269
PIK3CG	757	3.15654	-0.2252599	677	4.33116	-0.0045716
PIK3R1	897	2.85983	-0.2998912	750	2.20555	-0.5045673
PIK3R2	1060	3.0003	-0.2645588	599	2.35433	-0.4695706
PIK3R3	472	2.84602	-0.3033648	367	2.59477	-0.4130132
PIK3R4	417	3.37791	-0.1695787	282	2.4008	-0.4586397
PIK4CA	819	2.5437	-0.3794073	686	2.8916	-0.3431915
PIK4CB	668	4.0991	0.01182189	315	3.27316	-0.2534392
PIM1	792	4.35899	0.07719192	621	3.65724	-0.1630941
PIM2	479	4.57537	0.1316179	231	5.0234	0.15826027
PINK1	617	4.53658	0.12186107	534	4.26401	-0.0203669
PIP5K1A	645	2.94354	-0.2788357	494	2.25273	-0.4934694
PIP5K2A	687	4.00212	-0.0125715	585	3.58187	-0.180823
PIP5K2B	835	3.36069	-0.1739101	452	2.55424	-0.4225468
PIP5K2C	544	4.90047	0.21339018	385	5.61446	0.29729211
PIP5KL1	830	4.43682	0.09676847	695	4.05727	-0.0689972
PITPNM3	535	3.61482	-0.1099889	435	4.59593	0.05770882
PKIA	477	3.76428	-0.0723953	223	2.62976	-0.4047827
PKIB	348	1.93699	-0.5320128	164	1.56839	-0.654443
PKLR	863	3.32287	-0.1834229	711	2.75158	-0.3761276
PKM2	740	3.74442	-0.0773906	634	2.89772	-0.3417519
PKMYT1	911	4.11728	0.0163947	620	3.1251	-0.2882665
PKN3	185	2.46983	-0.3979878	173	2.44105	-0.4491719
PLK1	207	3.47984	-0.1439403	198	3.71567	-0.14935
PLK2	735	4.4282	-0.0141047	604	4.07652	-0.0379241
PLK3	771	3.19103	0.104802	514	3.79605	-0.1097491
PLK4	808	3.9368	-0.1272233	606	3.33487	-0.2170647
PME-1	1011	4.31119	0.00586724	746	3.60213	-0.1677425
PMVK	439	3.69332	-0.0902438	333	3.93888	-0.0968455
PNKP	748	3.89811	-0.038733	555	3.15459	-0.2813298
PON1	1160	3.76937	-0.124593	806	3.72272	-0.1391359
PON2	1147	3.63814	-0.1561908	865	3.62787	-0.1616364
PPAP2A	932	3.63921	-0.1559331	565	2.66605	-0.389801
PPAP2B	756	4.30043	0.00327644	718	3.613	-0.1651639
PPAP2C	708	4.3301	0.01042042	671	4.78815	0.11360728
PPEF1	1272	4.33555	0.01173268	891	4.23055	-0.0186676
PPEF2	705	4.42363	0.03294072	651	4.36243	0.01261723
PPM1A	1178	3.10755	-0.2839471	1034	3.12444	-0.2810609
PPM1B	1022	4.35535	0.01650016	680	3.53861	-0.1828108
PPM1D	1019	5.576	0.31041016	876	4.69719	0.09202959

PPM1E	1007	4.52127	0.05645063	868	4.57685	0.06348232
PPM1F	1058	6.51478	0.53645107	821	4.20761	-0.0241094
PPM1G	1020	5.39708	0.26732953	869	4.48252	0.04110519
PPM1L	788	4.97261	0.16512498	663	4.03392	-0.0653125
PPM2C	1219	3.64719	-0.1540117	1073	3.98999	-0.0757336
PPP1CA	871	5.90902	0.39059524	671	4.47703	0.03980285
PPP1CB	675	5.37291	0.26150984	538	4.6548	0.08197376
PPP1CC	1088	4.87842	0.14244577	847	4.03206	-0.0657537
PPP1R11	767	5.12922	0.20283378	460	3.98853	-0.07608
PPP1R16B	934	5.70245	0.34085699	770	5.43161	0.26625
PPP1R1B	1046	4.73802	0.10864004	722	4.0202	-0.0685672
PPP1R1B	767	4.67085	0.15563395	624	4.49893	0.03489204
PPP1R2	728	4.9287	0.15455226	644	5.08261	0.18345961
PPP1R3C	572	3.69359	-0.1428394	457	3.33267	-0.2316643
PPP1R7	753	7.05709	0.66702932	654	6.06493	0.41648729
PPP1R8	946	4.80664	0.12516247	822	4.90192	0.140596
PPP2CA	612	2.98869	-0.2674791	450	3.19912	-0.2708552
PPP2CA	929	3.39727	-0.2141878	821	3.50706	-0.1902952
PPP2CB	965	3.7368	-0.0793073	739	4.04301	-0.0723516
PPP2CB	831	3.73711	-0.1323606	895	4.15762	-0.0359682
PPP2R1A	534	2.26925	-0.4857942	372	2.18164	-0.5047136
PPP2R2A	602	3.87074	-0.100185	678	3.77134	-0.1276022
PPP2R2B	1082	4.80292	0.12426676	1134	3.52626	-0.1857405
PPP2R3A	952	5.23989	0.22948108	864	4.31913	0.00234553
PPP2R4	1002	3.86007	-0.1027541	845	3.6492	-0.1565764
PPP2R5A	674	5.84221	0.37450862	542	5.13152	0.19506212
PPP2R5B	1268	4.06583	-0.0532109	1021	3.6472	-0.1570509
PPP2R5C	1071	4.4001	0.02727513	791	4.24972	-0.01412
PPP2R5D	969	4.96935	0.16434003	846	5.31128	0.23770511
PPP2R5E	782	2.9847	-0.3135271	837	3.96769	-0.0810237
PPP3CA	1023	3.58935	-0.1679385	749	4.34275	0.00794871
PPP3CC	630	5.29825	0.24353309	706	4.74193	0.10264289
PPP3R1	1013	4.01001	-0.0666513	719	3.30046	-0.2393052
PPP4C	945	2.89497	-0.2910525	789	4.19594	-0.0363787
PPP4C	473	4.76356	0.1147896	847	4.26822	-0.0097314
PPP5C	674	5.28288	0.23983227	565	3.9072	-0.0953732
PPP6C	1015	4.14833	-0.0333464	976	3.13509	-0.2785345
PR48	862	5.60921	0.31840652	711	5.0817	0.18324373
PRKAA1	760	3.72987	-0.0810504	425	4.15519	-0.0459641
PRKAA2	945	3.54232	-0.1282248	555	4.80503	0.10689428
PRKACA	889	4.25415	0.05082156	793	3.32815	-0.2405042
PRKACB	616	3.48641	-0.1422878	480	2.56737	-0.4194583
PRKACG	711	4.86656	0.20486081	592	5.57422	0.28782667
PRKAG1	956	4.07254	0.00514127	665	3.78302	-0.1335076
PRKAG3	490	4.84047	0.1982984	316	4.96722	0.14504535

PRKAR1A	606	6.59353	0.6392449	383	7.78617	0.80813168
PRKAR2A	777	3.54026	-0.1287429	661	3.13449	-0.2860578
PRKAR2B	1077	4.41391	0.09100593	866	3.89282	-0.1076799
PRKCA	965	6.42731	0.59743565	846	5.50088	0.2705753
PRKCABP	464	4.22258	0.04288077	425	4.38298	0.00761775
PRKCB1	403	6.30161	0.56581838	246	4.9791	0.14783982
PRKCD	901	4.30135	0.06269376	542	4.45796	0.02525489
PRKCE	764	4.57544	0.13163551	658	3.91489	-0.1024885
PRKCG	922	4.73412	0.17154823	680	4.67072	0.07530127
PRKCH	964	2.52189	-0.3848931	681	3.51041	-0.1976322
PRKCI	1008	4.44302	0.09832796	818	3.97979	-0.0872224
PRKCL1	863	5.35646	0.32808517	737	5.70898	0.31952554
PRKCL2	932	4.29438	0.06094059	653	3.92139	-0.1009596
PRKCM	1112	3.29942	-0.1893213	846	3.2334	-0.2627917
PRKCN	545	3.15901	-0.2246386	315	3.3576	-0.2335768
PRKQC	883	4.56264	0.12841593	666	4.03713	-0.0737347
PRKCSH	674	3.68631	-0.092007	418	4.13561	-0.0505698
PRKCZ	987	4.45951	0.10247568	797	4.47292	0.02877385
PRKD2	902	4.26398	0.05329409	663	3.68254	-0.157143
PRKDC	660	5.02316	0.24425035	503	5.28189	0.21906347
PRKG1	847	3.78564	-0.0670226	517	3.72027	-0.1482679
PRKG2	939	4.34651	0.07405283	605	4.14625	-0.048067
PRKR	1179	2.31792	-0.4361976	1025	2.62633	-0.4055895
PRKRA	988	4.15868	0.02680803	809	4.1646	-0.0437506
PRKWNK1	868	4.23251	0.04537846	857	4.54803	0.04644156
PRKWNK2	881	4.70056	0.16310689	681	4.46934	0.02793174
PRKWNK3	1043	2.71415	-0.336534	1033	4.01243	-0.0795447
PRKX	687	4.02025	-0.0080112	511	5.43711	0.25557503
PRKY	478	4.26025	0.05235589	466	4.5632	0.05000992
PRPF4B	814	4.13283	0.02030599	808	3.95824	-0.0922915
PRPS1	859	5.46469	0.35530822	740	3.72291	-0.1476469
PRPS1L1	736	4.3901	0.08501701	684	4.25603	-0.022244
PRPS2	563	5.50911	0.36648116	477	5.77344	0.33468811
PRPSAP1	383	3.62031	-0.108608	359	4.80706	0.10737179
PRPSAP2	706	3.16716	-0.2225886	687	3.03027	-0.3105729
PSKH1	930	5.06166	0.25393424	852	4.70742	0.08393401
PSKH2	859	4.11005	0.01457614	579	3.77536	-0.1353094
PSPH	1087	3.357	-0.2238841	738	3.55203	-0.1796273
PTEN	1188	4.10498	-0.0437843	1031	3.44698	-0.2045474
PTK2	635	3.29776	-0.1897388	634	3.26429	-0.2555256
PTK2B	709	5.71222	0.41756934	558	6.15764	0.4250614
PTK6	922	3.77979	-0.068494	788	4.17761	-0.0406903
PTK7	778	5.44984	0.351573	781	5.31003	0.22568269
PTK9	649	6.29048	0.56301885	666	5.93458	0.3725922
PTK9L	862	4.08829	0.00910286	683	3.87614	-0.1116035

PTP4A1	820	3.5657	-0.173633	662	3.24452	-0.2525754
PTP4A2	1049	5.14915	0.20763256	868	4.02082	-0.0684201
PTP4A3	741	4.94228	0.15782208	526	4.78051	0.11179491
PTPDC1	1080	4.09395	-0.0464401	791	4.10359	-0.0487852
PTPLA	1063	4.15178	-0.0325157	844	4.87362	0.13388263
PTPN1	883	4.07589	-0.0507887	684	3.90525	-0.0958358
PTPN11	1033	4.75945	0.11379998	798	5.00756	0.16565611
PTPN12	1128	3.8279	-0.1105001	922	4.39325	0.01992841
PTPN13	986	3.53614	-0.1807505	771	3.41493	-0.2121504
PTPN14	980	2.65233	-0.3935556	599	3.30224	-0.2388829
PTPN18	753	4.83272	0.13144205	801	4.54569	0.05609049
PTPN2	943	4.17837	-0.0261134	951	4.08407	-0.0534158
PTPN21	577	4.2557	-0.0074937	616	4.63835	0.07807146
PTPN22	590	4.90006	0.14765628	639	4.40919	0.02370972
PTPN23	732	3.5676	-0.1731755	756	3.38654	-0.2188851
PTPN3	713	4.25636	-0.0073348	561	3.72664	-0.138206
PTPN4	650	4.71038	0.10198483	765	4.93734	0.1489984
PTPN5	362	4.33172	0.07033271	301	4.00923	-0.0802974
PTPN5	439	3.41014	-0.211089	481	4.20589	-0.0245175
PTPN6	754	3.66457	-0.1498269	685	4.549	0.0568757
PTPN7	725	4.14653	-0.0337798	760	4.09852	-0.049988
PTPN9	824	3.47623	-0.1951757	699	4.10034	-0.0495562
PTPRA	528	3.81438	-0.1137554	561	3.0335	-0.3026339
PTPRB	1108	4.38649	0.0239981	910	4.45332	0.03417832
PTPRC	989	4.19219	-0.0227858	896	4.26488	-0.0105238
PTPRD	1027	4.76518	0.11517966	751	4.45821	0.03533833
PTPRE	907	4.33774	0.01225999	821	3.77651	-0.1263757
PTPRF	684	4.21057	-0.0183602	712	3.9217	-0.0919335
PTPRG	564	3.18245	-0.2187427	564	3.03927	-0.3084559
PTPRG	840	4.36562	0.01897298	673	3.64602	-0.1573308
PTPRH	689	4.04869	-0.0573379	787	4.20572	-0.0245578
PTPRJ	523	3.18221	-0.2659703	476	3.35013	-0.2275224
PTPRJ	495	4.75731	0.1773812	456	4.61837	0.06298726
PTPRK	731	4.3744	0.02108705	721	3.19199	-0.2650366
PTPRM	1134	4.50364	0.05220566	879	4.43579	0.03001982
PTPRN	1110	4.53601	0.05999975	895	4.30912	-2.906E-05
PTPRN2	802	3.73807	-0.1321295	685	2.56583	-0.4135754
PTPRO	942	3.31562	-0.2338476	630	4.23212	-0.0182951
PTPRR	402	4.78924	0.18541254	461	4.18017	-0.0400881
PTPRR	827	5.06504	0.18738042	712	5.14972	0.19937956
PTPRS	855	4.23981	-0.0113197	850	3.65886	-0.1542849
PTPRT	1194	2.7066	-0.3804884	464	2.24278	-0.4902099
PTPRT	788	3.97979	-0.0181881	801	3.04617	-0.3068328
PTPRU	889	3.72635	-0.1349514	748	3.4425	-0.2056102
PTPRZ1	1144	3.68073	-0.1459359	855	4.23947	-0.0165516

PXK	585	3.67053	-0.0959762	411	4.17169	-0.0420829
PYCS	398	6.47438	0.60927515	430	6.40829	0.48402044
RAC1	461	4.87396	0.20672213	401	4.61829	0.06296844
RAF1	697	3.69764	-0.0891572	622	3.61093	-0.1739874
RAGE	602	4.16347	0.02801285	467	4.56269	0.04988996
RAPGEF3	489	7.25934	1.534773	500	7.88714	0.87210251
RAPGEF4	378	1.70189	-0.41862	417	3.12715	-0.2702834
RASGRF2	663	4.14334	0.02294956	599	4.06711	-0.0666826
RBKS	582	4.62312	0.0307652	675	3.88744	-0.0835951
RET	813	4.43234	-0.0131517	751	3.73704	-0.1199232
RFK	877	2.52696	-0.12861	727	3.36166	-0.2140016
RFP	593	4.66041	0.03934924	589	4.08544	-0.0357695
RIOK1	578	4.42213	-0.015502	549	4.07024	-0.039441
RIOK3	694	4.38726	-0.023529	801	3.22333	-0.2440064
RIPK1	859	3.63235	-0.1973067	706	2.98346	-0.3019454
RIPK2	485	3.75037	-0.1701389	786	2.59077	-0.396797
RIPK3	672	4.17994	-0.0712533	601	3.37223	-0.2080406
RNASEL	884	4.75266	0.06058488	670	4.09231	-0.0341101
RNGTT	842	4.09505	-0.0461753	842	4.56205	0.05997144
ROCK1	1105	4.11898	-0.0852861	918	3.74107	-0.1189498
ROCK2	888	4.5056	0.0037125	798	3.97544	-0.0623393
ROR1	757	5.21061	0.16600342	829	4.67606	0.10689075
ROR2	649	4.20402	-0.0657102	441	3.47077	-0.1842389
ROS1	538	4.47795	-0.0026524	479	3.84736	-0.0932762
RP2	781	4.75237	0.06051812	680	4.46941	0.05697583
RP6-213H19.1	727	4.55326	0.12605658	791	4.35105	0.00010703
RPS6KA1	555	4.62187	0.03047746	598	4.17261	-0.0147142
RPS6KA2	446	4.46994	-0.0044963	371	3.67187	-0.1356646
RPS6KA3	870	3.81968	-0.154184	674	3.12106	-0.268709
RPS6KA4	576	5.52455	0.23827135	624	4.78963	0.13432282
RPS6KA5	553	4.51235	0.00526632	508	4.36219	0.03107756
RPS6KA6	1060	4.3862	-0.023773	751	3.81377	-0.1013896
RPS6KB1	623	6.29107	0.41472167	599	4.66575	0.10440044
RPS6KB2	931	4.26624	-0.0513874	680	3.98442	-0.0601702
RPS6KC1	954	4.67882	0.04358716	846	3.57461	-0.1591571
RPS6KL1	728	5.5444	0.24284075	640	4.40196	0.04068374
RWDD2	1237	3.97017	-0.0762441	943	4.03479	-0.0651061
RYK	827	4.7622	0.06278095	737	3.94565	-0.0695349
SAG	719	5.60019	0.31623467	639	5.4168	0.26273675
SAST	180	5.98587	0.34446566	459	3.92152	-0.0753633
SBF1	832	4.22208	-0.0155888	897	4.63123	0.07638244
SCAP1	448	3.593	-0.2063649	377	2.6287	-0.3876353
SCYL1	658	3.94287	-0.1258261	730	3.06715	-0.2817306
SEPHS1	642	3.60514	-0.2035704	564	2.93845	-0.3128173
SEPHS2	688	4.78828	0.06878448	560	3.80714	-0.102991

SGK	1094	4.6036	0.02627177	958	3.88257	-0.0847714
SGK2	904	3.63157	-0.1974863	840	3.0816	-0.2782403
SGKL	1142	4.61778	0.02953595	1073	3.97469	-0.0625205
SHC1	1021	5.11787	0.14465499	799	4.03087	-0.0489506
SIK2	608	4.55082	0.01412199	521	3.39821	-0.2017653
SLK	709	5.57451	0.24977197	565	4.96465	0.17659772
SMAD7	1117	3.80013	-0.0633779	965	3.60975	-0.174265
SMG1	872	5.41576	0.21322826	760	5.09552	0.20820849
SNARK	538	4.7906	0.06931854	463	5.13705	0.21823978
SNF1LK	881	3.5768	-0.2100941	769	3.46512	-0.1856037
SNRK	875	6.47822	0.45780297	591	5.37684	0.27615944
SOCS1	739	4.35254	-0.0315214	732	4.40004	0.04021997
SOCS5	991	7.0469	0.58871119	671	4.90572	0.16236358
SPA17	518	6.36002	0.43059373	403	4.65805	0.10254055
SPEC2	776	3.78486	-0.1621994	631	3.00367	-0.2970638
SPHK1	558	5.14482	0.15085879	483	4.52409	0.07018342
SPHK2	856	5.37601	0.20407794	639	5.03171	0.19279561
SQSTM1	427	3.54711	-0.2169287	269	2.44659	-0.4316227
SRC	666	5.64291	0.26551742	438	4.10398	-0.0312913
SRMS	760	7.92945	0.79187122	288	6.78647	0.61664609
SRPK1	794	5.04639	0.12820053	761	4.07948	-0.0372091
SRPK2	736	4.73733	0.05705596	663	4.50018	0.06440812
SSH3	1146	4.66525	0.09111836	993	3.61781	-0.1640228
SSTK	996	5.55359	0.24495626	779	4.12195	-0.0269508
STK10	1045	4.65933	0.03910062	994	3.70134	-0.1285463
STK11	441	5.85706	0.31481403	460	5.17715	0.22792567
STK16	406	2.72683	-0.4057544	346	1.96832	-0.5471456
STK17A	664	5.21153	0.1662152	755	3.9414	-0.0705614
STK17B	911	4.65418	0.03791511	752	3.87707	-0.0860999
STK19	623	3.86602	-0.1435167	576	4.21304	-0.0049486
STK22B	786	3.94951	-0.1242975	645	3.68198	-0.1332226
STK22C	580	2.77501	-0.3946635	428	2.49825	-0.4191446
STK22D	706	2.63811	-0.4261774	678	1.96536	-0.5478606
STK23	1021	3.03	-0.3359656	863	2.85819	-0.3322035
STK24	810	4.32043	-0.038913	762	4.25834	0.00599329
STK25	759	4.8196	0.07599424	626	3.95517	-0.0672354
STK29	883	4.27161	-0.0501512	734	3.37184	-0.2081348
STK3	654	5.5398	0.24178185	873	4.35299	0.02885536
STK31	494	3.49319	-0.2293409	440	3.28494	-0.2291249
STK32A	770	3.63155	-0.1057808	663	3.3898	-0.2260026
STK32B	751	3.89049	0.350655	557	4.89036	0.15288264
STK32C	857	2.39131	-0.4177379	655	2.30779	-0.4805179
STK33	510	4.81061	0.07392477	528	4.68759	0.10967574
STK35	678	4.40209	-0.0201152	580	3.60037	-0.1529349
STK36	746	4.45266	-0.0084741	421	4.02941	-0.0493032

STK38	705	2.70309	-0.4112192	733	1.66487	-0.6204419
STK38L	643	3.58225	-0.2088396	830	2.75822	-0.3563506
STK39	639	2.36816	-0.488319	608	1.77336	-0.5942369
STK4	681	4.87119	0.08787008	497	3.69037	-0.131196
STK6	220	3.83255	-0.1512213	212	3.15685	-0.2600642
STYK1	546	1.54371	-0.47421	410	1.8344	-0.5805403
STYX	921	4.68898	0.09683211	804	3.83821	-0.1117392
SYK	480	5.4734	0.22649679	391	5.42226	0.28713034
SYNJ1	825	5.32643	0.25031831	631	4.32422	0.00355299
SYNJ2	675	5.43583	0.27665981	518	4.18786	-0.0287946
TAF1	576	4.83136	0.07870135	521	4.35393	0.02908241
TAF1L	679	4.21848	-0.0623816	571	4.44945	0.05215463
TAO1	605	3.93115	-0.0304225	637	2.82749	-0.3582717
TAO1	729	3.83774	-0.1500266	467	3.64285	-0.1426742
TBK1	557	3.46918	-0.2348679	615	3.73283	-0.1209401
TEC	793	4.28629	-0.0467719	726	4.31792	0.02038444
TEK	776	4.88534	0.09112736	740	3.76285	-0.113689
TENS1	882	3.1756	-0.2675619	570	2.8646	-0.3427006
TESK1	552	2.63881	-0.4260163	441	2.83851	-0.3369571
TESK2	826	3.429	-0.2441172	655	3.59994	-0.1530388
TEX14	437	3.91547	-0.1321334	435	3.77658	-0.1103726
TGFBR1	629	5.37391	0.20359453	584	4.42772	0.04690589
TGFBR2	876	5.82014	0.30631517	881	5.23721	0.24243276
THNSL1	868	2.69115	-0.0709	525	4.60387	0.08412574
TIE	780	4.14691	-0.0788567	513	3.45604	-0.1877969
TJP2	875	5.1559	0.15340936	736	3.71156	-0.1260777
TK1	818	5.50204	0.23308962	705	4.80596	0.13826722
TK2	759	3.81984	-0.1541471	606	2.74646	-0.3591912
TLK1	882	4.83303	0.07908578	813	4.00853	-0.0543466
TLK2	632	2.88127	-0.3702028	496	2.55571	-0.4052655
TLR1	865	3.69453	-0.1829931	1027	3.36247	-0.2103981
TLR3	447	4.96404	0.10924384	465	4.9923	0.18327639
TLR4	637	5.68652	0.2755563	527	4.65944	0.1028763
TLR6	432	5.15519	0.15324592	319	3.11514	-0.270139
TNFRSF10A	830	5.30526	0.18779153	811	4.02806	-0.0496293
TNIK	636	4.49204	0.11065794	599	4.29417	-0.0132725
TNK1	668	4.79639	0.07065137	636	4.55601	0.07789348
TNK2	576	2.44614	-0.15702	481	3.16398	-0.2614443
TNNI3K	952	3.21823	0.114363	870	4.13933	-0.0273627
TOPK	1073	6.39589	0.43885088	871	4.37154	0.03333599
TP53RK	708	3.20291	0.108978	861	3.35983	-0.2144408
TPK1	520	7.06157	0.59208817	474	6.08447	0.44708271
TPRXL	974	2.04794	-0.29698	899	2.53031	-0.4135236
TPTE	1155	3.78392	-0.1210896	1029	3.73411	-0.1364339
TPTE2	845	3.71451	-0.1378023	838	3.472	-0.1986121

TRIB1	669	1.73157	-0.40818	529	2.33119	-0.4613119
TRIB2	846	4.04246	-0.1029008	538	4.15876	-0.0180596
TRIB3	786	2.39797	-0.17395	664	2.57526	-0.4027357
TRIM	577	5.50278	0.23325997	525	4.64892	0.10033526
TRIO	852	4.05416	-0.1002075	598	3.73951	-0.1193266
TRIO	1106	4.70883	0.10161162	945	4.36879	0.01412596
TRPM6	878	5.41269	0.21252156	772	4.15101	-0.0199315
TRPM7	742	3.97128	-0.1192862	539	3.65129	-0.1406356
TSKS	589	4.9192	0.09892182	598	5.34718	0.26899527
TTBK1	874	3.7048	-0.180629	704	3.27006	-0.2327191
TTBK2	663	4.3291	-0.0369172	573	4.29948	0.01593038
TTK	415	5.32767	0.19295024	360	4.65376	0.10150433
TTN	864	3.63752	-0.1961166	836	3.43318	-0.1933186
TXK	698	6.45603	0.45269491	480	4.33546	0.02462111
TXNDC3	946	3.54823	-0.2166709	891	2.95296	-0.3093125
TYK2	690	3.51664	-0.2239428	592	2.46843	-0.4263474
TYRO3	893	5.70813	0.28053085	734	4.75159	0.12513451
UCK1	858	3.8915	-0.1376513	772	2.92095	-0.3170443
UGP2	962	4.41248	-0.0177234	757	3.64304	-0.1426283
UHMK1	1120	6.00919	0.49226609	933	5.81131	0.34359607
ULK1	1086	3.49649	-0.2285812	946	3.10806	-0.2718491
ULK2	1021	5.08813	0.13780894	747	4.40058	0.04035041
ULK4	728	3.45418	0.197297	640	3.67882	-0.137884
UMP-CMPK	946	4.40935	-0.0184439	752	3.46458	-0.1857341
UMPK	672	5.00157	0.11788312	583	3.30262	-0.2248544
URKL1	1018	4.43907	-0.0116025	718	3.91241	-0.0775638
VRK1	987	5.1418	0.15016359	761	4.06909	-0.0397188
VRK2	744	3.93042	-0.128692	546	3.69657	-0.1296985
VRK3	594	5.73358	0.28638935	764	4.58819	0.08566634
WEE1	124	4.65361	0.0377839	117	1.99754	-0.5400877
WIF1	857	4.20648	-0.0651439	711	3.06224	-0.2829166
WNK4	710	3.65008	-0.1011199	534	4.29129	-0.01395
XYLB	1023	3.99015	-0.1149424	806	3.04853	-0.2862282
YES1	938	4.86426	0.08627482	888	4.67583	0.10683519
YWHAH	876	5.85431	0.31418099	813	4.70456	0.11377473
YWHAQ	643	3.23731	-0.2882436	613	3.10872	-0.2716897
ZAK	920	4.90385	0.0953883	744	4.03619	-0.0476655
ZAP70	736	6.78755	0.52900969	735	6.48596	0.54405992
ZFH1B	1080	5.01317	0.17489108	125	4.9647	0.15548879

Table S1-8. Normalised data values (related to Figure 6-5) between NT5+BafA1 (-1) and NT5 (0). The table shows kinome and phosphatome results and deconvolution of 4 individual siRNAs (2 biological replicates, 2 technical replicates per biological replicate). Validated positive regulators are highlighted in orange, while negative are in green. Controls (ITGB1 and PAK1) are in dark red, NT5+BafA1 is in pink and NT5 is turquoise.

	K&Ph	siRNA1				siRNA2				siRNA3				siRNA4			
NT5	2E-17	-0.015	-0.09	0.1764	-0.092	-0.041	0.1007	0.0081	0.1118	-0.002	-0.008	0.168	0.0515	0.0584	-0.002	-0.353	-0.071
NT5+BafA1	-1	-0.991	-1.012	-0.957	-0.988	-1.028	-1.003	-1.026	-0.998	-0.954	-0.998	-0.994	-1.022	-1.027	-0.987	-1.022	-0.992
COPB2	-0.994	-0.982	-0.69	-1.098	-1.057	-0.944	-0.941	-1.121	-1.022	-0.971	-0.963	-0.985	-1.089	-0.999	-0.991	-1.115	-1.05
EPHB4	-0.615	-0.365	-0.324	-0.276	-0.347	-0.436	-0.273	-0.138	-0.205	-0.486	-0.47	-0.348	-0.117	-0.299	-0.232	-0.057	-0.08
DGKE	-0.613	0.0423	0.1026	-0.118	0.0577	-0.256	-0.237	-0.5	-0.31	-0.474	-0.402	-0.301	-0.517	-0.236	-0.2	0.076	0.0449
PKIB	-0.593	-0.529	-0.524	-0.102	-0.281	0.0435	-0.334	-0.171	-0.294	-0.091	-0.068	0.0506	-0.029	-0.198	-0.354	-0.443	-0.444
STK39	-0.541	-0.394	-0.554	-0.143	-0.294	-0.37	-0.571	-0.34	-0.16	0.4819	0.3519	0.4014	0.2261	-0.377	-0.353	-0.305	-0.426
STYK1	-0.527	0.0571	0.0061	0.242	0.122	0.2109	0.215	-0.193	-0.432	-0.442	-0.584	-0.668	-0.672	-0.661	-0.73	-0.87	-0.823
EPHA4	-0.525	-0.474	-0.432	-0.434	-0.403	-0.753	-0.693	-0.372	-0.454	-0.186	-0.159	-0.017	-0.067	-0.514	-0.456	-0.088	-0.214
DLG4	-0.513	-0.171	-0.033	0.0797	0.1952	-0.101	-0.247	-0.201	-0.219	-0.313	-0.36	-0.217	-0.396	-0.096	-0.175	0.1024	0.0802
GRK1	-0.512	-0.482	-0.601	-0.75	-0.727	-0.595	-0.391	-0.153	-0.291	-0.256	-0.281	-0.394	-0.268	0.1038	-0.078	-0.038	-0.06
PIK3C2A	-0.511	-0.005	-0.093	0.2796	0.1771	-0.095	-0.051	0.0673	-0.097	-0.418	-0.478	-0.136	-0.142	-0.703	-0.858	-0.796	-0.852
MAP3K1	-0.5	-0.287	-0.359	-0.369	-0.278	-0.883	-0.813	-0.732	-0.749	-0.45	-0.577	-0.39	-0.667	-0.234	-0.275	-0.036	-0.279
PPP2R1A	-0.495	-0.626	-0.725	-0.63	-0.595	-0.534	-0.565	-0.448	-0.483	-0.617	-0.599	-0.36	-0.359	-0.108	-0.082	-8E-04	-0.15
DUSP8	-0.484	-0.445	-0.311	-0.469	-0.443	-0.201	-0.169	0.0135	-0.186	-0.609	-0.314	-0.484	-0.517	-0.077	-0.031	0.1625	0.2264
FASTK	-0.484	-0.024	0.0378	0.3187	0.1515	-0.213	-0.308	0.0602	-0.467	-0.528	-0.533	-0.466	-0.308	-0.393	-0.091	-0.286	-0.271
NEK4	-0.481	-0.207	-0.194	0.0228	-0.104	-0.596	-0.688	-0.511	-0.564	0.1001	0.0883	0.6157	0.2789	-0.568	-0.139	-0.088	-0.302
STRADB	-0.459	-0.442	-0.471	-0.199	-0.339	0.097	-0.064	-0.095	-0.1	-0.463	-0.5	-0.381	-0.501	-0.074	-0.14	0.5553	0.179
ITGB1	-0.375	-0.409	-0.463	-0.327	-0.254	-0.278	-0.44	-0.345	-0.079	-0.355	-0.427	-0.458	-0.288	-0.393	-0.414	-0.33	-0.335
PAK1	-0.301	-0.084	-0.419	-0.357	-0.368	-0.574	-0.302	-0.561	-0.165	-0.01	-0.488	-0.415	-0.566	0.1461	-0.323	-0.755	-0.559
EPM2A	0.3692	-0.169	-0.291	-0.281	-0.391	0.0166	-0.217	-0.397	-0.388	0.22	-0.053	-0.111	-0.162	-0.176	-0.244	-0.383	-0.471
CDK16	0.3693	-0.616	-0.601	-0.398	-0.322	0.4333	0.4618	0.4697	0.1884	0.2865	0.1923	0.0137	-0.034	-0.223	-0.383	-0.45	-0.541
MET	0.3846	0.4056	0.2437	0.3624	0.1198	-0.322	-0.514	-0.384	-0.606	-0.279	-0.233	0.0411	-0.325	-0.229	-0.159	-0.345	-0.609
CIT	0.4073	0.1122	0.4256	0.5221	0.3319	-0.067	-0.14	-0.269	-0.121	-0.191	-0.13	0.0272	0.0269	-0.165	-0.025	-0.399	1.382
UHMK1	0.4179	0.7182	0.7955	1.2812	0.9996	-0.734	-0.921	-0.467	-0.941	-0.081	-0.029	0.0414	0.0619	-0.181	-0.239	-0.078	-0.104
PTK2B	0.4213	0.1416	0.2445	0.4784	0.4219	0.0407	-0.093	0.0479	-0.121	-0.222	-0.277	-0.151	-0.168	-0.069	-0.015	0.4306	0.1825
STKLD1	0.4355	0.3244	0.3108	0.0571	-0.096	-0.296	-0.214	-0.093	-0.057	-0.107	0.0193	0.2226	0.0842	-0.023	0.1739	-0.265	-0.01
NTRK2	0.4408	-0.304	-0.126	-0.038	-0.307	0.0014	0.2097	0.1121	-0.167	-0.173	-0.037	-0.054	0.0661	-0.205	-0.219	-0.075	-0.274
JAK3	0.4447	0.0843	0.2423	0.2412	0.3515	-0.53	-0.486	-0.361	-0.285	-0.105	0.0522	0.2274	0.1925	0.2713	0.4325	0.1206	0.5513

EPHB2	0.4588	0.2968	0.3597	0.3636	0.4135	0.4017	0.4557	0.7575	0.8816	-0.256	-0.181	-0.175	-0.475	-0.325	-0.058	-0.068	-0.087
TWF1	0.4678	-0.051	0.2283	0.0521	0.1656	-0.247	-0.003	0.1498	0.1094	-0.383	-0.243	-0.515	-0.369	-0.104	0.1199	-0.107	-0.04
SCYL3	0.4734	0.4213	0.6303	0.3042	0.4061	-0.388	-0.255	-0.24	-0.34	-0.274	-0.174	-0.224	-0.254	0.3264	0.22	0.1131	0.3321
MARK2	0.4979	0.0106	0.0092	0.1428	0.0575	0.2456	0.191	-0.18	-0.051	0.1958	0.1184	0.0126	-0.088	-0.034	-0.089	-0.37	-0.515
INSR	0.501	-0.111	-0.095	0.1217	0.1145	-0.197	-0.061	-0.17	0.0262	-0.237	0.0037	-0.333	-0.194	-0.164	-0.238	-0.208	-0.204
LIMK2	0.5035	-0.321	-0.195	0.4365	0.0778	-0.205	-0.004	-0.059	-0.047	0.0122	-0.184	0.3824	0.2632	0.059	0.2544	0.2151	0.4923
TPK1	0.5196	-0.033	-0.243	-0.183	-0.036	0.2687	-0.057	-0.138	0.03	0.3855	0.4098	0.5879	0.2826	-0.125	-0.221	-0.189	-0.078
ZAP70	0.5365	0.0761	0.1727	-0.223	0.0355	0.0955	0.0686	-0.103	-0.09	0.5419	0.7097	0.8333	0.6715	-0.047	-0.062	0.2106	0.1094
PPP1R7	0.5418	-0.048	0.1124	0.7163	0.2927	0.0044	-0.136	-0.095	0.3216	-0.152	-0.172	0.1845	0.1943	-0.044	0.1213	-0.096	0.2045
ALDH18A1	0.5466	-0.648	-0.436	-0.321	-0.033	-0.104	-0.033	0.0316	0.1356	0.5037	0.3973	0.8147	0.8141	0.1566	0.279	-0.245	0.3256
MARK3	0.5662	-0.106	-0.104	-0.492	-0.378	-0.041	0.0948	0.1619	0.2216	0.4659	0.5649	0.2939	0.4815	0.3595	0.3395	0.6171	0.4341
DCLK1	0.6011	0.6008	0.6723	-0.024	-0.235	-0.099	-0.052	0.0373	-0.133	0.2253	0.4129	-0.029	0.0113	0.1237	0.1103	-0.36	-0.276
CDK20	0.6717	-0.323	-0.296	-0.495	-0.703	0.4418	0.0784	0.2986	-0.261	1.3869	1.2967	0.5087	1.1763	-0.17	-0.087	-0.398	-0.495
AKAP11	0.6787	1.1855	0.8223	0.637	0.6142	0.0543	0.0336	-0.176	-0.069	-0.381	-0.411	-0.456	-0.227	-0.15	0.2388	-0.243	0.0912
SRMS	0.7043	0.864	0.7821	0.867	0.2247	0.9095	0.2846	0.4096	0.2749	-0.235	-0.201	-0.277	-0.214	-0.195	-0.258	0.1731	-0.134
PRKAR1A	0.7237	0.9788	1.1255	0.8608	0.2293	0.9939	0.8199	0.5287	0.3106	0.6619	0.5952	0.6658	0.5961	0.8007	0.6975	0.8086	0.7965
MPP3	0.7373	-0.348	-0.293	-0.161	-0.252	0.5109	0.3283	0.1424	0.1089	0.6348	0.536	0.3878	0.5883	0.8437	0.4547	0.6526	0.6338
CDKN3	0.7747	0.0321	0.1535	0.1547	0.0595	0.1201	-0.124	-0.276	-0.585	0.3904	0.1695	0.0816	-0.252	-0.589	-0.611	-0.581	-0.495
AURKB	0.8987	0.4885	0.2626	0.3085	0.1749	0.2721	0.4965	0.1842	0.5986	0.4126	0.107	0.5416	0.588	0.3389	0.0387	0.1453	0.0783
RAPGEF3	1.2034	-0.216	-0.277	-0.234	-0.318	0.125	-0.026	0.0052	0.1414	0.4797	0.4936	0.2905	0.1973	-0.121	0.0692	0.0904	-0.013